

This is to certify that the dissertation entitled

UNIVERSAL REALIZABLE ANISOTROPIC PRESTRESS CLOSURE FOR THE NORMALIZED REYNOLDS STRESS

presented by

KARUNA SREE KOPPULA

has been accepted towards fulfillment of the requirements for the

Ph.D degree in Chemical Engineering

Major Professor's Signature

MSU is an Affirmative Action/Equal Opportunity Employer

PLACE IN RETURN BOX to remove this checkout from your record.

TO AVOID FINES return on or before date due.

MAY BE RECALLED with earlier due date if requested.

DATE DUE	DATE DUE	DATE DUE
	_	
-		

5/08 K:/Proj/Acc&Pres/CIRC/DateDue.indd

UNIVERSAL RI AT FOR THE

In par

UNIVERSAL REALIZABLE ANISOTROPIC PRESTRESS CLOSURE FOR THE NORMALIZED REYNOLDS STRESS

Ву

KARUNA SREE KOPPULA

A DISSERTATION

Submitted to
Michigan State University
in partial fulfillment of the requirements
for the degree of

DOCTOR OF PHILOSOPHY

Chemical Engineering

2009

The Reynolds aver.

mod equation that relatively stress. The contribute stress. The contribute statistical closure for first existical closure model for himself them theory, the normalized diadic-valued, algorithms diadic-valued, algorithms.

The field velocity gradient, they stems from an analys

oral turbulent time scale, a

fectof a constant property

hastling closure can be

te class of benchmark

JE 2512

The foregoing low-or

Dian fluctuating veloci

ation correlations have

ABSTRACT

UNIVERSAL REALIZABLE ANISOTROPIC PRESTRESS CLOSURE FOR THE NORMALIZED REYNOLDS STRESS

By

Karuna Sree Koppula

The Reynolds averaged Navier-Stokes (RANS-) equation is an exact, albeit unclosed, equation that relates the mean velocity field to the mean pressure field and the Reynolds stress. The continuity equation and a Reynolds stress model provide a low-order statistical closure for the RANS-equation. This research has developed a new algebraic closure model for the Reynolds stress that is *realizable* for all turbulent flows. In the new theory, the normalized Reynolds (NR-) stress is a solution to an implicit, non-linear, dyadic-valued, algebraic equation that depends on the relative importance of a local turbulent time scale, a local viscous time scale, a local time scale related to the mean field velocity gradient, and a time scale associated with the frame of reference. The theory stems from an analysis of the dynamic equation governing the fluctuating velocity field of a constant property Newtonian fluid in a rotating frame of reference. Therefore, the resulting closure can be applied in either inertial or non-inertial frames regardless of the class of benchmark flows used to determine the phenomenological closure parameters.

The foregoing low-order closure model for the RANS-equation generalizes earlier research by Parks (1997) and Weispfennig (1997) based on an integral analysis of turbulent fluctuating velocity fields and the physical assumption that all space-time turbulent correlations have finite memories. In this research, the Parks-Weispfennig

great is extended to no Escapablem from the N resize fluctuations, and assathypition, siri shaft process to the N Emped and combined is Total realizable announce tion of other algebraic isse provides an answer Ander closure model them hows independen The URAPS-closus red The mapping depen alema a local scalar-

 \mathcal{Y}_{i}

Tate CRAPS-closure is formati flows: rotati

statise rotating fully-d.

and complementary dire

From its use as a closs

approach is extended to non-inertial frames. A preclosure equation shifts the turbulence closure problem from the NR-stress to a normalized prestress. The prestress is caused by pressure fluctuations and fluctuations in the instantaneous Reynolds stress. A self-consistent hypothesis, similar to the one for the pressure/strain rate correlation, is used to relate the prestress to the NR-stress. In the present research, a closure for the prestress is developed and combined with the preclosure equation for the NR-stress to produce a universal realizable anisotropic prestress (URAPS-) closure for the NR-stress. A critical review of other algebraic closure models in the literature indicates that the URAPS-closure provides an answer to one of the key questions in turbulence modeling: Can a low-order closure model for the NR-stress be formulated that is *realizable* for all turbulent flows independent of the specific benchmark flows used for calibration?

The URAPS-closure is formulated as a mapping of a non-negative operator into itself. The mapping depends on the rotational operator $\underline{\Omega}$ associated with the frame of reference, a local scalar-valued turbulent transport time scale τ_R , and an operator $<\underline{F}>(\equiv \nabla <\underline{u}>+2\underline{\Omega})$:

$$\underline{\underline{\mathfrak{R}}}(\underline{\underline{R}}, \tau_{R} < \underline{\underline{F}} >) = \underline{\underline{R}} \quad , \quad \underline{\underline{R}} \equiv \frac{<\underline{u}'\underline{u}'>}{\operatorname{tr}(<\underline{u}'\underline{u}'>)}.$$

The URAPS-closure is used to predict the components of the NR-stress for three benchmark flows: rotating homogeneous decay, rotating homogeneous shear, and spanwise rotating fully-developed channel flows. The URAPS-predictions are consistent with complementary direct numerical simulations of these flows and, thereby, partially supports its use as a closure model for the RANS-equation.

dedicated to my parents and my husband

East and foremost.

The Perty for his guide and received I would associated Professor Krishnan East Dr. Brigette Rosen.

Signification putting to get in

Lowe this dream to accourage and encourage and encourage and properties are tremendous strength.

is due to my brother V

The same helped me

Tean Kim for all of his

Special thanks are got allowing me to pursuate thank the Department

Special of Mechan

Mireconst Comp.

NSF 500 0331977 1 Ser a

ACKNOWLEDGEMENTS

First and foremost, I would like to express my deepest gratitude to Professor Charles Petty for his guidance, encouragement and continuing support throughout this entire research. I would also like to thank my committee members, Professor André Bénard, Professor Krishnamurthy Jayaraman, Professor Fahrad Jaberi, Professor Mei Zhuang, Dr. Brigette Rosendall and Professor John Foss for their oversight and helpful suggestions in putting together this dissertation.

I owe this dream to my mother and father who have given me their unlimited love, caring and encouragement. I need to specially thank my husband Prashanth who has given me tremendous strength and inspiration to help me finish this degree. Thanks are also due to my brother Vivekanand, my cousins and many friends at Michigan State University who helped me in various ways during this ride. I also would like to thank Dr. YoChan Kim for all of his support.

Special thanks are given to Bechtel National for the unique opportunities given to me, allowing me to pursue both my professional and academic goals. Finally, I would like to thank the Department of Chemical Engineering and Materials Science and the Department of Mechanical Engineering, and the National Science Foundation Industry/University Cooperative Research Center for Multiphase Transport Phenomena (NSF/ECC 0331977) for all their financial and technical support during the research

INTOFTABLES

WOFFIGURES .

ZZŒNOTATION

LNRODUCTION

- 11 Rationale for Tax
- 12 Tampience Closs.
- 13 The Normalized F 14 Objectives of This
- 15. Online of the D.s.

LITERATURE REVIEW

- 21 Introduction
- 22 Non-Rotating Fo
- 23 Rotating Fully-Di
- 24 Homogeneous S 25 Homogeneous D
- 26 Algebraic Mode
- 27 Conclusions

EURAPS-CLOSURI FO

- 3.1 Introduction .
- 32 Hydrodynamic 33 Prestress Closa
- 34 URAPS-Closus
- 35 Turbulant Rela
- 3.6 Transport Equa 37 Fixed-Point M
- 3.8 Conclusions...

AMODEL CALIBRAT

- 41 Introduction.
- 42 Dissipation (43 Turbulent Tra
- 44 Coefficients (
- 45 Production C
- 16 Contraction 4. Conclusions.

TABLE OF CONTENTS

LIST OF	TABLES	ix
LIST OF	FIGURES	x
LIST OF	NOTATION	xvi
1. INTR	ODUCTION	1
1.1	Rationale for Turbulence Modeling Research	1
1.2	Turbulence Closure Problem	2
1.3	The Normalized Reynolds Stress	7
1.4	Objectives of This Research	
1.5	Outline of the Dissertation	14
2. LITER	RATURE REVIEW	18
	Introduction	
2.2	Non-Rotating Fully-Developed Channel Flows	18
2.3	Rotating Fully-Developed Channel Flows	32
2.4	Homogeneous Simple Shear	52
2.5	Homogeneous Decay	
· 2.6	Algebraic Models for the NR-Stress	60
2.7	Conclusions	75
3. URAF	S-CLOSURE FOR THE NORMALIZED REYNOLDS STRESS	77
3.1	Introduction	77
3.2	Hydrodynamic Preclosure	
3.3	Prestress Closure and "Extra" Anisotropy	82
3.4	URAPS-Closure	
3.5	Turbulent Relaxation Time scale	97
3.6	Transport Equations for Turbulent Kinetic Energy and Dissipation	97
3.7	Fixed-Point Mapping and Solution Strategy of the URAPS-closure	98
3.8	Conclusions	100
4. MOD	EL CALIBRATION	103
4.1	Introduction	103
4.2	Dissipation Coefficient	
4.3	Turbulent Transport Time	
4.4	Coefficients of First and Second-Order "Extra" Anisotropy (α and β)	
4.5	Production Coefficient	
4.6	Contraction Mapping and "Extra" Anisotropy	
	Conclusions	

SEMOGENEOUS DEC 51 Introduction 🖸 Tuffulent Energie 33 Preclosure Opera 54 The NR-Stress F SS "Extra" Anisotro (if Condusions : ELMOGENEOUS SHI 61 Introduction 62 Dynamic Equation 63 Preclosure Opera-64 Asymptotic States 65 Asymptotic "Fatte hh Developing F. I Shear 67 Developing "I xir. of Conclusions TELLY-DEVELOPED (Il Introduction... 12 Preclosure Opera 13 Locus of States P 74 NR-Stress in the 75 NR-Stress in the % NR-Stress for Ze "Extra" Anisotro 3 Conclusions i CONCLUSIONS..... - RECOMMENDATION 91 Turbulent Trans 92 Extra Anisott 93 Espicie URAP A LYCTOSED FO. B LYCLOSED EOI C LYCLOSED EO D.INTEGRITY OF E REALIZABLE S F SPECTRAL AV COMBONENT I HPROGRAMS AV

5. HOM	OGENEOUS DECAY	127
5.1	Introduction	
5.2		
5.3	Preclosure Operator and URAPS-Closure	135
5.4	The NR-Stress: Results and Discussion	136
5.5	"Extra" Anisotropy: Results and Discussion	141
5.6	Conclusions	143
6. HOM	OGENEOUS SHEAR	145
6.1	Introduction	145
6.2	Dynamic Equation for $\tilde{\Gamma}$	145
6.3	Preclosure Operator and URAPS-Closure	147
6.4	Asymptotic States for $\tilde{\Gamma}$ and the NR-Stress: Results and Discussion	148
6.5		
	Developing $\tilde{\Gamma}$, \mathcal{P}/ϵ and the NR-Stress (shear component) for Homogen	neous
	Shear	
6.7	Developing "Extra" Anisotropy: Results and Discussion	168
6.8	Conclusions	171
7 FIUI	W DEVELOPED CHANNEL ELONG	17
	Y-DEVELOPED CHANNEL FLOWS	
7.1		
7.2		
7.3		
	NR-Stress in the Outer Region with $\tilde{\Omega} = 0$: Results and Discussion	
7.5		
7.6	NR-Stress for Zero Absolute Mean Intrinsic Vorticity: Results and Discu	
77	"Extra" Anisotropy with $\tilde{\Omega} = 0$: Results and Discussion	
	Conclusions	
7.0	Colletusions	200
8. CON	CLUSIONS	202
9. RECO	DMMENDATIONS	211
9.1		
9.2	•	
	Explicit URAPS-Closure	
A PPENI	DICES	219
	UNCLOSED EQUATION FOR THE REYNOLDS STRESS	
BI	JNCLOSED EQUATION FOR KINETIC ENERGY	223
C. 1	JNCLOSED EQUATION FOR DISSIPATION	226
	NTEGRITY OPERATORS	
	REALIZABLE SHIH CLOSURE FOR THE NR-STRESS	
	SPECTRAL ANALYSIS FOR ROTATING HOMOGENEOUS DECAY	
	COMPONENT EQUATIONS FOR THE URAPS-CLOSURE	
H. 1	PROGRAMS AND FLOW CHARTS	251

LBENCHMARK ST

EEDGRAPHY

I. BENCHMARK STATISTICS	
BIBLIOGRAPHY	

	Boundary (
13:11	Cross Flow 1 Non-Rotation
T2011	Iwamoto et al. Cross Flow V
	Stress for $\Omega_{\chi}^{*} \cong -0$ and
2013	DNS and I DNS (Breet). Speziale 1 (4)
हें: इ.स.	Optimum to Fix Shear.
£42	Summary of
343	Component.
विस्त	Component,
à:Sia	The Influent Figure 5.5 F
₹25.1b.	The Influent "Extra" And Closure
Piet la	Eigenvaluev
1	

Eigenvalues

LIST OF TABLES

Table 1.1	Boundary Characteristics of the L-Triangle (Parks, 1997; Weispfennig, 1997)
Table 2.1	Cross Flow Variation of $\tilde{\Gamma}_{DNS}$ and the Components of the NR-Stress for
	Non-Rotating, Fully-Developed, Channel Flow: (a) $\delta^+ \cong 300$, $\Omega_x^+ = 0$ (
	Iwamoto et al. 2002) ; (b) $\delta^+ \cong 2000$, $\Omega_X^+ = 0$ (Hoyas and Jimenez, 2006)
Table 2.2	Cross Flow Variation of $\tilde{\Gamma}_{DNS}$, $\tilde{\Omega}_{DNS}$, and the Components of the NR-
	Stress for Rotating, Fully-Developed, Channel Flow: $\delta^+ \cong 300$,
	$\Omega_{\mathbf{x}}^{+} \cong -0.0042$ (Wu and Kasagi, 2004)
Table 2.3	DNS and LES Results for Asymptotic Rotating Homogeneous Shear: DNS (Brethouwer, 2005); LES (Bardina et al., 1983 (as reported by Speziale, 1989; Salhi and Cambon, 1997))
Table 4.1	Optimum URAPS Closure Coefficients and Stress Components Compared with the Experimental Results of Asymptotic States for Homogeneous Shear
Table 4.2	Summary of calibration for the URAPS closure parameters 118
Table 4.3.	Components of $\underline{\underline{B}}$, $\underline{\underline{R}}$, and $\underline{\underline{\Delta}}$ ($\tilde{\Gamma}=4$ and $\tilde{\Omega}/\tilde{\Gamma}=0$)
Table 4.4.	Components of $\underline{\underline{B}}$, $\underline{\underline{R}}$, and $\underline{\underline{\Delta}}$ ($\tilde{\Gamma} = 11$ and $\tilde{\Omega}/\tilde{\Gamma} = -5/8$)
Table 5.1a.	The Influence of Rotation on the NR-Stress for Homogeneous Decay (see Figure 5.5 For Prolate States)
Table 5.1b.	The Influence of Rotation Number on the NR-Stress, the Prestress, and the "Extra" Anisotropy for Homogeneous Decay Predicted by The URAPS-Closure
Table 6.1a.	Eigenvalues of $\underline{\underline{B}}$, $\underline{\underline{R}}$, and $\underline{\underline{\Delta}}$ ($\tilde{\Gamma}=4$ and $\tilde{\Omega}/\tilde{\Gamma}=0$)
Table 6.1b.	Eigenvalues of B. R. and Δ ($\tilde{\Gamma} = 11$ and $\tilde{\Omega}/\tilde{\Gamma} = -5/8$)

- Eggeld Realizable S
- fall Definitions
- Em22. Total Shear Flows
- Emergy State
- First Anisotropic s
- Fire25 Kinetic Finer
- Epiclé Dissipation :
- Mean Dimich Developed ()
- Texal X Total Mean δ ≥ 300 and
- $\frac{75529}{\Omega_{\chi}^{2} \simeq -0.0632}$
- ign210 Energy State and $\Omega_{\chi}^{*} \cong -1$
- Anisotropic
 (6° ± 300 ani
- Kinetic Energy and $\Omega_{\chi}^{*} \cong -1$
- $\begin{array}{cc} \frac{1}{16\pi i^2} \frac{1}{2} & \text{Dissipation to} \\ \Omega_{\chi}^2 & \geq -0 \text{ total} \end{array}$
- Flows (6) 2 :

LIST OF FIGURES

Figure 1.1	Realizable States of the NR-Stress (Lumley, 1978)
Figure 2.1.	Definitions of Benchmark Flows
Figure 2.2.	Total Shear Stress Profile for Non-Rotating, Fully-Developed, Channel Flows
Figure 2.3.	Energy States for Non-Rotating, Fully-Developed, Channel Flows 24
Figure 2.4.	Anisotropic States for Non-Rotating, Fully-Developed, Channel Flows . 26
Figure 2.5.	Kinetic Energy for Non-Rotating, Fully-Developed, Channel Flows 28
Figure 2.6.	Dissipation for Non-Rotating, Fully-Developed, Channel Flows 29
Figure 2.7.	Mean Dimensionless Strain Rate $\tilde{\Gamma}_{DNS}$ for Non-Rotating, Fully-Developed Channel Flows
Figure 2.8	Total Mean Shear Stress Profile Across the Rotating Channel for $\delta^+ \cong 300$ and $\Omega_x^+ \cong -0.0042$
Figure 2.9	Mean Velocity and the Mean Velocity Gradient for $\delta^+\cong 300$ and $\Omega_x^+\cong -0.0042$
Figure 2.10	Energy States for Rotating, Fully-Developed, Channel Flow ($\delta^+ \cong 300$ and $\Omega_X^+ \cong -0.0042$)
Figure 2.11	Anisotropic States for Rotating, Fully-Developed, Channel Flows ($\delta^+\cong 300$ and $\Omega_x^+\cong -0.0042$)
Figure 2.12	Kinetic Energy for Rotating, Fully-Developed, Channel Flows ($\delta^+ \cong 300$ and $\Omega_x^+ \cong -0.0042$)
Figure 2.13	Dissipation for Rotating, Fully-Developed, Channel Flows ($\delta^+ \cong 300$ and $\Omega_x^+ \cong -0.0042$)
Figure 2.14	Transverse Profiles of $\tilde{\Gamma}_{DNS}$ for Rotating, Fully-Developed, Channel Flows ($\delta^+ \cong 300$ and $\Omega_v^+ \cong -0.0042$)

Ipalis Transverse Ecusion Egicl 16 Transverse Ratio, P. L Flows is Experimental [1997] Energy Disco Closure, and Figure 11 Eigenvalue m imit The influence Isass The influence fine14 The influence ign 35 The influence 19436 Universal B. $\beta(II_R,III_{\frac{p}{p}})$ 4237 Sammais of [42:4] Isotropic Ho ignate The Influence F243 Constrained Anisotropy Group, N The Influer

Optimization

Figure 2.15	Transverse Profiles of Ω_{DNS} for Rotating, Fully-Developed, Channel
	Flows ($\delta^+ \cong 300$ and $\Omega_X^+ \cong -0.0042$)
Figure 2.16	Transverse Profiles for Turbulent Production/Dissipation Ratio, $\mathcal{P}/\epsilon \equiv -2R_{yz}^{DNS}\tilde{\Gamma}_{DNS}$ for Rotating, Fully-Developed, Channel
	Flows ($\delta^+ \cong 300$ and $\Omega_X^+ \cong -0.0042$)
Figure 2.17	Experimental data of Comte-Bellot and Corrsin (1971) (also see Parks, 1997)
Figure 2.18	Energy Distribution and Anisotropic States for Non-Rotating Simple Shear Predicted by the Generalized Eddy Viscosity Closure, the Bilinear Closure, and the URIPS Closure for increasing values of $\tilde{\Gamma}$
Figure 3.1	Eigenvalue mapping from the λ_R - triangle to λ_B - triangle
Figure 3.2	The influence of λ_{R3} on α_{min} for $\lambda_{B3} = 1$
Figure 3.3	The influence of λ_{R3} on α_{max} for $\lambda_{B3} = 1/2$
Figure 3.4	The influence of λ_{R3} on β_{min} for $\lambda_{B3} = 1/3$ and $\alpha_{min} < \alpha < \alpha_{max} \dots 92$
Figure 3.5	The influence of λ_{R3} on β_{max} for $\lambda_{B3} = 1/2$ and $\alpha_{min} < \alpha < \alpha_{max} \dots 94$
Figure 3.6	Universal Bounds for the "Extra" Anisotropy Functions $\alpha(II_R, III_R)$ and $\beta(II_R, III_R)$
Figure 3.7	Summary of URAPS-Closure
Figure 4.1	Isotropic Homogeneous Decay in an Inertial Frame of Reference 105
Figure 4.2	The Influence of $\left \tilde{\Omega}\right (\equiv \left \Omega\right k/\epsilon)$ on the Turbulent Transport Time Scale
Figure 4.3	Constrained Optimization Strategy for Determining the "Extra" Anisotropy Coefficients, α and β , and the Dimensionless Transport Group, N_{Γ} , for Non-Rotating Asymptotic Homogeneous Shear
Figure 4.4	The Influence of the "Extra" Anisotropy Coefficient α on the Optimization Metric Ψ_{min}^{α}

- 13245 Parametric by the UR 3 Anisotropy 1484 Figure 1. The Develop Facil. The Influence k and k = 1isass. The Influence fants4. Influence of ign55. The Influence igns 6. The Influence The Develo Anisotropy: "Extra" Pres Schematic o Rates of alues of ૈકેત્સુ
 - Eggs46 The Devel and $\tilde{\Omega}$ $\tilde{\Gamma}$ -; objate = = 1:120
 - and $\bar{\Omega}$ $\bar{\Gamma}$ = $\Pi_{b} = 0 : .$
 - ign48 Prestress Co Homogeneou.

 - of Reynolds
 - Respect to the
 - Process for a First Order

 - - Asymptotic LES datas ...

Figure 4.5	by the URAPS-Closure for Different Values of the Second-Order "Extra" Anisotropy Coefficient (\(\frac{1}{2}\)—state, experiments, Tavoularis and Karnik, 1989;
Figure 4.6	The Development of Anisotropic Invariants of the NR-stress for $\tilde{\Gamma}=4$ and $\tilde{\Omega}/\tilde{\Gamma}=0$ from Different Initial States (initial states: isotropic \cdots ; oblate $$; prolate $$; ellipsoidal $$; iterations: $40 \diamondsuit$; $80 \diamondsuit$; $120 \bigcirc$; $\Pi_b^{\uparrow \downarrow}=0.1389$; $\Pi_b^{\uparrow \downarrow}=0.01525$)
Figure 4.7.	The Development of Anisotropic Invariants of the NR-Stress for $\tilde{\Gamma} = 11$ and $\tilde{\Omega}/\tilde{\Gamma} = -5/8$ from Different Initial States (same as Figure 4.6); $\Pi_b^{\frac{1}{12}} = 0.1190$; $\Pi_b^{\frac{1}{12}} = 0.01144$)
Figure 4.8	Prestress Coefficients α and β Determined From Asymptotic Homogeneous Shear flow
Figure 5.1.	The Influence of Rotation Number on the Decay of \tilde{k} and $\tilde{\epsilon}$
Figure 5.2.	\tilde{k} and $\tilde{\epsilon}$ Phase Plane Diagrams for Rotating Homogeneous Decay 131
Figure 5.3.	The Influence of Rotation on the Dimensionless Turbulent Time Scale.132
Figure 5.4.	Influence of Rotation on $\tilde{k}^2/\tilde{\epsilon}$
Figure 5.5.	The Influence of Rotation on the Temporal Variation of R_{xx} Component of Reynolds Stress for Homogeneous Decay (see Tables 5.1a,b) 137
Figure 5.6.	The Influence of Rotation on the Redistribution of Kinetic Energy with Respect to the Turbulent Time Scale
Figure 5.7.	The Development of "Extra" Prestress Anisotropy During the Decay Process for $\tilde{\Omega}_0 = 1$: a) Dynamic Response of the Second Invariants for the First Order and Second Order CH-Contributions to the "Extra" Prestress Anisotropy. b) Relative Changes of the First Order and Second Order "Extra" Prestress Anisotropies
Figure 6.1	Schematic of Rotating Homogeneous Shear Flow
Figure 6.2	Values of $\tilde{\tau}_R$ and $1/\tilde{\Gamma}$ for the Asymptotic States Characterized by $\tilde{\Omega}/\tilde{\Gamma}$
Figure 6.3	Asymptotic States of the Components of \underline{R} (Comparison with DNS and LES data)

- The Deve $\tilde{\Omega}/\tilde{\Gamma}=0$ eigenvalues 120 T. fix. Freehil Develope gasell Develops Tenedia Developi Freehla Ergennie Schema isterah Influenc
 - Egach S. The Devel $\tilde{\Omega} \tilde{\Gamma} = -5$
 - Egent alues $\frac{1}{2}$ and $\frac{1}{2}$
 - Fine Developing
 - Egith Temporal I)
 - finels Temporal I Initial $\hat{\Gamma}_{i}$
 - Temporal Results (E)

 - $\frac{1}{2}$ and

 - Ester 2a Locus (Ω ř =
 - Closure The Inf ÚĻ,

Figure 6.4	The Development of Extra-Anisotropy Eigenvalues for $\Gamma=4$ and $\tilde{\Omega}/\tilde{\Gamma}=0$ from an Isotropic State ((a) $\underline{\Delta}_1$ -eigenvalues; (b), $\underline{\Delta}_2$ -eigenvalues; λ_1 —; λ_2 ; λ_3 ····; iterations: 40 \diamondsuit ; 80 \triangle ; 120 \bigcirc ; fixed point, \overleftrightarrow{x}).
Figure 6.5.	The Development of Extra-Anisotropy Eigenvalues for $\tilde{\Gamma}=11$ and $\tilde{\Omega}/\tilde{\Gamma}=-5/8$ from an Isotropic State (see Figure 6.4 for notation) 156
Figure 6.6	Eigenvalues of the Extra-Anisotropy $\underline{\Delta}$ and Relative Contributions from $\underline{\Delta}_1$ and $\underline{\Delta}_2$ for Asymptotic Solutions
Figure 6.7	Developing $\tilde{\Gamma}$ Towards Asymptotic States for Various Initial $\tilde{\Gamma}_0$ 160
Figure 6.8	Temporal Development of $-R_{yz}$ for Different Initial $\tilde{\Gamma}_0$
Figure 6.9	Temporal Development of Production to Dissipation Ratio for Different Initial $\tilde{\Gamma}_0$
Figure 6.10	Temporal Development of NR-Stress Components Compared with DNS Results (Brethouwer, 2005) for High Initial Shear $\tilde{\Gamma}_0 = 18 \ (\tilde{\Omega}/\tilde{\Gamma} = 0).164$
Figure 6.11	Developing $\tilde{\Gamma}$ for Different Rotation Numbers for $\tilde{\Gamma}_0 = 1$
Figure 6.12	Developing R_{yz} for Different Rotation Numbers for $\tilde{\Gamma}_0 = 1167$
Figure 6.13	Developing \mathcal{P}/ϵ Ratio for Various Rotation Numbers for $\tilde{\Gamma}_0 = 1 \dots 169$
Figure 6.14	Eigenvlues of the Extra-Anisotropy $\underline{\Delta}$ and Relative Contributions from $\underline{\Delta}_1$ and $\underline{\Delta}_2$ for Developing Homogeneous Shear for $\tilde{\Gamma}_0 = 1$ and $\tilde{\Omega}/\tilde{\Gamma} = 0$.
Figure 7.1	Schematic of Fully Developed Channel Flow with Spanwise Rotation. 175
Figure 7.2a	Locus of URAPS-Closure States Parameterized by $\tilde{\Gamma}$ for $\tilde{\Omega}/\tilde{\Gamma}=0$ and $\tilde{\Omega}/\tilde{\Gamma}=-0.5$ (Zero Absolute Mean Vorticity, see Section 7.6)
Figure 7.2b	Influence of $\tilde{\Gamma}$ on the Components of NR-Stress Distribution for URAPS-Closure ($\tilde{\Omega}/\tilde{\Gamma}=0$)
Figure 7.3a	The Influence of $\tilde{\Omega}/\tilde{\Gamma}$ and $\tilde{\Gamma}$ on the Energy States for $\tilde{\Omega}/\tilde{\Gamma}<-0.5$ and $\tilde{\Omega}/\tilde{\Gamma}>0$

Figure 136. The Influence and $\tilde{\Omega}/\tilde{\Gamma}$: Figure 4. The Intiluer $-0.5 \cdot \tilde{\Omega}$ (Fully-Deve Epin 6 Spatial Var Developed Form Spatial Va based on ð = 30m. For Spatial Va $haved |_{\partial B}$ $\delta^* = 2m$ Family Spatial V Retating 6° ≥ 300 FRETTO URAPNO Fully-De TEETH URAPS Fully-D TEET 12 URAPS for F ΰ. ≆ isa 13 Influen. F = -20 TRAPS Spanis OF =

Figure 7.3b	The Influence of Ω/Γ and Γ on the Anisotropic States for $\Omega/\Gamma < -0.5$ and $\tilde{\Omega}/\tilde{\Gamma} > 0$
Figure 7.4	The Influence of $\tilde{\Omega}/\tilde{\Gamma}$ and $\tilde{\Gamma}$ on the Energy and Anisotropic States for $-0.5 < \tilde{\Omega}/\tilde{\Gamma} < 0$
Figure 7.5	The Influence of $\tilde{\Gamma}$ on the Components of NR-Stress for Non-Rotating Fully-Developed Channel Flows.
Figure 7.6	Spatial Variation of N_{Γ} and $\tilde{\tau}_R$ based on $\tilde{\Gamma}_{DNS}$ for Non-Rotating Fully-Developed Channel Flow
Figure 7.7	Spatial Variation of NR-Stress Components Predicted by URAPS-Closure based on $\tilde{\Gamma}_{DNS}$ for Non-Rotating Fully-Developed Channel Flows with $\delta^+=300$.
Figure 7.8	Spatial Variation of NR-Stress Components Predicted by URAPS-Closure based on $\tilde{\Gamma}_{DNS}$ for Non-Rotating Fully-Developed Channel Flows with $\delta^+=2000$
Figure 7.9	Spatial Variation of N_{Γ} , N_{Ω} and $\tilde{\tau}_{R}$ for Fully-Developed Spanwise Rotating Channel based on DNS Results for $\tilde{\Gamma}_{DNS}$ and $\tilde{\Omega}_{DNS}$ with $\delta^{+} \cong 300$, $\Omega^{+} \cong -0.0042$
Figure 7.10	URAPS-Closure Predictions for the R $_{yy}$ Component of the NR-Stress for Fully-Developed Spanwise Rotating Channel ($\delta^+ \cong 300$, $\Omega^+ \cong -0.0042$).
Figure 7.11	URAPS-Closure Predictions for the R_{zz} Component of the NR-Stress for Fully-Developed Spanwise Rotating Channel ($\delta^+ \cong 300$, $\Omega^+ \cong -0.0042$).
Figure 7.12	URAPS-Closure Predictions for the Shear Component of the NR-Stress for Fully-Developed Spanwise Rotating Channel ($\delta^+ \cong 300$, $\Omega^+ \cong -0.0042$).
Figure 7.13	Influence of $\tilde{\Omega}$ on the NR-Stress Distribution for URAPS-Closure when $\tilde{\Gamma} = -2\tilde{\Omega}$
Figure 7.14	URAPS-Closure Predictions in Comparison with DNS Results for Spanwise Rotating Channel, in the Linear Velocity Region where $\tilde{\Omega}/\tilde{\Gamma} = -0.5$ (Zero Absolute Mean Vorticity)

Entil Exm Ans

ELEVI URAPS-CL

Egn+2 URAPS+CS

Fully-Deve

Figure 7.15	Extra Anisotropy for Simple Shear Flow for $\tilde{\Omega} = 0$
Figure 9.1	URAPS-Closure Predictions of -R _{yz} for Non-Rotating Simple Shear. 214
Figure 9.2	URAPS-Closure Predictions of the Energy and Anisotropic States for Fully-Developed Spanwise Rotating Channel ($\delta^+ \cong 300$, $\Omega^+ \cong -0.0042$)

 $\sum_{i,j} = \int_{\mathbb{R}} m_i h_i \int_{\mathbb{R}} dx$ 1 = p′ B aj., r V

: n

= (n-mod.

= 45

= ac

LIST OF NOTATION

English Symbols

$$\underline{\underline{\mathbf{A}}}$$
 = preclosure operator, $\underline{\underline{\mathbf{A}}} = (\underline{\underline{\mathbf{I}}} + \underline{\underline{\mathbf{K}}})^{-1}$, dimensionless

$$\underline{\underline{B}} = \text{normalized prestress}, \frac{\langle \underline{\underline{f}'}\underline{\underline{f}'} \rangle}{\text{tr}(\langle \underline{\underline{f}'}\underline{\underline{f}'} \rangle)}$$

$$B_{n+1}$$
 = (n+1)-iteration for the normalized prestress defined by the APS-model

$$\underline{b}$$
 = anisotropic component of \underline{R} , $\underline{b} = \underline{R} - \frac{1}{3}\underline{I}$

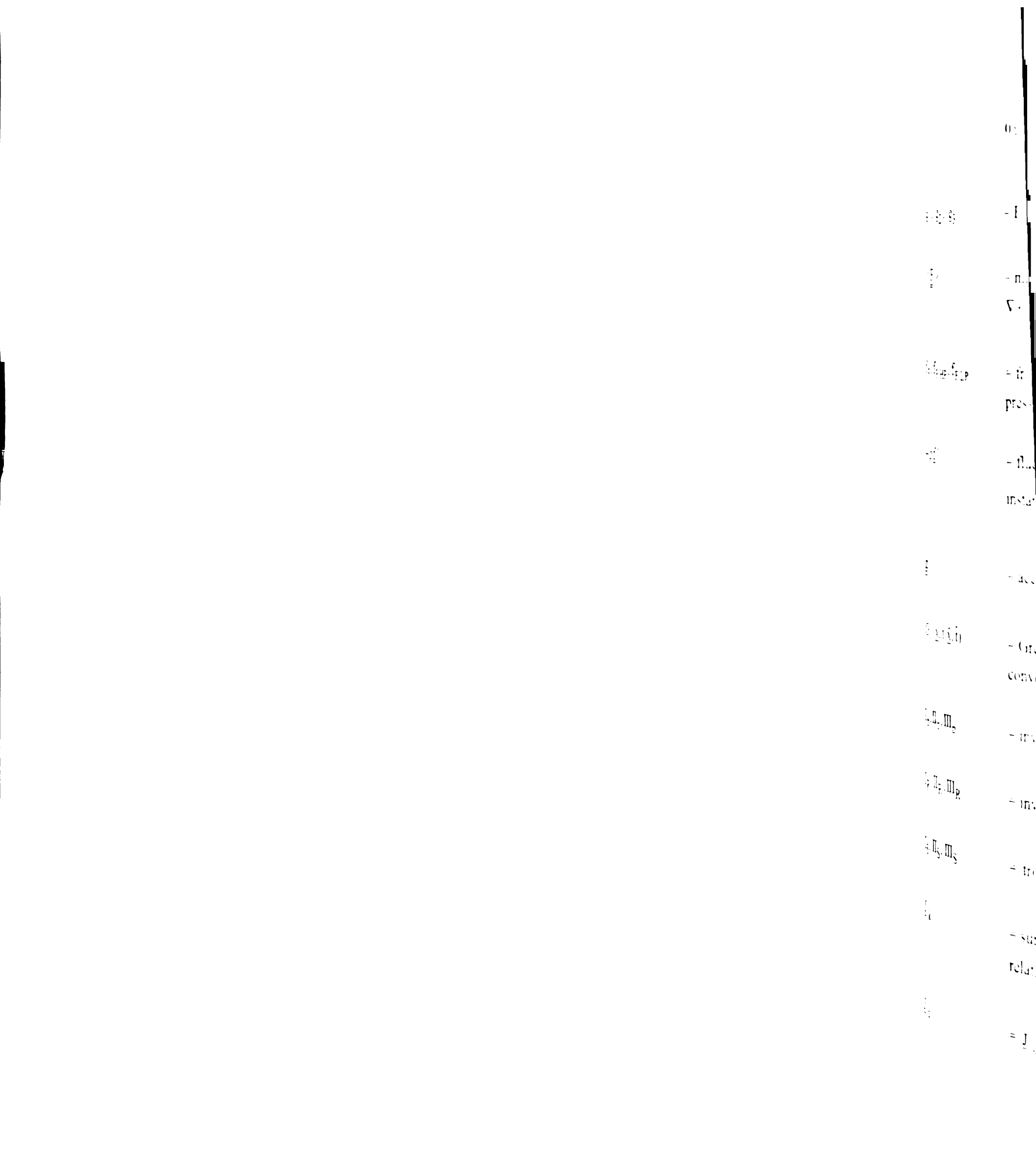
$$\underline{\underline{C}}$$
 = adj $(\underline{\underline{I}} + \underline{\underline{K}})$, preclosure operator (adj: adjugate, i.e. transpose of the minor)

$$C_P$$
 = "production" coefficient in the ε -equation

$$C_D$$
 = "dissipation" coefficient in the ε -equation

$$C_{\mu}$$
 = dimensionless turbulent transport time scale
$$C_{e} = C_{e}(\frac{k^{2}}{v_{c}}, \frac{k}{s} || < \frac{F}{s} > ||)$$

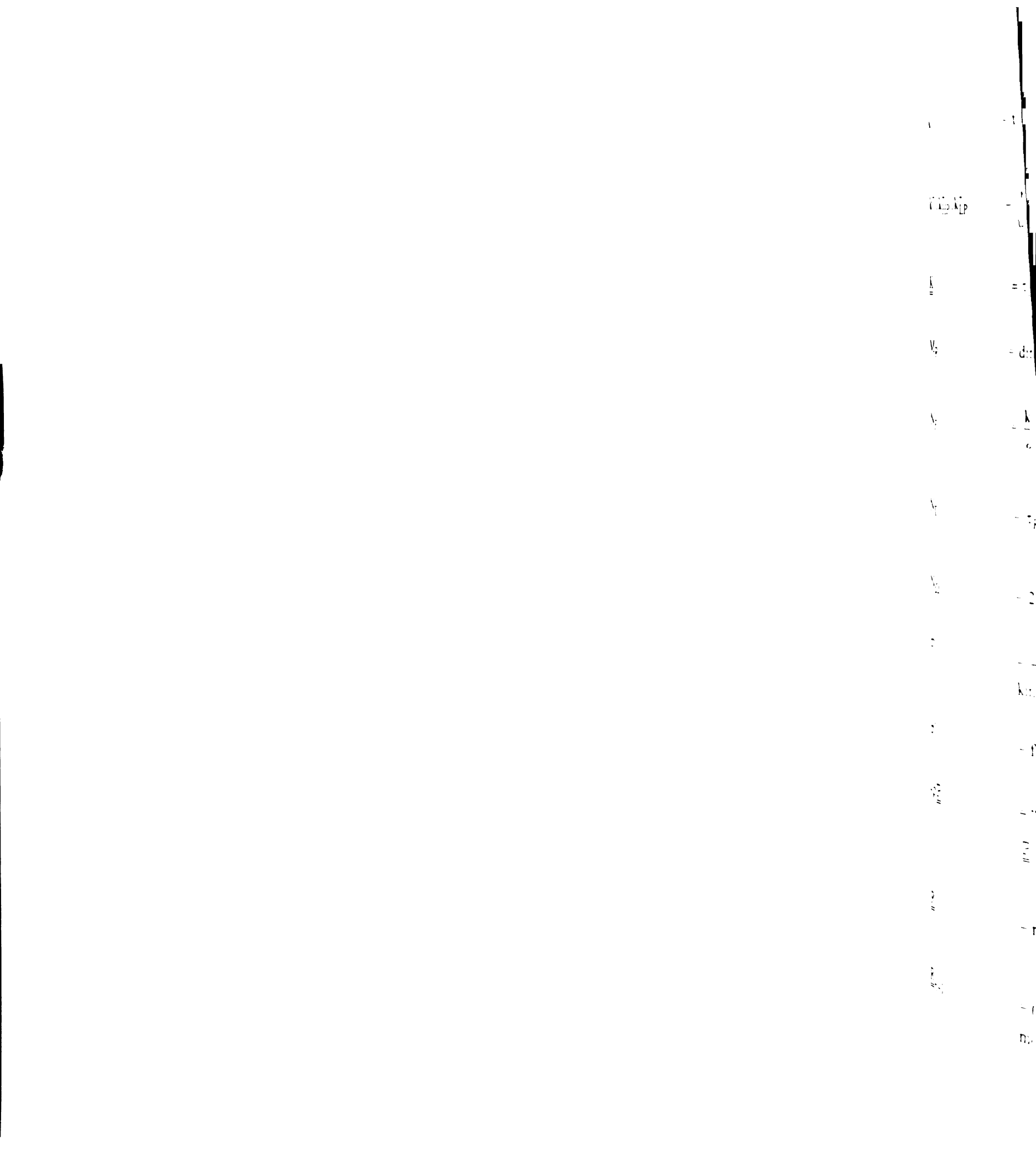
$$C_{CC}$$
 = correlation coefficient (Schwartz inequality),



$$0 \le C_{cc} \equiv \sqrt{\frac{R_{yz}^2}{R_{yy}R_{zz}}} \le 1$$

- \underline{e}_1 , \underline{e}_2 , \underline{e}_3 = Euclidean base vectors
- $<\underline{F}>$ = mean field kinematic variable in the preclosure operator $\underline{\underline{A}}$, $\nabla < \underline{u} > + 2\underline{\Omega}$, 1/t
- f_F , f_{FHP} , f_{FLP} = friction factor, based on the average, high pressure side and low pressure side shear stresses respectively.
- $-\rho \underline{f}' = \text{fluctuating force per unit volume induced by fluctuations in the}$ instantaneous turbulent stress $\underline{f}' \equiv \nabla \cdot (\frac{\underline{p}'}{\rho} \underline{I} + \underline{u}' \underline{u}' \langle \underline{u}' \underline{u}' \rangle), L/t^2$
- \underline{g} = acceleration due to gravity, L/t^2
- $G_{\nu}(\underline{x}, t | \underline{\hat{x}}, \hat{t})$ = Green's function associated with the mean field convective/viscous differential operator, $1/L^3$
- I_b, II_b, III_b = invariants of $\underline{\underline{b}}$: $tr(\underline{\underline{b}}), tr(\underline{\underline{b}} \cdot \underline{\underline{b}}), tr(\underline{\underline{b}} \cdot \underline{\underline{b}} \cdot \underline{\underline{b}})$, resp.
- $I_R, II_R, III_R \qquad \qquad = \text{invariants of } \underline{\underline{R}}: \ \text{tr}(\underline{\underline{R}}), \text{tr}(\underline{\underline{R}} \cdot \underline{\underline{R}}), \text{tr}(\underline{\underline{R}} \cdot \underline{\underline{R}} \cdot \underline{\underline{R}}) \ , \text{resp.}$
- $I_{S}, II_{S}, III_{S} = tr(\langle \underline{\underline{S}} \rangle \cdot \langle \underline{\underline{S}} \rangle), tr(\langle \underline{\underline{S}} \rangle \cdot \langle \underline{\underline{S}} \rangle \cdot \langle \underline{\underline{S}} \rangle)$
- \underline{J}_{k} = sum of the viscous and turbulent flux of turbulent kinetic energy relative to the mean velocity, $\underline{J}_{k} = -(v \underline{I} + \tau_{R} < \underline{u}'\underline{u}' >) \cdot \nabla k$, L^{3}/t^{3}

$$\underline{J}_{\varepsilon} = \underline{J}_{\varepsilon} \equiv -(\nu \underline{I} + \tau_{R} < \underline{u}'\underline{u}' >) \cdot \nabla \varepsilon, L^{3}/t^{4}$$



k = turbulent kinetic energy,
$$k = \frac{tr < \underline{u}'\underline{u}' >}{2}$$
, L^2/t^2

$$k^+, k_{HP}^+, k_{LP}^+$$
 = $\frac{k}{u}, \frac{k}{u_{HP}}, \frac{k}{u_{LP}}$, normalized by wall parameters.

$$\underline{\underline{K}}$$
 = $\tau_R (\nabla < u > + 2 \underline{\Omega})$, dimensionless kinematic operator.

$$M_R$$
 = dimensionless memory kernel

$$N_F$$
 = $\frac{k}{\epsilon} \| < \underline{F} > \|$, $\frac{\text{turbulent time scale}}{\text{kinematic time scale}}$

$$N_{\Gamma}$$
 = $\tau_R \Gamma_{yz} = C_{R1} \tilde{\tau}_R \tilde{\Gamma}$, turbulent time scale flow time scale

$$N_{\Omega}$$
 = $2\tau_R \Omega_x = 2C_{R1} \tilde{\tau}_R \tilde{\Omega}$

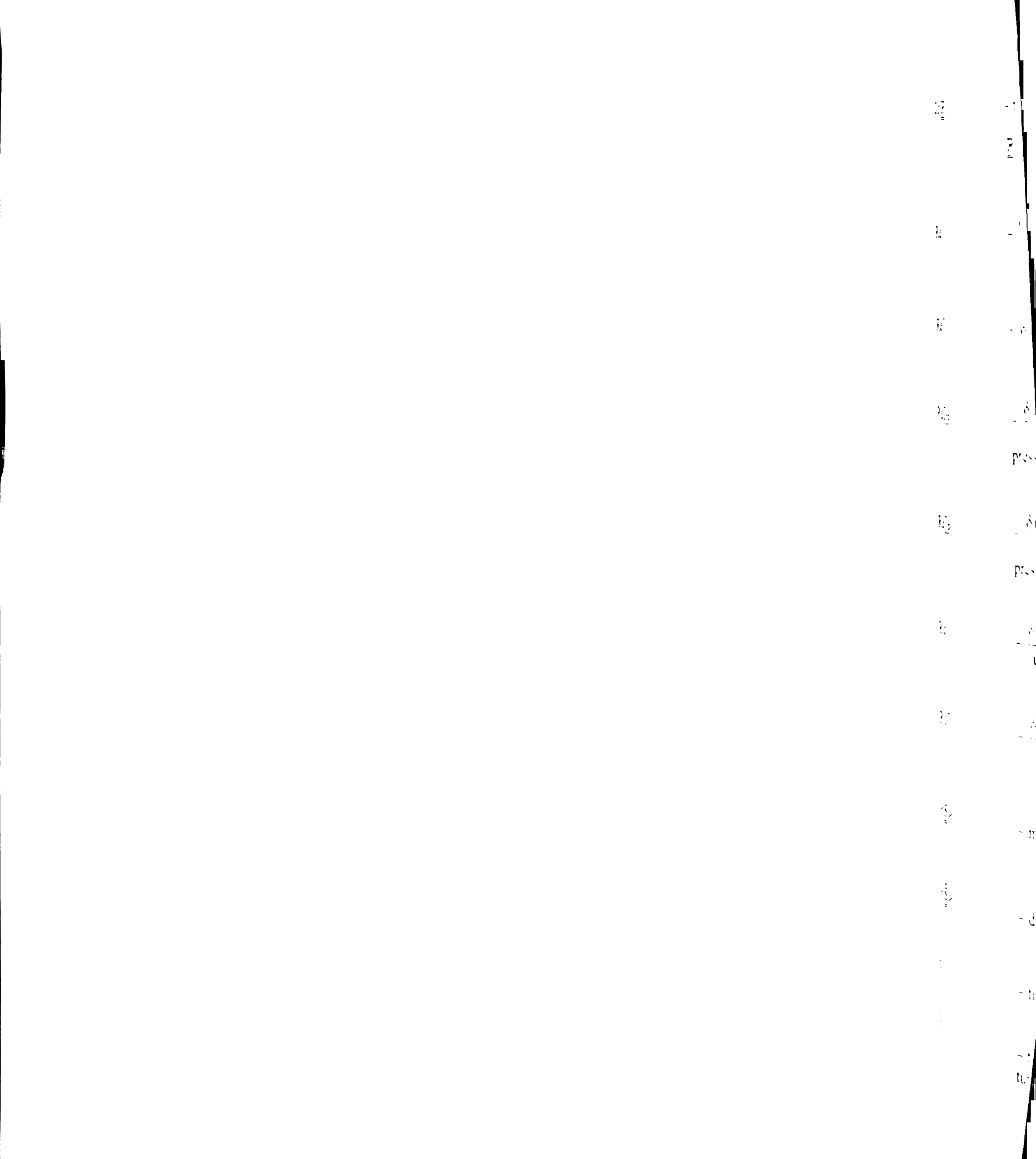
$$\mathcal{P} = -\langle \underline{\mathbf{u}}'\underline{\mathbf{u}}'\rangle : \langle \underline{\underline{\mathbf{S}}}\rangle = -2\,\mathbf{k}\,\,\underline{\underline{\mathbf{R}}} : \langle \underline{\underline{\mathbf{S}}}\rangle, \text{ "production" of turbulent kinetic energy, } \mathbf{L}^2/t^3$$

p' = fluctuating pressure,
$$M/L-t^2$$

$$\begin{array}{ll} -\rho \, \underline{\mathbb{P}} & = \text{``production'' of Reynolds stress,} \\ & \underline{\mathbb{P}} \, \equiv \, -<\underline{u}\, \underline{'}\underline{u}\, \overline{'}>\cdot \nabla <\underline{u}> - \left(\nabla <\underline{u}>\right)^T \cdot <\underline{u}\, \underline{'}\underline{u}\, \overline{'}> , \, L^2/t^3 \end{array}$$

$$\underline{\underline{R}}$$
 = normalized Reynolds stress, $\frac{\langle \underline{\underline{u}'}\underline{\underline{u}'}\rangle}{\operatorname{tr}(\langle \underline{\underline{u}'}\underline{\underline{u}'}\rangle)}$

$$\underline{R}_{n+1}$$
 = (n+1)-iteration for the normalized stress defined by the APS-model



 $2\rho \mathbb{R}$ = turbulent pressure/strain rate correlation,

$$\underline{\underline{\mathbb{R}}} = + < \frac{p'}{\rho} [\nabla \underline{u}' + (\nabla \underline{u}')^T] > , L^2/t^3$$

Re
$$=\frac{\delta u_b}{v}$$
, $\frac{\text{viscous time scale}}{\text{flow time scale}}$, Reynolds number

$$Re^+ = \delta^- = \frac{\delta u^*}{v}$$
, Reynolds number based on friction velocity.

$$Re_{HP}^{+}$$
 = $\frac{\delta u_{HP}^{*}}{v}$, Reynolds number based on friction velocity on the high pressure side.

$$Re_{LP}^{+}$$
 = $\frac{\delta u_{LP}^{*}}{v}$, Reynolds number based on friction velocity on the high pressure side.

$$R \ o \qquad \qquad = \frac{\delta \left| \underline{\Omega} \right|}{u_b} \ , \ \frac{flow \ timescale}{frame \ time \ scale} \ , \ Rossby \ number$$

$$R o^+ = \frac{\delta |\underline{\Omega}|}{u^*}$$

$$<\underline{\underline{S}}>$$
 = mean strain rate, $<\underline{\underline{S}}>=\frac{\nabla <\underline{u}>+(\nabla <\underline{u}>)^T}{2}$, $1/t$

$$< \tilde{\underline{S}} >$$
 = dimensionless mean strain rate, $< \tilde{\underline{S}} > \equiv \frac{k}{\varepsilon} < \underline{\underline{S}} >$

$$t = time, t$$

$$\hat{t}$$
 = time, $t - \hat{t} \ge 0$, instantaneous memory variable in space-time turbulent correlation, $1/t$

:: 1 - 1: į ą, = Rc 1, 1, -****

 $\rho \underline{\underline{\underline{T}}}$ = turbulent flux of turbulent momentum flux,

$$\frac{T}{=} = + < \underline{u}'\underline{u}'\underline{u}' > + \frac{1}{\rho} (< \underline{u}'p' > \underline{I} + \underline{I} < \underline{u}'p' >), L^3/t^3$$

 $\underline{\mathbf{u}}$ = instantaneous velocity, L/t

 $\underline{\mathbf{u}}$ = fluctuating velocity, L/t

 $\langle \underline{\mathbf{u}} \rangle$ = Reynolds average velocity (ensemble average)

 u_x, u_y, u_z = components of the instantaneous velocity in a Cartesian coordinate system

u* $= \sqrt{\frac{\tau_w}{\rho}} \text{ friction velocity (based on the average wall! shear stress}$ incase of rotating channel, $\sqrt{(u_{HP}^* + u_{LP}^*)/2}$), L/t

 $u_{HP}^* = \sqrt{\frac{\tau_{w \; HP}}{\rho}} \; , \; \text{friction velocity of the high pressure side in rotating} \\ \text{channel flow} \; , \; L/t$

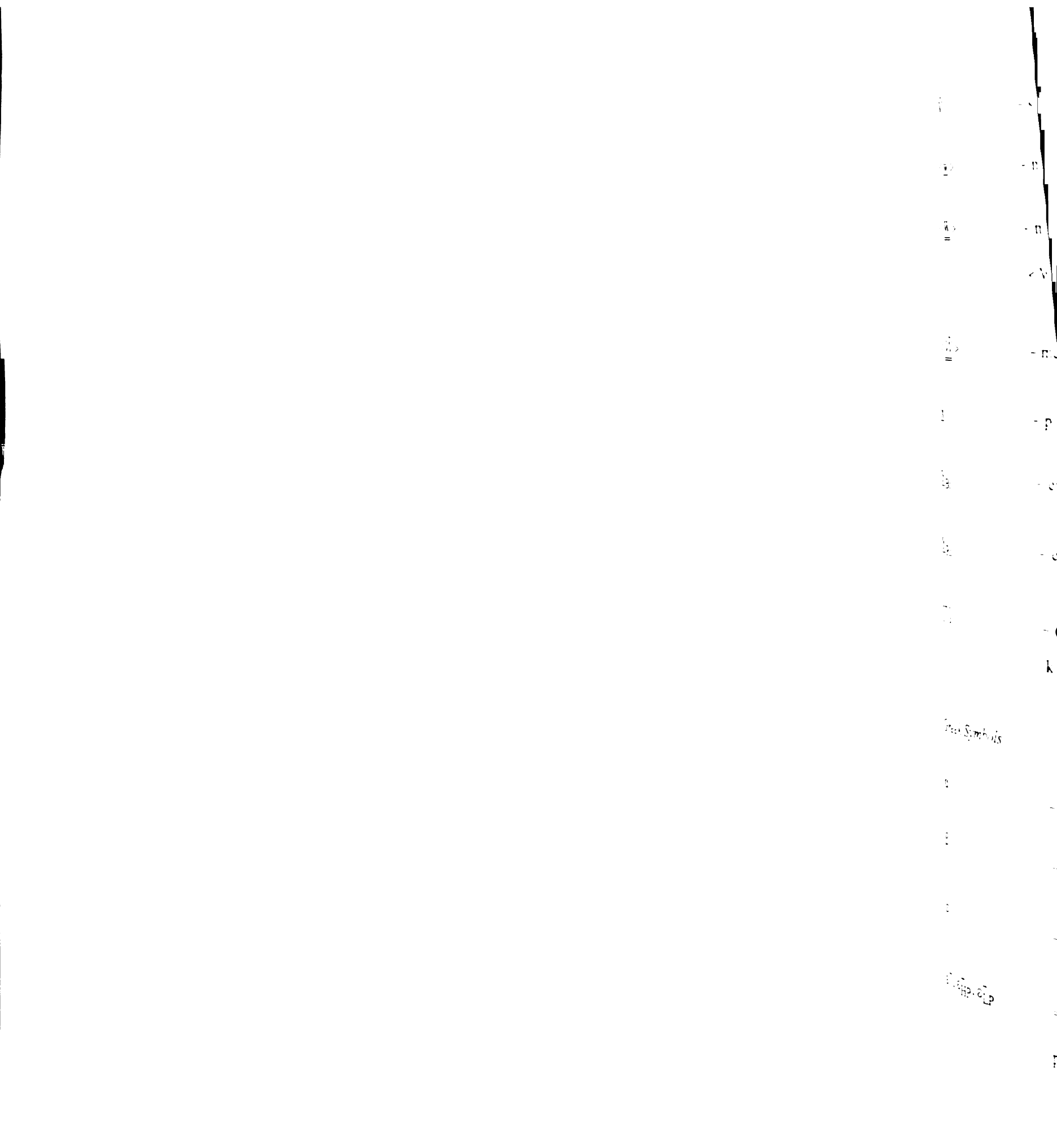
 $u_{LP}^* = \sqrt{\frac{\tau_{w\;LP}}{\rho}}$, friction velocity of the high pressure side in rotating channel flow , L/t

 $-<\underline{\mathbf{u}}'\underline{\mathbf{u}}'>$ = kinematic Reynolds stress, L^2/t^2

 $+ < \underline{\mathbf{u}}'\underline{\mathbf{u}}' >$ = kinematic Reynolds momentum flux, L^2/t^2

 $-\rho < u'u'>$ = Reynolds stress, M/L-t²

+ $\rho < \underline{u}'\underline{u}' >$ = Reynolds momentum flux, M/L- t^2



 \hat{V} = spatial domain in Green's function representation, L^3

 $< w > = mean vorticity, < w > \equiv \nabla \wedge < u > , 1/t$

< W > = mean rotational strain rate associated with the mean vorticity,

$$<\underline{\underline{W}}>\equiv \frac{\nabla <\underline{\underline{u}}>-(\nabla <\underline{\underline{u}}>)^{\mathrm{T}}}{2}$$
, $1/t$

 $< \underline{\tilde{W}} > = \text{mean intrinsic vorticity}, < \underline{\tilde{W}} > \equiv < \underline{W} > + \underline{\Omega}, 1/t$

 $\underline{\mathbf{x}}$ = position vector, L

 $\underline{\underline{y}}_{Bi}$ = eigenvector associated with $\underline{\underline{b}}$

 $\underline{\underline{y}}_{Ri}$ = eigenvector associated with $\underline{\underline{R}}$

[+] = (+ superscript), normalized by wall parameters, e.g. $k^{+} = \frac{k}{u^{*2}}, \quad \epsilon^{+} = \frac{\epsilon}{(u^{*4}/v)}$

Greek Symbols

α = anisotropic coefficient of the first kind in the URAPS closure

 β = anisotropic coefficient of the second kind in the URAPS closure

 ε = turbulent dissipation, $\varepsilon = v < (\nabla \underline{u}') : (\nabla \underline{u}')^T > L^2/t^3$

 ϵ^+ , ϵ_{HP}^+ , ϵ_{LP}^+ = $\frac{\epsilon}{(u^{*4}/v)}$, $\frac{\epsilon}{(u_{HP}^{*4}/v)}$, $\frac{\epsilon}{(u_{LP}^{*4}/v)}$, normalized by wall parameters.

3 : Eqi (Ži)

 $\underline{\underline{\mathcal{E}}}$ = dyadic-valued turbulent dissipation,

$$\underline{\underline{\mathcal{E}}} \equiv \nu \left[< (\nabla \underline{\mathbf{u}}^{\, \cdot}) \cdot (\nabla \underline{\mathbf{u}}^{\, \cdot})^T > + < (\nabla \underline{\mathbf{u}}^{\, \cdot})^T \cdot (\nabla \underline{\mathbf{u}}^{\, \cdot}) > \right], \, L^2/t^3$$

 $\underset{\equiv}{\epsilon}$ = permutation triadic

$$\underline{\underline{\varepsilon}} \equiv \underline{e}_1 \underline{e}_2 \underline{e}_3 + \underline{e}_3 \underline{e}_1 \underline{e}_2 + \underline{e}_2 \underline{e}_3 \underline{e}_1 - \underline{e}_3 \underline{e}_2 \underline{e}_1 - \underline{e}_2 \underline{e}_1 \underline{e}_3 - \underline{e}_1 \underline{e}_3 \underline{e}_2$$

 κ = wave number

 Φ = nth order integrity base associated with Φ for S-hypothesis,

Eq.(2.11)

Ψ = Optimization variable, (see Eq. 4.9)

 λ_{bi} = eigenvalue associated with \underline{b} , dimensionless

 λ_{Ri} = eigenvalue associated with \underline{R} , dimensionless

 $v = \text{kinematic viscosity of the fluid, } L^2/t$

 v_e = "eddy" viscosity, [=] L^2/t

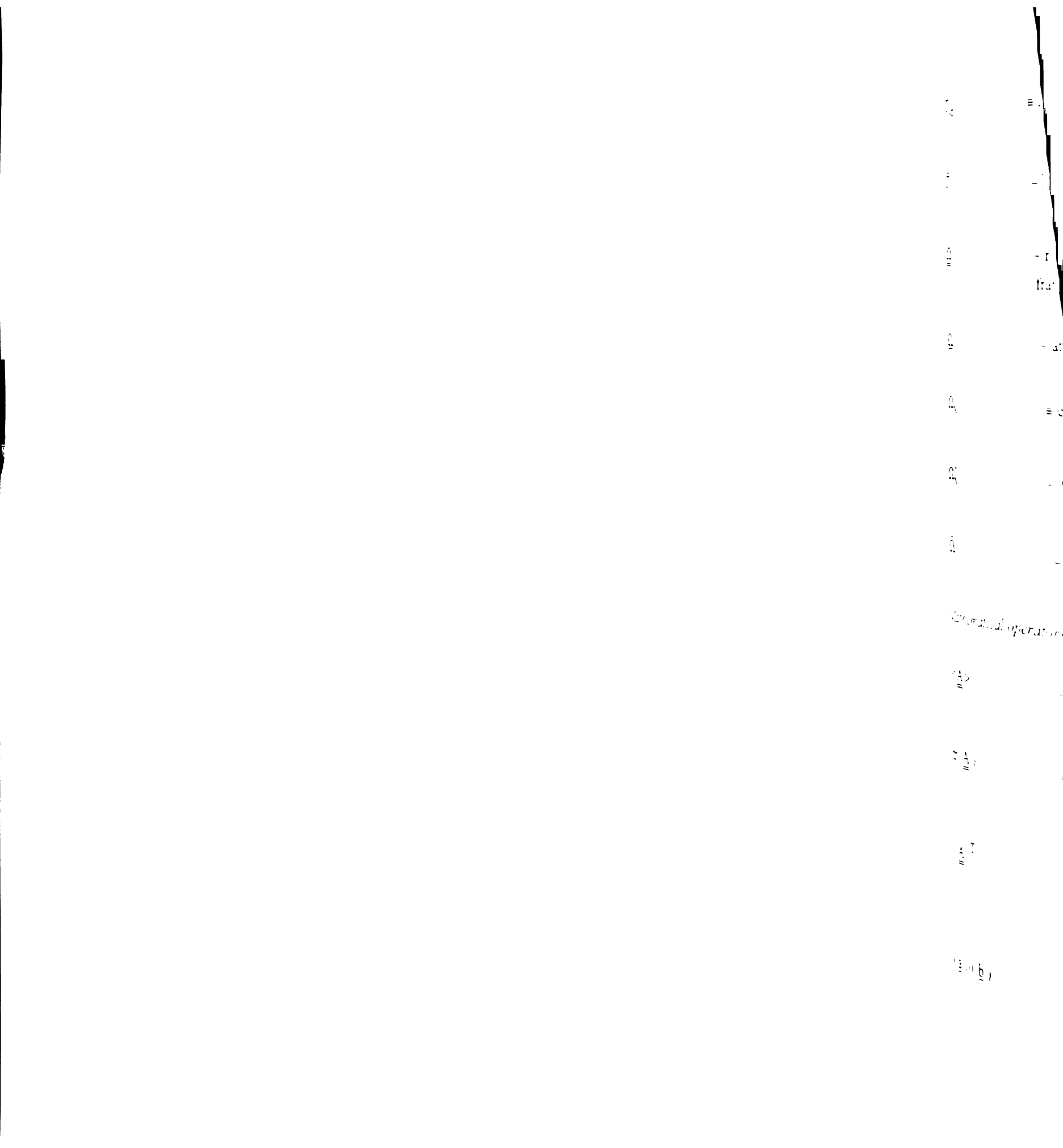
 ρ = mass density of the fluid, M/L³

 τ_t = turbulent transport time scale, $\tau_t = C_{\mu} \frac{k}{\epsilon}$, 1/t

 τ_R = turbulent relaxation time defined as follows

$$\tau_{R} = \int_{-\infty}^{t} M(\underline{x}, t | \underline{x}, \hat{t}) \left[\int_{\hat{V}} G(\underline{x}, t | \hat{\underline{x}}, \hat{t}) d\hat{V} \right] d\hat{t}$$

 χ (Σ ,t) = motion of a material particle, [=], L



$$\Gamma_{yz}$$
 $\equiv \underline{e}_{z}\underline{e}_{y}: \nabla < \underline{u} >$

$$\tilde{\Gamma} = [\underline{e}_z \underline{e}_y : \nabla < \underline{u} >] \frac{k}{\varepsilon} = \Gamma_{yz} \frac{k}{\varepsilon}$$

$$\underline{\underline{\Omega}} = \text{rotational operator}, \ \Omega_{x}[\underline{e}_{y}\underline{e}_{z} - \underline{e}_{z}\underline{e}_{y}] \text{ of a non-inertial rigid body}$$
frame, 1/t

$$\underline{\Omega}$$
 = angular velocity of a rigid body frame, $\Omega = \Omega_X \underline{e}_X$, $1/t$

$$\Omega_{X} \equiv \underline{e}_{z}\underline{e}_{y}:\underline{\Omega}$$

$$\Omega_{x}^{+} = \Omega_{x} v / (u^{*})^{2}$$

$$\tilde{\Omega}$$
 = $\Omega_x \frac{k}{\epsilon}$

Mathematical operators

$$< \underline{\underline{A}} >$$
 = Reynolds average (ensemble average) of $\underline{\underline{A}}$

$$\operatorname{tr}(\underline{\underline{A}})$$
 = $\sum_{i=1}^{3} A_{ii}$ trace of a dyadic-valued operator $\underline{\underline{A}}$

$$(\underline{\underline{A}})^{T} = (\sum_{i=1}^{3} \sum_{j=1}^{3} A_{ij} \underline{e}_{i} \underline{e}_{j})^{T} = \sum_{i=1}^{3} \sum_{j=1}^{3} A_{ij} \underline{e}_{j} \underline{e}_{i} \text{ transpose of a dyadic-valued operator } \underline{\underline{A}}$$

$$(\underline{a}) \cdot (\underline{b})$$
 = scalar product between two vectors \underline{a} and \underline{b}



ادر

= d_}

- (0 L = $\underline{\underline{A}}:\underline{\underline{B}}$ = double contraction (Gibbs convention) between two dyadic-valued operators $\underline{\underline{A}}$ and $\underline{\underline{B}}$

$$\|\underline{\underline{\mathbf{A}}}\|$$
 = norm of a real dyadic-valued operator,

$$\| < \underline{\underline{\mathbf{A}}} > \| \equiv \sqrt{< \underline{\underline{\mathbf{A}}} > : < \underline{\underline{\mathbf{A}}} >^{\mathsf{T}}}$$

$$\underline{\underline{I}}$$
 = dyadic-valued identity operator, $\underline{\underline{I}} \cdot \underline{\underline{a}} = \underline{\underline{a}}$

$$\frac{\partial}{\partial t}$$
 = time derivative, 1/t

$$\nabla$$
, $\nabla^2 \equiv \nabla \cdot \nabla$ = gradient operator, 1/L and Laplacian operator, 1/L²

E. Rabstale for T

Tax research

Mission retaining and

ngomed by the

Straight (Sex. Pro

- 1=1)

िक्त हु≡८७+३०

विद्यास्त्र १८६० हिल्ल

 $\frac{b}{2^{-1}b} = \frac{5}{I \cdot \delta}$

Ta independent v

^{म्याता} बार define

हुं s related to the

Estation triadic

5 = 0

For large R

and condition.

CHAPTER 1

INTRODUCTION

1.1 Rationale for Turbulence Modeling Research

This research is based on the premise that the instantaneous velocity and pressure fields for rotating and non-rotating turbulent flows of constant property Newtonian fluids are governed by the Navier-Stokes (NS-) equation and the continuity equation (see Greenspan, 1968; Piquet, 1999):

$$\frac{\partial \underline{\underline{u}}}{\partial t} + \underline{\underline{u}} \cdot \underline{\underline{F}} = -\nabla \left(\frac{p}{\rho} - \frac{\underline{\underline{x}} \cdot (\underline{\Omega} \cdot \underline{\Omega}^T) \cdot \underline{\underline{x}}}{2}\right) + \nu \nabla^2 \underline{\underline{u}} + \underline{\underline{g}}$$
(1.1)

$$\nabla \cdot \mathbf{u} = 0 \tag{1.2}$$

where $\underline{\underline{F}} \equiv \nabla \underline{\underline{u}} + 2\underline{\underline{\Omega}}$. Eqs.(1.1) and (1.2) imply that the instantaneous pressure distribution satisfies a Poisson equation:

$$-\nabla^{2}\left(\frac{p}{\rho} - \frac{\underline{x} \cdot (\underline{\Omega} \cdot \underline{\Omega}^{T}) \cdot \underline{x}}{2}\right) = \nabla \cdot (\underline{u} \cdot \underline{F})$$
(1.3)

The independent variables (\underline{x},t) and the dependent variables (\underline{u},p) in the above equations are defined relative to a non-inertial frame-of-reference. The rotation operator $\underline{\Omega}$ is related to the angular velocity of the frame by $\underline{\Omega} \equiv \underline{\varepsilon} \cdot \underline{\Omega}$, where $\underline{\varepsilon}$ denotes the permutation triadic. The same notation is used for an inertial frame-of-reference for which $\underline{\Omega} = \underline{0}$.

For large Reynolds numbers, solutions to Eqs.(1.1) and (1.2) subject to appropriate boundary conditions are unsteady, spatially three dimensional, and sensitive to initial conditions. A direct numerical simulation (DNS) of these equations is

at Meather than the analysis of the Residual Street of the Residual

replacedly inten-

sarah simple gu ti

%- der statistical in

Turbulence (

W,

The low-or street Navier-of Ensemble

\$20**1**8]

computationally intensive (see Chapter 1 and p. 349 in Pope, 2000) and is limited to relatively simple geometries. This situation has motivated the development and use of low-order statistical methods to study ensembles of solutions associated with Eqs.(1.1) and (1.2), rather than individual solutions.

An ensemble average of Eqs.(1.1) and (1.2) yields exact, albeit unclosed, equations for $\langle \underline{u} \rangle$ and $\langle p \rangle$ that depend on the turbulent momentum flux $\rho \langle \underline{u}\,\underline{u}' \rangle$. The fluctuating velocity \underline{u}' is defined as $\underline{u}' \equiv \underline{u} - \langle \underline{u} \rangle$. An analysis of turbulent flows based on low-order statistical moments has been an active area of research for more than a century. Previous studies have produced numerous and significant insights into the behavior of the Reynolds momentum flux $\rho \langle \underline{u}\,\underline{u}' \rangle$ or, equivalently, the Reynolds stress, $-\rho \langle \underline{u}\,\underline{u}' \rangle$ (see Chen and Jaw, 1999; Piquet, 1999; and, Pope, 2000). The Reynolds stress is fundamentally important in determining the behavior of all turbulent flows, including non-rotating flows with streamline curvature and rotating flows encountered in turbo-machinery, mixers, and fans (Gupta et al., 1984; Salhi and Cambon, 1997).

1.2 Turbulence Closure Problem

Unclosed Reynolds-Averaged Navier-Stokes Equation

The low-order statistical properties of turbulence are governed by the Reynolds-averaged Navier-Stokes (RANS-) equation and the Reynolds-averaged continuity equation. Ensemble averages of Eqs. (1.1), (1.2) and (1.3) yield the following unclosed equations:

- [MET < U > + 2 O

Menor is linear, com

五 ((こう)=(直):

g presidents

then the equ

Seech and is the pro

Probablish RANS-ed

Best due to the pr

state and may hi

Basier, for specific

to be mean pressur

Sak gaistically stat

Science, and statistical

More than a cer

विक्षिणीवे शावक सम्ब

Resistant rate and th

$$\frac{\partial <\underline{\mathbf{u}}>}{\partial t} + <\underline{\mathbf{u}}> <\underline{\underline{\mathbf{F}}}> = -\nabla(\frac{<\mathbf{p}>}{\rho} - \frac{\underline{\mathbf{x}}\cdot(\underline{\Omega}\cdot\underline{\Omega}^{\mathsf{T}})\cdot\underline{\mathbf{x}}}{2}) + \underline{\mathbf{g}} + \nu\nabla^{2} <\underline{\mathbf{u}}> -\nabla \cdot <\underline{\mathbf{u}}'\underline{\mathbf{u}}'> \quad (1.4)$$

$$\nabla \cdot \langle \mathbf{u} \rangle = 0 \tag{1.5}$$

$$-\nabla^{2}\left(\frac{\langle p\rangle}{\rho} - \frac{\underline{x}\cdot(\underline{\Omega}\cdot\underline{\Omega}^{T})\cdot\underline{x}}{\underline{2}}\right) = +\nabla\cdot[\langle\underline{u}\rangle\cdot\langle\underline{F}\rangle + \nabla\cdot\langle\underline{u}'\underline{u}'\rangle]. \tag{1.6}$$

These equations are fundamentally different from Eqs. (1.1), (1.2) and (1.3) due to the presence of the Reynolds stress, $-\rho < \underline{u}'\underline{u}' >$. The fluctuating velocity is $\underline{u}'(\underline{x},t)$ and $<\underline{\underline{F}}>(\equiv \nabla<\underline{\underline{u}}>+2\underline{\Omega})$ is an average kinematic operator. The ensemble-average operator is linear, commutes with spatial and temporal derivatives, and has the property that $\langle u \rangle = \langle u \rangle$; consequently, $\langle u'(x,t) \rangle = 0$. Clearly, the use of Eqs.(1.4) and (1.5) for engineering design and analysis requires a closure model for the specific momentum flux $\langle \underline{u}'\underline{u}' \rangle$. This closure problem is a major challenge for turbulence research and is the primary focus of this dissertation. Unlike the NS-equation, solutions to a closed RANS-equation at high Reynolds numbers are temporally and spatially smooth due to the presence of the Reynolds stress. The mean velocity field may be unsteady and may have three components that vary in all three spatial directions. However, for specific boundary conditions and initial conditions on the mean velocity and the mean pressure fields, the RANS-equation may also have periodic solutions, unique statistically stationary (i.e., steady state) solutions, multiple statistically stationary solutions, and statistically homogeneous solutions.

More than a century ago, Boussinesq (1877) used a phenomenological closure for the Reynolds stress that assumes that the turbulent momentum flux depends on the local m can strain rate and the local statistical properties of the fluctuating velocity. Turbulent

maily based on this id. In Joseph wherein -5.41 å.>=- 3.5 k] + 7 l de above equation istruju >1 2 i Th that can be related to demy scale or, equiazatanstic time scale $|\hat{\beta}_{z}|^{2}|\hat{\mu}_{z}=(\sqrt{k})\sqrt{k}|_{1}$ The received time sould See als the local disc Tax with the turbulent Theory can be Tancaing, fully-deve King ve may be se boss v. Deep in scary is less than th that Ve > 0 nc. la order to comple: is to models are need at the dimension less models based on this idea are often referred to as "eddy" viscosity closures (see, p. 359, Pope, 2000) wherein

$$-\rho < \underline{\mathbf{u}}'\underline{\mathbf{u}}' > = -\frac{2}{3}\rho \,\mathbf{k}\,\underline{\mathbf{I}} + 2\rho\,\mathbf{v}_{e} < \underline{\mathbf{S}} > , \quad \text{tr} < \underline{\mathbf{S}} > = 0. \tag{1.7}$$

In the above equation for the Reynolds stress, k is the turbulent kinetic energy $(k \equiv tr(\langle \underline{u}'\underline{u}' \rangle)/2)$. The parameter ρv_e is a scalar-valued turbulent "eddy" viscosity, which can be related to a local characteristic length scale and a local characteristic velocity scale or, equivalently, to the local turbulent kinetic energy and a local characteristic time scale:

$$v_e = \ell_c u_c = (\tau_c \sqrt{k}) \sqrt{k} = \tau_c k. \tag{1.8}$$

The transport time scale $\tau_c(\equiv C_\nu k/\epsilon)$ depends on the local turbulent time scale k/ϵ , where ϵ is the local dissipation of turbulent kinetic energy, $\epsilon \equiv v \operatorname{tr}(<(\nabla \underline{u}')\cdot(\nabla \underline{u}')^T>)$. Thus, with the turbulent Reynolds number defined as $\operatorname{Re}_t \equiv (k/\epsilon)/(v/k)$, the turbulent "eddy" viscosity can be formally expressed as $v_e/v = C_v \operatorname{Re}_t$. In the outer region of non-rotating, fully-developed channel flows, $\operatorname{Re}_t > 30$; thus, in some regions, the "eddy" viscosity v_e may be several orders of magnitude larger than the molecular kinematic viscosity v. Deep in the viscous sublayer near a solid/fluid interface, the "eddy" viscosity is less than the molecular kinematic viscosity. The no slip boundary condition implies that $v_e \to 0$ near a solid/fluid interface.

In order to complete the Boussinesq (B-) closure for the RANS-equation, additional closure models are needed for the turbulent kinetic energy k, the turbulent dissipation ϵ , and the dimensionless transport time scale $\tau_c \epsilon/k \equiv C_v$. Numerous closure models for

the time statistics of the latest of the lat

Tagan Egaci'i a

Added to an electrical design of the state o

Sign occurrent

istoration (see Ha

in place court. Prince

d Thilen kinen

ेरेडे हिंदांग्रह 10

्रेट्रोम्ह देशक्ष देशम् । विकास

ंद्रहरू कावा हाः The

these three statistical properties have emerged over the past forty years in support of computational fluid dynamic simulations based on the RANS-equation (see, esp., Chen and Jaw, 1999). The dimensionless group C_v is usually assumed to be an algebraic function of the local statistical state of the turbulence. Dimensional reasoning suggests that C_v depends on three distinct time scales: a viscous time scale, v/k, a turbulent time scale, k/ϵ , and mean field time scales related to the two nontrivial independent invariants of the local mean strain rate $\langle \underline{S} \rangle$ (i.e., $II_S \equiv tr(\langle \underline{S} \rangle \cdot \langle \underline{S} \rangle)$ and $III_S \equiv tr(\langle \underline{S} \rangle \cdot \langle \underline{S} \rangle)$. Based on this hypothesis, C_v depends on three independent dimensionless groups: the turbulent Reynolds number $(k/\epsilon)/(v/k)$; and, the two dimensionless time scales: $(k/\epsilon)II_S^{1/2}$ and $(k/\epsilon)III_S^{1/3}$.

Transport Equations for the Turbulent Kinetic Energy and the Turbulent Dissipation

Although an exact, albeit unclosed, equation for turbulent kinetic energy can be developed from the NS-equation (see Appendix B), the following phenomenological transport equation for the kinetic energy is used to support the research developed hereinafter (see Hanjalic, 1994):

$$\frac{\partial \mathbf{k}}{\partial t} + \langle \underline{\mathbf{u}} \rangle \cdot \nabla \mathbf{k} = + \nabla \cdot \{\underline{\mathbf{D}}_{\mathbf{v}} \cdot \nabla \mathbf{k}\} + \{-\langle \underline{\mathbf{u}}' \underline{\mathbf{u}}' \rangle : \langle \underline{\underline{\mathbf{S}}} \rangle \} - \{ \epsilon \}. \tag{1.9}$$

The three contributions in braces on the right-hand-side of Eq.(1.9) that cause changes in the turbulent kinetic energy include: 1) the viscous flux and the turbulent flux of kinetic energy relative to the mean velocity; 2) the "production" of kinetic energy due to the coupling between the Reynolds stress and the mean strain rate; and, 3) the dissipation of kinetic energy. The "production" term may be either positive or negative, depending on

13. 200 No i wasanat -<u>D</u>. Tk. acis wish.fi Aार्ट प्रदेश व विकास के i cho Lo i the turbulence

क्षा अर्था अध्या

I. The contr

हेल्लाका गरीब

द्धं अ क्षेष्ठ di

Bestini of

Bully for the

कृष्ट्रहाल्य edr

the local coupling between the Reynolds stress and the mean strain rate (see p. 180 in Pope, 2000; Nishino et al., 1996). The dissipation of energy is positive for all turbulent flows inasmuch as $\varepsilon \equiv v \operatorname{tr}(<(\nabla \underline{u}')\cdot(\nabla \underline{u}')^T>)>0$. The flux of turbulent kinetic energy, $-\underline{\underline{D}}_v \cdot \nabla k$, acts like mixing for all turbulent flows provided the dispersion operator $\underline{\underline{D}}_v$ satisfies the following conditions:

$$\underline{\underline{D}}_{v} \equiv v \underline{\underline{I}} + \tau_{R} < \underline{\underline{u}}' \underline{\underline{u}}' > , \quad \tau_{R} > 0 , \quad \underline{\underline{D}}_{v} : \nabla k \nabla k > 0 , \quad \forall \ \nabla k \ni \|\nabla k\| > 0. \tag{1.10}$$

Although an exact, albeit unclosed, equation for turbulent dissipation can also be developed from the NS-equation (see Appendix C), the following complementary phenomenological transport equation for the dissipation is used to support the research developed hereinafter (see Appendix C):

$$\frac{\partial \varepsilon}{\partial t} + \langle \underline{\underline{u}} \rangle \cdot \nabla \varepsilon = + \nabla \cdot \{\underline{\underline{\underline{D}}}_{v} \cdot \nabla \varepsilon\} + C_{P} \{\frac{-\langle \underline{\underline{u}}' \underline{\underline{u}}' \rangle : \langle \underline{\underline{S}} \rangle}{\tau_{R}}\} - C_{D} \{\frac{\varepsilon}{\tau_{R}}\}. \tag{1.11}$$

The three contributions in braces on the right-hand-side of Eq.(1.11) that cause changes in the turbulent dissipation include: 1) the viscous flux and the turbulent flux of turbulent dissipation relative to the mean velocity; 2) the "production" of turbulent dissipation; and, 3) the dissipation of turbulent dissipation. Rodi and Mansour (1993) give an assessment of the individual contributions to the exact equation for ε based on DNS results for non-rotating fully-developed channel flows. For a derivation of the exact dissipation equation, see Appendix C.

 $\tilde{\xi} = \frac{2 < \tilde{n}, \tilde{n}, >)}{< \tilde{n}, \tilde{n}, >} \quad .$

spiliantly, the NR-s

Emmissal vector spa

 $\int_{\mathbb{R}^{3}} |z| = \frac{1}{2} \sum_{i \in \mathbb{R}^{3}} |z|^{2} = \frac{1}{2} \sum_{i \in \mathbb{R}^{3}} |z|^{$

deg 1.13% which is e

Standing inequalities

Pals 1997; and, p. 5

recise solutions tha

रहार काकाष्ट्र, बरराजर ।

his information is c

जिल्ह्याह **ब** हामिन्द्रा (

tace for which

1.3 The Normalized Reynolds Stress

The foregoing results show that the Reynolds stress appears in the equations that govern the behavior of $<\underline{u}>$ and . The normalized Reynolds (NR-) stress, defined as follows

$$\underline{\underline{R}} = \frac{\langle \underline{\underline{u}'\underline{\underline{u}'}} \rangle}{\operatorname{tr}(\langle \underline{\underline{u}'\underline{u}'} \rangle)} , \quad \underline{\underline{R}}^{\mathrm{T}} = \underline{\underline{R}} \quad \operatorname{tr}(\underline{\underline{R}}) = 1,$$
 (1.12)

has real eigenvalues and real eigenvectors that are mutually orthogonal. Most significantly, the NR-stress is a non-negative, dyadic-valued operator inasmuch as its quadratic form $Q_R(\underline{z})$ is non-negative for arbitrary unit vectors in a Euclidean three-dimensional vector space:

$$Q_{R}(\underline{z}) = \underline{\underline{R}} : \underline{z}\underline{z} = \frac{\langle (\underline{z} \cdot \underline{u}')(\underline{u}' \cdot \underline{z}) \rangle}{\operatorname{tr} \langle u'u' \rangle} \ge 0 \quad , \quad \forall \underline{z} \in E^{3} \ni ||\underline{z}|| = 1.$$
 (1.13)

Ineq.(1.13), which is equivalent to Schwartz's inequalities for the components of the NR-stress, implies that the eigenvalues of the NR-stress are non-negative and satisfy the following inequalities: $0 \le \lambda_{R1} \le \lambda_{R2} \le \lambda_{R3} \le 1$ (cf., Schumann, 1977; Lumley, 1978; Parks, 1997; and, p. 51 and p. 401 in Pope, 2000). Closure models for the NR-stress that produce solutions that satisfy Ineq.(1.13) for all rotating and non-rotating turbulent flows are *universal* and *realizable*, but they may not be accurate or practical.

The diagonal components of the NR-stress represent the fraction of turbulent kinetic energy associated with each component of the instantaneous fluctuating velocity. This information is often displayed on a triangular diagram (or energy simplex), which represents a subset of positive points in a hyperplane of a three-dimensional Euclidean space for which $\sum_{i=1}^{3} R_{ii} = 1$. For states with energy equally distributed among the

7

specification of turbulances may not be till approaches of R are a

They and others (see which the states of turb.) $\frac{1}{16} \frac{R}{3} - \frac{1}{3} = \frac{1}{16} \frac{1}{16} = \frac{1}{16}$

Figure 1.1, whi

Beli defines the bo

terms of the arriver

tion of the inequal

Recomple invariants

Figure 1.1 provi

tamalized symm.

sees a specific

The eigenvalue simple

The of states on each

with the AB.

included The quadrated as one of the

velocity components, $R_{11} = R_{22} = R_{33} = 1/3$. This is a necessary condition for an *isotropic state* of turbulence, but it is not sufficient inasmuch as the eigenvalues of the NR-stress may not be the same even if the diagonal components of \underline{R} are the same. If the eigenvalues of \underline{R} are equal (i.e., $\lambda_{R1} = \lambda_{R2} = \lambda_{R3} = 1/3$), then the turbulent state is *isotropic*.

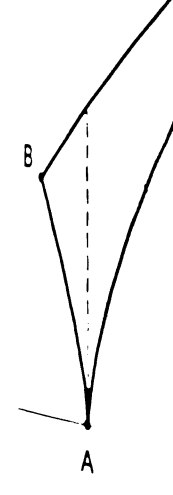
Figure 1.1, which is similar to the pseudo-triangular graphs introduced by Lumley and others (see Lumley, 1978; Reynolds, 1987; and, p. 401 in Pope, 2000), defines the states of turbulence in terms of the invariants of the anisotropic operator:

$$\underline{b} = \underline{R} - \frac{1}{3}\underline{I} \quad , \quad \underline{b}^{T} = \underline{b} \quad , \quad tr(\underline{b}) = 0 . \tag{1.14}$$

Table 1.1 defines the boundaries of the Lumley (L-) diagram in terms of the non-trivial invariants of the anisotropic operator and the eigenvalues of the NR-stress. For a derivation of the inequalities presented in Table 1.1, see Parks (1997). In this research, the anisotropic invariants are defined by the following three scalar parameters:

$$I_b \equiv tr(\underline{\underline{b}}) = 0$$
 , $II_b \equiv tr(\underline{\underline{b}} \cdot \underline{\underline{b}})$, $III_b \equiv tr(\underline{\underline{b}} \cdot \underline{\underline{b}} \cdot \underline{\underline{b}})$ (1.15)

Figure 1.1 provides a means to compare different anisotropic states associated with normalized, symmetric, non-negative operators. The eigenvalues of the NR-stress corresponding to specific anisotropic states on the L-diagram are located in the 1st Sextet of the eigenvalue simplex (see Table 1.1 and the inset on Figure 1.1). Table 1.1 identifies the type of states on each boundary of the L-diagram. For example, the quadratic forms associated with the AB- and AC-boundaries are oblate ellipsoids and prolate ellipsoids, respectively. The quadratic forms associated with the BC-boundary are planar ellipses in inasmuch as one of the eigenvalues of the NR-stress is zero. The quadratic forms



Realizabi.

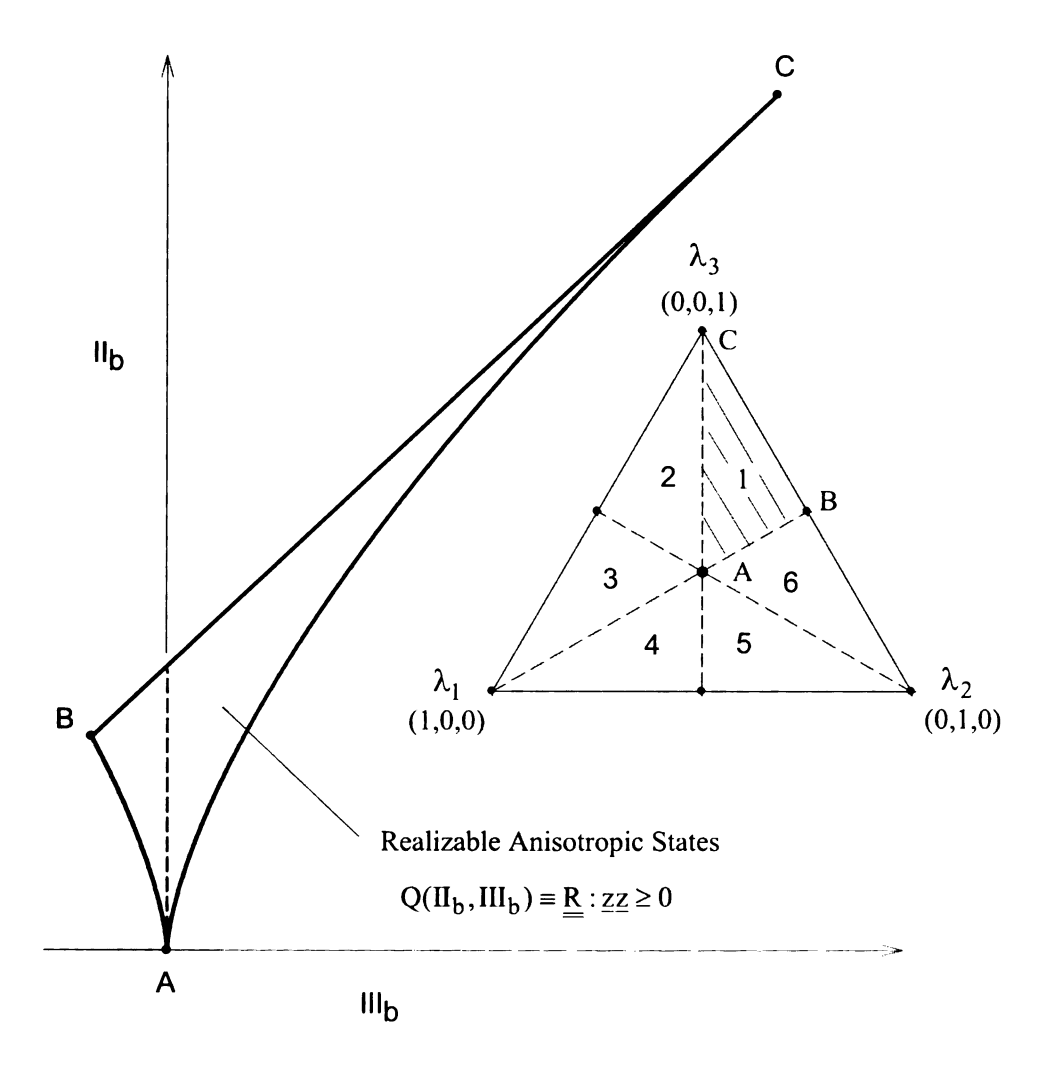


Figure 1.1 Realizable States of the NR-Stress (Lumley, 1978).

Töbil Boundar, 1997)

Visit pic News	QIII ₅ , III.
<u>A</u>	3D-Isotropio
B	2D45-75
(+ ID-IX 15-51
ارت <i>تن</i> ع	O-Cate
3(************************************	Planar
1.2022 10	Produce

Table 1.1 Boundary Characteristics of the L-Triangle (Parks, 1997; Weispfennig, 1997).

Anisotropic States	$Q(II_b,III_b)$	Eigenvalues of $\underline{\underline{R}}$	Invariants of $\underline{\underline{b}}$
Α	3D-Isotropic	$\lambda_{R1} = \lambda_{R2} = \lambda_{R3} = 1/3$	$III_b = 0, II_b = 0$
В	2D-Isotropic	$\lambda_{R1} = \lambda_{R2} = 1/2, \lambda_{R3} = 0$	$III_b = -1/36, II_b = 1/6$
С	1D-Isotropic	$\lambda_{R1} = 1, \lambda_{R2} = \lambda_{R3} = 0$	$III_b = 2/9, II_b = 2/3$
AB boundary	Oblate	$0 \le \lambda_{R1} \le 1/3 \le \lambda_{R2} = \lambda_{R3} \le 1/2$	$II_b = 6(-III_b/6)^{2/3},$ -1/36 \le III_b \le 0
BC boundary	Planar	$0 = \lambda_{R1} \le \lambda_{R2} \le 1/2 \le \lambda_{R3} \le 1$	$II_b = 2/9 + 2III_b$ -1/36 \le III_b \le 8/36
AC boundary	Prolate	$0 \le \lambda_{R1} = \lambda_{R2} \le 1/3 \le \lambda_{R3} \le 1$	$II_b = 6(III_b/6)^{2/3}$ $0 \le III_b \le 8/36$

ascared with the state the Beverning Country are in the Beverning of the Schwartz in the Schwa

4 Objectives of

The primary in the NR-stress that it is design and an a

minuter as the r

Totalis in this dissible URAPS-close

Etherenfication,

Acqui focus is or

The initiated earl

Prepris (199-)

The underly

 $^{\mathrm{dig}_{ij}}$ field and $_{\mathrm{tl}}$

associated with the states at the A-vertex are spheres; the quadratic forms associated with the states at the B-vertex are circles; and, the quadratic forms associated with the states at the C-vertex are infinitely elongated needles. The anisotropic states for which $0 \le II_b \le 2/9$ and $III_b = 0$ are associated with an NR-stress with eigenvalues that satisfy the following conditions: $0 \le \lambda_{R1} \le \lambda_{R2} = 1/3 \le \lambda_{R3} \le 1$. Anisotropic states that satisfy all of the Schwartz inequalities are either on the boundary or located within the L-diagram. Models that predict anisotropic states with (II_b, III_b) outside the L-diagram are unrealizable and, thereby, unphysical.

1.4 Objectives of This Research

The primary objective of this research is to develop an algebraic closure model for the NR-stress that supports the practical use of the RANS-equation (see Eq.(1.4) for rapid design and analysis of engineering processes. The new closure model is referred to hereinafter as the universal realizable anisotropic prestress (URAPS-) closure. The emphasis in this dissertation is on the theoretical development, calibration, and validation of the URAPS-closure. The implementation of the new closure in a computational code and the verification of the resulting computer code are not addressed in this research. The principal focus is on the further development of an algebraic closure model for the NR-stress initiated earlier by Parks (1997) for non-rotating homogeneous shear and by Weispfennig (1997) for non-rotating fully-developed channel flows.

The underlying premise of the research stems from the phenomenological idea that the Reynolds stress is determined by the local statistical properties of the fluctuating velocity field and the local mean field kinematics. This algebraic idea is similar to the

ignition proposed b

exemples areas exer

Mestess is formulate

TIPOV.

 $\sum_{k=1}^{\infty} \sum_{k=1}^{\infty} \sum_{k=1}^{\infty} \sum_{k=1}^{\infty} \int_{\mathbb{R}^{n}} \mathbf{1} \mathbf{f} \left[\sum_{k=1}^{\infty} \sum_{k=1}^{\infty} \sum_{k=1}^{\infty} \sum_{k=1}^{\infty} \mathbf{f} \left[\sum_{k=1}^{\infty} \sum_{k=1$

 $\lim_{x\to x} \underline{\underline{k}} = t_R < \underline{\underline{F}} > I_{\pi}:$

¹/₂>=7 < <u>u</u>> +2 <u>Ω</u> a

Ix ratio of the turn

hake I have when

esembon is to devel.

spilicantly, produces

it lan flows.

Clearly, the poet

Dien phenomena re strpic state in an in.

reciped hereinatter.

changes in th

Francis by Eqs.(1.9)

anisotropy that

itiel flows where

hypothesis proposed by Boussinesq in 1877, which has evolved into the class of "eddy" viscosity closures exemplified by Eqs.(1.7), (1.9), and (1.11) above. In what follows, the NR-stress is formulated as a non-nagative mapping of $\underline{\underline{R}}$ into itself with the following property:

$$\underline{\mathfrak{R}}(\underline{R},\underline{K}) = \underline{R}$$
, if $\underline{K} = \underline{0}$, then $\underline{R} = \frac{1}{3}\underline{I}$. (1.16)

where $\underline{\underline{K}} \equiv \tau_R < \underline{\underline{F}} >$ In the above hypothesis,

$$\langle \underline{F} \rangle = \nabla \langle \underline{u} \rangle + 2 \underline{\Omega} \text{ and } \tau_{R} = \tilde{\tau}_{R} (Re_{t}, \tilde{N}_{F}) \frac{k}{\varepsilon}.$$
 (1.17)

The ratio of the turbulent time scale k/ϵ and the mean field time scale is $\bar{N}_F \equiv k \| < \underline{F} > \| / \epsilon$ where $\| < \underline{F} > \|^2 \equiv tr(< \underline{F} > \cdot < \underline{F} >^T)$. The specific goal of this dissertation is to develop a closure for the NR-stress that satisfies Eq.(1.16) and, most significantly, produces solutions that satisfy Ineq.(1.13) for all rotating and non-rotating turbulent flows.

Clearly, the pseudo-steady state hypothesis expressed by Eq.(1.16) cannot explain turbulent phenomena related to the finite time required for the NR-stress to relax to an isotropic state in an inertial frame, if $\underline{K} \rightarrow \underline{0}$ instantaneously. Therefore, for the theory developed hereinafter, temporal changes in the NR-stress occur implicitly through temporal changes in the gradient of the mean velocity and the turbulent time scale k/ϵ governed by Eqs.(1.9) and Eq.(1.11) above. Furthermore, Eq.(1.16) cannot explain the weak anisotropy that occurs on the symmetry plane of non-rotating, fully-developed channel flows where $\underline{K} = \underline{0}$, yet $0 < R_{xx} = R_{yy} < 1/3 < R_{zz} < 1$. However, Eq.(1.16)

is mply that for rot. ally shot isotropic (la addition to "midution" and diss stig the new NR-sir. with minted to mon-Tank 1989, Parks, 19 at Pope, 2000). The Reliated to the These previous theory But Park and Chung. 1 As indicated above Maters that is aligned siteses four fundamen Tide 2) the selection (gramment of approxim ार्थ predictions relate In summary, with tikes tealizable solu South Sows, this res. seem that may have

does imply that for rotating homogeneous turbulent flows for which $\underline{\underline{K}} = 2\underline{\Omega}$, turbulence decay is not isotropic (see Chapter 5 hereinafter).

In addition to the development and calibration of the URAPS-closure, the "production" and dissipation coefficients C_P and C_D in Eq. (1.11) are estimated by using the new NR-stress model together with benchmark experimental data and DNS results related to non-rotating asymptotic homogeneous shear flows (Tavoularis and Karnik, 1989; Parks, 1997), and non-rotating homogeneous decay (see, esp., Parks, 1997; and, Pope, 2000). The dimensionless relaxation time $\tilde{\tau}_R$, formally introduced by Eq.(1.16), is related to the space-time structure of the local turbulence and is determined by using previous theoretical and computational results related to rotating homogeneous decay (Park and Chung, 1999).

As indicated above, the goal is to develop a new algebraic closure model for the NR-stress that is aligned with previous turbulent modeling principles. This dissertation addresses four fundamental issues related to this goal: 1) *realizabilty* of the closure model; 2) the selection of appropriate benchmark flows for calibration; 3) the practical development of approximate solutions to the URAPS-closure; and, 4) an assessment of model predictions related to the influence of frame rotation on the redistribution of energy.

In summary, with the discovery of an algebraic closure for the NR-stress that produces realizable solutions in rotating and non-rotating frames of reference for all turbulent flows, this research provides a unified and practical closure for the RANS-equation that may have a significant impact on engineering design, research and education.

is Outline of the D A review of the ត្តោះជា Chapter 2 milibility and redis all and other and ter verticity to the Ni ticks developed recent Terredictions of a real mis are used to partly at herodinamic procl Mestigning (1997) IN al

h Capter 3. 4. Realized to include th

To the NR-stress to

Tittess The proclassics \$116 above) and s

Ede NR-stress is a p

the depotical result.

et portotating totho!"

hish-cases and the Ca

te VR-stress and the p

Estral anisotropy

Fills, provides a m

1.5 Outline of the Dissertation

A review of the relevant literature that supports the objectives of this dissertation is given in Chapter 2. Previously developed algebraic models are discussed relative to realizability and redistribution of energy. Chapter 2 also includes a brief critique of Eq.(1.7) and other anisotropic models that relate the mean strain rate and the intrinsic mean vorticity to the NR-stress. The class of truncated explicit algebraic Reynolds stress models developed recently by Gatski and Jongen (2000) are also reviewed in Chapter 2. The predictions of a realizable algebraic model by Shih et al. (1994) are discussed and the results are used to partly justify the approach developed in this research. A summary of the hydrodynamic preclosure equation previously developed by Parks (1997) and by Weispfennig (1997) is also given in Chapter 2.

In Chapter 3, the preclosure result developed earlier by Parks et al. (1998) is generalized to include frame rotation. This is a key step in the development that directly links the NR-stress to another non-negative operator referred to hereinafter as the prestress. The preclosure mapping includes the hydrodynamic/kinematic operator \underline{K} (see Eq.(1.16) above) and satisfies the condition that if the prestress is a positive operator, then the NR-stress is a positive operator, which means that Ineq.(1.13) is satisfied. This *a priori* theoretical result, which does not depend on any calibration, holds for all rotating and non-rotating turbulent flows. In Chapter 3, the prestress is assumed to be caused by the NR-stress and the Cayley-Hamilton (CH-) theorem is used to relate the eigenvalues of the NR-stress and the prestress. The phenomenological CH-coefficients associated with the "extra" anisotropy of the prestress must be determined by benchmark flows, but Ineq.(1.13) provides a means to identify *universal* bounds on these parameters. Thus, the

Sing URAPS ales many and non-rote peficats are observe. ERANS-aquation as The URAPS-C Helefficients, α a actions, C_{p} and C_{p} money implies in Epititiabove. For Ital ad (33). The foregoin Briang three canonic Tizzy bemogeneous d The calibrated UR Assumen This airray earlows. The surpris tation is illuminated. Chapter 5 exam icas The URAPS-cho see all on the , Petits between the v Tally isotropic state Referred to the Muctu Totalli clearly demi resulting URAPS-closure is a non-linear mapping of the NR-stress into itself for all rotating and non-rotating turbulent flows, provided the *universal* bounds on the CH-coefficients are observed. This result provides a means to significantly broaden the use of the RANS-equation as a diagnostic tool for analyzing turbulent flows.

The URAPS-closure coefficients are estimated in Chapter 4. This includes two CH-coefficients, α and β , implicit in the hypothesis expressed by Eq.(1.16); two coefficients, C_P and C_D , associated with the ϵ -equation defined by Eq.(1.11); and, the parameters implicit in the turbulent transport group $\tilde{\tau}_R(Re_t, \tilde{N}_F)$, introduced by Eq.(1.17) above. For large Re_t , $\tilde{\tau}_R(\infty, \tilde{N}_F)$ depends on three coefficients: C_{R1} , C_{R2} , and C_{R3} . The foregoing seven URAPS-closure coefficients are estimated by using the following three canonical benchmark flows: 1) non-rotating homogeneous decay; 2) rotating homogeneous decay; and, 3) non-rotating asymptotic homogeneous shear.

The calibrated URAPS-equation can be solved by the method of successive substitution. This attractive numerical feature is demonstrated in Chapter 4 for simple shear flows. The surprising role of the "extra" anisotropy operator in solving the URAPS-equation is illuminated in Chapter 4.

Chapter 5 examines the influence of rotation on the NR-stress for homogeneous decay. The URAPS-closure predicts that for rotating homogeneous decay, the anisotropic states are all on the AB-boundary of the L-diagram (see Figure 1.1). Whence, the coupling between the velocity fluctuating field and the Coriolis acceleration causes an initially isotropic state to become anisotropic. For long times, the kinetic energy is transferred to the fluctuating velocity component that is co-linear with the rotation axis. This result clearly demonstrates that a return-to-isotropy upon the sudden removal of the

3% results for \tilde{N}_{i} exactly that the Carrely with the design totaling flow Thus, the ne hading velocity fi to fluctuating veloc Lating velocity f has captured essinamie kinema 7.Eq. (1.16).

tati ieloony gradio:

egalsohave implica k

is digment of these

minutely consistent

is we-mainly fully-

distress also used to

most verticity for i.

In Chapter 7, th

The influence of

mean velocity gradient only occurs in an inertial frame. This Coriolis-induced anisotropy may also have implications on scattering of electromagnetic fields in the atmosphere.

The influence of rotation on asymptotic homogeneous shear as well as on the development of these states is presented in Chapter 6. The URAPS-predictions are qualitatively consistent with DNS results and with other closure models in the literature.

In Chapter 7, the URAPS-closure is used to predict the redistribution of energy for non-rotating fully-developed channel flows ($\Gamma_{yz} = \underline{e}_z \underline{e}_y : \nabla < \underline{u} >$). The URAPSclosure is also used to predict the components of the NR-stress in the region of zero intrinsic vorticity for fully-developed channel flows with spanwise rotation ($\underline{\Omega} = \Omega_x \underline{e}_x$). DNS results for $\tilde{N}_F \equiv k \left\| < \frac{F}{E} > \right\| / \epsilon$ are used to predict the URAPS-results. It is noteworthy that the normal components predicted by the URAPS-closure agree qualitatively with the DNS results for non-rotating flows: $R_{yy} < R_{xx} < R_{zz}$; and, for spanwise rotating flows, $R_{zz} < R_{xx} < R_{yy}$. This behavior is also indicated in the DNS results. Thus, the new algebraic closure shows that the Coriolis coupling with the fluctuating velocity field causes a transfer of energy from the longitudinal component of the fluctuating velocity field to the cross flow (or transverse) component of the fluctuating velocity field. This prediction supports the conclusion that the URAPSclosure has captured the essential relationship between the NR-stress and the hydrodynamic/kinematic operator \underline{K} , as anticipated by the closure hypothesis expressed by Eq.(1.16).

(hapter १ द्वार

TAPS-closure and (

iiste (an be integra)

Chapter 8 gives a summary discussion of salient conclusions related to the URAPS-closure and Chapter 9 identifies additional research needed before the URAPS-closure can be integrated into a CFD code.

II Erroduction

In this chapter

need to the follower. raita fully-developed areautig, homogene comp homogeneous Ritard flows used a side the develop: frametological clos Milmark results are Raps-closure. A criv esection 2.6. The chi

Con-Rotating F

Sugar ton

ेव भाग बत

DNS results

haliped by Kim et

State (2003), Alam on Chapter 7 in

CHAPTER 2

LITERATURE REVIEW

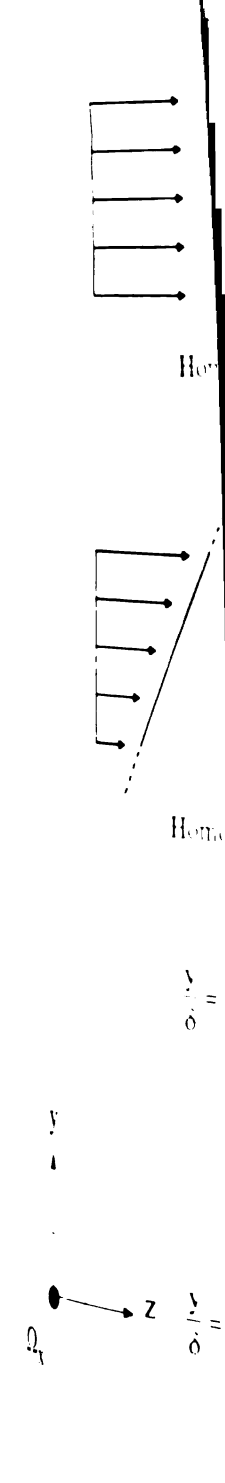
2.1 Introduction

In this chapter, direct numerical simulation (DNS) and experimental results related to the following canonical benchmark flows are reviewed: 1) rotating and non-rotating, fully-developed, turbulent channel flows (Sections 2.2 and 2.3); 2) rotating and non-rotating, homogeneous, turbulent shear flows (Section 2.4); and, 3) rotating and non-rotating, homogeneous turbulent decay (Section 2.5). Figure 2.1 illustrates the three benchmark flows used in this study. DNS results from the literature are used in Chapter 3 to guide the development of the URAPS-closure and in Chapter 4 to estimate the phenomenological closure coefficients introduced by the theory. In Chapters 5-7, DNS benchmark results are used to evaluate the predictions of the NR-stress based on the URAPS-closure. A critique of current algebraic closure models for the NR-stress is given in Section 2.6. The chapter concludes by restating the objectives of this research relative to the prior art.

2.2 Non-Rotating Fully-Developed Channel Flows

RANS-Equation

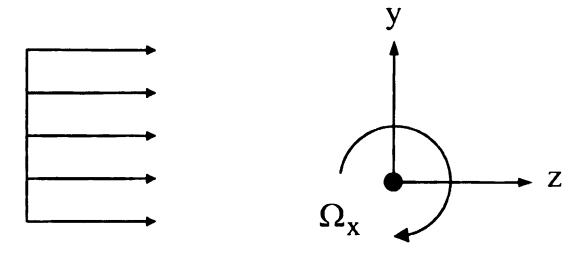
DNS results for non-rotating, fully-developed, channel flows have been eveloped by Kim et al.(1987), Moser et al.(1999), Iwamoto et al. (2002), Alamo and Jimenez (2003), Alamo et al.(2004), Hoyas and Jimenez (2006) and many others (see, Chapter 7 in Pope, 2000). The mean velocity has one component (i.e.,



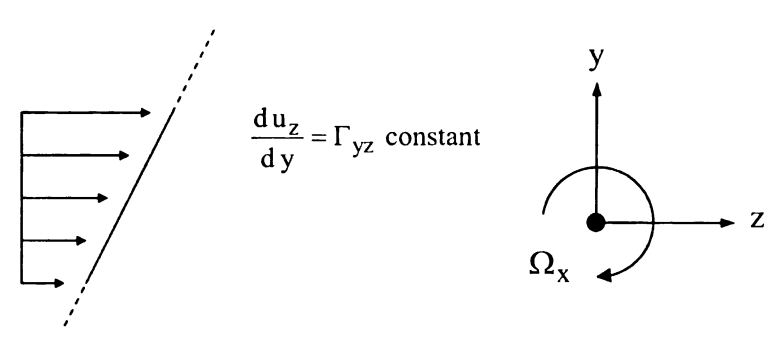
Definitions of

Hor

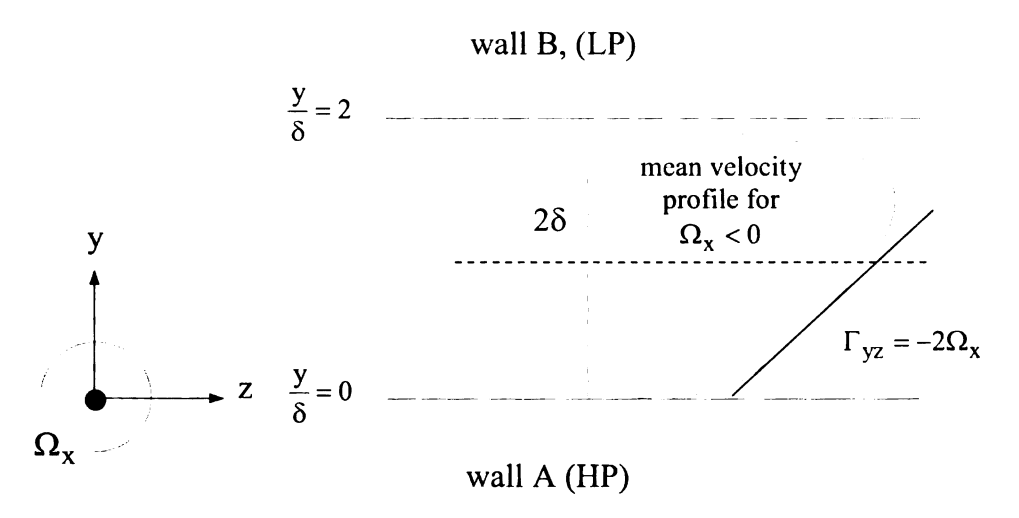
<u>;</u> = 0



Homogeneous decay with spanwise rotation



Homogeneous shear with spanwise rotation



Channel flow with spanwise rotation

Figure 2.1. Definitions of Benchmark Flows.

egy=(Uz >(y)ez) that is

Fin 21). The mean press

Fire 21, the symmetry :

firstel are located at y = 1

mads the solid fluid into

 $\frac{1}{2} = \xi_2 \xi_2$, and $\nabla < \underline{u} > = 1$

ANS-equation, defined by I

$$\frac{1}{\rho} \frac{1}{\partial x} \frac{\partial x}{\partial y} + \frac{d}{dy} \left[-2k \right]$$

$$\frac{1/(\rho_0)}{\rho/\rho_0} = \frac{d}{dy} [v]^{\frac{1}{2}}$$

Edeabore equations,

text velocity and the meat

$$||u_{z}\rangle||_{l} = \langle u_{z}\rangle(2\delta) = 0$$

ical implies that

$$p_{D} > (i,z) - \langle p_{D} > (0) \rangle$$

in no-slip on si

$$\frac{1}{2} e^{i(t)} = R_{yy}(2\delta) = 0 : th$$

desiminatry plane, max

 $^{\circ}$ accordinate $\mathbf{y}_{:}$

 $<\underline{u}>=<u_z>(y)\underline{e}_z$) that depends only on the transverse (cross flow) coordinate y (see Figure 2.1). The mean pressure depends on y and z: =(y,z). As indicated in Figure 2.1, the symmetry plane of the channel is located at $y=\delta$; the walls of the channel are located at y=0 and 2δ . Mean momentum is transported across the flow towards the solid/fluid interfaces by viscous and turbulent stresses. With $\underline{\Omega}=\underline{0}$, $\underline{g}=g_z\underline{e}_z$, and $\nabla<\underline{u}>=\Gamma_{yz}(y)\underline{e}_y\underline{e}_z$, the non-trivial components of the unclosed RANS-equation, defined by Eq. (1.4), are

$$0 = -\frac{1}{\rho} \frac{\partial \langle p_D \rangle}{\partial y} + \frac{d}{dy} [-2k R_{yy}] \quad , \quad 0 \le y \le 2\delta$$
 (2.1)

$$0 = -\frac{1}{\rho} \frac{\partial \langle p_D \rangle}{\partial z} + \frac{d}{dy} \left[v \frac{d \langle u_z \rangle}{dy} - 2k R_{yz} \right] , \quad 0 \le y \le 2\delta.$$
 (2.2)

In the above equations, $< p_D > (y,z) \equiv (y,z) - z \rho g_z$. Boundary conditions for the mean velocity and the mean pressure are

$$\langle \mathbf{u}_{\mathbf{z}} \rangle (0) = \langle \mathbf{u}_{\mathbf{z}} \rangle (2\delta) = 0 \quad , \quad -\frac{1}{\rho} \frac{\partial \langle \mathbf{p}_{\mathbf{D}} \rangle}{\partial z} = \text{constant} .$$
 (2.3)

Eq. (2.1) implies that

$$< p_D > (y,z) - < p_D > (0,z) \equiv \Delta_{PD}(y) = -2\rho \, k(y) \, R_{yy}(y) \le 0 \quad , \quad 0 \le y \le 2 \, \delta \, . \eqno(2.4)$$

Due to no-slip on solid/fluid interfaces and continuity, $k(0) = k(2\delta) = 0$ and $\mathbf{R}_{yy}(0) = \mathbf{R}_{yy}(2\delta) = 0$; therefore, Eq. (2.4) shows that $\langle p_D \rangle (0,z) = \langle p_D \rangle (2\delta,z)$. On **the** symmetry plane, $\max |\Delta_{PD}| = +\rho \langle \mathbf{u}_y' \mathbf{u}_y' \rangle (\delta) \neq 0$.

Eq. (2.2) and Eq. (2.3) imply that the total stress is a linear function of the cross flow coordinate y:

 $\frac{\sqrt{2g_2}}{dy} - 2kR_{yy} = -\left(-\frac{1}{y}\right)$

Exy=0 and 2δ , the shear

If implies that

$$\frac{1\hat{c} \cdot p_0}{\hat{c} \cdot \hat{c}z} \Big] 2\hat{o} = v \frac{d}{d}$$

The friction velocity u . det.

The DNS results

$$\int_{\mathbb{R}^2} g du \cdot dv = L^{M_{\Lambda_1}(n)}$$

(a) & Figure 2.2 shows (1)

We can function of ξ :

$$\int_{\mathbb{R}^{2}} J_{x} \cdot \mathbf{R}^{\lambda x} = \int_{-\infty}^{\lambda x} J_{x}(x) = \frac{1}{2}$$

in Rel = ô (= ô u° v) ≥ 3

That It is notewor

important no

Results stress determines

is auti-symmett

$$v \frac{d < u_z >}{dy} - 2k R_{yz} = -\left[-\frac{1}{\rho} \frac{\partial < p_D >}{\partial z} \right] y + v \frac{d < u_z >}{dy} \bigg|_{y=0}.$$
 (2.5)

For y = 0 and 2δ , the shear components of the Reynolds stress are zero; therefore, Eq. (2.5) implies that

$$+\left[-\frac{1}{\rho}\frac{\partial \langle p_{D}\rangle}{\partial z}\right]2\delta = v\frac{d\langle u_{z}\rangle}{dy}\bigg|_{y=0} - v\frac{d\langle u_{z}\rangle}{dy}\bigg|_{y=2\delta} \equiv 2(u^{*})^{2} > 0.$$
 (2.6)

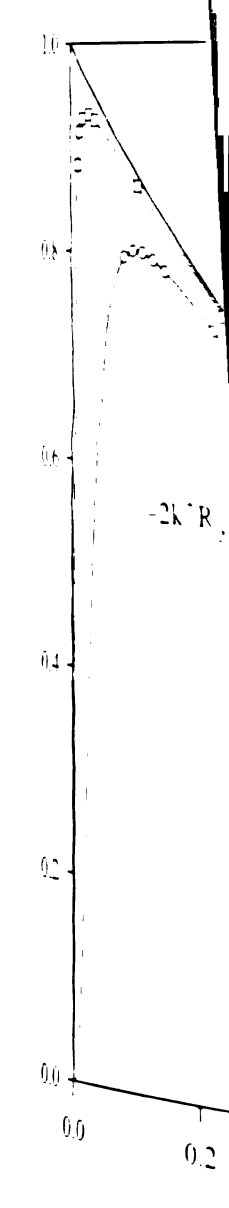
The friction velocity u*, defined by Eq. (2.6), is related to the axial pressure gradient or, equivalently, to the average wall shear stress.

Total Stress

The DNS results used herein are consistent with Eq. (2.5). With $\Gamma_{yz}^+ \equiv du^+/dy^+ = \Gamma_{yz} v/(u^*)^2 \,, \quad \Omega_x^+ \equiv \Omega_x v/(u^*)^2 \,, \quad k^+ \equiv k/(u^*)^2 \,, \quad y^+ \equiv y \, u^*/v \,, \quad \text{and}$ $\xi \equiv y/\delta \,, \text{ Figure 2.2 shows that the total dimensionless stress, defined as } \quad \Gamma_{yz}^+ - 2k^+ R_{yz} \,,$ is a linear function of ξ :

$$\Gamma_{vz}^{+} - 2k^{+} R_{vz} = \Gamma_{vz}^{+}(0) - \xi \quad , \quad 0 \le \xi \le 1 \quad , \quad \forall \ \delta^{+} > \delta_{c}^{+} \quad , \quad \Omega_{x}^{+} = 0.$$
 (2.7)

For $\text{Re}^+ = \delta^+ (\equiv \delta u^* / v) \cong 300$ and $\Omega_X^+ = 0$, the DNS results imply that $u_b / u^* \cong 17$ and $\Gamma_{yz}^+(0) = 1$. It is noteworthy that the viscous component of the total stress is **Quantitatively** important near the solid/fluid interface (viscous sublayer) and that the **Re**ynolds stress determines momentum transport in the outer region of the flow field. The **total** stress is anti-symmetric about the symmetry plane located at $\xi = 1$. These results are



Total Shear Flows

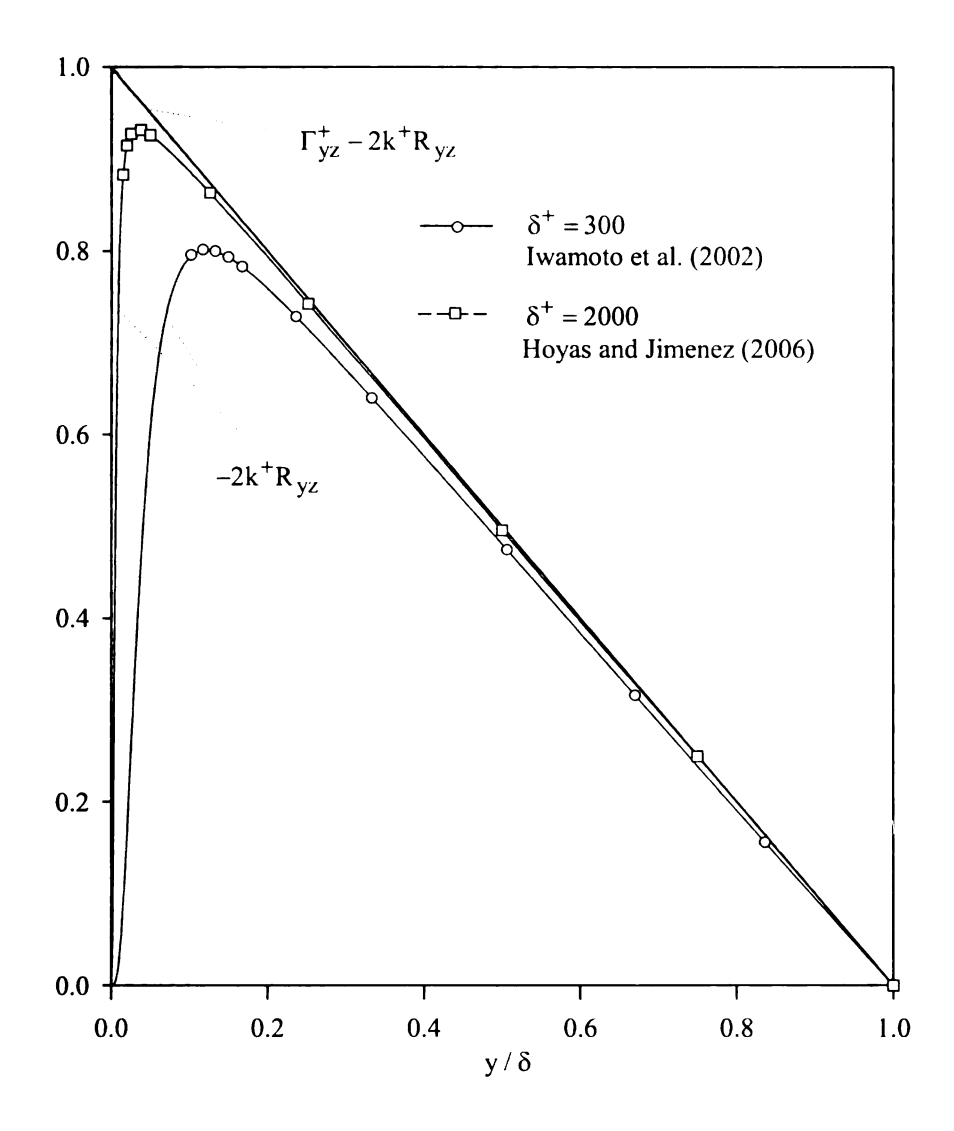


Figure 2.2. Total Shear Stress Profile for Non-Rotating, Fully-Developed, Channel Flows

fissall lie within the 2nd \

to low, the NR-stress has t

lin wordinate y (≡ y u v)

 $\frac{\beta = R_{11} e_1 e_2 + R_{12} e_2 e_3 + 1}{2}$

Determed slip at a solid film

 $\approx fory' = 0$ and $y'' = 2\alpha''$

and the NR-stres

aThin Menin and Yaglorn

 $\mathbb{R}^{H_{(0)} < K^{\infty}(0) < 1}$.

as the quadratic form

ace is a planar ellip.

Taratipsoid:

) (b) = Ry(6-) < 1 3 >

D/S results show:

Tage fully-developed. cl

 $^{\circ}$ Ry, and R $_{zz}$ to R $_{yy}$

consistent with the 1938 experiments of H. Reichardt for turbulent flow of air in a rectangular duct (see p.165 of Bird et al., 2007).

Energy States and Anisotropic Invariants

Figure 2.3 shows that the energy states for non-rotating, fully-developed, channel flows all lie within the 2nd Sextet of the energy simplex: $0 < R_{yy} \le R_{xx} < R_{zz} < 1$. For this flow, the NR-stress has three independent components that depend only on the cross flow coordinate $y^+ (\equiv y u^*/v)$:

$$\underline{R} = R_{xx} \underline{e}_{x} \underline{e}_{x} + R_{yy} \underline{e}_{y} \underline{e}_{y} + R_{zz} \underline{e}_{z} \underline{e}_{z} + R_{yz} \underline{e}_{y} \underline{e}_{z} + R_{zy} \underline{e}_{z} \underline{e}_{y}. \tag{2.8}$$

Due to no slip at a solid/fluid interface, all of the components of the Reynolds stress are zero for $y^+ = 0$ and $y^+ = 2\delta^+$. Continuity and the no-slip condition imply that the components of the NR-stress have the following properties at a solid/fluid interface (see p.279 in Monin and Yaglom, 1965, Weispfennig et al. 1999):

$$0 < R_{xx}(0) < R_{zz}(0) < 1$$
, $R_{yy} \propto (y^+)^2$ and $R_{yz} \propto y^+$ as $y^+ \to 0$ and $y^+ \to 2\delta^+$. (2.9)

Thus, the quadratic form associated with the NR-stress (QNR-form) at a solid/fluid interface is a planar ellipse. On the symmetry plane at $y^+ = \delta^+$, the QNR-form is a **Prolate ellipsoid**:

$$\mathbf{R}_{xx}(\delta^{+}) = \mathbf{R}_{yy}(\delta^{+}) < 1/3 < \mathbf{R}_{zz}(\delta^{+}) , \quad \mathbf{R}_{yz}(\delta^{+}) = 0.$$
 (2.10)

DNS results show that four qualitatively distinct energetic regions occur in a non- **TOtating**, fully-developed, channel flow. Near the wall $(0 < y^+ < 8)$, energy is transferred from R_{yy} and R_{zz} to R_{xx} as $y^+ \rightarrow 0$. A highly anisotropic region occurs for

R_M Children

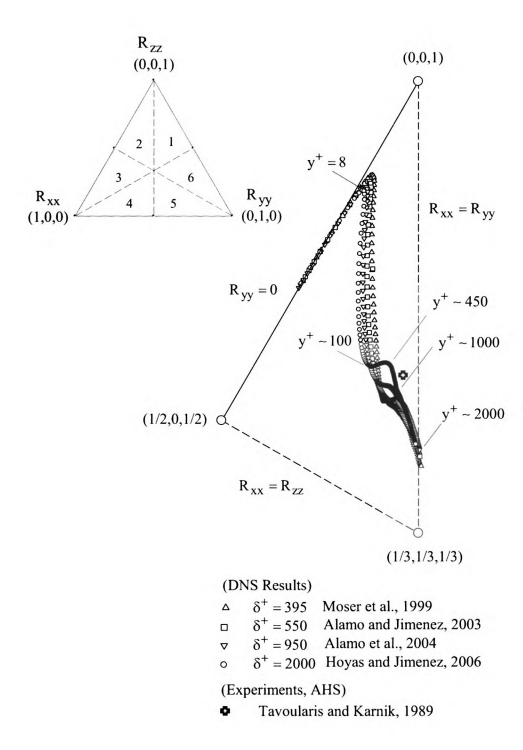


Figure 2.3. Energy States for Non-Rotating, Fully-Developed, Channel Flows

19 30 W E Carri # 1 . Ch R₀ ≥13 (4. $\frac{1}{2}$ (i) $[-R]_{yy}$ हेटी शुक्र $R_{g}(\mathbb{S}^{n}) = R_{g}$ Paris Tisking 33 apenns t 155. Bird et To Ministry The related व्यंत्रा व्याप्त Otplete des केंद्र के केंद्र इ Tractic to 14 SILP 1975 tong the three

Figure

Esperagio con

atalismopi,

 $8 < y^+ < 30$ with $max(R_{zz}) \cong 0.85$ and $max(\Gamma_{yz}^+) \cong 18$. For $30 < y^+ < 100$, $\Gamma_{yz}^+(y^+)$ decreases as y^+ increases and energy is transferred from R_{zz} to R_{xx} and R_{yy} . For $100 < y^+ < \delta^+$, energy continues to be transferred from R_{zz} to R_{yy} as $y^+ \to \delta^+$, but $R_{xx} \cong 0.3$ (see Figure 2.3). At the solid/fluid interface, $R_{yy}(0) = 0$, $R_{xx}(0) \cong 0.3$, $R_{zz}(0)1-R_{xx}\cong 0.7$, and $R_{yz}(0)=0$. At the symmetry plane (i.e., $y^+=\delta^+$), the mean velocity gradient is zero and the components of the NR-stress $R_{xx}(\delta^+) = R_{yy}(\delta^+) \cong 0.28$, $R_{zz}(\delta^+) = 1 - 2R_{xx}(\delta^+) \cong 0.44$, and $R_{yz}(\delta^+) = 0$. This weak anisotropic phenomenon on the symmetry plane is consistent with the classical 1938 experiments of H. Reichardt for turbulent flow of air in a rectangular duct (see p.165, Bird et al., 2007). A similar phenomenon is observed in axisymmetric pipe flows. This anisotropic energy state is contrary to the hypothesis expressed by Eq. (1.16) and may be related to the anisotropy in the normal components of the fluctuating pressure gradient correlation for wall bounded flows (i.e., $\langle \nabla p' \nabla p' \rangle$ for $y^+ = \delta^+$), or to an incomplete development of the flow field. It is noteworthy, however, that the fraction of energy in the spanwise component of the fluctuating velocity near the symmetry plane is comparable to the fraction of energy in the spanwise fluctuating velocity deep within the $\mathbf{viscous}$ sublayer (i.e., $R_{xx} \cong 0.3$). Clearly, the transverse redistribution of kinetic energy among the three components of the fluctuating velocity is significant.

Figure 2.4 shows the DNS results for the second and third invariants of the anisotropic component of the NR-stress for non-rotating, fully-developed channel flows.

The anisotropic states, defined by II_b and III_b, are all to the right of the anisotropic states



34:24. Anison

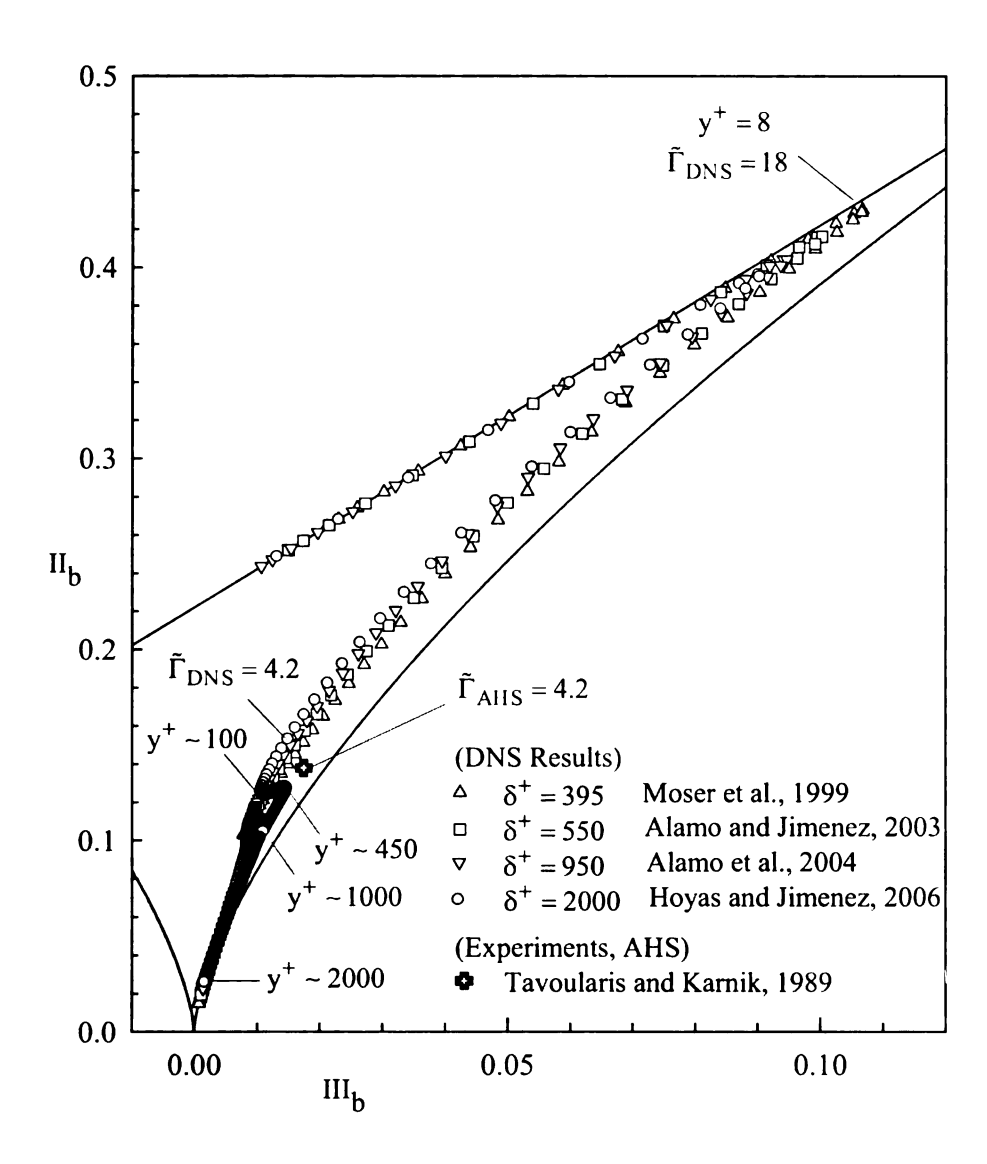


Figure 2.4. Anisotropic States for Non-Rotating, Fully-Developed, Channel Flows

Está I

For a Fyz

44.j0/25

ida in

santae h

70 7 1 King

j_{ny}=4.2

spring h

Acros # /B-313/

ें स्थान

35025 5EP/3

itay =

igate; F Throdix I

Figure

्यं(क्षत्रहु

Sec Tamble

for which $III_b=0$. These prolate-like states are parameterized by $y^+(\equiv yu^*/v)$ and $\tilde{\Gamma}_{DNS}(\equiv \Gamma_{yz}k/\epsilon \equiv \Gamma_{yz}^+k^+/\epsilon^+;\Gamma_{yz}^+\equiv du^+/dy^+)$. In the outer region (i.e., $100 < y^+ < \delta^+$), the anisotropic states are associated with prolate-like ellipsoidal quadratic forms. Figure 2.4 shows that the anisotropic state characteristic of non-rotating, asymptotic homogeneous shear (see Tavoularis and Karnik, 1989; and, Section 2.4 below) is located near the edge of the equilibrium core region in a channel flow (i.e., $\tilde{\Gamma}_{DNS}\cong 4.2$ for $y^+\cong 100$). This observation partly motivates the use of non-rotating asymptotic homogenous shear as a benchmark flow for model calibrations (see Chapter 4).

Across the core region (i.e., $30 < y^+ < 100$), the quadratic forms associated with the NR-stress (QNR-forms) change from a prolate-like structure to an elongated ellipsoidal structure as the turbulent kinetic energy increases near the wall. Within the viscous sublayer, viscous transport of momentum causes the elongated ellipsoidal QNR-form at $y^+ = 8$ to collapse to a planar elliptical form as $y^+ \to 0$. The DNS results used to construct Figures 2.3 and 2.4 are summarized in tabular form in Table I.1 and Table I.2 in Appendix I.

Turbulent Kinetic Energy and Turbulent Dissipation

Figure 2.5 shows the spatial distribution (inner and outer scaling) of turbulent kinetic energy (i.e., $k^+ \equiv k/(u^*)^2$) for δ^+ equal to 300 and 2,000. Figure 2.6 shows the spatial distribution (inner and outer scaling) of turbulent dissipation (i.e., $\epsilon^+ \equiv \epsilon v/(u^*)^4$)

ķ. 0.0

Em25. Kin

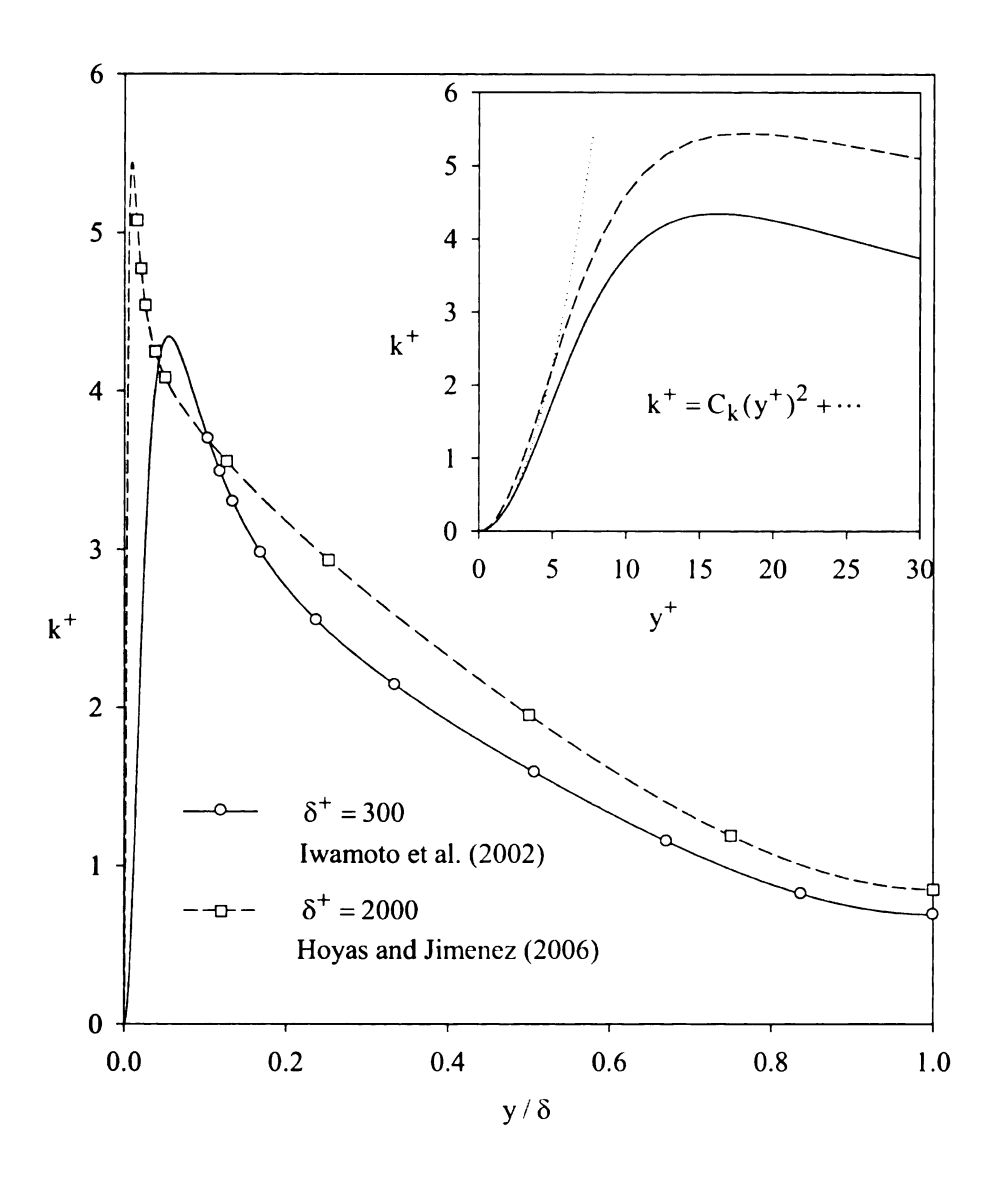


Figure 2.5. Kinetic Energy for Non-Rotating, Fully-Developed, Channel Flows

(120)

0.15

ý. j**í**j -

ŝ

9.06 **-**9.0

: \$326

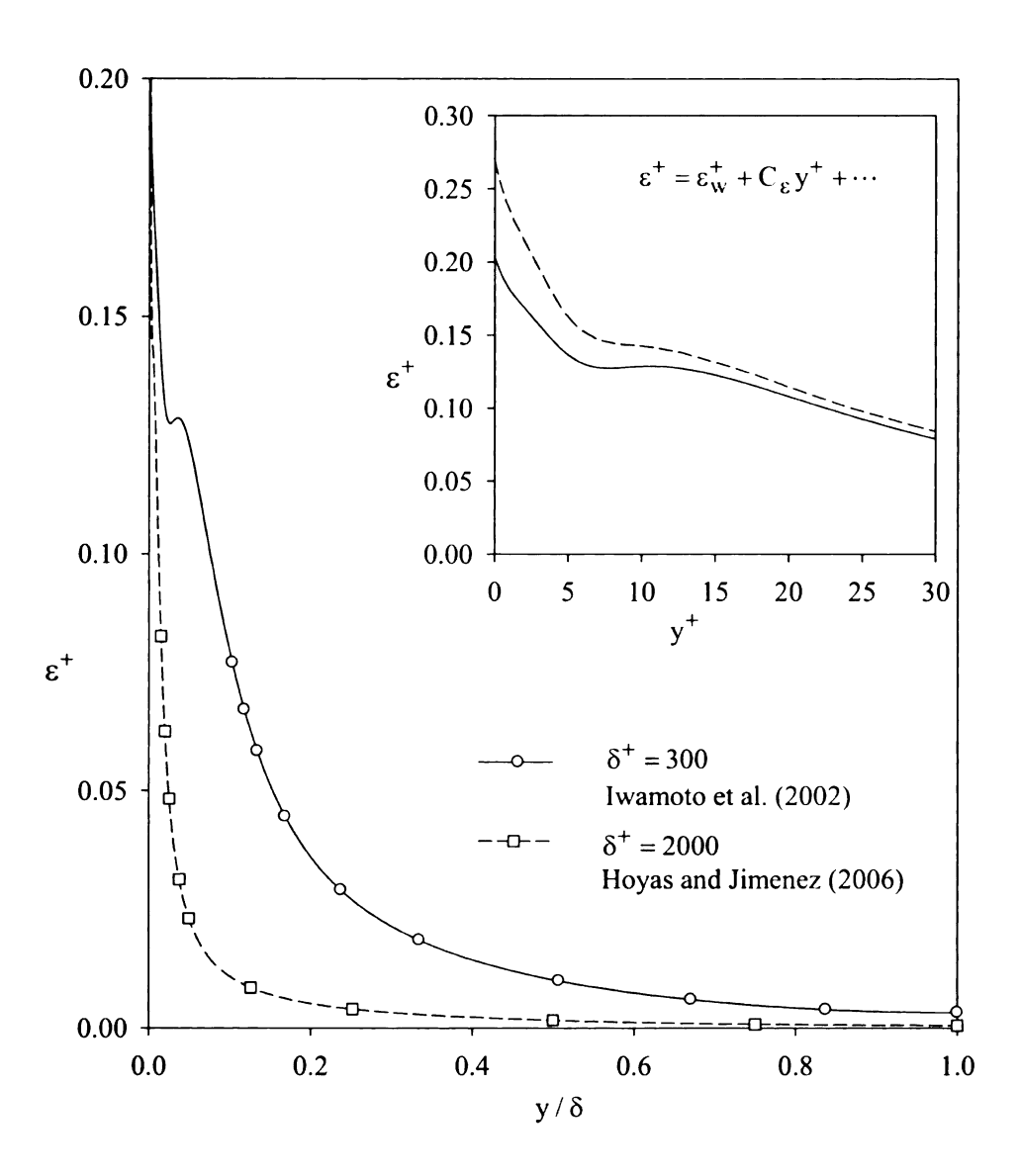


Figure 2.6. Dissipation for Non-Rotating, Fully-Developed, Channel Flows.

الشود كرج

y mer the h

Tabli Lauf B

Continu

: = : <mark>, - (, y</mark>

tacted of Fr

2258 to

F=39 and 2

เลียน: Value

a vietly, a

म्हाराताः । अधि

at åt cases

han katar

100000 T

ैंटें हैं Is a mai

Fizare

in bid ar

Eters, Re-

for δ^+ equal to 300 and 2,000. The DNS results for k^+ and ϵ^+ at different values of y^+ over the half width of the channel (i.e., $0 < y^+ < \delta^+$) are listed in Table I.1a and Table I.2a of Appendix I.

Continuity and the no-slip conditions imply that $k^+ = C_k(y^+)^2 + \cdots$ and $\varepsilon^+ = \varepsilon_w^+ + C_\varepsilon y^+ + \cdots$ near the wall, which is consistent with the DNS results shown on the inset of Figures 2.5 and 2.6. ($C_k\cong 0.09\,$ and $\,C_{\epsilon}\cong -0.03\,$) As $\,y^+\,$ increases, $\,k^+\,$ to $max(k^+) \cong 4.3$ and 5.4 respectively at $y^+ \cong 16$ and 18 for δ^+ = 300 and 2,000. However, as expected, the peak kinetic energy occurs at slightly different values of $\xi \equiv y/\delta$. For $\delta^+ = 300$, $k^+ \cong 3.7$ and $\epsilon^+ \cong 0.077$ at $y^+ = 30$ or, equivalently, at $\xi = 0.1$. For $\delta^+ = 2{,}000$, $k^+ \cong 5.1$ and $\epsilon^+ \cong 0.08$ at $y^+ = 30$ or, equivalently, at $\xi = 0.015$. Towards the center of the channel, $k^+ \cong 1$ and $\epsilon^+ \cong 0.01$. The maximum value of ϵ^+ occurs at the wall ($\epsilon^+_w \cong 0.2$ and $\epsilon^+_w \cong 0.27$ respectively for the two δ^+ cases). For $y^+ \sim 10$, ϵ^+ reaches a plateau (see inset of Figure 2.6) and then decreases monotonically to a positive minimum at the center of the channel. The plateau phenomenon related to the dissipation occurs in the region where the turbulent kinetic energy is a maximum.

Figure 2.7 compares the ratio of the local turbulent time scale k/ϵ and the local mean field time scale (i.e., $\tilde{\Gamma}_{DNS} \equiv \Gamma_{yz} \, k/\epsilon$) for $0 < \xi < 1$ at two different Reynolds numbers (Re⁺ = δ^+ = 300 and 2,000). The inset on Figure 2.7 shows the behavior of the

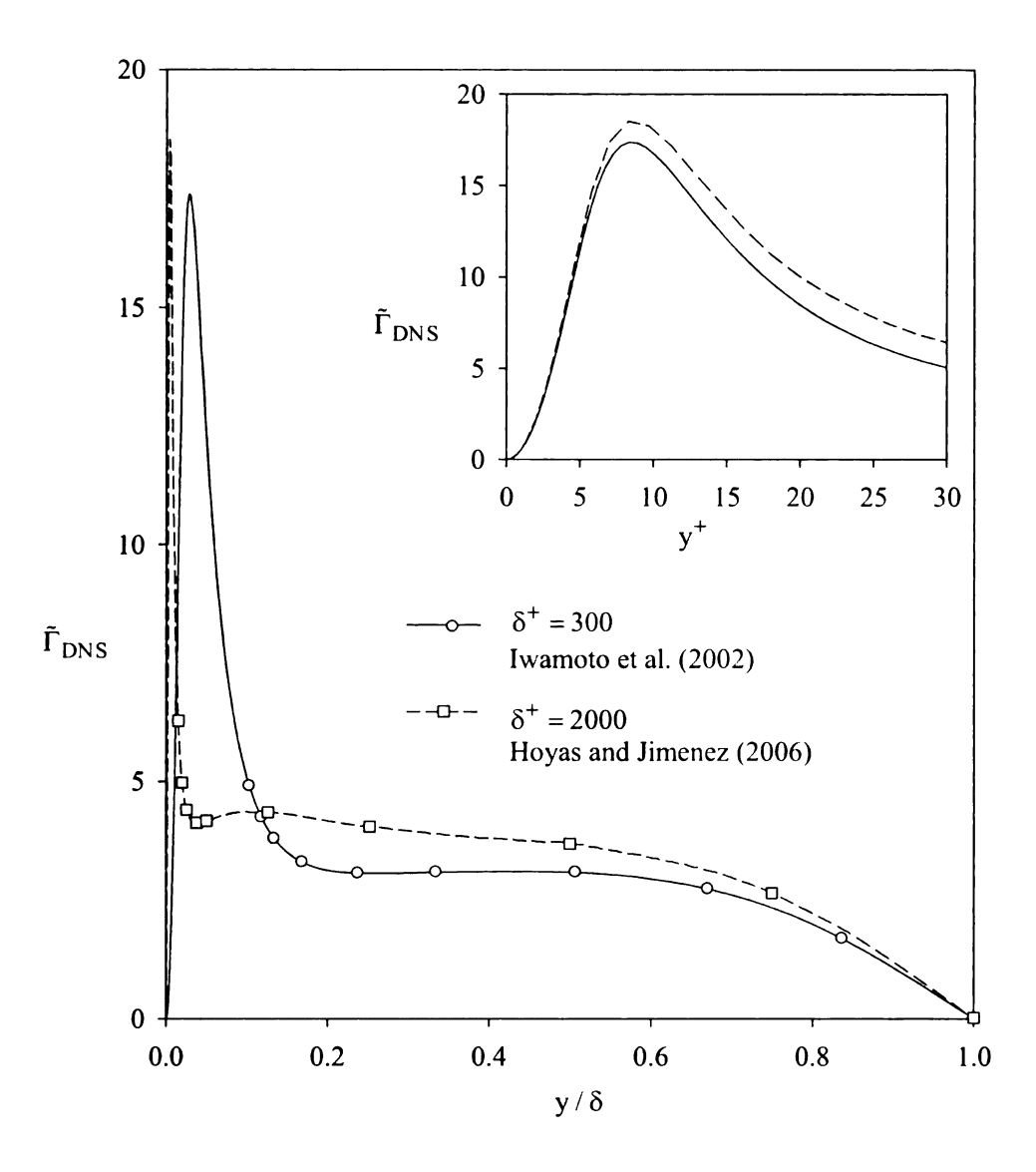


Figure 2.7. Mean Dimensionless Strain Rate $\tilde{\Gamma}_{DNS}$ for Non-Rotating, Fully-Developed Channel Flows.

ints: t_{os} a j = 1.10 0 म करं I u.P. ing g i in ¥457 4. 25, 0.7 13 Roans DN 3 1049 India Sin - CE: 30 ું હ્યુવરન -400 \$3.4(2b) द्राक्ति dimensionless shear rate group near the solid/fluid interface: $\tilde{\Gamma}_{DNS} \propto k^+ \sim (y^+)^2$. For $0 < y^+ < 10$, $\tilde{\Gamma}_{DNS}$ increases and peaks at $y^+ \cong 10$, where $\tilde{\Gamma}_{DNS} \cong 18$. For $y^+ > 10$, $\tilde{\Gamma}_{DNS}$ decreases. At $y^+ = 30$, $\tilde{\Gamma}_{DNS} \cong 4.9$ for $\delta^+ = 300$ and $\tilde{\Gamma}_{DNS} \cong 6.3$ for $\delta^+ = 2,000$. For $0.2 < \xi < 0.5$, $\tilde{\Gamma}_{DNS} \cong 4$. In this region, the local dissipation and the local production of turbulence kinetic energy approximately balance one another (see p. 281 in Pope, 2000). At the center of the channel, $\tilde{\Gamma}_{DNS} = 0$ inasmuch as the mean velocity gradient is zero due to symmetry. Table 2.1 tabulates the transverse variation of the dimensionless shear group $\tilde{\Gamma}_{DNS}$ and the components of the NR-stress for $30 \le y^+ \le \delta^+$. This information is used in Chapter 6 to evaluate predictions of the NR-stress for non-rotating fully-developed channel flow for $0 \le \tilde{\Gamma} \le 6$.

2.3 Rotating Fully-Developed Channel Flows

DNS results for fully-developed channel flows with spanwise rotation have been developed by Wu and Kasagi (2002, 2004), Alvelius (1999), and Grundestam et al. (2008). Simulations with and without spanwise rotation are performed with the same constant axial pressure drop or, equivalently, for the same average wall shear stress. Consequently, the friction velocity, defined by Eq. (2.18) below, is the same for all simulations. Comprehensive low-order statistical properties for the mean velocity, the components of the NR-stress, the turbulent kinetic energy, and the turbulent dissipation are available for $\delta^+ \equiv \delta u^*/v \cong 296$ and $\Omega_X^+ (\equiv \Omega_X v/(u^*)^2) = -0.0042$. The results of Wu and Kasagi (2004) are used in Chapter 7 to benchmark the predictions of the URAPS-

Table 2.1 Cross Flow Variation of $\tilde{\Gamma}_{DNS}$ and the Components of the NR-Stress for Non-Rotating, Fully-Developed, Channel Flow: (a) $\delta^+ \cong 300$, $\Omega_x^+ = 0$ (Iwamoto et al. 2002); (b) $\delta^+ \cong 2000$, $\Omega_x^+ = 0$ (Hoyas and Jimenez, 2006).

(a)

[y ⁺]	y/δ	$ ilde{\Gamma}_{ ext{DNS}}$	R _{xx}	R _{yy}	R _{zz}	R _{yz}
30	0.10	4.90	0.21	0.09	0.70	-0.11
35	0.12	4.24	0.22	0.11	0.67	-0.11
40	0.13	3.79	0.23	0.12	0.65	-0.12
45	0.15	3.49	0.24	0.14	0.62	-0.13
50	0.17	3.30	0.25	0.15	0.60	-0.13
70	0.24	3.06	0.27	0.18	0.55	-0.14
100	0.33	3.09	0.28	0.19	0.53	-0.15
150	0.51	3.08	0.28	0.21	0.51	-0.15
200	0.67	2.73	0.27	0.23	0.50	-0.14
250	0.84	1.69	0.27	0.26	0.47	-0.09
300	1.00	0.00	0.27	0.28	0.45	0.00

(b)

[y ⁺]	y/δ	$ ilde{\Gamma}_{ ext{DNS}}$	R _{xx}	R _{yy}	R _{zz}	R _{yz}
30	0.015	6.28	0.23	0.08	0.69	-0.09
40	0.02	4.98	0.25	0.10	0.65	-0.10
50	0.03	4.40	0.27	0.12	0.61	-0.10
75	0.04	4.13	0.27	0.14	0.59	-0.11
100	0.05	4.17	0.27	0.15	0.58	-0.11
250	0.13	4.35	0.25	0.16	0.59	-0.12
500	0.25	4.05	0.24	0.18	0.58	-0.13
1000	0.50	3.69	0.25	0.20	0.55	-0.13
1500	0.75	2.65	0.26	0.23	0.51	-0.10
2000	1.00	0.03	0.27	0.26	0.47	0.00

(sre Herem.

1107 En 11

Fer span

do=cb>ti

ger and the ki

Rights Ω

द्वार । शिल्ल

(F)=L··n

Sal companer

\$77.35 35

 $\Omega_{i} > \Omega_{i}$

[_ (,<p.

In the abo

19.71.21 EZ

हेत्स्याः conditi

ريد راء د الآ

closure. Hereinafter, a nominal value of $2\delta^+=600\,$ is used to refer to the DNS results for $2\delta^+=592$.

RANS-Equation

For spanwise rotation of a fully-developed channel flow, $\langle \underline{u} \rangle = \langle u_z \rangle (y) \underline{e}_z$ and $\langle p \rangle = \langle p \rangle (y,z)$. As illustrated by Figure 2.1 above, the symmetry plane is located at $y = \delta$ and the solid/fluid interfaces are located at y = 0 and 2δ . The angular velocity of the frame is $\underline{\Omega} = \Omega_x \underline{e}_x$, and the rotation operator is $\underline{\Omega} = \underline{\varepsilon} \cdot \underline{\Omega} = \Omega_x (\underline{e}_y \underline{e}_z - \underline{e}_z \underline{e}_y)$. The angular velocity of the frame is co-linear with the mean vorticity $\langle \underline{w} \rangle = \nabla \wedge \langle \underline{u} \rangle = \langle w_x \rangle \underline{e}_x$. With $\underline{g} = g_z \underline{e}_z$ and $\nabla \langle \underline{u} \rangle = \Gamma_{yz}(y) \underline{e}_y \underline{e}_z$, the two nontrivial components of the unclosed RANS-equation (see Eq. (1.4)) for this flow can be written as

$$-2 < u_z > \Omega_x = -\frac{\partial}{\partial y} \left[\frac{\langle p_D \rangle}{\rho} \right] + \frac{d}{dy} \left[-2kR_{yy} \right] , \quad 0 \le y \le 2\delta$$
 (2.11)

$$0 = -\frac{\partial}{\partial z} \left[\frac{\langle p_D \rangle}{\rho} \right] + \frac{d}{dy} \left[v \frac{d \langle u_z \rangle}{dy} - 2k R_{yz} \right] , \quad 0 \le y \le 2\delta.$$
 (2.12)

In the above equations, the dynamic pressure $\langle p_D \rangle (y, z)$ is defined as

$$\langle p_D \rangle (y,z) \equiv \langle p \rangle (y,z) - \rho \frac{(y^2 + z^2)\Omega_x^2}{2} - z\rho g_z.$$
 (2.13)

Boundary conditions for the mean velocity and the mean axial pressure gradient are

$$\langle \mathbf{u}_{\mathbf{Z}} \rangle (0) = \langle \mathbf{u}_{\mathbf{Z}} \rangle (2\delta) = 0$$
 , $-\frac{\partial \langle \mathbf{p}_{\mathbf{D}} \rangle}{\partial z} = \text{constant}$. (2.14)

la no

No. 15

Consta

हामुख्या १९

TERM

TITE

They.

h wall

kọn làs s

Fact p

2,=6;

452912

\$ (2)₆₁

£ <0. F;

The no-slip condition at solid/fluid interfaces implies that all the components of the Reynolds stress are zero on the channel walls. Therefore, for spanwise rotation, the Coriolis force, $2\rho < \underline{u} > \wedge \Omega$, acts in the transverse (cross flow) direction and, thereby, plays an explicit role in the force balance expressed by Eq. (2.11). As a consequence, the transverse component of the Reynolds stress and the Coriolis stress cause a cross flow variation in the dynamic pressure:

$$< p_D > (y,z) - < p_D > (0,z) \equiv \Delta_{PD}(y)$$

= $-2\rho k(y) R_{yy}(y) + 2\rho \Omega_x \int_0^y < \hat{u}_z > (\hat{y}) d\hat{y}$ (2.15)

The no-slip condition at a solid/fluid interface implies that the components of the Reynolds stress are zero at y=0 and 2δ ; therefore, unlike the non-rotating case, the dynamic pressure difference between the two solid/fluid interfaces is non-zero for $\Omega_x \neq 0$:

$$\Delta_{PD}(2\delta) = +2\rho\Omega_{x}\int_{0}^{2\delta} \langle u_{z} \rangle (\hat{y})d\hat{y} = +4\delta\rho\Omega_{x}u_{b} = [4\Omega_{x}^{+}\delta^{+}u^{*}/u_{b}]\rho u_{b}^{2}. \tag{2.16}$$

Eq. (2.16) shows that $\langle p_D \rangle$ (28,z) is smaller than $\langle p_D \rangle$ (0,z) if $\langle u_z \rangle$ (y) \geq 0 and $\Omega_x \langle 0$. For this configuration, the solid/fluid interface at $y=2\delta$ is the low pressure (LP-) interface and the solid/fluid interface at y=0 is the high pressure (HP-) interface. For $\delta^+=300$ and $\Omega_x^+\cong -0.0042$, the simulations predict that the bulk average velocity equals $u_b\cong 18u^+$ and the pressure difference across the channel is

Eq. (2.12) and E.

miserse coordinate y:

$$\sqrt{\frac{d \leq u_2}{dy}} - 2k R_{yz} = -[-]$$

For y = 0 and 2δ , the shoot

$$\frac{16(p_D)}{\rho} 2\delta = v \frac{d}{d}$$

_ (= -

标轴 the no-rotation cas

É mal pressure gradier

$$t = I_{L}(z^{n})Hb + (z^{n})Tb$$

Stear Stress

The DNS results of

ac 2000 are consisten

$$(x_{k}^{*}(u))^{2}$$
 and $y^{*} \equiv y_{k}$

Transform of $\xi = y \delta$

 0.5° and 0.5°

ેલ[©] ફ1.38. Figure 2.૪

Eq. (2.12) and Eq. (2.14) imply that the total stress is a linear function of the transverse coordinate y:

$$v \frac{d < u_z >}{dy} - 2k R_{yz} = -\left[-\frac{1}{\rho} \frac{\partial < p_D >}{\partial z} \right] y + v \frac{d < u_z >}{dy} \bigg|_{y=0}.$$
 (2.17)

For y = 0 and 2δ , the shear components of the Reynolds stress are zero; therefore,

$$+\left[-\frac{1}{\rho}\frac{\partial \langle p_{D}\rangle}{\partial z}\right]2\delta = v\frac{d\langle u_{z}\rangle}{dy}\bigg|_{y=0} -v\frac{d\langle u_{z}\rangle}{dy}\bigg|_{y=2\delta}.$$

$$=\frac{(\tau_{w})_{HP} + (\tau_{w})_{LP}}{\rho} = 2(u^{*})^{2}$$
(2.18)

As with the no-rotation case, the friction velocity u* for spanwise rotation is related to the axial pressure gradient or, equivalently, to the average wall shear stress (i.e.

$$u^* = \sqrt{[(\tau_w)_{HP} + (\tau_w)_{LP}]/(2\rho)} = [-\frac{\delta}{\rho} \frac{\partial < p_D >}{\partial z}]^{1/2}).$$

Total Shear Stress

The DNS results of Wu and Kasagi (2004) for $\delta^+ (\equiv \delta u^* / v = Re^+)$ equal to 300 and 2,000 are consistent with Eq. (2.17). For example, with $\Gamma_{yz}^+ \equiv du^+ / dy^+$, $k^+ \equiv k/(u^*)^2$, and $y^+ \equiv y \, u^* / v$, Figure 2.8 shows that $\Gamma_{yz}^+ - 2k^+ R_{yz}$ is approximately a linear function of $\xi \equiv y/\delta$ for $0 \le \xi \le 2$:

$$\Gamma_{yz}^{+}(\xi) - 2k^{+}R_{yz}^{-} = + \Gamma_{yz}^{+}(0) - \xi, \quad 0 \le \xi \le \delta^{+}, \quad \forall \delta^{+} > \delta_{c}^{+}, \quad -\infty < \Omega_{x}^{+} < +\infty. \tag{2.19}$$

For $\delta^+ = 300$ and $\Omega_X^+ \cong -0.0042$, the DNS results predict that $u_b/u^* \cong 18$ and $\Gamma_{vz}^+(0) \cong 1.38$. Figure 2.8 also illustrates that the viscous component of the total shear

05 -06 4 4)5 0.0 ð` <u>:</u>

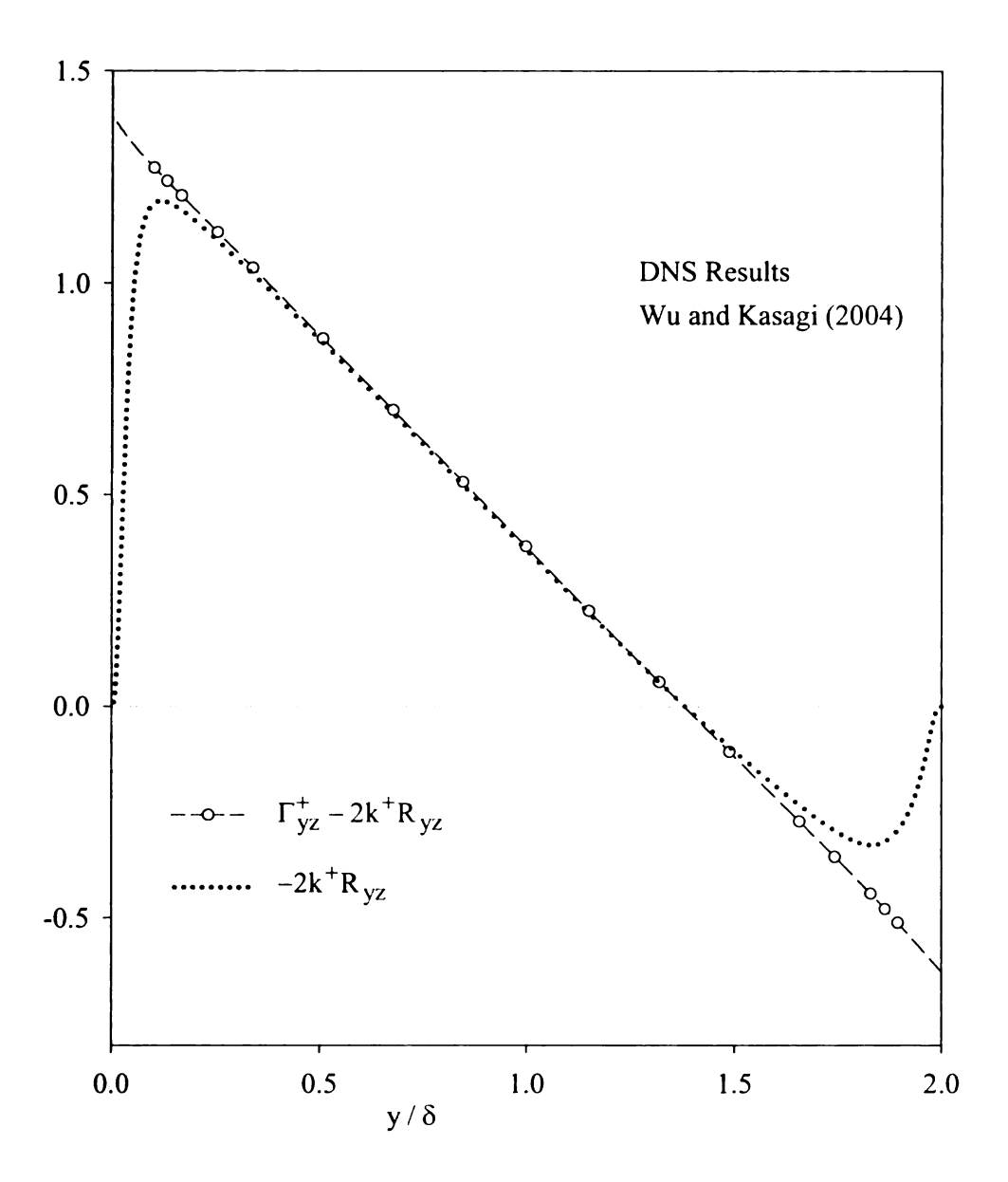


Figure 2.8 Total Mean Shear Stress Profile Across the Rotating Channel for $\delta^+ \cong 300 \text{ and } \Omega_x^+ \cong -0.0042 \ .$

eass is quantitatively in gamines transport of 2.77 for, equivalently, 2.57 for no rotation, the stass albeit linear in y=0 for Ω_{χ}^{2} shas that the total shear y=0 for no rotation stass is directly influx. Totation for the device

Bally Mean Vorte

As indicated

 $u_z > u^*$) is n

on the low pres

with is consistent w

is less than

 $L^{2}(\mathbb{S}) \geq L^{2}(\mathbb{S})^{\frac{1}{2}}.$

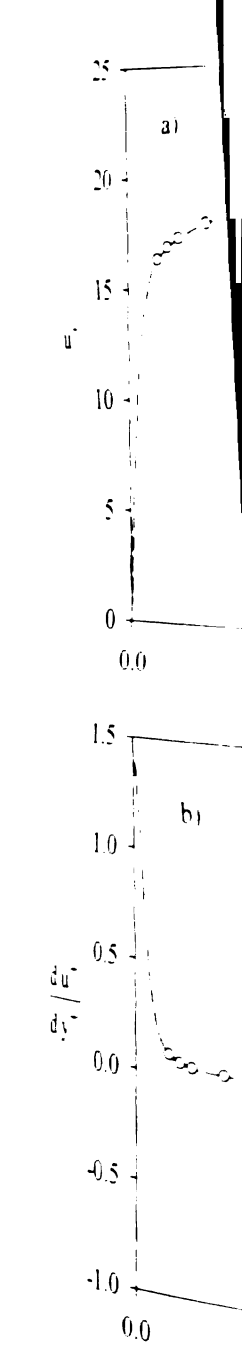
The mean velo

stress is quantitatively important near the solid/fluid interface and that the Reynolds stress determines transport of momentum in the outer region of the flow field. Although Eq. (2.17) (or, equivalently, Eq. (2.19)) for spanwise rotation is formally the same as Eq. (2.5) for no rotation, the DNS results summarized by Figure 2.8 show that the total shear stress, albeit linear in the transverse coordinate, is no longer anti-symmetric about $y = \delta$ (or, $\xi = 1$) for $\Omega_x^2 > 0$ (i.e., $\Gamma_{yz}^+(0) \cong 1.38$ and $\Gamma_{yz}^+(2) \cong -0.627$). Figure 2.8 also shows that the total shear stress is zero at $y_0 (\equiv \Gamma_{yz}^+(0) \delta) = 1.38 \delta$ for $\Omega_x^+ \cong -0.0042$; and $y_0 = \delta$ for no rotation inasmuch as $\Gamma_{yz}^+(0) = 1$. Eq. (2.19) implies that the Reynolds stress is directly influenced by the Coriolis force. This phenomenon provides ample motivation for the development of the URAPS-closure in Chapter 3.

Absolute Mean Vorticity

As indicated by Figure 2.9, the transverse (cross flow) variation of $u^+(\equiv < u_z > /u^*)$ is not symmetric about the symmetry plane. The maximum velocity occurs on the low pressure side of the flow field in the vicinity of $y^+ = 415$ ($\xi \cong 1.38$), which is consistent with the result that the wall shear stress at the LP-interface (i.e., $\xi = 2$) is less than the wall shear stress at the HP- interface (i.e., $\xi = 0$), i.e., $|\Gamma_{yz}^+(0)| > |\Gamma_{yz}^+(2)|$.

The mean velocity profile shows that the mean *intrinsic* vorticity operator (or, e-quivalently, the mean absolute vorticity) is approximately zero over a finite region of the flow field (also, see, p. 617 in Piquet, 1999; Hamba, 2006; and Grundestam et al., 2008).



 $\frac{\log_{2.9}}{\Omega_{x}^{2}} = \frac{\text{Mean } |\nabla_{e}|}{\Omega_{x}}$

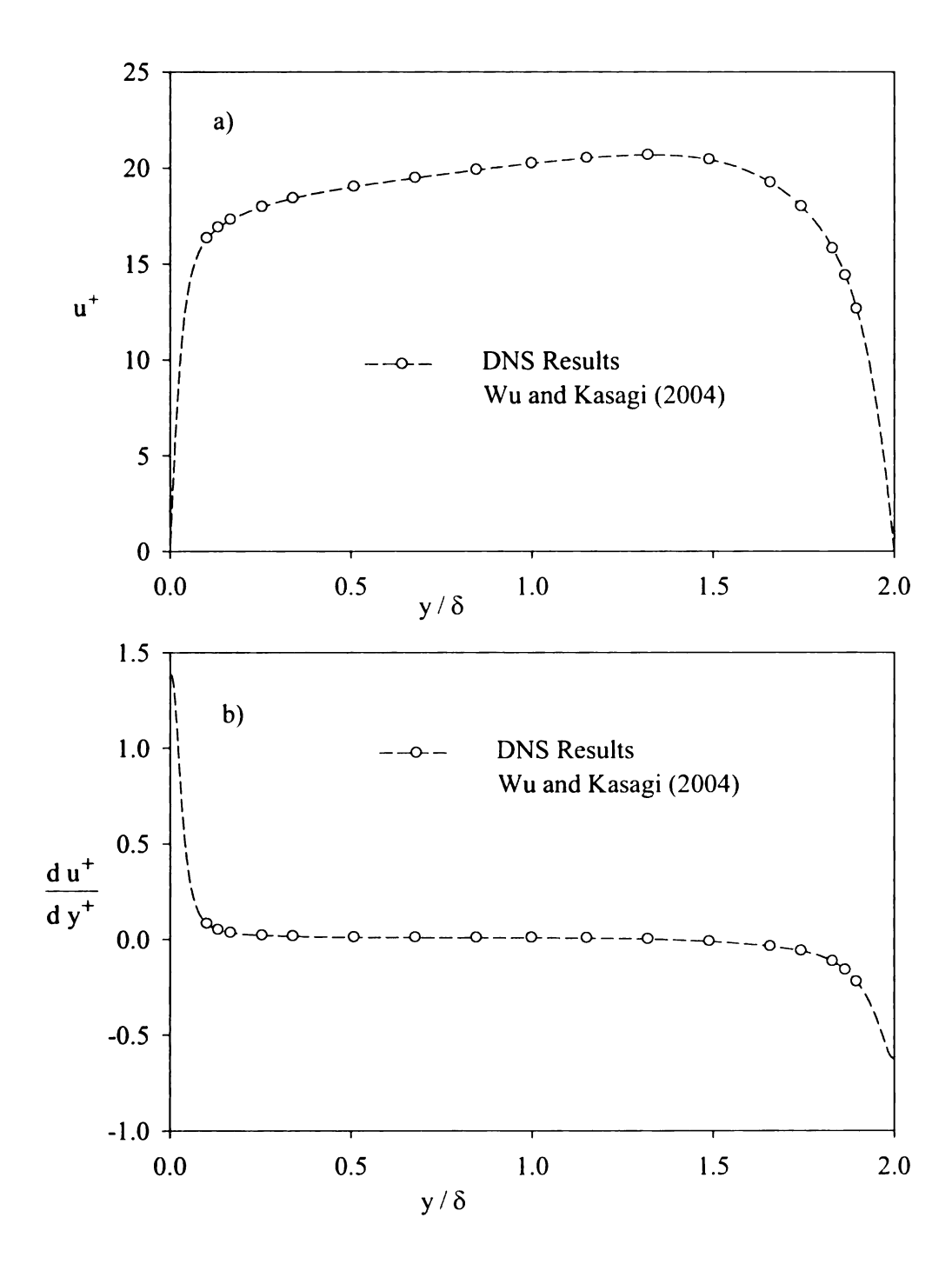


Figure 2.9 Mean Velocity and the Mean Velocity Gradient for $\delta^+\cong 300$ and $\Omega_x^+\cong -\,0.0042$.

for spanwise rotal

For $\delta' = 300$ and $\Omega_{\infty}^{+} \cong -$

shate region where the

$$\frac{ds^2}{ds^2} = \frac{1}{\delta^2} \frac{du^2}{d\xi} \cong -2\Omega_{\chi}^2$$

Every States, and Arrives

Similar to the notational statement only on the 1

E sold fluid interfaces

 $\delta y^* = 0 \text{ and } y^* = 2\delta^*.$

and no-slip i

exclensues:

 $\mathbb{R}_{v^{(i)}} < \mathbb{R}_{zz^{(i)}} < 1$

 $\frac{\partial R_{u}(2\delta^{2})}{\partial x} < R_{zz}(2\delta)$

 $^{\frac{1}{2}}$ $^{\frac{3}{2}}$ $^{\frac{3}{2}}$ $^{\frac{3}{2}}$ and $\Omega_{\chi}^{\frac{1}{2}}$

The HP-wall; and, R

Static forms associa

operate at the HP- and

For spanwise rotation, the intrinsic mean vorticity operator is

$$\langle \underline{\underline{\tilde{W}}} \rangle \equiv \langle \underline{\underline{W}} \rangle + \underline{\underline{\Omega}} \equiv \underline{\underline{\varepsilon}} \cdot (\frac{1}{2} \langle \underline{\underline{w}} \rangle + \underline{\Omega}) = (\frac{1}{2} \frac{d \langle \underline{u}_z \rangle}{dy} + \Omega_x) (\underline{\underline{c}}_y \underline{\underline{c}}_z - \underline{\underline{c}}_z \underline{\underline{c}}_y). \tag{2.20}$$

For $\delta^+ = 300$ and $\Omega_x^+ \cong -0.0042$, the DNS results (see Figure 2.9) show that there exist a finite region where the absolute mean vorticity is approximately zero:

$$\frac{du^{+}}{dy^{+}} = \frac{1}{\delta^{+}} \frac{du^{+}}{d\xi} \cong -2\Omega_{x}^{+} \cong +0.0084 \quad , \quad 0 < \xi^{\min} \cong 0.5 < \xi < \xi^{\max} \cong 1 < 2$$
 (2.21)

Energy States and Anisotropic Invariants

Similar to the no rotation case, the NR-stress has three independent components that depend only on the transverse coordinate $y^+ (\equiv y u^*/\nu)$. Due to the no slip condition at solid/fluid interfaces, all of the components of the Reynolds stress are zero for $y^+ = 0$ and $y^+ = 2\delta^+$. Deep in the viscous sublayers near the HP-wall and LP-wall, continuity and no-slip imply that the components of the NR-stress have the following characteristics:

$$0 < R_{xx}(0) < R_{zz}(0) < 1$$
, $R_{yy} \propto (y^+)^2$, $R_{yz} \propto y^+$, $y^+ \to 0$, (2.22)

$$0 < R_{xx}(2\delta^{+}) < R_{zz}(2\delta^{+}) < 1$$
, $R_{yy} \propto (2\delta^{+} - y^{+})^{2}$,
 $R_{yz} \propto (2\delta^{+} - y^{+})$, $y^{+} \rightarrow 2\delta^{+}$ (2.23)

For $\delta^+ \cong 300$ and $\Omega_X^+ \cong -0.0042$, Figure 2.10 shows that $R_{xx}(0) \cong 0.3$ and $R_{zz}(0) \cong 0.7$ at the HP-wall; and, $R_{xx}(600) \cong 0.2$ and $R_{zz}(600) \cong 0.8$ at the LP-wall. Thus, the quadratic forms associated with the NR-stress (QNR-form) are planar anisotropic (elliptical) at the HP- and LP-walls.



Energy St and $\Omega_{\chi}^{+} \ge$

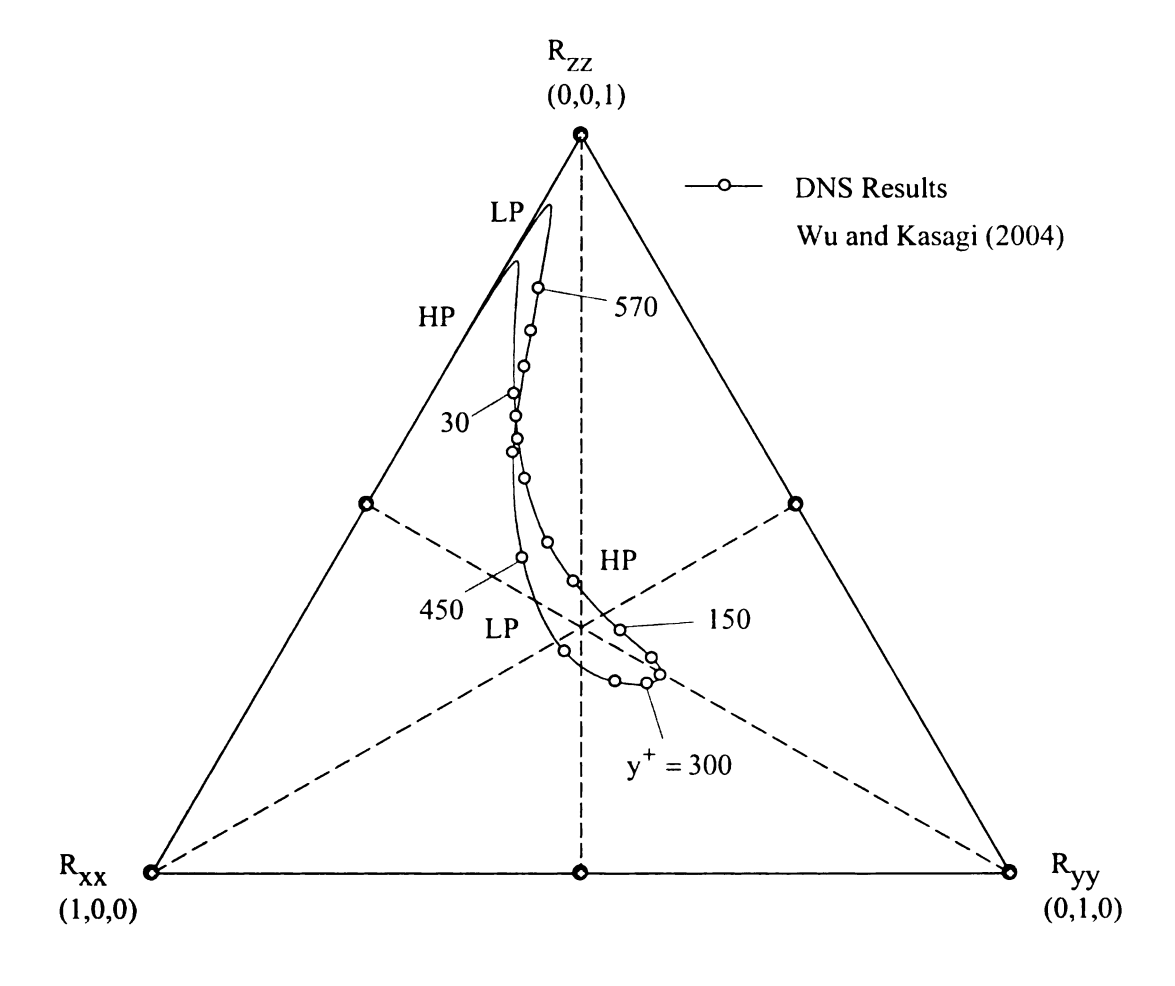


Figure 2.10 Energy States for Rotating, Fully-Developed, Channel Flow ($\delta^+\cong 300$ and $\Omega_x^+\cong -\,0.0042$).

√ ≥10 near the HP-wa

nerotation case (see Fig.

eeg simplex. On the

‡=1), the energy state

 $R_{2}=0.26$. At y =

 $R_{yz}(300) = -0.135$

and a y ≥ 415. The ma

 $\mathbb{E}^{\frac{1}{2}R_{j_2}(4|5)} \cong 0$. As inc

5 ≥ 415 are los

 $R_{W}(4|5) = 0.37$, $R_{yy}(4)$

Figure 2.10 show

exponents of the Re

Sept 5415) and the 1

at the HP-wall within

Sublayer (595 -

5→0 and 600, respec

\$17<30 and 570.

 $(20.8) \approx 0.8$ on the H

For $\delta^+\cong 300$ and $\Omega_x^+\cong -0.0042$, Figure 2.10 shows that $\max(R_{zz})\cong 0.8$ at $y^+\cong 10$ near the HP-wall and $\max(R_{zz})\cong 0.9$ at $y^+\cong 590$ near the LP-wall. Unlike the no-rotation case (see Figure 2.3), the energy states are distributed in all six sextets of the energy simplex. On the symmetry plane of the rotating channel (i.e., $y^+=\delta^+\cong 300$, or $\xi=1$), the energy state is in the 5th Sextet: $R_{xx}(300)=0.29$, $R_{yy}(300)=0.45$, and $R_{zz}(300)=0.26$. At $y^+\cong 300$, the cross correlation component of the NR-stress is non-zero: $R_{yz}(300)=-0.135$. As noted above, the total shear stress (i.e., $\Gamma_{yz}^+=2k^+R_{yz}$) is zero at $y^+\cong 415$. The mean velocity profile (see Figure 2.9) shows that $\Gamma_{yz}^+(415)\cong 0$ and $R_{yz}(415)\cong 0$. As indicated by Figure 2.10, the normal components of the NR-stress at $\delta^+\cong 415$ are located in the 4^{th} Sextet of the energy simplex: $R_{xx}(415)=0.37$, $R_{yy}(415)=0.29$, and $R_{zz}(415)=0.34$.

Figure 2.10 shows that the energy is distributed among the three normal components of the Reynolds stress differently on the HP-side of the channel $(0 \le y^+ \le 415)$ and the LP-side of the channel $(415 \le y^+ \le 600)$. As indicated above, near the HP-wall within the viscous sublayer $(0 < y^+ < 5)$ and the LP-wall within the viscous sublayer $(0 < y^+ < 5)$ and the LP-wall within the viscous sublayer $(595 < y^+ < 600)$ energy is transferred from R_{yy} and R_{zz} to R_{xx} as $y^+ \to 0$ and 600, respectively $(2^{nd}$ Sextet of the energy simplex). Within the regions $5 < y^+ < 30$ and $570 < y^+ < 595$, highly anisotropic QNR-forms develop with $\max(R_{zz}) \cong 0.8$ on the HP-side of the channel and $\max(R_{zz}) \cong 0.9$ on the LP-side of the

tantel 12nd Sextet of шку <570. energy : HP-wall and LP-wall incr ating the normal compo gy ≅300. Figure 2.10 istributed over the 5" aro in this region. This essin this region of th Figure 2.11 sha Takkiand $\Omega_{i}^{*} \equiv -0$ iows some similarities Sess is zero, the QN Famo whereas for) \$415. Figure 2.4 ; Ed Figure 2.11 show $I_{1}II_{2}) \ge (-0.03, -0.00)$ Stelle energy peaks (i. 21 Me ≥ -0.06 (see energy Peaks

 $T_{\rm s} \ge -0.44$, and $III_{\rm hos}$

channel (2^{nd} Sextet of energy simplex). Within the regions $30 < y^+ < 150$ and $440 < y^+ < 570$, energy is transferred from R_{zz} to R_{xx} and R_{yy} as the distance from the HP-wall and LP-wall increases. Within the region $150 < y^+ < 440$, energy is redistributed among the normal components R_{xx} , R_{yy} , and R_{zz} with the result that $\max(R_{yy}) \cong 0.45$ at $y^+ \cong 300$. Figure 2.10 shows that the energy states in the region $150 < y^+ < 300$ are distributed over the 5^{th} and 6^{th} -Sextets. The mean absolute vorticity is approximately zero in this region. This result is used in Chapter 7 to predict the components of the NR-stress in this region of the flow field.

Figure 2.11 shows the anisotropic states associated with the NR-stress for $\delta^+ \cong 300$ and $\Omega_X^+ \cong -0.0042$. A comparison with Figure 2.4 for the no-rotation case shows some similarities and some differences. Near the plane where the total mean shear stress is zero, the QNR-form for the no-rotation case is nearly prolate elliptical for $y^+ \cong 300$ whereas for the rotation case the QNR-form is nearly oblate elliptical for $y^+ \cong 415$. Figure 2.4 shows that for all y^+ , the invariant III_b is positive. On the other hand, Figure 2.11 shows that for $y^+ \cong 440$ on the LP-side the invariant III_b is negative: $(II_b, III_b) \cong (+0.03, -0.001)$. It is noteworthy that on the HP-side of the channel, the kinetic energy peaks (i.e., $\max(k) \cong 5.9$) at $y^+ \cong 15$ for which $\tilde{\Gamma}_{DNS} = 23$, $II_b \cong +0.33$, and $III_b \cong +0.06$ (see Figure 2.12 below). However, on the LP-side of the channel, the kinetic energy peaks (i.e., $\max(k) \cong 2.7$) at $y^+ \cong 582$ for which $\tilde{\Gamma}_{DNS} = -33$, $II_b \cong +0.44$, and $III_b \cong +0.11$ (see Figure 2.12 below). In the case of no rotation, the



Anisotrop
(67 ≥ 30)

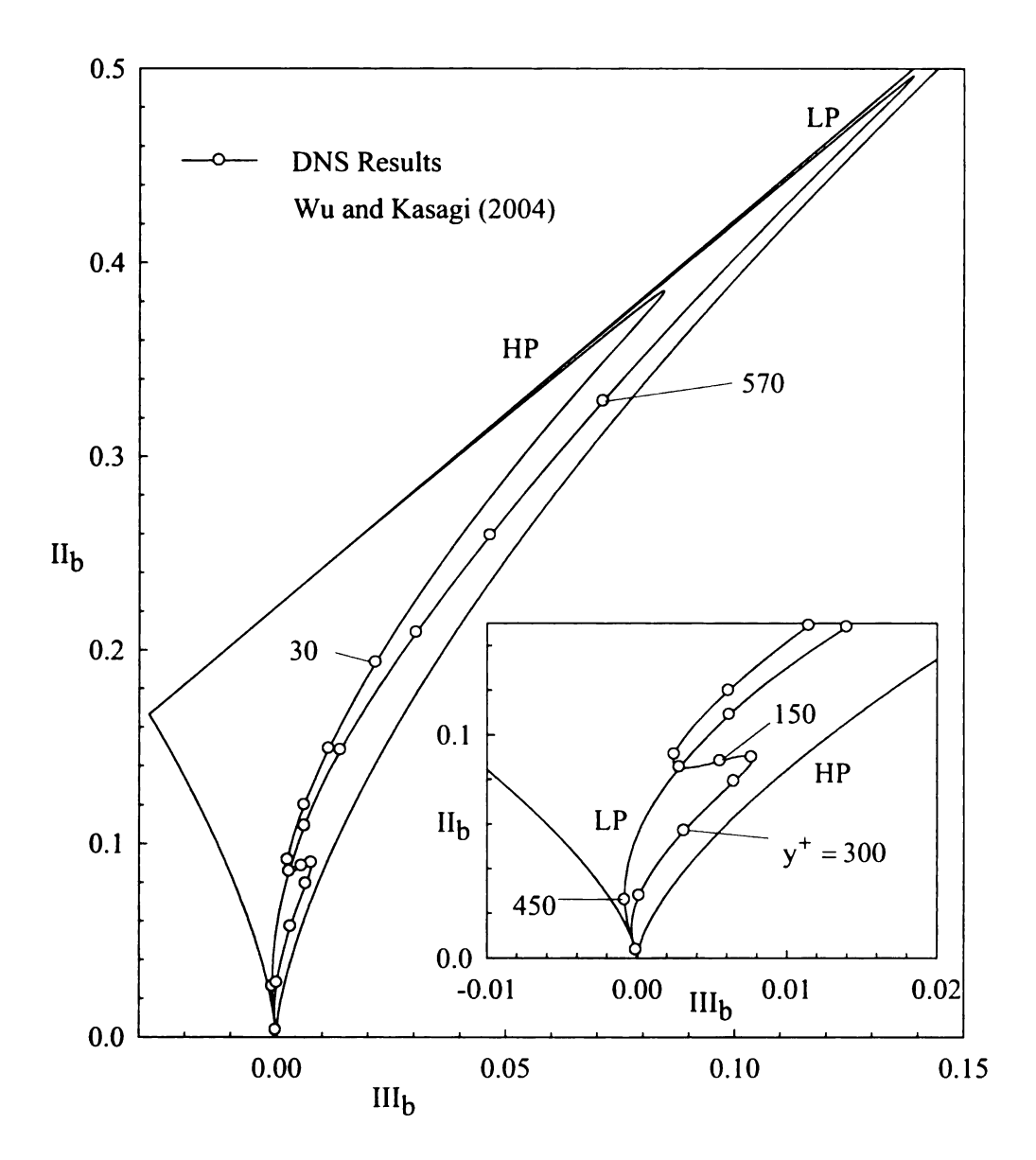


Figure 2.11 Anisotropic States for Rotating, Fully-Developed, Channel Flows $(\delta^+\cong 300 \text{ and } \Omega_x^+\cong -0.0042\,)$



Kinetic and Ω

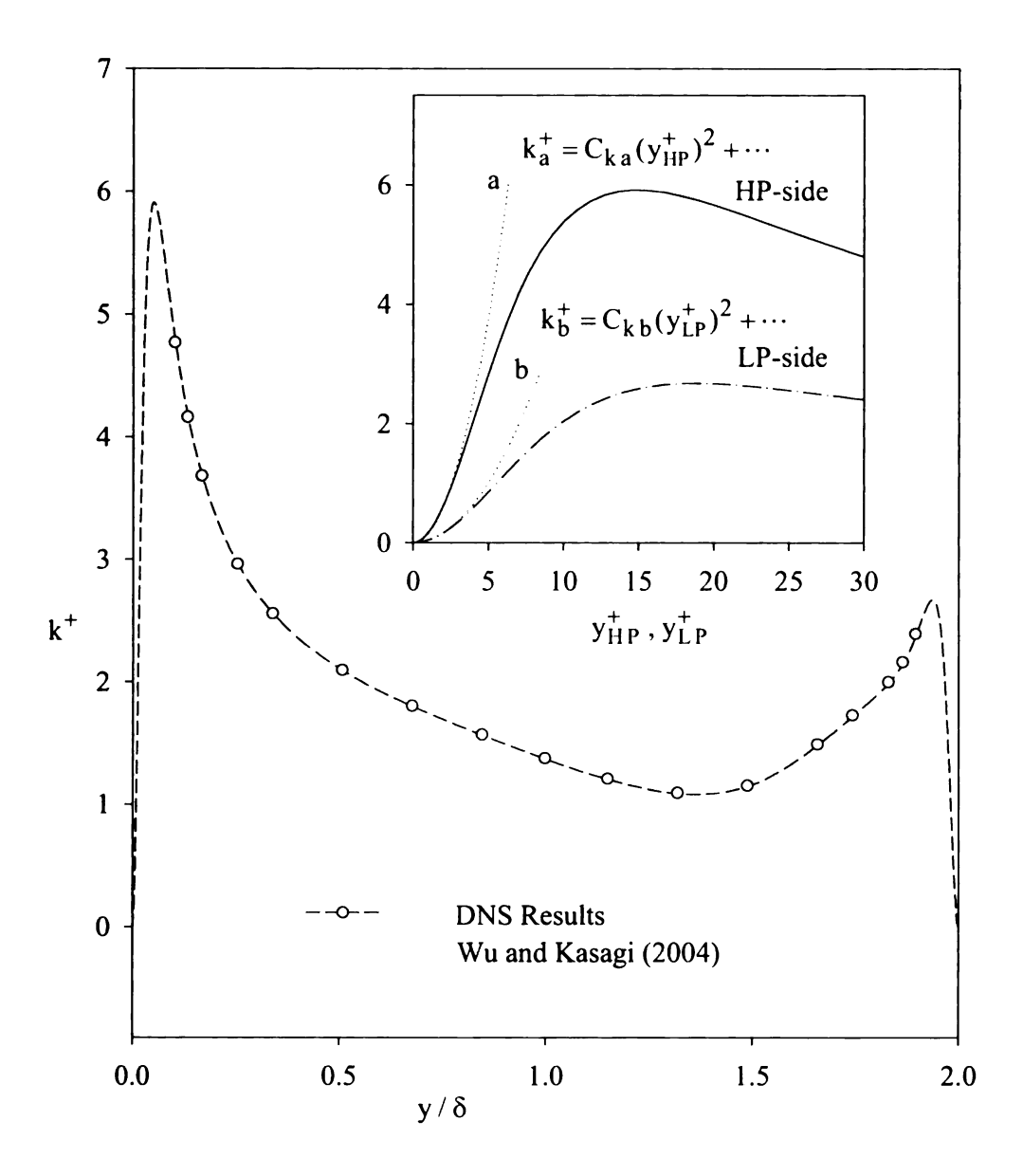


Figure 2.12 Kinetic Energy for Rotating, Fully-Developed, Channel Flows ($\delta^+ \cong 300$ and $\Omega_x^+ \cong -0.0042$).

erant ereally

1, ≥ -0.38 . 8

 $\overline{\mathbb{R}_{+}}(\mathbb{R}^{n}X)$

de turbalent)

Figure

 $i \in \Omega_{\lambda}^* \cong -0$.

.

esets by usin

HP- and LP-v

disofy

i =(; ...)

Court

(i) | ||p = 0||

(E) | [p = 1) ()

., ,

TAN 125

23 shows (

[ा]वं the tu

the total

#2.13 shay

kinetic energy peaks (i.e., max(k) \cong 4.3) at $y^+ \cong 16$ and $y^+ \cong 584$ for which $\tilde{\Gamma}_{DNS} = 12$, $II_b \cong +0.38$, and $III_b \cong +0.09$ (see Figure 2.4 above).

Turbulent Kinetic Energy and Turbulent Dissipation

Figures 2.12 and 2.13 show the spatial distributions (inner and outer scaling) of the turbulent kinetic energy, $k^+ \equiv k/(u^*)^2$, and the turbulent dissipation, $\epsilon^+ \equiv \epsilon v/(u^*)^4$, for $\Omega_x^+ \cong -0.0042$ for $\delta^+ = 300$. The results near the HP- and the LP-walls are shown as insets by using inner scaling parameters. The inset scale refers to the distance from the HP- and LP-walls in viscous wall units. The DNS results for k^+ and ϵ^+ at different values of y^+ are tabulated in Table I.4 of Appendix I.

Continuity and the no-slip conditions at a solid/fluid interface imply that $k^+ = C_k (y^+)^2 + \cdots$, and $\epsilon^+ = \epsilon_w^+ + C_\epsilon y^+ + \cdots$. At the HP-wall, $(C_k)_{HP} = 0.15$, $(\epsilon_w^+)_{HP} = 0.18$, and $(C_\epsilon)_{HP} \cong -0.02$; and, at the LP-wall, $(C_k)_{LP} = 0.04$, $(\epsilon_w^+)_{LP} = 0.05$, and $(C_\epsilon)_{LP} \cong -0.008$. Near the HP-wall at $y^+ \cong 15$ ($\xi = 0.05$), $\max(k^+) \cong 5.9$; and, near the LP-wall at $y^+ \cong 582$ ($\xi = 1.94$), $\max(k^+) \cong 2.7$. Figure 2.13 shows (see inset) that the turbulent dissipation profile has a plateau in the region where the turbulent kinetic energy has a local maximum. As noted above (see Figure 2.8), the total shear stress is zero at $\delta^+ = 415$ ($\xi = 1.38$). At this position, Figures 2.12 and 2.13 show that $\min(k^+) \cong 1.1$ and $\min(\epsilon^+) \cong 0.0025$.

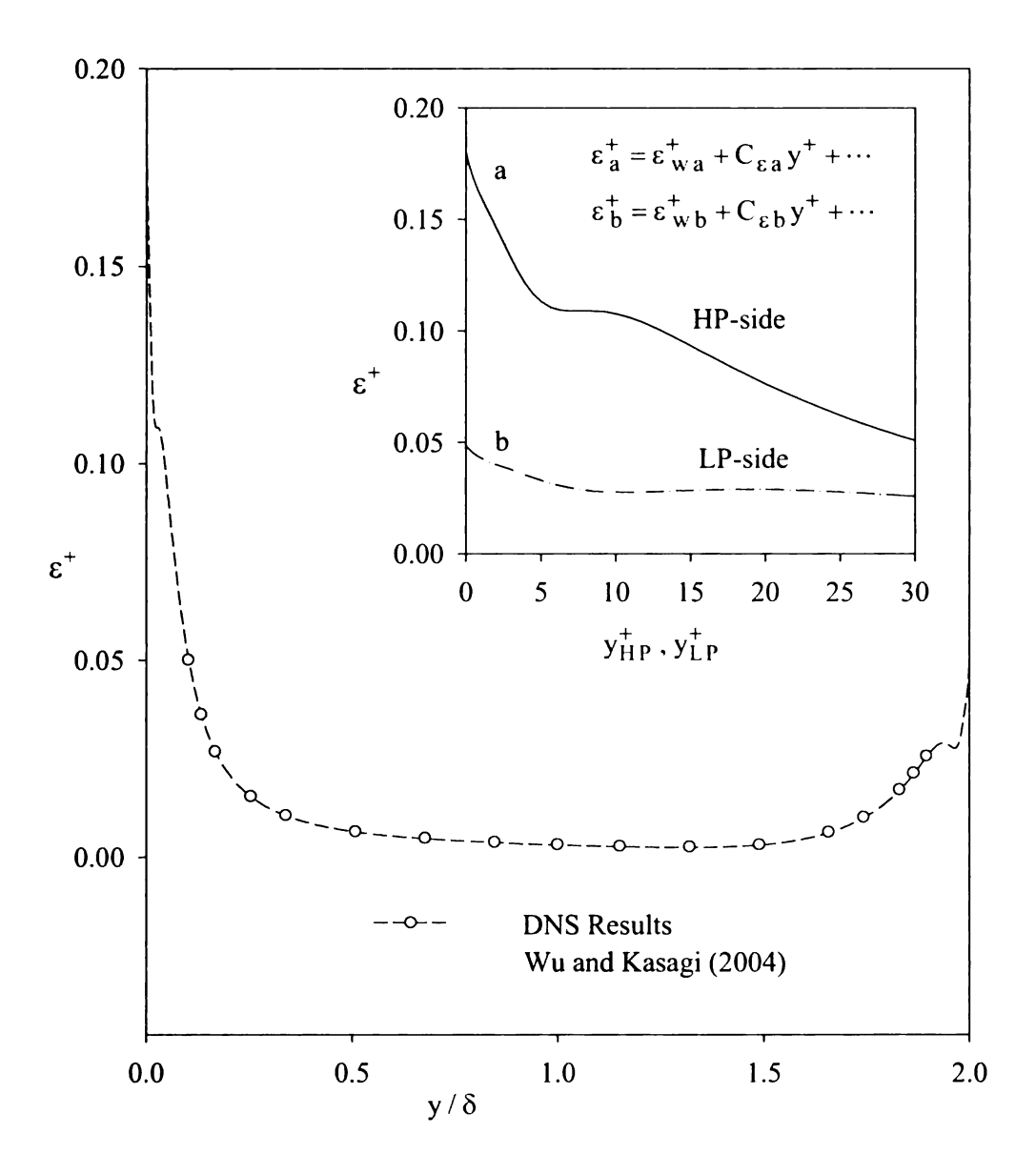


Figure 2.13 Dissipation for Rotating, Fully-Developed, Channel Flows ($\delta^+ \cong 300\,$ and $\Omega_x^+ \cong -\,0.0042$).

For 3

titien tin

 $\frac{1}{1000} \equiv \Gamma_{yz} I$

isos on the

für HP-wall (

is HP- and

T₁₂(1,3×3) =

For

ID Î

Tans 21-1

steef the fi

Can absolut

i34<ξ<2.

amponents.

and in Char

in grating fi

while m. Pr

Produ

क्रिक्ट क्षाम्बर्धाते हुन्। इतिहास

Fraimatio

For $\delta^+=300$ and $\Omega_x^+\cong-0.0042$, Figures 2.14 and 2.15 show the behavior of the turbulent time scale k/ϵ made dimensionless with the mean velocity gradient, $\tilde{\Gamma}_{DNS}\equiv\Gamma_{yz}\,k/\epsilon$, and with the angular velocity of the frame, $\tilde{\Omega}_{DNS}\equiv\Omega_x\,k/\epsilon$. The insets on the figures use inner scaling to highlight the behavior of $\tilde{\Gamma}_{DNS}$ and $\tilde{\Omega}_{DNS}$ near the HP-wall (0 < y⁺ < 30) and the LP-wall (570 < y⁺ < 600). The group $\tilde{\Gamma}_{DNS}$ is zero at the HP- and LP-walls because $k(0)=k(2\delta)=0$. It is also zero at $\xi\cong 1.38$ because $\Gamma_{yz}(1.38\delta)=0$.

For $y^+ \cong 12$ $(\xi \cong 0.04)$, $max(\tilde{\Gamma}_{DNS}) \cong +40$. At $y^+ \cong 588$ $(\xi \cong 1.96)$, $min(\tilde{\Gamma}_{DNS}) \cong -40$. Near the HP-wall, the mean absolute vorticity, defined as $(\tilde{\Gamma}_{DNS}/2) + \tilde{\Omega}_{DNS}$, is positive. For $0.5 < y/\delta < 1$, the mean absolute vorticity on the HP-side of the flow field is approximately zero. And, on the LP-side of the flow field, the mean absolute vorticity is negative inasmuch as $\tilde{\Gamma}_{DNS}$ and $\tilde{\Omega}_{DNS}$ are both negative for $1.34 < \xi < 2$. Table 2.2 tabulates the cross flow variation of $\tilde{\Gamma}_{DNS}$, $\tilde{\Omega}_{DNS}$, and the components of the NR-stress for $0.1 \le \xi^+ \le 1.9$ $(30 \le y^+ \le 570)$. This information is used in Chapter 7 to evaluate predictions of the NR-stress based on the URAPS-closure for rotating fully-developed channel flow.

Turbulent Production/Dissipation Ratio

Production is approximately balanced by dissipation in the outer region of the non-rotating channel. This feature is often applied in modeling for obtaining algebraic approximation for the Reynolds stress transport equation (this will be further discussed in

40 -

20 -T_{DN},

-20 -

40.

-60 . O

Figure 2.14

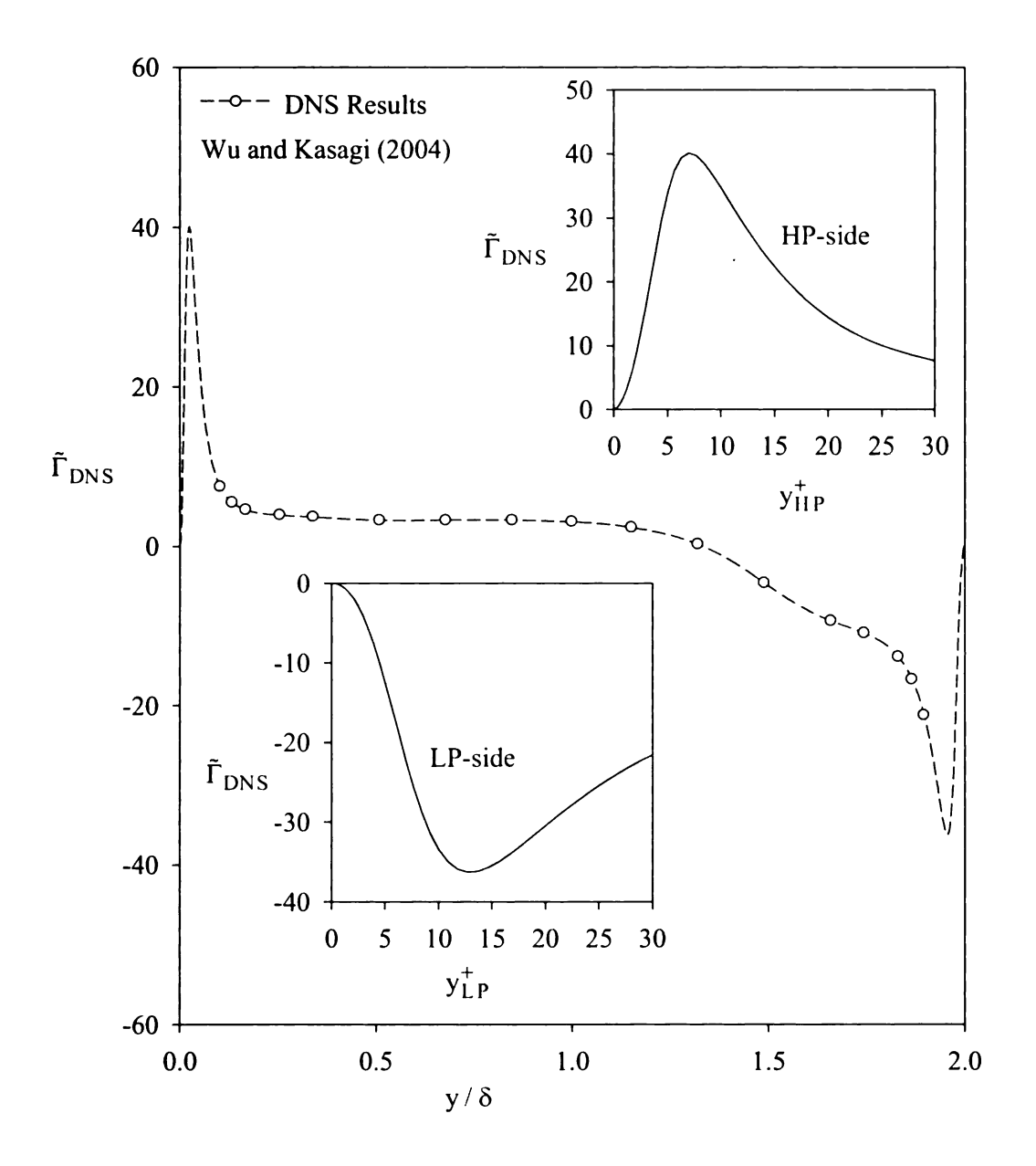


Figure 2.14 Transverse Profiles of $\tilde{\Gamma}_{DNS}$ for Rotating, Fully-Developed, Channel Flows ($\delta^+ \cong 300$ and $\Omega_x^+ \cong -0.0042$).

(),()

4).5

Ď_{ONS}

-1.0

-1.5

-2.0

-2.5 (

E11:2.15

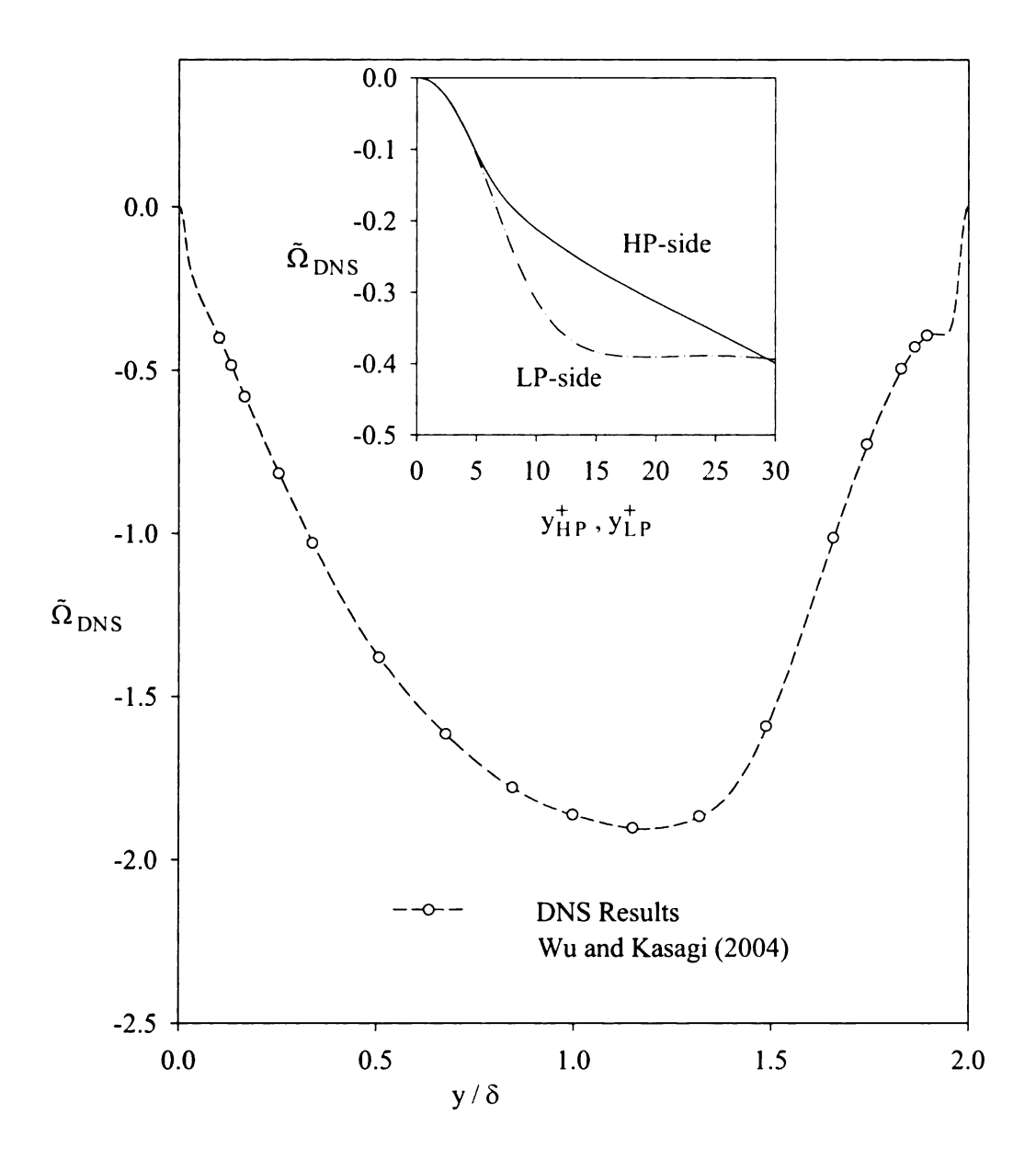


Figure 2.15 Transverse Profiles of $\tilde{\Omega}_{DNS}$ for Rotating, Fully-Developed, Channel Flows ($\delta^+ \cong 300$ and $\Omega_x^+ \cong -0.0042$).

Table 2.2 Cross Flow Variation of $\tilde{\Gamma}_{DNS}$, $\tilde{\Omega}_{DNS}$, and the Components of the NR-Stress for Rotating, Fully-Developed, Channel Flow: $\delta^+ \cong 300$, $\Omega_x^+ \cong -0.0042$ (Wu and Kasagi, 2004).

[y ⁺]	y/δ	$ ilde{\Gamma}_{ ext{DNS}}$	$ ilde{\Omega}_{ ext{DNS}}$	R _{xx}	R _{yy}	R _{zz}	R _{yz}
30	0.10	7.47	-0.40	0.25	0.10	0.65	-0.12
40	0.13	5.48	-0.49	0.28	0.13	0.59	-0.14
50	0.17	4.57	-0.58	0.30	0.17	0.53	-0.16
75	0.26	3.91	-0.82	0.31	0.24	0.45	-0.19
100	0.34	3.67	-1.03	0.31	0.29	0.40	-0.20
150	0.51	3.25	-1.38	0.29	0.38	0.33	-0.20
200	0.68	3.25	-1.62	0.27	0.44	0.29	-0.19
250	0.85	3.27	-1.78	0.27	0.46	0.27	-0.17
300	1.00	3.07	-1.86	0.29	0.45	0.26	-0.13
350	1.15	2.34	-1.90	0.33	0.41	0.26	-0.09
400	1.32	0.24	-1.87	0.37	0.33	0.30	-0.03
450	1.49	-4.62	-1.59	0.35	0.22	0.43	0.04
500	1.66	-9.40	-1.01	0.29	0.14	0.57	0.08
550	1.83	-13.92	-0.50	0.22	0.09	0.69	0.08
560	1.87	-16.74	-0.43	0.19	0.07	0.74	0.07
570	1.90	-21.23	-0.40	0.15	0.05	0.80	0.06

School 2.6

mang shar

2 (2) \$9

 $\Omega_{i}^{*} \geq -0.666$

nd then dec

sta the peal

14 Hymo

1. r.3 r.

Atrile shear

Expe

(480), and

对. Parks.

Regular fram

क्षेत्रकार क्षेत्र

Epit V

Etilent die

धी-शंजाविक ।

Ĭ √→x

Section 2.6). The production to dissipation ratio, \mathcal{P}/ϵ , for the rotating and the non-rotating channel is shown in Figure 2.16. For $\delta^+=300$ and $\Omega_{\rm X}^+=0$, a maximum value of \mathcal{P}/ϵ (\cong 1.8) occurs in the region where k^+ is a maximum. For $\delta^+=300$ and $\Omega_{\rm X}^+\cong-0.0042$, the production/dissipation ratio has a maximum value of 4.2 at $\xi=0.04$ and then decreases to zero at $\xi=1.38$, where the total shear stress is zero. Near the LP-side, the peak value of \mathcal{P}/ϵ is about 2.6 at $\xi=1.92$.

2.4 Homogeneous Simple Shear

Non-Rotating Frame of Reference

Experimental measurements of low order statistical properties of homogenous simple shear flows by Harris et al. (1977), Rohr et al. (1988), Tavoularis and Karnik (1989)) and others have been used to calibrate turbulent models (see Pope, 2000; and, esp., Parks, 1997). As illustrated by Figure 2.1, this statistically stationary flow in a noninertial frame of reference (i.e., $\Omega_{\rm x}=0$) is caused by a screen with a transverse resistance that produces an approximate homogenous shear environment downstream of the grid: $\nabla < \underline{\bf u} > : \underline{\bf e}_{\rm z} \, \underline{\bf e}_{\rm y} = \Gamma_{\rm yz} = {\rm constant}$. As $z \to \infty$, the turbulent kinetic energy and the turbulent dissipation become unbounded (i.e., $k \to \infty$ and $\epsilon \to \infty$) and the flow becomes self-similar with the following characteristics:

$$\tilde{\Gamma} = \Gamma_{yz} \frac{k}{\epsilon} \xrightarrow{z \to \infty} \tilde{\Gamma}_{AHS} = 4.18 \tag{2.24}$$

$$\underline{\underline{R}} \xrightarrow{z \to \infty} \underline{\underline{R}}^{AHS} = 0.236 \, \underline{e}_{x} \, \underline{e}_{x} + 0.197 \, \underline{e}_{y} \, \underline{e}_{y} + 0.567 \, \underline{e}_{z} \, \underline{e}_{z} \\
-0.165 \, \underline{e}_{y} \, \underline{e}_{z} - 0.165 \, \underline{e}_{z} \, \underline{e}_{y}$$
(2.25)



Ratio. P

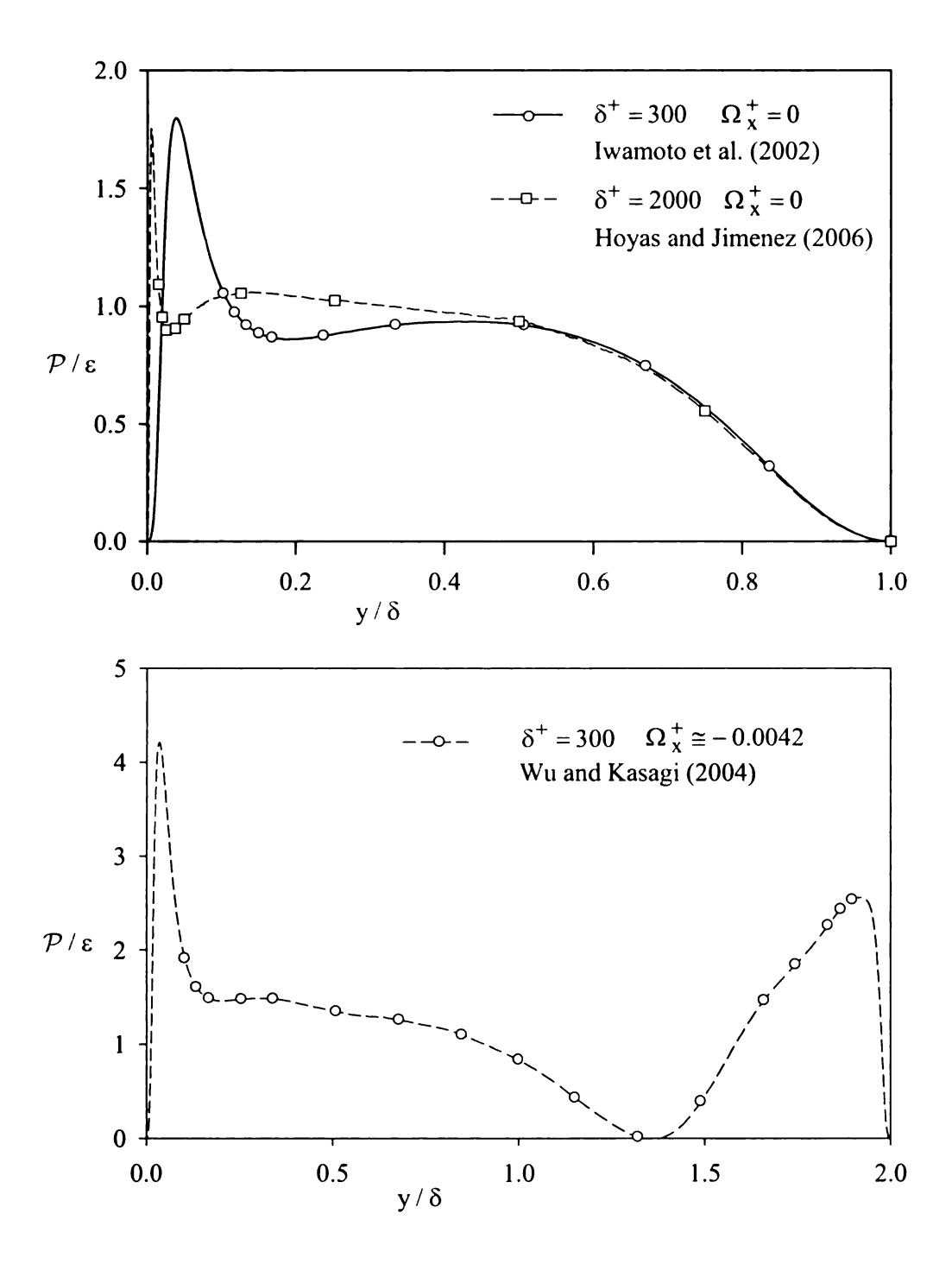


Figure 2.16 Transverse Profiles for Turbulent Production/Dissipation $Ratio, \mathcal{P}/\epsilon \equiv -2\,R_{yz}^{DNS}\,\tilde{\Gamma}_{DNS} \ \ \text{for Rotating, Fully-Developed,} \qquad Channel \\ Flows (\delta^+ \cong 300 \ \text{and} \ \Omega_X^+ \cong -0.0042 \).$

The xi-point on the figure 2-brind by Eqs. (2.24) a mixing, fully-develope. This observation justific braidmark flow. Eqs. (2.24) [PAPS-closure developed]

Easing Frame of Reten

Bardina et al. (i Ps) used large eddy s affect of spanwise rota havegeneous mean she

Email dimensionless

numbers: O

Ecked to develop

extranzed in Table 2

Selling of the URAI

Brethouwer (2)

to study, each simul.

To genous turbulent

The \$\frac{1}{2}\$-point on the energy simplex (see Figure 2.3 above) and on the anisotropic diagram (see Figure 2.4 above) shows that the asymptotic state for homogeneous shear, defined by Eqs.(2.24) and (2.25) above, is close to the turbulent states formed in non-rotating, fully-developed, channel flows near the outer edge of the equilibrium region. This observation justifies the use of asymptotic homogeneous shear flow statistics as a benchmark flow. Eqs.(2.24) and (2.25) are used in Chapter 4 below to calibrate the URAPS-closure developed in Chapter 3.

Rotating Frame of Reference

Bardina et al. (1983) and others (sec, esp., Speziale 1989; Salhi and Cambon, 1997) used large eddy simulations (LES) of the Navier-Stokes equation to determine the effect of spanwise rotation on the statistical properties of a statistically stationary, homogeneous mean shear flow (see Figure 2.1 above). The results were developed for an "initial" dimensionless shear rate of $\tilde{\Gamma}(0)\cong 3.3$. Simulations are available for three rotation numbers: $\tilde{\Omega}/\tilde{\Gamma}\equiv\Omega_{\rm X}/\Gamma_{\rm yz}=-1/2$, -1/4, and 0. The computations were allowed to develop for a dimensionless space-time of $t_{\rm u}\Gamma_{\rm yz}=5$, where $t_{\rm u}\equiv z/<{\rm u}_z>(0)$. The components of the NR-stress and $\tilde{\Gamma}$ for $t_{\rm u}\Gamma_{\rm yz}=5$ are summarized in Table 2.3. In Chapter 6, these LES results will be used to partially assess the ability of the URAPS-closure to predict the influence of rotation on the NR-stress.

Brethouwer (2005) also developed DNS results for $\tilde{\Omega}/\tilde{\Gamma}=-1/2$, -1/4, and 0. In this study, each simulation was initiated by suddenly setting $\tilde{\Gamma}(0)\cong 18$ in an otherwise homogenous turbulent field. The simulations were conducted over a finite development

	ΩĒ	(a;
DNS	0	
	-0.25	
,	-0.5	1
LES	0	1
	-0.25	-
	-0.5	-

Table 2.3 DNS and LES Results for Asymptotic Rotating Homogeneous Shear: DNS (Brethouwer, 2005); LES (Bardina et al., 1983 (as reported by Speziale, 1989; Salhi and Cambon, 1997)).

	$ ilde{\Omega}/ ilde{\Gamma}$	Γ̄ _o (appx)	t̃ (appx)	Γ̃(8) (appx)	R _{xx}	R _{yy}	R _{zz}	R _{yz}
DNS	0	18	12	12	0.210	0.120	0.670	-0.130
	-0.25	18	8	12	0.280	0.370	0.350	-0.320
	-0.5	18	14	12	0.394	0.553	0.053	-0.065
LES	0	3.3	5	-	0.294	0.073	0.633	-0.15
	-0.25	3.3	5	-	0.224	0.383	0.393	-0.35
	-0.5	3.3	5	-	0.344	0.583	0.073	-0.10

and $0 \le t_u \Gamma_{yz} < 15$. pore the experiment. ster to attain a self-sir emovimate asymptotic abilited results show. its streamwise compon imponent Note that distribution flips and R studations for spanwiss an absolute mean vorte Brethouwer (20) imageneous shear flow distribution numbers $ilde{\Omega}$ $\tilde{Q}[\tilde{Q}]_{mn} \leq (\tilde{Q}[\tilde{Q}]) \leq ($ The DNS results dev star behavior inasm 量量 components of ite i increases, but as indicated by T if the turb as the develop

^{ंच्या} produces two qu

time, $0 \le t_u \Gamma_{yz} < 15$. For $\Omega_x = 0$ and $t_u \Gamma_{yz} = 12$, $\tilde{\Gamma}(12) = 12$, which is significantly above the experimental value of $\tilde{\Gamma}_{AHS} = 4.2$. The simulation time may have been too short to attain a self-similar state. The components of the NR-stress listed in Table 2.3 are approximate asymptotic values extrapolated from the developing statistical results. The tabulated results show that as $\tilde{\Omega}/\tilde{\Gamma}$ becomes more negative, the energy is shifted from the streamwise component of the fluctuating velocity to the crossflow (or transverse) component. Note that for $\tilde{\Omega}/\tilde{\Gamma} = 0$, $R_{yy} < R_{zz}$; but, for $\tilde{\Omega}/\tilde{\Gamma} = -1/2$, the energy distribution flips and $R_{yy} > R_{zz}$. This redistribution of energy was also noted in the DNS simulations for spanwise rotation of channel flows (see Figure 2.4 above) in the region of zero absolute mean vorticity (see Eq. (2.21) above).

Brethouwer (2005) recently developed DNS simulations for spanwise rotation of homogeneous shear flows and showed that self-similar solutions occur over a finite range of rotation numbers $\tilde{\Omega}/\tilde{\Gamma}$:

$$(\tilde{\Omega}/\tilde{\Gamma})_{\min} < (\tilde{\Omega}/\tilde{\Gamma}) < (\tilde{\Omega}/\tilde{\Gamma})_{\max}. \tag{2.26}$$

The DNS results developed for $\tilde{\Omega}/\tilde{\Gamma}$ between $(\tilde{\Omega}/\tilde{\Gamma})_{min}$ and $(\tilde{\Omega}/\tilde{\Gamma})_{max}$ show self-similar behavior inasmuch as the turbulent kinetic energy, the turbulent dissipation, and all the components of the Reynolds stress increase as the dimensionless development time \tilde{t} increases, but $\tilde{\Gamma}$ and all the components of the NR-stress approach a self-similar state as indicated by Table 2.3. Brethouwer (2005) also noted that for $\tilde{\Omega}/\tilde{\Gamma}=-3/4$ and $\tilde{\Omega}/\tilde{\Gamma}=+1/4$ the turbulent kinetic energy k and the turbulent dissipation ε both decrease to zero as the development time increases. Therefore, spanwise rotation of homogeneous shear produces two qualitatively distinct flow regimes. A decay regime, defined as

 $\lim_{t_0 \to \infty} (k, \varepsilon) = (0, 0) \ni t$ for $(\tilde{\Omega})$

45d a self-similar reg≀

 $\lim_{k \to \infty} (k, \varepsilon) = (\infty, \infty) \Rightarrow 0$

for $(\tilde{\Omega}/\tilde{\Gamma})$

In Chapter 6 and in Sel

amogenous shear flow

dafferent closure mod

15 Homogeneous Da

VorBolating Frames ...

Experimental

and the second section of the section o

Ontsin (1971) and r

findamental ideas relat

ad Parks, 1997). DNS

emegenous decay and

¹⁸⁵: Yu et al. 200

_{r,ε,r}<ñ,ñ,> 5) au

me positive, are relat

3-=;;

$$\lim_{t_{\mathbf{u}}\to\infty} (\mathbf{k}, \varepsilon) = (0, 0) \ni \lim_{t_{\mathbf{u}}\Gamma_{\mathbf{y}z}\to\infty} \tilde{\Gamma} = \infty$$

$$\text{for } (\tilde{\Omega}/\tilde{\Gamma}) < (\tilde{\Omega}/\tilde{\Gamma})_{\text{min}} \text{ or } (\tilde{\Omega}/\tilde{\Gamma}) > (\tilde{\Omega}/\tilde{\Gamma})_{\text{max}}$$

$$(2.27)$$

And, a self-similar regime, defined as

$$\lim_{t_{U} \to \infty} (k, \varepsilon) = (\infty, \infty) \ni \lim_{t_{U} \Gamma_{yz} \to \infty} \tilde{\Gamma} = \tilde{\Gamma}_{AHS} < \infty$$

$$\text{for } (\tilde{\Omega}/\tilde{\Gamma})_{min} < (\tilde{\Omega}/\tilde{\Gamma}) < (\tilde{\Omega}/\tilde{\Gamma})_{max}$$
(2.28)

In Chapter 6 and in Section 2.6 below, the existence of self-similar states for rotating homogenous shear flows provides a means to validate and compare specific predictions of different closure models for the NR-stress.

2.5 Homogeneous Decay

Non-Rotating Frames of Reference

Experimental measurements of the low-order statistical properties of homogeneous decay in an inertial (non-rotating) frame of reference by Comte-Bellot and Corrsin (1971) and many others (see, esp., pg. 160, Pope 2000) confirm many fundamental ideas related to turbulent velocity fluctuations (see, Chapter 3, Piquet, 1999; and Parks, 1997). DNS and lattice Boltzmann simulations have also been developed for homogeneous decay and are consistent with experimental results (see, Mansour and Wray, 1993; Yu et al. 2005). For this flow (see Figure 2.1), the turbulent kinetic energy $k \ (\equiv tr < \underline{u} \ '\underline{u}' > /2)$ and the turbulent dissipation $\varepsilon \ (\equiv v \ tr < (\nabla \underline{u}') \cdot (\nabla \underline{u}')^T >)$, which are both positive, are related by (see Eq. (1.9) above)

$$\frac{\mathrm{d}\,\mathbf{k}}{\mathrm{d}\,\mathbf{t}} = -\varepsilon\,. \tag{2.29}$$

Figure 2.17 gives a significant the form of a likely curves are partially significant forms are partially significant forms are partially significant forms are Eqs. (1.9) with the phenomenous containing the phenomenous form and the phenomenous form are contained as $\frac{16}{61} = -C_D \frac{\epsilon}{7R}$.

Frame of Refer

Experimental resurbance reported by Ibbets of a 1999. They noted the stepy is decreased allowed in the integral standard. Complemental standard Speziale et al. (1995). Speziale et al. (1995).

The simulations were

relation number

Enliped from an initia

Figure 2.17 gives a summary of the experimental results (Comte-Bellot and Corrsin, 1971) in the form of a phase plane graph of $\tilde{k}(\tilde{t}) \equiv k(t)/k(0)$ and $\tilde{\epsilon}(\tilde{t}) \equiv \epsilon(t)/\epsilon(0)$. The decay curves are parameterized by the dimensionless time $\tilde{t} \equiv t \, \epsilon(0)/k(0)$. The non-viscous decay of turbulent kinetic energy has the feature that $0 \le \tilde{\epsilon}(\tilde{t}) \le \tilde{k}(\tilde{t}) \le 1$, which implies that $\tilde{k}/\tilde{\epsilon} \to \infty$ as $\tilde{t} \to \infty$. All NR-stress closure models that use $k-\epsilon$ transport equations (see Eqs.(1.9) and (1.11) use the results portrayed in Figure 2.17 to partially calibrate the phenomenological relaxation time τ_R governing the decay of turbulent dissipation (see Chapter 4 below):

$$\frac{\mathrm{d}\varepsilon}{\mathrm{d}t} = -C_{\mathrm{D}} \frac{\varepsilon}{\tau_{\mathrm{R}}} \ . \tag{2.30}$$

Rotating Frame of Reference

Experimental results for homogenous decay in a rotating frame of reference have been reported by Ibbetson and Tritton (1975), Weigland and Naguib (1978) and Jaquin et al. 1990. They noted that in the presence of rotation, rate of decay of turbulent kinetic energy is decreased along with a decrease in the dissipation. Although anisotropy was observed in the integral length scales, there was no significant Reynolds stress anisotropy reported. Complementary DNS and LES results were developed also by Bardina et al. (1985), Speziale et al. (1987) and Mansour et al. (1992) (see pg. 59 Gatski 1992). These earlier simulations were limited to relatively small decay times (i.e., $\tilde{t} < 10$) and low initial rotation numbers, $\tilde{\Omega}_0 = \Omega_x k(0)/\epsilon(0) < 75$). A weak prolate anisotropic state developed from an initial rotation number of $\tilde{\Omega}_0 \sim 1$; however, no discernable anisotropy



Experin 1997)

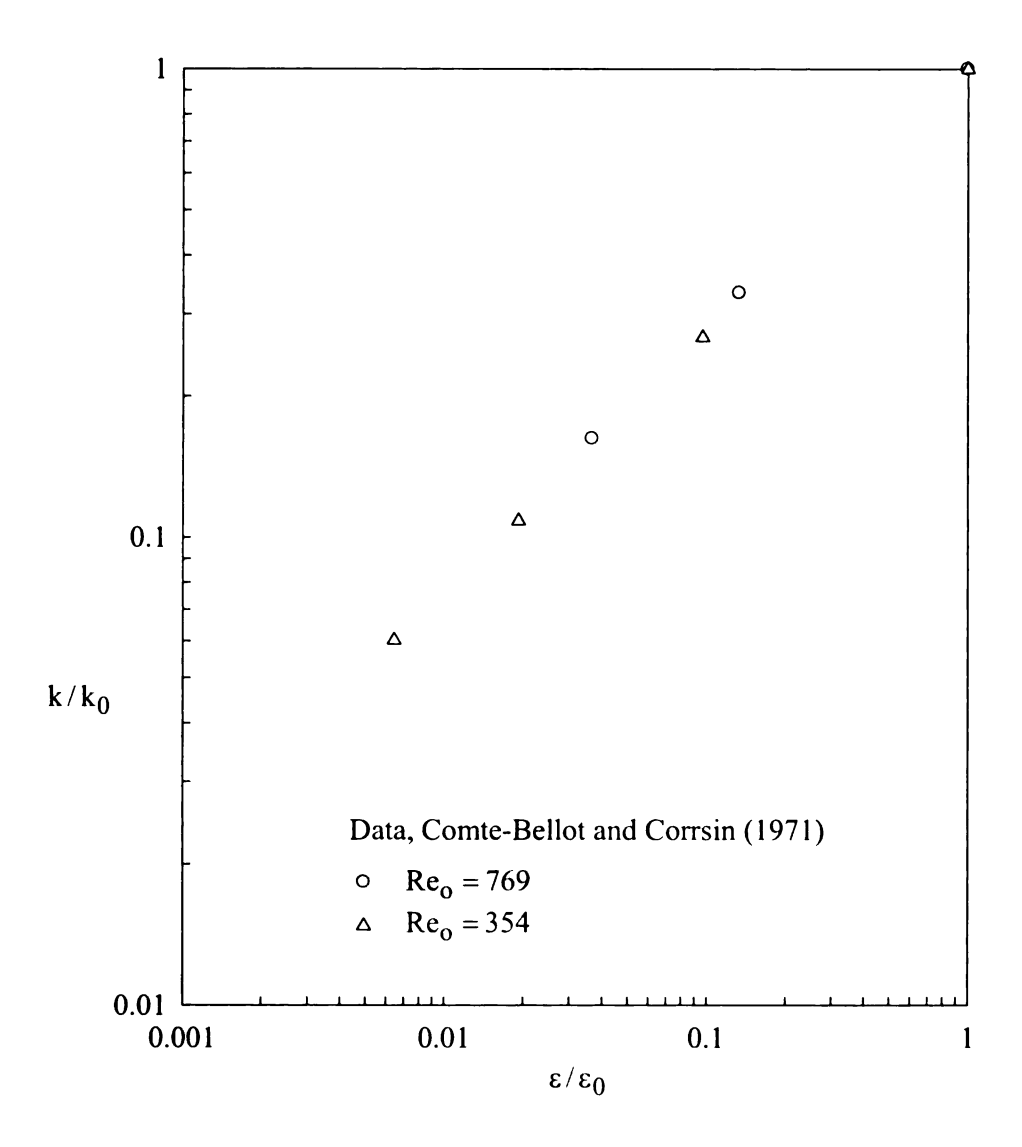


Figure 2.17 Experimental data of Comte-Bellot and Corrsin (1971) (also see Parks, 1997)

developed for large Baizmann, LES, and I Lastic energy among 1965. Bartello et al., Domanadzki, 2004). Ho Domanadzki (2004) use along simulation time show that the Q' mending on the initia Cambon et al., 1997; and The influence of t has studied theoretical keloped a relationship we number $\tilde{\Omega} \equiv \Omega$ nearth to determine so Appendix F provides a िक URAPS-closure ।

An algebraic Model

An algebraic class the normalized

ropenies of

Te telationship may

developed for large rotation rates. However, recent simulations based on lattice Boltzmann, LES, and DNS methods have indicated that rotation can redistribute turbulent kinetic energy among the three components of the fluctuating velocity (see Yu et al., 2005; Bartello et al., 1994; Cambon et al., 1997; Mornishi et al. 2001; and Yang and Domaradzki, 2004). However, significant anisotropy only occurs after $\tilde{t} >> 10$. Yang and Domaradzki (2004) used LES to show that an anisotropic state eventually develops after a long simulation time for rotation numbers ($\tilde{\Omega}_0 > 20$) and the results of Cambon et al. (1997) show that the QNR-form may be either an oblate ellipsoid or a prolate ellipsoid, depending on the initial conditions and the development time (see, esp., Figure 7 in Cambon et al., 1997; and Yang and Domaradzki, 2004).

The influence of frame rotation on the energy cascade in homogeneous decay has been studied theoretically by Zhou (1994) and Zeman (1995). Park and Chung (1999) developed a relationship between the relaxation time τ_R , defined by Eq. (2.29), and the rotation number $\tilde{\Omega} \equiv \Omega_x k/\epsilon$. The results of Park and Chung (PC-) are used in this research to determine several calibration parameters associated with the URAPS-closure. Appendix F provides a brief summary of the PC-paper needed to support the calibration of the URAPS-closure in Chapter 4 below.

2.6 Algebraic Models for the NR-Stress

An algebraic closure model for the NR-stress in a non-inertial frame of reference relates the normalized Reynolds stress to the local mean velocity gradient, to the local statistical properties of the fluctuating velocity, and to the angular velocity of the frame. The relationship may be either *implicit* or *explicit*. An *implicit* model is a non-linear

agebraic mapping of

E Clous

 $\underline{\underline{s}}^{\underline{l}}(\underline{\underline{R}},\underline{\underline{K}}) \rightarrow \underline{\underline{\underline{R}}}, \quad \underline{\underline{\underline{K}}}$

h general, the scalar

inensionless groups re

acil statistical state of

At applicit model provi

k and the NR-stress R

 $\underline{\underline{s}}^{\underline{r}}(\underline{\underline{k}}) \to \underline{\underline{R}} \ .$

5th implicit and explicit

la isotropic state can

 $\frac{\sqrt{3}}{2} = \frac{6}{2}$ in either Eq. (2.3)

tepossibility of a wea

stane flows (see Fig

Exponent for $\underline{\underline{K}} = \underline{0}$ i

Bosever, it is consiste

Telat a zero total str

appearent of the NR-st ad 19 above).

In Chapter 1. se

* Sections 2.2-2.5. e

anark flows were

algebraic mapping of $\underline{\underline{R}}$ into itself. A formal representation of this idea can be expressed as follows:

$$\underline{\mathfrak{R}}^{I}(\underline{\underline{R}},\underline{\underline{K}}) \to \underline{\underline{R}}, \quad \underline{\underline{K}} \equiv \tau_{R} < \underline{\underline{F}} >, \quad <\underline{\underline{F}} > \equiv \nabla < \underline{\underline{u}} > + 2\underline{\Omega}, \quad \tau_{R} \equiv C_{R} \, k \, / \, \epsilon. \tag{2.31}$$

In general, the scalar-valued dimensionless closure function C_R depends on two dimensionless groups related to the relative importance of time scales associated with the local statistical state of the turbulence, viz., $Re_t \equiv (k/\epsilon)/(v/k)$ and $\tilde{N}_F \equiv (k/\epsilon) \| < \underline{F} > \|$. An *explicit* model provides a direct link between the hydrodynamic/kinematic operator \underline{K} and the NR-stress \underline{R} :

$$\mathfrak{R}^{E}(\underline{K}) \to \underline{R} . \tag{2.32}$$

Both *implicit* and *explicit* algebraic models employ the assumption that deviations from a local isotropic state can only occur by a coupling with an external field. Therefore, if $\underline{K} = \underline{0}$ in either Eq. (2.31) or Eq. (2.32) above, then $\underline{R} = \underline{I}/3$. This hypothesis excludes the possibility of a weak anisotropic state on the symmetry plane for fully-developed channel flows (see Figure 2.3). It also excludes the possibility of a non-zero shear component for $\underline{K} = \underline{0}$ in fully-developed annular flows (see Churchill and Chan, 1995). However, it is consistent with DNS results for spanwise rotating channel flows that predict a zero total stress on the LP-side of the symmetry plane where the shear component of the NR-stress is zero and the mean velocity is a maximum (see Figures 2.8 and 2.9 above).

In Chapter 1, several theoretical properties for the NR-stress were identified and, in Sections 2.2-2.5, experimental and DNS results for the NR-stress for specific benchmark flows were noted. In this section, these observations are used to critique

geral algebraic clos equation (see Eq. (1) malable in the book b following nine charact

- Cl: The NR-s
- C2: The eigen flows.
- G: For non-re of the Figure
- C4: For spanse compore energy
- C5: In the abs flows n Figure
- C6: For spanw near the 2.11).
- C7: For non-redimens
- (§: For spanw self-sin of rotat

-J

C9: For rotati

several algebraic closure models presently used to support an analysis of the RANS-equation (see Eq. (1.4)). Additional information related to these specific models is available in the book by Pope (2000) and in the references cited in the bibliography. The following nine characteristics of the NR-stress will be used to benchmark algebraic closure models:

- C1: The NR-stress is real, symmetric ($\underline{\underline{R}}^T = \underline{\underline{R}}$), and normalized (tr($\underline{\underline{R}}$) = 1).
- C2: The eigenvalues of the NR-stress are non-negative real numbers for all flows.
- C3: For non-rotating, fully-developed, channel flows the normal components of the NR-stress are in the 2nd Sextet of the energy simplex (see Figure 2.3).
- C4: For spanwise rotation of fully-developed, channel flows, the normal components of the NR-stress are distributed in all six sextets of the energy simplex (see Figure 2.10).
- C5: In the absence of rotation, the QNR-form for fully-developed, channel flows near the isotropic state is nearly prolate (i.e., $III_b > 0$; also see Figure 2.4).
- C6: For spanwise rotation of fully-developed, channel flows, the QNR-form near the isotropic state is nearly oblate (i.e., III_b < 0; also see Figure 2.11).
- C7: For non-rotating homogenous shear, the NR-stress is self-similar and the dimensionless turbulent time scale, $\tilde{\Gamma} \equiv (k/\epsilon)\Gamma_{yz}$, is self-similar for sufficiently large development times.
- C8: For spanwise rotation of homogeneous shear, the NR-stress and $\tilde{\Gamma}$ are self-similar for sufficiently large development times for a finite range of rotation numbers:

$$-\infty < (\Omega_x / \Gamma_{vz})_{min} < (\Omega_x / \Gamma_{vz}) < (\Omega_x / \Gamma_{vz})_{max} < +\infty$$
.

C9: For rotating homogeneous decay, the energy distribution is anisotropic and, for long decay times, the QNR-form is stretched into a prolate or

was the Boussinesq (I

zd Boussinesq. 1877)

imponent of the Reyn

a ciplicit model for th

$$\frac{\mathbb{R}}{2} = \frac{\mathbb{R}}{2}^{\mathbb{E}} \left(\langle \tilde{\underline{S}} \rangle \right) = \frac{1}{3} \left[-\frac{1}{3} \right]$$

The dimensionless sca

and the turbulent

steal, C_v depends

Thank of $< \tilde{\underline{S}} >$.

RANS-equation (see Monting characterist

Eq. (2.33) cl

The eigenva

is realiz

provided

requires

oblate ellipsoid (see, Figure 7 in Cambon et al., 1997 and Yang and Domaradzki, 2004).

Closure Models Based on a Phenomenological Hypothesis

An "eddy" viscosity model for the Reynolds stress is analogous to the closure employed for the molecular stress of a Newtonian fluid. This idea, which is often referred to as the Boussinesq (B-) closure (see p. 162 in Bird et al., 2007; p. 93 in Pope, 2000; and, Boussinesq, 1877), has been used by numerous researchers to relate the anisotropic component of the Reynolds stress to the mean strain rate. The B-closure is an example of an *explicit* model for the NR-stress inasmuch as (see Eq. (1.7) above):

$$\underline{\underline{R}} = \underline{\underline{\mathfrak{R}}}^{E}(\langle \underline{\tilde{S}} \rangle) = \frac{1}{3}\underline{\underline{I}} + \underline{\underline{b}}, \quad \underline{\underline{b}} = -C_{\nu}\langle \underline{\tilde{S}} \rangle, \quad \langle \underline{\tilde{S}} \rangle = \frac{k}{\varepsilon}\langle \underline{\underline{S}} \rangle. \tag{2.33}$$

The dimensionless scalar-valued "eddy" viscosity coefficient C_{ν} links the mean strain rate and the turbulent time scale k/ϵ to the anisotropic component of the NR-stress. In general, C_{ν} depends on the turbulent Reynolds number, $Re_t = (k/\epsilon)/(\nu/k)$, and the invariants of $\langle \tilde{\underline{S}} \rangle$. Eq. (2.33) is widely used to support computational analyses of the RANS-equation (see Eq. (1.4)). The "eddy" viscosity closure for the NR-stress has the following characteristics.

- Eq. (2.33) clearly satisfies characteristic C1 above.
- The eigenvalues of $\langle \tilde{\underline{S}} \rangle$ and $\underline{\underline{R}}$ are related by $\lambda_{Ri} = -C_v \tilde{\lambda}_{Si} + 1/3$. Eq. (2.33) is realizable for all flows and, therefore, satisfies characteristic C2 above provided the invariants of $\underline{\underline{b}}$ are within the L-diagram (see Figure 1.1). This requires a phenomenological coefficient C_v that satisfies the following

inequality. been ider. rotating s flows. Ti inasmuch channel flo Eq. (2.33) car above. Eq. (2.33) p $III_{b} = 0$

coefficient For non-rotat

equally dis

Therefore,

however, t

the energy

NR-stress.

simple sh

 $0 \le \prod_{\beta} \le 3$

I see Figu

qualitativ The "product

be either

inequality $0 \le -C_v \tilde{\lambda}_{Si} + 1/3 \le 1$ for all flows. A specific form for C_v has been identified by Shih et al. (1995) using benchmark statistics for non-rotating simple shear, but a recalibration is needed for rotating simple shear flows. Therefore, Eq. (2.33) satisfies characteristic C2 provisionally inasmuch as the B-closure is not *universal* (i.e., a different "eddy" viscosity coefficient is needed for rotating flows).

- For non-rotating homogeneous shear and for non-rotating fully-developed channel flows, the B-closure predicts that the turbulent kinetic energy is equally distributed among the three components of the fluctuating velocity.

 Therefore, Eq. (2.33) is qualitatively inconsistent with C3 above.
- Eq. (2.33) can be "sensitized" to rotation through the turbulent time scale k/ε; however, the B-closure applied to a rotating simple shear still predicts that the energy is equally divided among the three normal components of the NR-stress. This theoretical prediction is qualitatively inconsistent with C4 above.
- Eq. (2.33) predicts that all the realizable anisotropic states for non-rotating simple shear flows have invariants that satisfy the following conditions:
 0 ≤ II_b ≤ 2/9 and III_b = 0. This result is qualitatively inconsistent with C5
 (see Figure 2.4). If Eq. (2.33) were used for rotating channel flows, then III_b = 0 would still be predicted for all anisotropic states. This prediction is qualitatively inconsistent with characteristic C6 above.
- The "production" term, $-\langle \underline{u}'\underline{u}'\rangle :< \underline{\underline{S}} >$, in the k-equation (see Eq. (1.9)) may be either positive or negative (see Pope, p.180, 2000; and Nishino et al.

1996). He

model for

inasmuch.

-< <u>u</u> '<u>u</u> '

Speziale (1991)

น aplicit second-orde

tilinear algebra with th

$$\frac{R}{3} = \frac{1}{3} - \frac{1}{3} = \frac{1}$$

The phenomenological

that and soft $< \frac{5}{2} > .dc$

 $\mathbb{E}(\mathfrak{g}(\Pi_S, \Pi_S) = 0, \text{ this}$

the Moreover, the

and be selected so the

ist for simple shear the

 $0 \le R_{yy} \le R_y$

transic operator for

Rivlin (1955) u

^{© develop} a general

Trailance properties.

Fied a similar app

syncids stress by a

1996). However, if the *realizable* B-closure (Shih et al., 1995) is used as a model for the Reynolds stress, energy "production" is positive for all flows inasmuch as $C_v > 0$ and

$$-<\underline{\mathtt{u}}\,'\underline{\mathtt{u}}\,'>:<\underline{\underline{S}}>=-2\,\epsilon\,\underline{\underline{R}}\,:<\underline{\tilde{\underline{S}}}>=+\,2\,\epsilon\,\,C_{\nu}<\underline{\tilde{\underline{S}}}>:<\underline{\tilde{\underline{S}}}>\geq0\,.$$

Speziale (1991) extended the *explicit* "eddy" viscosity model for the NR-stress to an *explicit* second-order model for the NR-stress by using the Cayley-Hamilton theorem of linear algebra with the result that

$$\underline{R} = \frac{1}{3}\underline{I} + \underline{b} = \frac{1}{3}\underline{I} + C_1 < \tilde{\underline{S}} > + C_2 \left(< \tilde{\underline{S}} > \cdot < \tilde{\underline{S}} > - II_S \underline{I}/3 \right). \tag{2.34}$$

The phenomenological coefficients $C_1(II_S, III_S)$ and $C_2(II_S, III_S)$ may depend on the invariants of $\langle \tilde{\underline{S}} \rangle$, defined as $II_S \equiv tr(\langle \tilde{\underline{S}} \rangle \cdot \langle \tilde{\underline{S}} \rangle)$ and $III_S \equiv tr(\langle \tilde{\underline{S}} \rangle \cdot \langle \tilde{\underline{S}} \rangle \cdot \langle \tilde{\underline{S}} \rangle)$. If $C_2(II_S, III_S) = 0$, then Eq. (2.34) reduces to Eq. (2.33). Clearly, Eq. (2.34) satisfies C1 above. Moreover, the phenomenological coefficients $C_1(II_S, III_S)$ and $C_2(II_S, III_S)$ could be selected so that $\underline{\underline{R}}$ is *realizable* (characteristic C2); however, Eq. (2.34) predicts that for simple shear flows, $R_{zz} = R_{yy}$. This result clearly does not agree with C3, which requires $0 \leq R_{yy} \leq R_{xx} \leq R_{zz} \leq 1$. Apparently, the mean strain rate is not an appropriate kinematic operator for the NR-stress.

Rivlin (1955) used the classical Cayley-Hamilton (CH) theorem of linear algebra to develop a general class of constitutive stress models for fluids that satisfy certain invariance properties. Pope (1975) and others (see p.452, Pope, 2000; Gatski, 2000) applied a similar approach to develop phenomenological models for the normalized Reynolds stress by assuming that \underline{b} , the anisotropic component of \underline{R} , depends on the

ariensionless strain

 $\lim_{n\to\infty} |x| \leq \frac{1}{n} > 1$

the NR-stress in rotation

 $\langle \underline{\hat{j}} \rangle$. With $\underline{\hat{b}} = \underline{\underline{B}} \hat{i}$

Fazer et al., 1960)

assotropic component!

$$\frac{3}{2} = \frac{1}{3} \mathbf{1} - \mathbf{b} = \frac{1}{3} \mathbf{1} + \sum_{n=1}^{10} \mathbf{0}$$

ील scalar-valued CH-

i the so-called integr

$$\langle \tilde{\xi} \rangle$$
 and $\langle \tilde{M} \rangle$ a

operators. If $|\mathbf{k}| |\epsilon|$

persions Φ_n are o

Times.

Comment on O

associated with

of reference. DN

stress depends c

not objective. T

the fluctuating,

the fluctuating.

dimensionless strain rate operator, $\langle \tilde{\underline{S}} \rangle$, and the dimensionless intrinsic vorticity operator, $\langle \underline{\tilde{W}} \rangle \equiv \langle \underline{\tilde{W}} \rangle + \underline{\tilde{\Omega}}$. Thus, a further generalization of Eq (2.33) assumes that the NR-stress in rotating and in non-rotating frames depends independently on $\langle \underline{\tilde{S}} \rangle$ and $\langle \underline{\tilde{W}} \rangle$. With $\underline{b} = \underline{\mathcal{B}}(\langle \underline{\tilde{S}} \rangle, \langle \underline{\tilde{W}} \rangle)$, an application of the Cayley-Hamilton theorem (see Frazer et al., 1960) yields the following explicit irreducible representation for the anisotropic component of the NR-stress (see p. 453 in Pope, 2000):

$$\underline{\underline{R}} = \frac{1}{3}\underline{\underline{I}} + \underline{\underline{b}} = \frac{1}{3}\underline{\underline{I}} + \sum_{n=1}^{10} C_n \underline{\underline{\Phi}}_n (\langle \underline{\tilde{S}} \rangle, \langle \underline{\tilde{W}} \rangle).$$
 (2.35)

The scalar-valued CH-coefficients C_n in Eq. (2.35) depend on the non-trivial invariants of the so-called *integrity* operators Φ_n (see Appendix D). The dimensional operators Φ_n are *objective*, symmetric, and traceless hydrodynamic/kinematic operators. If k/ϵ is assumed to be an *objective* scalar field, then all ten *integrity* operators Φ_n are *objective* and the ten CH-coefficients are scalar-valued *objective* functions.

Comment on *Objectivity*: The eigenvalues and the magnitude of the eigenvectors associated with an *objective* operator do not depend on the rotation of the frame of reference. DNS simulations in non-inertial frames clearly show that the NR-stress depends on the angular velocity of the frame. Therefore, the NR-stress is not *objective*. Theoretical support for this conclusion follows from the fact that the fluctuating velocity field $(\underline{u}^*)'$ in a *-frame (i.e., rotating frame) is related to the fluctuating velocity \underline{u}' and the fluctuating motion $\underline{\chi}'$ in a non-rotating frame

by the followin. arbitrary, time-d. unfortunately still 2001, Gatski, 200 Reynolds stress is flews. This idea st that $<(\bar{n})(\bar{n}),>$ stress in two diff $C_n = 0$ for $n \ge 3$, then $\frac{3}{3} = \frac{1}{1} - \frac{1}{9} = \frac{1}{3} = + C_{1}$ The hi-linear model ^{§त्राम}लांट and reduc genfied so the resu Cas. Eq. (2.36) pro Exist 0 < R yy <

fluctuating motion. If $C_n = 0$ for r

cans to account for

That $R_{\chi\chi} =$

assistant with the , indeveloped char by the following kinematic equation $(\underline{u}^*)' = \underline{Q} \cdot \underline{u}' + \dot{\underline{Q}} \cdot \underline{\chi}'$, where \underline{Q} is an arbitrary, time-dependent, orthogonal operator. An earlier impression that unfortunately still persist in the turbulence modeling literature (see, esp., Durst 2001, Gatski, 2004, Thais et al. 2005, Dafalias and Younis, 2007) is that the Reynolds stress is an *objective* statistical property of a turbulent ensemble of flows. This idea stems from an earlier theoretical argument by Speziale (1998) that $<(\underline{u}^*)'(\underline{u}^*)'>=\underline{Q}\cdot<\underline{u}'\underline{u}'>\cdot\underline{Q}^T$. This relationship between the Reynolds stress in two different equivalent frames is not correct inasmuch as the fluctuating motion χ' of a turbulent ensemble of flows is not zero.

If $C_n = 0$ for $n \ge 2$, then Eq. (2.35) reduces to Eq. (2.33) with $\Phi_1 = \langle \tilde{S} \rangle$. If $C_n = 0$ for $n \ge 3$, then

$$\underline{\underline{R}} = \frac{1}{3} \underline{\underline{I}} + \underline{\underline{b}} = \frac{1}{3} \underline{\underline{I}} + C_1 < \underline{\underline{\tilde{S}}} > + C_2 [< \underline{\underline{\tilde{S}}} > \cdot < \underline{\underline{\tilde{W}}} > + < \underline{\underline{\tilde{W}}} >^{\mathrm{T}} \cdot < \underline{\underline{\tilde{S}}} >].$$
 (2.36)

The bi-linear model defined by Eq. (2.36) was introduced by Shih et al. (1994) as a means to account for the anisotropic structure of the NR-stress. The model is clearly symmetric and reduces to $\underline{R} = \underline{I}/3$ if $\langle \tilde{\underline{S}} \rangle = \underline{0}$. The coefficients C_1 and C_2 can be specified so the resulting NR-stress is *realizable* (see Appendix E). For simple shear flows, Eq. (2.36) predicts that the energy states are in the 2^{nd} Sextet of the energy simplex: $0 < R_{yy} \le R_{xx} \le R_{zz} < 1$. However, for simple shear flows, Eq. (2.36) also predicts that $R_{xx} = 1/3$ and $III_b = 0$ for all values of $\tilde{\Gamma} \equiv \Gamma_{yz} k/\epsilon$, which is not consistent with the energy distribution and the anisotropic invariants associated with fully-developed channel flows (see Figures 2.18; also see Appendix E). Clearly, a

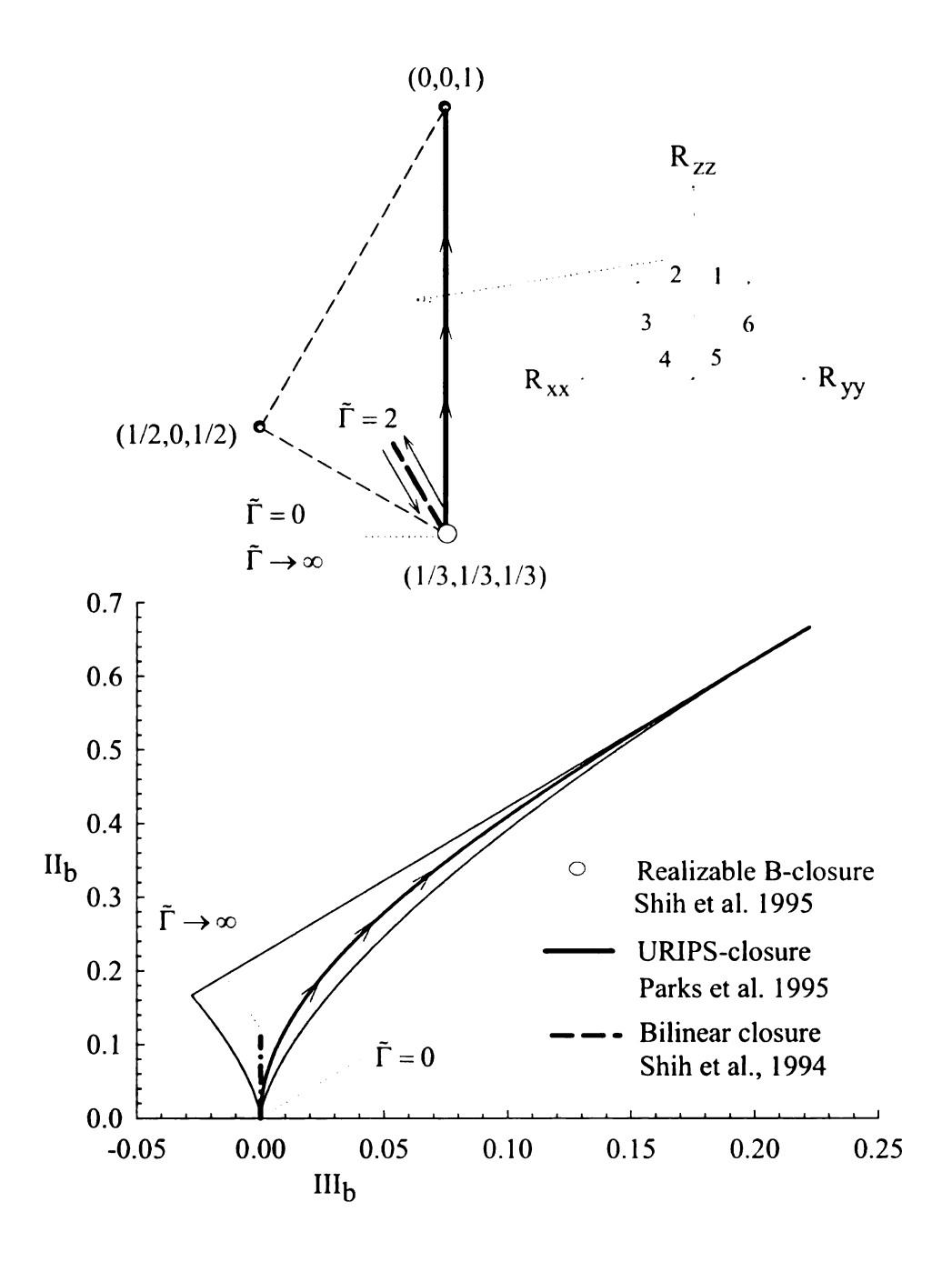


Figure 2.18 Energy Distribution and Anisotropic States for Non-Rotating Simple Shear Predicted by the Generalized Eddy Viscosity Closure, the Bilinear Closure, and the URIPS Closure for increasing values of $\tilde{\Gamma}$.

pteromenological ar agrare the low-order heavior for other flow Recently, Rahm in ogeneous shear fl. ed for axisymmetric-

Higher order c Eq. (2.35). For examp the NR-stress that inconficients were selec carnels, impinging j. appiduce the flows u-

stess model that consider sclar-valued turbulent stature near a solid il or the ratio of energy some model is cons

sected based on spec

Comment on t

assumption th ¹⁹⁸⁷, 1989, 1

assumption re

DNS results (

phenomenological approach based on the hypothesis that $\underline{\underline{b}} = \underline{\underline{\mathcal{B}}}(\langle \underline{\underline{\tilde{S}}} \rangle, \langle \underline{\underline{\tilde{W}}} \rangle)$ does not capture the low-order statistical phenomena of turbulent flows.

Higher order closure models have been developed by retaining additional terms in Eq. (2.35). For example, Craft et al. (1996) and Speziale (1996) developed a closure for the NR-stress that includes contributions from the cubic terms. The resulting six CH-coefficients were selected based on statistical properties related to flows through curved channels, impinging jet flows, and rotating pipe flows. Although the Craft-closure can reproduce the flows used to select the model parameters, it does not ensure *realizable* behavior for other flows.

Recently, Rahman and Siikonen (2006) developed an explicit non-linear algebraic stress model that considered the first four terms in Eq. (2.35). This quadratic model uses a scalar-valued turbulent transport time scale τ_R that accounts for the anisotropic turbulent structure near a solid/fluid interface. The authors assume that the CH-coefficients depend on the ratio of energy "production" and energy dissipation, $\mathcal{P}/\epsilon = -2 \epsilon \underline{R} :< \underline{\tilde{S}} >$. The closure model is consistent with characteristic C2 above for boundary layers and for homogeneous shear flows. It is also *realizable* for mean field planar-extensional flows and for axisymmetric-extensional flows. However, because the model coefficients were selected based on specific flows, *realizability* may not occur for other flows.

Comment on the Phenomenological Approach: Eq. (2.35) stems from the assumption that the NR-stress is an *objective* operator (see Spezialc, 1987, 1989, 1991). This conjecture, which was inspired by a similar assumption regarding the molecular stress of fluids, is not supported by DNS results (see Chen and Song, 1997; El-Samni and Kasagi, 2001;

Abid and Grundestam Nevertheless. principle to example. Gar Hutter, 2003; Unfortunately objective oper equation. The Chapter 3 h. negative mar benchmark 1 URAPS-clos ensure realiz the potentia

Some Models Bar

diagnostic to

The need for [972] (see pg. 449.

has to seek an alg

man differential c

Schonal can be de

Abid and Habibi, 2003; Grundestanm 2004; Brethouwer, 2005; Grundestam and Wallin, 2008; and Grundestam et al., 2008). Nevertheless, many researchers continue to use *objectivity* as a guiding principle to improve low-order turbulence closure models (see, for example, Gatski, 2000; p.19 in Piquet, 1999; Durst, 2001; Weis and Hutter, 2003; Girimaji 2004; Dafalias and Younis, 2007; Hamba, 2006). Unfortunately, the *explicit* representation of the NR-stress in terms of objective operators has not provided a practical closure for the RANSequation. The primary weakness has been characteristic C2 above. In Chapter 3 below, this problem is addressed by formulating a nonnegative mapping of R into itself that does not depend on specific benchmark flows used to calibrate closure parameters. Thus, once the URAPS-closure is calibrated, it does not need to be recalibrated to ensure realizable behavior for other flows. This theoretical approach has the potential of transforming the use of the RANS-equation as a diagnostic tool for engineering design and education.

Closure Models Based on a Weak Equilibrium Hypothesis

The need for an algebraic closure model for the Reynolds stress motivated Rodi (1972) (see pg. 449, Pope 2000; pg. 281, Piquet, 1999) and many others over the past 30 years to seek an algebraic model based on hydrodynamic principles. An unclosed, albeit exact, differential equation for the second-order moment of the velocity distribution functional can be developed from the Navier-Stokes equation (see p.387 in Pope, 2000).

The resulting month

mondes an explicit

([>(≡∇<<u>u</u>> +2Ω)

lewritten as follows:

<u>; ĉ</u> ĉt -< <u>u</u>>-∇ ji 2k <u>R</u>

-[v/C² < <u>u</u>'<u>u</u>'

+[-< \bu ,\bu ,> -

 $-2 \left[< \frac{p'}{\rho} \underbrace{s'}_{\text{redistribution}} \right]$

Numerous clos

137 have appeared

niduce a separate 1

Consequently, many

1488-equation. Unite

recable operators

Meriori for specific

Rodi (1972) re-

ising the following

Ec. 1.91 without the n

[2kR]=

The resulting moment equation requires three statistical closure models: one for "mixing", one for "redistribution", and another for "dissipation". The "production" term provides an explicit coupling to the frame rotation operator through the operator $\langle \underline{F} \rangle (\equiv \nabla \langle \underline{u} \rangle + 2 \underline{\Omega})$ and is already in closed form. The unclosed moment equation can be written as follows (see Appendix A for a derivation):

$$(\frac{\partial}{\partial t} + \langle \underline{\mathbf{u}} \rangle \cdot \nabla)(2k\underline{\mathbf{R}}) =$$

$$+ [\underline{\mathbf{v}}\nabla^{2} \langle \underline{\mathbf{u}}'\underline{\mathbf{u}}' \rangle - (\nabla \langle \underline{\mathbf{u}}'\underline{\mathbf{p}}' \rangle)^{T} - (\nabla \langle \underline{\mathbf{p}}'\underline{\mathbf{u}}' \rangle) - \nabla \cdot \langle \underline{\mathbf{u}}'\underline{\mathbf{u}}'\underline{\mathbf{u}}' \rangle]$$

$$= \underbrace{[-\langle \underline{\mathbf{u}}'\underline{\mathbf{u}}' \rangle \cdot \langle \underline{\mathbf{F}} \rangle - \langle \underline{\mathbf{F}} \rangle^{T} \cdot \langle \underline{\mathbf{u}}'\underline{\mathbf{u}}' \rangle]}_{\text{"production"}}$$

$$+ 2 [\langle \underline{\underline{\mathbf{p}}'}\underline{\underline{\mathbf{S}}'} \rangle] - 2[\underbrace{\mathbf{v} \langle (\nabla \underline{\mathbf{u}}')^{T} \cdot (\nabla \underline{\mathbf{u}}') \rangle]}_{\text{dissipation}}$$

$$(2.37)$$

Numerous closure models for the foregoing three statistical correlations in Eq. (2.37) have appeared in the literature (see Pope, 2000). Each set of closure models produce a separate transport equation for the NR-stress that must be calibrated. Consequently, many calibrated RSM transport models are available to support the RANS-equation. Unfortunately, a general assurance that any of these models produce realizable operators is not available. Realizability issues are generally handled a posteriori for specific classes of flows when they are deemed to be important.

Rodi (1972) reduced Eq. (2.37) to an *implicit* algebraic equation for the NR-stress by using the following *weak equilibrium hypothesis* (also see Gatski, 2000) together with Eq. (1.9) without the mixing contribution:

$$(\frac{\partial}{\partial t} + \langle \underline{u} \rangle \cdot \nabla)[2k\underline{R}] \cong 2\underline{R}(\frac{\partial}{\partial t} + \langle \underline{u} \rangle \cdot \nabla)[k] \cong 2(-2\underline{R} : \langle \underline{\tilde{S}} \rangle - 1) \varepsilon \underline{R}.$$
 (2.38)

E₄ (2.38) is partially

the NR-stress is app

agerraic Reynolds st

237) and using an 18-

 $(-2\underline{\underline{R}}) < \underline{\underline{\underline{S}}} > -1)\underline{\underline{R}} =$

Tie IARSM closure

activistion (Speziale et

$$\frac{\langle r_{\tilde{s}}^{\tilde{s}} \rangle}{\rho \epsilon} = \tilde{s}(\underline{R}. < \tilde{\underline{s}} > .$$

Solutions to Eqs.(2.39

ling et al. (1999), lare

Gatski (2000) a

is doping an explici

based on Eq. (2.35). In

h using "benchmark"

EARSM closure mod

the representation de

ine. The RSM "ho

taing frames. flo

liferturately, accord

ad Jongen, 2000: Ga

and may still prod

Eq. (2.38) is partially justified by the observation that in fully-developed channel flows, the NR-stress is approximately constant in the outer region. The following *implicit* algebraic Reynolds stress model (IARSM) follows by neglecting the mixing term in Eq. (2.37) and using an isotropic closure for the dissipation term:

$$(-2\underline{\underline{R}}:<\underline{\tilde{S}}>-1)\underline{\underline{R}}=-(\underline{\underline{R}}\cdot<\underline{\tilde{F}}>+<\underline{\tilde{F}}>^{T}\cdot\underline{\underline{R}})+\frac{\langle p'\underline{S}'>}{\rho\epsilon}-\frac{1}{3}\underline{\underline{I}}.$$
 (2.39)

The IARSM closure is completed by using a closure for the pressure/strain-rate correlation (Speziale et al. 1991, Girimaji, 1996; Craft and Launder, 1996):

$$\frac{\langle p'\underline{S}'\rangle}{\rho\varepsilon} = \underline{\mathfrak{I}}(\underline{\underline{R}}, \langle \underline{\tilde{S}}\rangle, \underline{\tilde{W}}). \tag{2.40}$$

Solutions to Eqs.(2.39) and (2.40) are generally difficult to develop and, according to Rung et al. (1999), are *unrealizable* for flows with strong streamline curvature.

Gatski (2000) addressed the dilemma associated with the IARSM type closures by developing an explicit algebraic Reynolds stress model (EASRM) for the NR-stress based on Eq. (2.35). In principle, the ten CH-coefficients in Eq. (2.35) can be determined by using "benchmark" flows generated by a closed moment equation for the NR-stress. EARSM closure models vary depending on the number of "integrity" operators used in the representation defined by Eq. (2.35) and the closure models used for Eq. (2.37) above. The RSM "benchmark" flows used in the calibration strategy include flows in rotating frames, flows with curvature, and other flows with difficult features. Unfortunately, according to Rung et al.(1999) and Gatski (see, esp., Gatski,1998; Gatski and Jongen, 2000; Gatski, 2004; and Gatski and Rumsey, 2006) a fully calibrated IASRM model may still produced *unrealizable* behavior. The IASRM and the EASRM class of

agebraic NR-stress common in support of

Courte Models Base

In a rotating

crainity equation, V

$$\frac{\partial}{\partial x} + \langle \bar{n} \rangle \cdot \nabla \bar{n} = A \Delta$$

t the above equation

ressure fluctuations ar

$$= \sum_{i=1}^{n} \frac{b_i}{b_i} = \overline{a_i} \cdot \overline{a_i} = -\infty$$

Aformal solution to the

क्ट fluctuations due t

freens function assoc

aftland side of Eq. (:

$$\frac{1}{2}(\tilde{y},t) = -\int_{-\infty}^{+\infty} d\tilde{t} \iiint_{t} d\tilde{t}$$

ेंग प्रका-inertial fram

the followin

ised on a smoothing

$$\frac{\mathbf{P}}{\mathbf{E}} = \underbrace{\mathbf{A}^{\mathsf{T}} \mathbf{B} \mathbf{A}}_{\mathbf{E}[\mathbf{A}^{\mathsf{T}}]} \mathbf{B} \mathbf{A}$$

algebraic NR-stress closure models do not provide a practical closure for the RANSequation in support of engineering design and analysis.

Closure Models Based on a Space-Time Smoothing Hypothesis

In a rotating frame of reference, turbulent velocity fluctuations satisfy the continuity equation, $\nabla \cdot \mathbf{u}' = 0$, and the following dynamic equation (Parks et al., 1998):

$$\frac{\partial \underline{\mathbf{u}}'}{\partial t} + \langle \underline{\mathbf{u}} \rangle \cdot \nabla \underline{\mathbf{u}}' - \nu \nabla^2 \underline{\mathbf{u}}' = -\underline{\mathbf{u}}' \cdot \langle \underline{\mathbf{F}} \rangle - \underline{\mathbf{f}}'. \tag{2.41}$$

In the above equation, the vector $\underline{\mathbf{f}}$ ' represents the fluctuating acceleration caused by pressure fluctuations and fluctuations in the *instantaneous* Reynolds stress:

$$\underline{\mathbf{f}}' \equiv \nabla \cdot \left[\frac{\mathbf{p}'}{\rho} \underline{\mathbf{I}} + \underline{\mathbf{u}}' \underline{\mathbf{u}}' - \langle \underline{\mathbf{u}}' \underline{\mathbf{u}}' \rangle \right]. \tag{2.42}$$

A formal solution to the above equation that neglects fluctuations due to initial conditions and fluctuations due to boundary conditions can be expressed in terms of a mean field Greens function associated with the convective/viscous parabolic operator defined by the left hand side of Eq. (2.41) above:

$$\underline{\underline{u}}'(\underline{x},t) = -\int_{-\infty}^{t} d\hat{t} \iiint_{V} d\hat{V} \left\{ G(\underline{x},t;\underline{\hat{x}},\hat{t}) \left[\underline{\underline{u}}'(\underline{\hat{x}},\hat{t}) \cdot \langle \underline{\underline{F}} \rangle (\underline{\hat{x}},\hat{t}) + \underline{\underline{f}}'(\underline{\hat{x}},\hat{t}) \right] \right\}$$
(2.43)

For non-inertial frames (i.e., $\langle \underline{F} \rangle = \nabla \langle \underline{u} \rangle$), Parks et al. (1998) used Eq. (2.43) and derived the following non-negative mapping between the prestress and the NR-stress based on a smoothing approximation:

$$\underline{\underline{R}} = \frac{\underline{\underline{A}}^{T} \cdot \underline{\underline{B}} \cdot \underline{\underline{A}}}{tr(\underline{\underline{A}}^{T} \cdot \underline{\underline{B}} \cdot \underline{\underline{A}})} , \quad \underline{\underline{A}} = [\underline{\underline{I}} + \tau_{R} < \underline{\underline{F}} >]^{-1} , \quad \underline{\underline{B}} = \frac{\langle \underline{\underline{f}} : \underline{\underline{f}} : \rangle}{tr < \underline{\underline{f}} : \underline{\underline{f}} : \rangle}.$$
 (2.44)

Gearly, if the prestra

thi satisfies C2 for a

has for the develope

Parks (1997) a

Suthe operator that

astame derivative:

$$\frac{\beta}{3} = \frac{1}{3} \left[-\frac{2}{3} \left(\frac{k}{\epsilon} < \frac{S}{2} > . \right) \right]$$

A generalized convect

of turbulent flows:

$$\frac{\delta_{1}\langle S \rangle}{\delta t} = \frac{\hat{c} \langle S \rangle}{\hat{c} t} + \langle$$

The above operator is

246; reduces to the c

If
$$\underline{B} = \underline{I} \cdot 3$$
.

Pestiess (URIPS-),

atoduced by Boussin

$$\frac{1}{2} = \frac{A^{T} \cdot A}{\text{tr}(A^{T} \cdot A)}$$

Fin simple shear flo

Sendary between

$$\frac{\text{deft een}}{\text{deft}} = R_{yy} \le 1.3$$

Clearly, if the prestress operator is non-negative, then Eq. (2.44) produces a NR-stress that satisfies C2 for all flows (see above model characteristics). This result provides the basis for the development of the URAPS-closure in Chapter 3.

Parks (1997) and Weispfennig (1997) assumed that the prestress operator $\underline{\underline{B}}$ is an *objective* operator that depends on the turbulent time scale k/ϵ , the mean strain rate, and its time derivative:

$$\underline{\underline{B}} = \frac{1}{3} \underline{\underline{I}} + \underline{\underline{B}} \left(\frac{k}{\varepsilon} < \underline{\underline{S}} >, \left(\frac{k}{\varepsilon} \right)^2 \frac{\delta_a < \underline{\underline{S}} >}{\delta t} \right). \tag{2.45}$$

A generalized convective derivative was used to account for mean field memory effects of turbulent flows:

$$\frac{\delta_{\mathbf{a}} < \underline{\underline{S}} >}{\delta t} = \frac{\partial < \underline{\underline{S}} >}{\partial t} + <\underline{\underline{u}} > \cdot \nabla < \underline{\underline{S}} > + <\underline{\underline{W}} > \cdot <\underline{\underline{S}} > + <\underline{\underline{W}} > \cdot <\underline{\underline{S}} > + <\underline{\underline{S}} > \cdot <\underline{\underline{W}} >^{\mathsf{T}}$$

$$+\zeta \left[<\underline{\underline{S}} > \cdot <\underline{\underline{S}} > + <\underline{\underline{S}} > \cdot <\underline{\underline{S}} > \right]$$

$$(2.46)$$

The above operator is *objective* (pg. 181, Parks, 1997) for $-\infty < \zeta < +\infty$. For $\zeta = 0$, Eq. (2.46) reduces to the classical Jaumann derivative (see pg. 250 in Bird et al., 2007).

If $\underline{\underline{B}} = \underline{\underline{I}}/3$, then Eq. (2.44) reduces to the universal, realizable, isotropic, prestress (URIPS-) closure and provides a significant generalization for Eq. (2.33) introduced by Boussinesq more than 130 years ago:

$$\underline{\underline{R}} = \frac{\underline{\underline{A}}^{T} \cdot \underline{\underline{A}}}{\operatorname{tr}(\underline{\underline{A}}^{T} \cdot \underline{\underline{A}})} , \quad \underline{\underline{A}} = [\underline{\underline{I}} + \underline{\underline{K}}]^{-1} , \quad \underline{\underline{K}} = \tau_{R} < \underline{\underline{F}} > , \quad \operatorname{tr}(\underline{\underline{K}}) = 0 .$$
(2.47)

For simple shear flows, the energy states for the URIPS-closure are all located on the boundary between the 1st and 2nd Sextets of the energy simplex: $0 \le R_{xx} = R_{yy} \le 1/3 \le R_{zz} \le 1$. For $\underline{K} = \underline{0}$, the NR-stress is isotropic, $\underline{R} = \underline{I}/3$. For no

rotation and as $\|\underline{K}\| \to \infty$, the turbulent energy is shifted to the axial component of the fluctuating velocity (i.e., $R_{zz} \to 1$). Also, for no rotation, the locus of anisotropic states predicted by the URIPS-closure follows the DNS results in the core region of the flow field: $10 \le y^+ \le 100$. For $\tilde{\Gamma} = 0$, the turbulence is isotropic (see Point A of Figure 1.1). As $\tilde{\Gamma} \to \infty$, the QNR-form is elongated into an infinite needle (see Point C of Figure 1.1).

If $\underline{\underline{K}} = \underline{0}$, Eq. (2.47) implies that $\underline{\underline{R}} = \underline{\underline{1}}/3$. If $0 < \|\underline{\underline{K}}\| \ll 1$, then a representation of the operator in terms of a power series of $\underline{\underline{K}}$ can be expressed as (see Kantorovich and Akilov, 1964)

$$\underline{\mathbf{A}} = \underline{\mathbf{I}} - \underline{\mathbf{K}} + \underline{\mathbf{K}} \cdot \underline{\mathbf{K}} + \cdots$$
 (2.48)

For small $\|\underline{\underline{K}}\|$, Eqs.(2.47) and (2.48) imply that

$$\underline{\underline{R}} = \frac{\underline{\underline{A}}^{T} \cdot \underline{\underline{A}}}{\operatorname{tr}(\underline{\underline{A}}^{T} \cdot \underline{\underline{A}})} \xrightarrow{\parallel \underline{\underline{K}} \parallel \to 0} \frac{1}{3} - \frac{2}{3} \tau_{R} < \underline{\underline{S}} > . \tag{2.49}$$

The Coriolis acceleration formally drops out of the representation at first order; therefore, the URIPS-closure reduces to the B-closure for $\|\underline{\underline{K}}\| \ll 1$.

2.7 Conclusions

DNS results and experimental data for channel flows with and without rotation show significant primary and secondary normal stress differences. In contrast to this evidence, the traditional B-closure predicts that the primary and secondary normal stress differences for simple shear are zero for non-rotating and for rotating simple shear flows. For non-rotating channel flows, the energy states are all in the 2nd Sextet Of the energy

simplex. However, for rotating simple shear flows, the normal components of the NR-stress are distributed among all six sextets in the energy simplex. For rotating simple shear, the anisotropic states may be prolate-like with $III_b > 0$, or oblate-like with $III_b > 0$. For rotating channel flows, the variation of $\tilde{\Gamma}$ is not symmetric about the center of the channel. On the HP-side of a fully-developed channel flow there is a region where the mean velocity profile is a linear function of the crossstream coordinate and the intrinsic absolute mean vorticity is zero. On the LP side of the channel, the maximum velocity occurs at the same position where the total shear stress is zero. On the LP-side of the channel, both $\tilde{\Gamma}$ and $\tilde{\Omega}$ are negative and the anisotropic states near the isotropic state are oblate-like.

DNS results clearly show that the NR-stress is not *objective*; therefore, the eigenvalues of the NR-stress depend on the angular velocity of a non-inertial frame. Closure models built on the hypothesis that the NR-stress is *objective* and, thereby, represented in terms of objective basis operators are inconsistent with the physical nature of a fluctuating velocity field governed by the Navier-Stokes equation.

The preclosure theory developed by Parks et al. (1998) is a fundamentally different approach which relates the NR-stress to the mean field based on a Green's function representation of the fluctuating velocity. The isotropic assumption for the prestress which lead to the URIPS-closure is realizable for all flows. The preclosure theory can be further developed to include anisotropy and also preserve the non-negative feature of the prestress to develop a universal and realizable algebraic closure for the NR-NR-stress.

CHAPTER 3

URAPS-CLOSURE FOR THE NORMALIZED REYNOLDS STRESS

3.1 Introduction

The preclosure theory by Parks et al. (1998) discussed in Chapter 2 provides an explicit relation for the NR-stress in terms of the prestress. This theory (see Eq. 2.44) is extended for rotating flows and a summary of the preclosure theory for non-inertial frames is presented in Section 3.2 below. This Chapter is focused on developing a closure for the prestress that appears in the preclosure equation. A hypothesis will be presented for closing the prestress in the following Section 3.3. An irreducible representation based on the Cayley- Hamilton theorem for the prestress resulting in an implicit algebraic relation for the NR-stress is developed. Further, the eigenvalues of the prestress closure are analyzed to understand the conditions of realizability for all flows. From a study of the various boundaries on the NR-eigenvalue simplex, a domain for the coefficients that appear in the prestress is identified such that the CH-mapping of the NR-stress into the prestress is non-negative for any choice of the coefficients within the domain. This ensures that the NR-stress from the preclosure theory is also realizable. A numerical strategy to solve the implicit closure relation is also discussed. The scalar-valued turbulent transport time scale introduced by the preclosure theory is used as the phenomenological transport time in the equation for the turbulent kinetic energy and in the equation for the turbulent dissipation.

3.2 Hydrodynamic Preclosure

Preclosure theory (Parks et al. 1998) briefly discussed in Chapter 2 is presented in detail for non-inertial frames in this section. Although the derivations are clearly presented in Parks (1997), and Weispfennig (1997), the derivation is also discussed in detail in this Chapter for non-inertial frames to understand the kinematic operators associated with rotating flows. Equation for the fluctuating velocity in Eq. (2.41) for rotating flows remains the same except for a term that involves the frame rotation dyad through $\langle \underline{F} \rangle (\equiv \nabla \langle \underline{u} \rangle + 2\underline{\Omega})$. The fluctuations within the flow domain in Eq. (2.41) are caused by (1) a convective coupling between the mean velocity gradient and the fluctuating velocity, (2) fluctuations in Coriolis forces (3) pressure fluctuations and (4) fluctuations in instantaneous Reynolds stress. A formal representation for the fluctuating velocity in terms of a Green's function has been presented in Eq. (2.43) discussed in Chapter 2. An unclosed equation for the fluctuating correlation $\langle \underline{u}'\underline{u}' \rangle \langle \underline{x}, t\rangle$ (i.e. Reynolds momentum flux) can be developed from Eq. (2.43).

Unclosed Integral Equation for the Reynolds Momentum Flux

An unclosed integral equation for $\langle \underline{u}'\underline{u}' \rangle (\underline{x}, t)$ can be developed from Eq. (2.43) by first multiplying with the fluctuating velocity and then averaging the result over the turbulent ensemble of realizations as shown in Eq. (3.1) below.

$$\langle \underline{\mathbf{u}}'\underline{\mathbf{u}}'\rangle(\underline{\mathbf{x}},\mathbf{t}) = -\int_{-\infty}^{\mathbf{t}} d\hat{\mathbf{t}} \iiint_{\mathbf{V}} d\hat{\mathbf{V}} G_{\mathbf{v}}(\underline{\mathbf{x}},\mathbf{t};\underline{\hat{\mathbf{x}}},\hat{\mathbf{t}}) [\langle \underline{\mathbf{u}}'\underline{\hat{\mathbf{u}}}'\rangle\langle\underline{\hat{\mathbf{f}}}'\rangle + \langle \underline{\mathbf{u}}'\underline{\hat{\mathbf{f}}}'\rangle] . \tag{3.1}$$

Eq. (3.1) shows that $<\underline{u}'\underline{u}'>(\underline{x},t)$ is caused by $<\underline{u}'\hat{\underline{u}}'>(\underline{x},t;\hat{\underline{x}},\hat{t})\cdot<\underline{\hat{\underline{F}}}>(\hat{\underline{x}},\hat{t})$ and $<\underline{u}'\underline{f}'>(\underline{x},t;\hat{\underline{x}},\hat{t})$. The convective/viscous Green's function, $G_{\nu}(\underline{x},t;\hat{\underline{x}},\hat{t})$ accounts for

the transport of momentum from $(\hat{\mathbf{x}},\hat{\mathbf{t}})$ to $(\underline{\mathbf{x}},\mathbf{t})$. The utility of Eq. (3.1), which is unclosed, is that it clearly identifies two space-time turbulent correlations (i.e., $<\underline{\mathbf{u}}'\hat{\mathbf{u}}'>(\underline{\mathbf{x}},\mathbf{t};\hat{\mathbf{x}},\hat{\mathbf{t}})$ and $<\underline{\mathbf{u}}'\hat{\mathbf{f}}'>(\underline{\mathbf{x}},\mathbf{t};\hat{\mathbf{x}},\hat{\mathbf{t}})$) as important factors in determining the local behavior of $<\underline{\mathbf{u}}'\underline{\mathbf{u}}'>(\underline{\mathbf{x}},\mathbf{t})$. In addition, and most significantly, Eq. (3.1) also shows that $<\underline{\mathbf{F}}>(\equiv\nabla<\underline{\mathbf{u}}>+2\underline{\Omega})$ is the primary connection between the mean field and the Reynolds stress. An analogous representation for the correlation $<\underline{\mathbf{f}}'\underline{\mathbf{u}}'>(\underline{\mathbf{x}},\mathbf{t})$ follows directly from Eq. (3.1):

$$\langle \underline{\mathbf{f}}'\underline{\mathbf{u}}' \rangle (\underline{\mathbf{x}}, \mathbf{t}) = -\int_{-\infty}^{\mathbf{t}} d\hat{\mathbf{t}} \iiint_{\mathbf{V}} d\hat{\mathbf{V}} G_{\mathbf{v}}(\underline{\mathbf{x}}, \mathbf{t}; \underline{\hat{\mathbf{x}}}, \hat{\mathbf{t}}) [\langle \underline{\mathbf{f}}'\underline{\hat{\mathbf{u}}}' \rangle \langle \underline{\hat{\mathbf{f}}} \rangle + \langle \underline{\mathbf{f}}'\underline{\hat{\mathbf{f}}}' \rangle].$$
(3.2)

Representations similar to Eq. (3.2) for the turbulent flux of a passive scalar near a solid/fluid interface have been used by Petty (1975), Hill and Petty (1996), and Parks and Petty (1999). Petty and Lyons (1985) also used a result analogous to Eq. (3.2) to study the effect of dilute polymer solutions on the Reynolds momentum flux.

Smoothing approximation

The single-point point correlations $<\underline{u}'\underline{u}'>$ and $<\underline{f}'\underline{u}'>$ given by Eqs. (3.1) and (3.2) depend on the space/time relaxation of the Green's function and the space/time relaxation of specific turbulent correlations. In a frame of reference moving with the mean velocity, the convective/viscous Green's function is spatially peaked for small values of $|t-\hat{t}|$. The Green's function acts like a delta distribution on a time scale for which turbulent correlations become uncorrelated. If the space/time turbulent correlations have finite memories and if a single scalar-valued memory function $M_R(\underline{x},|t-\hat{t}|)$ or time

scale is used to characterize all space/time correlations, then the application of a *spatial* smoothing approximation to Eqs. (3.1) and (3.2) yields the following algebraic equations for $\langle \underline{\mathbf{u}}'\underline{\mathbf{u}}' \rangle$ and $\langle \underline{\mathbf{f}}'\underline{\mathbf{u}}' \rangle$ (see Parks et al., 1998):

$$\langle \underline{\mathbf{u}}'\underline{\mathbf{u}}' \rangle (\underline{\mathbf{x}}, \mathbf{t}) = -\tau_{\mathbf{R}} [\langle \underline{\mathbf{u}}'\underline{\mathbf{u}}' \rangle \langle \underline{\mathbf{F}} \rangle + \langle \underline{\mathbf{u}}'\underline{\mathbf{f}}' \rangle]$$
(3.3)

$$\langle \underline{\mathbf{f}}'\underline{\mathbf{u}}' \rangle (\underline{\mathbf{x}}, \mathbf{t}) = -\tau_{R} [\langle \underline{\mathbf{f}}'\underline{\mathbf{u}}' \rangle \langle \underline{\mathbf{F}} \rangle + \langle \underline{\mathbf{f}}'\underline{\mathbf{f}}' \rangle]. \tag{3.4}$$

where τ_R is the turbulent relaxation time defined as below in Eq. (3.5)

$$\tau_{R} = \int_{-\infty}^{t} d\hat{t} \{ M_{R}(\underline{x}, |t - \hat{t}|) \iiint_{V} d\hat{V} G_{V}(\underline{x}, t; \hat{\underline{x}}, \hat{t}) \}.$$
(3.5)

Combining Eqs. (3.3) and (3.4), a relation between $\langle \underline{u}'\underline{u}' \rangle$ and $\langle \underline{f}'\underline{f}' \rangle$ can be obtained as in Eq. (3.6) below.

$$\langle \underline{\mathbf{u}}'\underline{\mathbf{u}}' \rangle = \tau_{\mathbf{R}}^2 \left(\underline{\mathbf{A}}^{\mathsf{T}} \cdot \langle \underline{\mathbf{f}}'\underline{\mathbf{f}}' \rangle \cdot \underline{\mathbf{A}} \right)$$
 (3.6)

where the operator $\underline{\underline{A}}$ (\equiv [$\underline{\underline{I}} + \tau_R < \underline{\underline{F}} >$]⁻¹) is related to the turbulent relaxation time τ_R , the mean velocity gradient and the frame rotation rate. Rearranging the Eq. (3.6) yields the preclosure relation presented in Eq. (2.44).

As discussed in Chapter 2, both the operators $\underline{\underline{R}} (\equiv \frac{\langle \underline{\underline{u}'\underline{u}'} \rangle}{\operatorname{tr} \langle \underline{\underline{u}'\underline{u}'} \rangle})$ and

 $\underline{\underline{B}} = \frac{\langle \underline{f}'\underline{f}' \rangle}{tr \langle \underline{f}'\underline{f}' \rangle}$ are symmetric and non-negative and have a unit trace. A relation for

the prestress should essentially be formulated to be symmetric and non-negative and would result in a realizable NR-stress closure. The kinematic operator $\underline{\underline{K}}$ and the preclosure operator $\underline{\underline{A}} = [\underline{\underline{I}} + \underline{\underline{K}}]^{-1}$ are important to understand the applicability of the

closure. The general preclosure operator for the benchmark flows discussed in Chapter 2 can be written as below (see Appendix G for details)

$$\underline{\underline{\underline{K}}} = \tau_{R} \Gamma_{yz} \underline{e}_{y} \underline{e}_{z} + 2\tau_{R} \Omega_{x} (\underline{e}_{y} \underline{e}_{z} - \underline{e}_{z} \underline{e}_{y})$$

$$= N_{\Gamma} \underline{e}_{y} \underline{e}_{z} + N_{\Omega} (\underline{e}_{y} \underline{e}_{z} - \underline{e}_{z} \underline{e}_{y})$$
(3.7)

where $N_{\Gamma} = \tau_R \Gamma_{yz}$ and $N_{\Omega} = 2 \tau_R \Omega_x$. The preclosure operator is,

$$\underline{\underline{A}} = \frac{(1 + N_{\Gamma}N_{\Omega} + N_{\Omega}^{2})\underline{c}_{x}\underline{e}_{x} + \underline{c}_{y}\underline{e}_{y} + \underline{e}_{z}\underline{c}_{z} - (N_{\Gamma} + N_{\Omega})\underline{c}_{y}\underline{e}_{z} + N_{\Omega}\underline{e}_{z}\underline{c}_{y}}{(1 + N_{\Gamma}N_{\Omega} + N_{\Omega}^{2})}.$$
(3.8)

The operator A above as shown has an inverse in the case when the denominator

$$(1+N_{\Gamma}N_{\Omega}+N_{\Omega}^2) \neq 0$$
. For $N_{\Omega} = \frac{-1\pm\sqrt{N_{\Gamma}^2-4}}{2}$, the inverse of $\underline{\underline{A}}$ does not exist.

Example of such points would be $(N_{\Gamma}, N_{\Omega}) = (3, -\frac{1}{2} \pm \frac{\sqrt{5}}{2}), (4, -\frac{1}{2} \pm \sqrt{3})$ etc. for rotating simple shear flows. However, to avoid this, the adjugate operator $\underline{C} = \operatorname{adj}(\underline{I} + \underline{K})$ is used so that the determinant is cancelled in the numerator and denominator in the limiting case of the determinant $\det(\underline{C}) = 0$. This is used in the subsequent numerical implementation of the preclosure theory.

$$\underline{\underline{R}} = \frac{\underline{\underline{A}}^{T} \cdot \underline{\underline{B}} \cdot \underline{\underline{A}}}{tr(\underline{\underline{A}}^{T} \cdot \underline{\underline{B}} \cdot \underline{\underline{A}})} = \frac{\underline{\underline{C}}^{T} \cdot \underline{\underline{B}} \cdot \underline{\underline{C}}}{tr(\underline{\underline{C}}^{T} \cdot \underline{\underline{B}} \cdot \underline{\underline{C}})} \quad ; \quad \underline{\underline{C}} = adj (\underline{\underline{I}} + \underline{\underline{K}})$$
(3.9)

The above operator for the specific benchmark flows will be discussed in the Chapters 5, 6 and 7.

3.3 Prestress Closure and "Extra" Anisotropy

The preclosure equation expressed by Eq. (3.9) shifts the closure problem from the normalized Reynolds stress $\underline{\underline{R}}$ to the normalized prestress $\underline{\underline{B}}$. Most significantly, $\underline{\underline{B}}$ must be modeled to be non-negative. So a closure for $\underline{\underline{B}}$, such that it is realizable and satisfies $Q(\underline{z}) = \underline{\underline{B}} : \underline{z}\underline{z} = \frac{\langle (\underline{\underline{f}} \cdot \underline{\underline{u}}')(\underline{\underline{f}} \cdot \underline{z}) \rangle}{\operatorname{tr} \langle \underline{\underline{u}}'\underline{\underline{u}}' \rangle} \ge 0$; $\operatorname{tr}(\underline{\underline{B}}) = 1$ should be developed.

Closure Hypothesis

As noted in Chapter 2, $\underline{\mathbf{f}}'$ represents the fluctuating acceleration caused by pressure fluctuations and fluctuations in the *instantaneous* Reynolds stress. The prestress $\underline{\mathbf{B}}$ is intrinsically related to the pressure fluctuations. As noted in Eq. (3.3), the correlation $<\underline{\mathbf{f}}'\underline{\mathbf{f}}'>$ is related to $<\underline{\mathbf{u}}'\underline{\mathbf{f}}'>$ through mean field operator $<\underline{\mathbf{F}}>$. It is interesting to note from the equation for fluctuating velocity that the correlation $(<\underline{\mathbf{u}}'\underline{\mathbf{f}}'>+<\underline{\mathbf{u}}'\underline{\mathbf{f}}'>)$ is linked to the pressure/strain-rate (pressure redistribution) term as shown in Eq. (3.10) below.

$$(\langle \underline{\mathbf{u}}'\underline{\mathbf{f}}'\rangle + \langle \underline{\mathbf{f}}'\underline{\mathbf{u}}'\rangle)$$

$$= \langle -\frac{1}{\rho}\nabla \cdot [(\underline{\mathbf{u}}'\mathbf{p}')\underline{\mathbf{I}} + \underline{\mathbf{I}}(\underline{\mathbf{u}}'\mathbf{p}')] + \frac{\mathbf{p}'}{\rho}[\nabla \underline{\mathbf{u}}' + (\nabla \underline{\mathbf{u}}')^{T}] - \nabla \cdot \underline{\mathbf{u}}'\underline{\mathbf{u}}'\underline{\mathbf{u}}'\rangle$$

$$= [-(\nabla \langle \underline{\mathbf{u}}'\frac{\mathbf{p}'}{\rho}\rangle)^{T} - (\nabla \langle \underline{\mathbf{p}}'\underline{\mathbf{u}}'\rangle) - \nabla \cdot \langle \underline{\mathbf{u}}'\underline{\mathbf{u}}'\underline{\mathbf{u}}'\rangle] + 2[\langle \underline{\mathbf{p}}'\underline{\mathbf{S}}'\rangle]$$
(3.10)

The first term in the LHS is related to the turbulent mixing and the second term is the pressure/strain-rate term in the transport equation for fluctuating Reynolds stress (see Eq. (2.37)). Because \underline{B} is closely linked to $\langle \underline{u}'\underline{f}' \rangle$ and hence to the pressure/strain

correlation (see Eq. 3.10), the prestress operator can be modeled using similar kinematic variables as for the pressure/strain-rate correlation.

In second order closure models, the pressure/strain-rate terms have also been modeled to be functions of the mean strain rate and the Reynolds stress itself as discussed in Chapter 2 (see esp. Eq. 2.40). A key hypothesis in this research is that the pre-stress operator \underline{B} is a dyadic-valued function of \underline{R} . With $\underline{B} = \underline{\mathfrak{B}}(\underline{R})$, which is similar to the Rotta-conjecture (Rotta, 1951) for the pressure/strain rate, the following CH representation forms the prestress closure. The hypothesis that $\underline{B} = \underline{\mathfrak{P}}(\underline{R})$ may provide a practical closure to the preclosure theory.

Cayley – Hamilton theorem and non-negative mapping

If $\underline{\underline{B}}$ is a continuous function of $\underline{\underline{R}}$, then an irreducible representation of $\underline{\underline{B}}$ in terms $\underline{\underline{R}}$ and its invariants can be developed by the application of the Cayley- Hamilton theorem from linear algebra (Frazer et al., 1960). An uncalibrated closure for the prestress can be written as

$$\underline{\mathbf{B}} = \mathbf{C}_0 \underline{\mathbf{I}} + \mathbf{C}_1 (\underline{\mathbf{R}}) + \mathbf{C}_2 (\underline{\mathbf{R}} \cdot \underline{\mathbf{R}}) \tag{3.11}$$

 C_0 , C_1 and C_2 can be functions of the invariants of $\underline{\underline{R}}$. Since $tr(\underline{\underline{B}}) = 1$ and $tr(\underline{\underline{R}}) = 1$, one of the three coefficients can be eliminated and with two coefficients remaining.

$$\underline{\underline{B}} = \frac{\underline{\underline{I}}}{3} + C_{1}(\underline{II}_{R}, \underline{III}_{R})(\underline{\underline{R}} - \frac{\underline{\underline{I}}}{3}) + C_{2}(\underline{II}_{R}, \underline{III}_{R})(\underline{\underline{R}} \cdot \underline{\underline{R}} - \underline{II}_{R} \stackrel{\underline{\underline{I}}}{3})$$
(3.12)

$$II_R = \sum_{i=1}^{3} \lambda_{R,i}^2 \text{ and } III_R = \sum_{i=1}^{3} \lambda_{R,i}^3$$
 (3.13)

The eigenvalues of these two real, symmetric, and non-negative operators are related to each by the following equation:

$$\lambda_{B,i} = \frac{1}{3} + C_1(\lambda_{R,i} - \frac{1}{3}) + C_2(\lambda_{R,i}^2 - \frac{II_R}{3}) , \quad i = 1, 2, 3$$
 (3.14)

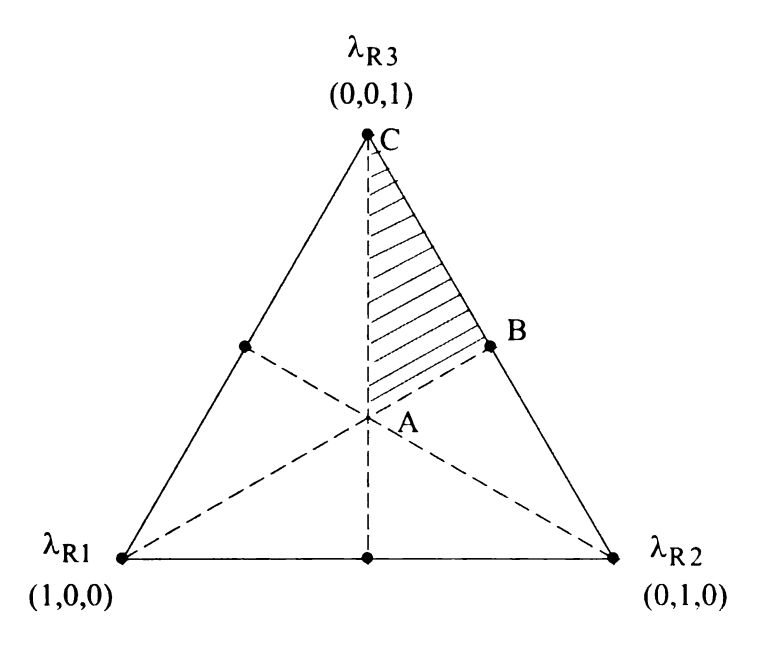
The three eigenvalues of \underline{B} and \underline{R} satisfy the following conditions: $0 \le \lambda_1 \le \lambda_2 \le \lambda_3 \le 1$ and $\lambda_1 + \lambda_2 + \lambda_3 = 1$. The non-negative mapping of \underline{R} into \underline{B} is equivalent to a mapping of the 1^{st} Sextet into itself, which also corresponds to a mapping of the L-diagram (see Figure 1.1) into itself. It follows from the above equation that the eigenvalues of \underline{R} on the vertices and in the center of the λ_R - triangle, map onto similar points on the λ_B - triangle (see Figure 3.1). The three boundaries of the λ_R - triangle are mapped onto corresponding boundaries of the λ_B - triangle, provided Eq. (3.15) below is satisfied.

$$C_1 + C_2 II_R = 1$$
 (only on the boundaries of the λ_R – triangle). (3.15)

One of the eigenvalues is zero on each of the boundaries of the λ_R - triangle. In order to map the boundaries of λ_R - triangle onto λ_B - triangle plane, then Eq. (3.15) results in Eq. (3.16) below by direct substitution of $\lambda_{B,3} = \lambda_{R,3} = 0$ (for one of the boundary lines).

$$\underline{\underline{B}} = \underline{\underline{R}} + \mathbf{C}_2(\underline{\underline{R}} \cdot \underline{\underline{R}} - \mathbf{II}_R \underline{\underline{R}}). \tag{3.16}$$

From the above result, without loss of generality, the mapping from λ_R -triangle to λ_R -triangle can now be expressed as in Eq. (3.17) where C_2 could be a function of the invariants as below.



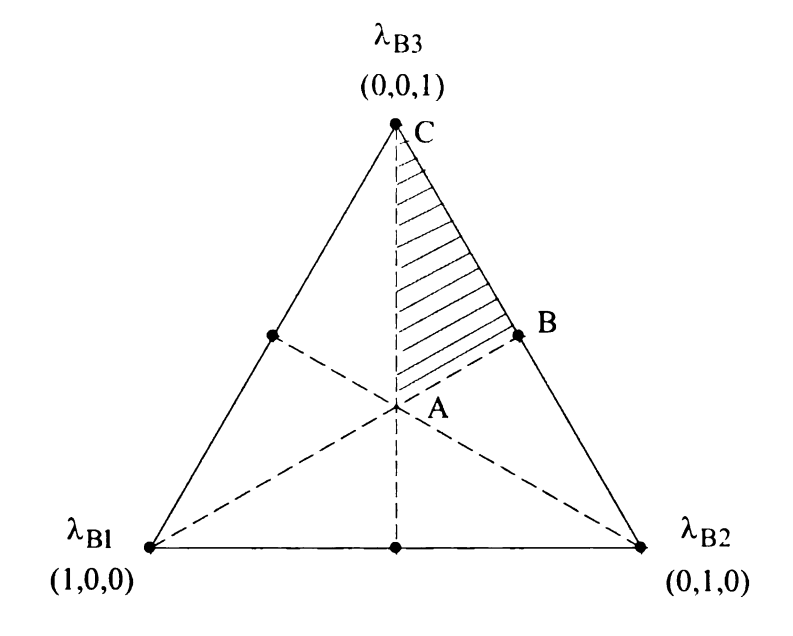


Figure 3.1 Eigenvalue mapping from the $\,\lambda_R^{}-\,$ triangle to $\,\lambda_B^{}-\,$ triangle

$$\underline{\underline{B}} = \underline{\underline{R}} + C_2(\underline{\underline{R}} \cdot \underline{\underline{R}} - II_R \underline{\underline{R}}) + \beta(\underline{\underline{R}} - \frac{1}{3}\underline{\underline{I}}) 27 \det(\underline{\underline{R}})$$
(3.17)

The coefficient C_2 is chosen to be a linear function of the second invariant II_R such that deviation of normal components of \underline{R} from isotropic states is along the $R_{xx} = R_{yy}$ line for simple shear flows. This is because DNS results for channel flow as discussed in Chapter 2 shows that the results close to the center of the channel are along $R_{xx} = R_{yy}$.

$$C_2 = -\alpha (II_R - \frac{1}{3})$$
 (3.18)

$$\underline{\underline{B}} = \underline{\underline{R}} - \alpha (\underline{II}_R - \frac{1}{3}) (\underline{\underline{R}} \cdot \underline{\underline{R}} - \underline{II}_R \underline{\underline{R}}) + \beta (\underline{\underline{R}} - \frac{1}{3} \underline{\underline{I}}) 27 \det(\underline{\underline{R}}). \tag{3.19}$$

The **above** representation is therefore associated with linear and nonlinear terms. The following discussion is related to developing the coefficients α and β such that Eq. (3.19) **above** is realizable.

Realizability Domain:

The eigenvalue relation for the prestress relation, Eq. (3.19) is,

$$\lambda_{Bi} = \lambda_{Ri} + \beta \left[27 \det(\underline{R}) (\lambda_{Ri} - \frac{1}{3}) \right] - \alpha \left[(II_R - \frac{1}{3}) (\lambda_{Ri}^2 - II_R \lambda_{Ri}) \right] , \quad i = 1, 2, 3. \quad (3.20)$$

In the following sections, the lower and upper bounds on α and β are determined from an analysis of Eq. (3.20) on the boundaries of the 1st sextet.

Lower bound on a:

The CH-mapping of \underline{R} into $\underline{\underline{B}}$ for planar anisotropic states (see BC-boundary of Figure 3.1) implies that

$$\lambda_{B3} = \lambda_{R3} - \alpha \left[\left(II_R - \frac{1}{3} \right) \left(\lambda_{R3}^2 - II_R \lambda_{R3} \right) \right] , \quad II_R = \left(1 - \lambda_{R3} \right)^2 + \lambda_{R3}^2 . \tag{3.21}$$

On the BC-boundary, $\lambda_{R1} = 0$, $\lambda_{R2} = 1 - \lambda_{R3}$, and $1/2 \le \lambda_{R3} \le 1$. By direct substitution, it follows from Eq. (3.21) that Point B is mapped into itself for all values of α ; and, Point C is mapped into itself for all values of the α . However, some interior points on the BC-boundary may not map onto the BC-boundary of the 1^{st} sextet if α is too small or too large. Eq. (3.22) can be used to determine a critical value of α that would give $\lambda_{B3} = 1$ for specific values of λ_{R3} :

$$\alpha_{\min} \equiv \frac{\lambda_{R3} - 1}{(II_R - 1/3)(\lambda_{R3}^2 - II_R \lambda_{R3})} , \quad \lambda_{R3} \xrightarrow{CH-\text{mapping}} \lambda_{B3} = 1.$$
 (3.22)

As indicated by Figure 3.2, a plot of α_{min} vs. λ_{R3} shows that $max(\alpha_{min}) = -3/2$, which is an *a priori* universal lower bound on the α -coefficient.

Upper bound on a:

Eq. (3.21) can also be used to eliminate redundancy in the CH-mapping. For example, a critical value of α can be determined that that would give $\lambda_{B3} = 1/2$ for specific values of λ_{R3} :

$$\alpha_{\text{max}} = \frac{\lambda_{\text{R3}} - 1/2}{(\text{II}_{\text{R}} - 1/3)(\lambda_{\text{R3}}^2 - \text{II}_{\text{R}}\lambda_{\text{R3}})}, \quad \lambda_{\text{R3}} \xrightarrow{\text{CH-mapping}} \lambda_{\text{B3}} = 1/2.$$
 (3.23)

As indicated by Figure 3.3, a plot of α_{max} vs. λ_{R3} shows that $min(\alpha_{max}) = +9$, which is an apriori universal upper bound on the α -coefficient. It is noteworthy that for $\alpha = 9$ the CH-mapping gives

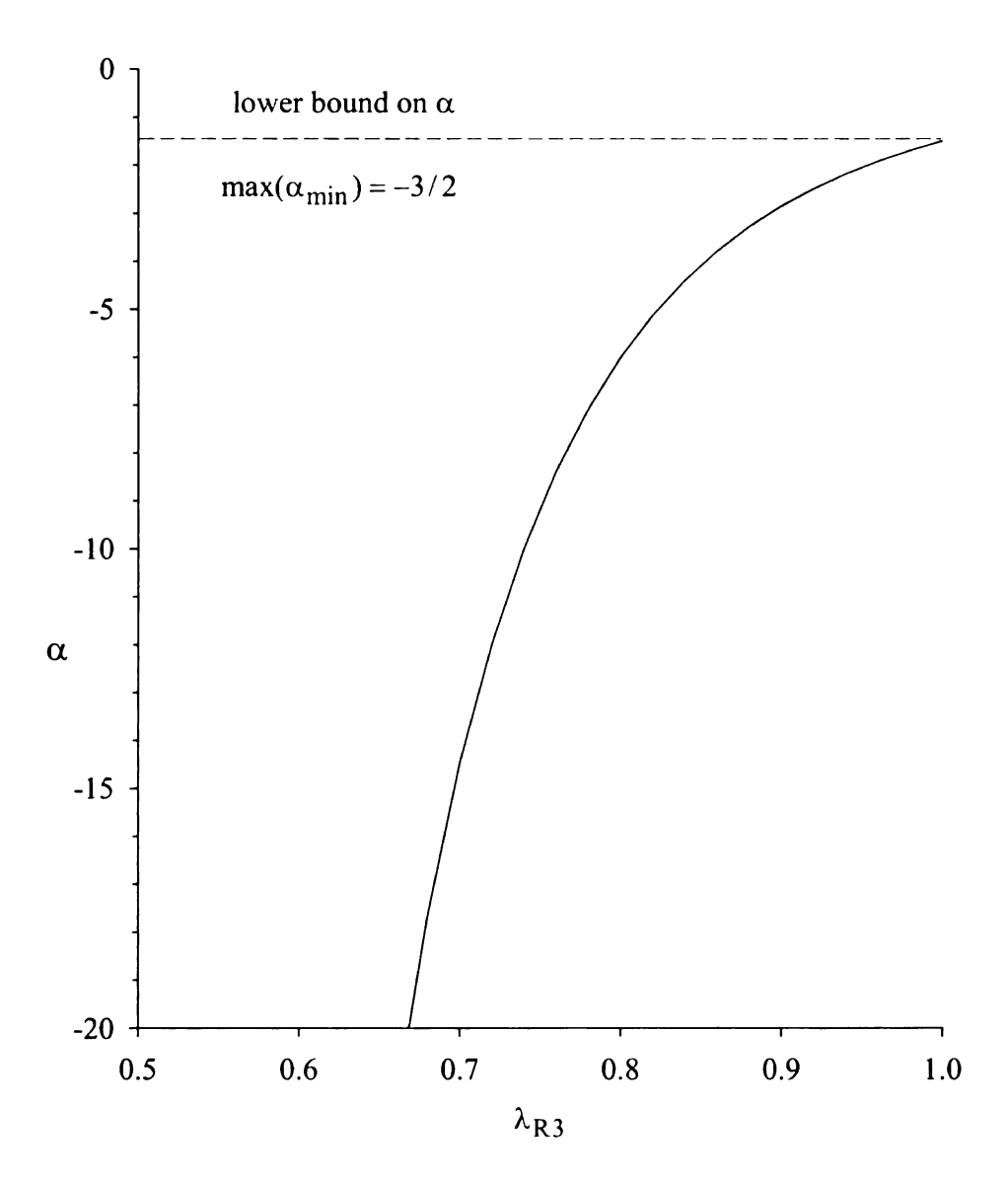


Figure 3.2 The influence of λ_{R3} on α_{min} for λ_{B3} = 1.

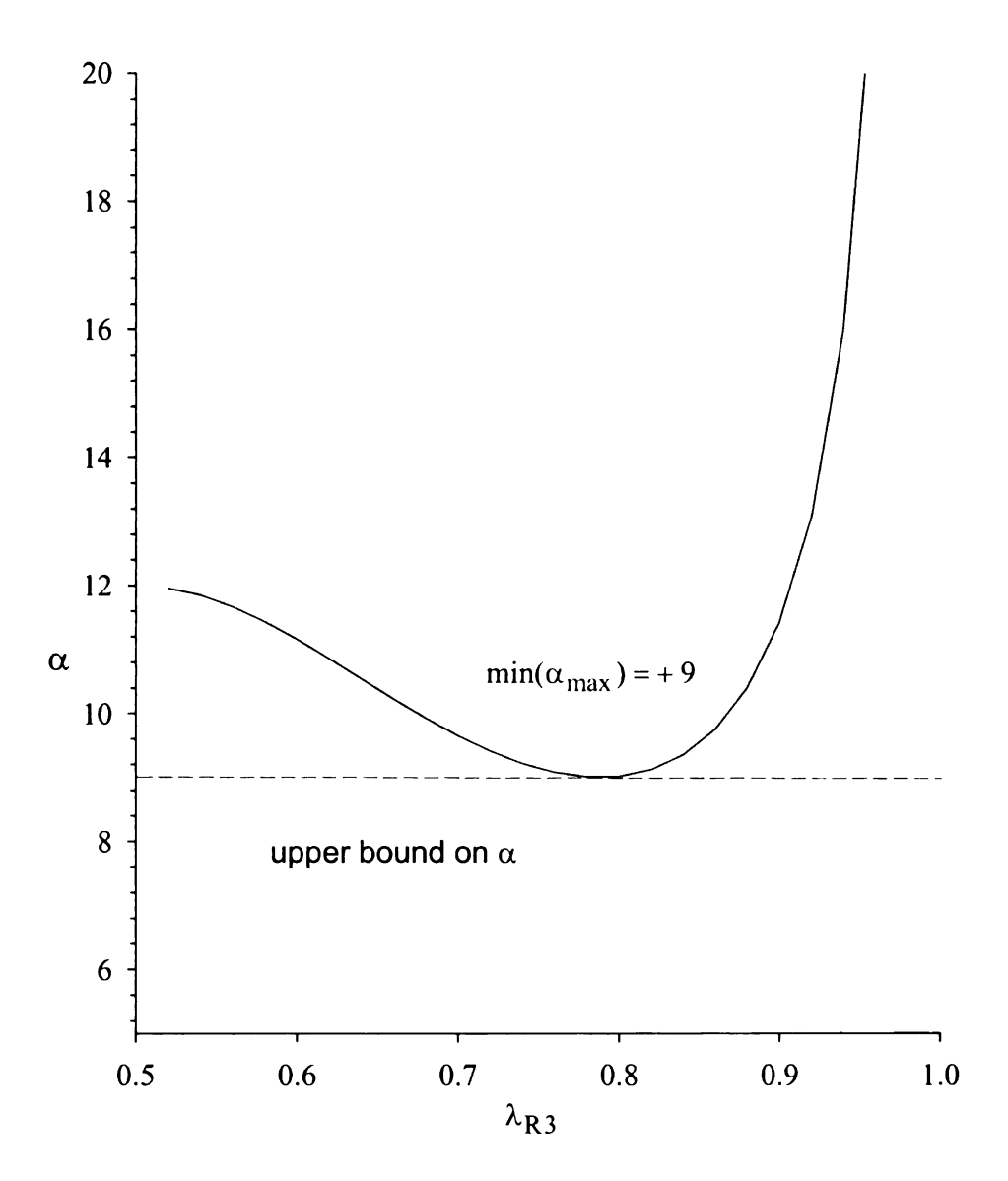


Figure 3.3 The influence of λ_{R3} on α_{max} for λ_{B3} = 1/2.

$$(\lambda_{R1}, \lambda_{R2}, \lambda_{R3}) = (0, 0.2, 0.8) \xrightarrow{\alpha = 9} (0, 0.5, 0.5) = (\lambda_{B1}, \lambda_{B2}, \lambda_{B3}).$$
 (3.24)

For $\alpha > 9$, points on the BC-boundary of the 1st Sextet would be mapped into planar anisotropic states associated with the 6th Sextet. Thus, the upper bound on the α -coefficient eliminates redundant non-negative states whereas the lower bound on the α -coefficient eliminates unrealizable states.

Lower bound on B

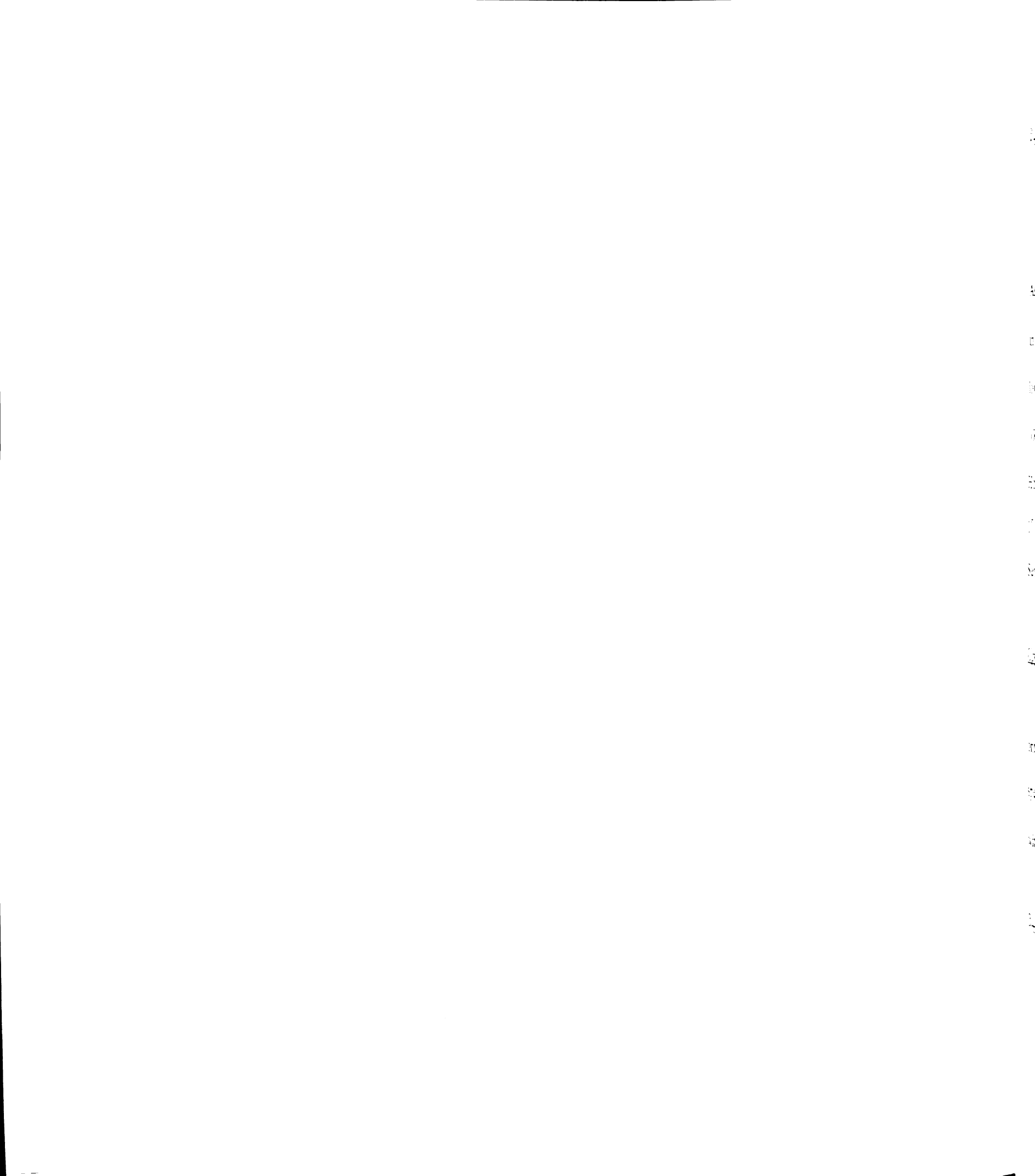
The CH-mapping of $\underline{\underline{R}}$ into $\underline{\underline{\underline{B}}}$ for oblate anisotropic states (see AB-boundary of Figure 3.1) implies that

$$\lambda_{B3} = \lambda_{R3} - \alpha \left[\left(II_R - \frac{1}{3} \right) (\lambda_{R3}^2 - II_R \lambda_{R3}) \right] + \beta \left[27 \det(\underline{\underline{R}}) (\lambda_{R3} - \frac{1}{3}) \right]$$

$$II_R = 2 \left(\frac{1 - \lambda_{R3}}{2} \right)^2 + \lambda_{R3}^2 , \quad \det(\underline{\underline{R}}) = \left(\frac{1 - \lambda_{R3}}{2} \right)^2 \lambda_{R3}$$

$$(3.25)$$

On the AB-boundary (see Figure 3.1), $\lambda_{R2} = \lambda_{R3}$, $\lambda_{R1} = 1 - 2\lambda_{R3}$, and $1/3 \le \lambda_{R3} \le 1/2$. By direct substitution, it follows from Eq. (3.25) that Point B is mapped into itself for all values of α and β ; and, Point A is mapped into itself for all values of the α and β . However, for $\alpha_{min} \le \alpha \le \alpha_{max}$, some interior points on the AB-boundary may not map onto the AB-boundary of the 1st Sextet if β is too small or too large. For a specific value of α and λ_{R3} , Eq. (3.25) implies that a minimum value of β for $\lambda_{B3} = 1/3$ is given by



$$\beta_{\min} = \frac{\frac{1/3 - \lambda_{R3} + \alpha \left[\left(II_R - \frac{1}{3} \right) \left(\lambda_{R3}^2 - II_R \lambda_{R3} \right) \right]}{\left[27 \det(\underline{\underline{R}}) \left(\lambda_{R3} - \frac{1}{3} \right) \right]}$$

$$\lambda_{R3} = \frac{\frac{\text{CH-mapping}}{\alpha_{\min} < \alpha < \alpha_{\max}} \lambda_{B3} = 1/3$$
(3.26)

As indicated by Figure 3.4, a plot of β_{min} vs. λ_{R3} shows that $\max(\beta_{min}) = -1$ for all α in the interval $\alpha_{min} < \alpha < \alpha_{max}$. The parameter $\max(\beta_{min})$ is an *a priori* universal lower bound on the β -coefficient. If $\beta = -1$, then

$$(\lambda_{R1}, \lambda_{R2}, \lambda_{R3}) \rightarrow (1/3, 1/3, 1/3) \Rightarrow (\lambda_{B1}, \lambda_{B2}, \lambda_{B3}) \rightarrow (1/3, 1/3, 1/3).$$
 (3.27)

However, if $\beta < -1$, then some oblate anisotropic states on the AB-boundary between the 1^{st} and 6^{th} Sextets will be mapped into prolate anisotropic states between the 3^{rd} and 4^{th} Sextets. The lower bound on β removes the redundancy of the CH mapping.

Upper bound on \beta

For $\alpha_{min} \leq \alpha \leq \alpha_{max}$, some interior points on the AB-boundary may not map onto the AB-boundary of the 1st Sextet if β is too large. Eq. (3.25) implies that for a specific value of α and λ_{R3} , a maximum value of β occurs for $\lambda_{B3} = 1/2$. Therefore, with $\lambda_{B3} = 1/2$, Eq. (3.25) can be used to define β_{max} as follows:

$$\beta_{\text{PDEx}} = \frac{1/2 - \lambda_{R3} + \alpha \left[(II_R - \frac{1}{3}) \left(\lambda_{R3}^2 - II_R \lambda_{R3} \right) \right]}{\left[27 \det(\underline{\underline{R}}) \left(\lambda_{R3} - \frac{1}{3} \right) \right]}$$

$$\lambda_{R3} \xrightarrow{\text{CH-mapping} \atop \alpha_{\text{min}} < \alpha < \alpha_{\text{max}}} \lambda_{B3} = 1/2$$
(3.28)

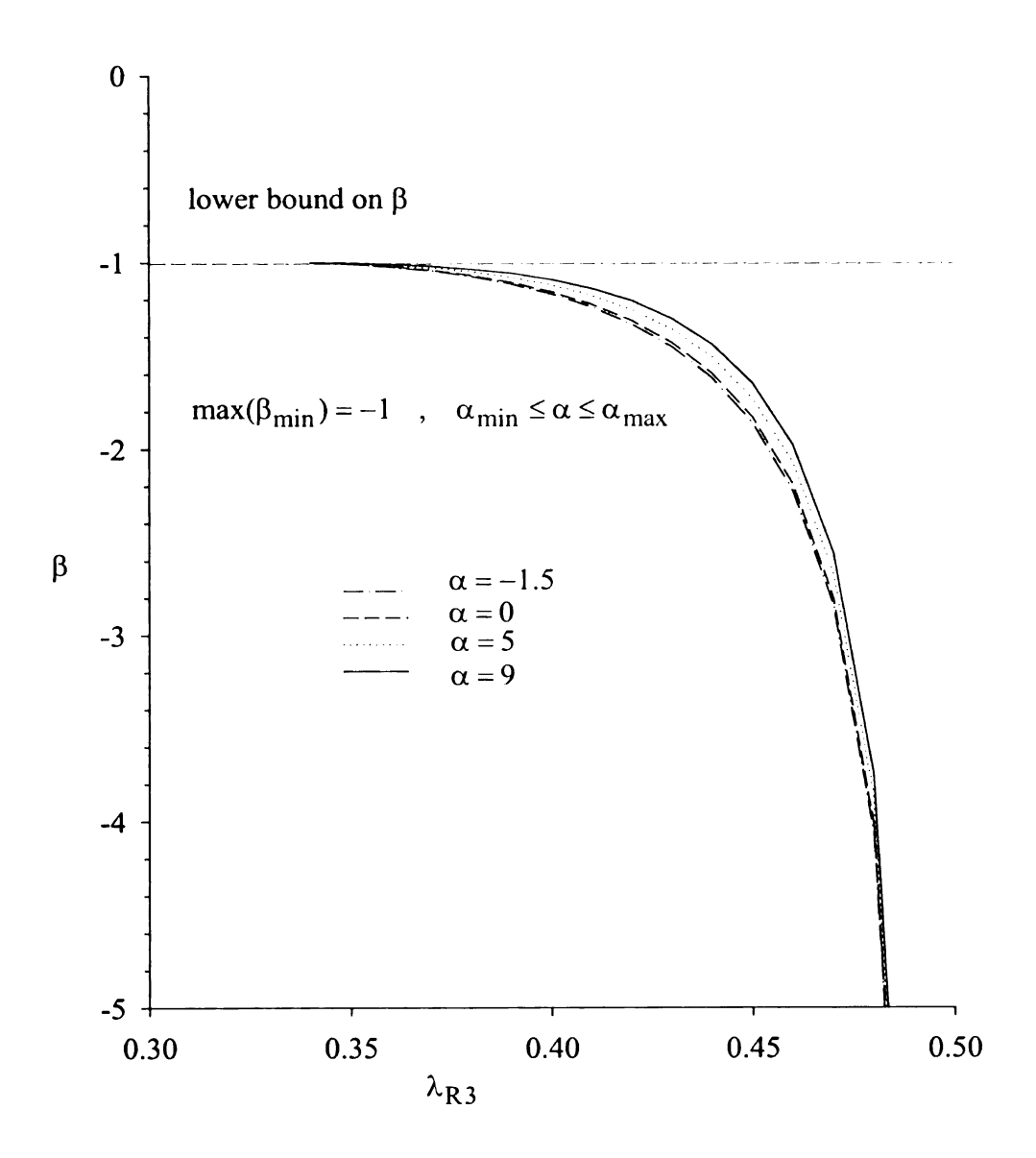


Figure 3.4 The influence of λ_{R3} on β_{min} for λ_{B3} = 1/3 and α_{min} < α < α_{max} .

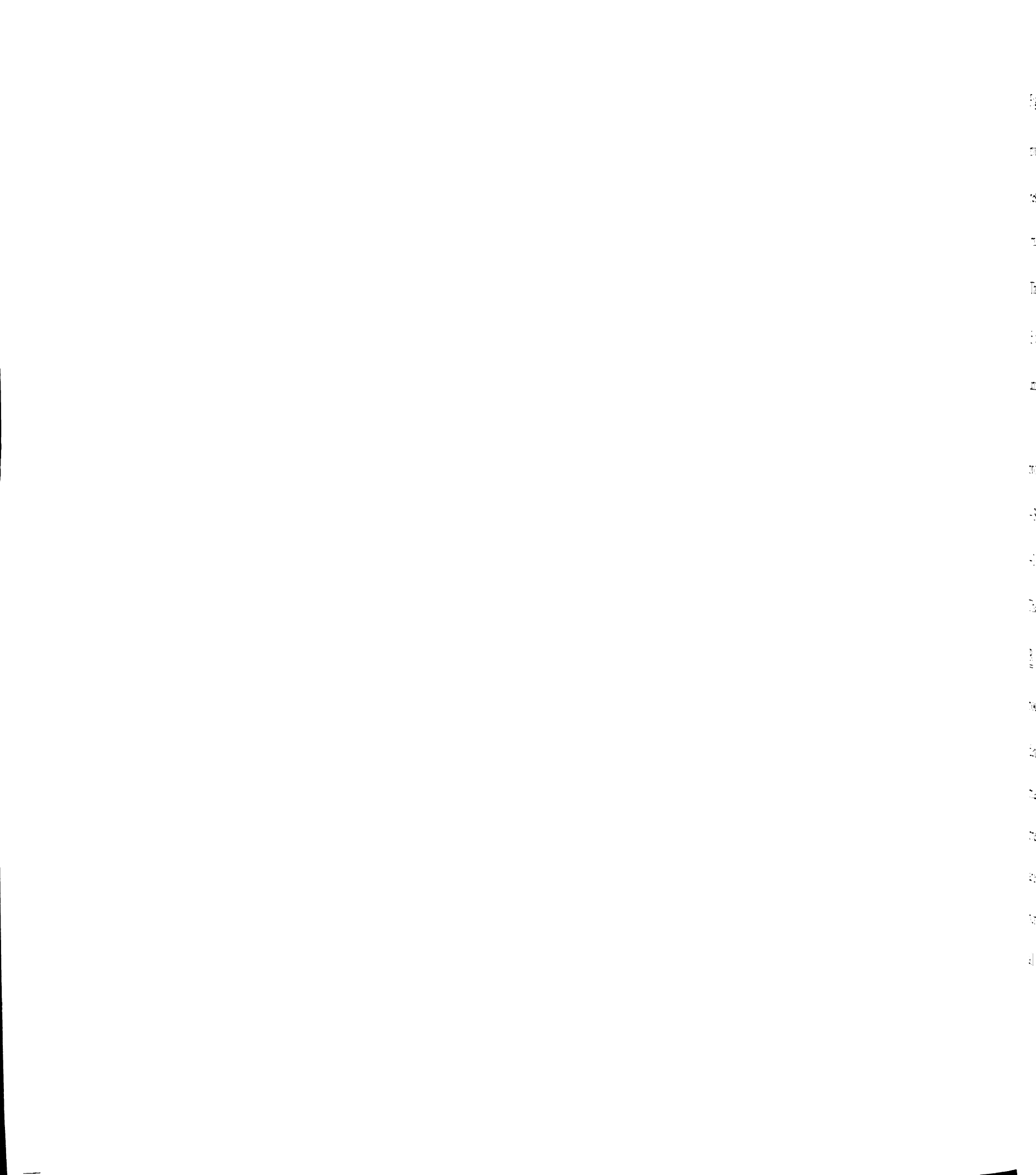


Figure 3.5 shows how β_{max} depends on λ_{R3} for specific values of α . Clearly, the minimum upper bound (i.e., $\min\beta_{max}$) occurs at $\lambda_{R3} \to 1/2$ and depends on α . The results shown in Figure 3.5 can be represented by a linear relation:

$$\min(\beta_{\max}) = \alpha/27 + 4/9$$
 , $\alpha_{\min} \le \alpha \le \alpha_{\max}$. (3.29)

The parameter $\min \beta_{max}$ is an *a priori* universal upper bound on the β -coefficient. If $\beta > \min \beta_{max}$, then a point on the AB-boundary of the 1st Sextet will be mapped into an unrealizable state.

In summary, Eq. (3.20) maps the 1st sextet of the eigenvalue simplex into itself provided α and β satisfy the following two inequalities:

$$-3/2 < \alpha < 9 \tag{3.30}$$

$$-1 < \beta < \alpha / 27 + 4 / 5$$
. (3.31)

The above theoretical inequalities are universal. Since $\underline{\underline{B}}$ has non negative eigenvalues, $\underline{\underline{R}}$ is a priory realizable with non-negative eigenvalues. Figure 3.6 identifies universal bounds for the "extra" anisotropy functions $\alpha(II_R, III_R)$ and $\beta(II_R, III_R)$, which must be determined from experimental and DNS results for benchmark flows. The physical and mathematical significance of Figure 3.6 is that the CH-mapping of the NR-stress into the prestress is non-negative for all turbulent flows provided the "extra" anisotropy functions are within the realizable region developed. This conclusion does not depend on the benchmark flow selected to calibrate the closure. The bounds are universal and apply for all inertial and non-inertial frames of reference.

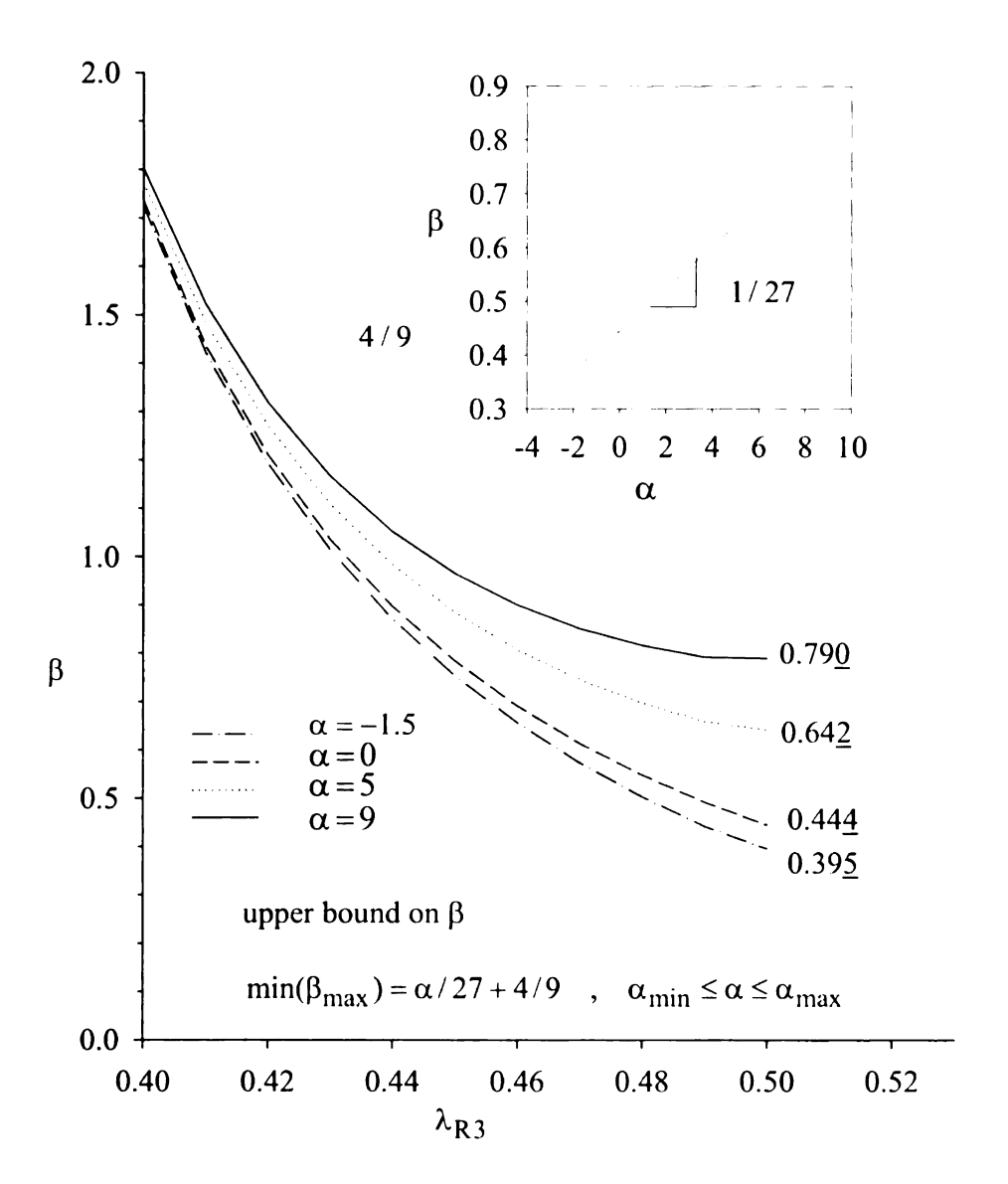


Figure 3.5 The influence of λ_{R3} on β_{max} for λ_{B3} = 1/2 and $\alpha_{min} < \alpha < \alpha_{max}$.

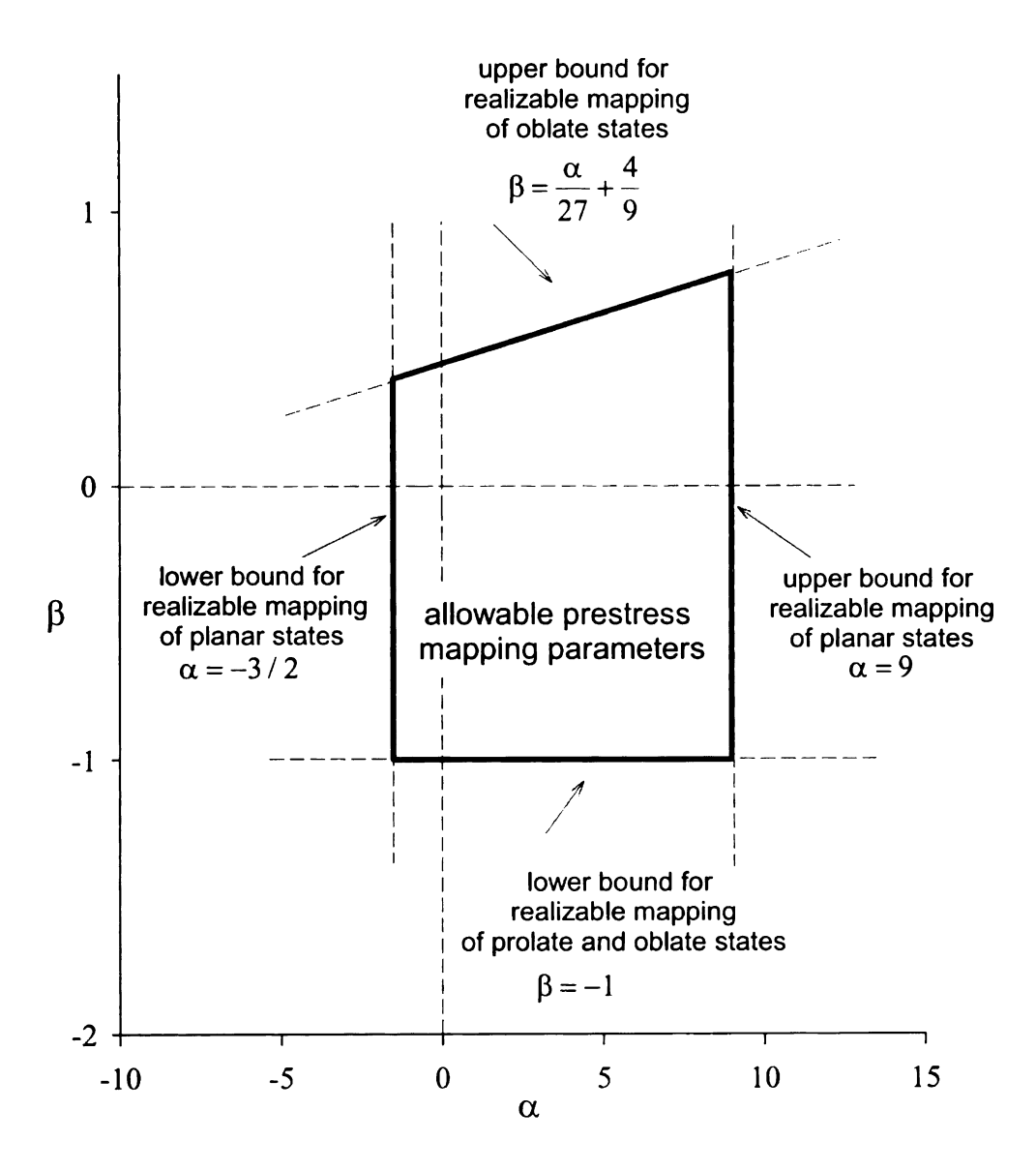


Figure 3.6 Universal Bounds for the "Extra" Anisotropy Functions $\alpha(II_R,III_R)$ and $\beta(II_R,III_R)$.

j. 1,5 31. 151 R 34 1:

্ৰ

T

Different classes of turbulent flows may have different "extra" anisotropy functions, but they must all conform to the universal bounds developed herein. In Chapter 4, non-rotating asymptotic homogeneous shear flow is used as a benchmark flow to estimate α and β . These estimates are used to predict the NR-stress for rotating asymptotic homogeneous shear in Chapter 6. All of the NR-stress solutions to the URAPS-closure are realizable.

3.4 URAPS-Closure

The preclosure equation (Eq. (3.9)) and the prestress closure (Eq. (3.12) can be combined to give a non-linear, implicit, algebraic equation for the NR-stress, referred to herein as the universal realizable anisotropic prestress (URAPS-) closure. The URAPS-closure is a significant generalization of the universal, realizable, isotropic prestress (URIPS-) closure. The resulting URAPS-closure can be formally expressed as

$$\underline{\underline{R}} = \frac{\underline{\underline{A}}^{T} \cdot \underline{\mathcal{B}}(\underline{\underline{R}}) \cdot \underline{\underline{A}}}{\operatorname{tr}(\underline{\underline{A}}^{T} \cdot \underline{\mathcal{B}}(\underline{\underline{R}}) \cdot \underline{\underline{A}})} = \underline{\underline{\mathcal{R}}}(\underline{\underline{K}}, \underline{\underline{R}}) . \tag{3.32}$$

The k- and ε - transport equations adopted for the URAPS-closure are briefly presented in the next section. An important requirement of these scalar-valued partial differential equations is that they should produce positive solutions inasmuch as the turbulent kinetic energy k and the turbulent dissipation ε are by definition positive within the flow domain.

The URAPS-closure is *universally realizable* inasmuch as the predicted NR-stress is *realizable* for all rotating and non-rotating rigid-body frames of reference. A calibrated URAPS-closure provides a means to predict the NR-stress for bounded and for

unbounded flows as well as for statistically stationary and non-stationary flows governed by the RANS-equation. Accuracy of the model for a specific class of flows will depend on the previous theoretical ideas and on the benchmark flows used to determine the closure parameters.

3.5 Turbulent Relaxation Time scale

A single time scale, τ_R has been introduced in the preclosure theory and the k and ϵ equations. Dimensional reasoning suggests that τ_R depends on three local time scales: a viscous time scale, v/k; a turbulent time scale, k/ϵ ; and, a mean field time scale, $\|\langle \underline{F} \rangle\|^{-1}$ that includes the time scale associated with the frame rotation.

$$\tau_{R} \equiv C_{R1} \frac{k}{\varepsilon} \tilde{\tau}_{R}, \text{ where } \tilde{\tau}_{R} = f_{R} (Re_{t}, N_{F})$$
(3.33)

Thus,
$$\tau_R = C_{R1} \tilde{\tau}_R (Re_t, N_F) k / \varepsilon \xrightarrow{Re_t >> 1} C_{R1} \tilde{\tau}_R (\infty, N_F) k / \varepsilon$$
, where $Re_t \equiv k^2 / (v\varepsilon)$,

$$N_F \equiv \frac{k}{\epsilon} \|\underline{\underline{F}}\| = \frac{\text{turbulent time scale}}{\text{mean field time scale}}$$
, and $\|<\underline{\underline{F}}>\| \equiv \sqrt{<\underline{\underline{F}}>:<\underline{\underline{F}}>^T}$. For turbulent flows

near a solid/fluid interface, the influence of the local Reynolds number will have an important impact on $\tilde{\tau}_R$. A model and calibration for $\tilde{\tau}_R$ will be presented in Chapter 4.

3.6 Transport Equations for Turbulent Kinetic Energy and Dissipation

An unclosed transport equation for the kinetic energy (see Appendix A) and unclosed equation for dissipation equation (see Appendix B) can be derived from the dynamic equation for the fluctuating velocity. However, in the k equation (see Eq. 1.9) the dispersion (or mixing) terms must be modeled as discussed in Chapter 1. Modeled

transport equation presented in Eq. (1.11) is used in this research. The URAPS-closure relies on positive solutions for the k and ε equations for all flows.

The dispersion operator in the k-equation and the ϵ -equation are the same. An interesting consequence of this assumption is that these equations support the existence of self-similar behavior. That is if $k(\underline{x},t)$ is proportional to $\epsilon(\underline{x},t)$ within a finite spacetime domain, then

$$\frac{\tau_{R}}{k/\epsilon} = \frac{C_{P} \mathcal{P} - C_{D} \epsilon}{\mathcal{P} - \epsilon} \quad , \quad \text{provided } \frac{k}{\epsilon} = \text{constant }.$$
 (3.34)

The calibration for the "production" and dissipation coefficients, C_P and C_D , as well as the turbulent transport time τ_R must be developed so that solutions to transport equations Eqs. (1.9) and (1.11) yield non-negative solutions for all turbulent flows. In the following chapter, these are determined from benchmark flows discussed in Chapter 2.

3.7 Fixed-Point Mapping and Solution Strategy of the URAPS-closure

Solutions to a calibrated URAPS-equation can be developed by successive substitution. Thus, if $\underline{\mathbb{R}}_n$ in a positive operator, then the following iterative algorithm yields another positive operator $\underline{\mathbb{R}}_{n+1}$ that converges to a fixed point of the closure equation.

$$\underline{\underline{R}}_{n+1} = \frac{\underline{\underline{A}}^{T} \cdot \underline{\underline{\mathcal{B}}}(\underline{\underline{R}}_{n}) \cdot \underline{\underline{A}}}{tr(\underline{\underline{A}}^{T} \cdot \underline{\underline{\mathcal{B}}}(\underline{\underline{R}}_{n}) \cdot \underline{\underline{A}})} = \underline{\underline{\mathcal{R}}}(\tau_{R} < \underline{\underline{F}} > , \underline{\underline{R}}_{n}) \quad . \tag{3.35}$$

An initial guess starting at the isotropic distribution of energy, the prestress for the IPS closure would also be isotropic.

$$\underline{\underline{R}}_{0} = \frac{\underline{\underline{I}}}{3} \implies \\
\underline{\underline{B}}_{1} = \underline{\underline{R}}_{0} + C_{1}(\underline{\underline{R}}_{0} - \frac{1}{3}\underline{\underline{I}}) + C_{2}(\underline{\underline{R}}_{0} \cdot \underline{\underline{R}}_{0} - II_{R_{0}} \underline{\underline{R}}_{0}) = \frac{\underline{\underline{I}}}{3}$$
(3.36)

$$\underline{\underline{R}}_{1} = \frac{\underline{\underline{A}}^{T} \cdot \underline{\underline{B}}_{1}(\underline{\underline{R}}_{0}) \cdot \underline{\underline{A}}}{\operatorname{tr}[\underline{\underline{A}}^{T} \cdot \underline{\underline{B}}_{1}(\underline{\underline{R}}_{0}) \cdot \underline{\underline{A}}]} = \frac{\underline{\underline{A}}^{T} \cdot \underline{\underline{A}}}{\operatorname{tr}[\underline{\underline{A}}^{T} \cdot \underline{\underline{A}}]} \quad (= \underline{\underline{K}}) \quad \Rightarrow \\
\underline{\underline{B}}_{2} = \underline{\underline{K}} + C_{1}(\underline{\underline{K}} - \frac{1}{3}\underline{\underline{I}}) + C_{2}(\underline{\underline{K}} \cdot \underline{\underline{K}} - II_{K} \underline{\underline{K}})$$
(3.37)

In subsequent iterations, re-distribution of energy starts to develop for $\underline{\underline{R}}$ which as a result yields anisotropic distribution in $\underline{\underline{B}}$.

$$\underline{\underline{R}}_{2} = \frac{\underline{\underline{A}}^{T} \cdot \underline{\underline{B}}_{2}(\underline{\underline{R}}_{1}) \cdot \underline{\underline{A}}}{\operatorname{tr}[\underline{\underline{A}}^{T} \cdot \underline{\underline{B}}_{2}(\underline{\underline{R}}_{1}) \cdot \underline{\underline{A}}]} \Rightarrow \\
\underline{\underline{B}}_{3} = \underline{\underline{R}}_{2} + C_{1}(\underline{\underline{R}}_{2} - \frac{1}{3}\underline{\underline{I}}) + C_{2}(\underline{\underline{R}}_{2} \cdot \underline{\underline{R}}_{2} - \operatorname{II}_{\underline{R}_{2}} \underline{\underline{R}}_{2})$$
(3.38)

.

The iterations are proceeded till the successive substitution has converged when each of the components of the Reynolds stress remain the same up to certain significant figures.

$$\underline{\underline{R}}_{n+1} = \frac{\underline{\underline{A}}^{T} \bullet \underline{\underline{B}}_{n+1}(\underline{\underline{R}}_{n}) \bullet \underline{\underline{A}}}{tr[\underline{\underline{A}}^{T} \bullet \underline{\underline{B}}_{n+1}(\underline{\underline{R}}_{n}) \bullet \underline{\underline{A}}]}$$
(3.39)

$$\underline{\underline{B}}_{n+1} = \underline{\underline{R}}_n + C_1(\underline{\underline{R}}_n - \frac{1}{3}\underline{\underline{I}}) + C_2(\underline{\underline{R}}_n \cdot \underline{\underline{R}}_n - II_{R_n}\underline{\underline{R}}_n)$$

$$\lim_{n \to \infty} \underline{\underline{R}}_n = \underline{\underline{R}}^{\hat{\gamma}_{r}} \ni \underline{\underline{\mathcal{R}}} (\tau_R < \underline{\underline{F}} > , \underline{\underline{R}}^{\hat{\gamma}_{r}}) = \underline{\underline{R}}^{\hat{\gamma}_{r}}$$
(3.40)

In the following Chapter 4, the iteration procedure is illustrated to converge to a fixed final solution independent of the realizable three component initial condition given, for simple shear flows.

3.8 Conclusions

- 1. Figure 3.7 presents a summary of the above URAPS-closure. The various steps in development of the implicit algebraic closure are shown starting from the Navier Stokes equation. An integral analysis of the equation for fluctuating velocity using Green's function is used to relate turbulent corrections to the mean field kinematics. A smoothing approximation based on the assumption that turbulent correlations have finite memories yields the preclosure theory.
- 2. The preclosure theory for non-inertial frames relates the Reynolds stress to the prestress though a kinematic operator, $\underline{\underline{K}} = \tau_R (\nabla < \underline{\underline{u}} > +2 \underline{\Omega})$ that takes into account both the mean velocity gradient and the angular velocity of the rotating frame. The preclosure time scale τ_R depends on the turbulent time scale, the mean field time—scale, the time scale associated with frame rotation, and a viscous time scale.
- 3. An implicit closure for the Reynolds stress is obtained by relating the prestress to the NR-stress stress itself. Based on this self-consistent hypothesis, the CH-theorem has been used to find an irreducible representation for the prestress (see Eq.(3.19)). In order for the resultant closure to provide realizable solutions for the NR-stress, CH-coefficients in the prestress relation must remain within the realizable bounds given by Ineq.(3.30) and Ineq.(3.31). The boundaries of the realizable domain are identified by analyzing the eigenvalue relation for R and B (see Eq. (3.20)) on the prolate and oblate anisotropic boundaries. The URAPS-closure is thus a priori realizable for all flows.

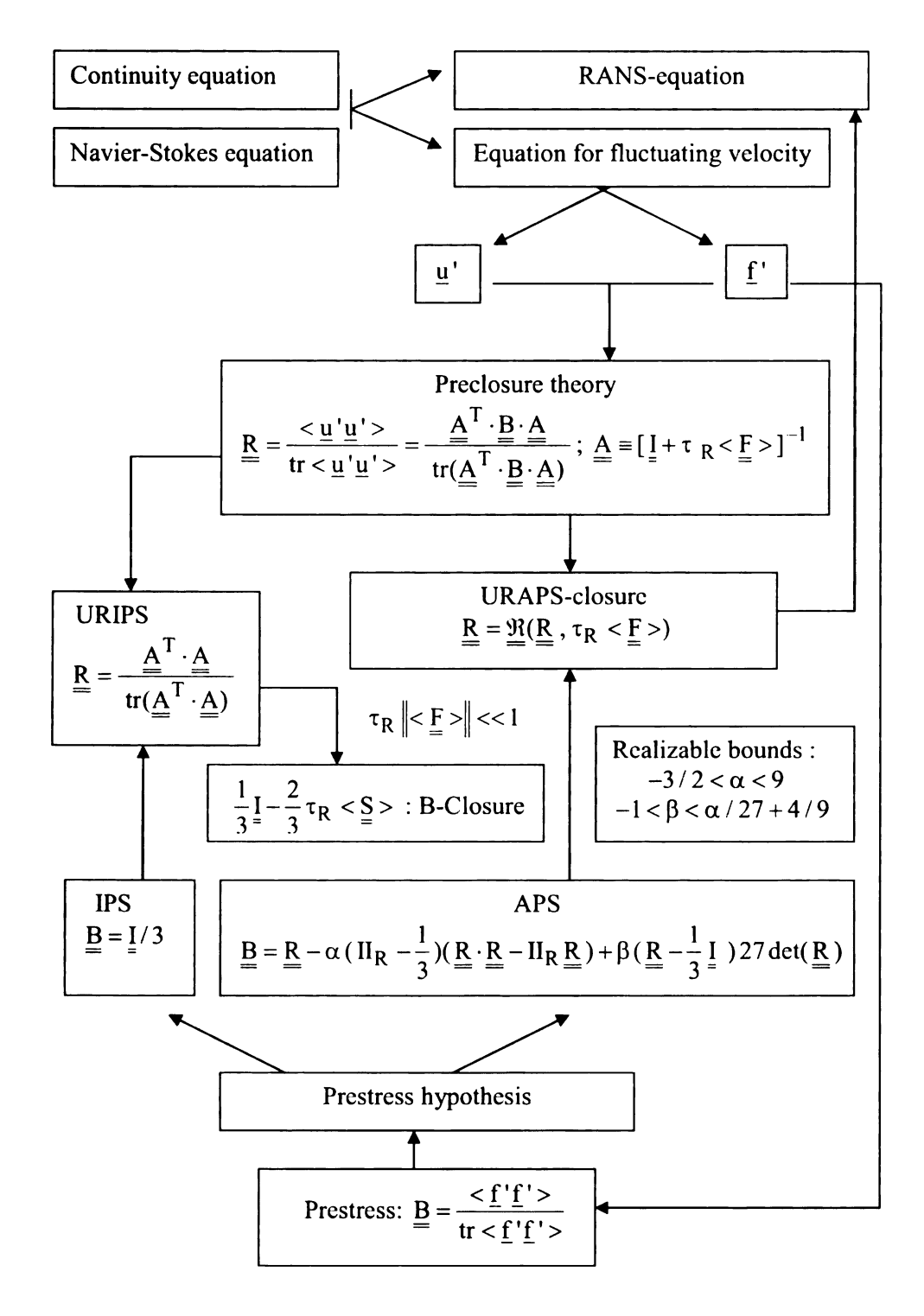


Figure 3.7 Summary of URAPS-Closure

4. Successive substitution method can be used to solve the URAPS-closure starting with an initial state say, isotropic state. The results for the prestress and subsequently the NR-stress are updated until a converged state for the NR-stress is obtained based on the convergence criteria used.

CHAPTER 4

MODEL CALIBRATION

4.1 Introduction

The URAPS-closure requires the determination of the following four dimensionless phenomenological parameters: α , β , C_P , C_D and a model for the turbulent timescale $\tau_{\mbox{\scriptsize R}}\,.$ In this chapter, the parameters for the URAPS-closure are estimated from the following benchmark flows. 1) non-rotating homogeneous decay; 2) rotating homogeneous decay; and, 3) non-rotating asymptotic homogeneous shear as discussed in Chapter 2. Transport equations for k and ε are simplified for homogeneous flows because of the absence of production and diffusive transport. The coefficient of dissipation is estimated from this flow as described in Section 4.2. From the theoretical analysis of energy spectrum in rotating homogeneous flows, the dimensionless turbulent time scale $\tilde{\tau}_R$ in Eq. (3.33) is formulated in Section 4.3, along with the specification of the coefficients. The coefficients α and β in the prestress relation are estimated using the components equations for the URAPS-closure and from the knowledge of asymptotic states described in Chapter 2 (see Eq. (2.25)) for homogeneous shear using an optimization procedure. Optimization also yields the value of C_{R1}, associated with model for τ_R in Eq. (3.33). Finally, the coefficient C_P is also evaluated from the asymptotic equation for homogeneous shear flows.

4.2 Dissipation Coefficient

For non-rotating isotropic homogeneous decay at high initial turbulent Reynolds numbers, the NR-stress is isotropic and the decay of turbulent kinetic energy and turbulent dissipation are governed by the differential equations, Eqs.(2.29) and (2.30) as described in Chapter 2. The turbulent time scale for this flow is $\tau_R = C_{R1} \frac{k}{\epsilon} \quad \text{for } Re_o \equiv \frac{k_0^2}{v\epsilon_0} \gg 1 \text{ (i.e., } \underline{\Omega} = \underline{0} \text{), } N_F = 0 \text{ , } \tilde{\tau}_R(N_F) = 1 \text{). If } C_D \text{ and } C_{R1}$

are constant, then the autonomous Eqs. (2.29) and (2.30) imply that

$$\frac{d\varepsilon}{dk} = +\frac{C_D}{C_{R1}} \frac{\varepsilon}{k} \implies \ln(\frac{\varepsilon}{\varepsilon_0}) = \frac{C_D}{C_{R1}} \ln(\frac{k}{k_0}), \qquad (4.2)$$

where $k(0) = k_0$ and $\epsilon(0) = \epsilon_0$. Figure 4.1 shows the decay process in the k- ϵ plane parameterized by the dimensionless decay time $\tilde{t} \equiv t \, \epsilon_0 / k_0$. The classical experimental data of Comte-Bellot and Corrsin (1971) for $Re_o = 354$ and 769 (see Figure 2.17) described in Chapter 2 are used to estimate the coefficient C_D/C_{R1} . The DNS results of Mansour and Wray (1994) and experimental results of Comte-Bellot and Corrsin (1971) imply that $C_D/C_{R1} \doteq 1.83$. Parks (1997) incorporated a Reynolds number dependence in the coefficient C_D/C_{R1} based on a comprehensive temporal analysis of the classical Kármán-Howarth equation together with the experimental data of Tavoularis et al. (1978) and the DNS results of Mansour and Wray (1992). In this research, C_D/C_{R1} is assumed to be a constant for $Re_t \gg 1$. For high Reynolds number homogeneous decay, $k(t) \geq \epsilon(t) \rightarrow 0$ and $Re_t \rightarrow \infty$ as $\tilde{t} \rightarrow \infty$. The temporal development of k and ϵ reconstructed for homogeneous flows as well as predictions for rotating homogeneous

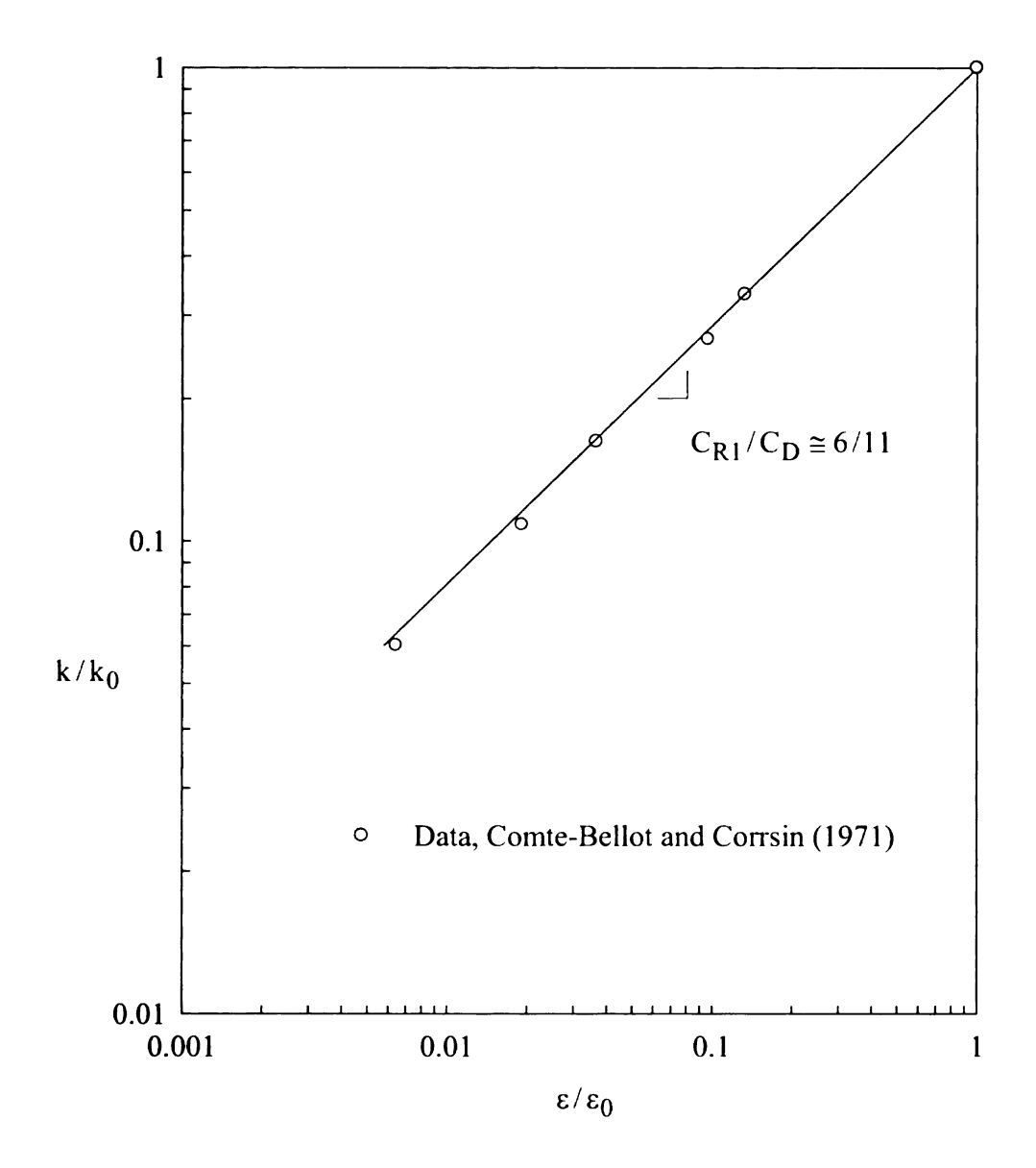


Figure 4.1 Isotropic Homogeneous Decay in an Inertial Frame of Reference

flows which include this coefficient $C_D/C_{R1} \doteq 1.83$, are presented in Chapter 5. In the following section 4.3, the model for turbulent transport time is discussed.

4.3 Turbulent Transport Time

Turbulent relaxation time scale τ_R is which appears in the preclosure theory in Eq. (3.33) is described as a function of the characteristic time scales of turbulence using dimensional reasoning. In Eq. (3.33), the dimensionless turbulent transport time $\tilde{\tau}_R(Re_t,N_F)$ is defined so that $\tilde{\tau}_R(\infty,0)=1$. $\tilde{\tau}_R$ needs to be determined so that solutions to the k-equation and the ϵ -equation are non-negative functions for all turbulent flows. Analysis of the energy spectrum provides information on the dependence of $\tilde{\tau}_R$ on rotation rate. For the case of rotating homogeneous turbulence, the energy spectrum deviates from the Kolmogorov's -5/3 dependence on wave number κ in inertial subrange and shows a κ^{-2} dependence instead (see Zeman, 1995 and Zhou, 1994). In the inertial subrange, the spectrum is represented as

$$E(\kappa) = C_K(\varepsilon)^{2/3} \kappa^{-5/3} \qquad \kappa >> (\Omega^3 / \varepsilon)^{1/2}$$
(4.3)

$$E(\kappa) = C_{\Omega}(\epsilon \Omega)^{1/2} \kappa^{-2} \qquad \kappa << (\Omega^{3}/\epsilon)^{1/2}$$
(4.4)

where κ is the wave number, C_K is Kolmogorov's constant and $C_\Omega = C_K^{3/4}$. From the spectrum equations (Eqs. 4.3 and 4.4), Park and Chung, (1999) derived an equation for k by integrating the energy spectrum over the entire range of wave length and also an equation for ϵ by differentiating the k equation with time. This analysis of the spectrum, identified the variation of the C_D/τ_R for the dissipation equation to vary with

dimensionless rotation rate $|\Omega| k/\epsilon$. The complete summary of the derivation of the key results are presented in Appendix F. Based on Eq. (F.42) for the coefficient of dissipation, a similar dependence on rotation rate is adopted into the model for turbulent time scale. A, non-unique, empirical equation for $\tilde{\tau}_R$ is proposed:

$$\tilde{\tau}_{R} = \frac{(1 + C_{R3} N_{F}^{n})}{(1 + C_{R2} N_{F}^{n})}.$$
(4.5)

The coefficients are assumed to be universal constants and can be determined by well-defined benchmark flow and applied to any other flow. In the limiting cases, $\tilde{\tau}_R(N_F \to 0) = 1 \quad \text{and} \quad \tilde{\tau}_R(N_F \to \infty) = C_{R3}/C_{R2}. \text{ The dependence } \tilde{\tau}_R \text{ on the group}$ $\frac{k}{\epsilon} \| \underline{F} \| \quad \text{can be deduced from Eq.}(F.42) \text{ to be } 3/2 \text{ since for homogeneous flows,}$ $\frac{k}{\epsilon} \| \underline{F} \| = 2\sqrt{2} |\Omega| k/\epsilon.$

Figure 4.2 shows the variation of $\frac{C_D}{C_{R1}} \frac{1}{\tilde{\tau}_R}$ in Eq. (F.42) with $|\Omega| k/\epsilon$. The following are

the noticeable features of the Figure 4.2.

$$\frac{C_{D}}{C_{R1}} \frac{1}{\tilde{\tau}_{R}} = \begin{cases}
\frac{11}{6} &, & \text{for } |\Omega| \, k/\epsilon = 0 \quad (N_{F} = 0) \\
2 &, & \text{for } |\Omega| \, k/\epsilon = 1 \quad (N_{F} = 2\sqrt{2}) \\
\frac{8}{3} &, & \text{for } |\Omega| \, k/\epsilon = \infty \quad (N_{F} \to \infty)
\end{cases} \tag{4.6}$$

(Note that from the above points, it can be seen that $\frac{C_D}{C_{R1}} \frac{(1 + C_{R2}(2\sqrt{2})^{3/2})}{(1 + C_{R3}(2\sqrt{2})^{3/2})} = 2$ and

$$\frac{C_D}{C_{R1}} \frac{C_{R2}}{C_{R3}} = \frac{8}{3}$$
). From Eq. (4.6), with $\frac{C_D}{C_{R1}} = \frac{11}{6}$, the estimates for the coefficients are:

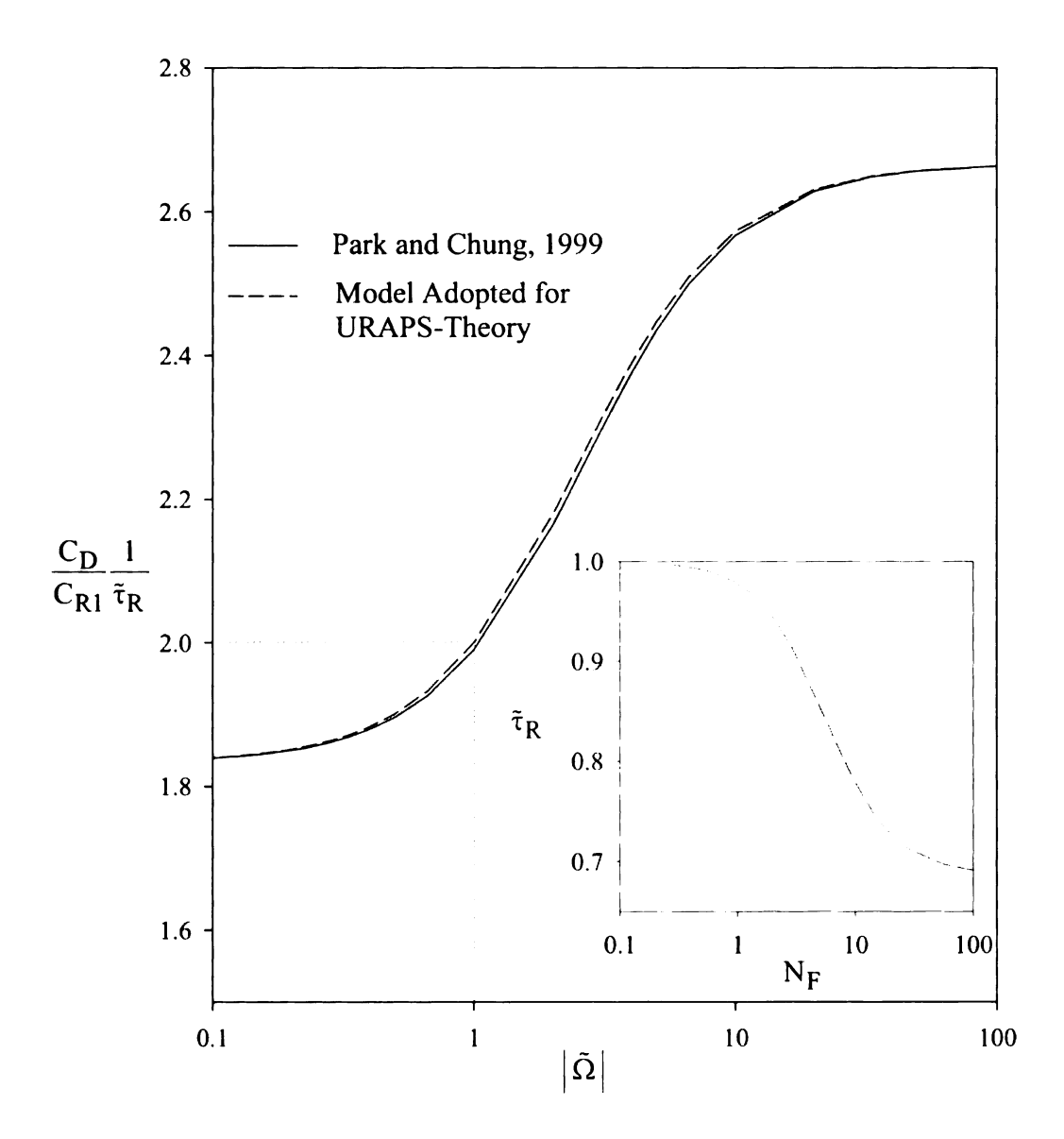


Figure 4.2 The Influence of $\left|\tilde{\Omega}\right| (\equiv \left|\Omega\right| k/\epsilon)$ on the Turbulent Transport Time Scale

$$(C_{R2}, C_{R3}) = (0.0764, 0.0526)$$
 (4.7)

The variation of $\tilde{\tau}_R$ with N_F with the above coefficients and n=3/2 is shown in the Figure 4.2. For $0 < N_F < \infty$, $\tilde{\tau}_R$ varies as $0.69 < \tilde{\tau}_R < 1$ with smaller values of $\tilde{\tau}_R$ corresponding to larger values of N_F . The model reconstruction in the phase plane of k and ϵ for the limiting cases discussed in Eq. (4.6) are discussed in Chapter 5 along with predictions for NR-stress distribution for rotating homogeneous flows using the above calibrated model for turbulent time scale. In the forgoing Section 4.4, the two CH-coefficients related to the "extra" anisotropy terms in the prestress are determined.

4.4 Coefficients of First and Second-Order "Extra" Anisotropy (α and β)

In the following analysis, first the ratio of β/α is obtained from the analysis of the component equations of URAPS-equation for homogeneous shear and using the experimental results described in Table 4.1. All the NR-stress components from the experimental data for asymptotic states cannot be exactly satisfied by the URAPS closure. So an optimization strategy is used to find the coefficients (α and C_{R1}) that closely recover the experimental values.

For non-rotating asymptotic homogeneous shear, the algebraic URAPS-equation depends on three dimensionless groups: N_{Γ} ($\equiv C_{R1}\tilde{\tau}_R \tilde{\Gamma}$); α ; and, β . For simple shear, a relation for the "extra" anisotropy coefficients and the components of the NR-stress can be obtained from an analysis of the component equations of URAPS-equation as shown in Eq. (4.8) below. For details of the derivation, see Appendix G (Eq. G.30)

Table 4.1 Optimum URAPS Closure Coefficients and Stress Components Compared with the Experimental Results of Asymptotic States for Homogeneous Shear.

Model Statistic →	N _F	R _{xx}	R _{yy}	R _{zz}	-R _{yz}	N _Γ	α	-β	C_{R1}
experimental data (Tavoularis and Karnik, 1989)	4. <u>2</u>	0.2 <u>4</u>	0.20	0.5 <u>6</u>	0.1 <u>7</u>	n/a	n/a	n/a	n/a
APS-closure	4. <u>2</u>	0.2 <u>5</u>	0.20	0.5 <u>5</u>	0.1 <u>9</u>	0.01 <u>3</u>	0.1 <u>0</u>	0.01 <u>0</u>	0.003 <u>6</u>

$$\frac{\beta}{\alpha} = +3 \frac{(II_R - \frac{1}{3})}{27 \det(\underline{R})} \frac{R_{xx} R_{yy}}{(R_{xx} - R_{yy})} (R_{xx} - R_{yy} - \frac{R_{yz}^2}{R_{yy}}). \tag{4.8}$$

where $II_R = \underline{R} : \underline{R} = R_{xx}^2 + R_{yy}^2 + R_{zz}^2 + 2R_{yz}^2$ and $det(\underline{R}) = R_{xx} R_{yy} R_{zz} - R_{xx} R_{yz}^2$ Eq.(4.8) is used herein to estimate β/α from self-similar (asymptotic) homogeneous shear measurements of Tavoularis and Karnik (1989) with $\tilde{\Gamma} = N_F = 4.2$ summarized in Table 4.1. The components of the Reynolds stress listed in Table 4.1 imply that $\lambda_{R1} = 0.134$; $\lambda_{R2} = 0.236$; and, $\lambda_{R3} = 0.630$. Thus, $det(\underline{R}) = 0.020$ and $II_R = 0.47$. Therefore, the CH-ratio, defined by Eq.(4.8), is $\beta/\alpha = -0.096$. The important conclusion from this estimate is that $\beta/\alpha < 0$; and, $\beta/\alpha \cong -0.1$. For non-rotating simple shear flows, the primary normal stress difference, $R_{zz} - R_{yy}$, is positive; and, the secondary normal stress difference, $R_{yy} - R_{xx}$, is negative (i.e., $R_{yy} < R_{xx} < R_{xx}$) as discussed in Chapter 2. This observation implies that the CH-coefficients α and β for homogeneous simple shear satisfy the following inequalities: $\alpha > 0$ and $\beta < 0$.

The remaining two groups N_{Γ} and α (with $\beta=-0.1\,\alpha$) are estimated by minimizing the following optimization metric over a two dimensional domain where the components of the NR-stress are $R_{xx}^{exp}=0.24$, $R_{yy}^{exp}=0.2$, $R_{zz}^{exp}=0.56$, and $R_{yz}^{exp}=-0.17$ listed in Table 4.1.

 $\Psi(N_{\Gamma},\alpha,\beta)$

$$\equiv \left[\left(\frac{R_{xx}^{APS} - R_{xx}^{exp}}{R_{xx}^{exp}} \right)^2 + \left(\frac{R_{yy}^{APS} - R_{yy}^{exp}}{R_{yy}^{exp}} \right)^2 + \left(\frac{R_{zz}^{APS} - R_{zz}^{exp}}{R_{zz}^{exp}} \right)^2 + \left(\frac{R_{yz}^{APS} - R_{yz}^{exp}}{R_{yz}^{exp}} \right)^2 \right]^{1/2} (4.9)$$

A search is conducted over a two dimensional domain defined as $0 \le N_{\Gamma} \le 1$, $0 < \alpha \le 9$, $\beta = -0.1\alpha$. Figure 4.3 shows several graphs of how $\Psi(N_{\Gamma}, \alpha, \beta)$ depends on N_{Γ} for a fixed value of α . The search is conducted subject to the constraint implied by Eq.(4.9) above. The method of successive substitution is used to find the solution to the URAPS-equation for each value of N_{Γ} . Figures 4.3 and 4.4. show how the optimization is done. Figure 4.3 shows the influence of the "extra" anisotropy coefficient α on the constrained optimization metric Ψ_{min}^{α} , defined as follows

$$\Psi_{\min}^{\alpha} \equiv \min_{N_R} (\Psi|_{\alpha}) , \quad \beta = -0.1 \alpha = \text{constant}.$$
(4.10)

For each fixed value α , the URAPS-equation for the NR-stress was solved for several values of N_{Γ} in order to determine Ψ^{α}_{min} . Figure 4.3 shows an example of various curves constructed with $\alpha=0.25,0.1,1,5$ and $0< N_{\Gamma}<1$. There appears a Ψ^{α}_{min} for each α . The $(N_{\Gamma})^{\alpha}_{min}$ corresponding to each of those Ψ^{α}_{min} are also shown in the figure. Figures 4.3 and 4.4 show that the minimum of $\Psi(N_{\Gamma},\alpha,\beta)$ subject to the constraint defined by Eq.(4.9) is almost the same for α in the range $0<\alpha<1$ with $\min(\Psi^{\alpha}_{min})\cong 0.153\pm 0.05$.

Figure 4.5 shows the locus of anisotropic states of the NR-stress predicted by the URAPS-closure for four different values of the second-order "extra" anisotropy

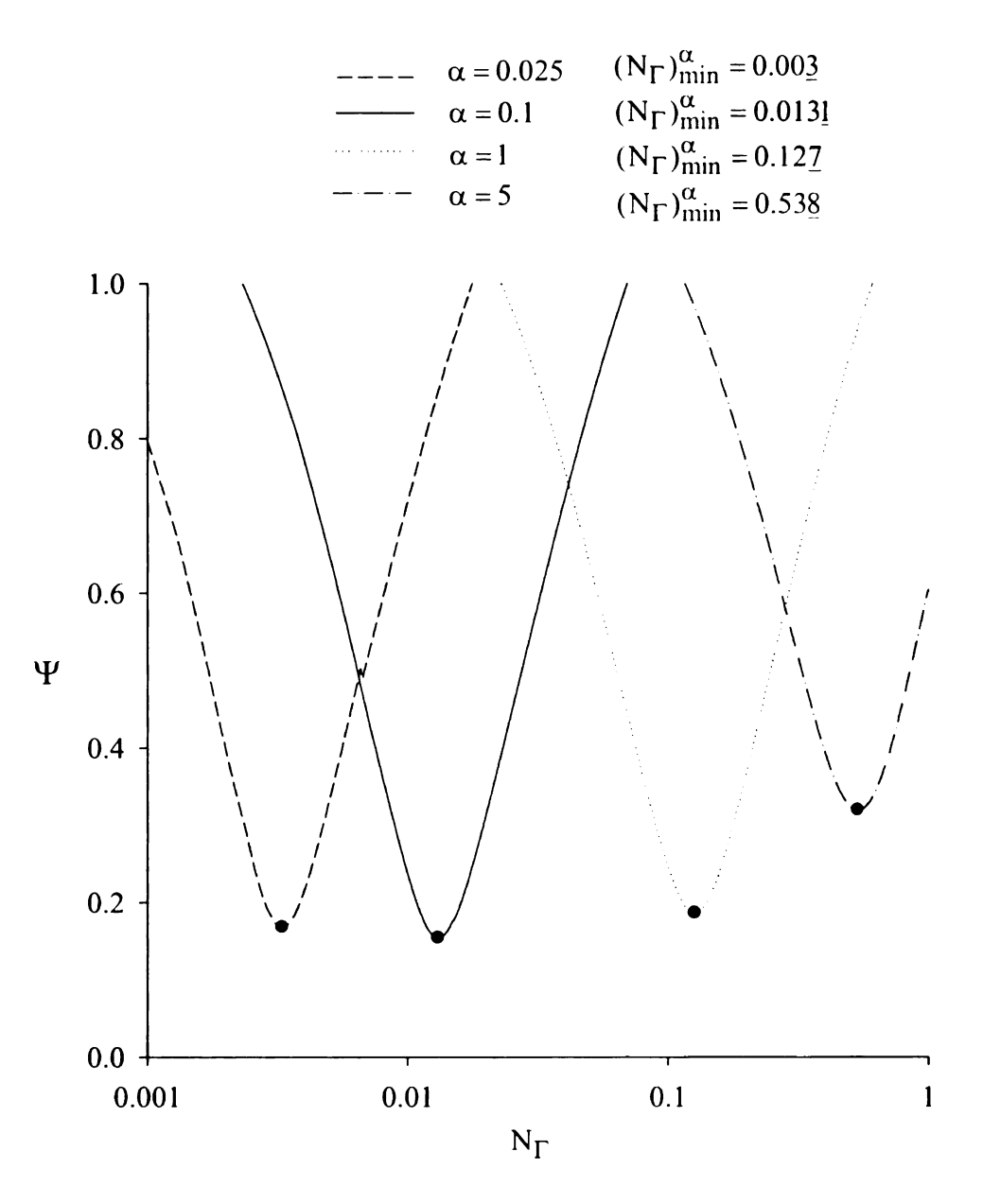


Figure 4.3 Constrained Optimization Strategy for Determining the "Extra" Anisotropy Coefficients, α and β , and the Dimensionless Transport Group, N_{Γ} , for Non-Rotating Asymptotic Homogeneous Shear.

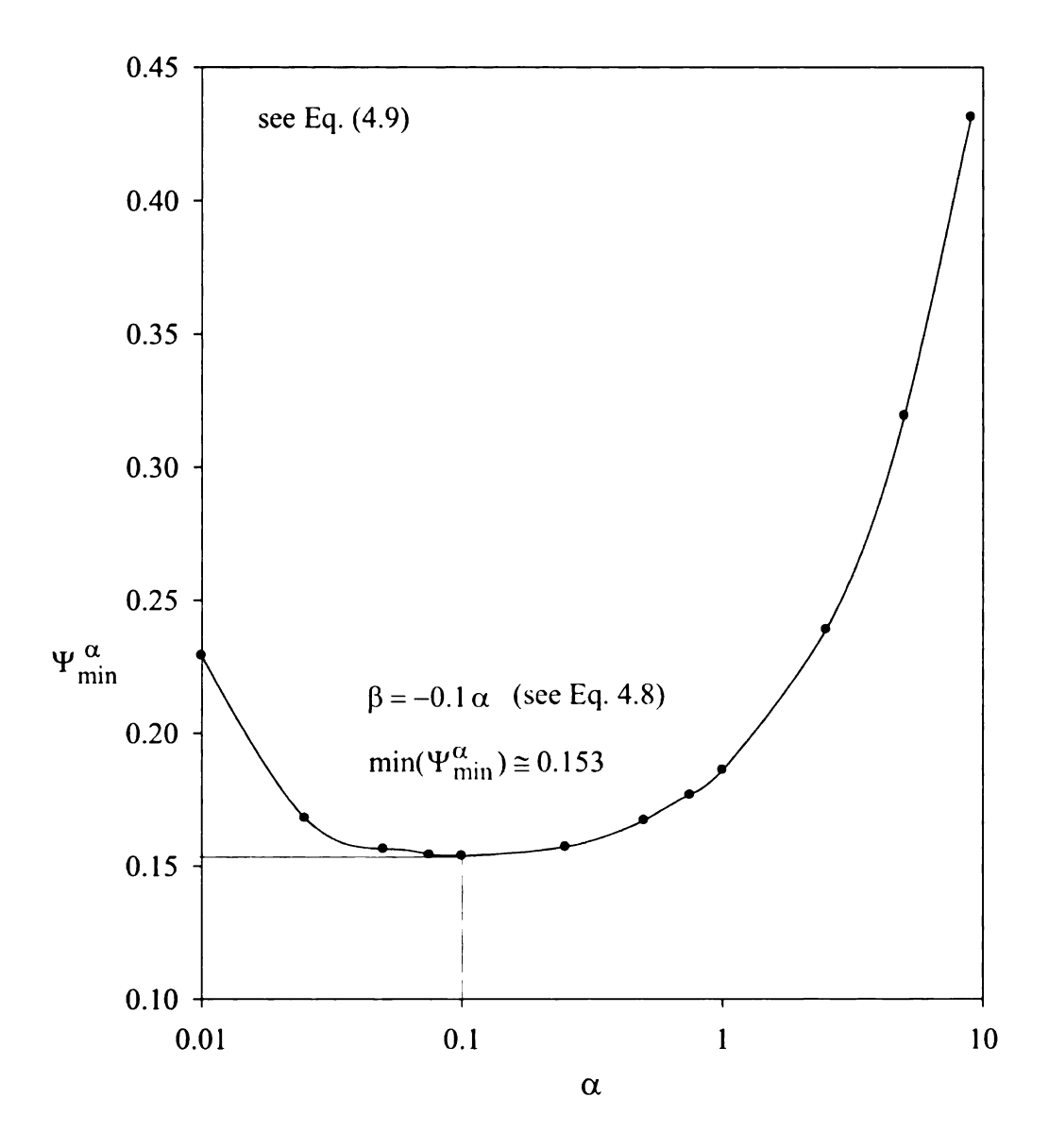
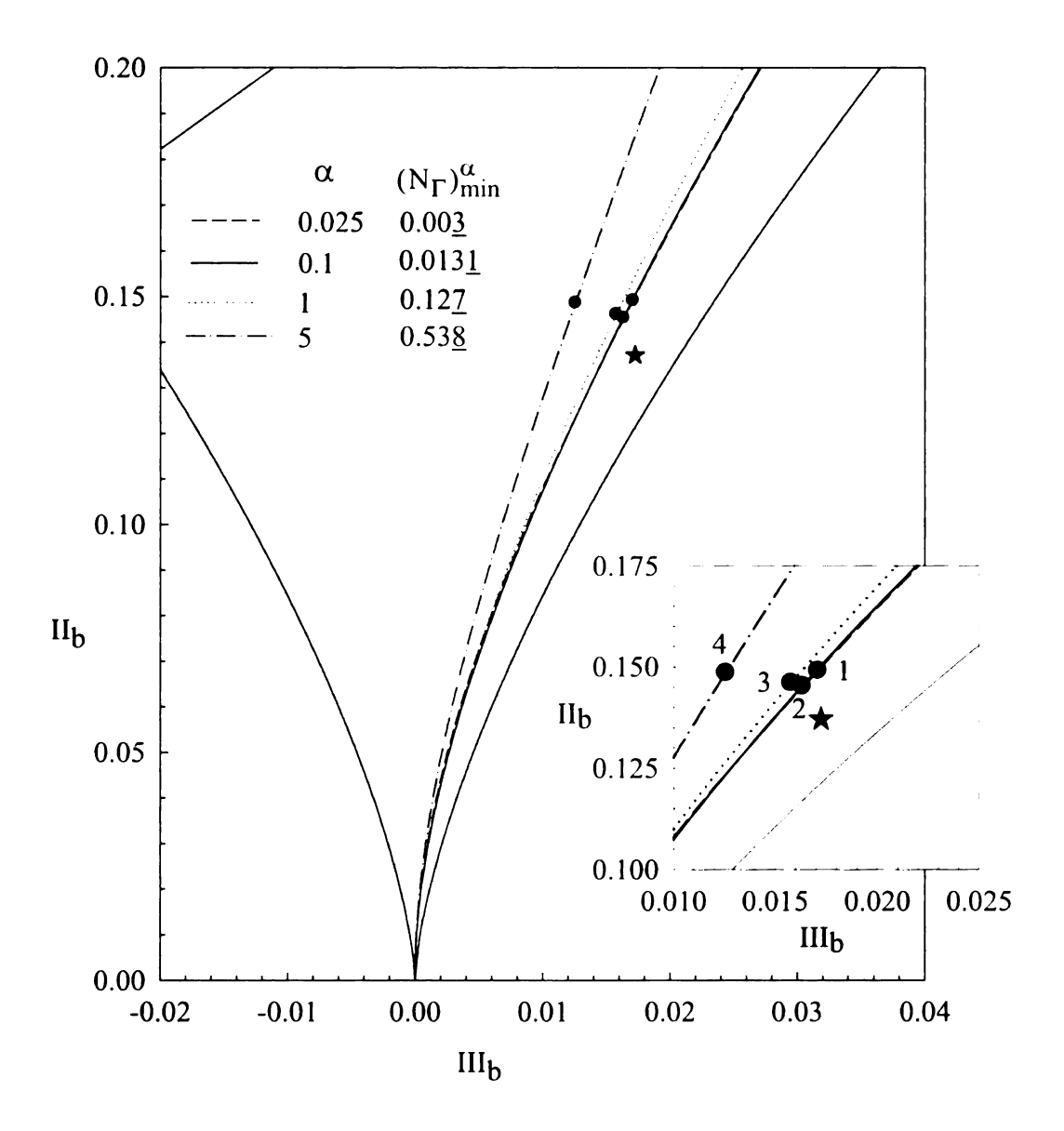


Figure 4.4 The Influence of the "Extra" Anisotropy Coefficient α on the Optimization Metric Ψ^{α}_{min}



Parametric Sensitivity of the Anisotropic States of the NR-Stress Predicted by the URAPS-Closure for Different Values of the Second-Order "Extra" Anisotropy Coefficient (☆-state, experiments, Tavoularis and Karnik, 1989;

coefficient α . Each α -curve is parameterized by $N_{\Gamma} = C_{R1} \tilde{\tau}_R \tilde{\Gamma}$. The values of N_{Γ} identified in the caption correspond to the local minima of the optimization metric $\Psi(N_{\Gamma})$ defined by Eq.(4.9). Each α -curve has a minimum value of Ψ . The ' $\dot{\approx}$ ' state corresponds to the experimental results for asymptotic homogeneous shear in a non-rotating frame of reference. By definition, $\Psi=0$ at the ' $\dot{\approx}$ ' state. The inset in Figure 4.5 shows the behavior of the α -curve for $0 \le N_{\Gamma} \le 1$.

The parameter optimization strategy yields the following result:

$$\min_{N_{\Gamma}, \alpha} \Psi(N_{\Gamma}, \alpha) \cong 0.15\underline{3} \Rightarrow \alpha \cong +0.1 , \beta \cong -0.01 , N_{\Gamma} \cong +0.01\underline{3}.$$
 (4.11)

Table 4.1 compares the components of the NR-stress predicted by the calibrated URAPS-closure with the experimental results for asymptotic homogeneous shear in a non-rotating rame of reference. The URAPS-closure optimized state differs from the experiments by 0.01 for the normal components and by about 0.02 for the shear component.

The coefficient C_{R1} can be estimated from the following relationship between N_{Γ} and $\tilde{\Gamma}.$

$$\begin{split} N_{\Gamma} &= C_{R1} \tilde{\Gamma} \, \tilde{\tau}_{R}(\infty, N_{F}) \\ &= C_{R1} \tilde{\Gamma} \frac{(1 + C_{R3} \, N_{F}^{n})}{(1 + C_{R2} \, N_{F}^{n})} \, . \end{split} \tag{4.12}$$

For homogenous shear with no rotation, $N_F = \tilde{\Gamma} = 4.2$ (see Table 4.1) and $N_\Gamma = 0.013$ (from optimization). Eq.(4.12) implies that $C_{R1} = 0.0036$. The three coefficients C_{R1} , α and β are assumed to be universal constants. In the section below, the coefficient of production in dissipation equation is determined.

4.5 Production Coefficient

The k and Equations for the k and ε yield a relation for the turbulent time scale as a function of the production to dissipation ratio as described earlier in Eq. (3.34). This relation is used to determine the model coefficient C_P/C_{R1} inasmuch as

$$C_P/C_{R1} = \frac{C_D/C_{R1} + ([P/\epsilon] - 1)\tilde{\tau}_R(\infty, N_F)}{[P/\epsilon]}$$
, $[P/\epsilon] = -2N_F R_{yz}^{APS}(N_\Gamma)$ (4.13)

Eq.(4.13) and the experimental data in Table 4.1 for $N_F=4.2$ indicate that $\tilde{\tau}_R(\infty,4.2)=0.8\underline{8}$. With $N_\Gamma=0.01\underline{3}$, $R_{yz}^{APS}=-0.1\underline{9}$ (see Table 4.1), it follows directly from Eq.(4.13) that $[\mathcal{P}/\epsilon]=1.596$. Finally, with $C_D/C_{R1}=1.\underline{8}$, Eq.(4.13) implies that $C_P/C_{R1}=1.\underline{5}$.

In summary, Table 4.2 lists the eight URAPS closure coefficients for $Re_t \to \infty$. The specific benchmark flows used for evaluation along with the calibrated coefficients are shown. In the forthcoming Chapters 5, 6, and 7 on application of the URAPS closure, the above closure coefficients are used assuming them to be universal constants.

4.6 Contraction Mapping and "Extra" Anisotropy

The following two cases for shear flow are illustrated. These cases appear in Ch.6 and the significance of anisotropy will be discussed in Ch.6, for this specific flow case along with the relevant equations.

Case 1:
$$\tilde{\Omega}/\tilde{\Gamma} = 0$$
 and $\tilde{\Gamma} = 4$;

Case2:
$$\tilde{\Omega}/\tilde{\Gamma} = -5/8$$
 and $\tilde{\Gamma} = 11$.)

Table 4.2 Summary of calibration for the URAPS closure parameters.

Parameter	Benchmark Flow					
$\frac{C_{\mathbf{D}}}{C_{\mathbf{R}1}} \doteq 1.\underline{8}$	Non-rotating homogeneous decay. Parameter selected using high Reynolds number, initial decay data (Batchelor and Townsend,1948, Comte-Bellot and Corrsin,1971). Independent of other calibration parameters.					
$\mathbf{n} = \frac{3}{2}$	Rotating homogeneous decay . Parameter selected based on theoretical analysis of energy spectrum (Park and Chung, 1999).					
$(C_{R2}, C_{R3}) = (0.076, 0.053)$	Rotating homogeneous decay. Parameters selected based on energy spectrum analysis (Park and Chung, 1999). Depends only on an estimate for C_D/C_{R1} .					
$\frac{\beta}{\alpha} = -0.1$	Non-rotating simple shear. Parameter selected based on URAPS closure and the components of R for asymptotic homogeneous shear (Tavoularis and Karnik, 1989). Independent of other parameters.					
○ = 0. <u>1</u>	Non-rotating homogeneous simple shear. Parameter selected based on the components of R for asymptotic homogeneous shear (Tavoularis and Karnik, 1989) Depends on all the above parameter estimates.					
$C_{\mathbf{R}_{1}} = 0.003\underline{6}$	Non-rotating homogeneous simple shear. Parameter selected based on APS transport time consistent with the Reigenvalues of the asymptotic anisotropic state (Tavoularis and Karnik, 1989). Depends on all the above parameter estimates.					
$\frac{\mathbf{C_{P}}}{\mathbf{C_{R1}}} = 1.\underline{5}$	Non-rotating homogeneous simple shear. Parameter selected based on asymptotic behavior of k and ε (Tavoularis and Karnik, 1989). This parameter does not depend on the estimate for C_{R1} , but it does depend on all the other parameters listed above.					

The components of the prestress, the NR-stress, and the extra-anisotropic operator \mathbf{are} listed in Table 4.3 for non-rotating simple shear flows with $\tilde{\Omega}/\tilde{\Gamma}=0$ and $\tilde{\Gamma}=4$. For this case, $N_F=4$, $\tilde{\tau}_R=0.8818$ and $N_{\Gamma}=0.01259$. Figure 4.6 shows the locus of anisotropic invariants (II_b , III_b) associated with several solution paths produced by URAPS-theory. The invariants of the fixed-point (i.e., \hat{z} on Figure 4.6) are $II_b^{\hat{z}}=0.1389$ and $III_b^{\hat{z}}=0.01525$, which corresponds to the anisotropic state for asymptotic homogeneous shear for case 1. The following initial operators were selected to produce the four solution paths illustrated in Figure 4.6:

$$\underline{\underline{\mathbf{R}}} \quad \mathbf{O} \Rightarrow \frac{1}{3}\underline{\mathbf{e}}_{\mathbf{x}}\underline{\mathbf{e}}_{\mathbf{x}} + \frac{1}{3}\underline{\mathbf{e}}_{\mathbf{y}}\underline{\mathbf{e}}_{\mathbf{y}} + \frac{1}{3}\underline{\mathbf{e}}_{\mathbf{z}}\underline{\mathbf{e}}_{\mathbf{z}}, \quad \mathbf{II}_{\mathbf{b}} = 0, \text{ isotropic state}$$
 (4.14)

$$\underline{\underline{R}}$$
 $_{\mathbf{O}} \Rightarrow \frac{9}{20} \underline{e}_{x} \underline{e}_{x} + \frac{9}{20} \underline{e}_{y} \underline{e}_{y} + \frac{9}{20} \underline{e}_{z} \underline{e}_{z}$, $II_{b} = 0.0817$, $III_{b} = -0.0095$, oblate state; (4.15)

$$\underline{\mathbf{R}} \quad \mathbf{O} \Rightarrow \frac{1}{10} \underline{\mathbf{e}}_{x} \underline{\mathbf{e}}_{x} + \frac{1}{10} \underline{\mathbf{e}}_{y} \underline{\mathbf{e}}_{y} + \frac{8}{10} \underline{\mathbf{c}}_{z} \underline{\mathbf{c}}_{z}, \quad \text{II}_{b} = 0.3267, \text{III}_{b} = 0.0762, \text{ prolate state;} \quad (4.16)$$

$$\underline{\mathbf{R}} \quad \mathbf{O} \Rightarrow 0.2 \, \underline{\mathbf{e}}_{\mathbf{x}} \, \underline{\mathbf{e}}_{\mathbf{x}} + 0.3 \, \underline{\mathbf{e}}_{\mathbf{y}} \, \underline{\mathbf{e}}_{\mathbf{y}} + 0.5 \, \underline{\mathbf{e}}_{\mathbf{z}} \, \underline{\mathbf{e}}_{\mathbf{z}} + 0.1 \, \underline{\mathbf{e}}_{\mathbf{x}} \, \underline{\mathbf{e}}_{\mathbf{y}} + 0.1 \, \underline{\mathbf{e}}_{\mathbf{y}} \, \underline{\mathbf{e}}_{\mathbf{x}} \\
-0.3 \, \underline{\mathbf{e}}_{\mathbf{x}} \, \underline{\mathbf{e}}_{\mathbf{z}} - 0.3 \, \underline{\mathbf{e}}_{\mathbf{z}} \, \underline{\mathbf{e}}_{\mathbf{x}} - 0.2 \, \underline{\mathbf{e}}_{\mathbf{y}} \, \underline{\mathbf{e}}_{\mathbf{z}} - 0.2 \, \underline{\mathbf{e}}_{\mathbf{z}} \, \underline{\mathbf{e}}_{\mathbf{y}} ; \qquad \text{, ellipsoidal state.}$$

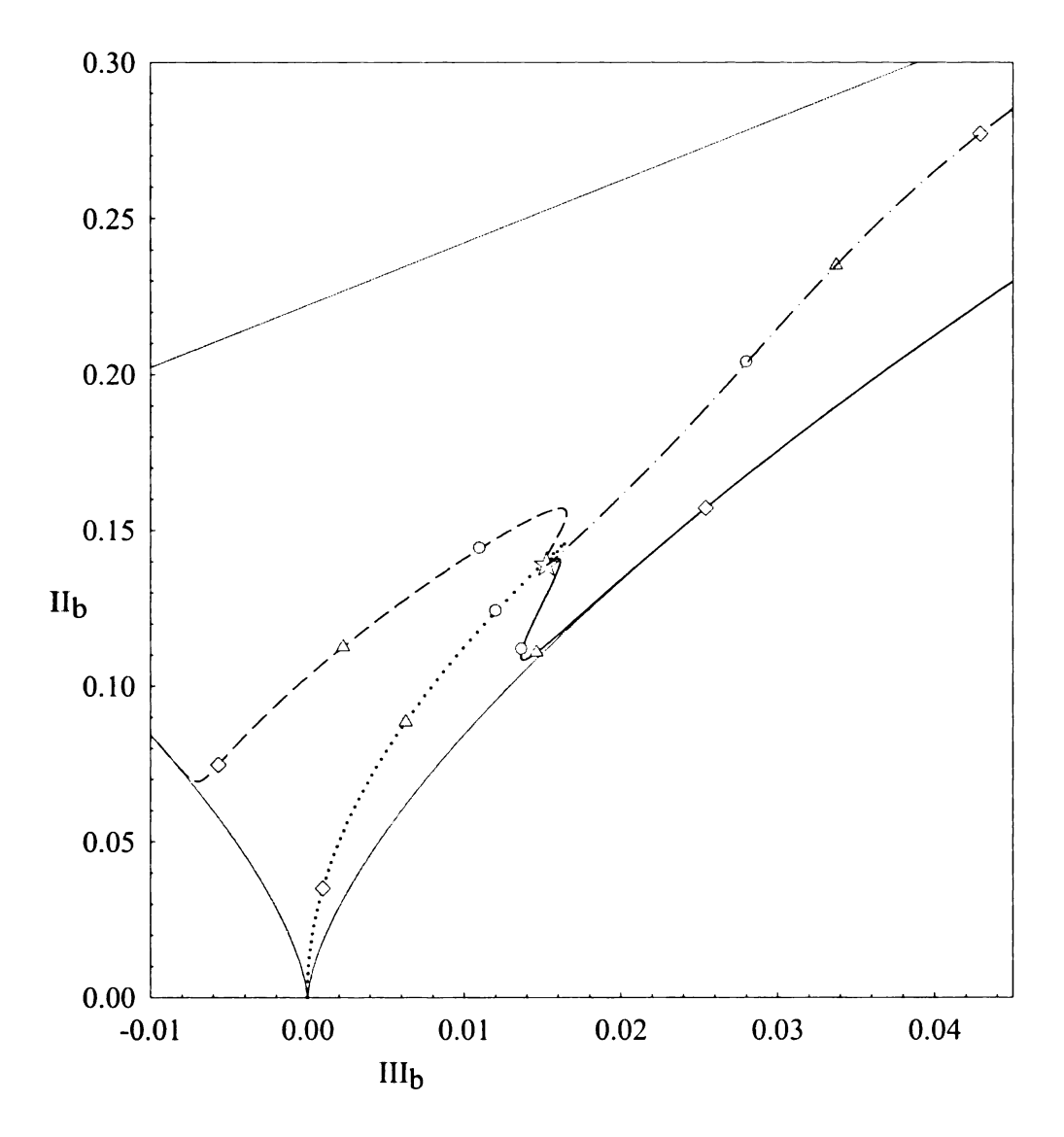
$$\mathbf{II}_{\mathbf{b}} = 0.3267 \, , \, \mathbf{III}_{\mathbf{b}} = 0.0582$$

The eigenvalues of \underline{R}_0 associated with the ellipsoidal state are $\lambda_1^R = 0.0127$, $\lambda_2^R = 0.2000$, and $\lambda_3^R = 0.7873$. Figure 4.6 shows that all the solution paths are in the vicinity of the fixed-point in about 120 iterations. More than 600 iterations are needed to satisfy the convergence criterion $|(\underline{R}_{n+1} - \underline{R}_n) : \underline{c}_i \underline{c}_j| \le 10^{-5} \, \underline{R}_n : \underline{c}_i \underline{c}_j$ for i = x, y, z and j = x, y, z. However, within about 200 iterations, all the solutions are close a single unique solution. The specific number of iterations depend on the initial

Table 4.3. Components of $\underline{\underline{B}}$, $\underline{\underline{R}}$, and $\underline{\underline{\Delta}}$ ($\tilde{\Gamma} = 4$ and $\tilde{\Omega}/\tilde{\Gamma} = 0$)

component	xx	уу	ZZ	yz	χ_B and χ_R
<u>B</u>	+ 0.253705	+ 0.202491	+ 0.543804	- 0.185129	+ 0.557892
<u>R</u>	+ 0.252520	+ 0.201545	+ 0.545935	- 0.186801	+ 0.563148
$\underline{\underline{\Delta}} = \underline{\underline{B}} - \underline{\underline{R}}$	+ 0.001185	+ 0.000946	- 0.002131	+ 0.001672	n/a

$$\chi_{\mathbf{R}} \equiv \left| R_{yz} \right| / \sqrt{R_{yy} R_{zz}} \; ; \; \chi_{B} \equiv \left| B_{yz} \right| / \sqrt{B_{yy} B_{zz}}$$



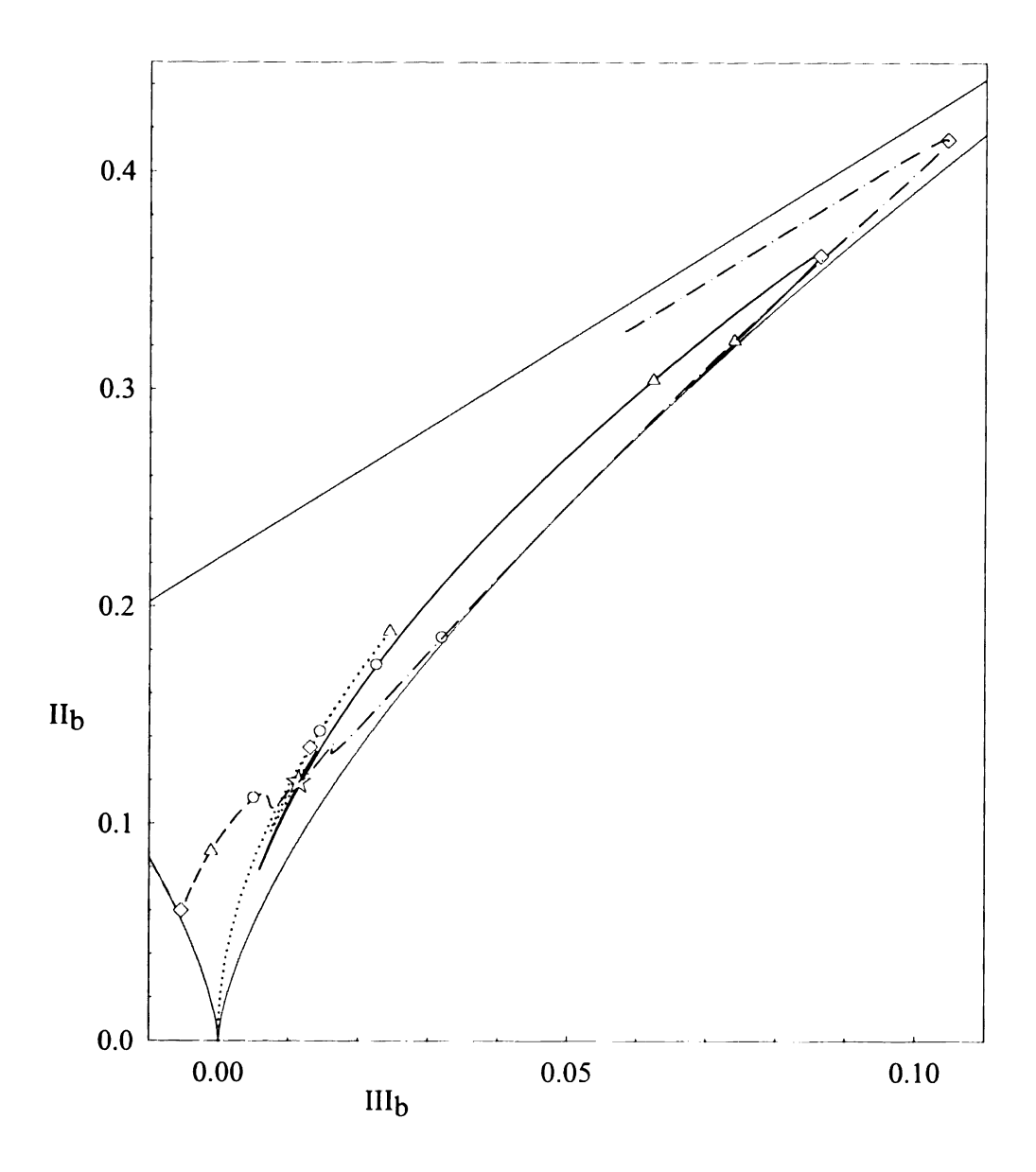
The Development of Anisotropic Invariants of the NR-stress for $\tilde{\Gamma}=4$ and $\tilde{\Omega}/\tilde{\Gamma}=0$ from Different Initial States (initial states: isotropic · · · · · ; oblate - - - ; prolate — ; ellipsoidal - · · · · ; iterations: $40 \diamondsuit$; $80 \diamondsuit$; $120 \bigcirc$; $11b \diamondsuit$ = 0.1389; $111b \diamondsuit$ = 0.01525).

condition. Figure 4.7, shows solution trajectories from the initial conditions in Eqs. (4.14) (4.17) for case 2. The components of \underline{B} , \underline{R} , and $\underline{\Delta}$ are listed in Table 4.4. The components of $\underline{\Delta}$ are of the order of 10^{-3} . For this case $(\tilde{\Omega}/\tilde{\Gamma}=-5/8)$ and $\tilde{\Gamma}=11$, $N_F=14$, $\tilde{\tau}_R=0.7506$, $N_\Gamma=0.02948$, and $N_\Omega=-0.03685$. Although the trajectories seem to intersect at some point for the case 2, the components are all unique and finally reach single solution.

4.7 Conclusions

The URAPS-closure coefficients have been estimated using benchmark flows described in Chapter 2 assuming them to be universal constants. Following is a summary of the calibration described in Table 4.2.

- 1. The ratio C_D/C_{R1} , which appears in the in the ϵ -equation, has been calibrated to be 1.8 from experimental data (see Figure 2.17) for non-rotating homogeneous flow for high initial Reynolds number. In this research, C_D/C_{R1} is assumed to be a universal constant
- 2. The turbulent time scale for the URAPS closure is based on an empirical formulation for the dimensionless timescale $\tilde{\tau}_R = \frac{(1+C_{R3}\,N_F^{3/2})}{(1+C_{R2}\,N_F^{3/2})}$ which has been proposed from the understanding derived from the analysis of Park and Chung (1999) presented in Appendix F. The analysis of energy spectrum for homogeneous flows in the presence of rotation shows the dependence of dissipation equation on rotation (see Eq.(F.42)). This information is used to derive



The Development of Anisotropic Invariants of the NR-Stress for $\tilde{\Gamma} = 11$ and $\tilde{\Omega}/\tilde{\Gamma} = -5/8$ from Different Initial States (same as Figure 4.6); $II_b^{\dot{\alpha}} = 0.1190$; $III_b^{\dot{\alpha}} = 0.01144$).

Table 4.4. Components of $\underline{\underline{B}}$, $\underline{\underline{R}}$, and $\underline{\underline{\Delta}}$ ($\tilde{\Gamma} = 11$ and $\tilde{\Omega}/\tilde{\Gamma} = -5/8$)

component	xx	уу	ZZ	yz	χ_B and χ_R
<u>B</u>	+ 0.264508	+ 0.592243	+ 0.143249	- 0.066540	+ 0.228447
<u>R</u>	+ 0.263520	+ 0.594788	+ 0.141692	- 0.067148	+ 0.231303
$\underline{\underline{\Delta}} = \underline{\underline{B}} - \underline{\underline{R}}$	+ 0.000988	- 0.002545	+ 0.001557	+ 0.000608	n/a

$$\chi_{\mathbf{R}} \equiv \left| R_{yz} \right| / \sqrt{R_{yy}R_{zz}} \; ; \; \chi_{B} \equiv \left| B_{yz} \right| / \sqrt{B_{yy}B_{zz}}$$

the coefficients $(C_{R2},C_{R3})=(0.0764,0.0526)$ in order to include the dependence on mean field time scale. The power on the group N_F , i.e. n=3/2, is adopted from the dependence of time scale on the rotation rate observed in the energy spectrum analysis. For $0 < N_F < \infty$, $\tilde{\tau}_R$ varies between the limits $0.69 < \tilde{\tau}_R < 1$.

- 3. The URAPS relation for simple shear and experimental data for asymptotic states flows has been used to estimate the ratio $\beta/\alpha \cong -0.1$. URAPS-closure component equations cannot exactly satisfy all the experimental data in Table 4.1 for asymptotic homogeneous shear. Consequently, an optimization strategy was used to minimize the metric defined by Eq. (4.9). The resulting coefficients $\alpha = +0.1$ and $C_{R1} \cong 0.0036$ minimized the error between the model predictions and the experimental data. The coefficient of production ($C_P/C_{R1} \cong 1.5$) was estimated from the asymptotic relation for the turbulent time scale. The summary of the parameters listed in Table 4.2 will be used for the application of URAPS-closure for predicting the NR-stress. Figure 4.8 shows the realizable choice of $\alpha = +0.1$ and $\beta = -0.01$ from the calibration procedure to be within the realizable bounds discussed in Chapter 3.
- 4. Successive substitution method for finding the URAPS-closure solution is illustrated for two cases of simple shear flows: Case 1: $\tilde{\Omega}/\tilde{\Gamma} = 0$ and $\tilde{\Gamma} = 4$; and, Case 2: $\tilde{\Omega}/\tilde{\Gamma} = -5/8$ and $\tilde{\Gamma} = 11$. It is shown that for different initial anisotropic states in Eqs. (4.14) to (4.17) show a convergence towards a unique final ' $\dot{\Xi}$ ' state shown in Figures 4.6 and 4.7 for a specific convergence criteria.

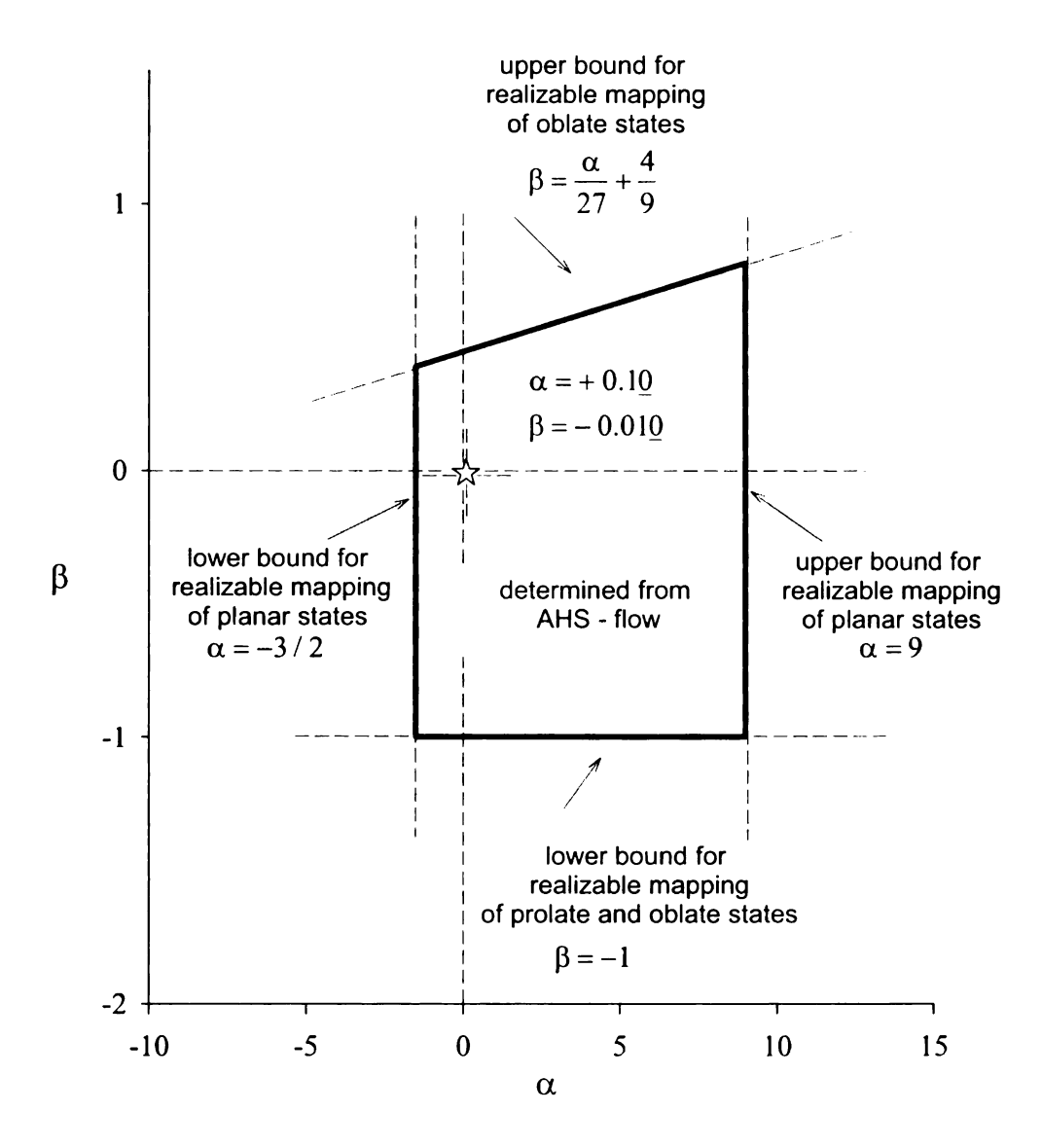


Figure 4.8 Prestress Coefficients α and β Determined From Asymptotic Homogeneous Shear flow.

CHAPTER 5

HOMOGENEOUS DECAY

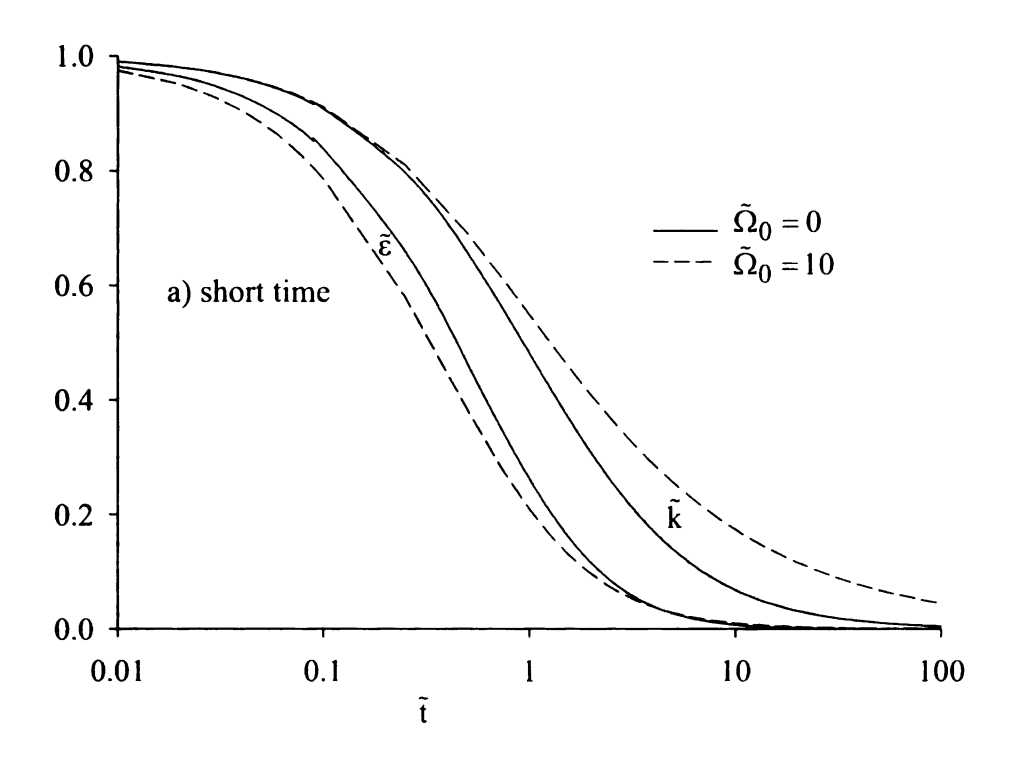
5.1 Introduction

In the absence of spatial gradients in the mean velocity, turbulence decays. This flow field which is referred to as homogeneous decaying turbulence, is often used as a benchmark flow for studying turbulence models. Eq. (2.29) and Eq. (2.30), which are autonomous non-linear dynamic equations for $\tilde{k} (\equiv k/k_0)$ and $\tilde{\epsilon} (\equiv \epsilon/\epsilon_0)$, define the decay dynamics as discussed in Chapter 4. The dimensionless turbulent time scale $\tilde{\tau}_R$ described in Eq. (4.5) has been modeled in Chapter 4 to include the time scale associated with the rotation of the frame through the group $N_F \equiv k \| \langle \underline{F} \rangle \| / \epsilon$. In Section 5.2, the reconstruction of some of the results used in the calibration along with a further parametric analysis for various important turbulent quantities like the turbulent time scale $\tilde{k}/\tilde{\epsilon}$, and the turbulent dispersion $\tilde{k}^2/\tilde{\epsilon}$ are discussed to understand the temporal development of $\tilde{\Omega}$ ($\equiv \tilde{\Omega}_0 \tilde{k}$)/ $\tilde{\epsilon}$). The focus of Chapter 5 is on the development of the Reynolds stress anisotropy in the presence of rotation for high initial turbulent Reynolds numbers $(k_0^2/(v\epsilon_0) >> 1)$. The URAPS-closure component equations are simplified for this case because of no shear. These are discussed in Section 5.3. The temporal development of the NR-stress for the URAPS-closure estimated from the temporal variation of $\tilde{\Omega}$ is discussed in Section 5.4. The temporal development of the 'extra' anisotropy terms is studied in Section 5.5 to understand their role in energy redistribution.

5.2 Turbulent Energy and Turbulent Dissipation: Results and Discussion

The dimensionless time \tilde{t} is defined as $\epsilon_0 t/k_0$ and the rotational operator is related to the angular velocity by $\underline{\Omega} = \Omega_x (\underline{e}_y \underline{e}_z - \underline{e}_z \underline{e}_y)$. For $\tilde{t} = 0$, $\tilde{k} = 1$ and $\tilde{\epsilon} = 1$, the initial value problem (defined by Eq. (2.29) and (2.30)) was solved for a wide range of rotation numbers by using a fourth-order Runge-Kutta algorithm implemented in MatLab® (Appendix H provides the flowchart and Matlab program). Summary of the influence of $\tilde{\Omega}_0$ on the decay process as discussed below.

In the presence of rotation for decay of homogeneous turbulent flow, the rate of decay of k is hindered by rotation with a decrease in dissipation (Bardina et al. 1985, Speziale et al. 1987, Cambon et al. 1997) as discussed in the literature in Chapter 2. Figure 5.1 shows the decay dynamics for $0 < \tilde{\Omega}_0 < 10$ all lie between the two curves. Although turbulence decays monotonically for all rotation rates, the decay rate of k decreases with increasing rotation. During the initial stage (i.e., $0 < \tilde{t} < 0.1$), an enhanced rate-of-decay of $\tilde{\epsilon}$ in Eq. (2.30) arises due to a decrease in the dimensionless turnover time $\tilde{\tau}_R$ as the rotation number $N_F (= 2\sqrt{2}~\tilde{\Omega}_0 \tilde{k} \,/\, \tilde{\epsilon})$ increases as discussed in Chapter 4 (see Figure 4.2). The influence of rotation on \tilde{k} is relatively small during the initial stage. However, during the intermediate stage (i.e., $0.1 < \tilde{t} < 4$), the rate of decay of \tilde{k} is mitigated by the smaller dissipation that is developed during the initial stage. For the final (non-viscous) decay period (i.e., $\tilde{t} > 4$), the rate-of-decay of $\tilde{\epsilon}$ decreases due to the persistence of a relatively large value of \tilde{k} as $\tilde{k}/\tilde{\epsilon} \to \infty$. Thus, for $\tilde{t} \gg 4$, $N_F \to \infty$ and $\tilde{\tau}_R \to C_{R3}/C_{R2} = 11/16$. Figure 5.1b shows that the dissipation for $\tilde{\Omega}_0 = 10$ eventually



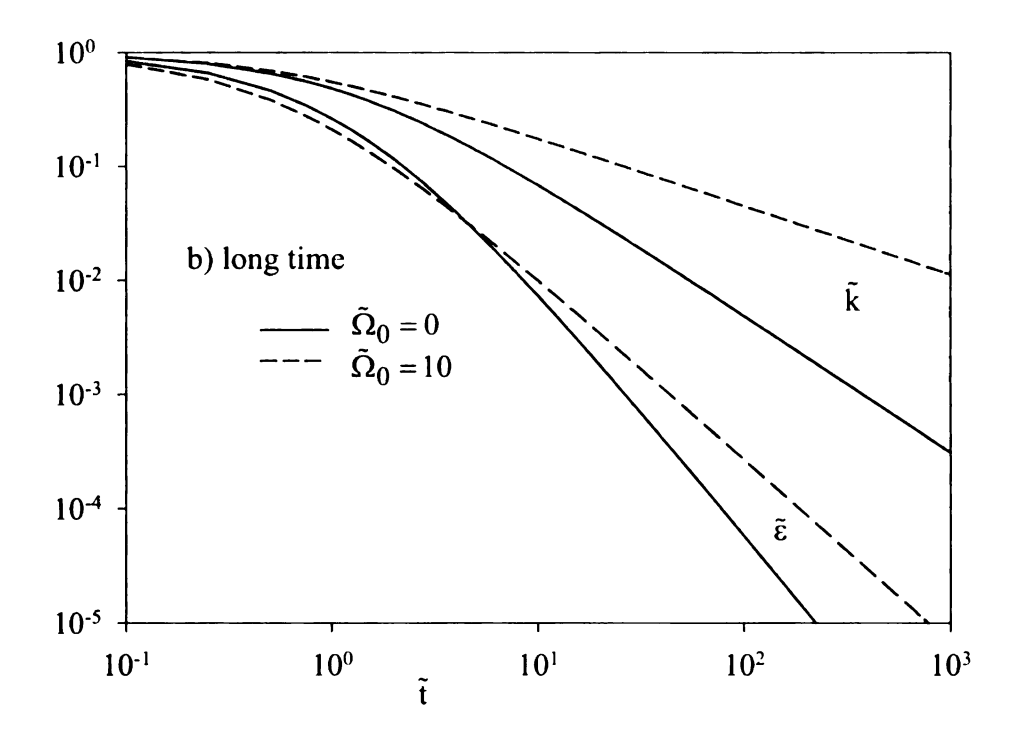


Figure 5.1. The Influence of Rotation Number on the Decay of \tilde{k} and $\tilde{\epsilon}$.

exceeds the dissipation for $\tilde{\Omega}_0 = 0$. This feature, which was not noted by Park and Chung (1999) shows that rotation actually retards the rate-of-decay of dissipation during the final stage of the decay process.

Figure 5.2 shows the decay dynamics in a phase plane. The decay process starts at $\tilde{k} = \tilde{\epsilon} = 1$ and decays with time asymptotically approaching zero with $\tilde{k} \ge 0$, and $\tilde{\epsilon} \ge 0$ for all times. During the initial decay period, the slope of the curves in the phase plane shown in this figure are related to the coefficients in Eq.(5.1) below, which is obtained by combining Eqs. (2.29) and (2.30).

$$\frac{\mathrm{d}\,\tilde{\epsilon}}{\mathrm{d}\,\tilde{k}}_{\tilde{t}=0} = -\frac{C_{\mathrm{D}}}{C_{\mathrm{R}1}} \frac{1}{\tilde{\tau}_{\mathrm{R}}} \frac{\tilde{\epsilon}}{\tilde{k}} = -\frac{C_{\mathrm{D}}}{C_{\mathrm{R}1}} \frac{1}{\tilde{\tau}_{\mathrm{R}}}$$
(5.1)

For $\tilde{\Omega}_0 = 0$, $\frac{C_D}{C_{R1}} \frac{1}{\tilde{\tau}_R} = \frac{11}{6}$ since $\tilde{\tau}_R(N_F \to 0) = 1$ for no rotation. For very large rotation

rates, where
$$\tilde{\Omega}_0 \to \infty$$
, the slope is $\frac{C_D}{C_{R1}} \frac{1}{\tilde{\tau}_R} \to \frac{8}{3}$ since $\tilde{\tau}_R(N_F \to \infty) \to 11/16$. These

limiting values are a consequence of the model for $\tilde{\tau}_R$ in Chapter 4. Figure 5.3 shows that the turbulent time scale increases monotonically for increasing rotation rates. The initial slopes of the curves are positive and continue to remain so during the entire decay process as described by Eq. (5.2) for turbulent time scale below.

$$\frac{\mathrm{d}}{\mathrm{d}\,\tilde{\mathrm{t}}}\left(\frac{\tilde{\mathrm{k}}}{\tilde{\epsilon}}\right)\Big|_{\forall\,\tilde{\mathrm{t}}} = -1 + \frac{C_{\mathrm{D}}}{C_{\mathrm{R}1}} \frac{1}{\tilde{\tau}_{\mathrm{R}}} \tag{5.2}$$

$$\frac{C_D}{C_{R1}} \frac{1}{\tilde{\tau}_R} > 1 \quad \forall \ \tilde{\Omega}_0 \text{ and so } -1 + \frac{C_D}{C_{R1}} \frac{1}{\tilde{\tau}_R} > 0 \text{ i.e. positive slope for any rotation rate.}$$

The decay dynamics in the presence of rotation has a qualitatively different response compared with its non-rotating counterpart. Figure 5.4 shows that turbulent

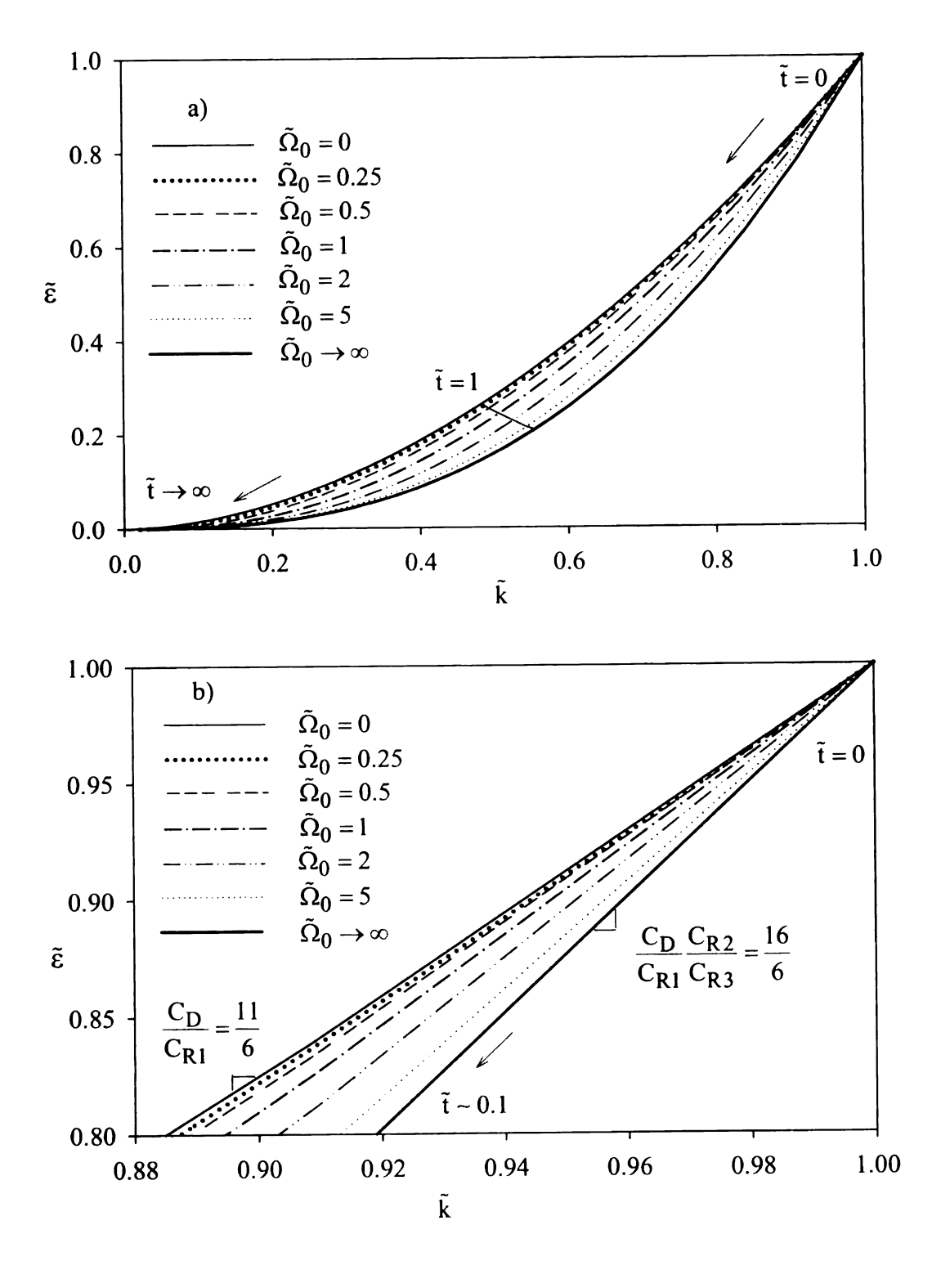


Figure 5.2. \tilde{k} and $\tilde{\epsilon}$ Phase Plane Diagrams for Rotating Homogeneous Decay.

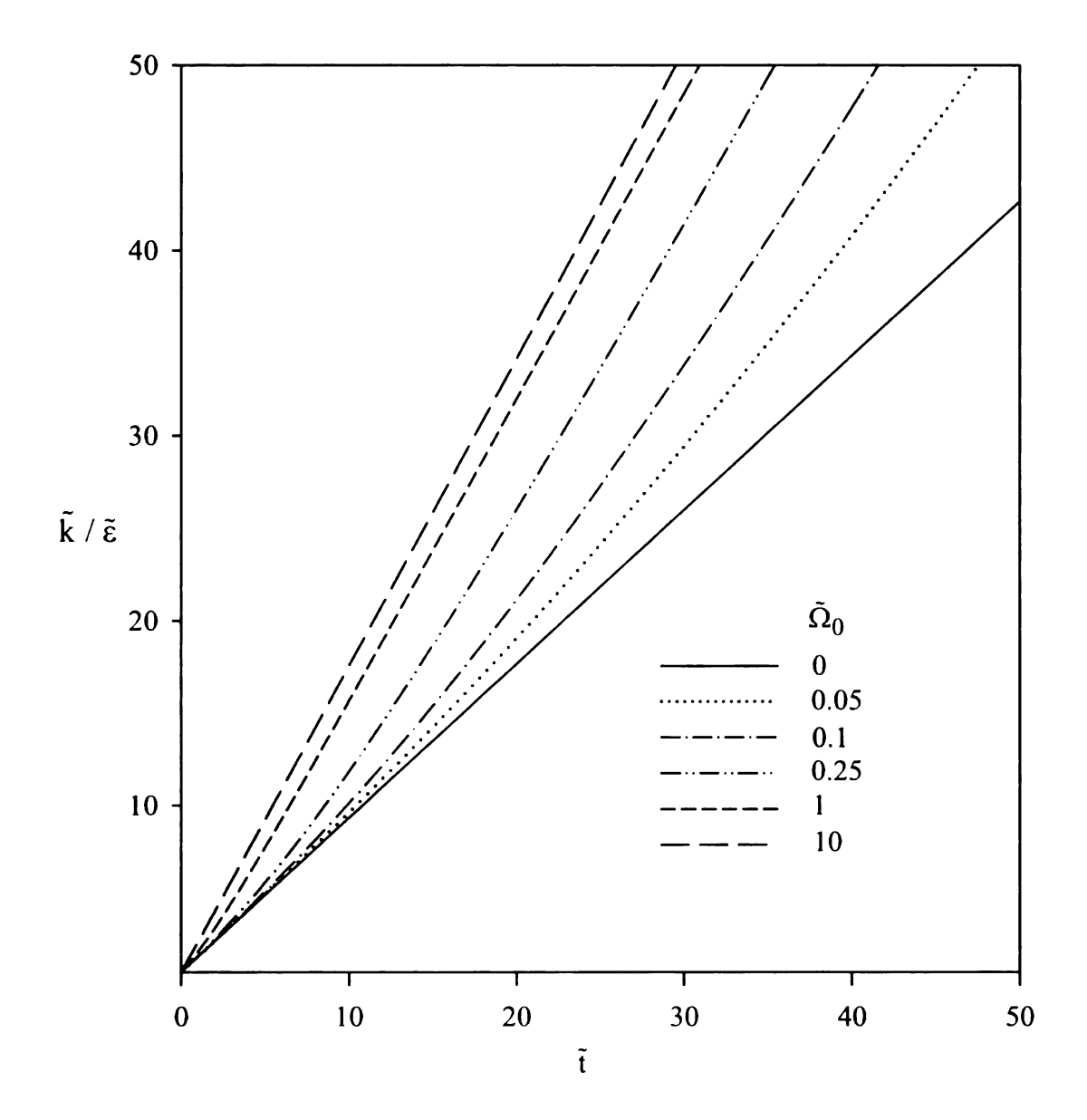


Figure 5.3. The Influence of Rotation on the Dimensionless Turbulent Time Scale.

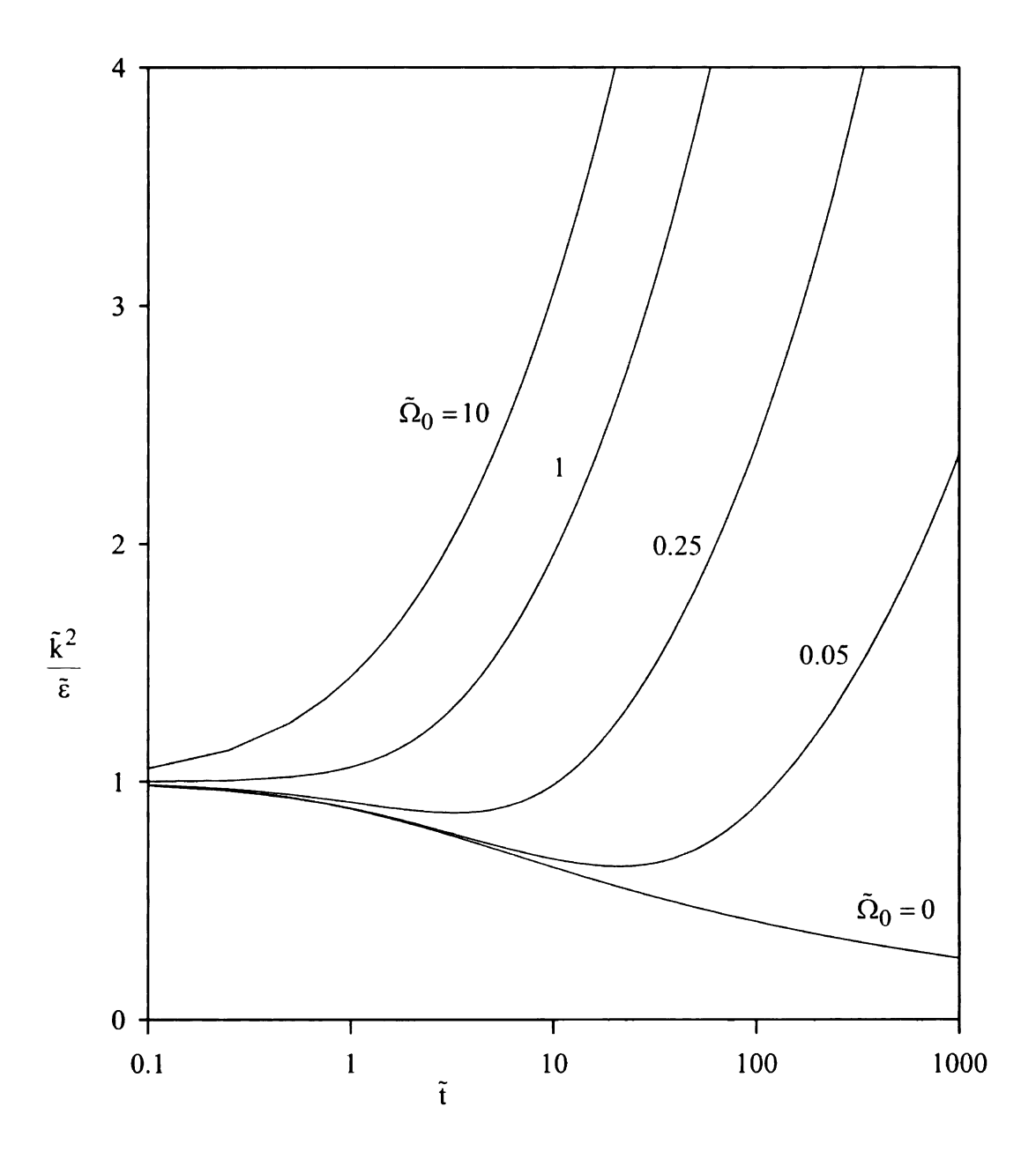


Figure 5.4. Influence of Rotation on $\,\tilde{k}^{\,2}\,/\,\tilde{\epsilon}\,.$

dispersion (i.e., $\tilde{k}^2/\tilde{\epsilon}$) variation with \tilde{t} for various rotation rates. In the absence of rotation, $\tilde{k}^2/\tilde{\epsilon}$ decreases monotonically as \tilde{k}^2 decreases faster than $\tilde{\epsilon}$. However, in the presence of rotation, although \tilde{k} and $\tilde{\epsilon}$ decrease monotonically, $\tilde{k}^2/\tilde{\epsilon}$ becomes unbounded for large rotation numbers (see Figure 5.4). For $0<\tilde{\Omega}_0<1$, $\tilde{k}^2/\tilde{\epsilon}$ first decreases and then increases and becomes unbounded for long times while for $\tilde{\Omega}_0\geq 1$, there is a monotonic increase. This can be explained by the Eq. (5.3) below for the rate of change of turbulent dispersion which gives the initial slope of $\tilde{k}^2/\tilde{\epsilon}$ vs. \tilde{t} .

$$\frac{\mathrm{d}}{\mathrm{d}\,\tilde{t}}\left(\frac{\tilde{k}^2}{\tilde{\epsilon}}\right)\bigg|_{\tilde{t}=0} = -2 + \frac{C_{\mathrm{D}}}{C_{\mathrm{R}1}} \frac{1}{\tilde{\tau}_{\mathrm{R}}}.\tag{5.3}$$

The initial slope is negative for $0 < \tilde{\Omega}_0 < 1$ since $\frac{11}{6} < \frac{C_D}{C_{R1}} \frac{1}{\tilde{\tau}_R} < 2$. For $\tilde{\Omega}_0 \ge 1$, the

initial slope is positive as $\frac{C_D}{C_{R1}} \frac{1}{\tilde{\tau}_R} > 2$ and so $\tilde{k}^2 / \tilde{\epsilon}$ increases monotonically.

From the above information on the \tilde{k} and $\tilde{\epsilon}$, the group $\tilde{\Omega} = \tilde{\Omega}_0 \tilde{k} / \tilde{\epsilon}$ increases for all rotation numbers during the decay process. Viscous effects are negligible for all initial rotation numbers $\tilde{\Omega}_0 \geq 1$ and for $0 < \tilde{\Omega}_0 < 1$ during long times since $\tilde{k}^2 / (v\tilde{\epsilon})$ increases monotonically in this region as discussed above. The following Section illustrates the simplified URAPS-closure component equations and the Reynolds stress anisotropy predicted by the URAPS-equation.

5.3 Preclosure Operator and URAPS-Closure

For rotating homogeneous flows, the preclosure operator $\underline{\underline{A}}$ is defined by the following equations Eq.(5.4) and Eq.(5.5). (See Appendix G. for more detailed derivations).

$$\underline{\underline{A}}^{-1} = \underline{\mathbf{e}}_{\mathbf{x}} \underline{\mathbf{e}}_{\mathbf{x}} + \underline{\mathbf{e}}_{\mathbf{y}} \underline{\mathbf{e}}_{\mathbf{y}} + \underline{\mathbf{e}}_{\mathbf{z}} \underline{\mathbf{e}}_{\mathbf{z}} + \mathbf{N}_{\Omega} \underline{\mathbf{e}}_{\mathbf{y}} \underline{\mathbf{e}}_{\mathbf{z}} - \mathbf{N}_{\Omega} \underline{\mathbf{e}}_{\mathbf{z}} \underline{\mathbf{e}}_{\mathbf{y}}$$
(5.4)

$$\underline{\underline{A}} = \frac{(1 + N_{\Omega}^2) \underline{e}_x \underline{e}_x + \underline{e}_y \underline{e}_y + \underline{e}_z \underline{e}_z - N_{\Omega} \underline{e}_y \underline{e}_z + N_{\Omega} \underline{e}_z \underline{e}_y}{(1 + N_{\Omega}^2)}$$
(5.5)

where $N_{\Omega}=2\,C_{R1}\,\tilde{\tau}_R\,\frac{\tilde{k}}{\tilde{\epsilon}}\,\tilde{\Omega}_0=2\,C_{R1}\,\tilde{\tau}_R\,\tilde{\Omega}$. For $\nabla<\underline{u}>=\underline{0}$ and $0<\tilde{\Omega}_0<\infty$, an analysis URAPS-closure predicts that if $B_{xy}=0$ and $B_{xz}=0$, then $R_{xy}=0$ and $R_{xz}=0$. Furthermore, if $B_{yz}=0$ and $B_{yy}=B_{zz}$, then $R_{yz}=0$. Therefore, for rotating homogeneous decay, URAPS closure can be written in the component form (See Appendix G. Case3).

$$\kappa R_{xx} = (1 + N_{\Omega}^2)^2 B_{xx}$$
 (5.6)

$$\kappa R_{yy} = B_{yy} + N_{\Omega}^2 B_{zz} \tag{5.7}$$

$$\kappa R_{zz} = N_{\Omega}^2 B_{yy} + B_{zz} \tag{5.8}$$

$$\kappa \equiv (1 + N_{\Omega}^2)(1 + N_{\Omega}^2 B_{xx}) \tag{5.9}$$

The components of the prestress operator for rotating homogeneous decay are also presented in Appendix G. Eqs.(5.7) and (5.8) imply that if $B_{yy} = B_{zz}$, then $R_{yy} = R_{zz}$. This is consistent with the closure expressed by URAPS-theory. Therefore, with $B_{yy} = B_{zz} = (1 - B_{xx})/2$ and $R_{yy} = R_{zz} = (1 - R_{xx})/2$, URAPS-equations implies that

$$R_{xx} = \frac{(1 + N_{\Omega}^2)B_{xx}}{(1 + N_{\Omega}^2B_{xx})}.$$
 (5.10)

Based on the simplified URAPS-closure result in Eq. (5.10), the NR-stress variation with rotation is discussed in the following Section.

5.4 The NR-Stress: Results and Discussion

Eq. (5.10) shows that for $N_{\Omega}=0$, $R_{xx}=B_{xx}$. For the non-rotating case, three solutions to URAPS equations exist: $R_{xx}=0$; 1/3; and ,1. For $N_{\Omega}=\pm\infty$, Eq.(5.10) implies that $R_{xx}=1$; therefore, $B_{xx}=1$ also. Thus, as the rotation number increases, the URAPS-closure predicts that the Coriolis force causes a transfer of energy from the fluctuating velocity components in the plane orthogonal to the rotating axis (i.e. y and z components) into the fluctuating velocity aligned with the angular velocity (i.e. x component). If $-\infty < N_{\Omega} < \infty$, prolate anisotropic states also exist. The prolate anisotropic form produced is characterized by the following inequality: $0 \le R_{yy} = R_{zz} < 1/3 < R_{xx} \le 1$.

Figures 5.5 and 5.6 summarize the solutions to URAPS-equations for different rotation numbers, $\tilde{\Omega}_0$. Temporal variation of the rotation group, $N_\Omega = 2C_{R1}\tilde{\tau}_R \, (\Omega_0\tilde{k})/\tilde{\epsilon}$ are calculated based on the decay dynamics discussed earlier. Thus from Eq. (5.10), the URAPS-closure predicts that the Coriolis force causes a redistribution of energy from an initial isotropic state to a prolate state as the turbulent kinetic energy decays. The algebraic nature of the URAPS-closure causes a rapid (instantaneous) redistribution of energy at $\tilde{t}=0$ followed by a slower transfer of energy

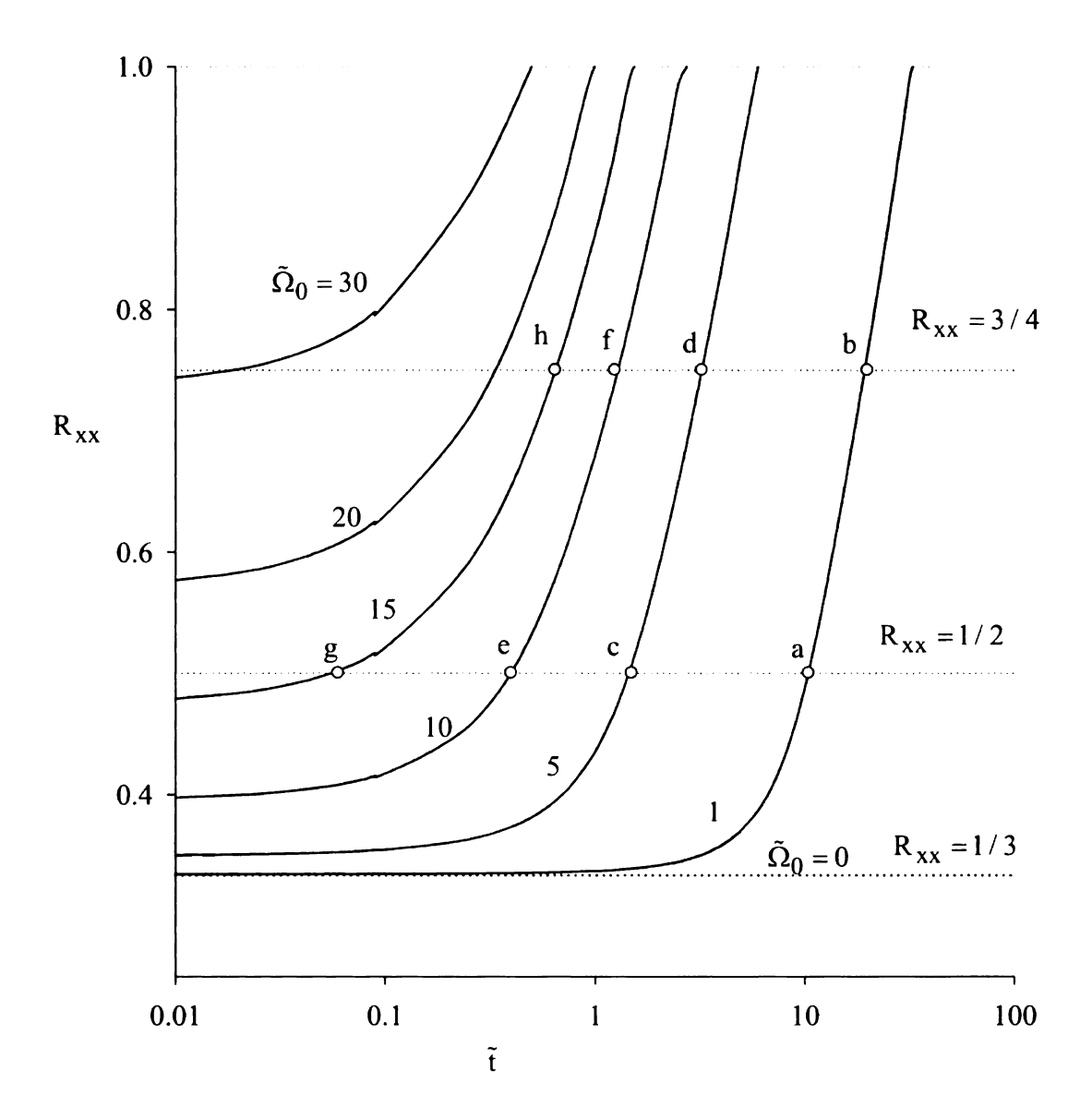


Figure 5.5. The Influence of Rotation on the Temporal Variation of R_{xx} Component of Reynolds Stress for Homogeneous Decay (see Tables 5.1a,b).

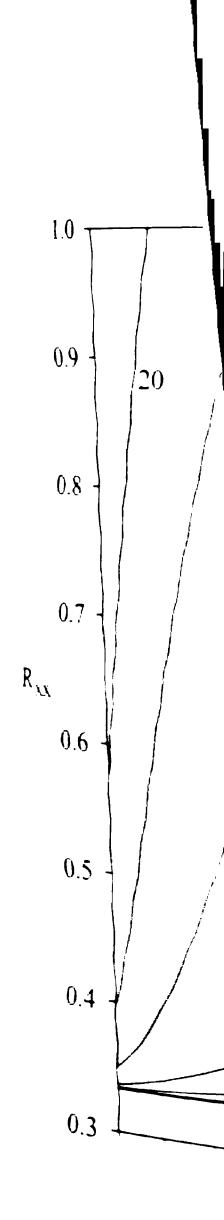


Figure 5.6. The Res

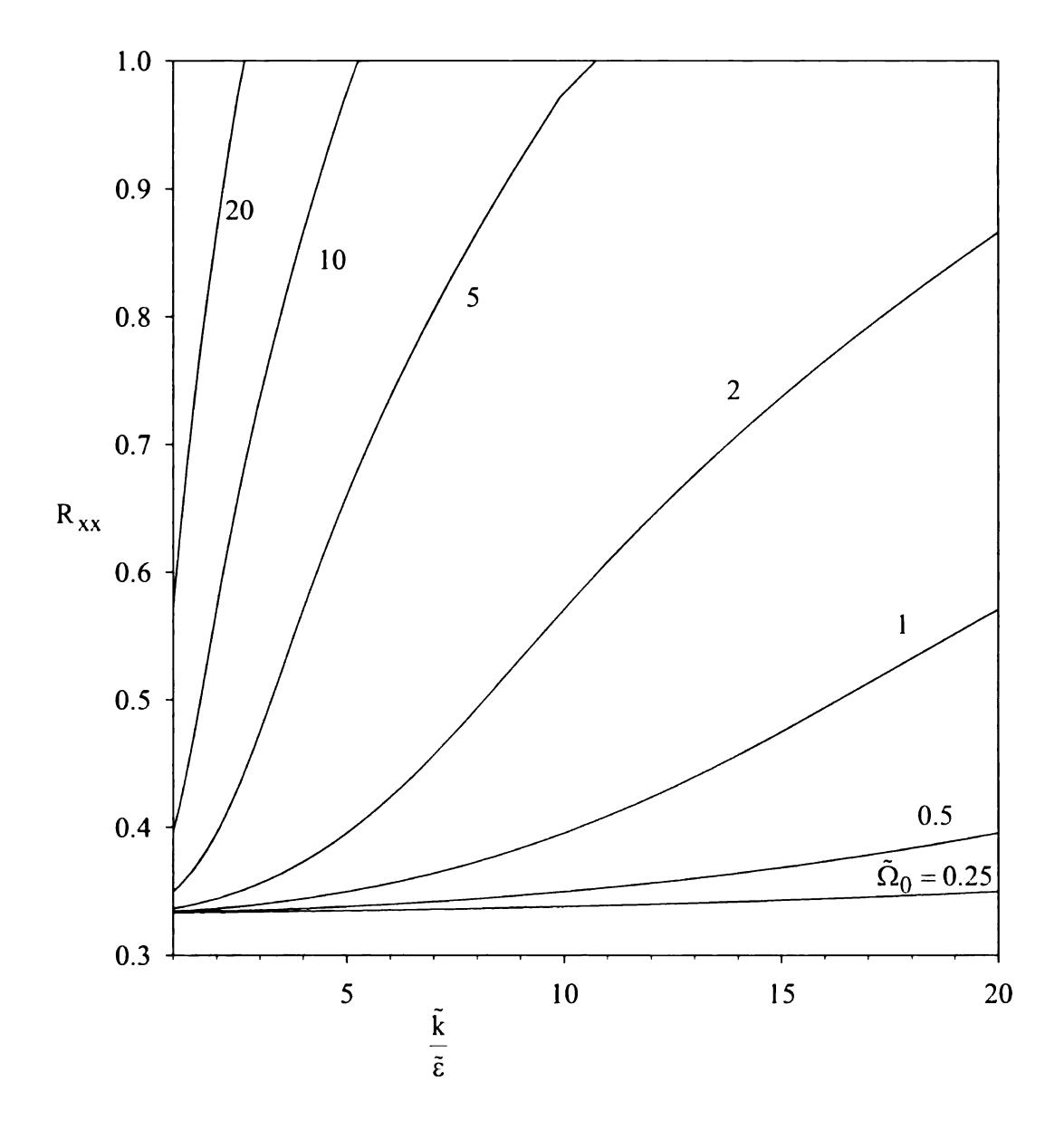


Figure 5.6. The Influence of Rotation on the Redistribution of Kinetic Energy with Respect to the Turbulent Time Scale.

for t>0. During the changes from a spheric of $2R_{xx}(1-R_{xx})$. The in Figure 5.5 for which The anisotropic states $R_{xx} = 3$ 4 all have qui details of values of each time increases (i.e., τ effectively completed (5.5 shows that the tim rotation number $ilde{\Omega}_0$. However, for $\tilde{\Omega}_0 = 1$ From the abo state is isotropic () states $0 < R_{yy} = F$ among the velocit intrinsic accelerat etergy. Transport puely reorganiza effecting the eq knowledge of lit for $\tilde{t}>0$. During the decay process, the quadratic form associated with the NR-stress changes from a spherical isotropic form to a prolate ellipsoidal form with an aspect ratio of $2R_{xx}/(1-R_{xx})$. Table 5.1 lists the anisotropic states identified as 'a', 'c', 'e', and 'g' in Figure 5.5 for which $R_{xx}=1/2$ all have quadratic forms with an aspect ratio of 2:1. The anisotropic states identified as 'b', 'd', 'f', and 'h' in Figure 5.5 for which $R_{xx}=3/4$ all have quadratic forms with an aspect ratio of 6:1. (See Table 5.1 for the details of values of each of URAPS variables for these states). As the turbulent transport time increases (i.e., $\tau_R >> \Omega_x^{-1}$), the energy redistribution process continues and is effectively completed (i.e., $R_{xx} \cong 1$) in a finite amount of time $\tilde{t}_f = t_f \epsilon_0/k_0 < \infty$. Figure 5.5 shows that the time needed to shift the energy to the R_{xx} component depends on the rotation number $\tilde{\Omega}_0$. For $\tilde{\Omega}_0 = 1$, the transfer time is significant inasmuch as $\tilde{t}_f \cong 33$. However, for $\tilde{\Omega}_0 = 15$, $\tilde{t}_f \cong 1.8$.

From the above discussion, it can be seen that for URAPS-closure, if the initial state is isotropic ($R_{xx} = R_{yy} = R_{zz} = 1/3$) and homogeneous, then prolate anisotropic states ($0 < R_{yy} = R_{zz} < 1/3 < R_{xx} < 1$) develop due to strong non-linear interactions among the velocity components (i.e., $\|\underline{\mathbf{f}}'(\underline{\mathbf{x}},t)\| \cong \|\underline{\mathbf{u}}'(\underline{\mathbf{x}},t)\cdot\underline{\Omega}\|$). The action of the intrinsic acceleration $\underline{\mathbf{f}}'(\underline{\mathbf{x}},t)$ is fundamental in this reorganization of turbulent kinetic energy. Transport equation for the Reynolds stress shows that the effect of rotation is purely reorganization of turbulent kinetic energy into an axisymmetric form, without effecting the equation for k directly (see Piquet, 1999) This is consistent with the knowledge of literature presented in Chapter 2, indicating that the Reynolds anisotropy is

Table 5.1b.

prolate s 'see Figur

a.c.

b.d,f

Table 5.1a. The Influence of Rotation on the NR-Stress for Homogeneous Decay (see Figure 5.5 For Prolate States).

$ ilde{\Omega}_0$	$R_{xx} \cong 1$ \tilde{t}_{f}	prolate state	ĩ	$\tilde{k}/\tilde{\epsilon}$	N _F	$ ilde{ au}_{ m R}$
1	3 <u>3</u>	a	1 <u>1</u>	1 <u>6</u>	46. <u>2</u>	0.7 <u>0</u>
		b	2 <u>0</u>	3 <u>2</u>	87. <u>5</u>	0.6 <u>9</u>
5	6. <u>0</u>	С	1. <u>5</u>	3. <u>3</u>	46. <u>2</u>	0.7 <u>0</u>
		d	3. <u>3</u>	6. <u>2</u>	87. <u>5</u>	0.6 <u>9</u>
10	2. <u>8</u>	e	0.4 <u>0</u>	1. <u>6</u>	46. <u>2</u>	0.7 <u>0</u>
		f	1. <u>3</u>	3. <u>0</u>	87. <u>5</u>	0.6 <u>9</u>
15	1. <u>8</u>	g	0.06 <u>0</u>	1. <u>1</u>	46. <u>2</u>	0.7 <u>0</u>
		h	0.6 <u>5</u>	2. <u>0</u>	87. <u>5</u>	0.6 <u>9</u>

Table 5.1b. The Influence of Rotation Number on the NR-Stress, the Prestress, and the "Extra" Anisotropy for Homogeneous Decay Predicted by The URAPS-Closure.

prolate states (see Figure 5.5)	N_{Ω}	R _{xx}	B_{xx}	Δ_{xx}
a,c,e,g	+ 0.082	+ 0.500	+ 0.498	- 0.0017
b,d,f,h	+ 0.15	+ 0.750	+ 0.746	- 0.0042

ensitive to the initial indicated $R_{XX} > 1/3$ demonstrated by Camb distribution among the

for long time simulat

anisotropy for pure rot

Thus, for three clearly anisotropic an R_{xx} component in $\frac{1}{2}$

 $\tilde{\Omega}_0 = 1$).

55 "Extra" Anis

The normali

$$\frac{1}{2} = \frac{B}{B} - \frac{R}{R} = C_1 \left(\frac{R}{R} - \frac{1}{R} \right)$$

$$= \beta \left(\frac{R}{R} - \frac{1}{R} \right)$$

$$= \Delta_1 + \Delta_2$$

The second invaria

and
$$\Pi_{\Delta_2} \equiv \underline{\Delta}_2 : \underline{\Delta}_2$$

57, although II 3

intiponents of th

sensitive to the initial conditions and may be either oblate or prolate. DNS results indicated $R_{xx} > 1/3$ for simulations with $\tilde{\Omega}_0 = 25$ (see page 71, Gatski, 1992). As demonstrated by Cambon et al. (1997) and Yang and Domaradzki (2004), anisotropic distribution among the normal components of NR-stress could be either prolate or oblate for long time simulations. Rapid Distortion Theory (RDT) theory which indicates no anisotropy for pure rotation case is incorrect (see Piquet, 1999).

Thus, for three-dimensional rotating homogeneous decay, the Reynolds stress is clearly anisotropic and the URAPS-closure predicts anisotropy shifting the energy to R_{xx} component in a finite time (although long time $\tilde{t}_f \cong 33$ for small rotation rates $\tilde{\Omega}_0 = 1$).

5.5 "Extra" Anisotropy: Results and Discussion

The normalized prestress and the NR-stress have anisotropic components. The "extra" anisotropy $\underline{\Delta}$ in the CH-representation is defined by

$$\underline{\underline{\Delta}} = \underline{\underline{B}} - \underline{\underline{R}} = C_1 (\underline{\underline{R}} - \underline{\underline{I}}/3) + C_2 (\underline{\underline{R}} \cdot \underline{\underline{R}} - II_R \underline{\underline{R}})$$

$$= \beta (\underline{\underline{R}} - \frac{1}{3}\underline{\underline{I}}) 27 \det(\underline{\underline{R}}) - \alpha (II_R - \frac{1}{3}) (\underline{\underline{R}} \cdot \underline{\underline{R}} - II_R \underline{\underline{R}}). \tag{5.11}$$

$$= \underline{\underline{\Delta}}_1 + \underline{\underline{\Delta}}_2$$

The second invariants of the "extra" anisotropic operators are defined as $II_{\Delta_1} = \underline{\Delta}_1 : \underline{\Delta}_1^T$ and $II_{\Delta_2} = \underline{\Delta}_2 : \underline{\Delta}_2^T$. The second invariant associated with $\underline{\Delta}$ is $II_{\Delta} = \underline{\Delta} : \underline{\Delta}^T$. In Figure 5.7, although II_{Δ} is small compared with the second invariants of the anisotropic components of the normalized prestress and the NR-stress, the presence of $\underline{\Delta}$ in

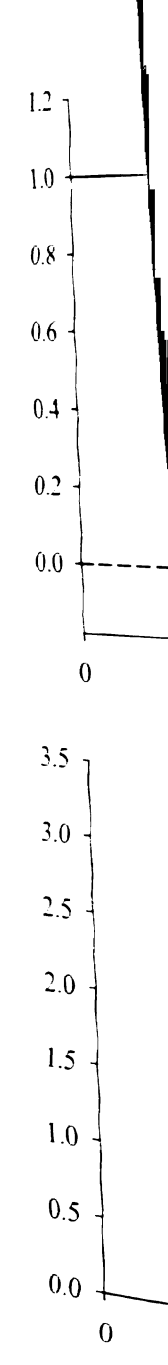


Figure 5.7.

The
Proc
First
Anis

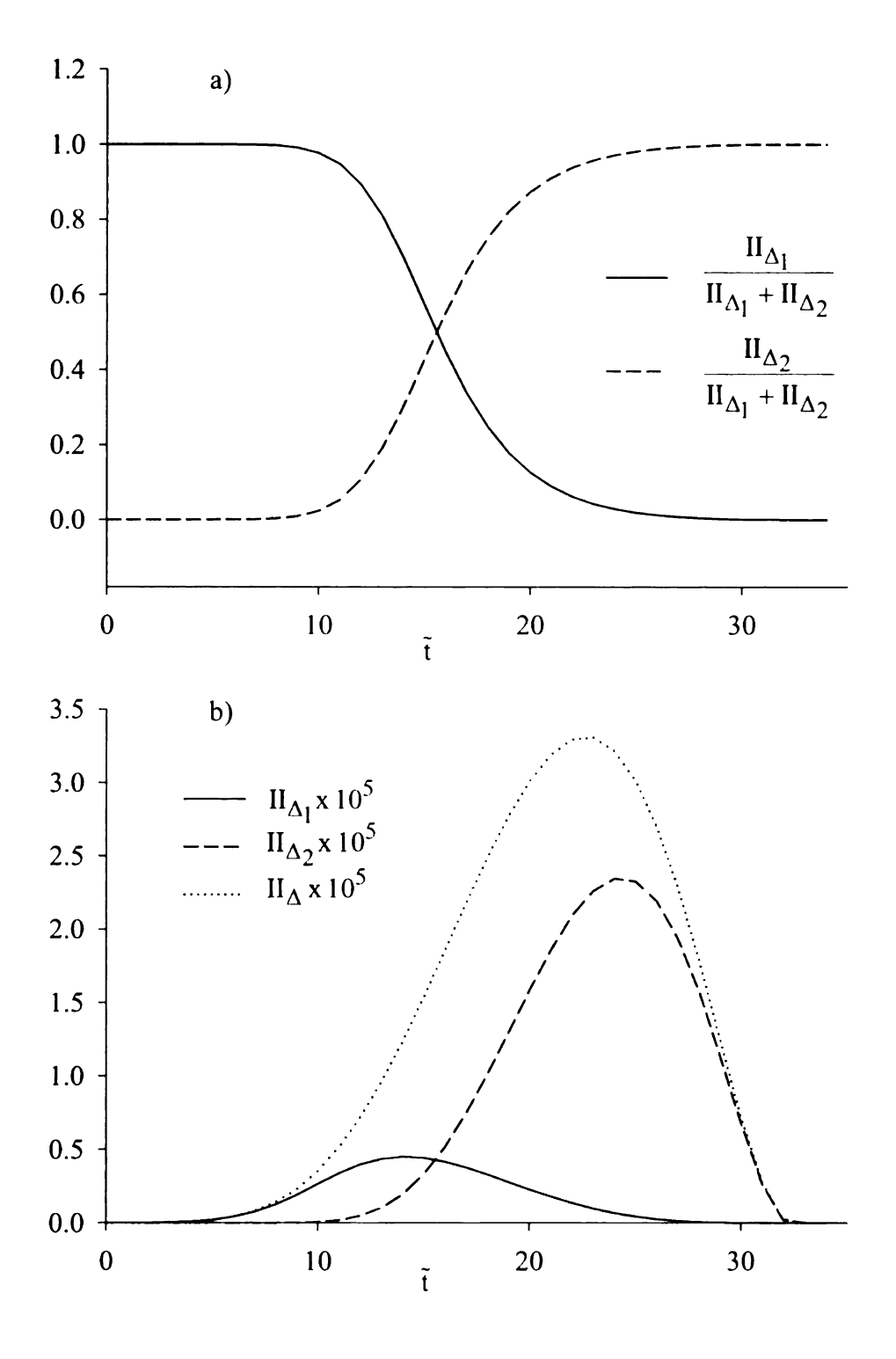


Figure 5.7. The Development of "Extra" Prestress Anisotropy During the Decay Process for $\tilde{\Omega}_0 = 1$: a) Dynamic Response of the Second Invariants for the First Order and Second Order CH-Contributions to the "Extra" Prestress Anisotropy. b) Relative Changes of the First Order and Second Order "Extra" Prestress Anisotropies.

Eq.(5.11) is neverthely ealy prolate solution of the first-order and the During the initial stage during the final stage transfer of energy from

- 5.6 Conclusions

 In this chapte
- $\tilde{\epsilon},\,\tilde{k},\tilde{\epsilon}$ and \tilde{k}^2 , $\tilde{\epsilon}$,
 - decay for a there is decay (i.e., $0 < \tilde{t}$ decrease i
 - mitigates
 - exceeds th
 - 2. The turbu homogene
 - $|\tilde{k}^2/\tilde{\epsilon}|_{bec}$

Eq.(5.11) is nevertheless fundamentally important. It is noteworthy that if $\underline{\Delta} = \underline{0}$, then the only prolate solution is $\underline{R} = \underline{B} = \underline{e}_x \, \underline{e}_x$. Figure 5.7 also shows that the relative importance of the first-order and the second-order anisotropic operators on the local anisotropic state. During the initial stage of the decay process ($\tilde{t} <<1$), the first-order anisotropic operator $\underline{\Delta}_1$ controls the redistribution of energy (see Figure 5.7a and Figure 5.7b). However, during the final stage ($\tilde{t} >>1$), the second-order anisotropic operator $\underline{\Delta}_2$ controls the transfer of energy from the transverse plane to the longitudinal axis.

5.6 Conclusions

In this chapter, the NR-stress distribution, along with the dynamic behavior of \tilde{k} , $\tilde{k}/\tilde{\epsilon}$ and $\tilde{k}^2/\tilde{\epsilon}$, for rotating homogeneous flows is studied for various rotation rates.

- 1. The decay of \tilde{k} and $\tilde{\epsilon}$ shown in the phase plane indicates that both \tilde{k} and $\tilde{\epsilon}$ decay for all rotation rates. The decay dynamics in the initial stage indicate that there is decreased dissipation rate with increased rotation. During the initial stage (i.e., $0 < \tilde{t} < 0.1$), an enhanced rate-of-decay of $\tilde{\epsilon}$ is observed because of the decrease in $\tilde{\tau}_R$. However, during the final stage for $\tilde{t} > 4$, where rotation mitigates the rate of decay of dissipation, dissipation for $\tilde{\Omega}_0 = 10$ eventually exceeds the dissipation for $\tilde{\Omega}_0 = 0$ (see Figure 5.1b).
- 2. The turbulent time scale and dispersion monotonically decrease for non-rotating homogeneous decay. However, in the presence of rotation, turbulent dispersion, $\tilde{k}^2/\tilde{\epsilon}$ becomes unbounded for all rotation rates (see Figure 5.4) with the initial

slopes defined rotation numb.

3. In rotating how the NR-stress

Coriolis acceled that product $-\alpha < N_{\Omega} = 20$ 4. For $\tilde{\Omega}_0 < 1$, transfer time $\tilde{\Omega}_0 > 1$, the

5. The extra-a energy in

second ord

- slopes defined in Eq. (5.3), to be either positive or negative depending the initial rotation number $\tilde{\Omega}_0$.
- 3. In rotating homogeneous decay, the anisotropic quadratic form associated with the NR-stress is elongated by a coupling between velocity fluctuations and the Coriolis acceleration. The component equation for R_{xx} (see Eq.(5.10)) shows that prolate anisotropic states exist for the rotation group $-\infty < N_{\Omega} = 2C_{R1}\tilde{\tau}_{R}\tilde{\Omega} < \infty \,.$
- 4. For $\tilde{\Omega}_0$ < 1, energy is shifted slowly to the R_{xx} component (R_{xx} = 1). The transfer time is significant inasmuch as $\tilde{t}_f > 30$. However, for rotation rates $\tilde{\Omega}_0 > 1$, the redistribution of energy from an isotropic initial state is attained in a relatively short time (e.g. $\tilde{\Omega}_0 = 15$, $\tilde{t}_f \cong 1.8$).
- 5. The extra-anisotropy terms in the preclosure play the role of this transfer of energy in URAPS-closure. During the initial and final decay stages, first and second order anisotropic contributions to the prestress control the transfer process (see Figure 5.7).

Introduction

mitial conditions

 $^{\circ n}$ understanding

As discussifisimilar beha

CHAPTER 6

HOMOGENEOUS SHEAR

6.1 Introduction

Statistically homogenous shear flow is characterized by constant or uniform mean shear independent of spatial position. Self similar solutions obtained for this flow observed in experiments (Rohr at al., 1988, Tavoularis and Karnik, 1989) as well as DNS and LES simulations (see Salhi and Cambon, 1997, Brethouwer, 2005) for rotating homogeneous shear discussed in Chapter 2, are often used in turbulence modeling to calibrate and validate closures for low-order statistical properties. Figure 6.1 illustrates the idea of a homogeneous shear with rotation. The shear rate Γ_{yz} is constant and the rotation rate is $\underline{\Omega} = \Omega_x e_x$. In this chapter, the dynamic equation for $\tilde{\Gamma} = \Gamma_{yz} k / \epsilon$ and the URAPS-closure component equations are presented in Sections 6.2 and 6.3. In Section 6.4, the asymptotic states for different values of Ω_x / Γ_{yz} are determined by solving the dynamic equation for $\tilde{\Gamma} = \Gamma_{yz} k / \epsilon$ and the URAPS-equation. The predictions are also compared with the literature discussed in Chapter 2. The NR-stress results for various initial conditions (i.e., $\tilde{\Gamma}_{o}$) are discussed in Section 6.6. Sections 6.5 and 6.7 are focused on understanding the contribution of the "extra" anisotropy terms in the URAPS-closure.

6.2 Dynamic Equation for $\tilde{\Gamma}$

As discussed in Chapter 3, the k and epsilon equations support the existence of self-similar behavior. That is, if k(x,t) is proportional to $\epsilon(x,t)$ within a finite space-

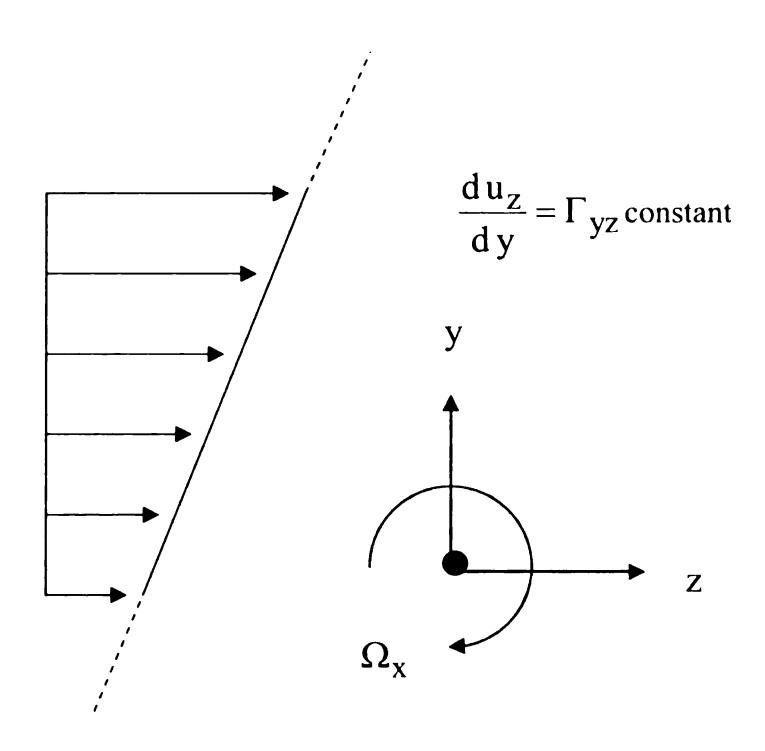


Figure 6.1 Schematic of Rotating Homogeneous Shear Flow

time domain (i.e., k &

field time scale \(\bar{\Gamma}\) sat

$$\frac{d\hat{\Gamma}}{d\hat{t}} = \left(-2\hat{\Gamma} \underline{R} : \underline{e}_z \underline{e}_y - \frac{1}{\hat{\tau}_{\mu}}\right)$$
$$= ([\mathcal{P} \ \epsilon] - 1) - \frac{1}{\hat{\tau}_{\mu}}$$

where
$$\tilde{\Gamma} \equiv \tilde{\Gamma}_0 \frac{\tilde{k}}{\tilde{\epsilon}}$$
 ,

This flow shows an

equation can be rearra

$$\hat{z}_{R}(x, N_{F}) = \frac{\tilde{C}_{P}[\mathcal{P}]}{[\mathcal{P}]}$$

where $\zeta^b \equiv C^b \cdot C^B$

kinetic energy to di

asymptotic states.

component of NR-

logether with the U

tat Eq. (6.2) is sa

discussed in the following

Preclosure (

Asymptotic

which the angular

time domain (i.e., k/ϵ is a constant), then the ratio of the turbulent time scale to the mean field time scale $\tilde{\Gamma}$ satisfies the following non-linear algebraic equation:

$$\frac{d\tilde{\Gamma}}{d\tilde{t}} = \left\{ -2\tilde{\Gamma} \underline{R} : \underline{e}_{z} \underline{e}_{y} - 1 \right\} - \left\{ \tilde{C}_{P} \frac{-2\tilde{\Gamma} \underline{R} : \underline{e}_{z} \underline{e}_{y}}{\tilde{\tau}_{R}} - \tilde{C}_{D} \frac{1}{\tilde{\tau}_{R}} \right\}
= ([\mathcal{P}/\epsilon] - 1) - \frac{1}{\tilde{\tau}_{R}} (\tilde{C}_{P} [\mathcal{P}/\epsilon] - \tilde{C}_{D}) = 0$$
(6.1)

$$\text{where } \tilde{\Gamma} \equiv \tilde{\Gamma}_o \frac{\tilde{k}}{\tilde{\epsilon}} \quad , \quad \tilde{\Gamma}_o \equiv \Gamma_{yz} \frac{k_o}{\epsilon_o} \qquad \tilde{t} \equiv \Gamma_{yz} t_u \text{ and } \quad t_u \equiv \frac{z}{< u_z > (0)} \, .$$

This flow shows an asymptotic solution that $\frac{d\tilde{\Gamma}}{d\tilde{t}} = 0$, (i.e. $\tilde{\Gamma}^a = \text{constant}$) The above equation can be rearranged as below in Eq. (6.2)

$$\tilde{\tau}_{R}(\infty, N_{F}) = \frac{\tilde{C}_{P}[\mathcal{P}/\epsilon] - \tilde{C}_{D}}{[\mathcal{P}/\epsilon] - 1} , \quad [\mathcal{P}/\epsilon] = -2 \,\tilde{\Gamma}(\underline{\underline{R}} : \underline{e}_{z}\underline{e}_{y})$$
(6.2)

where $\tilde{C}_P \equiv C_P/C_{R1}$, $\tilde{C}_D \equiv C_D/C_{R1}$ and \mathcal{P}/ϵ is the ratio of production of turbulent kinetic energy to dissipation. It should be noted that \mathcal{P}/ϵ is also a constant for the asymptotic states. The above Eq. (6.1) however, needs the information of the shear component of NR-stress that can be computed from the URAPS-closure. Eq. (6.1) together with the URAPS-closure can be solved for developing homogeneous flows so that Eq. (6.2) is satisfied in the asymptotic region. The URAPS-closure equations are discussed in the following section.

6.3 Preclosure Operator and URAPS-Closure

Asymptotic homogeneous shear (AHS-) flow in a rotating frame of reference for which the angular velocity is co-linear with the mean field vorticity has the following

URAPS equations (s

ease). The preclosure

$$\frac{1}{4}^{-1} = \frac{1}{2} + \tau_R < \frac{F}{E} > =$$

$$\begin{split} &\underline{A}^{-1} = \underline{I} + \tau_R < \underline{F} > = \\ &\underline{A} = \frac{\underline{C}}{\det(\underline{I} + \tau_R < \underline{F} >)} \\ &= \frac{(I + N_\Gamma N_\Omega + N_\Omega^2)}{2} \end{split}$$
 where $N_\Gamma \equiv \tilde{\tau}_R \tilde{\Gamma}$ and

$$=\frac{(1+N_{\Gamma}N_{\Omega}+N_{\Omega}^{2})}{1+N_{\Gamma}N_{\Omega}+N_{\Omega}^{2}}$$

 $\tilde{\Gamma}$ and $\tilde{\Omega}$ or for asym:

simplify the compon

asymptotic states, the r

change with time. Sol

No were determined

agonithm converges t

with invariants withir

Asymptotic S

The self-simi in simultaneously so

that RHS of Eq. (6.

solving the above

URAPS equations (see Appendix G for URAPS equations with $N_{\Gamma} \neq 0$ and $N_{\Omega} \neq 0$ case). The preclosure operator for this flow is,

$$\underline{\underline{A}}^{-1} = \underline{\underline{I}} + \tau_{R} < \underline{\underline{F}} > = \underline{\underline{e}}_{x} \underline{\underline{e}}_{x} + \underline{\underline{e}}_{y} \underline{\underline{e}}_{y} + \underline{\underline{e}}_{z} \underline{\underline{e}}_{z} + (N_{\Gamma} + N_{\Omega}) \underline{\underline{e}}_{y} \underline{\underline{e}}_{z} - N_{\Omega} \underline{\underline{e}}_{z} \underline{\underline{e}}_{y}$$
(6.3)

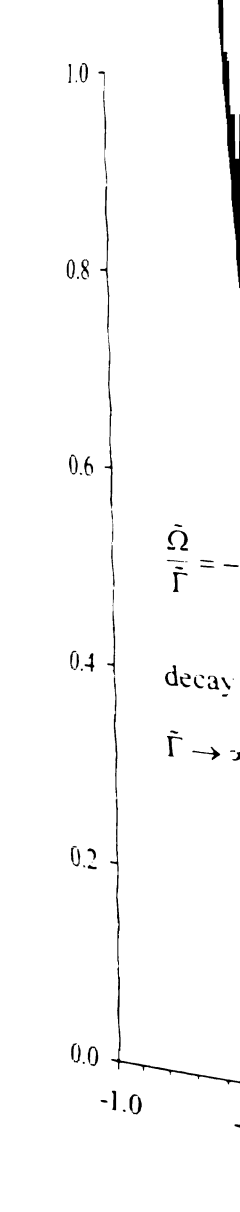
$$\underline{\underline{A}} = \frac{\underline{\underline{C}}}{\det(\underline{\underline{I}} + \tau_{R} < \underline{\underline{F}} >)}$$

$$= \frac{(1 + N_{\Gamma}N_{\Omega} + N_{\Omega}^{2}) \underline{e}_{x} \underline{e}_{x} + \underline{e}_{y}\underline{e}_{y} + \underline{e}_{z}\underline{e}_{z} - (N_{\Gamma} + N_{\Omega})\underline{e}_{y}\underline{e}_{z} + N_{\Omega}\underline{e}_{z}\underline{e}_{y}}{(1 + N_{\Gamma}N_{\Omega} + N_{\Omega}^{2})}$$
(6.4)

where $N_{\Gamma} \equiv \tilde{\tau}_R \tilde{\Gamma}$ and $N_{\Omega} \equiv 2 \, \tilde{\tau}_R \, \tilde{\Omega}$. URAPS-closure can be fully defined by specifying $\tilde{\Gamma}$ and $\tilde{\Omega}$ or for asymptotic homogeneous shear. N_{Γ} and N_{Ω} defined above are used to simplify the component equations. Through the developing flow region towards asymptotic states, the ratio $\frac{1}{2} \frac{N_{\Omega}}{N_{\Gamma}} (= \frac{\tilde{\Omega}}{\tilde{\Gamma}} = \frac{\Omega_x}{\Gamma_{yz}})$ remains constant although N_{Γ} and N_{Ω} change with time. Solutions to URAPS-closure equations for a given value of N_{Γ} and N_{Ω} were determined by successive substitution. For rotating simple shear flows, the algorithm converges to a unique solution for any initial non-negative operator (i.e., n=0) with invariants within the L-diagram (see Figures 4.6 and 4.7)

6.4 Asymptotic States for $\tilde{\Gamma}$ and the NR-Stress: Results and Discussion

The self-similar solutions summarized in this section were developed numerically by simultaneously solving Eq.(6.1) and the URAPS-closure equations for long times such that RHS of Eq. (6.1) is essentially zero. Appendix H has the flowchart and program for solving the above equations. Figure 6.2 shows that non-trivial, self-similar solutions



hgure 6.2 Valu

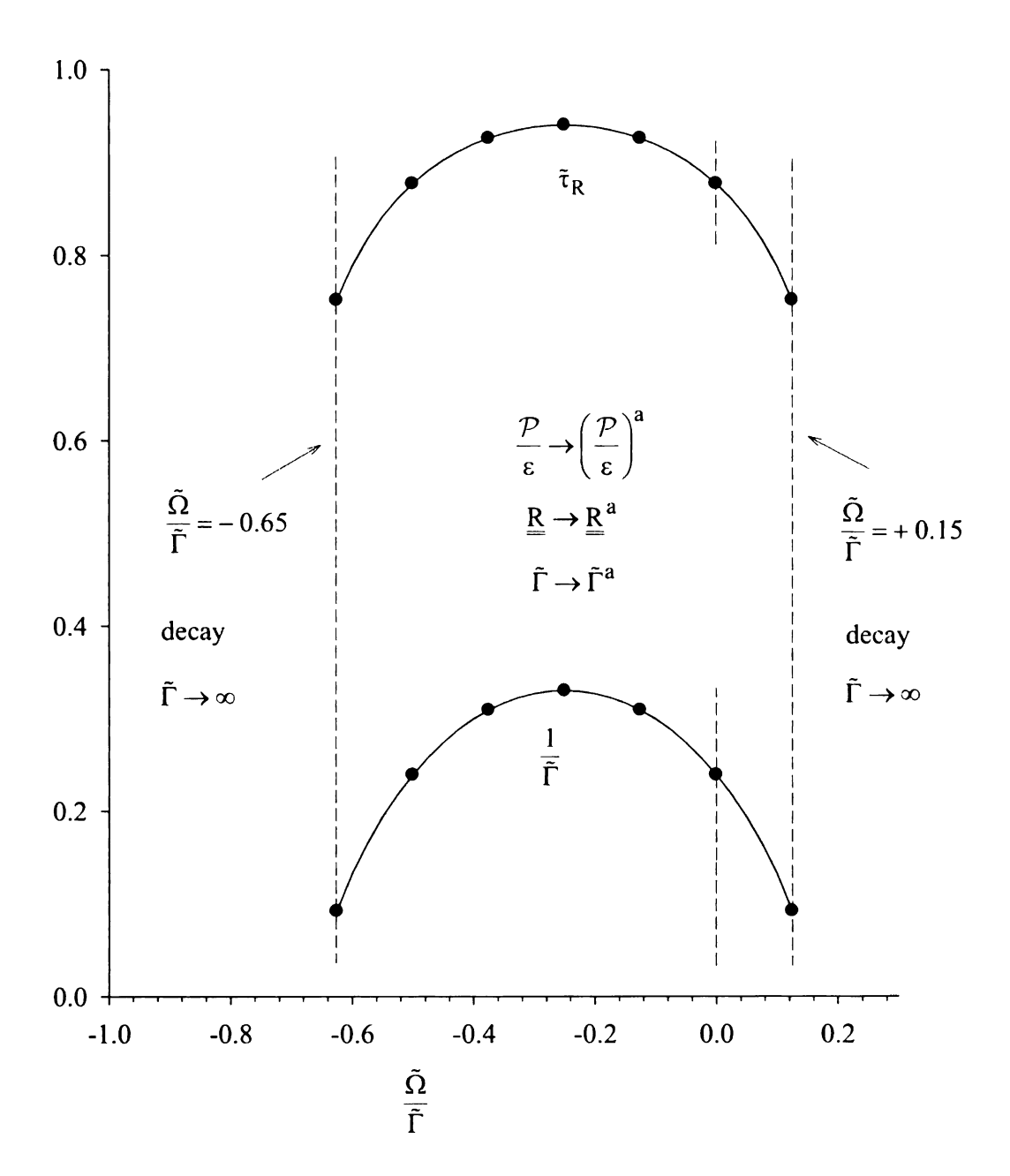


Figure 6.2 Values of $\tilde{\tau}_R$ and $1/\tilde{\Gamma}$ for the Asymptotic States Characterized by $\tilde{\Omega}/\tilde{\Gamma}$.

The lower curve in II upper curve shows the the rotation number. However, near the upper $\hat{\Omega}$ $\hat{\Gamma}$ decreases minimum.

Figure 6.3 illu

occur for a finite ra

turbulent kinetic energy data all the anisotropy temoved from the constitution of the street about 0.60 as $\tilde{\Omega}$ if decreases from 0.53 decreases from 0.53 decreases from 0.53 figure components. Figure 6.3).

occur for a finite range of rotation numbers: $-0.65 = (\frac{\tilde{\Omega}}{\tilde{\Gamma}})_{min} < \frac{\tilde{\Omega}}{\tilde{\Gamma}} < (\frac{\tilde{\Omega}}{\tilde{\Gamma}})_{max} = +0.15$. The lower curve in Figure 6.2 shows the effect of the rotation number on $\tilde{\Gamma}^{-1}$ and the upper curve shows the effect of $\tilde{\Omega}/\tilde{\Gamma}$ on the dimensionless transport time $\tilde{\tau}_R$. Clearly, the rotation number has a large effect on $\tilde{\Gamma}$. For example, with $\tilde{\Omega}=0$, $\tilde{\Gamma}=4.2$. However, near the upper and lower bounds on $\tilde{\Omega}/\tilde{\Gamma}$ (see States 1 and 7), $\tilde{\Gamma}$ is about 11. As $\tilde{\Omega}/\tilde{\Gamma}$ decreases from 0 to -1/4, $\tilde{\Gamma}$ decreases from 4.2 to 3, which is a local minimum.

Figure 6.3 illustrates the effect of rotation on the redistribution of the normalized turbulent kinetic energy and on the anisotropic invariants. The URAPS-closure predicts that all the anisotropic states are prolate-like (i.e., $\Pi I_b > 0$). For $\tilde{\Omega}/\tilde{\Gamma} > 0$, the energy is removed from the cross-flow and span-wise components of the fluctuating velocity and shifted into the stream-wise component. For $\tilde{\Omega}/\tilde{\Gamma} = 0$, R_{zz} is about 0.55 and increase to about 0.60 as $\tilde{\Omega}/\tilde{\Gamma}$ increases to +1/8. However, as $\tilde{\Omega}/\tilde{\Gamma}$ decreases to -8/5, R_{zz} decreases from 0.55 to 0.14; and, R_{yy} increases from 0.20 to 0.60. As shown in Figure 6.3, the predicted shift in the turbulent energy by the URAPS-closure is qualitatively consistent with results observed in DNS and LES studies (see Bardina et al., 1983; Piquet, p. 213, 1999; Brethouwer, 2005) (The solution is extrapolated from the short time simulations). The widely used B-closure predicts an equipartition of energy among the three components of the fluctuating velocity for all values of the rotation group (see Figure 6.3).

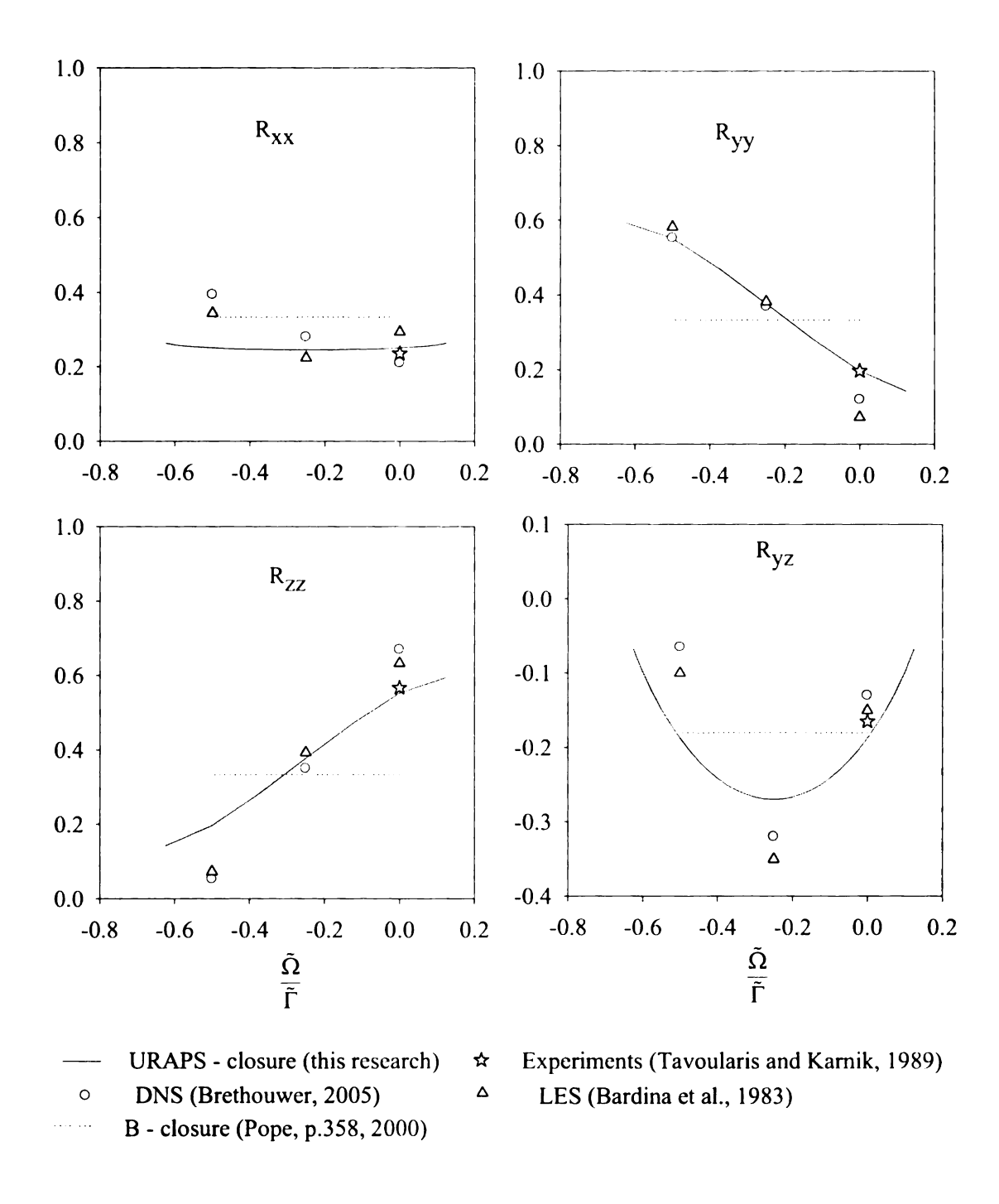


Figure 6.3 Asymptotic States of the Components of $\underline{\underline{R}}$ (Comparison with DNS and LES data)

It is especial!

absolute vorticity distribution with R

URAPS-closu

(Speziale et al., 199

dosures which prediction

asymptotic states in

Piquet, p.259, 1999

region which distin

90 self similar solu

(995) predict self's

i approaches a co

of DNS and LES r

ange of rota

त्राता which cause

equired. Further

of the algebraic me

states for all rotation

It is especially interesting to note that $\tilde{\Omega}/\Gamma=-0.5$ corresponds to the zero mean absolute vorticity discussed in Chapter 2. This region occurs in the HP side of spanwise rotating channel (see Chapter 7). The results for the asymptotic solution in this region and the results in rotating channel (see Table I.4, Appendix I) show the same trend of energy distribution with $R_{yy} > R_{zz}$.

URAPS-closure predictions are qualitatively consistent with the second-order closures which predict asymptotic solutions for $-0.53 = (\frac{\tilde{\Omega}}{\tilde{\Gamma}})_{min} < \frac{\tilde{\Omega}}{\tilde{\Gamma}} < (\frac{\tilde{\Omega}}{\tilde{\Gamma}})_{max} = +0.09$ (Speziale et al., 1996, Piquet, p.259, 1999). Rapid Distortion Theory (RDT) predicts asymptotic states in the region of about $-0.6 < \frac{\tilde{\Omega}}{\tilde{\Gamma}} < 0.2$ (see Salhi and Cambon, 1997, Piquet, p.259, 1999). Standard B-closure based models cannot predict this bifurcation region which distinguishes region of self-similar solutions with regions where there are no self similar solutions. Linear and Bilinear Shih models (Shih et al. 1994, Shih et al. 1995) predict self similar solutions for $-\infty < \frac{\tilde{\Omega}}{\tilde{\Gamma}} < \infty$. For all values of $\frac{\tilde{\Omega}}{\tilde{\Gamma}}$, the value of $\tilde{\Gamma}$ approaches a constant within a finite time, which is not consistent with the knowledge of DNS and LES results. Incase of URAPS-closure, asymptotic states are observed for a finite range of rotations. The effect of rotation on the Eq. (6.1) through the production term which causes this phenomenon of asymptotic states for finite rotation rates is captured. Further details of why the asymptotic states occur for URAPS and not for some of the algebraic models will be clearer at the end of this chapter after studying developing states for all rotation rates.

65 Asymptotic "I In this section extra anisotropy in at Later, the extra aniso

illustrated in Chapter

that the fixed point

 $\tilde{\Gamma}$ =4: Case2: $\tilde{\Omega}$ $\tilde{\Gamma}$ The component

m Table 4.3, and the

simple shear flows

 $N_{\Gamma} = 0.01259$. The

are more than two c

the NR-stress. The

and for $\underline{\underline{R}}$ (i.e., γ

eigenvalues for $\underline{\underline{B}}$,

½ are two orders of

nevertheless plays

a shown by Figur

ettra-anisotropic oj

hear the fixed-poin

few iterations whe

6.5 Asymptotic "Extra" Anisotropy: Results and Discussion

In this section, first the convergence of URAPS closure theory and the role of extra anisotropy in attaining a unique state is discussed for two of the asymptotic states. Later, the extra anisotropy contributions for all the asymptotic states are discussed. (Note that the fixed point mapping trajectory for the two cases presented below has been illustrated in Chapter 4, Section 4.7, for various initial conditions. Case 1: $\tilde{\Omega}/\tilde{\Gamma} = 0$ and $\tilde{\Gamma} = 4$; Case2: $\tilde{\Omega}/\tilde{\Gamma} = -5/8$ and $\tilde{\Gamma} = 11$.)

The components of the prestress, the NR-stress were discussed in earlier Chapter in Table 4.3, and the extra-anisotropic operator are listed in Table 6.1a for non-rotating simple shear flows with $\tilde{\Omega}/\tilde{\Gamma}=0$ and $\tilde{\Gamma}=4$. For this case, $N_F=4$, $\tilde{\tau}_R=0.8818$ and $N_{\Gamma} = 0.01259$. The results show that the components of the extra-anisotropic operator are more than two orders of magnitude smaller than the components of the prestress and the NR-stress. The correlation coefficients for $\underline{\underline{B}}$ (i.e., $\chi_B \equiv \left|B_{yz}\right|/\sqrt{B_{yy}B_{zz}} = 0.558$) and for $\underline{\underline{R}}$ (i.e., $\chi_R = \left| R_{yz} \right| / \sqrt{R_{yy}R_{zz}} = 0.563$) are comparable. Table 6.1 gives the eigenvalues for \underline{B} , \underline{R} , and $\underline{\Delta}$. Although the eigenvalues of the extra-anisotropic operator $\underline{\Delta}$ are two orders of magnitude smaller than the eigenvalues of \underline{B} and \underline{R} , the $\underline{\Delta}$ -operator nevertheless plays a fundamental role in determining the fixed-point solutions to URAPS as shown by Figures 6.4 and 6.5. As illustrated by Figure 6.4, the eigenvalues of the extra-anisotropic operators, $\underline{\Delta}_1$ and $\underline{\Delta}_2$, determine the fine structure of the solution path near the fixed-point. Figure 6.4a shows that the eigenvalues of $\underline{\Delta}_1$ begin to appear after a few iterations whereas the eigenvalues of $\underline{\Delta}_2$ do not appear until after 20 iterations. If

Table 6.1a. Eigenva

eigenvalue	7.
i=1	+ 0.12
i=2	+ 0.25
i=3	+ 0.6

Table 6.1b. Eigenv

eigenvalue	λ_{A}^{B}
j=]	+ 0.13
i=2	+ 0.26
j=3	+ 0.60

Table 6.1a. Eigenvalues of $\underline{\underline{B}}$, $\underline{\underline{R}}$, and $\underline{\underline{\Delta}}$ ($\tilde{\Gamma} = 4$ and $\tilde{\Omega} / \tilde{\Gamma} = 0$)

eigenvalue	λ_{i}^{B}	λ_{i}^{R}	$\lambda_i^{\Delta} \times 10^3$
i =1	+ 0.121361	+ 0.119680	+ 1.681
i=2	+ 0.253705	+ 0.252520	+ 1.185
i=3	+ 0.624934	+ 0.627800	- 2.866

Table 6.1b. Eigenvalues of $\underline{\underline{B}}$, $\underline{\underline{R}}$, and $\underline{\underline{\Delta}}$ ($\tilde{\Gamma} = 11$ and $\tilde{\Omega}/\tilde{\Gamma} = -5/8$)

eigenvalue	λ_{i}^{B}	λ_i^R	$\lambda_i^{\Delta} \times 10^3$
i=1	+ 0.133596	+ 0.131950	+ 1.646
i=2	+ 0.264508	+ 0.263520	+ 0.988
i=3	+ 0.601896	+ 0.604530	- 2.634

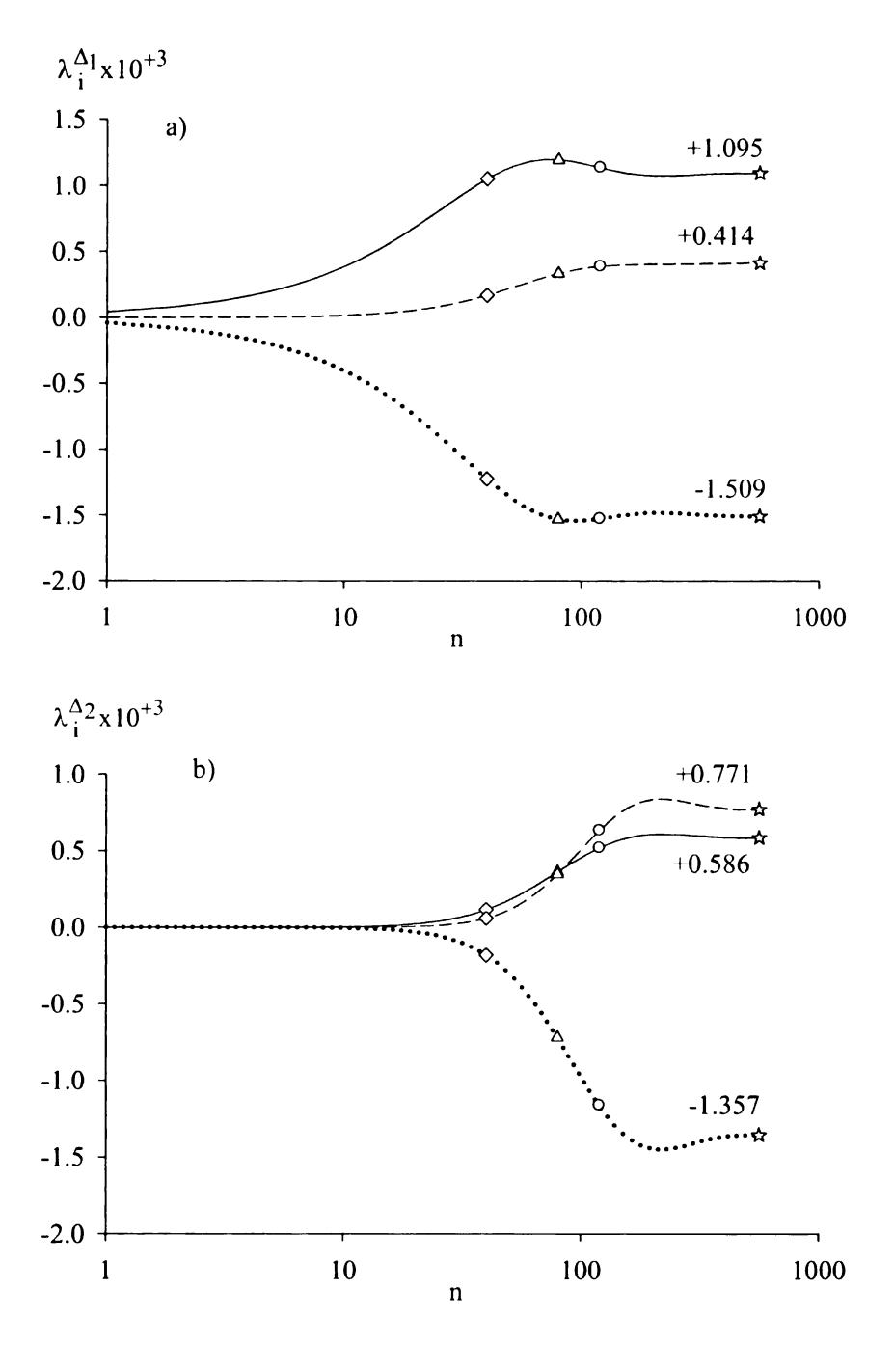


Figure 6.4 The Development of Extra-Anisotropy Eigenvalues for $\tilde{\Gamma}=4$ and $\tilde{\Omega}/\tilde{\Gamma}=0$ from an Isotropic State ((a) $\underline{\Delta}_1$ -eigenvalues; (b), $\underline{\Delta}_2$ -eigenvalues; λ_1 ——; λ_2 ——; λ_3 ·····; iterations: 40 \diamondsuit ; 80 \triangle ; 120 \bigcirc ; fixed point, $\dot{\Xi}$).

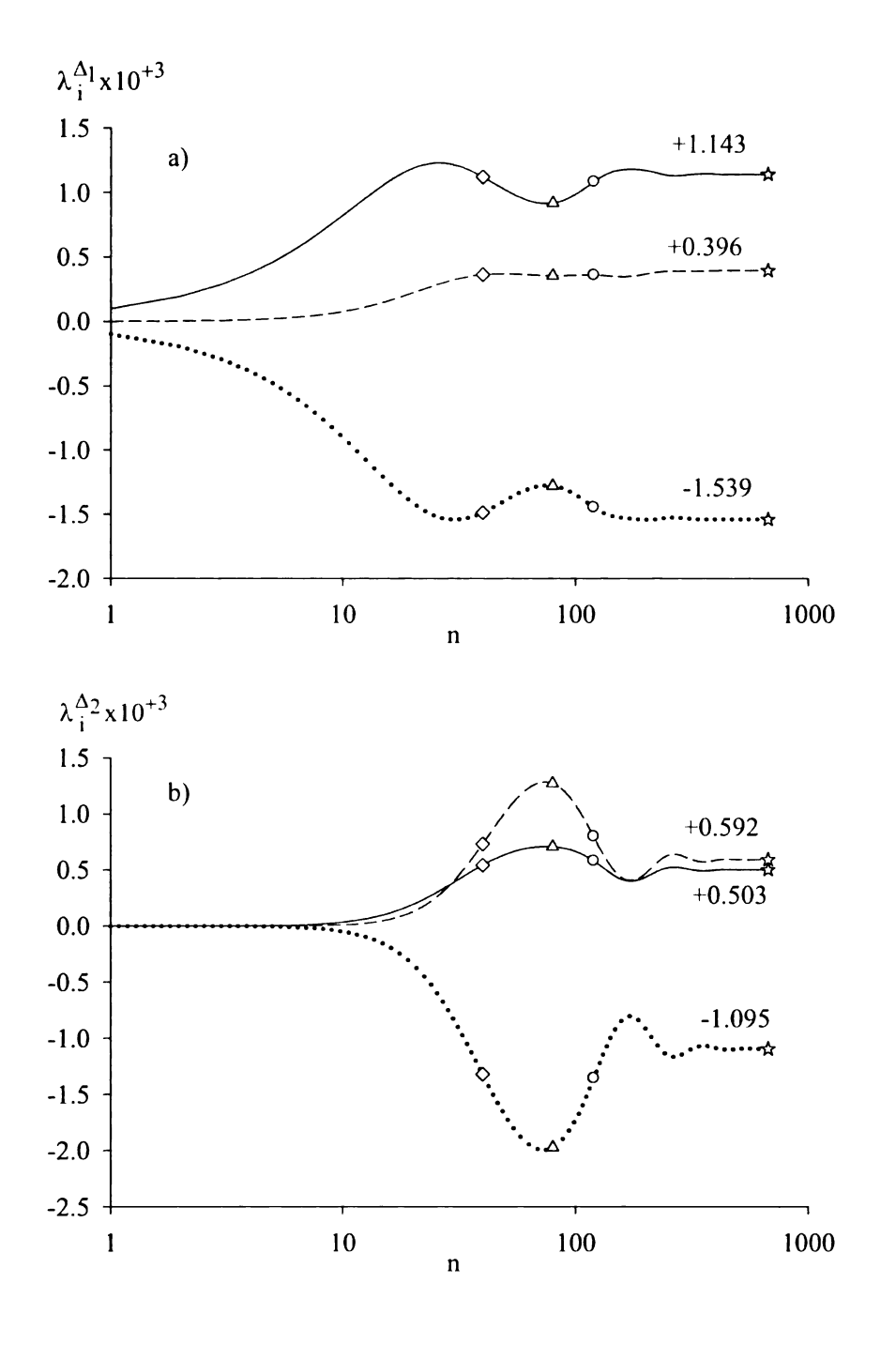


Figure 6.5. The Development of Extra-Anisotropy Eigenvalues for $\tilde{\Gamma}=11$ and $\tilde{\Omega}/\tilde{\Gamma}=-5/8$ from an Isotropic State (see Figure 6.4 for notation).

the extra-anisotropic operator were turned off for n > 120 (i.e., $\alpha = 0$ and $\beta = 0$), a fixed-point to URAPS still exist, but it moved to a different ellipsoidal state with $II_b = 0.6662$ and $III_b = 0.2220$. This is significantly different than the $\frac{1}{100}$ -point for which $II_b = 0.1389$ and $III_b = 0.01525$ with $\alpha = 1/10$ and $\beta = -1/100$. Thus, the prestress extra-anisotropy, albeit small, plays an important quantitative role in determining the prestress and, thereby, the NR-stress.

The components of \underline{B} , \underline{R} , and $\underline{\Delta}$ are listed earlier in Table 4.4 for rotating simple shear flows with $\tilde{\Omega}/\tilde{\Gamma}=-5/8$ and $\tilde{\Gamma}=11$. For this case, $N_F=14$, $\tilde{\tau}_R=0.756$, $N_\Gamma=0.02948$, and $N_\Omega=-0.03685$. The results in Figure 6.5 also show that the fixed-point components of the extra-anisotropic operator are more than two orders of magnitude smaller than the components of the prestress and the NR-stress. The correlation coefficients for \underline{B} and \underline{R} are comparable (i.e., $\chi_B=0.228$ and $\chi_R=0.231$), but significantly smaller than the non-rotating example above. Table 6.1b gives the eigenvalues for the rotating example. Like the non-rotating case, the eigenvalues of $\underline{\Delta}$ are two orders of magnitude smaller than the eigenvalues of \underline{B} and \underline{R} ; and, as illustrated by Figures 6.4 and 6.5, the $\underline{\Delta}$ -operator plays a fundamental and quantitative role in determining the NR-stress.

The eigenvalue contributions from the extra-anisotropy $\underline{\Delta}$ are of the order of 10^{-3} for all the asymptotic states as can be seen in Figure 6.6. Two of the eigenvalues are positive while the other is negative. One of the eigenvalues remains almost approximately the same for all the rotation variations at about 1.5×10^{-3} . The variation in

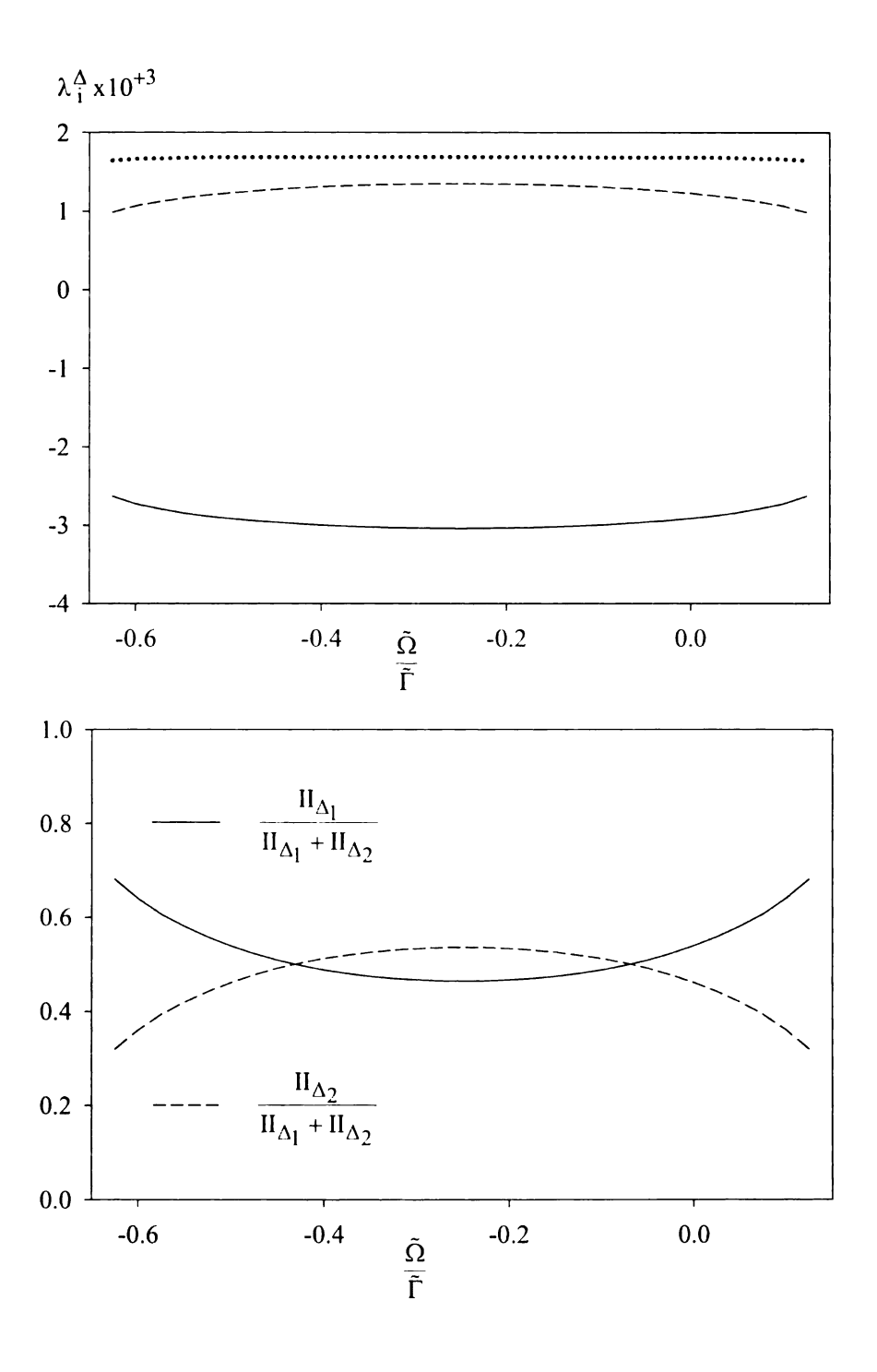


Figure 6.6 Eigenvalues of the Extra-Anisotropy $\underline{\underline{\Delta}}$ and Relative Contributions from $\underline{\underline{\Delta}}_1$ and $\underline{\underline{\Delta}}_2$ for Asymptotic Solutions.

the other two although small, causes different energy states for the NR-distribution. The normal components of NR are different for $\frac{\tilde{\Omega}}{\tilde{\Gamma}}=0$ and -0.5 because of the different energy contributions in the R $_{yy}$ and R $_{zz}$. However, the eigenvalues associated with these states are the same as there is a shift in the energy states without change in the values. This is reflected in the eigenvalues of the extra anisotropy too as the eigenvalue distribution is symmetric about $\frac{\tilde{\Omega}}{\tilde{\Gamma}}=-0.25$, with the same eigenvalues for 0 and -0.5 etc. The relative contributions from $\underline{\Delta}_1$ and $\underline{\Delta}_2$ can be seen in Figure 6.6. The relative values of the second invariant contributions show that contributions from $\underline{\Delta}_2$ are significant in the range between $-0.45 < \frac{\tilde{\Omega}}{\tilde{\Gamma}} < 0.05$. At these limits, both the contributions are almost equal. Outside this range, $\underline{\Delta}_1$ eigenvalues are more important for the anisotropic distribution.

6.6 Developing $\tilde{\Gamma}$, \mathcal{P}/ϵ and the NR-Stress (shear component) for Homogeneous Shear

Eq. (6.2) along with the URAPS-closure discussed in Sections 6.2 and 6.6 are studied for different initial conditions of $\tilde{\Gamma}_0 = 0.5, 1, 2, 5, 10$ and 15 and for different rotation rates to understand the development towards asymptotic states which occurs only for the finite range of $\frac{\tilde{\Omega}}{\tilde{\Gamma}}$ discussed in Section 6.4. Figure 6.7 presents variation of the dimensionless shear $\tilde{\Gamma}$ from different initial values of $\tilde{\Gamma}_0$. Although at $\tilde{t}=0$, the states

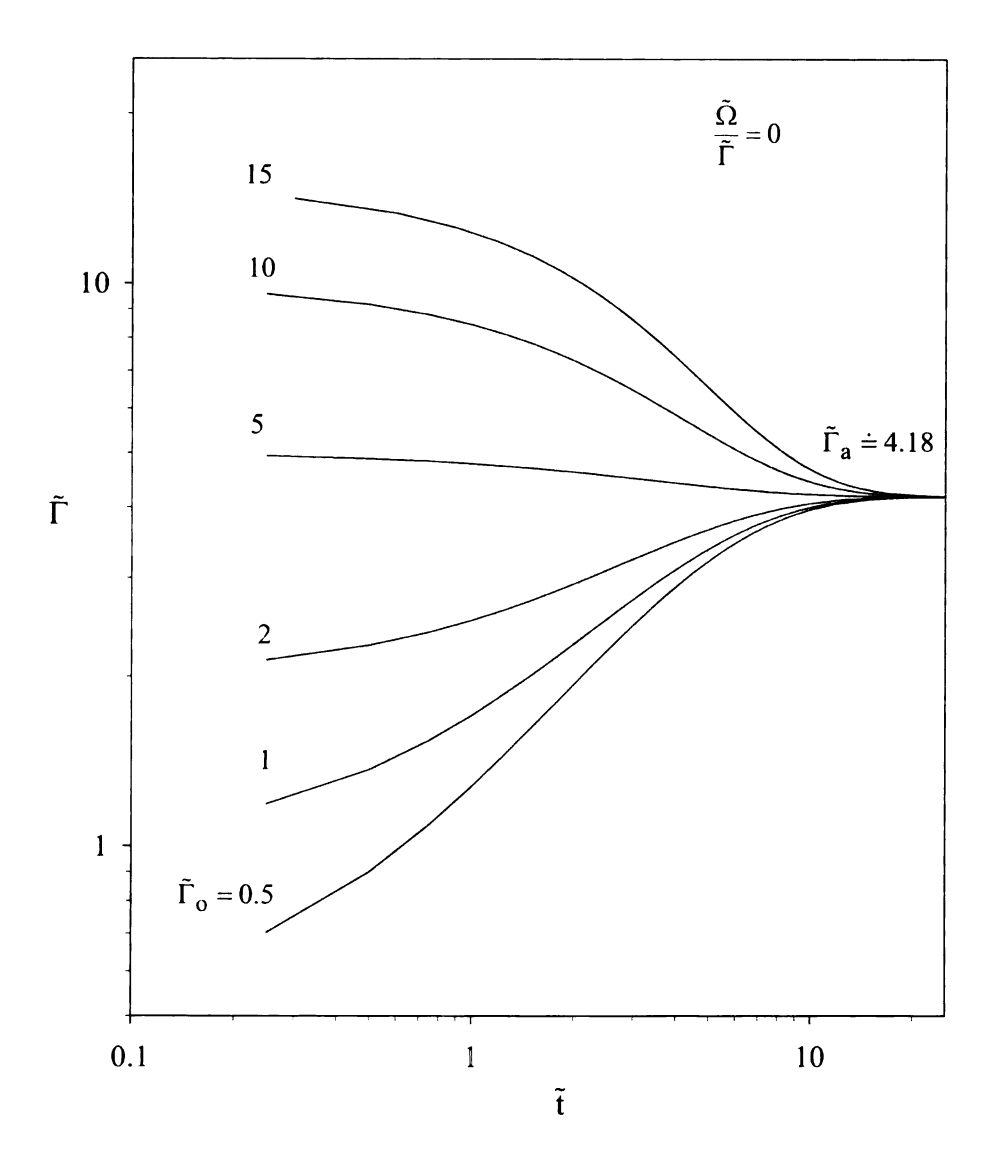


Figure 6.7 Developing $\tilde{\Gamma}$ Towards Asymptotic States for Various Initial $\tilde{\Gamma}_{o}$.

are all different, all the curves rapidly attain a final asymptotic state of $\tilde{\Gamma}_a \cong 4.2$. Independent of the initial condition, $\tilde{\Gamma}$ attains an asymptotic state that does not vary any further with the downstream distance in $\tilde{t}\cong 10$. Development of the shear component for different initial values of $\tilde{\Gamma}_o$ mentioned above are presented in Figure 6.8. Depending on the initial shear, as shown in the small graph, the initial R_{yz} is different. For an increase of $\tilde{\Gamma}_o$ from 0.5 to 5, there is an increase in the initial value ($\tilde{t}<0.3$) of the shear component ($-R_{yz}$) from 0.08 to 0.19, while for $\tilde{\Gamma}_o$ variation from 5 to 10, the initial values of ($-R_{yz}$) are smaller (see Figure 6.8). However, independent of the initial values, the curves rapidly attain a final asymptotic state of $-R_{yz}^a \doteq 0.19$ (in $\tilde{t}\sim 11$). As shown in Figure 6.9, the ratio of production to dissipation (\mathcal{P}/ϵ) also approaches a constant value in a finite time. The initial values range from 0 to 5 for the initial values of $\tilde{\Gamma}_o$ chosen. The final states of $(\mathcal{P}/\epsilon)^a \doteq 1.57$ are attained for all the initial conditions.

The development of NR-stress to asymptotic states is presented for high initial shear $\tilde{\Gamma}_0$ = 18 in Figure 6.10. DNS results from Brethouwer (2005) are also shown in this figure for comparison. The URAPS closure predicts NR stress distribution instantaneously to imposed shear like other algebraic models. So the initial values of NR-stress distribution is anisotropic compared to the isotropic initial condition in the DNS simulations. The simulations show development towards constant values, which however may need more simulation time steps to further develop into asymptotic states. The extrapolation of DNS results seem to be directed towards the final states predicted by the URAPS-closure (see Figure 6.10).

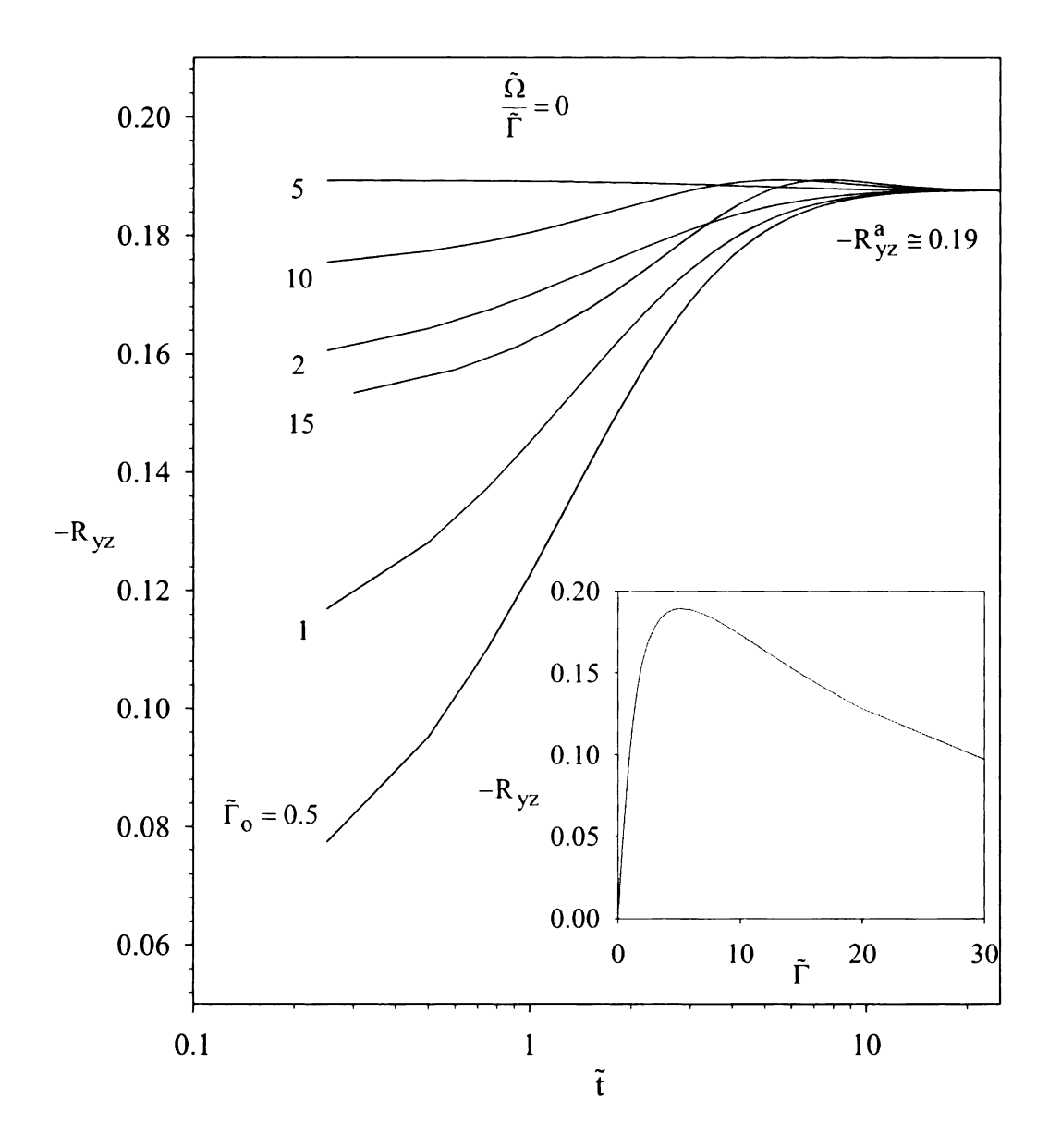


Figure 6.8 Temporal Development of $-R_{yz}$ for Different Initial $\tilde{\Gamma}_o$.

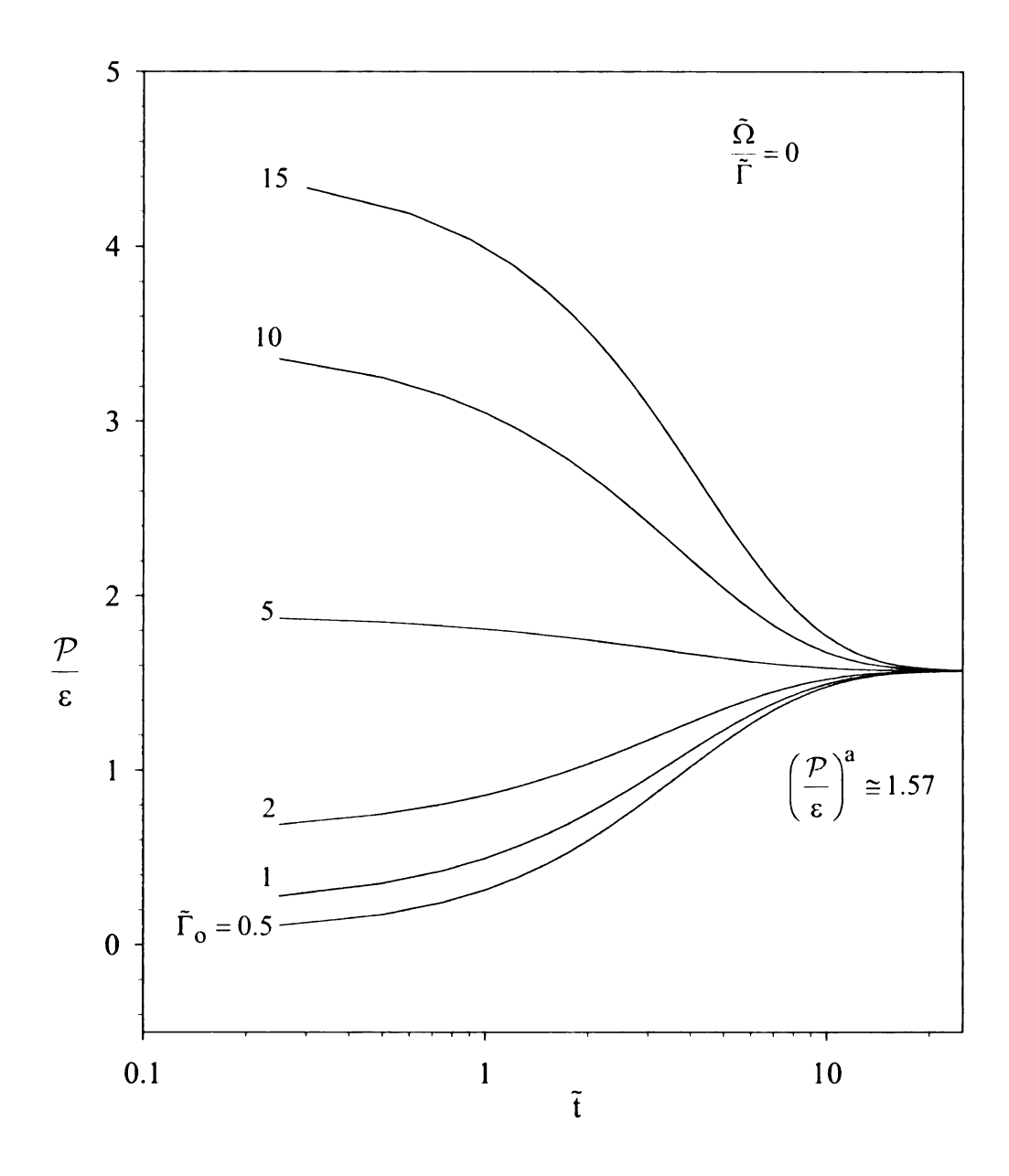


Figure 6.9 Temporal Development of Production to Dissipation Ratio for Different Initial $\tilde{\Gamma}_o$.

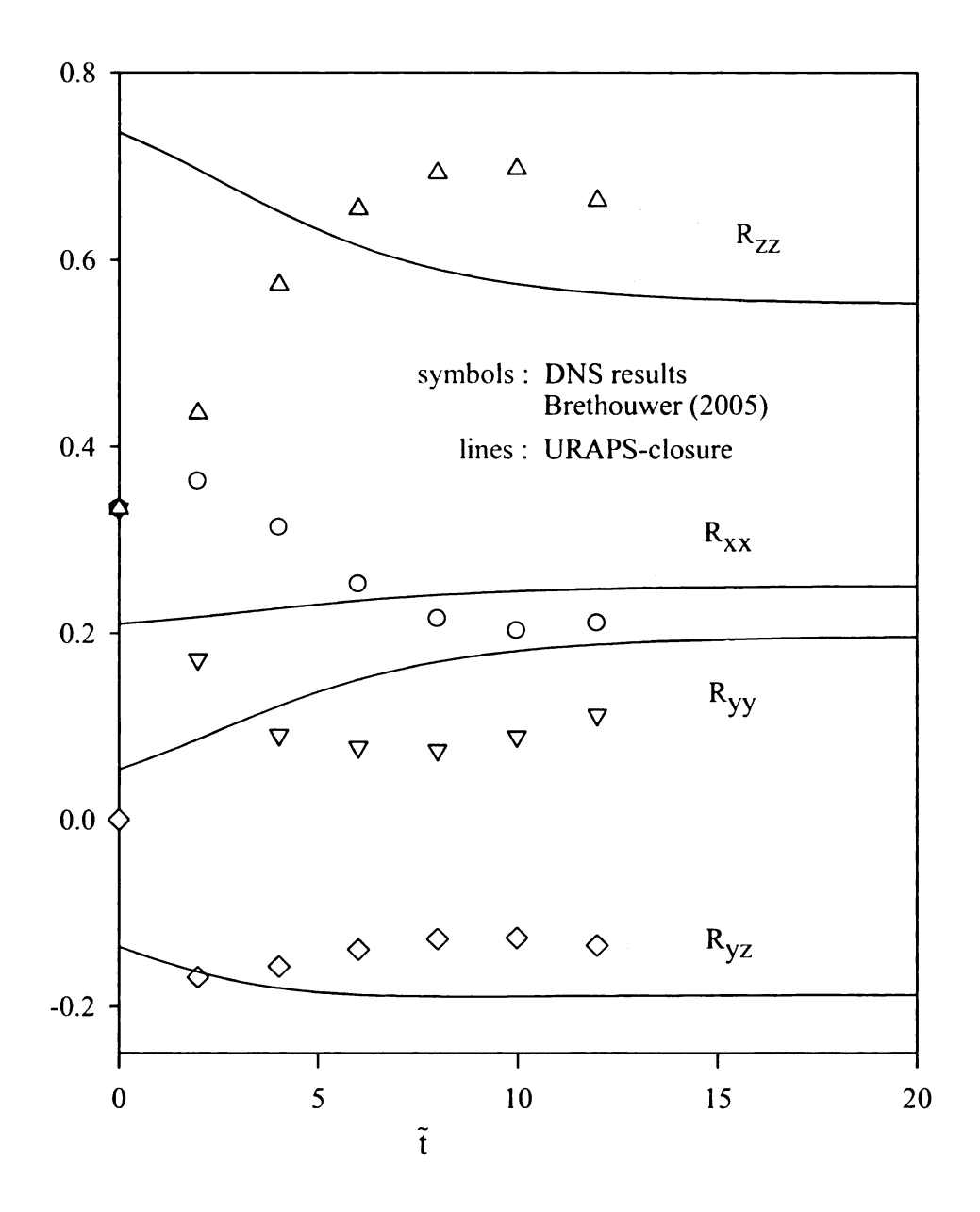


Figure 6.10 Temporal Development of NR-Stress Components Compared with DNS Results (Brethouwer, 2005) for High Initial Shear $\tilde{\Gamma}_0 = 18 \ (\tilde{\Omega}/\tilde{\Gamma} = 0)$.

The asymptotic states exist for $\tilde{\Omega}/\tilde{\Gamma} = 0$ for all initial values described above. The following discussion shows the temporal development for various values of $\tilde{\Omega}/\tilde{\Gamma}=-0.75-0.5, -0.25, -0.1, 0, 0.1, 0.25, 1$, covering beyond the range for which asymptotic solutions exist (AS-range). The initial value is fixed at $\tilde{\Gamma}_0 = 1$ for all the above cases of rotation. Interesting features below explain why there are no asymptotic states in a certain region. Figure 6.11 describes the downstream development of dimensionless shear for a fixed initial $\tilde{\Gamma}_0$, for different values of rotation rates. As discussed in the Section 6.4 of this Chapter $\frac{\tilde{\Omega}}{\tilde{\Gamma}} = -0.5, -0.25, -0.1, 0$, and 0.1, have asymptotic states as they are range between the maximum and minimum discussed previously. However, the asymptotic states are different with $\tilde{\Gamma}^{a}$ being the minimum for -0.25. For the range of $\frac{\tilde{\Omega}}{\tilde{\Gamma}} = -0.75, 0.25, 1$, and 2, which are outside the AS-range, $\tilde{\Gamma}$ increases monotonically, with slopes equal to Eq.(6.5) below, where the slopes depend on the rotation rate through $\tilde{\tau}_R$.

$$\frac{d\tilde{\Gamma}}{d\tilde{t}}\bigg|_{t\to\infty} = (\frac{\tilde{C}_D}{\tilde{\tau}_R}) - 1 \tag{6.5}$$

Eq. (6.5) is a consequence of understanding that $R_{yz} \to 0$ as $\tilde{\Gamma} \to \infty$ as can be seen in Figure 6.12. For $R_{yz} \to 0$, Eq. (6.1) becomes Eq. (6.5). Figure 6.12 describes the downstream development of the shear component of the Reynolds Stress. The initial values seem to be different for the same $\tilde{\Gamma}_0 = 1$ because of the rotation rates. R_{yz} attains different asymptotic states in a finite time for the rotation rates within the AS-range

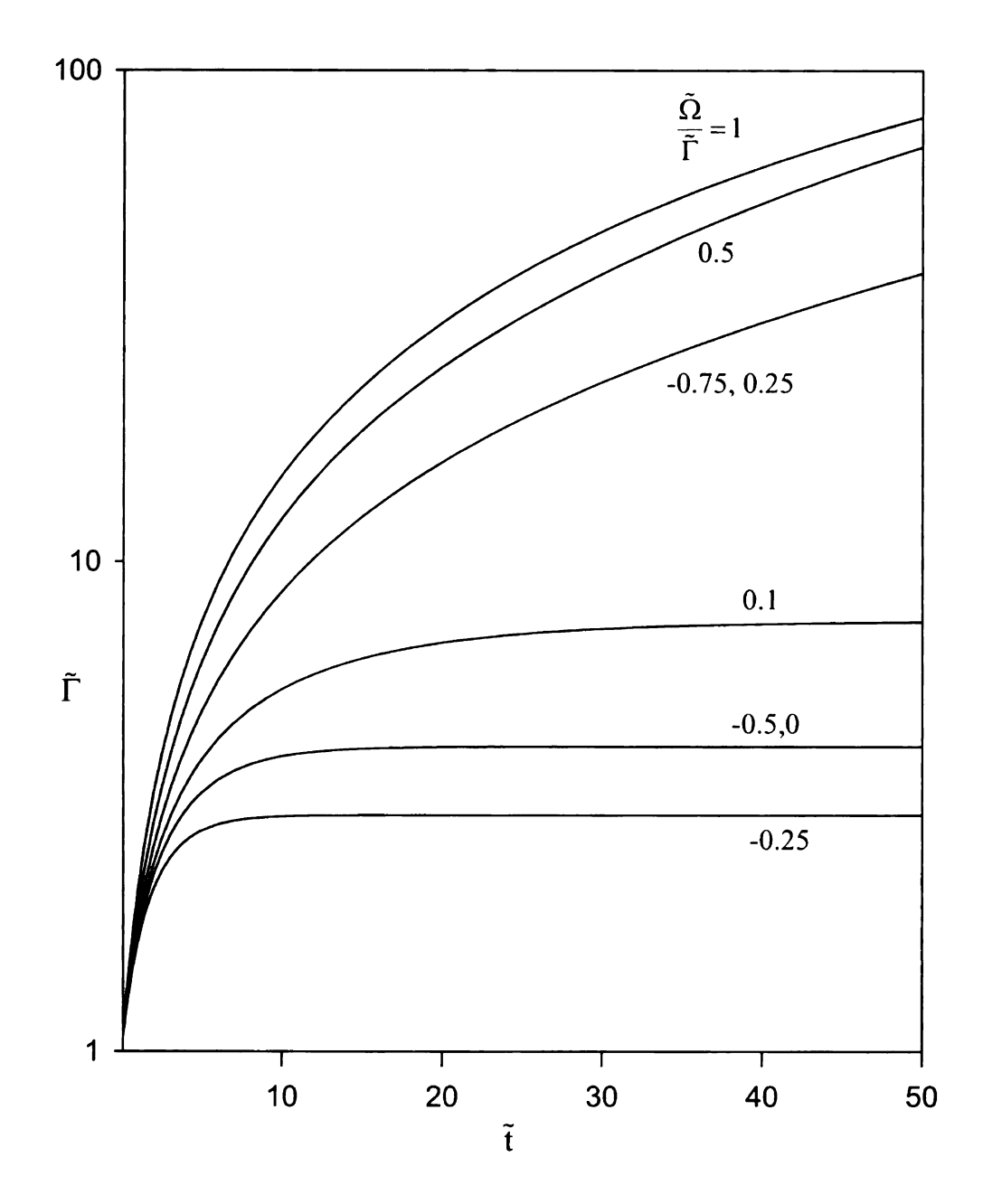


Figure 6.11 Developing $\tilde{\Gamma}$ for Different Rotation Numbers for $\tilde{\Gamma}_o = 1$.

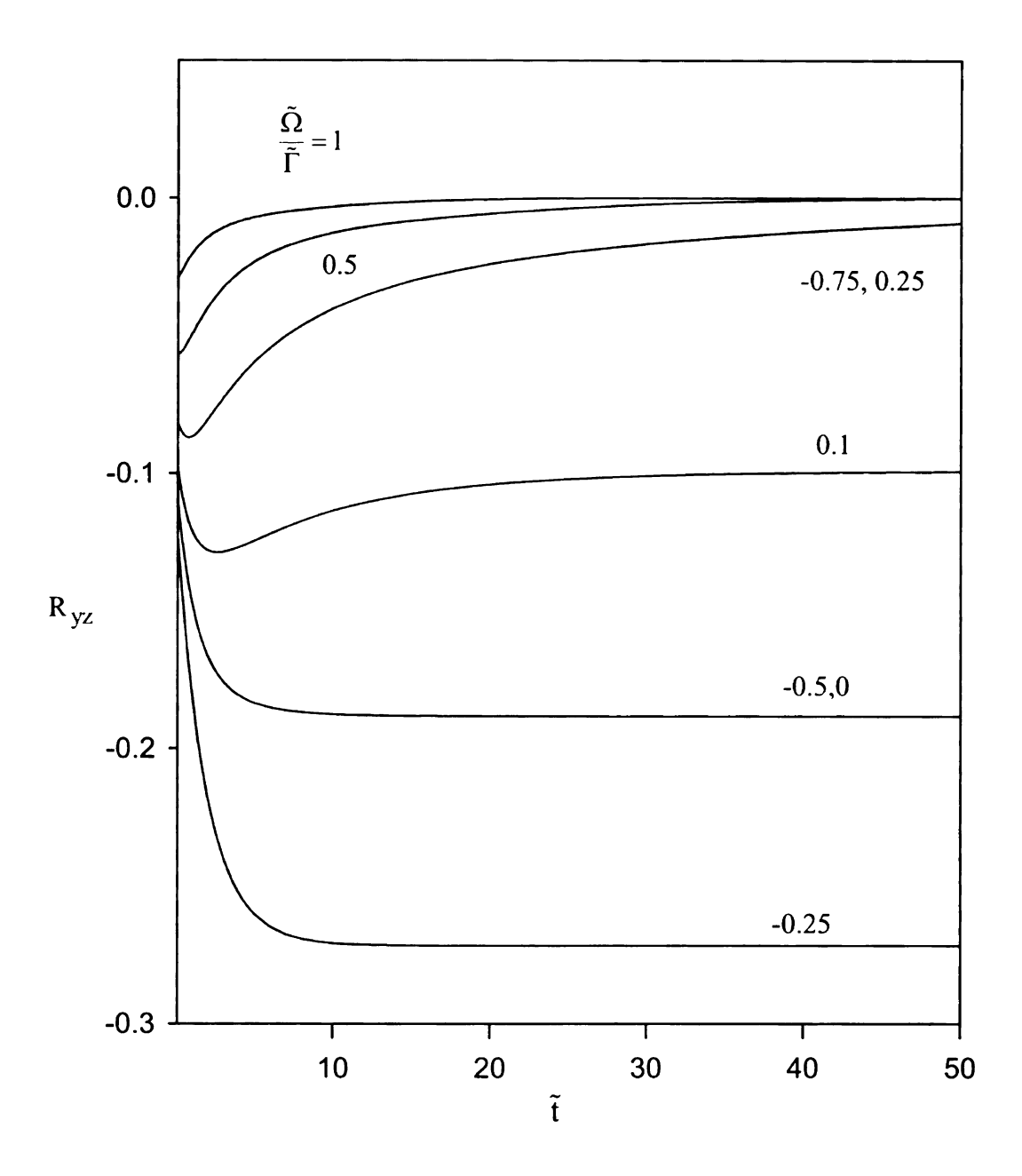


Figure 6.12 Developing R_{yz} for Different Rotation Numbers for $\tilde{\Gamma}_o = 1$.

described earlier. Outside this range, $R_{yz} \to 0$. The development of the \mathcal{P}/ϵ ratio is shown in Figure 6.13 for various rotations for an initial $\tilde{\Gamma}_0 = 1$. Within the AS-range, \mathcal{P}/ϵ approaches a constant (The asymptotic states are all between 1.45 and 1.65 as shown in the inset to Figure 6.13. For the rotation rates outside the asymptotic range, \mathcal{P}/ϵ approaches zero because R_{yz} approaches zero.

From the knowledge of the above discussion for rotation rates outside the AS-range, it can be seen that since URAPS closure and Eq. (6.1) yield $R_{yz} \rightarrow 0$ and so $\mathcal{P}/\epsilon \, (= 2\,\tilde{\Gamma}\,R_{yz}) \rightarrow 0 \,. \, \frac{d\,\tilde{\Gamma}}{d\,\tilde{t}} \bigg|_{t\,\to\,\infty} \ \text{approaches a constant value depending on the rotation}$ rate as described in Eq. (6.5). For rotation rates within the AS-range, Eq. (6.1) proceeds till the rate of change $\frac{d\,\tilde{\Gamma}}{d\,\tilde{t}} = 0$. For the bilinear model by Shih et al. (1994) and some of the other non linear models (see Piquet 1999) which cannot predict effect of rotation through the R_{yz} component predict that all the range of rotation rates have asymptotic states and that \mathcal{P}/ϵ and the normal components of NR-stress always approach a constant. Realizable model by Shih et al. (1995) can predict variation of the normal components of NR-stress with rotation but not the shear component as shown in Appendix E.

6.7 Developing "Extra" Anisotropy: Results and Discussion

The extra anisotropy in the URAPS-closure is studied for the following case of developing flow. $\tilde{\Gamma}_0 = 1$ and $\tilde{\Omega}/\tilde{\Gamma} = 0$. Figure 6.14 shows the eigenvalues of the extra-

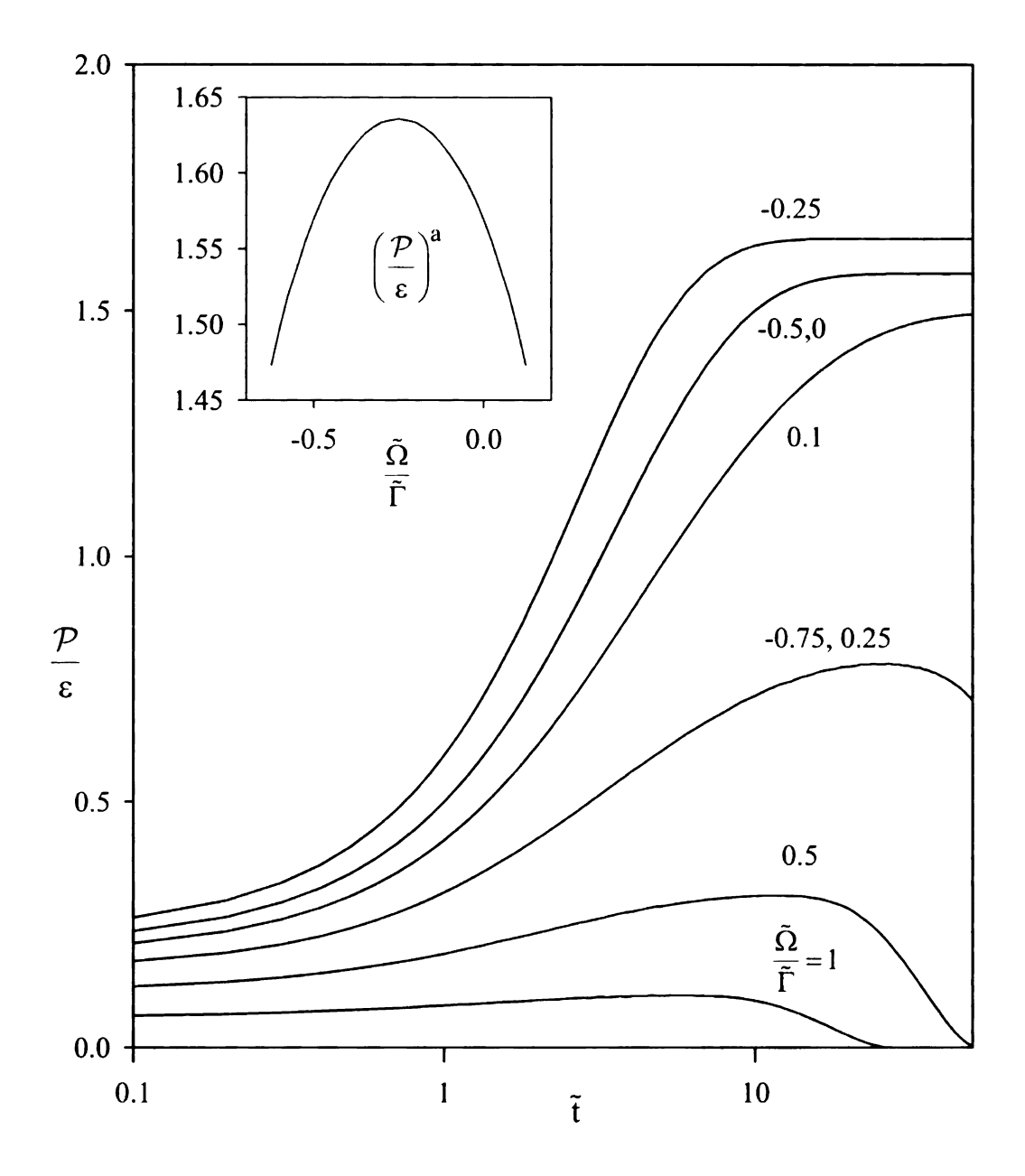


Figure 6.13 Developing P/ϵ Ratio for Various Rotation Numbers for $\tilde{\Gamma}_0 = 1$

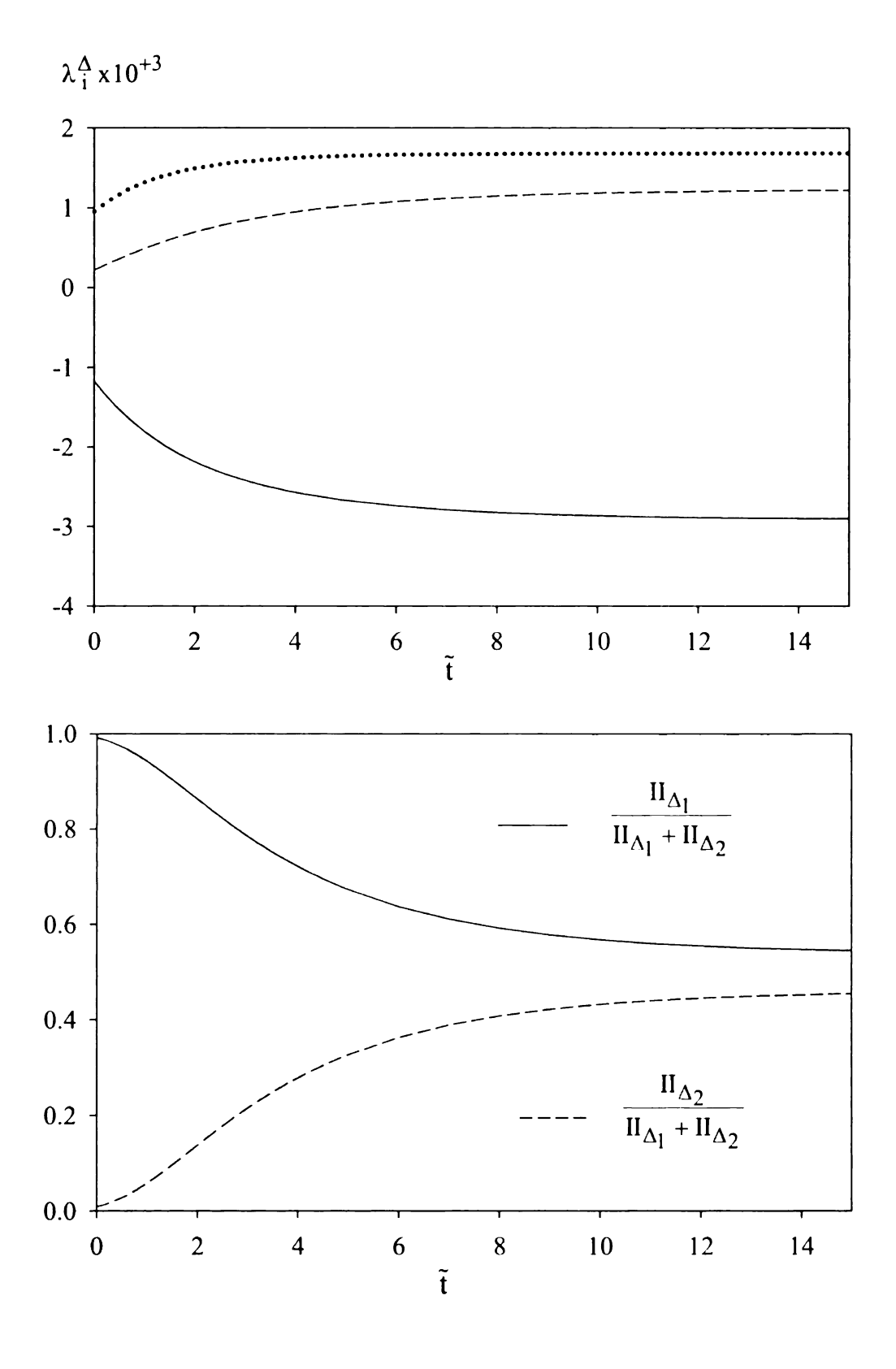


Figure 6.14 Eigenvlues of the Extra-Anisotropy $\underline{\Delta}$ and Relative Contributions from $\underline{\Delta}_1$ and $\underline{\Delta}_2$ for Developing Homogeneous Shear for $\tilde{\Gamma}_0=1$ and $\tilde{\Omega}/\tilde{\Gamma}=0$.

anisotropy $\underline{\underline{\Delta}}$ start with an initial distribution corresponding to the initial \underline{R} at $\tilde{t}=0$ and $\tilde{\Gamma}_0 = 1$. (i.e. $\Delta \times 10^3 = 0.22 \, \underline{e}_x \, \underline{e}_x + 0.22 \, \underline{e}_y \, \underline{e}_y - 0.44 \, \underline{e}_z \, \underline{e}_z + 0.10 \, \underline{e}_y \, \underline{e}_z + 1.01 \, \underline{e}_z \, \underline{e}_y$ and the eigenvalues are $\lambda_i^{\Delta} \times 10^3 = (-1.17, 0.22, 0.95)$). As the time proceeds, with the variation in $\tilde{\Gamma}$ towards the asymptotic state, the eigenvalues of $\underline{\underline{\Delta}}$ also approach the asymptotic approaches a constant $(\Delta \times 10^3 =$ state Δ as $1.2\underline{3}\,\underline{e}_{x}\,\underline{e}_{x} + 0.97\,\underline{e}_{y}\,\underline{e}_{y} - 2.2\,\underline{e}_{z}\,\underline{e}_{z} + 0.10\,\underline{e}_{y}\,\underline{e}_{z} + 1.67\,\underline{e}_{z}\,\underline{e}_{y}$ and eigenvalues $\lambda_i^{\Delta} \times 10^3 = (-2.91, 1.23, 1.69)$). The eigenvalues contribution from the second order terms $\underline{\underline{\Delta}}_2$ are almost zero initially as can be seen from the ratio of the second invariants in Figure 6.14b. However, both become significant during the final development time $(\tilde{t} > 15)$ as Δ approaches its asymptotic values (see in Figure 6.14), with the ratio $II_{\Delta_1}/(II_{\Delta_1}+II_{\Delta_2})$ being about 0.539. This value is also evident in earlier Figure 6.6 which showed the asymptotic states for several rotation rates. The values for $\tilde{\Omega}/\tilde{\Gamma}=0$ on Figure 6.6 are the final states of $\tilde{t} > 15$ in Figure 6.14.

6.8 Conclusions

The transport equations for k and ϵ , along with the URAPS-closure predict self-similar states for homogeneous shear. The range of rotations for which asymptotic states exist is qualitatively consistent with known literature results (Brethouwer 2005).

1. The observed anisotropy for the URAPS-closure shows a transfer of energy from R_{yy} to R_{zz} for increasing $\frac{\tilde{\Omega}}{\tilde{\Gamma}}$ in the range

 $-0.65 = (\frac{\tilde{\Omega}}{\tilde{\Gamma}})_{min} < \frac{\tilde{\Omega}}{\tilde{\Gamma}} < (\frac{\tilde{\Omega}}{\tilde{\Gamma}})_{max} = +0.15 \text{, which is similar to the trend in DNS and}$ LES simulations (see Figure 6.3b). For this range of rotation rates the dynamic states approach asymptotic values, $\tilde{\Gamma} \to \tilde{\Gamma}^a$, $\mathcal{P}/\varepsilon \to (\mathcal{P}/\varepsilon)^a$ and $\underline{R} \to \underline{R}^a$. This occurs because Eq. (6.2) balances in the asymptotic range (AS-). However, outside the AS- range, the turbulent kinetic energy, the turbulent dissipation, and the shear component of the NR-stress relax to zero. (i.e., $R_{yz} \to 0$). The ratio \mathcal{P}/ε also decays. So the dynamic equation for $\tilde{\Gamma}$ for $t \to \infty$ becomes Eq. (6.5) resulting in monotonically increasing values of $\tilde{\Gamma}$.

The effect of rotation predicted by the URAPS-closure agrees with the DNS and LES results (see Figure 6.3b), with the energy shift from the R_{zz} to R_{yy} component as $\tilde{\Omega}/\tilde{\Gamma}$ changes from + 0.15 to -0.65. The distribution of energy in the case of $\tilde{\Omega}/\tilde{\Gamma}=-0.5$, which corresponds to the zero absolute mean vorticity, with $R_{yy}>R_{zz}$, is consistent with the knowledge of NR-stress distribution in spanwise rotating channel in similar region (see Table I.4). Distinctly larger with maximum values of $1/\tilde{\Gamma}^a \cong 0.33$, $(\mathcal{P}/\epsilon)^a \cong 1.64$, and $-R_{yz}^a \cong 0.27$ for $\tilde{\Omega}/\tilde{\Gamma}=-0.25$ occur in the AS-region, which is also consistent with literature (Brethouwer 2005). The URAPS- closure accounts for the effect of rotation on the R_{yz} component which is important for the finite range of asymptotic states observed.

3. The development towards asymptotic states occurs within $\tilde{t} \sim 11$ for various initial $\tilde{\Gamma}_0$ ranging from 0.5 to 15 for the dimensionless shear rate, NR-stress and the "production" to dissipation ratio. For the case of $\tilde{\Gamma}_0 = 1$ and $\tilde{\Omega}/\tilde{\Gamma} = 0$, during the initial time of development towards AS-states, $\underline{\Delta}_1$ contributions to the NR-stress are large compared to $\underline{\Delta}_2$. However, both the contributions are almost equal towards the asymptotic solution. In the asymptotic range, for $-0.45 < \tilde{\Omega}/\tilde{\Gamma} < 0.05$, $\underline{\Delta}_2$ is important compared to $\underline{\Delta}_1$.

CHAPTER 7

FULLY-DEVELOPED CHANNEL FLOWS

7.1 Introduction

The RANS-equation and important flow characteristics for non-rotating and spanwise rotating channel flow for a constant streamwise pressure gradient have been discussed in Chapter 2. Low-order statistics ($<\underline{u}>^+,k^+,\epsilon^+,\Gamma_{yz}^+$) from DNS results available in literature have also been discussed in Chapter 2 for δ^+ = 300 and 2000 (see Figures 2.5, 2.6 and 2.7) for non-rotating channel and also for $\delta^+ = 300$ with rotation number $\Omega^+ = -0.0042$ (see Figures 2.9 to 2.14). The mean statistics are not symmetric about the center of the channel in the case of rotating channel. These results in the core region of the channel have been tabulated in Appendix I (Tables I.1 to I.3). Apart from these, the linear velocity region results for various rotations have also been presented in Appendix I (Table I.4) and discussed in Section 7.6. The DNS results for the NR-stress are compared with the NR-stress predicted by the URAPS-theory. In this chapter, the URAPS-closure predictions for NR-stress in a fully developed channel flow with and without rotation are presented. DNS results are used to test the closure performance. Influence of rotation on the NR-stress is also compared with the DNS results in the zero absolute mean vorticity region and in the core region of a spanwise rotating channel. The closure prestress and its components are studied to understand their contributions to the NR-stress predictions. Figure 7.1 presents a schematic of fully-developed channel flow with z as the streamwise direction and y as the crossflow direction ($<\underline{u}_z>(y)$). The

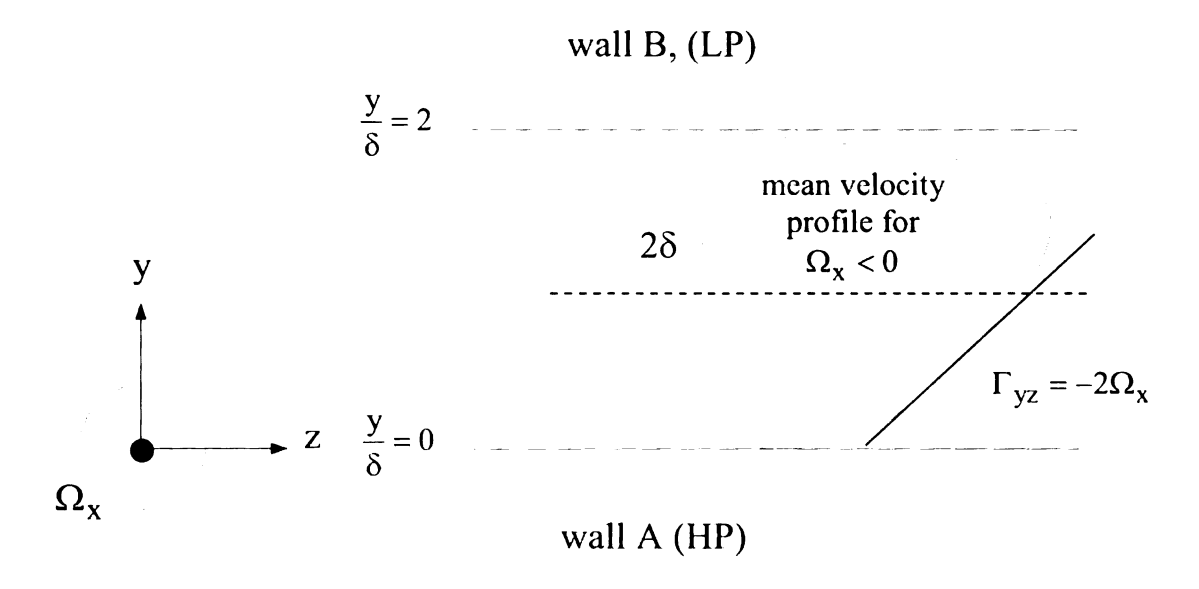


Figure 7.1 Schematic of Fully Developed Channel Flow with Spanwise Rotation.

rotation vector is aligned along the vorticity direction ($\underline{\Omega} = \Omega_x \underline{e}_x$). The cross length of the channel is from $y/\delta = 0$ to $y/\delta = 2$ where δ is the half-width of the channel.

7.2 Preclosure Operator and URAPS-Closure

The preclosure operator for URAPS for non-rotating simple shear has been presented in Appendix G, Eq. (G.7). Eqs. (G.12)-(G.20) are the URAPS-closure NR-stress component equations. For simple shear flow without rotation, the simplified URAPS equations have been presented in Case 2 (i.e. $N_{\Gamma} \neq 0$ & $N_{\Omega} = 0$). The equations show that there is a mechanism to transfer energy from one component to the other through the prestress components depending on the shear group N_{Γ} . Case 4 represents the case when $N_{\Gamma} = -N_{\Omega}$ (i.e. $\Gamma_{yz}^+ = -2\Omega_x^+$). It is interesting to note that the preclosure operator for Case 2 (i.e. non rotation simple shear) and Case 4 (i.e. linear velocity profile region of rotating channel) are the transpose of each other (compare Eqs. (G.22) and (G.44)). The resulting URAPS component equations for NR-stress are also the similar except for a change in the yy and zz component equations (see Eqs.(G.24)-(G.27) and Eqs.(G.46)-(G.49) in Appendix G).

7.3 Locus of States Predicted by URAPS-Closure for Simple Shear Flows

Solution to the URAPS-equation for the NR-stress can be obtained by successive substitution, as described in Chapter 4. Locus of states predicted by URAPS-closure equations for a range of $\tilde{\Gamma}$ and $\tilde{\Omega}$ are presented below. The study can be simplified by fixing the ratio $\tilde{\Omega}/\tilde{\Gamma}$ and varying $\tilde{\Gamma}$. Figure 7.2a shows the locus of URAPS-closure

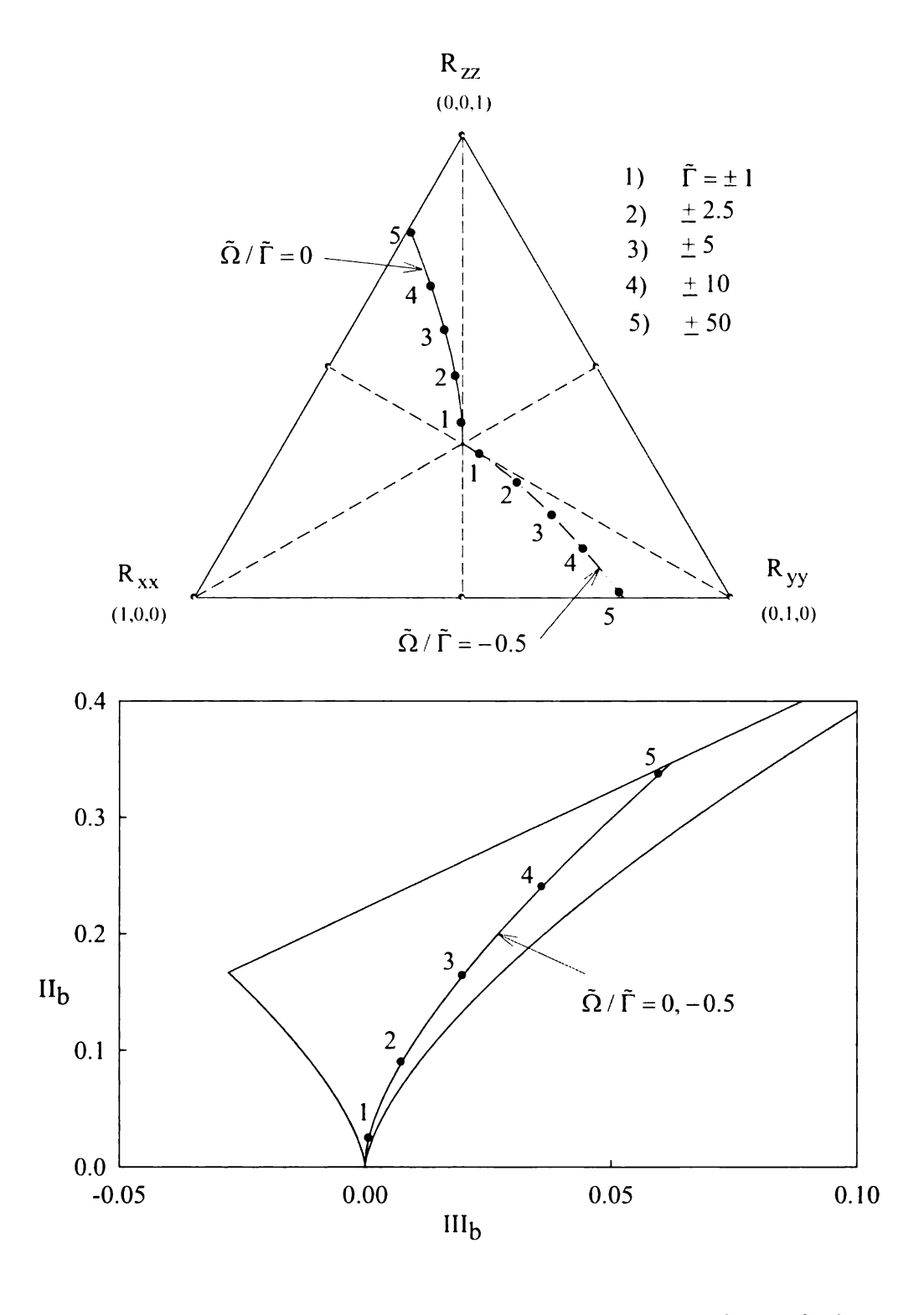


Figure 7.2a Locus of URAPS-Closure States Parameterized by $\tilde{\Gamma}$ for $\tilde{\Omega}/\tilde{\Gamma}=0$ and $\tilde{\Omega}/\tilde{\Gamma}=-0.5$ (Zero Absolute Mean Vorticity, see Section 7.6).

theory for non-rotation case (i.e. $\tilde{\Omega}/\tilde{\Gamma}=0$) and for the case $\tilde{\Omega}/\tilde{\Gamma}=-0.5$. As discussed earlier, since the preclosure operator \underline{A} for the above cases is the transpose of one other, URAPS-equations predict same anisotropic states, except for a flip in energy states R_{vv} and R_{zz} for the two cases. The energy simplex reflects the above feature with states in the 2nd sextet and 5th sextet respectively for the two cases. Figure 7.2b complements Figure 7.2a showing the component distribution with variation in $\tilde{\Gamma}$. Components of \underline{R} with a variation in the dimensionless shear $-\infty < \tilde{\Gamma} (= \Gamma_{yz} k \, / \, \epsilon) < +\infty$, show that for $\tilde{\Gamma} = 0$, there is equi-distribution of energy with no shear component to the NR-stress. But as $|\tilde{\Gamma}| \to \infty$, the energy is transferred from the R_{xx} and R_{yy} components to the R_{zz} components. For negative values of $\tilde{\Gamma}$, there is a positive R_{yz} and for positive $\tilde{\Gamma}$ negative R_{yz} occurs with peak value of about $\left|R_{yz}\right| = 0.19$ occurring at $\left|\tilde{\Gamma}\right| \cong 5$. Typically the normal components are close to the two component energy state $R_{zz} = 0.8$ and $R_{yy} = 0.2$ for $|\tilde{\Gamma}| \cong 50$. However, the shear component relaxes to zero asymptotically for $\left|\tilde{\Gamma}\right| >> 50$. In the case of $\tilde{\Omega}/\tilde{\Gamma} = -0.5$, the energy distribution approaches the two component state where $R_{zz} = 0.2$ and $R_{yy} = 0.8$, for $|\tilde{\Gamma}| \approx 50$. However, the anisotropic states for both the cases are the same because of the values being the same.

Locus of states for $\tilde{\Omega}/\tilde{\Gamma}>0$ and $\tilde{\Omega}/\tilde{\Gamma}<-0.5$ are presented in Figures 7.3a and 7.3b. For $\tilde{\Omega}/\tilde{\Gamma}>0$, the energy distribution shifts from the 2^{nd} and 3^{rd} sextet and approaches the single component state $R_{xx}=1$ with increasing values of $|\tilde{\Gamma}|$. As noted

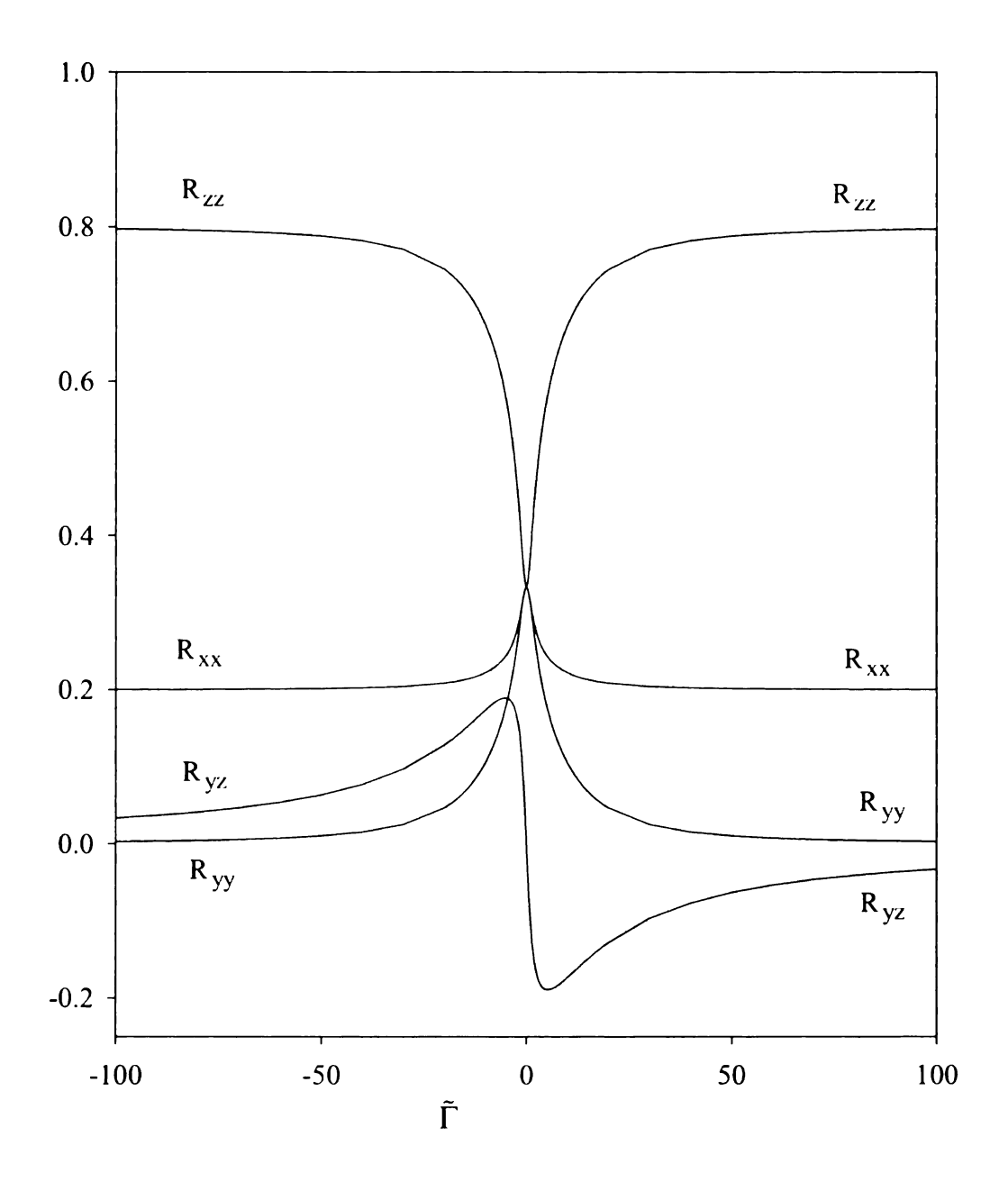


Figure 7.2b Influence of $\tilde{\Gamma}$ on the Components of NR-Stress Distribution for URAPS-Closure ($\tilde{\Omega}/\tilde{\Gamma}=0$).

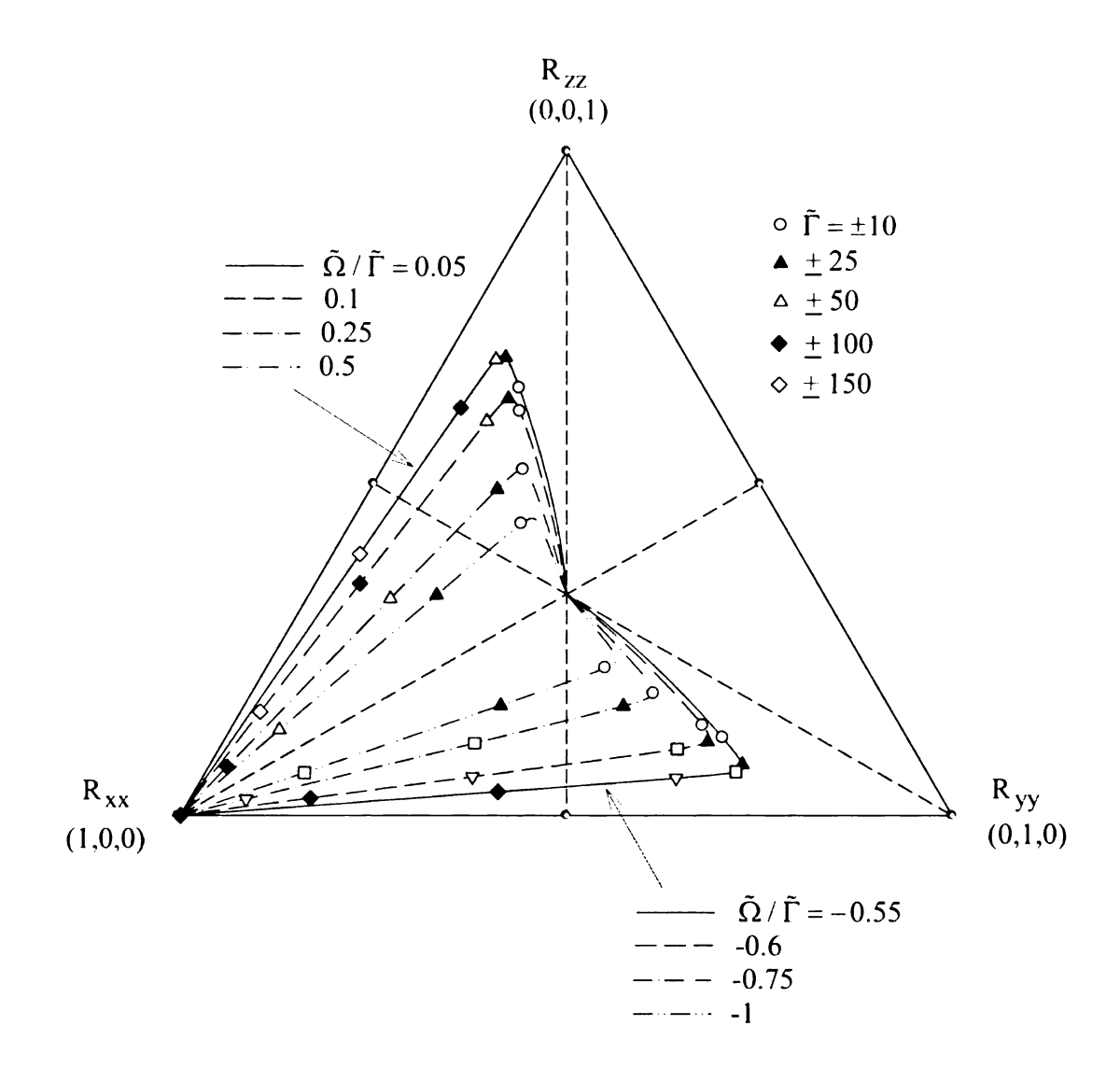


Figure 7.3a The Influence of $\tilde{\Omega}/\tilde{\Gamma}$ and $\tilde{\Gamma}$ on the Energy States for $\tilde{\Omega}/\tilde{\Gamma}<-0.5$ and $\tilde{\Omega}/\tilde{\Gamma}>0$.

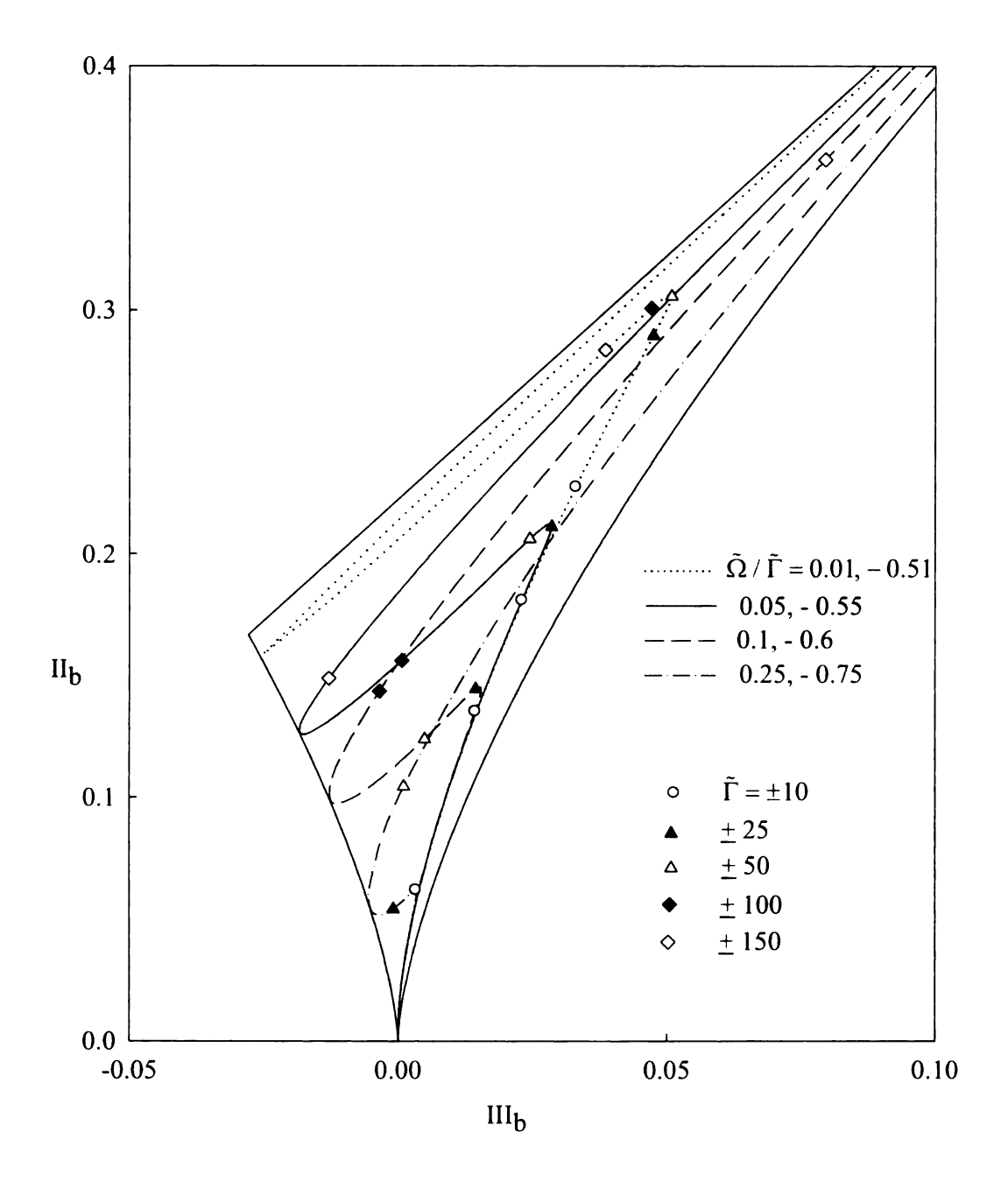


Figure 7.3b The Influence of $\tilde{\Omega}/\tilde{\Gamma}$ and $\tilde{\Gamma}$ on the Anisotropic States for $\tilde{\Omega}/\tilde{\Gamma}<-0.5$ and $\tilde{\Omega}/\tilde{\Gamma}>0$.

earlier, if $\tilde{\Gamma} > 0$, then $R_{yz} < 0$ and vice versa. However, the magnitude of the shear component is the same. So as shown in the Figure 7.3a, for both positive and negative values of $\tilde{\Gamma}$, the locus of states remain the same in the energy simplex. For $\tilde{\Omega}/\tilde{\Gamma} < -0.5$, the energy shifts from the 5th sextet to the 4th sextet approaching $R_{xx} = 1$ for large values of $|\tilde{\Gamma}|$. The anisotropic states for each value of $\tilde{\Omega}/\tilde{\Gamma} > 0$, remains the same as for $-0.5 - \tilde{\Omega}/\tilde{\Gamma}$. For example, the anisotropic states are the same for $\tilde{\Omega}/\tilde{\Gamma} = 0.05$ and $\tilde{\Omega}/\tilde{\Gamma} = -0.55$ (see states Figure 7.3b). This is because although there is a shift in the energy distribution, the eigenvalues are the same. It can be seen that the states can be either prolate like distribution ($III_b > 0$) or towards oblate like states ($III_b < 0$) depending on the magnitude of $|\tilde{\Gamma}|$. Each of the constant $\tilde{\Omega}/\tilde{\Gamma}$ lines start at the isotropic state for $|\tilde{\Gamma}| = 0$ and pass through the oblate state, which typically is associated with $\tilde{\Gamma}$ corresponding to the $R_{xx} = R_{zz}$ and $R_{xx} = R_{yy}$ in energy plane for $\tilde{\Omega}/\tilde{\Gamma} > 0$ and $\tilde{\Omega}/\tilde{\Gamma} < -0.5$, respectively. This is because of the shear component being small compared to the normal components. Unlike other eddy viscosity based linear and bilinear closure models (see Chapter 2), the URAPS-closure states occupy both $III_b > 0$ and $III_b < 0$ states depending on the rotation rate and magnitude of the shear rate, which is expected from the previous knowledge of DNS results for rotating simple shear flows.

For $-0.5 < \tilde{\Omega}/\tilde{\Gamma} < 0$, the locus of states are restricted to $R_{xx} < 1/3$ in the energy simplex (see Figure 7.4). The locus of states starting at the equi-distribution of energy approach $R_{xx} = 0$ for increasing values of $\left| \tilde{\Gamma} \right|$ from 0 to 20 as shown in the Figure 7.4. For $\tilde{\Omega}/\tilde{\Gamma} = -0.25$, $R_{yy} = R_{zz}$. All the states for $\tilde{\Omega}/\tilde{\Gamma} > -0.25$ are in the region

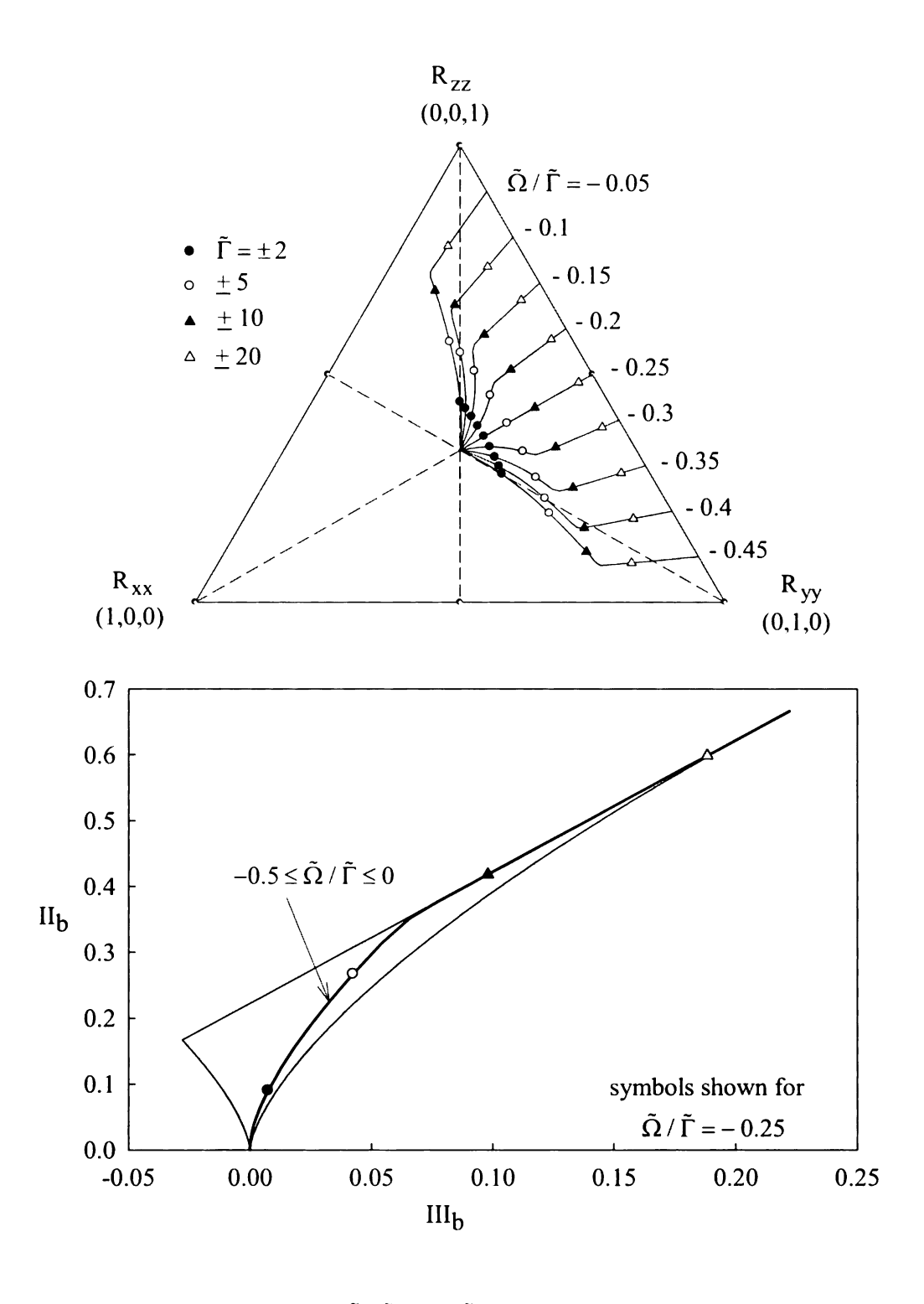


Figure 7.4 The Influence of $\tilde{\Omega}/\tilde{\Gamma}$ and $\tilde{\Gamma}$ on the Energy and Anisotropic States for $-0.5 < \tilde{\Omega}/\tilde{\Gamma} < 0$.

 $R_{yy} < R_{zz}$. For $\tilde{\Omega}/\tilde{\Gamma} < -0.25$, the states are in $R_{zz} < R_{yy}$ of the energy plane. However, interestingly, for all $\tilde{\Omega}/\tilde{\Gamma}$ in this range, the anisotropic states follow a single curve in the Lumley's diagram. Each $\tilde{\Omega}/\tilde{\Gamma}$ is characterized by different $\left|\tilde{\Gamma}\right|$ for any given state along this curve.

7.4 NR-Stress in the Outer Region with $\tilde{\Omega} = 0$: Results and Discussion

The URAPS-equation needs the group $N_{\Gamma} (\equiv \tau_R \Gamma_{yz} = C_{R1} \tilde{\tau}_R \tilde{\Gamma})$ to give the NR-stress distribution for non rotating simple shear. This can be calculated from the $\tilde{\Gamma}_{DNS} (= \Gamma_{yz} k/\epsilon)_{DNS}$ group from the DNS simulations as a preliminary analysis without solving the boundary value problem. $\tilde{\Gamma}_{DNS}$ calculated from the DNS statistics has been presented in Chapter 2 (see Figure 2.7 and Table 2.1 discussed in Chapter 2). From this the $\tilde{\tau}_R$ and N_{Γ} for URAPS theory are calculated.

Figure 7.5 presents the URAPS closure predictions for components of R with a variation in the dimensionless shear $0 < \tilde{\Gamma} < +\infty$. DNS results corresponding to each $\tilde{\Gamma}$ are also shown for comparison. For $\tilde{\Gamma} = 0$, there is equi-distribution of energy with no shear component to the NR-stress, while DNS results show weak anisotropy (with $R_{zz} > R_{yy} = R_{xx}$). The qualitative shift of energy to R_{zz} component for $\tilde{\Gamma} > 0$, which is seen in the DNS results, is also observed in the URAPS-closure results. For $\delta^+ = 300$ and 2000, there is a sudden change in the energy distribution occurring at $\tilde{\Gamma} \cong 3$ and 4 respectively. In this region, DNS results show different NR-stress variations for the same values of $\tilde{\Gamma}$. Although URAPS- closure predicts unique values of NR-stress distribution

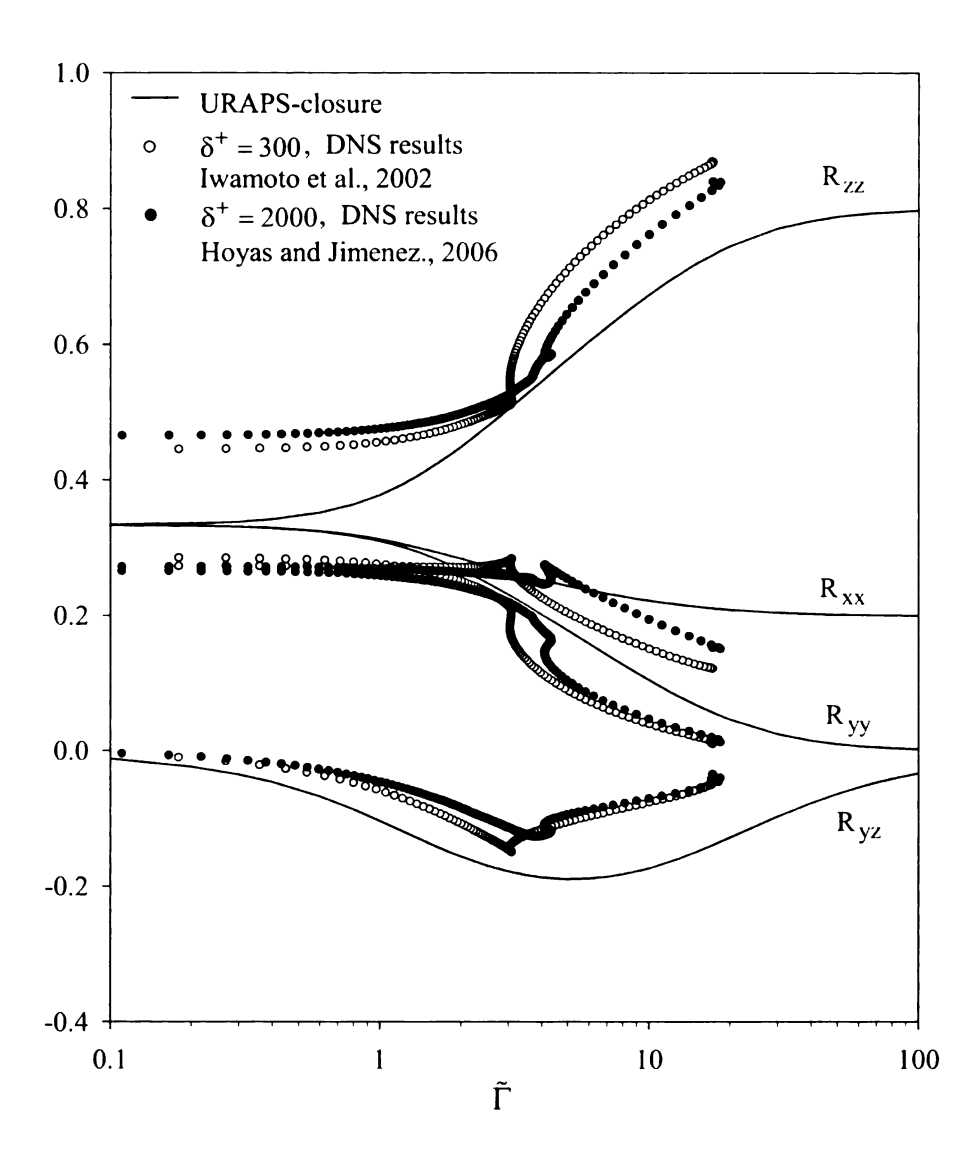


Figure 7.5 The Influence of $\tilde{\Gamma}$ on the Components of NR-Stress for Non-Rotating Fully-Developed Channel Flows.

for each $\tilde{\Gamma}$, the values in this region agree closely with DNS results. URAPS-closure for $\tilde{\Gamma}=4$ predicts $R_{xx}=0.25$, $R_{yy}=0.20$, $R_{zz}=0.55$ and $R_{zz}=-0.187$. DNS results show $R_{xx}=0.25$, $R_{yy}=0.18$, $R_{zz}=0.57$ and $R_{zz}=-0.13$ for $\delta^+=2000$. The minimum value of the shear component R_{yz} in the DNS results is of the order of -0.15 for $\delta^+=300$ while the URAPS closure has minimum of about -0.19. There is a significant qualitative agreement with the DNS results for the NR-stresses. Typically the normal components are close to the two component energy state $R_{zz}=0.8$ and $R_{yy}=0.2$ for $\tilde{\Gamma}\cong 50$. $(R_{yz})_{DNS}$ relaxes to zero for $\tilde{\Gamma}<50$, while for the URAPS-closure, the shear component relaxes to zero asymptotically for $\tilde{\Gamma}>100$.

The shear group $N_{\Gamma}(=C_{R1}\bar{\tau}_R\tilde{\Gamma})$, which appears in the URAPS-closure equation, determines the NR-stress variation. So the variation of the group along with the $\bar{\tau}_R$ is presented in Figure 7.6 with respect to the wall coordinates. For y/δ , where $\tilde{\Gamma}=0$, $\bar{\tau}_R=1$. Away from the center of the channel (i.e., $0 < y/\delta < 1$), the dimensionless time is influenced by the increasing shear rate. For $\tilde{\Gamma}>0$ the mean field time scale affects the timescale associated with turbulent transport. These effects are maximum when $\tilde{\Gamma}\cong 18$ (see Figure 2.7, Chapter 2) which occurs at $y^+\sim 10$ for $y/\delta < 0.05$ (Note that $\bar{\tau}_R$ has not been calibrated to include the Re_t dependence and so the near wall effects are not discussed). N_{Γ} typically reflects the $\tilde{\Gamma}$ variation with increasing values from $y/\delta=0$ to $y/\delta=0.05$. The URAPS-closure predictions of the NR-stress, calculated from the group $\tilde{\Gamma}_{DNS}$ (for $\delta^+\cong 300$), are presented in Figure 7.7. The redistribution of energy with

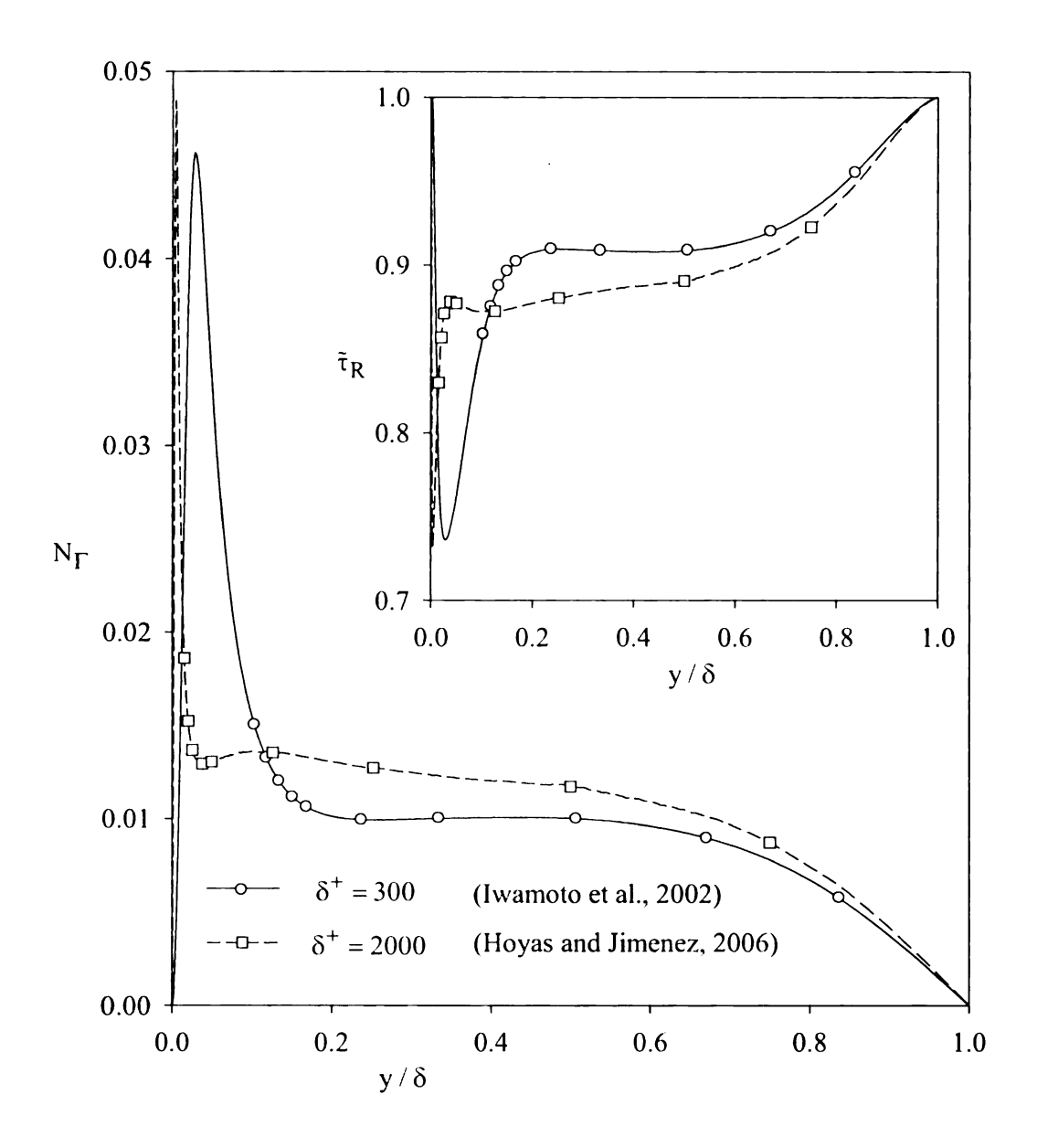


Figure 7.6 Spatial Variation of N_Γ and $\tilde{\tau}_R$ based on $\tilde{\Gamma}_{DNS}$ for Non-Rotating Fully-Developed Channel Flow

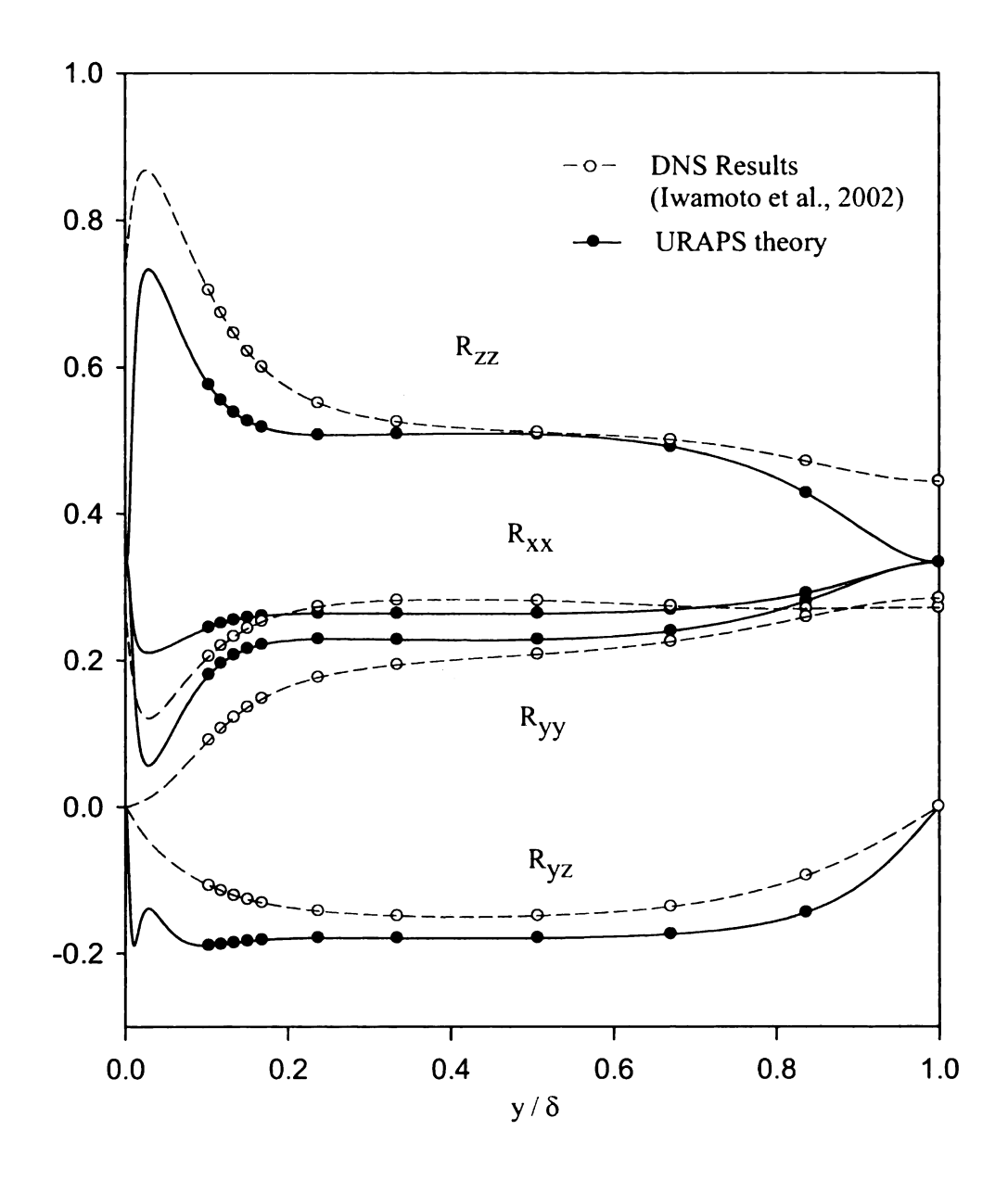


Figure 7.7 Spatial Variation of NR-Stress Components Predicted by URAPS-Closure based on $\tilde{\Gamma}_{DNS}$ for Non-Rotating Fully-Developed Channel Flows with $\delta^+=300$.

 $R_{zz} > R_{xx} > R_{yy}$ is predicted by the URAPS-closure. At the center of the channel for $\tilde{\Gamma}_{DNS} = 0$, there is no anisotropy predicted unlike the DNS results, but the states in the core region of the channel remain in close agreement with the DNS results. The symbols correspond to the specific points presented in Table I.1c (Appendix I.). R_{yz} component is slightly higher for the URAPS compared to the DNS results (See Table I.1c for the values). The statistics of the URAPS closure for Reynolds stress components for $\delta^+ \cong 2000$ are also presented in Figure 7.8. The overall predictions in the core region of the channel flow are in qualitatively agreement with the DNS results. The |Ryz| predicted by URAPS closure has a maximum of 0.19 while the DNS data has 0.15 for this case. The near wall region needs further modeling.

7.5 NR-Stress in the Outer Region with $\tilde{\Omega} \neq 0$: Results and Discussion

DNS results by Wu and Kasagi, 2004 for spanwise rotating channel is presented in Table I.3. in Appendix I. for $Re^+ \cong 300$, $\Omega^+ \cong -0.0042$ and the dimensionless time scales associated with the shear and rotation numbers, $\tilde{\Gamma}$ and $\tilde{\Omega}$, are discussed in Chapter 2. The shear and rotation groups $N_{\Gamma} = C_{R1} \tilde{\tau}_R \tilde{\Gamma}$ and $N_{\Omega} = 2 C_{R1} \tilde{\tau}_R \tilde{\Omega}$ give the relative degree of each of the effects (i.e shear and rotation) in the URAPS-equations. As shown in Figure 7.9, N_{Γ} values vary between 0.02 and -0.04 in the core region of the channel while N_{Ω} values reach to a maximum of about -0.012. So the effect of rotation may be small. $\tilde{\tau}_R$ as seen on the Figure 7.9 has a smaller value at $y/\delta = 1.5$ compared to $y/\delta = 0.5$. Since both $\tilde{\Gamma}$ and $\tilde{\Omega}$ are negative at $y/\delta = 1.5$, the value of N_F is larger and

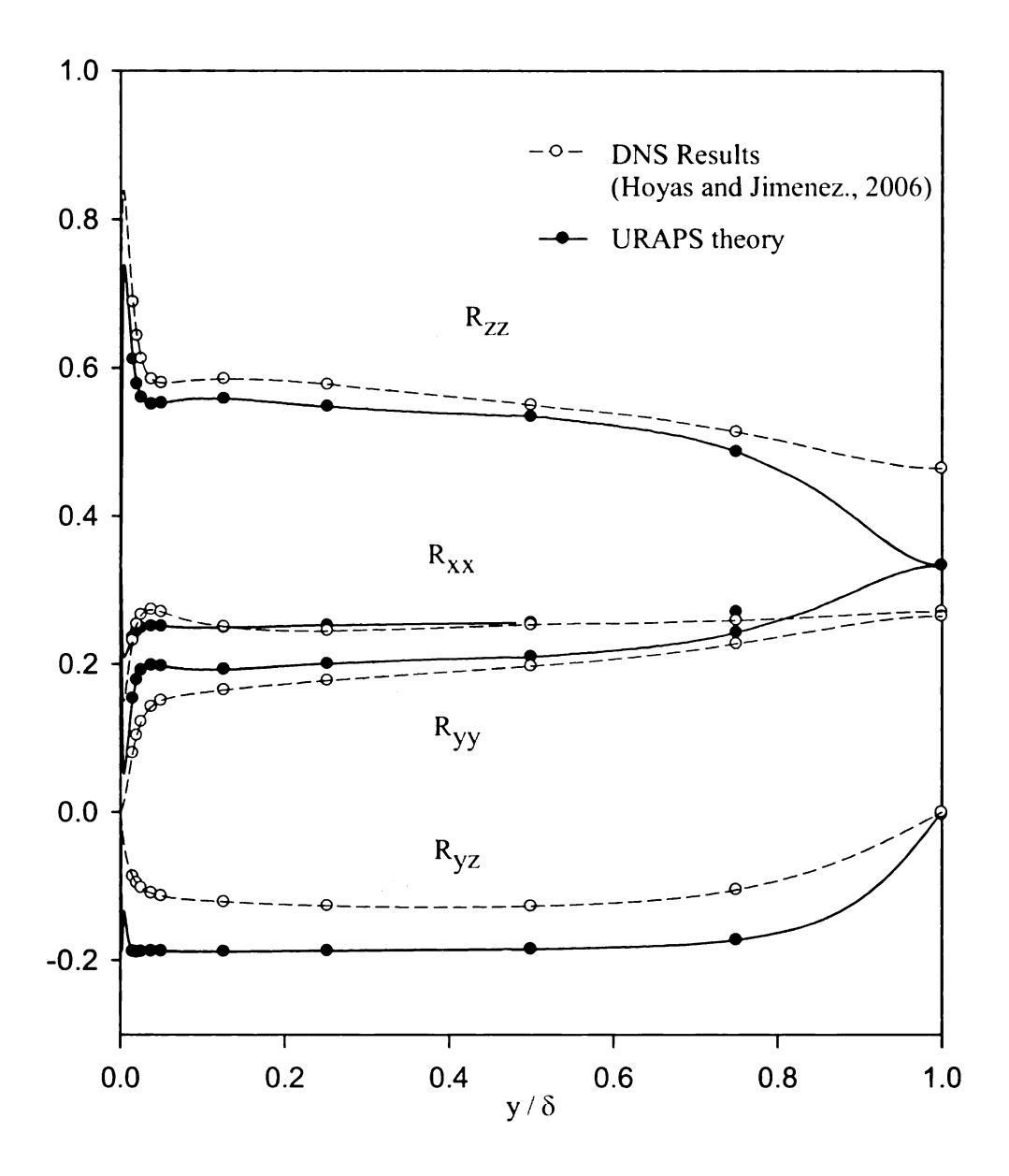


Figure 7.8 Spatial Variation of NR-Stress Components Predicted by URAPS-Closure based on $\tilde{\Gamma}_{DNS}$ for Non-Rotating Fully-Developed Channel Flows with $\delta^+ = 2000\,.$

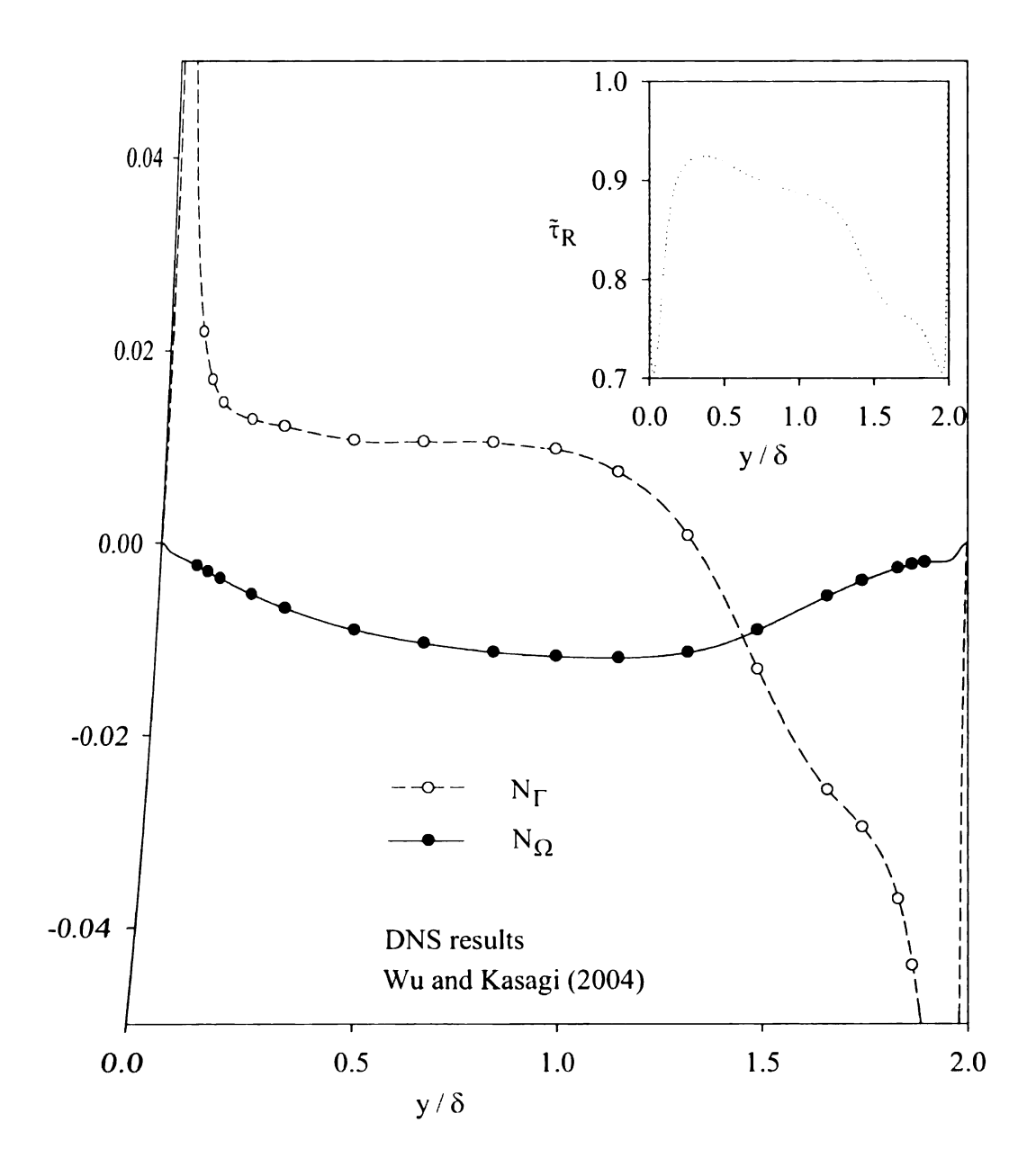


Figure 7.9 Spatial Variation of N_Γ , N_Ω and $\tilde{\tau}_R$ for Fully-Developed Spanwise Rotating Channel based on DNS Results for $\tilde{\Gamma}_{DNS}$ and $\tilde{\Omega}_{DNS}$ with $\delta^+ \cong 300$, $\Omega^+ \cong -0.0042$.

the value of $\tilde{\tau}_R$ is smaller compared to the corresponding values at $y/\delta=0.5$. URAPS-closure can essentially be computed from the knowledge of the two groups $\tilde{\Gamma}_{DNS}$ and $\tilde{\Omega}_{DNS}$. The URAPS-closure states can be computed by successive substitution. The converged solution predicts a distribution of turbulent kinetic energy among the normal components. The predictions of R_{yy} , R_{zz} and R_{yz} are shown in Figures 7.10, 7.11 and 7.12 respectively. The results for each of the components in the LP-side of the channel (i.e. $1 < y/\delta < 2$) are in close agreement with the DNS results. This is the region where both $\tilde{\Gamma}$ and $\tilde{\Omega}$ are negative. Qualitative agreement is also observed for the normal components in HP side of the channel (i.e. $0.1 < y/\delta < 1$). At $y/\delta \cong 0.75$, it can be seen that $R_{yy} > R_{zz}$ unlike the case of channel without rotation. However deviation from the DNS predictions seem to occur at $y/\delta = 0.1$ ($y^+ \sim 30$), possibly due to influence of wall (viscous effects).

7.6 NR-Stress for Zero Absolute Mean Intrinsic Vorticity: Results and Discussion

Data presented by Grundestam et al. (2008) in the core region of the channel is compared with the URAPS-closure predictions. Results reported by Grundestam et al. (2008) in this region which falls mostly in the $0 < y/\delta < 1$ region (HP-side where kinetic energy peaks) are presented in Table I.4 of Appendix I. It is interesting to note that asymptotic homogeneous shear discussed earlier in Chapter 6 for $\tilde{\Omega}/\tilde{\Gamma} = -0.5$ also represents zero absolute mean vorticity region and represents similar features of NR-stress distribution which will be discussed below.

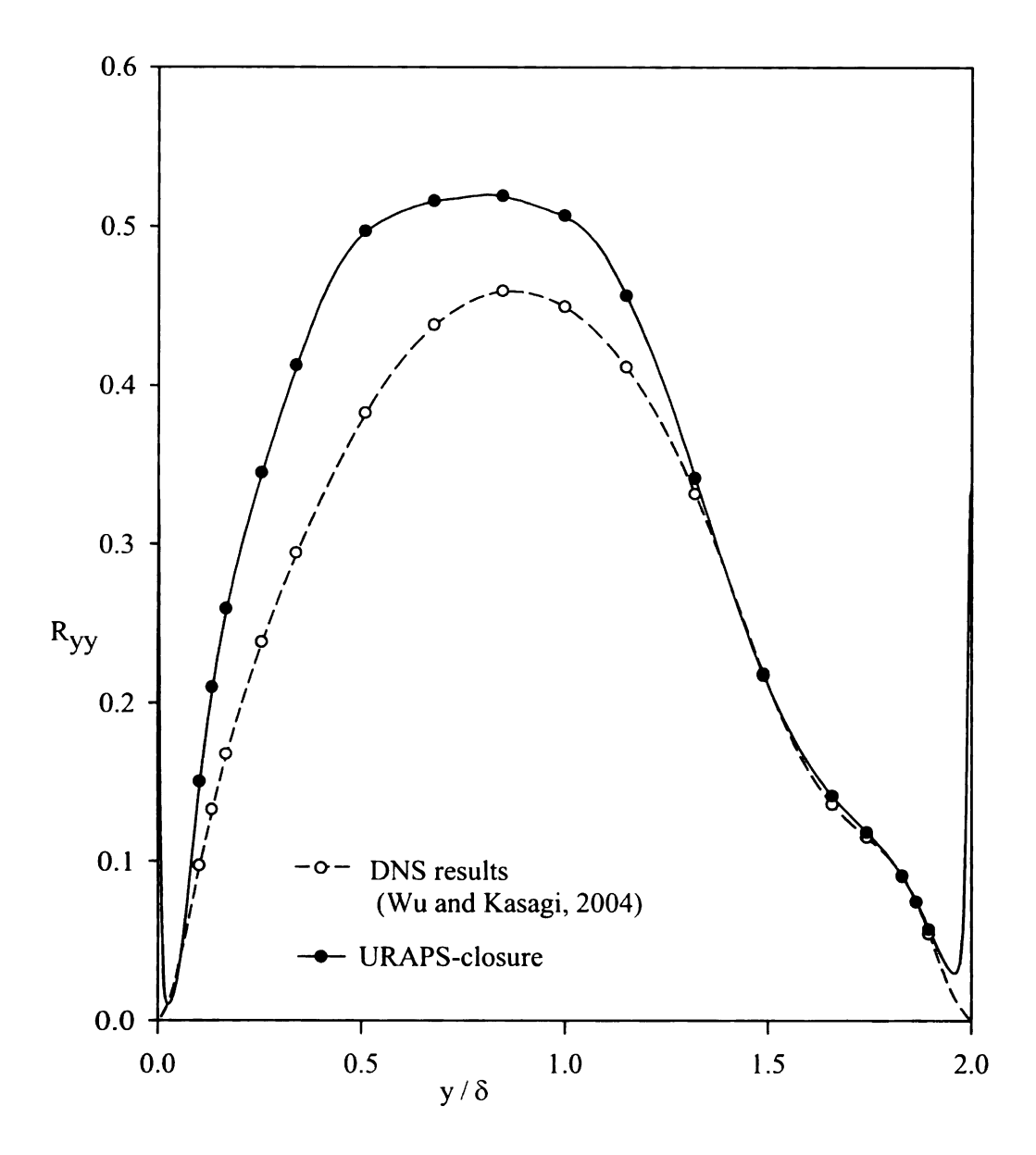


Figure 7.10 URAPS-Closure Predictions for the R_{yy} Component of the NR-Stress for Fully-Developed Spanwise Rotating Channel ($\delta^+ \cong 300$, $\Omega^+ \cong -0.0042$).

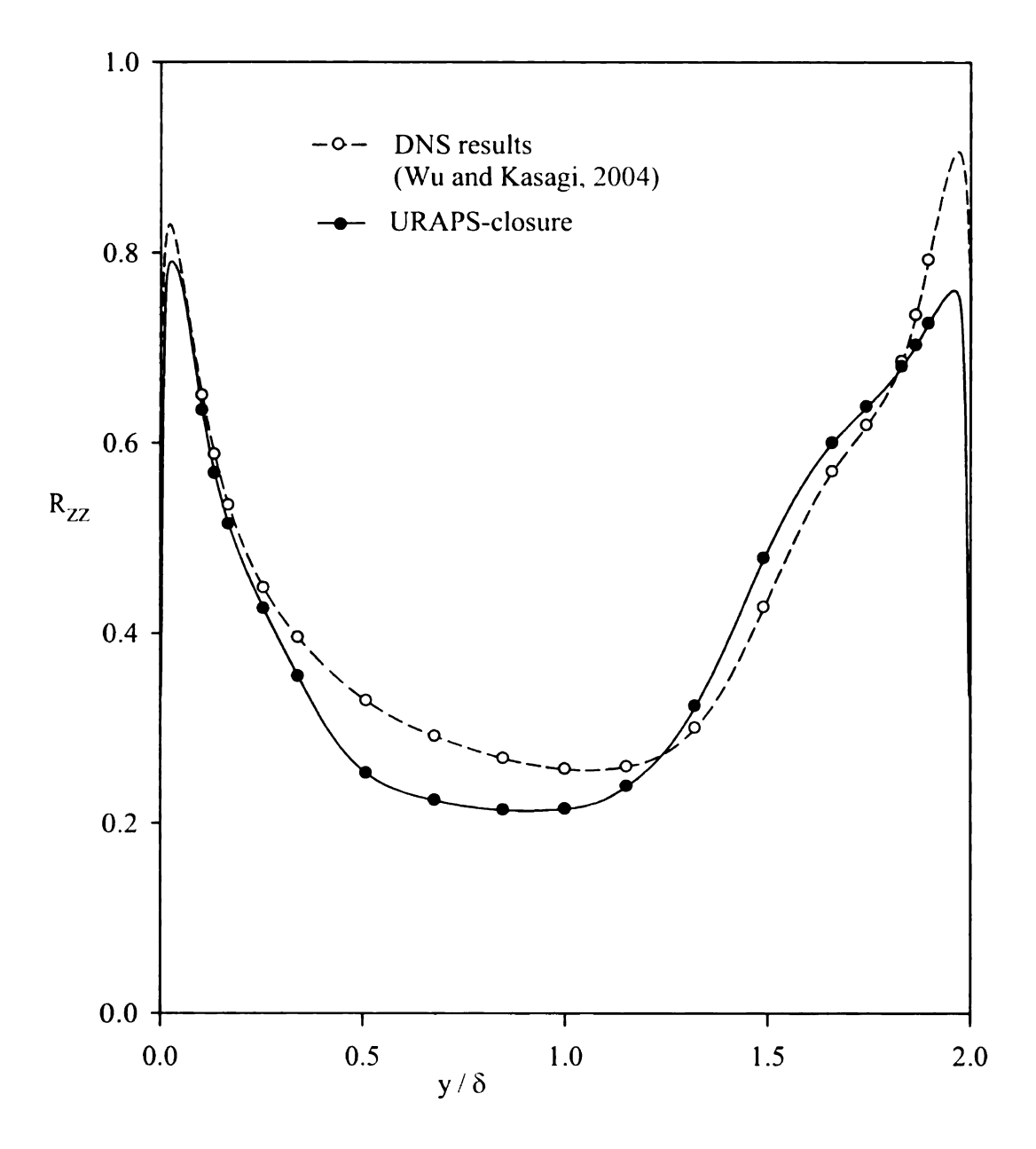


Figure 7.11 URAPS-Closure Predictions for the R_{zz} Component of the NR-Stress for Fully-Developed Spanwise Rotating Channel ($\delta^+ \cong 300$, $\Omega^+ \cong -0.0042$).

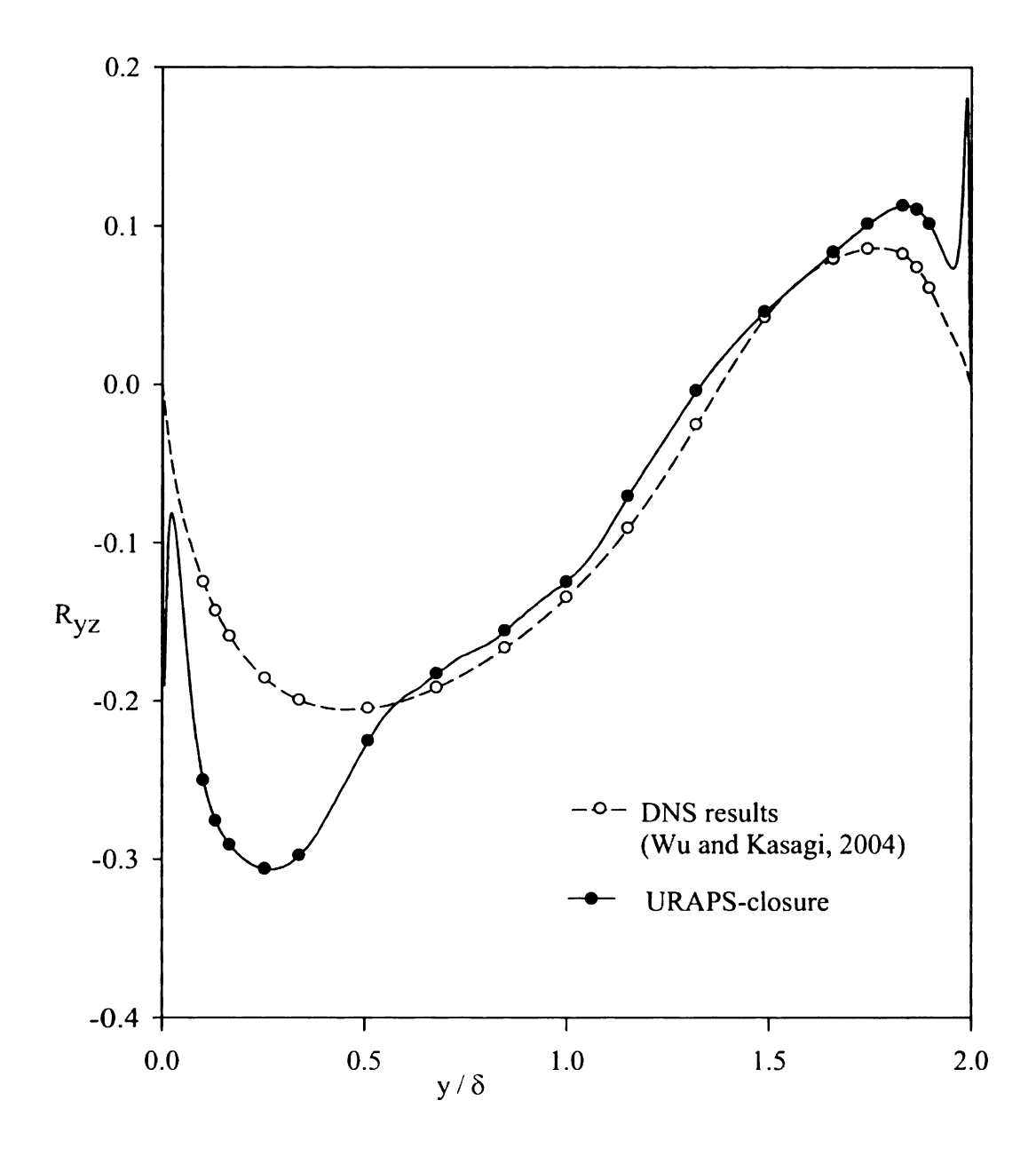


Figure 7.12 URAPS-Closure Predictions for the Shear Component of the NR-Stress for Fully-Developed Spanwise Rotating Channel ($\delta^+ \cong 300$, $\Omega^+ \cong -0.0042$).

The zero absolute mean vorticity has the feature discussed in Case 4 of Appendix G. The URAPS closure equations for this case also show a similarity with the nonrotating channel equations as discussed earlier in Figure 7.2. The predictions in this case shown in Figure 7.13 indicate that energy is concentrated in the R_{yy} component unlike the R $_{zz}$ component for the non-rotating case. For $\tilde{\Omega}=0\,,$ there is equi-distribution of energy and this shifts to $\,R_{\,yy}\,$ component when $\left|\,\tilde{\Omega}\,\right|>0\,.$ For about $\left|\,\tilde{\Omega}\,\right|\cong50\,,$ the energy is all in the R_{vv} and R_{xx} components. The shear component is negative for negative values of $\tilde{\Omega}$ and visc versa with a maximum value of 0.19 occurring at $|\tilde{\Omega}| \cong 2.5$. As summarized in Figure 7.14, for the case when $\tilde{\Gamma} = -2\tilde{\Omega}$, with increasing values of $\tilde{\Gamma}$ (or $-2\tilde{\Omega}$), the energy is transferred from R_{zz} to R_{yy}. DNS results from literature (open symbols) for rotating channel from different simulations with different rotation rates in this region show that $R_{yy} > R_{zz}$. Also note that the previous results for asymptotic homogenous shear (see Figure 6.3) discussed in Chapter 6, with $\tilde{\Omega}/\tilde{\Gamma} = -0.5$ also show that $R_{yy} > R_{zz}$. Corresponding predictions by URAPS closure (closed symbols in Figure 7.14) show that the redistribution of energy consistent with the trend observed in DNS results.

7.7 "Extra" Anisotropy with $\tilde{\Omega} = 0$: Results and Discussion

Figure 7.15 indicates that as the value of $\tilde{\Gamma}$ increases from 0 to 5, the magnitude of the eigenvalues of the extra anisotropy tensor also increase. From $\tilde{\Gamma}=5$ to 50, one of the eigenvalues decreases to zero. This is the region where the NR-stress approaches the

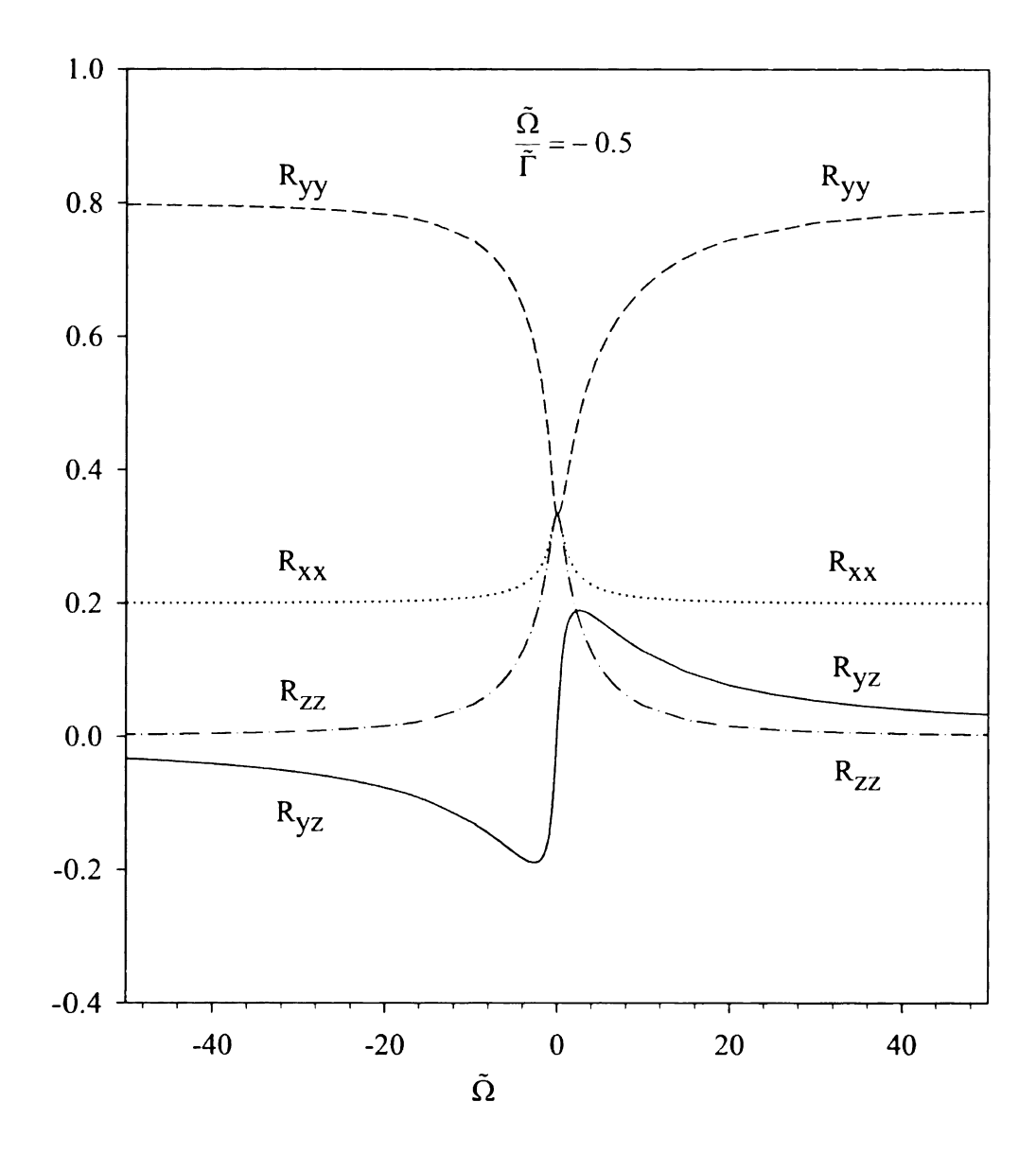


Figure 7.13 Influence of $\tilde{\Omega}$ on the NR-Stress Distribution for URAPS-Closure when $\tilde{\Gamma}=-2\tilde{\Omega}$

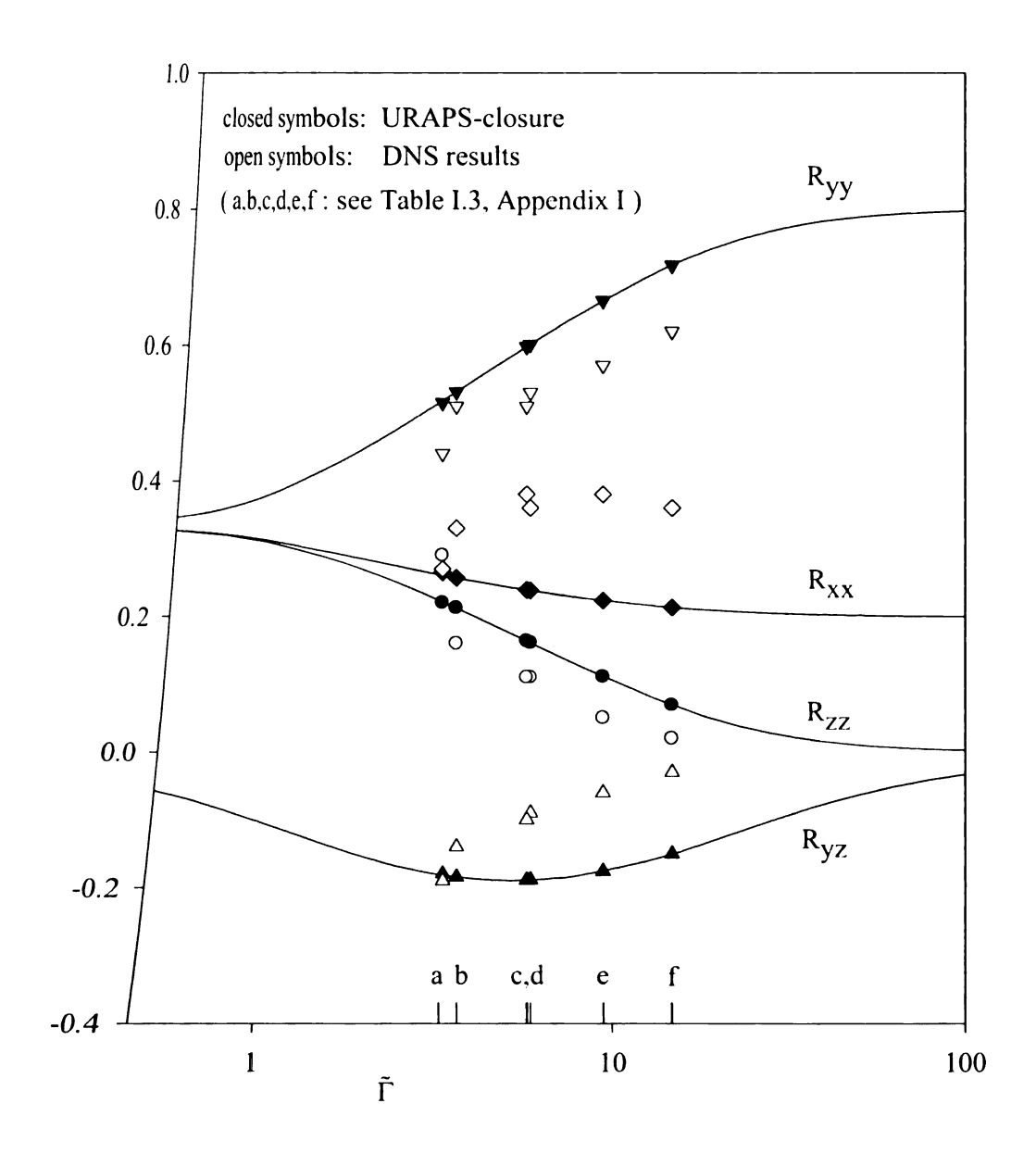


Figure 7.14 URAPS-Closure Predictions in Comparison with DNS Results for Spanwise Rotating Channel, in the Linear Velocity Region where $\tilde{\Omega}/\tilde{\Gamma}=-0.5$ (Zero Absolute Mean Vorticity).

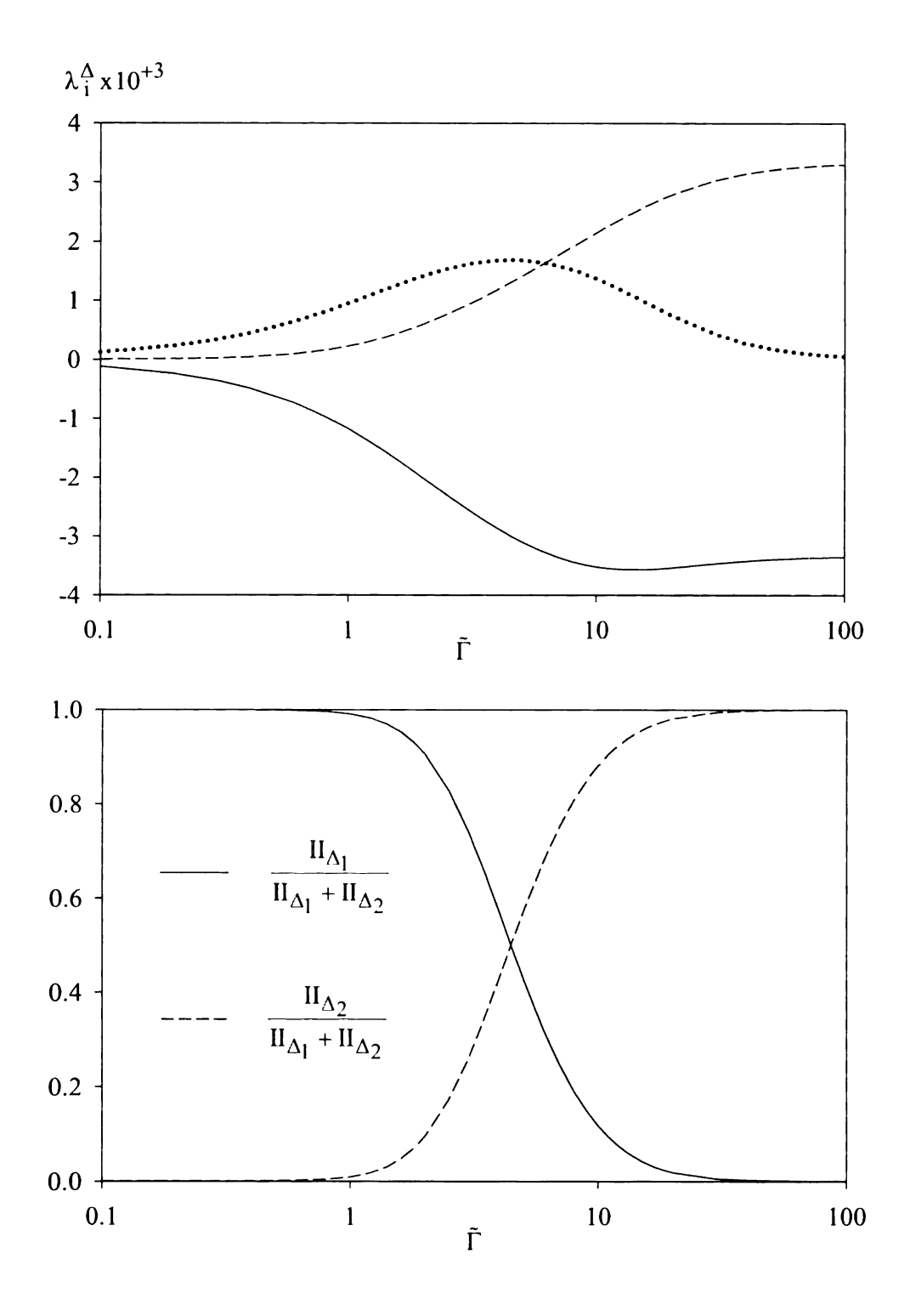


Figure 7.15 Extra Anisotropy for Simple Shear Flow for $\tilde{\Omega} = 0$.

two component anisotropic state where the shear component eventually decreases to zero. The first order linear term of the extra anisotropy is important for smaller values of $\tilde{\Gamma}$ up to about 5. For $\tilde{\Gamma} > 5$, the second order extra anisotropy has a dominating role in controlling the NR-stress anisotropy towards the two component anisotropic states.

7.8 Conclusions

The URAPS-closure with the parameters calibrated in Chapter 4 has been used to predict the NR-stress distribution for simple shear flows using DNS results for the dimensionless shear time and the dimensionless rotation time. Key features for this flow are as below.

- 1. For simple shear flows without rotation, the energy distribution predicted by the URAPS-closure is consistent with the DNS results in the core region of the channel. The anisotropic states $III_b > 0$ starting with the isotropic state for $\tilde{\Gamma} = 0$ and reaching a two component state for $\tilde{\Gamma} > 10$ are also consistent with the DNS results. Near wall results indicate that further evaluation is needed so the NR-stress near a solid/fluid interface is qualitatively consistent with current knowledge.
- 2. As expected, in the case of rotating simple shear, the states predicted by the URAPS- closure are within the L-diagram for all rotations. For the range of $-0.5 < \tilde{\Omega}/\tilde{\Gamma} < 0 \text{, the locus of states are in the region for which } R_{xx} < 1/3 \text{ in the energy simplex and the anisotropic states fall on the curve as for the case of no rotation with } III_b > 0 \text{, although the } \tilde{\Gamma} \text{ is different for each specific state. For } III_b > 0$

- rotation rates $\tilde{\Omega}/\tilde{\Gamma}<-0.5$ and $\tilde{\Omega}/\tilde{\Gamma}>0$, the locus of anisotropic states span the entire L-diagram with $III_b>0$ as well as with $III_b<0$.
- 3. URAPS-closure results for rotating channel flows with $\tilde{\Gamma}_{DNS}$ and $\tilde{\Omega}_{DNS}$ from DNS results for $Re^+ \cong 300$, $\Omega^+ \cong -0.0042$ show a close agreement with the DNS NR-stress results on the LP-side of the channel where both $\tilde{\Gamma}$ and $\tilde{\Omega}$ are negative. Qualitative agreement is also observed on the HP-side of the channel although the predicted values for the normal components differ by about 0.1 for the R_{yy} when compared with DNS results. The shear component in this region needs improvement by studying the near wall viscous effects and taking into account for the URAPS-closure through the turbulent relaxation time.
- 4. Zero absolute mean vorticity region of the channel which is towards the HP-side of the channel, for various rotation rates show a consistent trend that $R_{yy} > R_{zz}$ as indicated through DNS results for Ω^+ ranging from -0.004 to -0.3 (Table I.4, Appendix I). This is also observed in the asymptotic region of rotating homogeneous shear (see Figure 6.3b). URAPS-closure correctly predicts this feature (see Figure 7.14).
- 5. First order and second order extra-anisotropy terms are important for the convergence of URAPS-closure states. The first order anisotropy contribution is more important for smaller values of $\tilde{\Gamma} < 5$ while second order terms are more important for larger values, for the case of non-rotating simple shear flows (see Figure 7.15).

CHAPTER 8

CONCLUSIONS

A universal realizable anisotropic prestress (URAPS-) closure for the normalized Reynolds (NR-) stress has been formulated for the first time as part of this research. This result has much potential as a *practical* and *dependable* closure model for the Reynolds averaged Navier-Stokes (RANS-) equation. *Practicality* stems from the algebraic nature of the URAPS-equation. The new closure is formulated as a non-negative algebraic mapping of the NR-stress into itself. Consequently, the method of successive substitution yields a local solution to the URAPS-equation that is *realizable*. A calibrated URAPS-closure is *dependable* inasmuch as all solutions are non-negative operators. This feature holds for all turbulent flows in inertial and non-inertial frames of reference.

Unlike other commonly encountered algebraic models for the NR-stress, realizability for the URAPS-closure does not depend on the selection of benchmark flows used to determine phenomenological coefficients in the closure. Once the model has been benchmarked against a class of turbulent flows, it yields a realizable NR-stress for all other flows. Thus, the assurance of realizability (dependability feature) together with the simplicity of constructing solutions to a non-linear equation by using a successive substitution algorithm (practicality feature) strongly support the use of the URAPS-closure as a turbulence model for the RANS-equation.

Synopsis of the URAPS-Closure

The URAPS-closure depends on two fundamentally important physical ideas: 1) all turbulent space-time correlations have finite memories; and, 2) the normalized prestress operator is phenomenologically determined by the normalized Reynolds stress. As demonstrated in Chapter 3, the first idea supports the use of a *smoothing approximation* to obtain a local algebraic preclosure mapping between the NR-stress and the normalized prestress:

$$\underline{\underline{R}} = \frac{\underline{\underline{A}^{T} \cdot \underline{B} \cdot \underline{A}}}{\operatorname{tr}(\underline{\underline{A}^{T} \cdot \underline{B} \cdot \underline{A}})}, \quad \underline{\underline{A}} = [\underline{\underline{I}} + \tau_{R} < \underline{\underline{F}} >]^{-1}, \quad <\underline{\underline{F}} > = \nabla < \underline{\underline{u}} > + 2\underline{\underline{\Omega}}.$$
(8.1)

In the above equation, the NR-stress $\underline{\underline{R}}$ and the normalized prestress $\underline{\underline{B}}$ are defined as follows:

$$\underline{\underline{R}} = \frac{\langle \underline{\underline{u}'\underline{\underline{u}'}} \rangle}{\operatorname{tr}(\langle \underline{u'u'}\rangle)} , \quad \underline{\underline{B}} = \frac{\langle \underline{\underline{f}'\underline{f'}}\rangle}{\operatorname{tr}(\langle \underline{f'f'}\rangle)} , \quad \underline{\underline{f}'} = \nabla \cdot [\frac{\underline{p'}}{\rho} + \underline{\underline{u}'\underline{\underline{u}'}} - \langle \underline{\underline{u}'\underline{\underline{u}'}}\rangle]. \tag{8.2}$$

It is noteworthy that the NR-stress and the normalized prestress are symmetric, normalized, and non-negative operators. Eq.(8.1) is clearly a non-negative mapping of B into R.

The second idea noted above provides an additional equation that completes the formal URAPS-closure:

$$\underline{\underline{B}} = \underline{\underline{\mathfrak{B}}}(\underline{\underline{R}}) = \underline{\underline{R}} + C_1(\underline{\underline{R}} - \frac{1}{3}\underline{\underline{I}}) + C_2(\underline{\underline{R}} \cdot \underline{\underline{R}} - II_R\underline{\underline{R}}). \tag{8.3}$$

The coefficients in Eq.(8.3) may be functions of the invariants of the NR-stress and, without loss of generality, can be expressed as (see Chapter 3 for a rationale)

$$C_1 \equiv +\beta \ 27 \det(\underline{\underline{R}}) \quad , \quad C_2 \equiv -\alpha \left(II_R - \frac{1}{3} \right).$$
 (8.4)

A major finding in Chapter 3 is the discovery that Eq.(8.3) is also a non-negative mapping of $\underline{\underline{R}}$ into $\underline{\underline{B}}$ provided the dimensionless coefficients α and β in Eq.(8.4) satisfy the following universal inequalities:

$$-3/2 < \alpha < 9$$
 and $-1 < \beta < \alpha / 27 + 4/5$. (8.5)

Specific functional forms for $\alpha(II_R, III_R)$ and $\beta(II_R, III_R)$ can be determined by appropriate benchmark flows. However, they must satisfy the upper and lower universal bounds to insure that all solutions to the URAPS-closure are non-negative operators.

About fifty-eight years ago, Rotta (see p. 422 in Pope, 2000) used a self-consistent approximation wherein the pressure/strain rate correlation was assumed to depend on the anisotropic component of the Reynolds stress. Rotta's conjecture provided an algebraic closure for a correlation that appears in the second-order moment equation for the NR-stress (see the redistribution term in Eq.(A.11). The research developed herein uses a similar strategy for the normalized prestress. Thus, Eq.(8.3) completes the closure for the preclosure equation given by Eq.(8.1) above. The URAPS-closure generalizes previous work of Parks (1997) and of Weispfennig (1997) by assuming that the prestress is phenomenologically connected to the NR-stress and that the preclosure operator $\underline{\underline{A}}$, defined by Eq.(8.1) above, provides an appropriate coupling between the NR-stress and the normalized prestress for all rigid body frames of reference.

As noted in Chapter 2, other phenomenological algebraic closures for the NR-stress incorrectly relate the NR-stress to *objective* operators, such as the mean strain rate and the intrinsic vorticity operator. This approach misrepresents the underlying physics of the simplest turbulent flows and should be avoided. Therefore, extensions of the prestress closure hypothesis employed in this dissertation should not be based on representation

theorems based on *objective* operators, as proposed earlier by Parks (1997) and, by Weispfennig (1997). However, an appropriate extension of the URAPS-closure could be made based on the URIPS-closure (see Eq.(2.47)) developed previously by Parks et al. (1998). For example,

$$\underline{\underline{B}} = \underline{\underline{\mathcal{B}}}(\underline{\underline{R}}, \underline{\underline{R}}^{o}) \quad , \quad \underline{\underline{R}}^{o} = \frac{\underline{\underline{A}}^{T} \cdot \underline{\underline{A}}}{\operatorname{tr}(\underline{\underline{A}}^{T} \cdot \underline{\underline{A}})}. \tag{8.6}$$

This hypothesis is not developed in the research reported herein.

URAPS-Closure Calibration

The URAPS-closure for the NR-stress requires an estimate of five phenomenological statistical properties: a turbulent transport time τ_R ; the "extra" anisotropic prestress coefficients α and β ; and, the dissipation and production coefficients, C_D and C_P , in the transport equation for the turbulent dissipation. Table 4.3 gives a summary of the calibration results.

In this research, a scalar-valued turbulent transport time τ_R was defined in terms of the space-time structure of the local turbulent state (see Eq. (3.5)). The theoretical development suggests that τ_R depends on three distinct time scales associated with the local turbulent state: a viscous time scale, v/k; a turbulent time scale, k/ϵ ; and, a mean field time scale, $1/\|<\underline{F}>\|$. An analysis of the energy spectrum for rotating and nonrotating homogeneous decay shows that $\tau_R\epsilon/k$ depends on the dimensionless group $N_F \equiv (k/\epsilon)\sqrt{\underline{F}:\underline{F}^T}$ (see Section 4.3; Appendix F; and, Koppula et al., 2009). The three coefficients C_{R2} , C_{R3} , and the exponent 'n' in Eq.(4.3) were determined by recovering

the results of Park and Chung (1998) for rotating homogeneous decay. The dissipation coefficient $C_{\rm D}/C_{\rm R1}$ was estimated by using experimental and DNS results related to non-rotating homogeneous decay.

The "extra" anisotropy coefficients α and β , the coefficient C_{R1} , and the production coefficient C_P are calibrated based on self-similar states in non-rotating homogeneous shear. Optimal values of the coefficients are chosen so that the NR-stress components for self-similar states are recovered with minimum deviation from the experimental data used. The optimized choice of α = +0.1 and β = -0.01 from the realizable domain ensures that the predicted normalized Reynolds stress is non-negative for all flows.

Solution Strategy for the URAPS-equation: Successive Substitution

The mathematical significance of the URAPS-closure for the NR-stress is that a solution can be obtained by successive substitution. If the hydrodynamic/kinematic operator $\tau_R < \underline{F} >$ is known locally, then a solution to the URAPS-closure can be determined by the application of the following algorithm: $\underline{R}_{n+1} = \underline{\mathfrak{R}}(\underline{R}_n)$. The algorithm converges within 600 iterations (i.e., $|(\underline{R}_{n+1} - \underline{R}_n) : \underline{e}_i \underline{e}_j| \le 10^{-5} \underline{R}_n : \underline{e}_i \underline{e}_j$) for rotational simple shear flows. This result occurs for any initial non-negative operator \underline{R}_0 . If this solution method converges for all flows (conjecture), then the URAPS-closure will provide a practical closure of the RANS-equation in rotating and in non-rotating frames of reference.

Homogeneous Decay

For rotating homogeneous decay, the Coriolis acceleration couples with the fluctuating velocity field and causes a redistribution of turbulent kinetic energy into the fluctuating velocity component co-linear with the angular velocity of the frame. The URAPS-closure predicts this redistribution of energy from an initial isotropic state. The resulting quadratic form associated with the NR-stress is a prolate ellipsoid. The prolate anisotropic states $(0 < R_{zz} = R_{zz} < 1/3 < R_{xx} < 1)$ exist for all non-zero rotation numbers. This phenomenon is consistent with DNS and LES simulations of rotating homogeneous decay. Thus, there is no return to isotropy in non-inertial frames. For small rotation rates (i.e., $\tilde{\Omega}_0$ < 1), the URAPS-closure predicts that energy is shifted slowly to the R_{xx} component with a large transfer time of $\tilde{t}_f > 30$. For larger rotation rates (i.e., $\tilde{\Omega}_0$ = 15), the redistribution of energy occurs for $\tilde{t}_f \cong 1.8$. The "extra" anisotropic operator Δ_1 triggers the reorganization of energy during the initial stage of decay ($\tilde{t} << 4$) and the "extra" anisotropic operator $\underline{\Delta}_2$ completes the energy transfer during for the final stage of the decay ($\tilde{t} >> 4$).

Unbounded Rotating Homogeneous Shear

For unbounded rotating homogeneous shear, the transport equations for k and ϵ together with the URAPS-closure for the NR-stress have self-similar solutions for $-0.65 = (\tilde{\Omega}/\tilde{\Gamma})_{min} < (\tilde{\Omega}/\tilde{\Gamma}) < (\tilde{\Omega}/\tilde{\Gamma})_{max} = +0.15. \text{ As the rotation group decreases from } 0 \text{ to } -1/2, \text{ energy is shifted from } R_{zz} \text{ to } R_{yy}. \text{ For } \tilde{\Omega}/\tilde{\Gamma} = -1/4, \ 1/\tilde{\Gamma}^a, \ (P/\epsilon)^a, \text{ and } R_{zz} = -1/4, \ 1/\tilde{\Gamma}^a, \ (P/\epsilon)^a, \text{ and } R_{zz} = -1/4, \ 1/\tilde{\Gamma}^a, \ (P/\epsilon)^a, \text{ and } R_{zz} = -1/4, \ 1/\tilde{\Gamma}^a, \ (P/\epsilon)^a, \text{ and } R_{zz} = -1/4, \ 1/\tilde{\Gamma}^a, \ (P/\epsilon)^a, \text{ and } R_{zz} = -1/4, \ 1/\tilde{\Gamma}^a, \ (P/\epsilon)^a, \text{ and } R_{zz} = -1/4, \ 1/\tilde{\Gamma}^a, \ (P/\epsilon)^a, \text{ and } R_{zz} = -1/4, \ 1/\tilde{\Gamma}^a, \ (P/\epsilon)^a, \text{ and } R_{zz} = -1/4, \ 1/\tilde{\Gamma}^a, \ (P/\epsilon)^a, \text{ and } R_{zz} = -1/4, \ 1/\tilde{\Gamma}^a, \ (P/\epsilon)^a, \text{ and } R_{zz} = -1/4, \ 1/\tilde{\Gamma}^a, \ (P/\epsilon)^a, \text{ and } R_{zz} = -1/4, \ 1/\tilde{\Gamma}^a, \ (P/\epsilon)^a, \text{ and } R_{zz} = -1/4, \ 1/\tilde{\Gamma}^a, \ (P/\epsilon)^a, \$

-R_{yz} show a maximum compared to other rotation numbers. The URAPS-predictions are qualitatively consistent with DNS and LES results. Algebraic models that cannot account for the rotation dependence on the shear component of the NR-stress cannot predict the finite asymptotic region and the energy redistribution phenomenon.

For rotating homogeneous shear flows, the eigenvalues associated with the "extra" anisotropy operators $\underline{\Delta}_1$ and $\underline{\Delta}_2$ are several orders of magnitude smaller than the eigenvalues associated with the anisotropic component of the NR-stress. Nevertheless, these operators play an important role in attaining the self-similar states. For $\tilde{\Omega}/\tilde{\Gamma}=0$ and $\tilde{\Gamma}_0=1$, the $\underline{\Delta}_1$ -operator is prominent during the early stage of development towards a self-similar state; however, during the final stage of development, both "extra" anisotropic operators are important.

Fully-Developed Channel Flows with Spanwise Rotation

For simple shear flow, there are no energy states in the 1^{st} -Sextet or the 2^{nd} -Sextet of the energy simplex (see Figure 7.3a) for rotation rates $\tilde{\Omega}/\tilde{\Gamma}<-0.5$ and $\tilde{\Omega}/\tilde{\Gamma}>0$. However, the anisotropic states span the entire L-diagram (III_b may be either positive or negative) as indicated by Figure 7.3b. However, for $-0.5<\tilde{\Omega}/\tilde{\Gamma}\leq0$, there are no energy states in the 3^{rd} -Sextet and the 4^{th} -Sextet (see Figure 7.4). The third invariant of the anisotropic stress is always positive and all anisotropic states, (II_b, III_b), fall on the same curve within the L-diagram (see Figure 7.4). URAPS-closure predictions for non-rotating and rotating fully-developed channel flows depend on two groups $\tilde{\Gamma}$ and $\tilde{\Omega}$ that vary across the channel. Both groups are zero at a solid/fluid interface. The shear

group $\tilde{\Gamma}$ is zero where the mean velocity is a maximum. The magnitude of the rotation group (i.e., $\left|\tilde{\Omega}\right|$) is non-zero within the flow domain inasmuch as $k/\epsilon > 0$.

For non-rotating flows ($\tilde{\Omega}$ =0), the energy states are all in the 2nd-Sextet and the second invariant of the anisotropic stress is positive for all states (i.e., III_b > 0). These predictions are in good qualitative agreement with DNS results for fully-developed channel flows (see Figures 7.5, 7.7, and 7.8). The invariants of the "extra" anisotropy operators $\underline{\Delta}_1$ and $\underline{\Delta}_2$ indicate that $\underline{\Delta}_1$ is more important for $\tilde{\Gamma}$ < 5, while $\underline{\Delta}_2$ is more important for larger values of the local shear group (see Figure 7.15).

As indicated by Figure 7.14, the URAPS-closure predictions in the region where $\tilde{\Gamma} = -2\tilde{\Omega}$ are in good qualitative agreement with DNS results. Note that the Coriolis phenomenon has shifted the energy to the transverse component in the region where the intrinsic vorticity is zero. This is a significant conclusion and strongly supports the use of the URAPS-closure as a practical and physical closure for the RANS equation.

As indicated by Figures 7.10, 7.11, and 7.12, the local components of the NR-stress predicted by the URAPS-closure based on the local values of $\tilde{\Gamma}_{DNS}$ and $\tilde{\Omega}_{DNS}$ are qualitatively consistent with the DNS results. The URAPS-closure predictions on the LP-side of the channel are in close agreement with the DNS results for $Re^+ \cong 300$ and $\Omega^+ \cong -0.0042$. Qualitative agreement is also observed on the HP-side of the channel. The shear component on the HP-side (see Figure 7.12) needs to be improved by either modifying τ_R near the solid/fluid interface and/or by modifying the "extra" anisotropic prestress coefficients near the solid/fluid interface. In conclusion, the remarkable qualitative agreement between the URAPS-closure and the DNS results strongly supports

the conclusion that Eq. (3.32) will provide a low-order closure model for the RANS-equation.

•

CHAPTER 9

RECOMMENDATIONS

The following three problems will complement the research results developed herein and will support the use of the URAPS-closure as a low-order closure model for the RANS-equation.

9.1 Turbulent Transport Time for Low Turbulent Reynolds Numbers

The turbulent transport time τ_R introduced by the preclosure equation (see Eq.(3.5)) depends on the turbulent Reynolds number $\text{Re}_t = (k/\epsilon)/(v/k)$ and the shear group $N_F \equiv (k/\epsilon) \| < \frac{F}{\epsilon} > \|$. In this research (see Section 4.3), the URAPS-closure for the NR-stress was calibrated for unbounded turbulent flows for which

$$(k/\epsilon)\gg (\nu/k)$$
 and $\tau_R=C_{R1}\tilde{\tau}_R(\infty,N_F)k/\epsilon$.

For wall-bounded flows, turbulent transport time will be influenced significantly by the turbulent Reynolds number. A method for including a Reynolds number dependence in the preclosure equation was proposed earlier by Weispfennig (1997) for the URIPS-closure. This approach can also be used for the URAPS-closure.

For fully-developed channel flows, the turbulent Reynolds number Re_t is large in the outer region and small near the walls. Viscous transport of mean momentum compared with turbulent transport of mean momentum is negligible in the core of the flow field; however, close to the wall, viscous effects dominate the transport of mean momentum as can be seen in the total shear stress profiles portrayed by Figures 2.2 and 2.8. The near wall influence of the turbulent Reynolds number can be included in the

turbulent transport time by developing a functional dependence of $\tilde{\tau}_R$ on Re_t. In the near wall region (i.e., $0 < y^+ < 30$) major differences between DNS and the URAPS-closure are observed for the shear stress for both rotating and non-rotating flows (see Figure 7.7, 7.8 and 7.12). Accurate predictions of the shear component of the NR-stress in the near wall region are critical for predicting the mean velocity profile. Hence, the following analysis based on a previous study by Weispfennig (1997) may provide a framework to include the influence of the turbulent Reynolds number on the turbulent transport time: $\tilde{\tau}_R = \tilde{\tau}_R \left(Re_t, N_F \right)$.

Near a solid/fluid interface, continuity and the no-slip boundary condition imply that (see Monin and Yaglom, 1965; Weispfennig, 1997):

$$< u_x' u_x' > = (u^*)^2 [C_{xx}(y^+)^2 + \cdots]$$
 (9.1)

$$\langle u_{y}'u_{y}' \rangle = (u^{*})^{2} [C_{yy}(y^{+})^{4} + \cdots]$$
 (9.2)

$$< u_z' u_z' > = (u^*)^2 [C_{zz}(y^+)^2 + \cdots]$$
 (9.3)

$$\langle u_{y}'u_{z}' \rangle = -(u^{*})^{2} [C_{yz}(y^{+})^{3} + \cdots]$$
 (9.4)

$$k^{+} = C_{k} (y^{+})^{2} + \cdots$$
 (9.5)

$$\varepsilon^{+} = \varepsilon_{w}^{+} + C_{\varepsilon} y^{+} + \cdots \tag{9.6}$$

DNS results for rotating and non-rotating channel flows are consistent with Eqs.(9.1)-(9.6). Eqs. (9.4) and (9.5) imply that

$$-Ryz = C_{yz} y^{+} + \cdots. \tag{9.7}$$

Figure 9.1 shows the variation of $-R_{yz}$ with $N_{\Gamma} (\equiv \tau_R \Gamma_{yz})$ for the URAPS-closure. For $N_{\Gamma} >> 1$, it can be seen that $-R_{yz} \propto 1/N_{\Gamma}$. Thus, Eq. (9.7) implies that

$$N_{\Gamma} \propto 1/y^{+} \text{ as } y^{+} \rightarrow 0.$$
 (9.8)

An empirical expression for $\tilde{\tau}_R(Re_t, N_F)$ consistent with this behavior of N_Γ is

$$N_{\Gamma} = \tau_{R} \Gamma_{yz} = C_{R1} \tilde{\tau}_{R} (Re_{t}, N_{F}) \frac{k}{\varepsilon} \Gamma_{yz} \quad \text{where}$$

$$\tilde{\tau}_{R} (Re_{t}, N_{F}) = (1 + C_{W} Re_{t}^{-3/4}) \frac{(1 + C_{R3} N_{F}^{3/2})}{(1 + C_{R2} N_{F}^{3/2})}$$
(9.9)

Near wall statistical data can be used to determine the dependence of the wall function $C_{\rm W}$ on Re_t and N_F subject to the following two conditions:

$$C_{W}(Rc_{t}, N_{F}) \rightarrow \begin{cases} C_{W}(0,0) = C_{W}^{0} < \infty \\ C_{W}(\infty, N_{F}) = 0 \end{cases}$$
 (9.10)

9.2 "Extra" Anisotropy Coefficients

Although the components of the NR-stress predicted by the high Reynolds number URAPS-closure are qualitatively consistent with DNS, an improved quantitative agreement is nevertheless needed in the near wall region where the anisotropy associated with the NR-stress is large. The "extra" anisotropic coefficients α and β in the URAPS-theory (see Section 3.3) were calibrated in this research based on experimental data associated with asymptotic homogeneous shear (see Section 4.4), which is a relatively weak anisotropic state by comparison with the near-wall region. The near wall URAPS-results portrayed in Figure 7.12 were calculated based on the assumption that α and β are universal constants. This assumption is probably not correct and needs to be

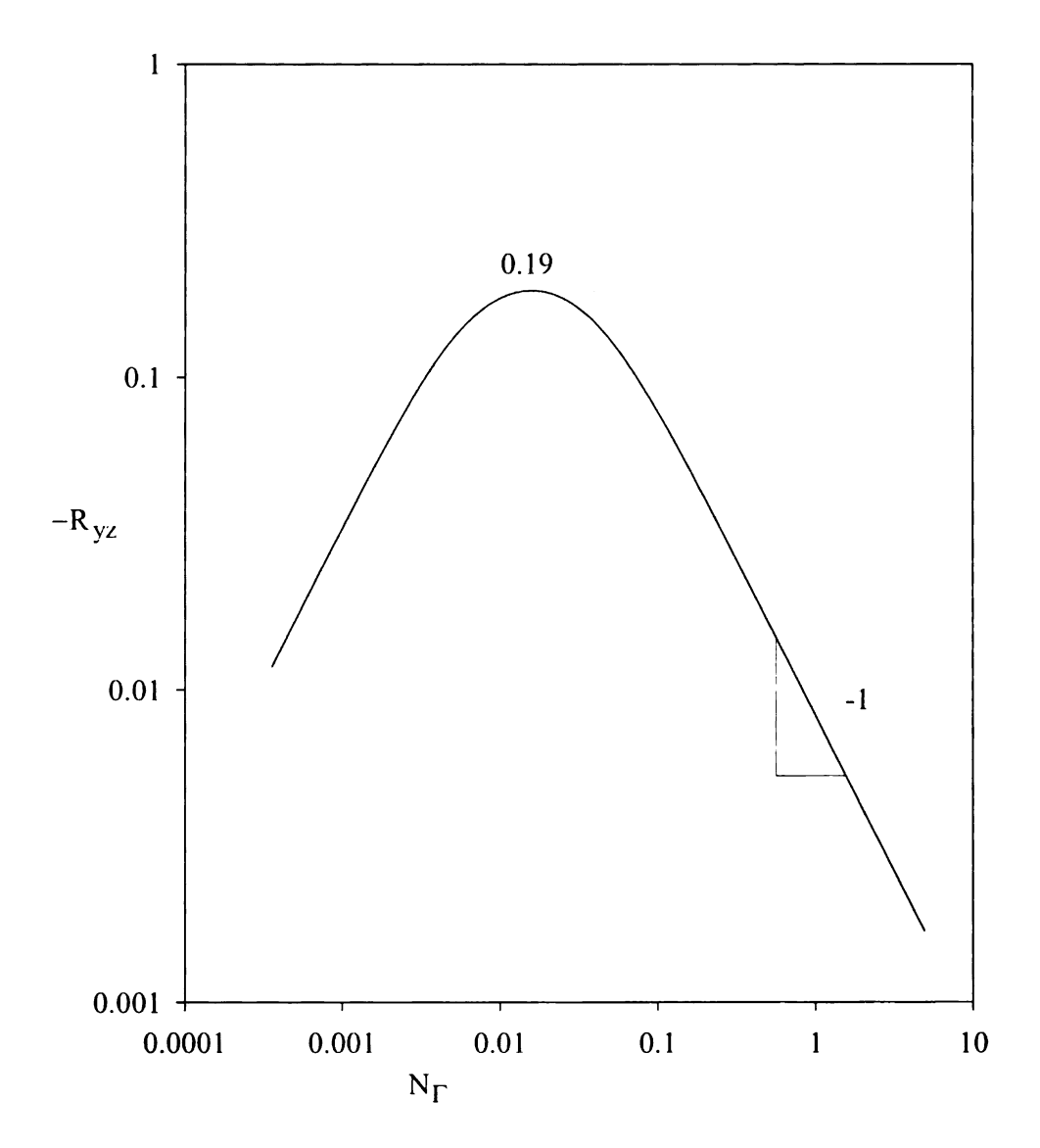


Figure 9.1 URAPS-Closure Predictions of $-R_{yz}$ for Non-Rotating Simple Shear.

examined carefully. An approach forward based on the theoretical finding portrayed by Figure 3.6 is proposed below.

For simple shear flows in an inertial frame of reference, the maximum value of $-R_{yz}$ predicted by the URAPS-closure is about $+0.19\,$ for $\,\tilde{\Gamma}\cong 5$. This is the maximum value for all $\,\delta^+$. This is too large. DNS results show that $\, max(-R_{yz}) = +0.15 \,$ for $\, \tilde{\Gamma} \cong 3 \,$ and $\delta^+=300$. For $\delta^+=2000$, DNS results show that $max(-R_{yz})=+0.13$ for $\tilde{\Gamma}\cong 4$. The URAPS-prediction of this statistical property can be improved by further exploring the assumption that the "extra" anisotropy coefficients α and β depend on the local invariants of the NR-stress: $\alpha(II_R, III_R)$ and $\beta(II_R, III_R)$. The only theoretical restriction on these coefficients is the universal bounds portrayed by Figure 3.6. This type of point re-calibration could also improve the near wall predictions of the URAPSclosure inasmuch as the invariants II_R and III_R change significantly across a wallbounded flow field. Figure 9.2 shows the URAPS-prediction for the energy distribution and the anisotropic states for fully-developed channel flows with spanwise rotation based on the assumption that α and β are constants. A comparison of Figure 9.2 with Figures 2.10 and 2.11 provides ample motivation for dropping the assumption that the "extra" anisotropic coefficients α and β are universal constants. The proposed re-calibration under the constraint expressed by Figure 3.6 should improve the quantitative agreement between the DNS results and the URAPS-closure predictions.

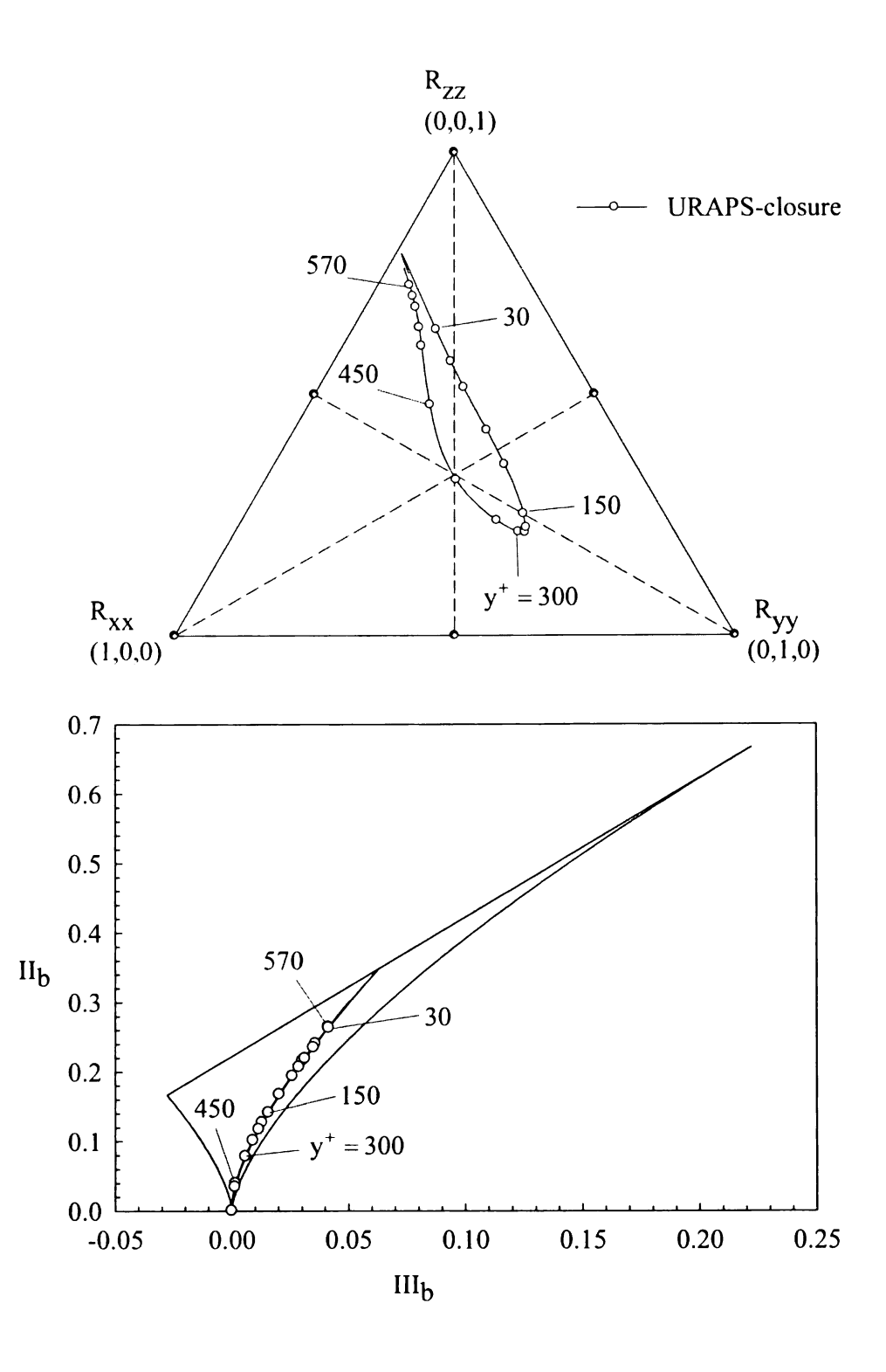


Figure 9.2 URAPS-Closure Predictions of the Energy and Anisotropic States for Fully-Developed Spanwise Rotating Channel ($\delta^+ \cong 300$, $\Omega^+ \cong -0.0042$)

9.3 Explicit URAPS-Closure

The URAPS-closure, defined by Eq.(3.32), is an *implicit* equation for the NRstress. As demonstrated in this research, Eq.(3.32) can easily be solved by using a method of successive substitution. This result occurs in part because the URAPS-closure is a mapping of the NR-stress into itself for all turbulent flows (i.e., all $\tau_R < \underline{F} >$). The convergence of the successive substitution algorithm depends on the choice of the initial operator in the space of non-negative operators. For simple shear flows with spanwise rotation, this research demonstrated that any initial non-negative operator will converge to a unique NR-stress by applying a successive substitution algorithm to Eq.(3.32). This global contraction property is highly desirable and would support the need for rapid solution methods in CFD applications. However, for more complex flows, the choice of the initial condition for the successive substitution algorithm to converge may be restricted to a "neighborhood" of the NR-stress operator that satisfies Eq.(3.32). For example, this will surely occur for statistically stationary flows with multiple solutions. This issue can be addressed by formulating an *explicit* URAPS-closure wherein the nonnegative prestress operator is directly related to the hydrodynamic/kinematic operator $\tau_R < \underline{\underline{F}} > \text{ by a non-linear algebraic equation. Previous research by Parks (1997) and}$ Weispfennig (1997) used the assumption that the normalized prestress could be approximated as an isotropic operator, but this approach could not explain the energy distribution for non-rotating, fully-developed channel flows. A proposed alternative to the Parks-Weispfennig conjecture is to use the URIPS-stress as an appropriate hydrodynamic/kinematic operator. This idea is briefly discussed below.

An example of an *explicit* representation for the NR-stress follows by combining the preclosure equation (see Eq.(2.44) and Eq.(3.9)) with the following hypothesis:

$$\underline{\underline{B}} = \underline{\underline{\mathcal{B}}}(\underline{\underline{R}}^{IPS}) , \underline{\underline{R}}^{IPS} = \underline{\underline{\underline{A}}^T \cdot \underline{\underline{A}}} = \underline{\underline{\underline{C}}^T \cdot \underline{\underline{C}}} = \underline{\underline{\underline{C}}^T \cdot \underline{\underline{C}}} . \tag{9.11}$$

The application of the non-negative Cayley-Hamilton mapping theorem developed in this research yields the following representation for the prestress (cf., Eq.(3.19)),

$$\underline{\underline{B}} = \underline{\underline{R}}^{\text{URIPS}} - \alpha (II_{R^{\text{IPS}}}, III_{R^{\text{IPS}}}) [II_{R^{\text{IPS}}} - \frac{1}{3}] [\underline{\underline{R}}^{\text{IPS}} \cdot \underline{\underline{R}}^{\text{IPS}} - II_{R^{\text{IPS}}} \underline{\underline{R}}^{\text{IPS}}]$$

$$+ \beta (II_{R^{\text{IPS}}}, III_{R^{\text{IPS}}}) 27 \det(\underline{\underline{R}}^{\text{IPS}}) [\underline{\underline{R}}^{\text{IPS}} - \frac{1}{3}\underline{I}]$$

$$(9.12)$$

The calibration of the two "extra" anisotropic prestress coefficients with appropriate benchmark flows is subject to the following universal bounds (see Figure 3.6):

$$-\frac{3}{2} < \alpha(II_{R IPS}, III_{R IPS}) < +9$$

$$-1 < \beta(II_{R IPS}, III_{R IPS}) < \frac{1}{27}\alpha(II_{R IPS}, III_{R IPS}) + \frac{4}{9}$$
(9.13)

The proposed *explicit* URAPS-closure is defined by

$$\underline{\underline{R}} = \frac{\underline{\underline{A}}^{T} \cdot \underline{\mathfrak{B}}(\underline{\underline{R}}^{IPS}) \cdot \underline{\underline{A}}}{tr(\underline{\underline{A}}^{T} \cdot \underline{\mathfrak{B}}(\underline{\underline{R}}^{IPS})\underline{\underline{A}})}.$$
(9.14)

The above EURAPS-closure does not require a numerical search for a solution. Once $\tau_R < \underline{F} >$ has been specified locally, then Eq.(9.14) yields a prediction of the local NR-stress.

APPENDICES

APPENDIX A

UNCLOSED EQUATION FOR THE REYNOLDS STRESS

The equation for fluctuating velocity can be derived by subtracting the ensemble average equation from the instantaneous equation. A transport equation for the Reynolds stress can be developed by multiplying with the fluctuating velocity and ensemble averaging it. An unclosed equation for the Reynolds stress in a rotating frame of reference is presented in this appendix. The governing equation for fluid flow in a non-inertial frame of reference is as follows:

$$\frac{\partial \underline{u}}{\partial t} + \underline{u} \cdot \underline{F} = -\nabla \left(\frac{p}{\rho} - \frac{\underline{x} \cdot (\underline{\Omega} \cdot \underline{\Omega}^T) \cdot \underline{x}}{2}\right) + \nu \nabla^2 \underline{u} + \underline{g}$$
(A.1)

$$\nabla \cdot \underline{\mathbf{u}} = 0 \tag{A.2}$$

Upon ensemble averaging,

$$\frac{\partial <\underline{\mathbf{u}}>}{\partial t} + <\underline{\mathbf{u}}> <\underline{\mathbf{F}}> = -\nabla(\frac{<\mathbf{p}>}{\rho} - \frac{\underline{\mathbf{x}}\cdot(\underline{\Omega}\cdot\underline{\Omega}^{\mathsf{T}})\cdot\underline{\mathbf{x}}}{2}) + \underline{\mathbf{g}} + \nu\nabla^{2} <\underline{\mathbf{u}}> -\nabla \cdot <\underline{\mathbf{u}}'\underline{\mathbf{u}}'> \text{ (A.3)}$$

$$\nabla \cdot < \underline{\mathbf{u}} > = 0 \tag{A.4}$$

The equation for fluctuating velocity can be obtained by subtracting Eq.(a.3) from Eq. (A.1) as shown in Eq. (A.5)

$$\frac{\partial \underline{\mathbf{u}}'}{\partial t} + \langle \underline{\mathbf{u}} \rangle \cdot \nabla \underline{\mathbf{u}}' - \nu \nabla^2 \underline{\mathbf{u}}' = -\underline{\mathbf{u}}' \cdot \langle \underline{\mathbf{F}} \rangle - \nabla \cdot (\frac{\mathbf{p}'}{\rho} \underline{\mathbf{I}} + \underline{\mathbf{u}}' \underline{\mathbf{u}}' - \langle \underline{\mathbf{u}}' \underline{\mathbf{u}}' \rangle)$$

$$I \qquad II \qquad IIV \qquad V \qquad VI \qquad VII$$
(A.5)

where $\langle \underline{F} \rangle = \nabla \langle \underline{u} \rangle + 2 \underline{\Omega}$. Upon pre-multiplication and post multiplication of the above equation with u' the resulting equations are

$$\underline{\mathbf{u}}'\left[\frac{\partial \underline{\mathbf{u}}'}{\partial t} + <\underline{\mathbf{u}}> \cdot \nabla \underline{\mathbf{u}}' - \mathbf{v}\nabla^2 \underline{\mathbf{u}}'\right] = \underline{\mathbf{u}}'\left[-\underline{\mathbf{u}}' \cdot <\underline{\mathbf{F}}> -\nabla \cdot (\frac{\mathbf{p}'}{\rho}\underline{\mathbf{I}} + \underline{\mathbf{u}}'\underline{\mathbf{u}}' - <\underline{\mathbf{u}}'\underline{\mathbf{u}}'>)\right] \tag{A.6}$$

$$\left[\frac{\partial \underline{\mathbf{u}}'}{\partial t} + \langle \underline{\mathbf{u}} \rangle \cdot \nabla \underline{\mathbf{u}}' - \nu \nabla^2 \underline{\mathbf{u}}'\right] \underline{\mathbf{u}}' = \left[-\underline{\mathbf{u}}' \cdot \langle \underline{\mathbf{F}} \rangle - \nabla \cdot (\frac{\mathbf{p}'}{\rho} \underline{\mathbf{I}} + \underline{\mathbf{u}}' \underline{\mathbf{u}}' - \langle \underline{\mathbf{u}}' \underline{\mathbf{u}}' \rangle)\right] \underline{\mathbf{u}}' \tag{A.7}$$

Adding the above two equations, the equation for fluctuating momentum can be obtained.

$$\begin{split} I: & \qquad (\underline{u}'\frac{\partial\,\underline{u}'}{\partial\,t} + \frac{\partial\,\underline{u}'}{\partial\,t}\,\underline{u}') & = & \frac{\partial}{\partial\,t}(\underline{u}'\underline{u}') \\ II: & \qquad \underline{u}'(<\underline{u}>\cdot\nabla\underline{u}') + (<\underline{u}>\cdot\nabla\underline{u}')\,\underline{u}' & = & <\underline{u}>\cdot\nabla(\underline{u}'\underline{u}') \\ III: & \qquad -\nu\left[\underline{u}'(\nabla^2\underline{u}') + (\nabla^2\underline{u}')\,\underline{u}'\right] & = & -\nu\nabla^2(\underline{u}'\underline{u}') + 2\nu\left[(\nabla\underline{u}')^T\cdot(\nabla\underline{u}')\right] \\ IV: & \qquad \underline{u}'(-\underline{u}'\cdot<\underline{F}>) - (\underline{u}'\cdot<\underline{F}>)\,\underline{u}' & = & -\underline{u}'\underline{u}'\cdot<\underline{F}> - <\underline{F}>^T\cdot\underline{u}'\underline{u}' \\ V: & \qquad -\underline{u}'\nabla\cdot(\frac{\underline{p}'}{\rho}\underline{I}) - (\nabla\cdot(\frac{\underline{p}'}{\rho}\underline{I}))\,\underline{u}' & = & \\ & \qquad \qquad -\frac{1}{\rho}\nabla\cdot\left[(\underline{u}'\underline{p}')\,\underline{I} + \underline{I}\,(\underline{u}'\underline{p}')\right] + \frac{\underline{p}'}{\rho}\left[\nabla\underline{u}' + (\nabla\underline{u}')^T\right] \\ VI: & \qquad -\underline{u}'\nabla\cdot(\underline{u}'\underline{u}') - (\nabla\cdot(\underline{u}'\underline{u}'))\,\underline{u}' & = & -\nabla\cdot\underline{u}'\underline{u}'\underline{u}' \\ VII: & \qquad \underline{u}'\nabla\cdot<\underline{u}'\underline{u}'> + (\nabla\cdot<\underline{u}'\underline{u}'>)\,\underline{u}' = \nabla\cdot(\underline{u}'<\underline{u}'\underline{u}'>) \end{split}$$

The resultant equation is the transport equation for instantaneous Reynolds stress

$$\begin{split} \frac{\partial}{\partial t} (\underline{u}'\underline{u}') + &< \underline{u} > \cdot \nabla (\underline{u}'\underline{u}') - \nu \nabla^2 (\underline{u}'\underline{u}') = \\ & I \qquad III_{a} \\ & - 2\nu \left[(\nabla \underline{u}')^T \cdot (\nabla \underline{u}') \right] - \left[(\underline{u}'\underline{u}') \cdot < \underline{F} > + < \underline{F} >^T \cdot (\underline{u}'\underline{u}') \right] \\ & III_{b} \qquad IV \\ & - \frac{1}{\rho} \nabla \cdot \left[(\underline{u}'p') \underline{I} + \underline{I} (\underline{u}'p') \right] + \frac{p'}{\rho} \left[\nabla \underline{u}' + (\nabla \underline{u}')^T \right] \\ & V_{a} \qquad V_{b} \end{split} \tag{A.9}$$

Ensemble averaging Eq. (A.9) results in Eq. (A.10) below. Note that $VII: <\nabla \cdot (\underline{\mathbf{u}}' < \underline{\mathbf{u}}'\underline{\mathbf{u}}' >)> = \nabla \cdot (<\underline{\mathbf{u}}' > <\underline{\mathbf{u}}'\underline{\mathbf{u}}' >) = 0.$

$$\frac{\partial}{\partial t} < \underline{u}'\underline{u}' > + < \underline{u} > \cdot \nabla < \underline{u}'\underline{u}' > - \nu \nabla^{2} < \underline{u}'\underline{u}' > =$$

$$I \qquad III \qquad III_{a}$$

$$- < \underline{u}'\underline{u}' > \cdot < \underline{F} > - < \underline{F} >^{T} \cdot < \underline{u}'\underline{u}' >$$

$$IV$$

$$-\frac{1}{\rho} \nabla \cdot (< \underline{u}'\underline{p}' > \underline{I} + \underline{I} < \underline{u}'\underline{p}' >) + < \frac{\underline{p}'}{\rho} [\nabla \underline{u}' + (\nabla \underline{u}')^{T}] >$$

$$V_{a} \qquad V_{b}$$

$$-\nabla \cdot < \underline{u}'\underline{u}'\underline{u}' > -2\nu [(\nabla \underline{u}')^{T} \cdot (\nabla \underline{u}') >]$$

$$VI \qquad III_{b}$$

$$(A.10)$$

Eq. (A.10) can be further re-arranged showing the physical significance of each term as

$$\frac{\partial}{\partial t} < \underline{u}'\underline{u}' > + < \underline{u} > \cdot \nabla < \underline{u}'\underline{u}' > =$$

$$+ \left[\underline{v}\nabla^{2} < \underline{u}'\underline{u}' > - (\nabla < \underline{u}'\frac{p'}{\rho} >)^{T} - (\nabla < \frac{p'}{\rho}\underline{u}' >) - \nabla \cdot < \underline{u}'\underline{u}'\underline{u}' >\right]$$

$$+ \underbrace{\left[- < \underline{u}'\underline{u}' > \cdot < \underline{F} > - < \underline{F} >^{T} \cdot < \underline{u}'\underline{u}' >\right]}_{\text{"production"}}$$

$$+ 2 \underbrace{\left[< \frac{p'}{\rho} \underline{S}' >\right] - 2 \underbrace{\left[\underline{v} < (\nabla \underline{u}')^{T} \cdot (\nabla \underline{u}') >\right]}_{\text{dissipation}}$$
(A.11)

Eq. (A.11) has been discussed in the context of algebraic closures derived from the Reynolds stress transport equation (based on a weak equilibrium hypothesis, see Eq. (2.38)) and also in deriving the equation for turbulent kinetic energy.

APPENDIX B

UNCLOSED EQUATION FOR KINETIC ENERGY

The exact equation for turbulent kinetic energy ($k = \langle \underline{u}' \cdot \underline{u}' \rangle / 2$) can be obtained by taking the trace of the exact transport equation for Reynolds stress (A.11). The resulting transport equation in a rotating frame of reference is presented in this appendix. The individual terms after taking the trace of Eq. (A.10) are as below.

I:
$$\frac{\partial}{\partial t} < \underline{\mathbf{u}}' \cdot \underline{\mathbf{u}}' >) = 2 \frac{\partial \mathbf{k}}{\partial t}$$

II:
$$\langle \underline{\mathbf{u}} \rangle : \nabla \langle \underline{\mathbf{u}}' \underline{\mathbf{u}}' \rangle = 2 \langle \underline{\mathbf{u}} \rangle : \nabla \mathbf{k}$$

III_a:
$$-\nabla \nabla^2 < \underline{\mathbf{u}} \cdot \underline{\mathbf{u}}' > = -2 \nabla^2 \mathbf{k}$$

III_b:
$$-2v[(\nabla \underline{u}')^T:(\nabla \underline{u}')>]=2\varepsilon$$

IV:
$$-\langle \underline{\mathbf{u}}'\underline{\mathbf{u}}' \rangle : \langle \underline{\underline{\mathbf{F}}} \rangle - \langle \underline{\underline{\mathbf{F}}} \rangle^{T} : \langle \underline{\mathbf{u}}'\underline{\mathbf{u}}' \rangle =$$

$$-\langle \underline{\mathbf{u}}'\underline{\mathbf{u}}' \rangle : (\nabla \langle \underline{\mathbf{u}} \rangle + 2 \underline{\Omega}) - ((\nabla \langle \underline{\mathbf{u}} \rangle)^{T} - 2 \underline{\Omega})) \cdot \langle \underline{\mathbf{u}}'\underline{\mathbf{u}}' \rangle$$

$$= -\langle \underline{\mathbf{u}}'\underline{\mathbf{u}}' \rangle : (\nabla \langle \underline{\mathbf{u}} \rangle) - (\nabla \langle \underline{\mathbf{u}} \rangle)^{T}) : \langle \underline{\mathbf{u}}'\underline{\mathbf{u}}' \rangle$$

$$= -2\langle \underline{\mathbf{u}}'\underline{\mathbf{u}}' \rangle : \langle S \rangle$$

(Note:
$$<\underline{\mathbf{u}}'\underline{\mathbf{u}}'>: 2\underline{\Omega}=2\underline{\Omega}: <\underline{\mathbf{u}}'\underline{\mathbf{u}}'>=0$$
)

$$V_{a}: \qquad (-\frac{1}{\rho}\nabla:(<\underline{u}'p'>\underline{I}+\underline{I}<\underline{u}'p'>))=-2\frac{1}{\rho}\nabla\cdot(<\underline{u}'p'>+<\underline{u}'p'>)$$

VI:
$$-\nabla :< \underline{\mathbf{u}}'\underline{\mathbf{u}}'\underline{\mathbf{u}}'> = -\nabla \cdot < \underline{\mathbf{u}}'\mathbf{k}>$$

$$V_b: \qquad \operatorname{tr}\left[<\frac{p'}{\rho}(\nabla \underline{u}' + (\nabla \underline{u}')^T)>\right] = <\frac{p'}{\rho}(\nabla \cdot \underline{u}' + (\nabla \cdot \underline{u}')^T)> = 0$$

Dividing by 1/2, the transport equation for turbulent kinetic energy is thus,

$$\frac{\partial k}{\partial t} + \langle \underline{u} \rangle \cdot \nabla k - \nu \nabla^{2} k = -\nu \langle (\nabla \underline{u}') : (\nabla \underline{u}')^{T} \rangle - \langle \underline{u}'\underline{u}' \rangle : \langle \underline{\underline{S}} \rangle$$
(dissipation rate) (production due to mean strain)
$$I \qquad III \qquad III_{a} \qquad III_{b} \qquad IV$$

$$-\frac{1}{\rho} \nabla \cdot \langle \underline{u}'\underline{p}' \rangle - \nabla \cdot \langle \underline{u}'\frac{(\underline{u}'\underline{u}')}{2} \rangle$$

$$V \qquad VI$$
(B.1)

Eq. (B.1) is exact and unclosed. A model for $\langle \underline{u}' \frac{(\underline{u}' \cdot \underline{u}')}{2} \rangle$ is needed. This can be simplified as defining $\phi = \frac{(\underline{u}' \cdot \underline{u}')'}{2}$ (can be considered as fluctuating part of kinetic energy).

$$<\underline{u}'\frac{(\underline{u}'\underline{u}')}{2}> = <\underline{u}'k> + <\underline{u}'\phi> = <\underline{u}'>k+ <\underline{u}'\phi> = <\underline{u}'\phi>$$
(B.2)

So closure for $\langle \underline{u}' \phi \rangle$ is needed. Equation for ϕ can be written by subtracting the equation for $k = \langle \underline{u}' \cdot \underline{u}' \rangle / 2$ from $(\underline{u}' \cdot \underline{u}') / 2$. Taking the trace of Eq. (B.4),

$$\frac{\partial}{\partial t} \frac{(\underline{\mathbf{u}}' \cdot \underline{\mathbf{u}}')}{2} + \langle \underline{\mathbf{u}} \rangle \cdot \nabla \frac{(\underline{\mathbf{u}}' \cdot \underline{\mathbf{u}}')}{2} - \nu \nabla^2 \frac{(\underline{\mathbf{u}}' \cdot \underline{\mathbf{u}}')}{2} = -(\underline{\mathbf{u}}' \underline{\mathbf{u}}') : \langle \underline{\underline{\mathbf{S}}} \rangle - \frac{1}{\rho} \nabla \cdot [(\underline{\mathbf{u}}' \mathbf{p}')]
- \nabla \cdot \underline{\mathbf{u}}' \frac{(\underline{\mathbf{u}}' \cdot \underline{\mathbf{u}}')}{2} - \nu [(\nabla \underline{\mathbf{u}}') : (\nabla \underline{\mathbf{u}}')^T] + \nabla \cdot (\underline{\mathbf{u}}' \mathbf{k})$$
(B.3)

Substracting Eq. (B.6) from Eq. (B.8),

$$\begin{split} \frac{\partial}{\partial} \, \frac{\varphi}{t} + & <\underline{u} > \cdot \nabla \, \varphi - \nu \, \nabla^2 \, \varphi = -(\underline{u}\, \underline{u}\, \underline{u}\, - <\underline{u}\, \underline{u}\, \underline{u}\, >) : <\underline{\underline{S}} > -\frac{1}{\rho} \nabla \cdot (\underline{u}\, \underline{p}\, \underline{u}\, \underline{u}\, \underline{u}\, \underline{u}\,) \\ & -\nu < (\nabla \underline{u}\, \underline{u}\, \underline{u}\, \underline{u}\, \underline{u}\, \underline{u}\,)^T > + \, \underline{u}\, \underline{u}\, \nabla \, k \end{split} \tag{B.4}$$

Now, re-arrangine Eq. (B.9), with the explicit Laplace term,

$$\mathcal{L}(\phi) = \underline{\mathbf{u}} \cdot \nabla \mathbf{k} - \mathbf{f}_{\mathbf{k}}'$$

$$\mathcal{L} \equiv \frac{\partial}{\partial t} + \langle \underline{\mathbf{u}} \rangle \cdot \nabla - \mathbf{v} \nabla^{2}$$

$$\mathbf{f}_{\mathbf{k}}' = (\underline{\mathbf{u}}' \underline{\mathbf{u}}' - \langle \underline{\mathbf{u}}' \underline{\mathbf{u}}' \rangle) : \langle \underline{\underline{\mathbf{S}}} \rangle + \frac{1}{2} \nabla \cdot (\underline{\mathbf{u}}' \mathbf{p}')' - \nabla \cdot (\underline{\mathbf{u}}' \frac{(\underline{\mathbf{u}}' \cdot \underline{\mathbf{u}}')}{2})' + \mathbf{v} \langle (\nabla \underline{\mathbf{u}}') : (\nabla \underline{\mathbf{u}}')^{\mathsf{T}} \rangle$$
(B.5)

Now applying the Green's function analysis and smoothing approximation as discussed in Chapter 3 (also see Weispfenning, 1997),

$$k'(\underline{x},t) = -\int_{-\infty}^{t} d\hat{t} \iiint d\hat{V} \underbrace{G(\underline{x},t;\hat{\underline{x}},\hat{t})}_{\uparrow} [\underline{u}' \cdot \nabla k - f'_{k}](\hat{\underline{x}},\hat{t})$$

$$< \underline{u}'k' > = -\int_{-\infty}^{t} d\hat{t} \iiint d\hat{V} \underbrace{G(\underline{x},t;\hat{\underline{x}},\hat{t})}_{\uparrow} [\underline{u}' \cdot \nabla k - f'_{k}](\hat{\underline{x}},\hat{t})$$
(B.6)

Applying smoothing approximation and introducing a time scale,

$$\langle \underline{\mathbf{u}}'\mathbf{k}' \rangle = -\tau_{\mathbf{R}} \langle \underline{\mathbf{u}}'\underline{\mathbf{u}}' \rangle \cdot \nabla \mathbf{k} - \tau_{\mathbf{R}} \langle \underline{\mathbf{u}}'\mathbf{f}_{\mathbf{k}}' \rangle$$
 (B.7)

Similarly,

$$\langle \underline{\mathbf{u}}' \mathbf{f}_{\mathbf{k}}' \rangle = -\tau_{\mathbf{R}} \langle \underline{\mathbf{u}}' \mathbf{f}_{\mathbf{k}}' \rangle \cdot \langle \underline{\mathbf{F}} \rangle - \tau_{\mathbf{R}} \langle \underline{\mathbf{f}}' \mathbf{f}_{\mathbf{k}}' \rangle$$
 (B.8)

Rearranging, Eqs. (B.7) and (B.8),

$$\langle \underline{\mathbf{u}}'\mathbf{k}' \rangle = -\tau_{\mathbf{R}} \langle \underline{\mathbf{u}}'\underline{\mathbf{u}}' \rangle \cdot \nabla \mathbf{k} - \tau_{\mathbf{R}}^2 \langle \underline{\mathbf{f}}'\mathbf{f}_{\mathbf{k}}' \rangle \cdot \underline{\mathbf{A}}$$
 (B.9)

$$<\underline{\mathbf{u}}'\mathbf{k}'> \approx -\tau_{\mathbf{R}} <\underline{\mathbf{u}}'\underline{\mathbf{u}}'>\cdot\nabla\mathbf{k}$$
 (B.10)

The unclosed exact equation presented in Eq. (B.1) together with Eq. (B.10) are used in describing the transport of turbulent kinetic energy in a rotating frame of reference (see Eqs. (1.9) and (1.10)).

APPENDIX C

UNCLOSED EQUATION FOR DISSIPATION

Exact turbulent dissipation equation can be derived from the transport equation for fluctuating velocity (see Eq. (A.5)) (Eq. (A.5) is presented again in Eq. (C.1) below for convenience).

$$\frac{\partial \underline{\mathbf{u}'}}{\partial t} + \langle \underline{\mathbf{u}} \rangle \cdot \nabla \underline{\mathbf{u}'} - \nu \nabla^2 \underline{\mathbf{u}'} = -\underline{\mathbf{u}'} \cdot \langle \underline{\mathbf{F}} \rangle - \nabla \cdot (\frac{\underline{\mathbf{p}'}}{\rho} \underline{\mathbf{I}} + \underline{\mathbf{u}'} \underline{\mathbf{u}'} - \langle \underline{\mathbf{u}'} \underline{\mathbf{u}'} \rangle)$$

$$I \qquad II \qquad III \qquad IV \qquad V \qquad VI \qquad VII$$
(C.1)

where $\langle \underline{F} \rangle = \nabla \langle \underline{u} \rangle + 2 \, \underline{\Omega}$. The Roman numerals represent individual terms. The following operations are performed in the order, on the above equation to finally derive the equation for ε . 1) gradient operator is applied 2) scalar multiplication with $(\nabla \underline{u}')^T$ is carried 3) trace operator is applied 4) multiplied by 2ν and 5) ensemble average is performed.

I:
$$(\nabla \underline{\mathbf{u}}')^{\mathrm{T}} : \nabla \frac{\partial \underline{\mathbf{u}}'}{\partial t} = \frac{1}{2} \nu \frac{\partial}{\partial t} ((\nabla \underline{\mathbf{u}}')^{\mathrm{T}} : \nabla \underline{\mathbf{u}}')$$

$$2\nu < \frac{1}{2}\nu \frac{\partial}{\partial t} ((\nabla \underline{\mathbf{u}}')^{\mathrm{T}} : \nabla \underline{\mathbf{u}}') > = \frac{\partial \varepsilon}{\partial t}$$

II:
$$(\nabla \underline{u}')^T : \nabla (< \underline{u} > \cdot \nabla \underline{u}') = (\nabla \underline{u}')^T : (\nabla < \underline{u} > \cdot \nabla \underline{u}') + (\nabla \underline{u}')^T : (< \underline{u} > \cdot \nabla \nabla \underline{u}')$$

$$= (\nabla \underline{u}')^T : (\nabla < \underline{u} > \cdot \nabla \underline{u}') + \frac{1}{2} < \underline{u} > \cdot \nabla (\nabla \underline{u}' : (\nabla \underline{u}')^T)$$

$$= (\nabla \underline{u}') \cdot (\nabla \underline{u}')^T : \nabla < \underline{u} > + \frac{1}{2} < \underline{u} > \cdot \nabla (\nabla \underline{u}' : (\nabla \underline{u}')^T)$$

Note that $(\nabla \underline{\mathbf{u}}') \cdot (\nabla \underline{\mathbf{u}}')^T : \nabla < \underline{\mathbf{u}} > = (\nabla \underline{\mathbf{u}}') \cdot (\nabla \underline{\mathbf{u}}')^T : \nabla < \underline{\mathbf{u}} >$

$$\Rightarrow II: \qquad 2\mathbf{v} < (\nabla \underline{\mathbf{u}}') \cdot (\nabla \underline{\mathbf{u}}')^T : < \underline{\mathbf{S}} > + \frac{1}{2} < \underline{\mathbf{u}} > \cdot \nabla (\nabla \underline{\mathbf{u}}' : (\nabla \underline{\mathbf{u}}')^T) >$$

$$= 2\mathbf{v} < (\nabla \underline{\mathbf{u}}') \cdot (\nabla \underline{\mathbf{u}}')^T : < \underline{\mathbf{S}} > + \mathbf{v} < \underline{\mathbf{u}} > \cdot \nabla \mathbf{\epsilon}$$

$$III: \qquad (\nabla \underline{\mathbf{u}}')^T : \nabla (-\mathbf{v} \nabla^2 \underline{\mathbf{u}}') = -\mathbf{v} (\nabla \underline{\mathbf{u}}')^T : (\nabla \nabla^2 \underline{\mathbf{u}}')$$

$$= -\mathbf{v} \nabla \cdot ((\nabla \underline{\mathbf{u}}')^T : (\nabla \nabla \underline{\mathbf{u}}')) + \mathbf{v} (\nabla \cdot (\nabla \underline{\mathbf{u}}')^T : (\nabla \nabla \underline{\mathbf{u}}'))$$

$$= -\frac{1}{2}\mathbf{v} \nabla^2 ((\nabla \underline{\mathbf{u}}')^T : \nabla \underline{\mathbf{u}}') + \mathbf{v} \nabla (\nabla \underline{\mathbf{u}}')^T : \nabla (\nabla \underline{\mathbf{u}}')^T$$

$$2\mathbf{v} < -\frac{1}{2}\mathbf{v} \nabla^2 ((\nabla \underline{\mathbf{u}}')^T : \nabla \underline{\mathbf{u}}') + \mathbf{v} \nabla (\nabla \underline{\mathbf{u}}')^T : \nabla (\nabla \underline{\mathbf{u}}')^T >$$

$$= -\mathbf{v} \nabla^2 \mathbf{\epsilon} + 2\mathbf{v}^2 \nabla < (\nabla \underline{\mathbf{u}}')^T : \nabla (\nabla \underline{\mathbf{u}}')^T : \nabla (\nabla \underline{\mathbf{u}}')^T >$$

$$IV: \qquad (\nabla \underline{\mathbf{u}}')^T : \nabla (-\mathbf{u}' \cdot < \underline{\mathbf{f}} >) = -(\nabla \underline{\mathbf{u}}')^T : \nabla (\underline{\mathbf{u}}' \cdot < \underline{\mathbf{f}} >)$$

$$= -(\nabla \underline{\mathbf{u}}')^T : (\nabla \underline{\mathbf{u}}' \cdot < \underline{\mathbf{f}} >) - (\nabla \underline{\mathbf{u}}')^T : \nabla (\underline{\mathbf{u}}' \cdot \nabla < \underline{\mathbf{f}} >)$$

$$= -(\nabla \underline{\mathbf{u}}')^T : (\nabla \underline{\mathbf{u}}' \cdot < \underline{\mathbf{f}} >) - ((\nabla \underline{\mathbf{u}}')^T : \underline{\mathbf{u}}' \cdot \nabla < \underline{\mathbf{f}} >)$$

$$= -(\nabla \underline{\mathbf{u}}')^T : (\nabla \underline{\mathbf{u}}' \cdot < \underline{\mathbf{f}} >) - ((\nabla \underline{\mathbf{u}}')^T : \underline{\mathbf{u}}' \cdot \nabla < \underline{\mathbf{f}} >)$$

$$= -(\nabla \underline{\mathbf{u}}')^T : (\nabla \underline{\mathbf{u}}' \cdot < \underline{\mathbf{f}} >) - ((\nabla \underline{\mathbf{u}}')^T : \underline{\mathbf{u}}' \cdot \nabla < \underline{\mathbf{f}} >)$$

$$= -(\nabla \underline{\mathbf{u}}')^T : (\nabla \underline{\mathbf{u}}' \cdot < \underline{\mathbf{f}} >) - ((\nabla \underline{\mathbf{u}}')^T : \underline{\mathbf{u}}' \cdot \nabla < \underline{\mathbf{f}} >)$$

$$= -(\nabla \underline{\mathbf{u}}')^T : (\nabla \underline{\mathbf{u}}' \cdot < \underline{\mathbf{f}} >) - ((\nabla \underline{\mathbf{u}}')^T : \underline{\mathbf{u}}' \cdot \nabla < \underline{\mathbf{f}} >)$$

$$= -(\nabla \underline{\mathbf{u}}')^T : (\nabla \underline{\mathbf{u}}' \cdot < \underline{\mathbf{f}} >) - ((\nabla \underline{\mathbf{u}}')^T : \underline{\mathbf{u}}' \cdot \nabla < \underline{\mathbf{f}} >)$$

$$= -((\nabla \underline{\mathbf{u}}')^T : (\nabla \underline{\mathbf{u}}' \cdot)) : < \underline{\mathbf{f}} > - ((\nabla \underline{\mathbf{u}}')^T : (\nabla \underline{\mathbf{u}}' \cdot)) : < \underline{\mathbf{f}} >$$

$$= -((\nabla \underline{\mathbf{u}}')^T : (\nabla \underline{\mathbf{u}}' \cdot)) : < \nabla < \underline{\mathbf{u}} > - \mathbf{v} < (\nabla \underline{\mathbf{u}}' \cdot)^T : (\nabla \underline{\mathbf{u}}' \cdot) > : < (\nabla < \underline{\mathbf{u}} >)^T$$

$$\Rightarrow IV: \qquad = -((\nabla \underline{\mathbf{u}}')^T : (\nabla \underline{\mathbf{u}}' \cdot)) : < \underline{\mathbf{f}} > - ((\nabla \underline{\mathbf{u}}')^T : \underline{\mathbf{u}}' \cdot \nabla) : (\nabla < \underline{\mathbf{u}} > + 2 : \underline{\Omega})$$

$$= -((\nabla \underline{\mathbf{u}}')^T : (\nabla \underline{\mathbf{u}}' \cdot)) : < \underline{\mathbf{f}} > - ((\nabla \underline{\mathbf{u}}')^T : \underline{\mathbf{u}}' \cdot \nabla) : (\nabla < \underline{\mathbf{u}} > + 2 : \underline{\Omega})$$

$$= -2\mathbf{v} < ((\nabla \underline{\mathbf{u}}')^T : (\nabla \underline{\mathbf{u}}' \cdot)) : < \underline{\mathbf{f}} > - ((\nabla \underline{\mathbf{u}}')^T : \underline{\mathbf{u}}' \cdot \nabla) : (\nabla < \underline{\mathbf{u}} > + 2 : \underline{\Omega})$$

$$= -2\mathbf$$

$$\begin{split} V: & (\nabla \underline{u}')^T : \nabla (-\nabla \cdot (\frac{p'}{\rho}\underline{I})) = -(\nabla \underline{u}')^T : \nabla \nabla (\frac{p'}{\rho}) \\ & = -(\nabla \nabla (\frac{p'}{\rho}) : (\nabla \underline{u}')^T = -(\nabla \cdot (\nabla (\frac{p'}{\rho}) : (\nabla \underline{u}')^T) \\ & 2\nu < \nabla \cdot (\nabla (\frac{p'}{\rho}) : (\nabla \underline{u}')^T >= 2\nu \nabla \cdot < (\nabla (\frac{p'}{\rho}) : (\nabla \underline{u}')^T > \\ VI & -(\nabla \underline{u}')^T : \nabla (\nabla \cdot \underline{u}'\underline{u}') = -(\nabla \underline{u}')^T : \nabla (\underline{u}' \cdot \nabla \underline{u}') \\ & = -[(\nabla \underline{u}')^T \cdot (\nabla \underline{u}')] : (\nabla \underline{u}') - (\nabla \underline{u}')^T : (\underline{u}' \cdot \nabla (\nabla \underline{u}')) \\ & = -((\nabla \underline{u}')^T \cdot (\nabla \underline{u}')) : (\nabla \underline{u}') - \frac{1}{2} \underline{u}' \cdot \nabla ((\nabla \underline{u}')^T : (\nabla \underline{u}')) \\ & 2\nu < -((\nabla \underline{u}')^T \cdot (\nabla \underline{u}')) : (\nabla \underline{u}') - \frac{1}{2} \underline{u}' \cdot \nabla ((\nabla \underline{u}')^T : (\nabla \underline{u}')) > \\ & = 2\nu < (\nabla \underline{u}')^T \cdot (\nabla \underline{u}')) : \underline{S}' > -\nu \nabla \cdot < \underline{u}' \cdot \nabla ((\nabla \underline{u}')^T : (\nabla \underline{u}')) > \\ & \approx 2\nu < (\nabla \underline{u}')^T \cdot (\nabla \underline{u}')) : \underline{S}' > -\nu \nabla \cdot < \underline{u}' \cdot ((\nabla \underline{u}')^T : (\nabla \underline{u}')) > \\ & VII: & (\nabla \underline{u}')^T : \nabla (\nabla \cdot < \underline{u}'\underline{u}' >) = (\nabla \underline{u}')^T : \nabla < \underline{u}' \cdot \nabla \underline{u}' > \\ & = 0 \end{split}$$

Arranging all the above terms to obtain the exact equation for the dissipation,

$$\begin{split} \frac{\partial \epsilon}{\partial t} + &<\underline{u}> \cdot \nabla \epsilon - \nu \nabla^2 \epsilon = \\ & I \quad III_b \quad IIIa \\ & -2\nu < (\nabla \nabla (\frac{p'}{\rho}): (\nabla \underline{u}')^T> - \nu < \underline{u}' \cdot \nabla ((\nabla \underline{u}')^T: (\nabla \underline{u}'))> \\ & \quad V \quad VIb \\ & -2\nu < (\nabla \underline{u}')^T \cdot (\nabla \underline{u}')> :<\underline{S}> -2\nu < (\nabla \underline{u}') \cdot (\nabla \underline{u}')^T> :<\underline{S}> \\ & \quad IV_a \quad II_a \\ & -2\nu < (\nabla \underline{u}')^T \underline{u}' \cdot \nabla > : (\nabla < \underline{u}> + 2\underline{\Omega}) - 2\nu < (\nabla \underline{u}')^T \cdot (\nabla \underline{u}')]:\underline{S}'> \\ & \quad IVb \quad VIa \\ & -2\nu^2 \nabla < (\nabla \underline{u}')^T \vdots \nabla (\nabla \underline{u}')^T> \\ & \quad IIIb \end{split}$$

Upon rearranging:

$$\frac{\partial \varepsilon}{\partial t} + < \underline{\mathbf{u}} > \cdot \nabla \varepsilon \qquad = \qquad$$

rate of change of dissipation relativeto the mean velocity

$$-\nabla \cdot \{\underbrace{-\nu \nabla \varepsilon}_{\text{viscous flux of dissipation}} + 2\nu < \nabla (\frac{\underline{p'}}{\rho}) \cdot \nabla \underline{u'} > + \nu < \underline{u'}[(\nabla \underline{u'}) : (\nabla \underline{u'})^T] > \}$$

$$\underline{-2\nu < (\nabla \underline{u'}) \cdot (\nabla \underline{u'})^T > : < \underline{S} > } -2\nu < (\nabla \underline{u'})^T \cdot (\nabla \underline{u'}) > : < \underline{S} > }$$

$$\underline{-2\nu < (\nabla \underline{u'})^T \cdot (\nabla \underline{u'}) > : < \underline{S} > }$$

$$\underline{-2\nu < (\nabla \underline{u'})^T \cdot (\nabla \underline{u'}) > : < \underline{S} > }$$

$$\underline{-2\nu < (\nabla \underline{u'})^T \cdot (\nabla \underline{u'}) > : < \underline{S} > }$$

$$\underline{-2\nu < (\nabla \underline{u'}) \cdot (\nabla \underline{u'}) > : < \underline{S} > }$$

$$\underline{-2\nu < (\nabla \underline{u'}) \cdot (\nabla \underline{u'}) T : \underline{S'} > }$$

$$\underline{-2\nu < (\nabla \underline{u'}) \cdot (\nabla \underline{u'}) T : \underline{S'} > }$$

$$\underline{-2\nu < (\nabla \underline{u'}) \cdot (\nabla \underline{u'}) T : \underline{S'} > }$$

$$\underline{-2\nu < (\nabla \underline{u'}) \cdot (\nabla \underline{u'}) T : \underline{S'} > }$$

$$\underline{-2\nu < (\nabla \underline{u'}) \cdot (\nabla \underline{u'}) T : \underline{S'} > }$$

$$\underline{-2\nu < (\nabla \underline{u'}) \cdot (\nabla \underline{u'}) T : \underline{S'} > }$$

$$\underline{-2\nu < (\nabla \underline{u'}) \cdot (\nabla \underline{u'}) T : \underline{S'} > }$$

$$\underline{-2\nu < (\nabla \underline{u'}) \cdot (\nabla \underline{u'}) T : \underline{S'} > }$$

$$\underline{-2\nu < (\nabla \underline{u'}) \cdot (\nabla \underline{u'}) T : \underline{S'} > }$$

$$\underline{-2\nu < (\nabla \underline{u'}) \cdot (\nabla \underline{u'}) T : \underline{S'} > }$$

$$\underline{-2\nu < (\nabla \underline{u'}) \cdot (\nabla \underline{u'}) T : \underline{S'} > }$$

$$\underline{-2\nu < (\nabla \underline{u'}) \cdot (\nabla \underline{u'}) T : \underline{S'} > }$$

$$\underline{-2\nu < (\nabla \underline{u'}) \cdot (\nabla \underline{u'}) T : \underline{S'} > }$$

$$\underline{-2\nu < (\nabla \underline{u'}) \cdot (\nabla \underline{u'}) T : \underline{S'} > }$$

$$\underline{-2\nu < (\nabla \underline{u'}) \cdot (\nabla \underline{u'}) T : \underline{S'} > }$$

$$\underline{-2\nu < (\nabla \underline{u'}) \cdot (\nabla \underline{u'}) T : \underline{S'} > }$$

$$\underline{-2\nu < (\nabla \underline{u'}) \cdot (\nabla \underline{u'}) T : \underline{S'} > }$$

$$\underline{-2\nu < (\nabla \underline{u'}) \cdot (\nabla \underline{u'}) T : \underline{S'} > }$$

$$\underline{-2\nu < (\nabla \underline{u'}) \cdot (\nabla \underline{u'}) T : \underline{S'} > }$$

$$\underline{-2\nu < (\nabla \underline{u'}) \cdot (\nabla \underline{u'}) T : \underline{S'} > }$$

$$\underline{-2\nu < (\nabla \underline{u'}) \cdot (\nabla \underline{u'}) T : \underline{S'} > }$$

$$\underline{-2\nu < (\nabla \underline{u'}) \cdot (\nabla \underline{u'}) T : \underline{S'} > }$$

$$\underline{-2\nu < (\nabla \underline{u'}) \cdot (\nabla \underline{u'}) T : \underline{S'} > }$$

$$\underline{-2\nu < (\nabla \underline{u'}) \cdot (\nabla \underline{u'}) T : \underline{S'} > }$$

$$\underline{-2\nu < (\nabla \underline{u'}) \cdot (\nabla \underline{u'}) T : \underline{S'} > }$$

$$\underline{-2\nu < (\nabla \underline{u'}) \cdot (\nabla \underline{u'}) T : \underline{S'} > }$$

$$\underline{-2\nu < (\nabla \underline{u'}) \cdot (\nabla \underline{u'}) T : \underline{S'} > }$$

$$\underline{-2\nu < (\nabla \underline{u'}) T : \underline{S'} > }$$

$$\underline{-2\nu < (\nabla \underline{u'}) T : \underline{S'} > }$$

$$\underline{-2\nu < (\nabla \underline{u'}) T : \underline{S'} > }$$

$$\underline{-2\nu < (\nabla \underline{u'}) T : \underline{S'} > }$$

$$\underline{-2\nu < (\nabla \underline{u'}) T : \underline{S'} > }$$

$$\underline{-2\nu < (\nabla \underline{u'}) T : \underline{S'} > }$$

$$\underline{-2\nu < (\nabla \underline{u'}) T : \underline{S'} > }$$

$$\underline{-2\nu < (\nabla \underline{u'}) T : \underline{S'} > }$$

$$\underline{-2\nu < (\nabla \underline{u'}) T : \underline{S'} > }$$

$$\underline{-2\nu < (\nabla \underline{u'}) T : \underline{S'} > }$$

$$\underline{-2\nu$$

Often the following terms are modeled as: (see Launder and Spalding, 1972; Rodi and Mansour, 1992)

$$v < 2(\nabla \underline{\mathbf{u}}')^{\mathrm{T}} \cdot \nabla (\frac{\mathbf{p}'}{\Omega}) > -v < \underline{\mathbf{u}}'[(\nabla \underline{\mathbf{u}}') : (\nabla \underline{\mathbf{u}}')^{\mathrm{T}}] > \} = -\tau_{\mathrm{R}} < \underline{\mathbf{u}}'\underline{\mathbf{u}}' > \cdot \nabla \varepsilon$$
 (C.4)

$$\begin{split} -2\nu < &(\nabla \underline{u}') \cdot (\nabla \underline{u}')^T > :< \underline{\underline{S}} > -2\nu < &(\nabla \underline{u}')^T \cdot (\nabla \underline{u}') > :< \underline{\underline{S}} > \\ &-2\nu < &(\nabla \underline{u}')^T \underline{u}' > : \nabla \nabla < \underline{u} > -2\nu < &(\nabla \underline{u}') \cdot (\nabla \underline{u}')^T : \underline{\underline{S}}' > = C_P \frac{-<\underline{u}'\underline{u}' > : \nabla < \underline{u} >}{\tau_R} \end{split}$$

$$2v^{2} < \nabla(\nabla \underline{\mathbf{u}}')^{T} : \nabla(\nabla \underline{\mathbf{u}}')^{T} > = + C_{D} \frac{\varepsilon}{\tau_{R}}$$
(C.6)

A transport equation resulting from Eqs. (C.3) to (C.6), which is similar to the transport equation for turbulent kinetic energy is used for describing the turbulent dissipation (see Eq. (1.11)).

APPENDIX D

INTEGRITY OPERATORS

Complete Set of Symmetric, Anisotropic, Objective Operators $\underline{\underline{\Phi}}_n$ described in Eq. (2.35) (see Pope 2000) are presented in this appendix.

n	$(\underline{\Phi}^{(n)})^{T} = \underline{\Phi}^{(n)}$ symmetric; $tr(\underline{\Phi}^{(n)}) = 0$ anisotropic; $\underline{Q}^{T} \cdot [\underline{\Phi}^{(n)}] \cdot \underline{Q} = \underline{\Phi}^{(n)}$
1	$\underline{\underline{\Phi}}^{(1)} = \langle \tilde{\underline{S}} \rangle$
2	$\left[< \tilde{\underline{S}} > \cdot < \tilde{\underline{S}} > -1/3 \operatorname{tr}(< \tilde{\underline{S}} > \cdot < \tilde{\underline{S}} >) \underline{\underline{I}} \right]$
3	$\left[\langle \tilde{\underline{S}} \rangle \cdot \langle \tilde{\underline{\mathcal{W}}} \rangle - \langle \tilde{\underline{\mathcal{W}}} \rangle^{T} \cdot \langle \tilde{\underline{S}} \rangle\right]$
4	$\left[< \underline{\tilde{\mathcal{W}}} > \cdot < \underline{\tilde{\mathcal{W}}} > -1/3 \text{ tr}(< \underline{\tilde{\mathcal{W}}} > \cdot < \underline{\tilde{\mathcal{W}}} >) \underline{\mathbf{I}} \right]$
5	$\left[< \underline{\underline{\tilde{\mathcal{W}}}} > \cdot < \underline{\tilde{S}} > \cdot < \underline{\tilde{S}} > + < \underline{\tilde{S}} >^{T} \cdot < \underline{\tilde{S}} >^{T} \cdot < \underline{\underline{\tilde{\mathcal{W}}}} >^{T} \right]$
6	$< \underline{\tilde{\mathcal{W}}} > \cdot < \underline{\tilde{\mathcal{W}}} > \cdot < \underline{\tilde{\mathbf{S}}} > + < \underline{\tilde{\mathbf{S}}} >^{T} \cdot < \underline{\tilde{\mathcal{W}}} >^{T} \cdot < \underline{\tilde{\mathcal{W}}} >^{T}$ $- 2/3 \operatorname{tr}(< \underline{\tilde{\mathcal{W}}} > \cdot < \underline{\tilde{\mathcal{W}}} > \cdot < \underline{\tilde{\mathbf{S}}} >) \underline{\mathbf{I}}$
7	$\left[< \underline{\underline{\tilde{\mathcal{W}}}} > \cdot < \underline{\underline{\tilde{S}}} > \cdot < \underline{\underline{\tilde{\mathcal{W}}}} > \cdot < \underline{\underline{\tilde{\mathcal{W}}}} > + < \underline{\underline{\tilde{\mathcal{W}}}} >^{T} \cdot < \underline{\underline{\tilde{\mathcal{W}}}} >^{T} \cdot < \underline{\underline{\tilde{\mathcal{W}}}} >^{T} \right]$
8	$\left[<\underline{\tilde{\mathbb{S}}} > \cdot <\underline{\tilde{\mathcal{W}}} > \cdot <\underline{\tilde{\mathbb{S}}} > \cdot <\underline{\tilde{\mathbb{S}}} > + <\underline{\tilde{\mathbb{S}}} >^T \cdot <\underline{\tilde{\mathbb{S}}} >^T \cdot <\underline{\tilde{\mathbb{W}}} >^T \cdot <\underline{\tilde{\mathbb{S}}} >^T \right]$
9	$< \underline{\tilde{\mathcal{W}}} > \cdot < \underline{\tilde{\mathcal{W}}} > \cdot < \underline{\tilde{\mathbb{S}}} > \cdot < \underline{\tilde{\mathbb{S}}} > + < \underline{\tilde{\mathbb{S}}} >^{T} \cdot < \underline{\tilde{\mathbb{S}}} >^{T} \cdot < \underline{\tilde{\mathcal{W}}} >^{T} \cdot < \underline{\tilde{\mathcal{W}}} >^{T}$ $-2/3 \operatorname{tr}(< \underline{\tilde{\mathcal{W}}} > \cdot < \underline{\tilde{\mathcal{W}}} > \cdot < \underline{\tilde{\mathbb{S}}} > \cdot < \underline{\tilde{\mathbb{S}}} >) \underline{\mathbb{I}}$
10	$<\underline{\tilde{\mathcal{W}}}>\cdot<\underline{\tilde{\mathbf{S}}}>\cdot<\underline{\tilde{\mathbf{S}}}>\cdot<\underline{\tilde{\mathcal{W}}}>\cdot<\underline{\tilde{\mathcal{W}}}>+<\underline{\tilde{\mathcal{W}}}>^{T}\cdot<\underline{\tilde{\mathcal{W}}}>^{T}\cdot<\underline{\tilde{\mathbf{S}}}>^{T}\cdot<\underline{\tilde{\mathbf{S}}}>^{T}\cdot<\underline{\tilde{\mathbf{S}}}>^{T}\cdot<\underline{\tilde{\mathcal{W}}}>^{T}$

APPENDIX E

REALIZABLE SHIH CLOSURE FOR THE NR-STRESS

Shih et al. (1994) developed a realizable bilinear eddy viscosity closure. A linear version of this model (Shih et al., 1995) is widely used in commercial codes. This appendix summarizes the model and also presents the scope or locus of the states for simple shear flows in rotating and non-rotating cases.

$$\langle \underline{\underline{S}} \rangle = \frac{1}{2} [\nabla \langle \underline{\underline{u}} \rangle + (\nabla \langle \underline{\underline{u}} \rangle)^{T}]$$
 (E.1)

$$\langle \underline{\underline{W}} \rangle = \frac{1}{2} [\nabla \langle \underline{\underline{u}} \rangle - (\nabla \langle \underline{\underline{u}} \rangle)^{\mathrm{T}}]$$
 (E.2)

$$\underline{\underline{R}} = \frac{1}{3} \underline{\underline{I}} - C_{\mu} \frac{k}{\varepsilon} < \underline{\underline{S}} > + C_2 \frac{k^2}{\varepsilon^2} [-\langle \underline{\underline{S}} \rangle \cdot \langle \underline{\underline{W}} \rangle + \langle \underline{\underline{W}} \rangle \cdot \langle \underline{\underline{S}} \rangle]$$
 (E.3)

where the coefficients are as below:

$$C_{\mu} = \frac{1}{A_0 + A_s(U_{\epsilon}^k)}, \quad A_0 = 6.5, \qquad C_2 = \frac{\sqrt{1 - 9C_{\mu}^2(\frac{Sk}{\epsilon})^2}}{C_0 + 6(\frac{Sk}{\epsilon})(\frac{Wk}{\epsilon})}, \quad C_0 = 1, \quad A_s^* = \sqrt{6}\cos\phi,$$

$$3\phi = \cos^{-1}(\sqrt{6}X), X = \frac{\operatorname{tr}(\langle \underbrace{S} > \cdot \langle \underbrace{S} > \cdot \langle \underbrace{S} >)}{(S)^{3/2}}, S = \sqrt{\langle \underbrace{S} > : \langle \underbrace{S} >}, W = \sqrt{\langle \underline{W} > : \langle \underline{W} >} \rangle^{T}},$$

and
$$U = \sqrt{\langle \underline{\underline{S}} \rangle : \langle \underline{\underline{S}} \rangle + \langle \underline{\underline{W}} \rangle : \langle \underline{\underline{W}} \rangle^T}$$
.

In non-inertial frames, the model is modified. $\underline{\underline{W}}$ is replaced by $<\underline{\underline{\tilde{W}}}>$ defined by

$$\langle \tilde{\mathcal{W}} \rangle = \underline{\mathbf{W}} + \underline{\mathbf{\Omega}}$$
 (E.4)

Apart from this, U is modified particularly as \tilde{U}

$$\tilde{\mathbf{U}} = \sqrt{\langle \underline{\underline{S}} \rangle : \langle \underline{\underline{S}} \rangle + (\langle \underline{\tilde{W}} \rangle + 2\underline{\Omega}) : (\langle \underline{\tilde{W}} \rangle + 2\underline{\Omega})^{\mathrm{T}}}$$
(E.5)

The K and epsilon equations for this model are:

$$\left(\frac{\hat{c}}{\partial t} + <\underline{\mathbf{u}}> \cdot \nabla - \mathbf{v}\nabla^{2}\right)\mathbf{k} = \frac{\mathbf{v}_{t}}{\sigma_{k}}\nabla^{2}\mathbf{k} - <\underline{\mathbf{u}}'\underline{\mathbf{u}}'> :<\underline{\underline{\mathbf{S}}}> -\varepsilon$$
(E.6)

$$\left(\frac{\partial}{\partial t} + \langle \underline{\mathbf{u}} \rangle \cdot \nabla - \mathbf{v} \nabla^{2}\right) \varepsilon = \frac{\mathbf{v}_{t}}{\sigma_{\varepsilon}} \nabla^{2} \varepsilon - C_{\varepsilon 1} \frac{\varepsilon}{k} \langle \underline{\mathbf{u}}' \underline{\mathbf{u}}' \rangle : \langle \underline{\underline{\mathbf{S}}} \rangle - C_{\varepsilon 2} \frac{\varepsilon^{2}}{k}$$
(E.7)

$$C_{\epsilon 1} = 1.44$$
; $C_{\epsilon 2} = 1.92$; $\sigma_k = 1$; $\sigma_{\epsilon} = 1.3$

Component equations for NR-stress for simple shear flows

$$R_{zz} = \frac{1}{3} + C_2 \frac{1}{2} \tilde{\Gamma} (\tilde{\Gamma} + 2\tilde{\Omega})$$
 (E.8)

$$R_{yy} = \frac{1}{3} - C_2 \frac{1}{2} \tilde{\Gamma} (\tilde{\Gamma} + 2\tilde{\Omega})$$
 (E.9)

$$R_{XX} = \frac{1}{3} \tag{E.10}$$

$$R_{yz} = -C_{\mu} \frac{1}{2} \tilde{\Gamma} \tag{E.11}$$

where $\tilde{\Gamma} = \frac{k}{\epsilon} \frac{d < u_z >}{dy}$. It is evident that the states on an energy diagram would be on the

line of $R_{xx} = 1/3$. Further more, the coefficients reduce to

$$X = 0 \Rightarrow \phi = \frac{\pi}{6} \Rightarrow A_s^* = \sqrt{6}\cos(\frac{\pi}{6}) = \frac{3}{\sqrt{2}}, \quad C_{\mu} = \frac{1}{6.5 + \frac{3}{\sqrt{2}}(\frac{U^*k}{\epsilon})}, \quad C_2 = \frac{\sqrt{1 - 9C_{\mu}^2(\frac{Sk}{\epsilon})^2}}{1 + 6(\frac{Sk}{\epsilon})(\frac{W^*k}{\epsilon})},$$

$$U^* \frac{k}{\varepsilon} = \sqrt{\frac{\tilde{\Gamma}^2}{2} + \frac{(\tilde{\Gamma} + 6\tilde{\Omega})^2}{2}}, \quad \frac{Sk}{\varepsilon} = \frac{\tilde{\Gamma}}{\sqrt{2}} \text{ and } \frac{W^*k}{\varepsilon} = \frac{1}{\sqrt{2}}(\tilde{\Gamma} + 2\tilde{\Omega}).$$

In an inertial frame, as $\tilde{\Gamma} \rightarrow 0$, $R_{xx}, R_{yy}, R_{zz} \rightarrow 1/3$ and $Ryz \rightarrow 0$. As $\tilde{\Gamma} \rightarrow \infty$, $C_{\mu} \rightarrow \frac{\sqrt{2}}{3} \frac{1}{\tilde{\Gamma}}, \quad C_2 \rightarrow 0 \quad , \quad R_{xx}, R_{yy}, R_{zz} \rightarrow 1/3 \quad \text{and} \quad Ryz \rightarrow -\frac{1}{3\sqrt{2}} \quad (III_b = 0 = 0, \quad II_b = 2 + 1/9 = 0.111).$

The above closure based on the hypothesis that NR-stress is *objective*, has been discussed in Section 2.6 (see Chapter 2). The locus of energy and anisotropic states for the above closure for non-rotating simple shear are shown in Figure 2.18.

APPENDIX F

SPECTRAL ANALYSIS FOR ROTATING HOMOGENEOUS DECAY

This appendix presents details of the derivations of equations in Park and Chung (1999) that are used in modeling $\tilde{\tau}_R(N_F)$ for the relaxation time for the URAPS theory. The model energy spectrum in the presence of rotation is represented by Eqs. (F.1), (F.2), and (F.3). (Speziale, 1998, Zhou , 1995 and Zeman, 1994). (See Figure F.1). In the following discussion, κ_L and κ_η are wave numbers associated with the inverse of energy containing scale $(k^{3/2}/\epsilon)$ and the Kolmogorov scale $(v^3/\epsilon)^{1/4}$). In the small wave number range or the energy containing scales ($\kappa < \kappa_L$), the spectrum is

$$E(\kappa) = B\kappa^{m} \tag{F.1}$$

In the inertial subrange ($\kappa_L < \kappa < \kappa_\eta$), the spectrum is represented as

$$E(\kappa) = C_{\Omega}(\epsilon \Omega)^{1/2} \kappa^{-2} \qquad \kappa << (\Omega^{3}/\epsilon)^{1/2}$$
 (F.2)

$$E(\kappa) = C_K(\varepsilon)^{2/3} \kappa^{-5/3} \qquad \kappa >> (\Omega^3/\varepsilon)^{1/2}$$
 (F.3)

where $C_K = 25/9$ is the Kolmogorov constant and $C_\Omega = C_K^{3/4}$. Let κ_M be the wave number where the two functions in Eq.(F.2) and (F.3) meet ($\kappa_M = C_K^{-3/4} \kappa_\Omega$). In the absence of rotation, Eq. (F.3) holds in the inertial subrange as well as dissipation range of the spectrum. The turbulent kinectic energy for homogeneous flows can be obtained by the integral of the energy spectrum over the entire wave number space.

$$k = \int_{0}^{\infty} E(\kappa) d\kappa$$
 (F.4)

Case I: No rotation

$$k = \int_{0}^{\kappa_L} B \kappa^m + \int_{\kappa_L}^{\kappa_{\eta}} C_K(\varepsilon)^{2/3} \kappa^{-5/3}$$
 (F.5)

$$k = \frac{B \kappa_L^{m+1}}{m+1} - \frac{3}{2} C_K(\varepsilon)^{2/3} (\kappa_{\eta}^{-2/3} - \kappa_L^{-2/3})$$
 (F.6)

In the region where the two spectrum functions Eq. (F.1) and Eq. (F.3) meet,

$$C_{K}(\varepsilon)^{2/3} \kappa_{L}^{-2/3} = B \kappa_{L}^{m+1}$$
(F.7)

Substituting the (F.7) in the third term of Eq. (F.6),

$$k = \frac{(3m+5)}{2(m+1)} B \kappa_L^{m+1} - \frac{3}{2} C_K(\epsilon)^{2/3} (\kappa_{\eta}^{-2/3})$$
 (F.8)

Eq. (F.7) can be rearranged as below for a representation for κ_L .

$$\Rightarrow (\kappa_L)^{m+1} = \left(\frac{C_K(\epsilon)^{2/3}}{B}\right)^{\frac{3(m+1)}{(3m+5)}}$$
(F.9)

Also, $\kappa_{\eta} = \frac{1}{\eta} = (\frac{v^3}{\epsilon})^{-1/4}$. So inserting κ_{L} and κ_{η} in Eq. (F.8),

$$k = \frac{(3m+5)}{2(m+1)} B \left(\frac{C_K(\epsilon)^{2/3}}{B} \right)^{\frac{3(m+1)}{(3m+5)}} - \frac{3}{2} C_K(\epsilon)^{2/3} (\frac{v^3}{\epsilon})^{1/6}$$
 (F.10)

Rearranging to get a relation between k and ε ,

$$k = \frac{(3m+5)}{2(m+1)} B\left(\frac{C_K}{B}\right)^{\frac{3(m+1)}{(3m+5)}} (\epsilon)^{\frac{2(m+1)}{(3m+5)}} - \frac{3}{2} C_K(\nu)^{1/2} (\epsilon)^{1/2}$$
 (F.11)

Now differentiating the above equation,

$$\frac{\partial \mathbf{k}}{\partial t} = \left(\mathbf{B} \left(\frac{\mathbf{C_K}}{\mathbf{B}} \right)^{\frac{3(m+1)}{(3m+5)}} (\epsilon)^{\frac{2(m+1)}{(3m+5)}-1} - \frac{3}{4} \mathbf{C_K}(\mathbf{v})^{1/2} (\epsilon)^{-1/2} \right) \frac{\partial \epsilon}{\partial t}$$
 (F.12)

Comparing the above equation with the standard model equations in homogeneous decaying turbulence,

$$\frac{\partial \mathbf{k}}{\partial t} = -\varepsilon \tag{F.13}$$

$$\frac{d\varepsilon}{dt} = -C_{\varepsilon 2} \frac{\varepsilon^2}{k} \quad (= -\frac{C_D}{C_{R1}} \frac{1}{\tau_R} \frac{\varepsilon^2}{k})$$
 (F.14)

Substituting F. (13) and F.(14) (and also (F.9) for simplification), in the L.H.S and R.H.S of Eq. (12),

$$C_{\epsilon 2} = \frac{\left(\frac{(3m+5)}{2(m+1)} B \kappa_L^{m+1} - \frac{3}{2} C_K(\nu)^{1/2} (\epsilon)^{1/2}\right)}{(k)(\epsilon)}$$
(F.15)

Replacing k in the denominator of Eq. (15) with Eq. (11),

$$C_{\varepsilon 2} = \frac{\left(\frac{(3m+5)}{2(m+1)}B\kappa_L^{m+1} - \frac{3}{2}C_K(\nu)^{1/2}(\varepsilon)^{1/2}\right)}{\left(B\kappa_L^{m+1} - \frac{3}{4}C_K(\nu)^{1/2}(\varepsilon)^{1/2}\right)}$$
(F.16)

Eq. (16) can be rearranged to be a function of turbulence Reynolds number as following.

Substituting Eq. (F.7) and dividing numerator and denominator by $C_K(\epsilon)^{2/3} \kappa_L^{-2/3}$,

$$C_{\varepsilon 2} = \frac{\left(\frac{(3m+5)}{2(m+1)} - \frac{3}{2}(\nu)^{1/2}(\varepsilon)^{-1/6} \kappa_{L}^{2/3}\right)}{\left(1 - \frac{3}{4} C_{K}(\nu)^{1/2}(\varepsilon)^{-1/6} \kappa_{L}^{2/3}\right)}$$
(F.17)

Now substitute, $\kappa_L = \frac{\varepsilon}{k^{3/2}}$

$$C_{\varepsilon 2} = \frac{\left(\frac{(3m+5)}{2(m+1)} - \frac{3}{2}(\nu)^{1/2}(\varepsilon)^{1/2}k^{-1}\right)}{\left(1 - \frac{3}{4}(\nu)^{1/2}(\varepsilon)^{1/3}k^{-1}\right)}$$
(F.18)

Replacing $k^2/(v\epsilon)$ with Re_t ,

$$C_{\varepsilon 2} = \frac{\left(\frac{(3m+5)}{2(m+1)} - \frac{3}{2} Re_{t}^{-1/2}\right)}{\left(1 - \frac{3}{4} Re_{t}^{-1/2}\right)}$$
(F.19)

Case II: Intermediate rotation rates

$$k = \int_{0}^{\kappa_{L}} B \kappa^{m} + \int_{\kappa_{L}}^{\kappa_{M}} C_{\Omega}(\epsilon \Omega)^{1/2} \kappa^{-2} + \int_{\kappa_{M}}^{\kappa_{\eta}} C_{K}(\epsilon)^{2/3} \kappa^{-5/3}$$
 (F.20)

$$k = \frac{B \kappa_L^{m+1}}{m+1} - C_{\Omega}(\epsilon \Omega)^{1/2} (\kappa_M^{-1} - \kappa_L^{-1}) - \frac{3}{2} C_K(\epsilon)^{2/3} (\kappa_{\eta}^{-2/3} - \kappa_M^{-2/3})$$
 (F.21)

In the region where the two spectrum functions Eq. (F.1) and (F.2) meet,

$$B \kappa_{L}^{m} = C_{\Omega}(\epsilon \Omega)^{1/2} \kappa_{L}^{-2}$$
 (F.22)

In the region where the two spectrum functions Eq. (F.2) and (F.3) meet,

$$C_{\Omega}(\varepsilon\Omega)^{1/2}\kappa_{M}^{-2} = C_{K}(\varepsilon)^{2/3}\kappa_{M}^{-5/3}$$
(F.23)

Substituting Eqs. (F. 22) and (F. 23) in Eq. (F. 21),

$$k = \frac{m+2}{m+1} B \left[\frac{C_{\Omega}(\epsilon \Omega)^{1/2}}{B} \right]^{\frac{m+1}{m+2}} + \frac{1}{2} C_{\Omega}(\epsilon \Omega)^{1/2} \kappa_{M}^{-1} - \frac{3}{2} C_{K}(\epsilon)^{2/3} (\kappa_{\eta}^{-2/3})$$
 (F.24)

Now, substituting, the wave numbers, $\kappa_{\rm M} = C_{\rm K}^{-3/4} \kappa_{\Omega}$, $\kappa_{\Omega} = (\frac{\Omega^3}{\epsilon})^{1/2}$, and

$$\kappa_{\eta} = \frac{1}{\eta} = \left(\frac{v^3}{\varepsilon}\right)^{-1/4},$$

$$k = \frac{m+2}{m+1} B \left[\frac{C_{\Omega}(\Omega)^{1/2}}{B} \right]^{\frac{m+1}{m+2}} \frac{1 (m+1)}{(\epsilon)^{2(m+2)}} + \frac{1}{2} C_{\Omega} C_{K}^{3/4}(\Omega)^{-1}(\epsilon) - \frac{3}{2} C_{K} v^{1/2}(\epsilon)^{1/2}. \quad (F.25)$$

Now differentiating the above equation for k,

$$\frac{\partial \mathbf{k}}{\partial \mathbf{t}} = \left(\frac{1}{2} \mathbf{B} \left[\frac{\mathbf{C}_{\Omega}(\Omega)^{1/2}}{\mathbf{B}} \right]^{\frac{m+1}{m+2}} \frac{1}{(\epsilon)^{\frac{1}{2}(m+2)} - 1} + \frac{1}{2} \mathbf{C}_{\Omega} \mathbf{C}_{K}^{3/4}(\Omega)^{-1} - \frac{3}{4} \mathbf{C}_{K} \mathbf{v}^{1/2}(\epsilon)^{-1/2} \right) \frac{\partial \epsilon}{\partial \mathbf{t}}$$
(F.26)

Comparing the above equation with the standard model equations in homogeneous decaying turbulence Eqs (F.13) and (F.14),

$$C_{\varepsilon 2} = \frac{\left(\frac{m+2}{m+1}B\left[\frac{C_{\Omega}(\Omega)^{1/2}}{B}\right]^{\frac{m+1}{m+2}}\frac{1(m+1)}{(\varepsilon)^{\frac{2(m+2)}{2(m+2)}}} + \frac{1}{2}C_{\Omega}C_{K}^{3/4}(\Omega)^{-1}(\varepsilon) - \frac{3}{2}C_{K}v^{1/2}(\varepsilon)^{1/2}\right)}{\left(\frac{1}{2}B\left[\frac{C_{\Omega}(\Omega)^{1/2}}{B}\right]^{\frac{m+1}{m+2}}\frac{1(m+1)}{(\varepsilon)^{\frac{2(m+1)}{2(m+2)}}} + \frac{1}{2}C_{\Omega}C_{K}^{3/4}(\Omega)^{-1} - \frac{3}{4}C_{K}v^{1/2}(\varepsilon)^{-1/2}\right)\varepsilon}$$
(F.27)

Now substituting, B $\kappa_L^{m+2} = C_{\Omega}(\epsilon \Omega)^{1/2}$ (derived from Eq. F.22),

$$C_{\epsilon 2} = \frac{\left(\frac{m+2}{m+1}B\left[\kappa_{L}\right]^{m+1} + \frac{1}{2}C_{\Omega}C_{K}^{3/4}(\Omega)^{-1}(\epsilon) - \frac{3}{2}C_{K}v^{1/2}(\epsilon)^{1/2}\right)}{\left(\frac{1}{2}B\left[\kappa_{L}\right]^{m+1} + \frac{1}{2}C_{\Omega}C_{K}^{3/4}(\Omega)^{-1}(\epsilon) - \frac{3}{4}C_{K}v^{1/2}(\epsilon)^{1/2}\right)}$$
(F.28)

Now dividing both numerator and denominator by $B \, \kappa_L^{m+1} = C_\Omega(\epsilon\Omega)^{1/2} \, \kappa_L^{-1}$ and substituting, $\kappa_L = \frac{\epsilon}{k^{3/2}}$,

$$C_{\varepsilon 2} = \frac{\left(\frac{m+2}{m+1} + \frac{1}{2}C_{K}^{3/4}(\frac{\varepsilon}{\Omega k})^{3/2} - \frac{3}{2}C_{K}(\frac{\varepsilon}{\Omega k})^{1/2}(\frac{k^{2}}{\nu\varepsilon})^{-1/2}\right)}{\left(\frac{1}{2} + \frac{1}{2}C_{K}^{3/4}(\frac{\varepsilon}{\Omega k})^{3/2} - \frac{3}{4}C_{K}(\frac{\varepsilon}{\Omega k})^{1/2}(\frac{k^{2}}{\nu\varepsilon})^{-1/2}\right)}$$
(F.29)

Replacing $k^2/(\nu\epsilon)$ with Re_t and $\epsilon/\Omega k$ with Ro_l

$$C_{\varepsilon 2} = \frac{\left(\frac{m+2}{m+1} + \frac{1}{2}C_K^{3/4}(Ro_l)^{3/2} - \frac{3}{2}C_K(Ro_l)^{1/2}(Re_t)^{-1/2}\right)}{\left(\frac{1}{2} + \frac{1}{2}C_K^{3/4}(Ro_l)^{3/2} - \frac{3}{4}C_K(Ro_l)^{1/2}(Re_t)^{-1/2}\right)}$$
(F.30)

Case III: For high rotation rate

In this case, the inertial range of energy spectrum function Eq.(F.2) extends till the dissipation range of spectrum.

$$k = \int_{0}^{\kappa_{L}} B \kappa^{m} + \int_{\kappa_{L}}^{\kappa_{\eta}} C_{\Omega}(\epsilon \Omega)^{1/2} \kappa^{-2}$$
 (F.31)

$$k = \frac{B \kappa_L^{m+1}}{m+1} - C_{\Omega}(\epsilon \Omega)^{1/2} (\kappa_{\eta}^{-1} - \kappa_L^{-1})$$
 (F.32)

At κ , where the two functions in F.2 and F.3 meet,

$$B \kappa_{L}^{m} = C_{\Omega}(\epsilon \Omega)^{1/2} \kappa_{L}^{-2}$$
 (F.33)

From Eq. (33), it can be seen that $C_{\Omega}(\epsilon\Omega)^{1/2}\kappa_L^{-1}=B\,\kappa_L^{m+1}$ and also eliminating $\kappa_L^{m+2}=(C_{\Omega}(\epsilon\Omega)^{1/2})/B$. So using these relations in Eq. (F.32),

$$k = \frac{m+2}{m+1} B \left[\frac{C_{\Omega}(\epsilon \Omega)^{1/2}}{B} \right]^{\frac{m+1}{m+2}} - C_{\Omega}(\epsilon \Omega)^{1/2} \kappa_{\eta}^{-1}$$
 (F.33)

Substituting, the wave numbers, $\kappa_{\eta} = \frac{1}{\eta} = (\frac{v^3}{\epsilon})^{-1/4}$ in Eq. (F.33),

$$k = \frac{m+2}{m+1} B \left[\frac{C_{\Omega}(\epsilon \Omega)^{1/2}}{B} \right]^{\frac{m+1}{m+2}} - C_{\Omega}(\epsilon \Omega)^{1/2} (\frac{v^3}{\epsilon})^{1/4}$$
 (F.34)

Rearranging for a relation between k and ε

$$k = \frac{m+2}{m+1} B \left[\frac{C_{\Omega}(\Omega)^{1/2}}{B} \right]^{\frac{m+1}{m+2}} \frac{1 (m+1)}{(\epsilon)^{2 (m+2)}} - C_{\Omega}(\Omega)^{1/2} (\nu^{3})^{1/4} (\epsilon)^{1/4}$$
 (F.35)

Differentiating the above equation for k,

$$\frac{\partial \mathbf{k}}{\partial \mathbf{t}} = \left(\frac{1}{2} \mathbf{B} \left[\frac{\mathbf{C}_{\Omega}(\Omega)^{1/2}}{\mathbf{B}} \right]^{\frac{m+1}{m+2}} \frac{\mathbf{1} \cdot (m+1)}{(\varepsilon)^{2 \cdot (m+2)}} - \mathbf{C}_{\Omega}(\Omega)^{1/2} (\mathbf{v})^{3/4} (\varepsilon)^{-3/4} \right] \frac{\partial \varepsilon}{\partial \mathbf{t}}$$
(F.36)

Comparing the above equation with the standard model equations in homogeneous decaying turbulence Eqs (F.13) and (F.14),

$$C_{\varepsilon 2} = \frac{\left(\frac{m+2}{m+1}B\left[\frac{C_{\Omega}(\Omega)^{1/2}}{B}\right]^{\frac{m+1}{m+2}}\frac{1(m+1)}{(\varepsilon)^{\frac{1}{2}(m+2)}} - C_{\Omega}(\Omega)^{1/2}(\nu)^{\frac{3}{4}}(\varepsilon)^{\frac{1}{4}}}{\left(\frac{1}{2}B\left[\frac{C_{\Omega}(\Omega)^{1/2}}{B}\right]^{\frac{m+1}{m+2}}\frac{1(m+1)}{(\varepsilon)^{\frac{1}{2}(m+2)}} - C_{\Omega}(\Omega)^{\frac{1}{2}}(\nu)^{\frac{3}{4}}(\varepsilon)^{-\frac{3}{4}}}\right)}$$
(F.37)

The above equation can be simplified and rearranged using, Eq. (F.33) as following

$$C_{\varepsilon 2} = \frac{\left(\frac{m+2}{m+1}B\left[\kappa_{L}\right]^{m+1} - C_{\Omega}(\Omega)^{1/2}(\nu)^{3/4}(\varepsilon)^{1/4}\right)}{\left(\frac{1}{2}B\left[\kappa_{L}\right]^{m+1} - C_{\Omega}(\Omega)^{1/2}(\nu)^{3/4}(\varepsilon)^{1/4}\right)}$$
(F.38)

Now dividing both numerator and denominator by $B \, \kappa_L^{m+1} = C_\Omega(\epsilon\Omega)^{1/2} \, \kappa_L^{-1}$ and substituting, $\kappa_L = \frac{\epsilon}{k^{3/2}}$,

$$C_{\varepsilon 2} = \frac{\left(\frac{m+2}{m+1} - (\frac{v\varepsilon}{k^2})^{3/4}\right)}{\left(\frac{1}{2} - (\frac{v\varepsilon}{k^2})^{3/4}\right)}$$
(F.39)

$$C_{\epsilon 2} = \frac{\left(\frac{m+2}{m+1} - Re_t^{-3/4}\right)}{\left(\frac{1}{2} - Re_t^{-3/4}\right)}$$
 (F.40)

<u>Summary:</u> Results form Cases I, II and III, (See Eq. (F. 19), (F.30) and (F.40) have been used to formulate the following relation by Park and Chung for all rotation rates for m=2.

$$C_{\varepsilon 2} = \left(\frac{C_D}{\tau_R}\right)_{URAPS} = \frac{4}{3} + \frac{\left(\frac{4}{3} + C_K^{3/4} Ro_l^{3/2}\right)}{\left(1 + 2C_K^{3/4} Ro_l^{3/2}\right)}$$
(F.41)

This can be re-arranged as

$$\left(\frac{C_{D}}{\tau_{R}}\right)_{URAPS} = \frac{4}{3} + \frac{\left(1 + \frac{2}{3}C_{K}^{-3/4}(|\Omega|k/\epsilon)^{3/2}\right)}{\left(1 + \frac{1}{2}C_{K}^{-3/4}(|\Omega|k/\epsilon)^{3/2}\right)}$$
(F.42)

The asymptotic behavior of the above equation is as shown in

$$\frac{d\varepsilon}{d\tilde{t}} = \begin{cases}
-\frac{11}{6} \frac{\varepsilon^2}{k}, & \text{for } Ro_1 = \infty \\
-2 \frac{\varepsilon^2}{k}, & \text{for } Ro_1 = 1 \\
-\frac{16}{6} \frac{\varepsilon^2}{k}, & \text{for } Ro_1 = 0
\end{cases}$$
(F.43)

This asymptotic behavior in Eq. (F.42) is incorporated into the model for $\tilde{\tau}_R$ in the URAPS theory (see Chapter 4).

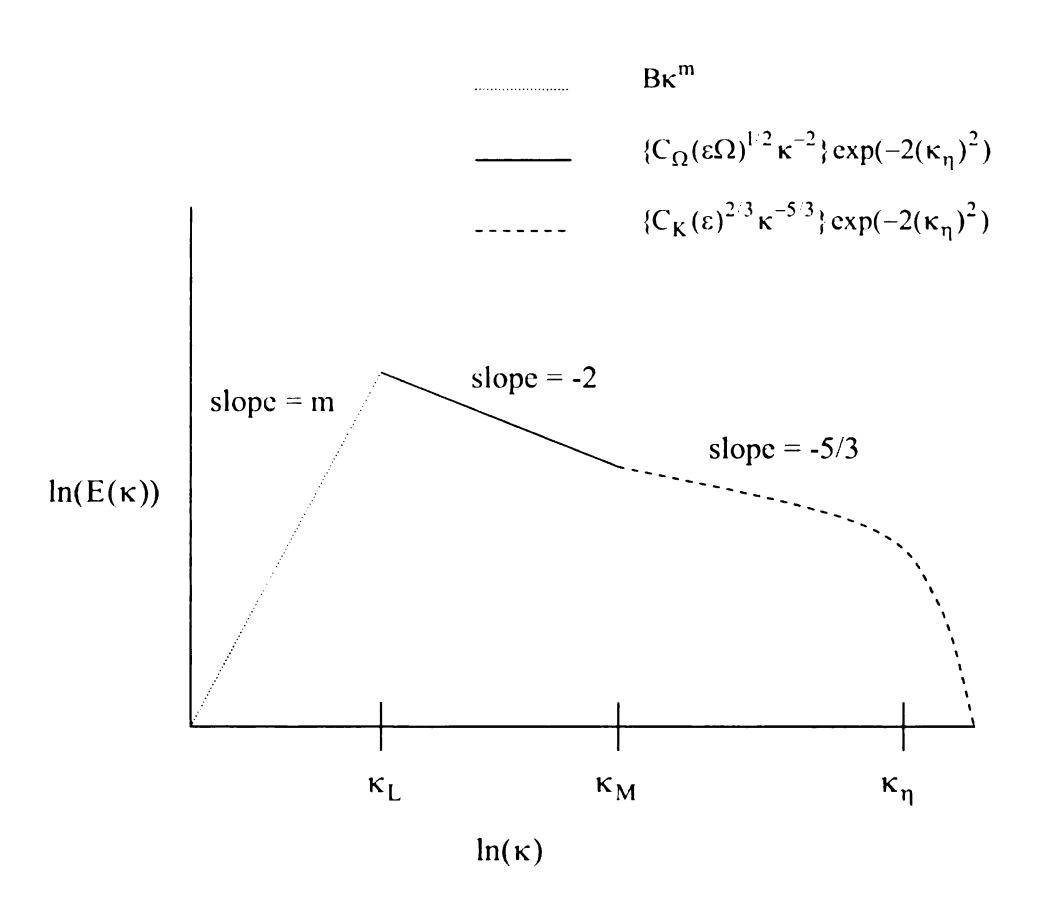


Figure F.1 Model Spectrum in the Presence of Rotation (Park and Chung, 1999)

APPENDIX G

COMPONENT EQUATIONS FOR THE URAPS-CLOSURE

The URAPS-closure component equations are described for specific benchmark flows (see Chapters 5, 6 and 7) in this appendix. For rotating simple shear flows with z as the flow direction and y as the cross flow direction, and with axis of rotation aligned in the direction of vorticity, the URAPS closure equations can be simplified as shown in this appendix.

$$\nabla < \underline{u} > \xrightarrow{\text{simple shear flows}} \frac{d < u_z >}{dy} \underline{e}_y \underline{e}_z = \Gamma_{yz} \underline{e}_y \underline{e}_z$$
 (G.1)

$$\underline{\underline{\Omega}} = \underline{\underline{\varepsilon}} \cdot \underline{\underline{\Omega}} \xrightarrow{\underline{\Omega} \text{ is colinear with } <\underline{w}>} \Omega_{X} \ (\underline{e}_{y}\underline{e}_{z} - \underline{e}_{z}\underline{e}_{y})$$
(G.2)

$$\nabla < \underline{\mathbf{u}} > + 2 \underline{\Omega} = \Gamma_{yz} \underline{\mathbf{e}}_{y} \underline{\mathbf{e}}_{z} + 2 \Omega_{x} (\underline{\mathbf{e}}_{y} \underline{\mathbf{e}}_{z} - \underline{\mathbf{e}}_{z} \underline{\mathbf{e}}_{y})$$
(G.3)

The inverse of the preclosure operator defined in Eq. (2.44) is related to the mean field kinematics as shown in Eq. (G.4) below.

$$\underline{\underline{A}}^{-1} = \underline{\underline{I}} + \tau_{R} (\nabla < \underline{\underline{u}} > + 2 \underline{\underline{\Omega}}) = \underline{\underline{I}} + \underline{\underline{K}}$$

$$= \underline{\underline{e}}_{X} \underline{\underline{e}}_{X} + \underline{\underline{e}}_{Y} \underline{\underline{e}}_{Y} + \underline{\underline{e}}_{Z} \underline{\underline{e}}_{Z} + (N_{\Gamma} + N_{\Omega}) \underline{\underline{e}}_{Y} \underline{\underline{e}}_{Z} - N_{\Omega} \underline{\underline{e}}_{Z} \underline{\underline{e}}_{Y}$$
(G.4)

where the two groups appearing in the above Eq. (G.4) are

$$N_{\Gamma} \equiv \tau_{R} \Gamma_{yz} = C_{R1} \tilde{\tau}_{R} \tilde{\Gamma} \tag{G.5}$$

$$N_{\Omega} = 2 \tau_{R} \Omega_{X} = 2C_{R1} \tilde{\tau}_{R} \tilde{\Omega}$$
 (G.6)

Then, Eq. (G.2) can be rewritten in terms of the adjugate operator $\underline{\underline{C}} = \operatorname{adj}(\underline{\underline{I}} + \tau_R < \underline{\underline{F}} >)$

$$\underline{\underline{A}} = \frac{\underline{\underline{C}}}{\det(\underline{\underline{I}} + \tau_R < \underline{\underline{F}} >)}$$

$$= \frac{(1 + N_{\Gamma}N_{\Omega} + N_{\Omega}^2) \underline{e}_x \underline{e}_x + \underline{e}_y \underline{e}_y + \underline{e}_z \underline{e}_z - (N_{\Gamma} + N_{\Omega}) \underline{e}_y \underline{e}_z + N_{\Omega} \underline{e}_z \underline{e}_y}{(1 + N_{\Gamma}N_{\Omega} + N_{\Omega}^2)}$$
(G.7)

Also, the normalized turbulent relaxation time scale is defined as below.

$$\tilde{\tau}_{R} = \frac{(1 + C_{R3} N_{F}^{3/2})}{(1 + C_{R2} N_{F}^{3/2})} \tag{G.8}$$

$$N_{F} = \left\| \langle F \rangle \right\| k / \varepsilon = +\sqrt{(\tilde{\Gamma} + 2\tilde{\Omega})^{2} + (2\tilde{\Omega})^{2}}$$
(G.9)

where the two dimensionless timescales are

$$\tilde{\Gamma} \equiv \Gamma_{VZ} \, k / \varepsilon \tag{G.10}$$

$$\tilde{\Omega} \equiv \Omega_{\mathbf{x}} \, \mathbf{k} / \varepsilon \tag{G.11}$$

The component equations from the URAPS closure $\underline{\underline{R}} = \frac{\underline{\underline{A}}^T \cdot \underline{\underline{B}} \cdot \underline{\underline{A}}}{tr(\underline{\underline{A}}^T \cdot \underline{\underline{B}} \cdot \underline{\underline{A}})} = \frac{\underline{\underline{C}}^T \cdot \underline{\underline{B}} \cdot \underline{\underline{C}}}{tr(\underline{\underline{C}}^T \cdot \underline{\underline{B}} \cdot \underline{\underline{C}})}$

follow as in Eq (G.12) to Eq. (G.16)

$$\kappa R_{xx} = (1 + N_{\Gamma} N_{O} + N_{O}^{2})^{2} B_{xx}$$
 (G.12)

$$\kappa R_{vv} = B_{vv} + 2 N_{\Omega} B_{vz} + N_{\Omega}^{2} B_{zz}$$
 (G.13)

$$\kappa R_{zz} = (N_{\Gamma} + N_{\Omega})^2 B_{yy} - 2(N_{\Gamma} + N_{\Omega}) B_{yz} + B_{zz}$$
 (G.14)

$$\kappa R_{yz} = B_{yz} - (N_{\Gamma} + N_{\Omega}) B_{yy} - (N_{\Gamma} + N_{\Omega}) N_{\Omega} B_{yz} + N_{\Omega} B_{zz}$$
 (G.15)

The parameter κ is defined as follows

$$\kappa = (1 + N_{\Gamma} N_{\Omega} + N_{\Omega}^{2})^{2} B_{xx} + (1 + (N_{\Gamma} + N_{\Omega})^{2}) B_{yy} + (1 + N_{\Omega}^{2}) B_{zz} - 2 N_{\Gamma} B_{yz}. \quad (G.16)$$

Furthermore, the CH-mapping of $\underline{\underline{R}}$ into $\underline{\underline{\underline{B}}}$ (see Eq.(4.1)) implies that

$$B_{xx} = R_{xx} + C_1(R_{xx} - \frac{1}{3}) + C_2(R_{xx}^2 - II_R R_{xx})$$
 (G.17)

$$B_{yy} = R_{yy} + C_1(R_{yy} - \frac{1}{3}) + C_2(R_{yy}^2 + R_{yz}R_{zy} - II_RR_{yy})$$
 (G.18)

$$B_{zz} = R_{zz} + C_1(R_{zz} - \frac{1}{3}) + C_2(R_{zz}^2 + R_{zy}R_{yz} - II_RR_{zz})$$
 (G.19)

$$B_{vz} = [I + C_1 + C_2(R_{vv} + R_{zz} - II_R)]R_{vz}.$$
(G.20)

where $C_1 \equiv 27\beta \det(\underline{R})$, $C_2 \equiv -\alpha (II_R - \frac{1}{3})$. Four specific cases of the above general set of equations for simple shear flows in the presence of rotation are discussed below. Case1: $N_{\Gamma} = 0$ and $N_{\Omega} = 0$; Case 2: $N_{\Gamma} = 0$ and $N_{\Omega} \neq 0$ Case 3: $N_{\Gamma} = 0$ and $N_{\Omega} \neq 0$ and Case 4: $N_{\Gamma} = -N_{\Omega}$. Case 4 here refers to the zero absolute mean vorticity region discussed in Chapters 2, 6, and 7.

Case 1: $N_{\Gamma} = 0$ and $N_{\Omega} = 0$

This case is for Homogeneous flows in a non-inertial frame where $\underline{\underline{K}} = \underline{\underline{0}}$ and $\underline{\underline{A}} = \underline{\underline{I}}$. It follows directly from URAPS-equations that $\underline{\underline{R}} = \underline{\underline{B}}$ and $\underline{\underline{\Delta}} = \underline{\underline{0}}$. Consequently, $\underline{\underline{R}} = \underline{\underline{I}}/3$. The following cases illustrate the equations for rotating homogeneous flows and shear flow with and without rotation.

$\underline{CASE\ 2:}\quad N_{\Gamma}\neq 0\ \ and\ \ N_{\Omega}=0\ ;$

The equations below apply to homogeneous shear and for simple shear flows without rotation.

$$\underline{\underline{K}} = N_{\Gamma} \underline{e}_{y} \underline{e}_{z} \tag{G.21}$$

$$\underline{\mathbf{A}} = \underline{\mathbf{e}}_{\mathbf{x}} \underline{\mathbf{e}}_{\mathbf{x}} + \underline{\mathbf{e}}_{\mathbf{y}} \underline{\mathbf{e}}_{\mathbf{y}} + \underline{\mathbf{e}}_{\mathbf{z}} \underline{\mathbf{e}}_{\mathbf{z}} - \mathbf{N}_{\Gamma} \underline{\mathbf{e}}_{\mathbf{y}} \underline{\mathbf{e}}_{\mathbf{z}}$$
 (G.22)

$$N_{F} = \left\| \langle F \rangle \right\| k / \varepsilon = +\sqrt{\tilde{\Gamma}^{2}}$$
(G.23)

The preclosure equations in Eq.(G.12) to Eq.(G.16) can be simplified as below

$$\kappa R_{xx} = B_{xx} \tag{G.24}$$

$$\kappa R_{yy} = B_{yy} \tag{G.25}$$

$$\kappa R_{zz} = N_{\Gamma}^2 B_{yy} - 2 N_{\Gamma} B_{yz} + B_{zz}$$
 (G.26)

$$\kappa R_{yz} = B_{yz} - N_{\Gamma} B_{yy} \tag{G.27}$$

The parameter κ is defined as follows

$$\kappa \equiv 1 + N_{\Gamma}^2 B_{vv} - 2 N_{\Gamma} B_{vz}. \tag{G.28}$$

It should be noted that in this case for shear flows without rotation (homogeneous or simple shear), the URAPS-equations have a feature that

$$\frac{R_{xx}}{R_{yy}} = \frac{B_{xx}}{B_{yy}} = \frac{R_{xx} + C_1(R_{xx} - \frac{1}{3}) + C_2(R_{xx}^2 - II_R R_{xx})}{R_{yy} + C_1(R_{yy} - \frac{1}{3}) + C_2(R_{yy}^2 + R_{yz} R_{zy} - II_R R_{yy})}.$$
 (G.29)

This results in the following equation for the ratio the two CH-related extra anisotropy coefficients

$$\frac{\beta}{\alpha} = +3 \frac{(II_R - \frac{1}{3})}{27 \det(\underline{R})} \frac{R_{xx} R_{yy}}{(R_{xx} - R_{yy})} (R_{xx} - R_{yy} - \frac{R_{yz}^2}{R_{yy}}). \tag{G.30}$$

Case 3: $N_{\Gamma} = 0$ and $N_{\Omega} \neq 0$;

This case if for homogeneous flows in inertial frames (i.e. rotating flows)

$$\underline{\underline{K}} = N_{\Omega} \left(\underline{e}_{y} \underline{e}_{z} - \underline{e}_{z} \underline{e}_{y} \right) \tag{G.31}$$

$$\underline{\underline{A}} = \frac{(1 + N_{\Omega}^2) \underline{e}_x \underline{e}_x + \underline{e}_y \underline{e}_y + \underline{e}_z \underline{e}_z - N_{\Omega} \underline{e}_y \underline{e}_z + N_{\Omega} \underline{e}_z \underline{e}_y}{(1 + N_{\Omega}^2)}$$
(G.32)

$$N_{F} = \| \langle F \rangle \| k / \epsilon = +\sqrt{(2\tilde{\Omega})^{2} + (2\tilde{\Omega})^{2}} = +2\sqrt{2\tilde{\Omega}^{2}}$$
 (G.33)

For this case,

$$\nabla < \underline{\mathbf{u}} > = \underline{\underline{\mathbf{0}}}, \text{ and } \underline{\underline{\Omega}} = \underline{\underline{\varepsilon}} \cdot \underline{\Omega} = \Omega_{\mathbf{x}} (\underline{\mathbf{c}}_{\mathbf{y}} \underline{\mathbf{c}}_{\mathbf{z}} - \underline{\mathbf{e}}_{\mathbf{z}} \underline{\mathbf{c}}_{\mathbf{y}}).$$
 (G.34)

Furthermore, if $B_{yz} = 0$ and $B_{yy} = B_{zz}$, then $R_{yz} = 0$, (URAPS closure prediction for this flow field),

$$\kappa R_{xx} = (1 + N_{\Omega}^2)^2 B_{xx}$$
 (G.35)

$$\kappa R_{yy} = B_{yy} + N_{\Omega}^2 B_{zz} \tag{G.36}$$

$$\kappa R_{zz} = N_{\Omega}^2 B_{yy} + B_{zz} \tag{G.37}$$

The parameter κ is defined as follows

$$\kappa = (1 + N_{\Omega}^{2})^{2} B_{xx} + (1 + N_{\Omega}^{2}) B_{yy} + (1 + N_{\Omega}^{2}) B_{zz}.$$
 (G.38)

$$B_{xx} = R_{xx} + C_1(R_{xx} - 1/3) + C_2(R_{xx}^2 - II_R R_{xx})$$
(G.39)

$$B_{yy} = R_{yy} + C_1(R_{yy} - 1/3) + C_2(R_{yy}^2 - II_R R_{yy})$$
(G.40)

$$B_{zz} = R_{zz} + C_1(R_{zz} - 1/3) + C_2(R_{zz}^2 - II_R R_{zz}).$$
 (G.41)

In the above equations, $II_R \equiv \underline{\underline{R}} : \underline{\underline{R}} = R_{xx}^2 + R_{yy}^2 + R_{zz}^2$ inasmuch as the shear components of $\underline{\underline{R}}$ are zero. Eqs.(G.26) and (G.27) imply that if $B_{yy} = B_{zz}$, then

 $R_{yy} = R_{zz}$ which means that $B_{yy} = B_{zz} = (1 - B_{xx})/2$ and $R_{yy} = R_{zz} = (1 - R_{xx})/2$.

So, Eq.(G.26) results in

$$R_{xx} = \frac{(1 + N_{\Omega}^2)B_{xx}}{(1 + N_{\Omega}^2B_{xx})}.$$
 (G.42)

Case 4: $N_{\Gamma} = -N_{O}$.

This case is specifically occurs in the zero absolute mean vorticity region of channel.

$$\underline{K} = N_{\Gamma} \underline{e}_{\nu} \underline{e}_{z} + N_{\Omega} (\underline{e}_{\nu} \underline{e}_{z} - \underline{e}_{z} \underline{e}_{\nu})$$
(G.43)

$$\underline{\underline{A}} = \underline{e}_{x} \underline{e}_{x} + \underline{e}_{y} \underline{e}_{y} + \underline{e}_{z} \underline{e}_{z} + N_{\Omega} \underline{e}_{z} \underline{e}_{y}$$
(G.44)

It can be noted that the pre-closure operator for Case 2 non-rotating channel is the transpose of the operator for rotating channel where the velocity profile is linear.

$$N_{F} = \left\| \langle \underline{F} \rangle \right\| k / \varepsilon = +\sqrt{(2\tilde{\Omega})^{2}}$$
(G.45)

$$\kappa R_{xx} = B_{xx} \tag{G.46}$$

$$\kappa R_{yy} = B_{yy} + 2 N_{\Omega} B_{yz} + N_{\Omega}^{2} B_{zz}$$
 (G.47)

$$\kappa R_{77} = B_{77}$$
 (G.48)

$$\kappa R_{yz} = B_{yz} + N_{\Omega} B_{zz} \tag{G.49}$$

The parameter κ is defined as follows

$$\kappa = 1 + (N_{\Omega}^2) B_{zz} - 2 N_{\Gamma} B_{yz}.$$
(G.50)

It is important to note that the equations for Case 2 and Case 4 are quite similar, except for a change/ flip in R_{yy} and R_{zz} equations. The component equations of the URAPS-closure for the specific cases described in this appendix are used in Chapter 5 (Case 2:

 $N_\Gamma=0$ and $N_\Omega\neq 0$) and in Chapters 6 and 7 (Case 3: $N_\Gamma=0$ and $N_\Omega\neq 0$; and Case 4: $N_\Gamma=-N_\Omega$).

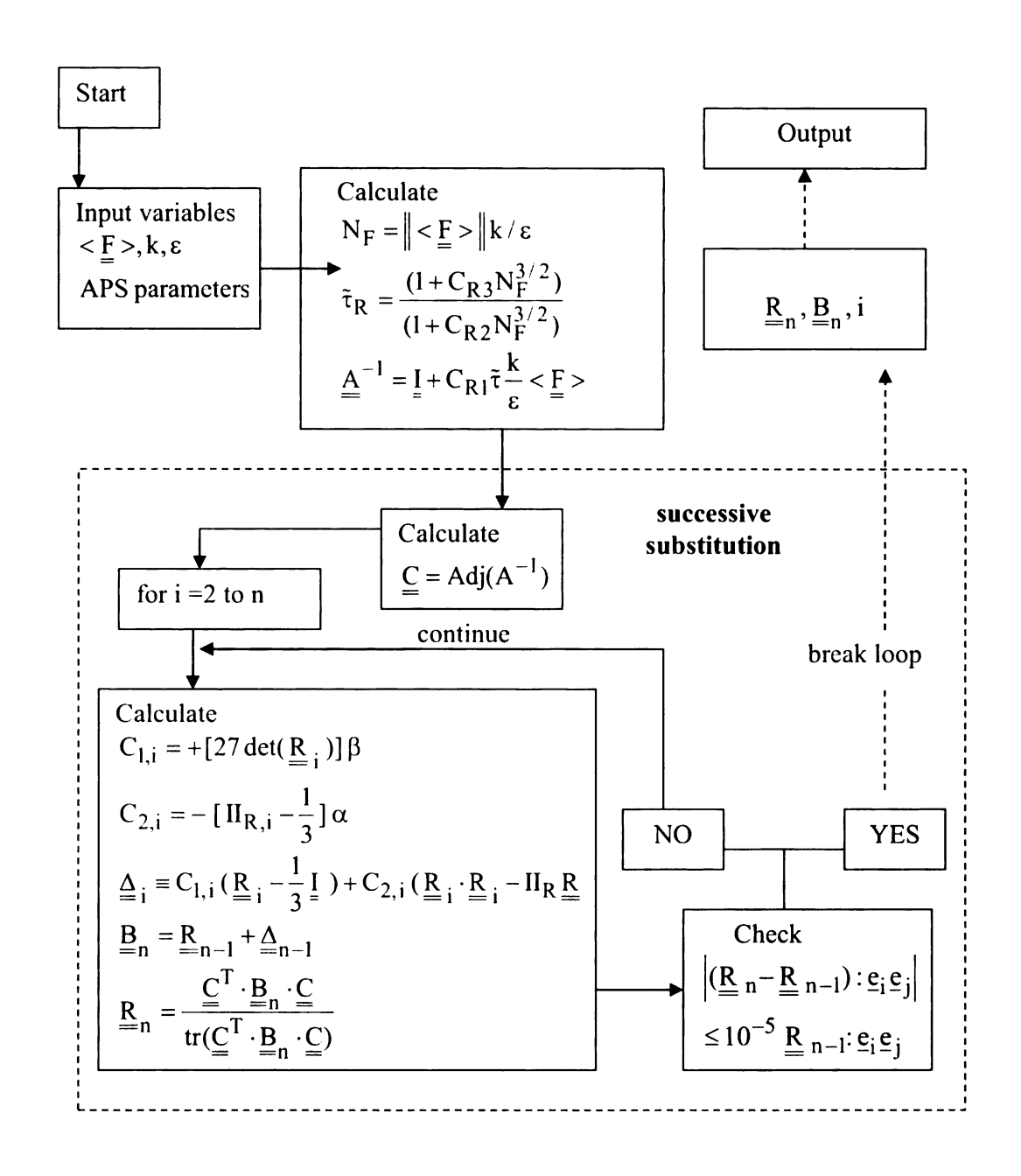
APPENDIX H

PROGRAMS AND FLOW CHARTS

The following programs are used in different chapters of the dissertation:

- H.1 General URAPS Closure Calculation Subprogram
- H.2 Optimization of APS Parameters
- H.3 Homogeneous decay
- H.4 Homogeneous Shear

H.1 General URAPS Closure Calculation Subprogram

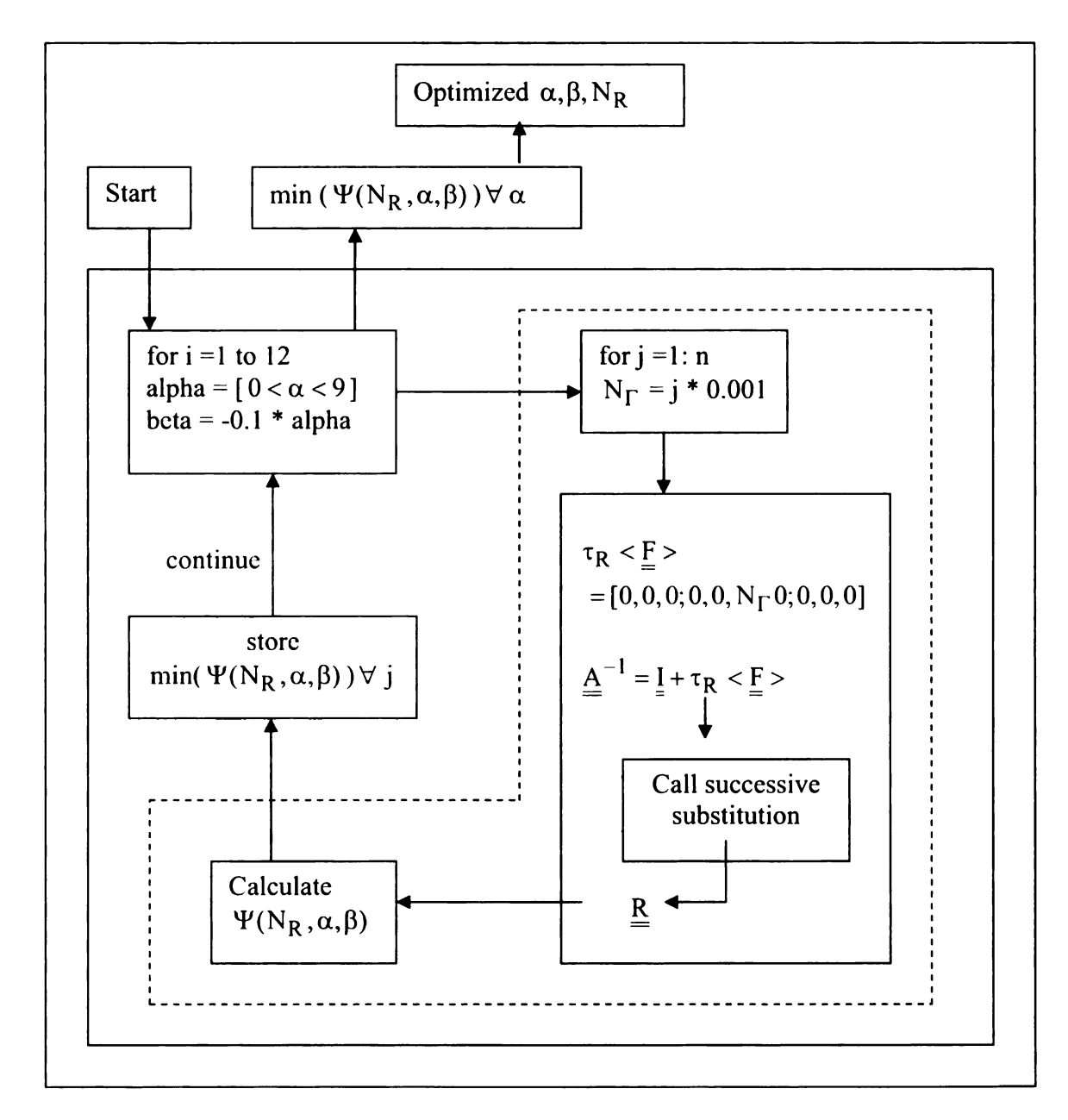


```
% Input variable needed
% F=[0 0; 0 0 Gam yz; 0 0 0] (in the form a matrix)
% k (kinetic energy)
% eps (dissipation)
3 \text{ APSpar} = [0.1, -0.01, 0.00357, 0.0764, 0.0526, 3/2]  (APS parameters)
% Call the following matlab program
% [R,B,it,Tau] = aps_gen_funl(F,k,eps,APSpar);
function[R,B,it,Tau] = aps gen funl(F,k,eps,APSpar)
alpha= APSpar(1);
beta = APSpar(2);
cr1= APSpar(3);
cr2= APSpar(4);
cr3 = APSpar(5);
n= APSpar(6);
I = [1 \ 0 \ 0; \ 0 \ 1 \ 0; \ 0 \ 0 \ 1];
NF=k/eps*sqrt(trace(F*(F)'));
T2 = (1 + cr2 * (NF) ^ (n));
T3 = (1 + cr3 * (NF) ^ (n));
Tau=T3/T2;
TauR=crl*Tau*(k/eps);
& A inverse
Ain=I+TauR*F;
%Calling the successive substitution function
[R,B,it] = aps gen fun2(Ain,alpha,beta);
end
function [R,B,i] = aps gen fun2(Ain, alpha, beta)
I = [1 \ 0 \ 0; \ 0 \ 1 \ 0; \ 0 \ 0 \ 1];
Cxx=Ain(2,2)*Ain(3,3)-Ain(3,2)*Ain(2,3);
Cxy = (-1) * (Ain(2,1) * Ain(3,3) - Ain(3,1) * Ain(2,3));
Cxz = Ain(2,1) * Ain(3,2) - Ain(3,1) * Ain(2,2);
Cyx = (-1) * (Ain (1, 2) * Ain (3, 3) - Ain (3, 2) * Ain (1, 3));
Cyy = Ain(1,1) * Ain(3,3) - Ain(3,1) * Ain(1,3);
Cyz = (-1) * (Ain (1,1) * Ain (3,2) - Ain (3,1) * Ain (1,2));
Czx=Ain(1,2)*Ain(2,3)-Ain(2,2)*Ain(1,3);
Czy=(-1)*(Ain(1,1)*Ain(2,3)-Ain(2,1)*Ain(1,3));
Czz=Ain(1,1)*Ain(2,2)-Ain(2,1)*Ain(1,2);
rxx(1) = 1/3;
ryy(1) = 1/3;
rzz(1)=1/3;
ryz(1) = 0;
rxy(1) = 0;
rxz(1) = 0;
% (note that C adjugate which is Transpose of the minor
C=[Cxx Cxy Cxz; Cyx Cyy Cyz; Czx Czy Czz]';
```

```
R=[rxx(1) rxy(1) rxz(1); rxy(1) ryy(1) ryz(1); rxz(1) ryz(1)];
for i=2:4000
IIR = trace(R*R);
detr=det(R);
cl=beta*(27*detr);
c2=-alpha*(IIR -1/3);
B = R + c1*(R-I/3) + c2*(R*R - IIR*R);
CT=C';
D=(CT*B)*C;
tr=trace(D);
R=D/tr;
        rxx(i) = R(1,1);
        ryy(i) = R(2,2);
        rzz(i) = R(3,3);
        rxy(i) = R(1,2);
        rxz(i) = R(1,3);
        ryz(i) = R(2,3);
errl= abs((rxx(i)-rxx(i-1))/rxx(i-1));
err2= abs((ryy(i)-ryy(i-1))/ryy(i-1));
err3 = abs((rzz(i)-rzz(i-1))/rzz(i-1));
err4= abs((rxy(i)-rxy(i-1))/rxy(i-1));
err5= abs((rxz(i)-rxz(i-1))/rxz(i-1));
err6= abs((ryz(i)-ryz(i-1))/ryz(i-1));
   if ((err1<0.00001) && (err2<0.00001) &&
                                                      (err3<0.00001)
                                                                       & &
(err4<0.00001) && (err5<0.00001) && (err6<0.00001))
    break
   end
end
```

end

H.2 Optimization of APS Parameters



Note:

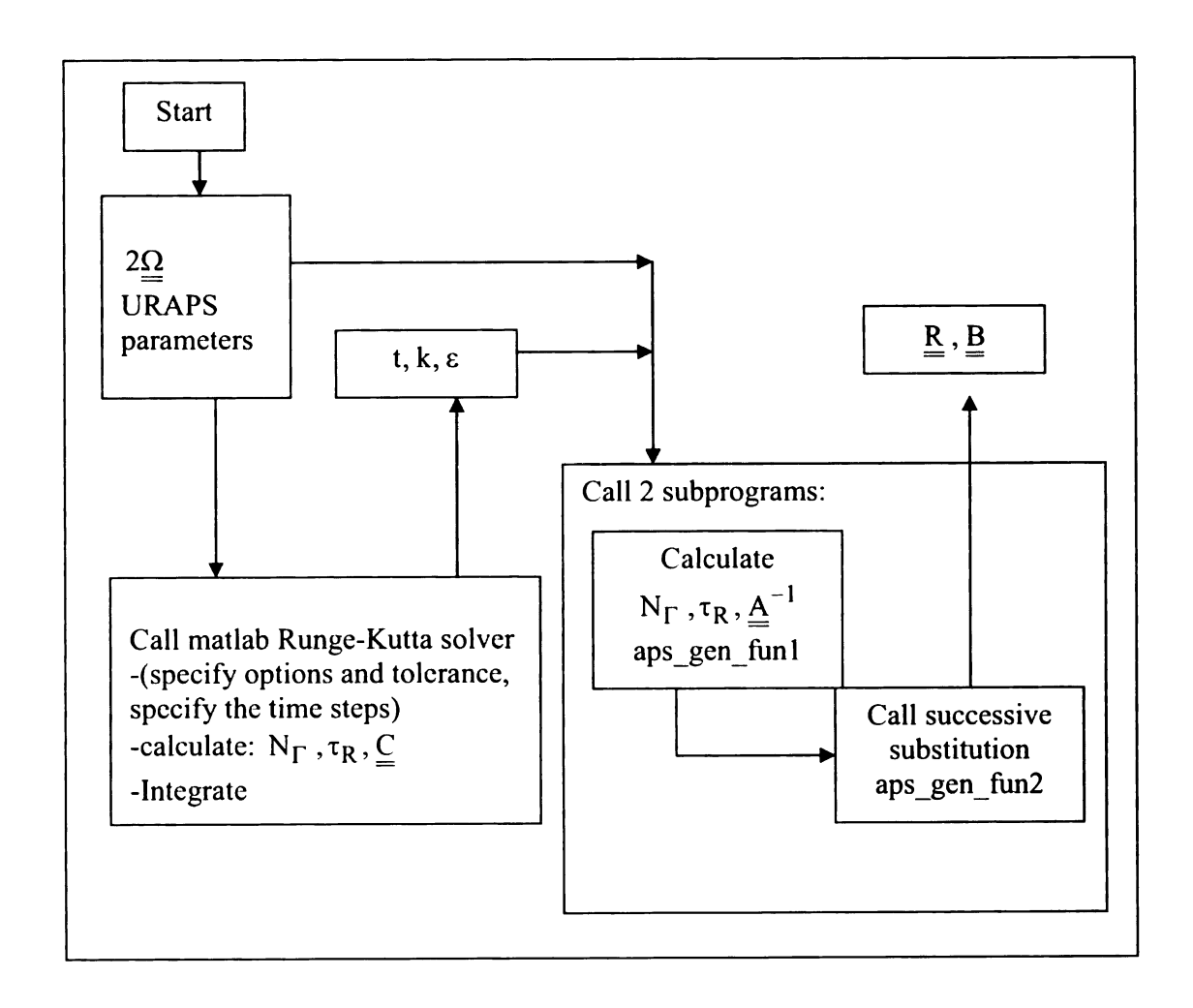
$$\Psi(N_R,\alpha,\beta) \equiv$$

$$\left[(\frac{R_{xx}^{APS} - R_{xx}^{exp}}{R_{xx}^{exp}})^2 + (\frac{R_{yy}^{APS} - R_{yy}^{exp}}{R_{yy}^{exp}})^2 + (\frac{R_{zz}^{APS} - R_{zz}^{exp}}{R_{zz}^{exp}})^2 + (\frac{R_{yz}^{APS} - R_{yz}^{exp}}{R_{yz}^{exp}})^2 \right]^{1/2}$$

```
I=[1 0 0; 0 1 0; 0 0 1];
for a=1:12
    alpha = [0.01, 0.025, 0.05, 0.075, 0.1, 0.25, 0.5, 0.75, 1, 2.5, 5, 9];
    beta(a) = -0.1 \times alpha(a);
    if (alpha(a) < 1)
    step=0.0001;
        else if (alpha(a) >= 1)
        step=0.001;
        end
    end
         for i=1:1001
              Nq(i) = (i-1) * step;
              Ngam=[0 \ 0 \ 0; \ 0 \ 0 \ Ng(i); \ 0 \ 0 \ 0];
               I = [1 \ 0 \ 0; \ 0 \ 1 \ 0; \ 0 \ 0 \ 1];
              Ain=I + Ngam;
               [R,B,it] = aps gen fun2(Ain,alpha(a),beta(a));
              Rxx ss=R(1,1);
              Ryy ss=R(2,2);
              Rzz ss=R(3,3);
              Ryz ss=R(2,3);
              d(i) = sqrt((Rxx ss-0.236)/0.236)^2
                           + ((Ryy ss-0.197)/0.197)^2
                           + ((Ryz ss+0.165)/0.165)^2
                           + ((Rzz ss-0.567)/0.567)^2);
             data(i)=d(i);
             data2(i) = Ng(i);
             data3(i)=i;
             data4(i) = Rxx ss;
             data5(i)=Ryy ss;
             data6(i)=Rzz ss;
             data7(i)=Ryz ss;
         end
         mini(a,1) = alpha(a);
         [y,v]=min(data); %y is the value and v is the index
         mini(a, 2) = data2(v);
         mini(a, 3) = data(v);
         mini(a, 4) = y;
         mini(a,7) = data4(v);
         mini(a, 8) = data5(v);
         mini(a, 9) = data6(v);
         mini(a, 10) = data7(v);
      R=[data4(v) \ 0 \ 0; \ 0 \ data5(v) \ data7(v); \ 0 \ data7(v) \ data6(v)];
      b=R-I/3;
      IIb(a) = trace(b*b);
      IIIb(a) = trace(b*b*b);
      x(i) = (data6(v) + 2*data5(v))/2;
      y(i) = 0.5*sqrt(3)*data6(v);
```

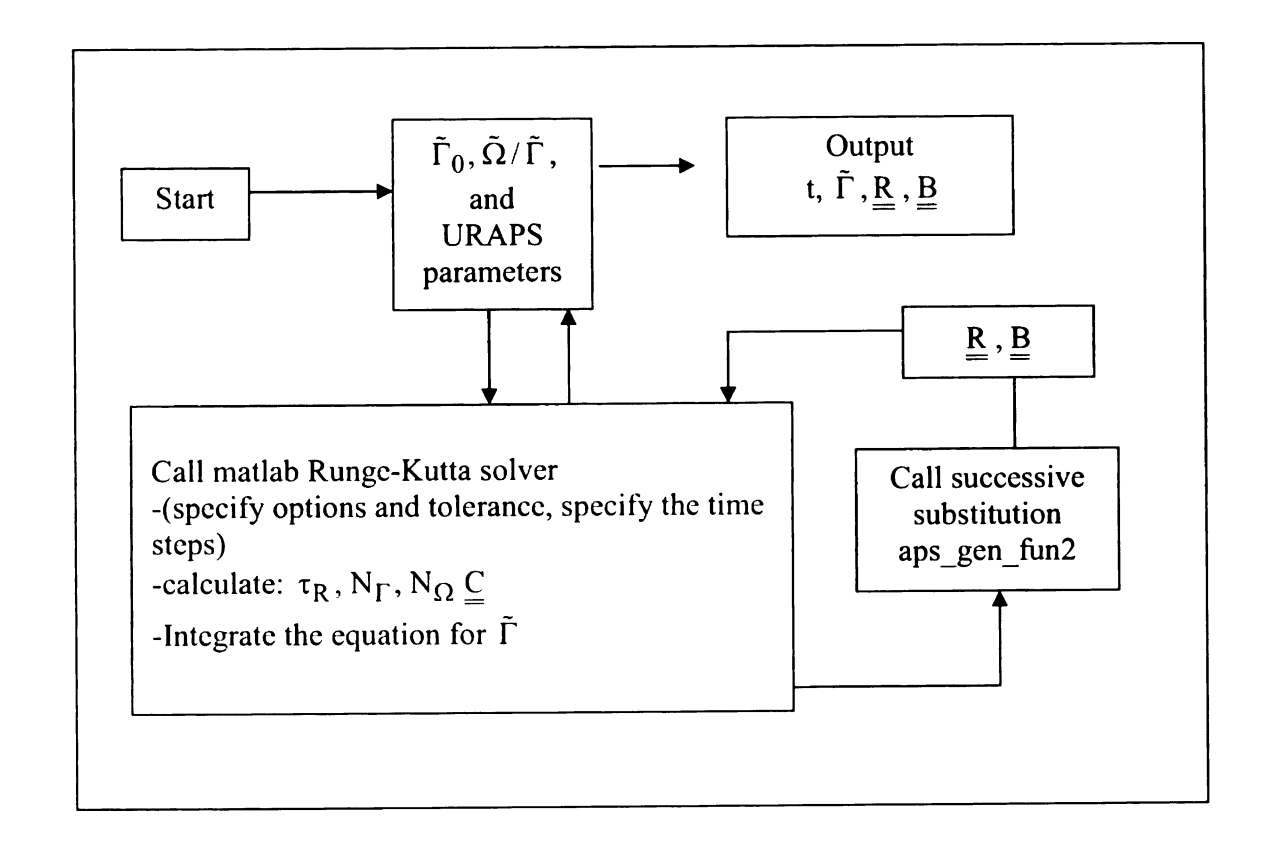
end

H.3 Homogeneous Decay



```
APSpar=[0.1, -0.01, 0.00357, 0.0764, 0.0526, 3/2];
omg x=0.25;
yz = \overline{2} * omg x;
zy=-2*omq x;
F = [0 \ 0 \ 0; \ 0 \ 0 \ yz; \ 0 \ zy \ 0];
I = [1 \ 0 \ 0; \ 0 \ 1 \ 0; \ 0 \ 0 \ 1];
[t,y]=homogeneous decay(F,APSpar);
for i=1:101
k = y(i, 1);
eps=y(i,2);
[R,B,it,Tau] = aps gen funl(F, k, eps, APSpar);
Rxx(i) = R(1,1); Ryy(i) = R(2,2); Rzz(i) = R(3,3);
Rxy(i) = R(1,2); Rxz(i) = R(1,3); Ryz(i) = R(2,3);
B=R-I/3;
IIb aps(i)=trace(B*B);
IIIb aps(i)=trace(B*B*B);
Bxx(i) = B(1,1); Byy(i) = B(2,2); Bzz(i) = B(3,3);
Bxy(i) = B(1,2); Bxz(i) = B(1,3); Byz(i) = B(2,3);
end
function[t,y]=homogeneous decay(F,APSpar);
Cd cr1=11/6; Cp cr1=1.486;
alpha= APSpar(1);
beta = APSpar(2);
crl= APSpar(3);
cr2= APSpar(4);
cr3 = APSpar(5);
n= APSpar(6);
options = odeset('RelTol', 1e-4, 'AbsTol', [1e-6 1e-6]);
[t,y] =
ode45(@isodecay1,[0:0.1:1,1.2:0.2:5,5.5:0.5:25,26:1:40,45:5:60,70:10:17
0],[1 1],options);
function dydt = isodecayl(t,y)
NF = (y(1)/y(2) * sgrt(trace(F*(F)')+0.00000000001));
T2 = (1 + cr2 * (NF) ^ (n));
T3 = (1 + cr3 * (NF) ^ (n));
Tau = (y(1)/y(2)) *T3/T2;
dydt(1) = -y(2);
dydt(2) = -Cd_cr1/(Tau) * y(2);
end
end
```

H.4 Homogeneous Shear



```
APSpar=[0.1, -0.01, 0.00357, 0.0764, 0.0526, 3/2];
Omg Gam =-0.25;
Gamo=1;
Cd cr1=11/6;
Cp cr1=1.486;
alpha= APSpar(1);
beta = APSpar(2);
crl= APSpar(3);
cr2= APSpar(4);
cr3= APSpar(5);
n= APSpar(6);
[t,y]=homogeneous_shear(Gamo,Omg_Gam,APSpar);
num=size(t);
for i=1:num
Gam=y(i);
I = [1 \ 0 \ 0; \ 0 \ 1 \ 0; \ 0 \ 0 \ 1];
D=sqrt((1+2*Omg_Gam)^2+(2*Omg_Gam)^2);
NF=Gam*D;
T2 = (1 + cr2 * (NF) ^ (n));
T3 = (1 + cr3 * (NF) ^ (n));
Tau=cr1 *T3/T2;
yz=1+2*Omg Gam;
zy=-2*Omg Gam;
Fke=y(i) * [0 0 0; 0 0 yz; 0 zy 0];
Ain=I+Tau*Fke;
[R,B,iter]=aps_gen_fun2(Ain, alpha, beta);
  Rxx(i) = R(1,1); Ryy(i) = R(2,2); Rzz(i) = R(3,3);
  Rxy(i) = R(1,2); Rxz(i) = R(1,3); Ryz(i) = R(2,3);
end
```

```
function [t,y]=homogeneous shear(Gamo,Omg Gam,APSpar);
Cd cr1=11/6;
Cp cr1=1.486;
alpha= APSpar(1);
beta= APSpar(2);
cr1= APSpar(3);
cr2= APSpar(4);
cr3= APSpar(5);
n= APSpar(6);
D=sqrt((1+2*Omg Gam)^2+(2*Omg Gam)^2);
[t,y] = ode45(@isodecay1,[0:0.5:1000],[Gamo]);
function dydt = isodecay1(t,y)
Gam=y;
I = [1 \ 0 \ 0; \ 0 \ 1 \ 0; \ 0 \ 0 \ 1];
NF=Gam*D;
T2 = (1 + cr2 * (NF) ^ (n));
T3 = (1 + cr3 * (NF) ^ (n));
Tau=cr1*T3/T2;
⊱TauR⊬Tau′γ;
A invarse
yz=1+2*Omg Gam;
zy=-2*Omg Gam;
Fke=y*[0 0 0; 0 0 yz; 0 zy 0];
Ain=I+Tau*Fke;
[R,B,i]=aps_gen_fun2(Ain, alpha, beta);
  Rxx=R(1,1); Ryy=R(2,2); Rzz=R(3,3);
  Rxy=R(1,2); Rxz=R(1,3); Ryz=R(2,3);
dydt= (-2*y*Ryz-1) - (Cp_cr1*cr1*(-2*y*Ryz)/Tau-Cd_cr1*cr1/(Tau));
end
yf = y(2001);
zer=(-2*Ryz*yf)-(Cd crl*crl-Tau)/(Cp crl*crl-Tau);
end
```

APPENDIX I

BENCHMARK STATISTICS

The following Tables are the DNS results for non-rotating and rotating channel used in Chapters 2 and 7. The information of $\tilde{\Gamma}$ and $\tilde{\Omega}$ from the DNS results is used in the URAPS-closure equations to predict the NR-stress. A comparison of DNS results and URAPS-closure results is presented in Chapter 7.

Table I.1a: DNS data in the core region of non rotating channel (Iwamoto, 2002, Iwamoto et al. 2002).

[y ⁺]	y ⁺	y/δ	p ⁺	u ⁺	$\frac{d u^+}{d y^+}$	k ⁺	ε+	Γ	Re ⁺	Ρ/ε
30	30.72	0.10	0.56	13.64	0.102	3.70	0.077	4.90	177.64	1.05
35	35.18	0.12	0.67	14.04	0.082	3.49	0.067	4.24	181.62	0.97
40	39.91	0.13	0.75	14.39	0.067	3.30	0.058	3.79	186.59	0.92
45	44.92	0.15	0.80	14.70	0.057	3.13	0.051	3.49	192.48	0.88
50	50.21	0.17	0.85	14.98	0.049	2.98	0.045	3.30	199.12	0.87
70	70.74	0.24	0.88	15.82	0.035	2.55	0.029	3.06	224.20	0.87
100	99.65	0.33	0.83	16.70	0.027	2.14	0.018	3.09	248.48	0.92
150	151.07	0.51	0.66	17.86	0.019	1.59	0.010	3.08	254.39	0.92
200	199.84	0.67	0.52	18.67	0.014	1.16	0.006	2.73	222.71	0.75
250	249.37	0.84	0.43	19.23	0.008	0.82	0.004	1.69	173.70	0.32
300	297.90	1.00	0.39	19.43	0.000	0.69	0.003	0.00	147.44	0.00

Table I.1 b.: DNS data of Table I.1a continued.

y/δ	R _{xx}	R _{yy}	R _{zz}	R _{yz}	λ_{R1}	λ_{R2}	λ_{R3}	III _b	II _b
0.10	0.21	0.09	0.70	-0.11	0.07	0.21	0.72	0.039	0.236
0.12	0.22	0.11	0.67	-0.11	0.08	0.22	0.70	0.031	0.206
0.13	0.23	0.12	0.65	-0.12	0.10	0.23	0.67	0.024	0.182
0.15	0.24	0.14	0.62	-0.13	0.10	0.24	0.66	0.020	0.162
0.17	0.25	0.15	0.60	-0.13	0.11	0.25	0.64	0.016	0.146
0.24	0.27	0.18	0.55	-0.14	0.13	0.27	0.60	0.010	0.116
0.33	0.28	0.19	0.53	-0.15	0.14	0.28	0.58	0.008	0.104
0.51	0.28	0.21	0.51	-0.15	0.15	0.28	0.57	0.007	0.094
0.67	0.27	0.23	0.50	-0.14	0.17	0.27	0.56	0.006	0.080
0.84	0.27	0.26	0.47	-0.09	0.22	0.27	0.51	0.004	0.046
1.00	0.27	0.28	0.45	0.00	0.28	0.27	0.45	0.001	0.018

Table I.1c: URAPS predictions

y/δ	ĩ	N _Γ	R _{xx}	R _{yy}	R _{zz}	R _{yz}	λ_{R1}	λ_{R2}	λ _{R3}	III _b	II _b
0.10	0.859	0.015	0.24	0.18	0.58	-0.19	0.10	0.24	0.66	0.019	0.162
0.12	0.875	0.013	0.25	0.20	0.55	-0.19	0.12	0.25	0.63	0.016	0.145
0.13	0.888	0.012	0.25	0.21	0.54	-0.19	0.12	0.25	0.63	0.014	0.133
0.15	0.896	0.011	0.26	0.22	0.52	-0.18	0.14	0.26	0.60	0.013	0.124
0.17	0.902	0.011	0.26	0.22	0.52	-0.18	0.14	0.26	0.60	0.012	0.118
0.24	0.910	0.010	0.26	0.23	0.51	-0.18	0.14	0.26	0.60	0.010	0.110
0.33	0.909	0.010	0.26	0.23	0.51	-0.18	0.14	0.26	0.60	0.011	0.111
0.51	0.909	0.010	0.26	0.23	0.51	-0.18	0.14	0.26	0.60	0.011	0.111
0.67	0.920	0.009	0.27	0.24	0.49	-0.17	0.15	0.27	0.58	0.009	0.098
0.84	0.955	0.006	0.29	0.28	0.43	-0.14	0.20	0.29	0.51	0.003	0.055
1.00	1.000	0.000	0.33	0.33	0.34	0.00	0.33	0.33	0.34	0.000	0.000

Table I.2a: DNS data in the core region of non rotating channel (Hoyas and Jimenez, 2006).

[y ⁺]	y ⁺	y/δ	u ⁺	$\frac{du^+}{dy^+}$	k ⁺	ε+	Γ̈́	Re ⁺	Ρ/ε
30	30.56	0.015	13.49	0.102	5.08	0.083	6.28	312.05	1.09
40	40.39	0.02	14.28	0.065	4.77	0.063	4.98	364.64	0.95
50	51.27	0.03	14.88	0.047	4.54	0.048	4.40	427.23	0.90
75	75.86	0.04	15.79	0.030	4.25	0.031	4.13	576.87	0.91
100	100.16	0.05	16.44	0.024	4.09	0.023	4.17	722.93	0.95
250	252.71	0.13	18.75	0.010	3.56	0.009	4.35	1488.97	1.06
500	505.16	0.25	20.61	0.005	2.93	0.004	4.05	2161.31	1.02
1000	1002.11	0.50	22.61	0.003	1.95	0.002	3.69	2327.16	0.94
1500	1503.02	0.75	23.82	0.002	1.19	0.001	2.65	1777.16	0.56
2000	2004.30	1.00	24.29	0.000	0.85	0.001	0.03	1333.08	0.00

Table I.2 b: DNS data of Table I.2a continued.

y/δ	R _{xx}	R _{yy}	R _{zz}	R _{yz}	λ _{R1}	λ_{R2}	λ_{R3}	III _b	II _b
0.015	0.23	0.08	0.69	-0.09	0.07	0.23	0.70	0.030	0.216
0.02	0.25	0.10	0.65	-0.10	0.09	0.25	0.66	0.019	0.173
0.03	0.27	0.12	0.61	-0.10	0.10	0.27	0.63	0.014	0.148
0.04	0.27	0.14	0.59	-0.11	0.12	0.27	0.61	0.011	0.127
0.05	0.27	0.15	0.58	-0.11	0.12	0.27	0.61	0.011	0.124
0.13	0.25	0.16	0.59	-0.12	0.13	0.25	0.62	0.014	0.128
0.25	0.24	0.18	0.58	-0.13	0.14	0.25	0.61	0.015	0.124
0.50	0.25	0.20	0.55	-0.13	0.16	0.25	0.59	0.011	0.104
0.75	0.26	0.23	0.51	-0.10	0.19	0.26	0.55	0.007	0.071
1.00	0.27	0.26	0.47	0.00	0.27	0.27	0.46	0.002	0.026

Table I.2c: URAPS predictions

y/δ	ĩ	N _Γ	R _{xx}	R _{yy}	R _{zz}	R _{yz}	λ _{R1}	λ_{R2}	λ_{R3}	III _b	II _b
0.015	0.830	0.019	0.24	0.15	0.61	-0.19	0.08	0.24	0.68	0.025	0.190
0.02	0.857	0.015	0.24	0.18	0.58	-0.19	0.10	0.24	0.66	0.020	0.163
0.03	0.871	0.014	0.25	0.19	0.56	-0.19	0.11	0.25	0.64	0.017	0.150
0.04	0.878	0.013	0.25	0.20	0.55	-0.19	0.12	0.25	0.63	0.016	0.142
0.05	0.877	0.013	0.25	0.20	0.55	-0.19	0.12	0.25	0.63	0.016	0.144
0.13	0.872	0.014	0.25	0.19	0.56	-0.19	0.11	0.25	0.64	0.017	0.148
0.25	0.881	0.013	0.25	0.20	0.55	-0.19	0.12	0.25	0.63	0.015	0.140
0.50	0.891	0.012	0.26	0.21	0.53	-0.18	0.13	0.26	0.61	0.014	0.130
0.75	0.923	0.009	0.27	0.24	0.49	-0.17	0.15	0.27	0.58	0.008	0.095
1.00	1.000	0.000	0.33	0.33	0.34	0.00	0.33	0.33	0.34	0.000	0.000

Table I.3a: DNS data for Spanwise rotating channel in the linear velocity profile region.

a: Wu and Kasagi, 2002, Wu and Kasagi, 2004. b,c: Alvelius, 1999 (as reported by Grundestam et al. 2008) d,e,f:Grundestam et al., 2008:

	a	b	С	d	e	f
$Ro = \frac{\delta\Omega_{x}}{u_{b}}$ $Re_{b} = \frac{u_{b}\delta}{v}$ $Ro^{+} = \frac{\delta\Omega_{x}}{u_{b}^{*}}$	-0.0687	-0.215	-0.385	-0.49	-0.75	-1.03
$Re_b = \frac{u_b \delta}{v}$	5378	~3100	~3470	4026	6592	9605
$Ro^{+} \equiv \frac{\delta\Omega_{x}}{u^{*}}$	-1.25	-3.71	-7.41	-11	-27.5	-55
$Re^{+} \equiv \frac{\delta u^{*}}{v}$	295.5	180	180	180	180	180
$\frac{y}{\delta}$	0.7	0.5	0.5	0.25	0.25	0.25
< u'zu'z >+	1.00	1.1	1.05	1.1	0.6	0.1
< u'yu'y >+	1.55	3.6	4.9	5.3	6.3	3.6
$< u_X^{'} u_X^{'} > ^+$	0.95	2.3	3.3	3.9	4.2	2.1
<u'yu'z>+</u'yu'z>	-0.67	-0.95	-0.85	-1.05	-0.7	-0.2
k ⁺	1.75	3.5	4.625	5.15	5.55	2.9
ε+	0.0045	0.04	0.065	0.11	0.18	0.12
$\frac{\mathrm{d}u^+}{\mathrm{d}y^+} = 2\left \Omega_x^+\right $	0.0084	0.04	0.08	0.12	0.31	0.61
$\tilde{\Gamma} = \frac{du^+}{dy^+} \frac{k^+}{\epsilon^+}$	3.30	3.61	5.86	5.72	9.42	14.77
$\tilde{\Omega} = \Omega_{X} \frac{k^{+}}{\epsilon^{+}}$	-1.65	-1.80	-2.93	-2.86	-4.71	-7.38
$\frac{\Omega_{x}}{\Gamma_{yz}}$	-0.5	-0.5	-0.5	-0.5	-0.5	-0.5

Table I.3b: DNS data for spanwise rotating channel in the linear velocity profile region and the corresponding APS predictions for the Reynolds stress components.

		a	b	С	d	e	f
DNS	$\tilde{\Gamma} = \frac{du^+}{dy^+} \frac{k^+}{\epsilon^+}$	3.30	3.61	5.86	5.72	9.42	14.77
:	$\tilde{\Omega} = \Omega_{x} \frac{k^{+}}{\varepsilon^{+}}$	-1.65	-1.80	-2.93	-2.86	-4.71	-7.38
	R_{zz}	0.29	0.16	0.11	0.11	0.05	0.02
	R_{yy}	0.44	0.51	0.53	0.51	0.57	0.62
	R _{xx}	0.27	0.33	0.36	0.38	0.38	0.36
	R _{yz}	-0.19	-0.14	-0.09	-0.10	-0.06	-0.03
URAPS	R _{zz}	0.22	0.21	0.16	0.16	0.11	0.07
	R _{yy}	0.51	0.53	0.60	0.60	0.67	0.72
	R _{xx}	0.27	0.26	0.24	0.24	0.22	0.21
	R _{yz}	-0.18	-0.18	-0.19	-0.19	-0.18	-0.15

Table I.4a: DNS data for Spanwise rotating channel (Wu and Kasagi, 2002, Wu and Kasagi, 2004).

[y ⁺]	y ⁺	y/δ	p ⁺	u ⁺	$\frac{d u^+}{d y^+}$	k ⁺	ε+	Γ	$ ilde{\Omega}$
570	560.53	1.90	2.09	12.65	-0.223	2.39	0.026	-21.23	-0.40
560	551.41	1.87	2.09	14.38	-0.162	2.16	0.021	-16.74	-0.43
550	541.20	1.83	2.06	15.79	-0.117	1.99	0.017	-13.92	-0.50
525	515.53	1.74	1.88	17.98	-0.063	1.72	0.010	-10.91	-0.73
500	490.34	1.66	1.62	19.23	-0.039	1.49	0.006	-9.40	-1.01
450	440.45	1.49	1.13	20.42	-0.012	1.15	0.003	-4.62	-1.59
400	390.49	1.32	0.97	20.66	0.001	1.09	0.002	0.24	-1.87
350	340.45	1.15	1.08	20.50	0.005	1.20	0.003	2.34	-1.90
300	295.50	1.00	1.25	20.21	0.007	1.37	0.003	3.07	-1.86
250	250.55	0.85	1.42	19.88	0.008	1.56	0.004	3.27	-1.78
200	200.52	0.68	1.60	19.47	0.009	1.80	0.005	3.25	-1.62
150	150.55	0.51	1.81	19.01	0.010	2.09	0.006	3.25	-1.38
100	100.66	0.34	2.12	18.40	0.015	2.55	0.010	3.67	-1.03
75	75.47	0.26	2.35	17.96	0.021	2.96	0.015	3.91	-0.82
50	49.80	0.17	2.65	17.30	0.034	3.68	0.027	4.57	-0.58
40	39.59	0.13	2.76	16.89	0.049	4.16	0.036	5.48	-0.49
30	30.47	0.10	2.81	16.32	0.080	4.76	0.050	7.47	-0.40

Table I.4b: DNS data of Table I.4a continued.

y/δ	Ret	P/e	R _{xx}	R _{yy}	R _{zz}	R _{yz}	λ _{RI}	λ_{R2}	λ _{R3}	Шь	II _b
1.90	222.86	2.53	0.15	0.05	0.80	0.06	0.05	0.15	0.80	0.07	0.33
1.87	219.42	2.43	0.19	0.07	0.74	0.07	0.07	0.19	0.74	0.05	0.26
1.83	234.19	2.26	0.22	0.09	0.69	0.08	0.08	0.22	0.70	0.03	0.21
1.74	296.48	1.84	0.27	0.12	0.61	0.09	0.10	0.27	0.63	0.01	0.15
1.66	356.79	1.46	0.29	0.14	0.57	0.08	0.12	0.29	0.58	0.01	0.11
1.49	432.43	0.39	0.35	0.22	0.43	0.04	0.21	0.35	0.44	0.00	0.03
1.32	481.39	0.01	0.37	0.33	0.30	-0.03	0.29	0.35	0.37	0.00	0.00
1.15	541.56	0.43	0.33	0.41	0.26	-0.09	0.22	0.33	0.45	0.00	0.03
1.00	603.95	0.83	0.29	0.45	0.26	-0.13	0.19	0.29	0.52	0.00	0.06
0.85	658.33	1.10	0.27	0.46	0.27	-0.17	0.17	0.27	0.56	0.01	0.08
0.68	687.73	1.26	0.27	0.44	0.29	-0.19	0.16	0.27	0.57	0.01	0.09
0.51	683.05	1.35	0.29	0.38	0.33	-0.20	0.15	0.29	0.56	0.01	0.09
0.34	622.05	1.48	0.31	0.29	0.40	-0.20	0.14	0.31	0.55	0.00	0.09
0.26	571.60	1.47	0.31	0.24	0.45	-0.19	0.13	0.31	0.56	0.00	0.09
0.17	506.61	1.48	0.30	0.17	0.53	-0.16	0.11	0.30	0.59	0.01	0.12
0.13	478.37	1.60	0.28	0.13	0.59	-0.14	0.09	0.28	0.63	0.01	0.15
0.10	454.12	1.91	0.25	0.10	0.65	-0.12	0.07	0.25	0.68	0.02	0.19

Table I.4c: URAPS predictions

y/δ	ĩ	ΝΓ	N_{Ω}	R _{xx}	R _{yy}	R _{zz}	R _{yz}
1.90	0.723	-0.055	-0.002	0.22	0.06	0.72	0.101
1.87	0.735	-0.044	-0.002	0.22	0.07	0.71	0.110
1.83	0.746	-0.037	-0.003	0.23	0.09	0.68	0.113
1.74	0.760	-0.030	-0.004	0.24	0.12	0.64	0.101
1.66	0.766	-0.026	-0.006	0.26	0.14	0.60	0.083
1.49	0.797	-0.013	-0.009	0.30	0.22	0.48	0.046
1.32	0.854	0.001	-0.011	0.34	0.34	0.32	-0.004
1.15	0.880	0.007	-0.012	0.31	0.46	0.23	-0.071
1.00	0.888	0.010	-0.012	0.28	0.51	0.21	-0.125
0.85	0.894	0.010	-0.011	0.27	0.52	0.21	-0.156
0.68	0.904	0.011	-0.010	0.26	0.52	0.22	-0.183
0.51	0.918	0.011	-0.009	0.25	0.50	0.25	-0.225
0.34	0.924	0.012	-0.007	0.23	0.41	0.36	-0.298
0.26	0.918	0.013	-0.005	0.23	0.34	0.43	-0.306
0.17	0.893	0.015	-0.004	0.23	0.26	0.51	-0.291
0.13	0.866	0.017	-0.003	0.22	0.21	0.57	-0.276
0.10	0.822	0.022	-0.002	0.22	0.15	0.63	-0.250

(P.T.O. Table I.4c contd.)

Table I.4c continued: URAPS predictions

y/δ	λ_{R1}	λ_{R2}	λ_{R3}	III _b	II _b
1.90	0.04	0.22	0.74	0.04	0.26
1.87	0.06	0.22	0.72	0.04	0.24
1.83	0.07	0.23	0.70	0.03	0.22
1.74	0.10	0.24	0.66	0.02	0.17
1.66	0.13	0.26	0.61	0.01	0.13
1.49	0.21	0.30	0.49	0.00	0.04
1.32	0.32	0.34	0.34	0.00	0.00
1.15	0.22	0.31	0.48	0.00	0.03
1.00	0.17	0.28	0.55	0.01	0.08
0.85	0.15	0.27	0.58	0.01	0.10
0.68	0.14	0.26	0.60	0.01	0.12
0.51	0.12	0.25	0.63	0.02	0.14
0.34	0.08	0.23	0.68	0.03	0.19
0.26	0.08	0.23	0.69	0.03	0.21
0.17	0.07	0.23	0.70	0.03	0.22
0.13	0.06	0.22	0.72	0.03	0.24
0.10	0.04	0.22	0.74	0.04	0.26

Tabl

Tal

Table I.5 DNS Results for Developing Homogeneous Shear (Brethouwer, 2005)($\tilde{\Omega}/\tilde{\Gamma}=0$); $\tilde{\Gamma}_o=18$

ĩ	R _{xx}	R yy	R _{zz}	R _{yz}
0	0.333	0.333	0.334	0.000
2	0.436	0.172	0.392	-0.169
4	0.573	0.091	0.336	-0.157
6	0.654	0.078	0.268	-0.139
8	0.693	0.075	0.232	-0.128
10	0.697	0.089	0.214	-0.127
12	0.663	0.112	0.225	-0.135

Table I.6 Self Similar States for Homogeneous Shear (DNS- Brethouwer, 2005; LES- Bardina et al., 1983 (see Salhi and Cambon, 1997))

	$ ilde{\Omega}/ ilde{\Gamma}$	Γ̄ _o (appx)	t̃ (appx)	Γ̃(8) (appx)	R _{xx}	R yy	R _{zz}	R _{yz}
DNS	0	18	12	12	0.210	0.120	0.670	-0.130
	-0.25	18	8	12	0.280	0.370	0.350	-0.320
	-0.5	18	14	12	0.394	0.553	0.053	-0.065
LES	0	3.3	5	-	0.294	0.073	0.633	-0.15
	-0.25	3.3	5	-	0.224	0.383	0.393	-0.35
	-0.5	3.3	5	-	0.344	0.583	0.073	-0.1

BIBLIOGRAPHY

BIBLIOGRAPHY

- Abid, R., and R. Habibi, 2003, "Analysis of Reynolds Stress Equations for Stratified Rotating Homogeneous Shear Flow", International Journal of Engineering Science 41, 1869-1881.
- Akylas, E., C. A. Langer, S. C. Kassinos, and E. Demostheneous, 2007, "On the linear Stability of Turbulent Plane Strain Flow in a Rotating Frame", Phys. Fluids, 19, 075108, 1-11.
- Alamo, J. D. C. and J. Jimenez, 2003, "Spectra of the Very Large Anisotropic Scales in Turbulent Channels", Phys. Fluids, 15 (6), L41-L44.
- Alamo, J. C. D., J. Jimenez, P. Zandonade, and R. D. Moser, 2004, "Scaling of the Energy Spectra of Turbulent Channels", J. Fluid Mech., Vol. 500, pp. 135-144.
- Alvelious K., 1999, "Studies of Turbulence and its Modelling Through Large Eddy- and Direct Numerical Simulation", Ph.D., Royal Institute of Technology, Sweden.
- Andereck, C., S. Lin, and H. Swinney, 1986, "Flow regimes in a Circular Couette System With Independently Rotating Cylinders", J. Fluid Mech., 164, 155.
- Bagheri, M. and K. S. Surana, 2000, "P-Version Least Squares Finite Element Formulation of Extended K-ε Model of Turbulence for Fully Developed Flow", Commun. Numer. Meth. Engg., 16, 83-95.
- Baglietto, E. and H. Ninokata, 2006, "Anisotropic Eddy Viscosity Modeling for Application to Industrial Engineering Internal Flows", I. J. Trans. Phenomena, 8, 85-101.
- Bardina, J, J. H. Ferziger, and W. C. Reynolds, 1983, "Improved Turbulence Models Based on Large-Eddy Simulation of Homogeneous, Incompressible, Turbulent Flows", TF-19, Stanford University.
- Bardina, J., J. H. Ferziger, and R. S. Rogallo, 1985, "Effect of Rotation on Isotropic Turbulence: Computational and Modelling", J. Fluid Mech., 154, 321-336.
- Bartello P., O. Metais, and M. Lesieur, 1994, "Coherent Structures in Rotating Three-Dimensional Turbulence", J. Fluid Mech., 273, 1-29.
- Batchelor, G. and A. Townseed, 1948, "Decay of Turbulence in the Initial Period", Proc. Roy. Soc., A 194, 527.
- Bird, R. B., W. E. Stewart, and E. N. Lightfoot, 2007, **Transport Phenomena**, Second Edition, John Wiley & Sons.

- Biswas G., and V. Eswaran, 2002, "Turbulent Flows: Fundamentals, Experiments and Modelling", ISBN 1-84265-067-X.
- Boussinesq, J., 1877, "Theorie De l'Ecoulement Toubillant", Me'moires Pre'sente's Par Divers Savants a' l'Acade'mie des Sciences, 23, 46-50.
- Brethower B., 2005, "The Effect of Rotation on Rapidly Sheared Homogeneous Turbulence and Passive Scalar Transport. Linear Theory and Direct Numerical Simulation", J. Fluid Mech., 542, 305-342.
- Brodkey, R.S., S. G. Nychas, J.L. Taraba, and J. M. Wallace, 1973, "Turbulent energy production, dissipation, and transfer", Phys. Fluids, 14, No. 11, 2010-2011. Also see Bradshaw, P., 1974, Phys. Fluids, 17, No. 11, 2149; and Brodkey, R.S. and J.L. Taraba, Phys. Fluids, 17, No. 11, 2150.
- Cambon C., N. N. Mansour, F. S. Godefrerd, 1997, "Energy Transfer in Rotating Turbulence", J. Fluid Mech., 337, 303-332.
- Cambon, C., and J. F. Scott, 1999, "Linear and Nonlinear Models of Anisotropic Turbulence", Annu. Rev. Fluid Mech., 31, 1-53.
- Chen, C.-J. and S.-Y. Jaw, 1999, Fundamentals of Turbulence Modeling, Taylor & Francis, Washington, D. C.
- Chen, W., and F. Song, 1997, "Reynolds Stress Modeling of Turbulent Rotating Flows", Acta Mechanica Sinica (English Series), The Chinese Society of Theoretical and Applied Mechanics, 13 (4), 323-330.
- Churchill, S. W., and C. Chan, 1995, "Turbulent Flow in Channels in Terms of Local Turbulent Shear and Normal Stresses", AIChE J., 41 (12), 2513-2521.
- Churchill, S. W., 1996, "A Critique of Predictive and Correlative Models for Turbulent Flow and Convection", Ind. Eng. Chem. Res., 35 (9), 3122-3140.
- Comte-Bellot G. and S. Corrsin, 1971, "Simple Eulerian Time Correlation of Full and Narrow Band Velocity Signals in Grid Generated Isotropic Turbulence", J. Fluid Mech., 48, 273.
- Corrsin, S., 1974, "Limitations of Gradient Transport Models in Random Walks and in Turbulence", Advances in Geophysics, 18A, 25-71.
- Craft, T. J., B. E. Lander, K. Suga, 1996, "Development and Application of a Cubic Eddy-Viscosity Model of Turbulence", Int. J. Heat and Fluid flow, 17 (2), 108-115.
- Craft, T. J. and B. E. Lander, 1996, "A Reynolds Stress Closure Designed for Complex Geometries", Int. J. Heat and Fluid flow, 17 (3), 245-254.

- Craft, T. J., 1998, "Developments in a low-Reynolds-Number Second-Moment closure and its Application to Separating and Reattaching Flows", Int. J. Heat and Fluid Flow 19, 541-548.
- Craft, T. J., and B. E. Launder, 2001, "Principles and Performance of TCL-Based Second -Moment Closures, Flow, Turbulence and Combustion, 66, 355-372.
- Dafalias, Y. F., and B. A. Younis, 2007, "Objective Tensorial Representation of the Pressure-Strain Correlations of Turbulence", Mechanics Research Communications, 34, 319-324.
- Daoud, M. and A. Naguib, 2004, "Stochastic Estimation of the Flow Structure Downstream of a Separating/Reattaching Flow Using Wall-Pressure-Array Measurements", ASME Heat Transfer/Fluids Engineering Summer Conference, paper no. HT-FED04-56816, Charlotte, NC, July 11 15.
- DOE, 1999, "Chemical Industry of the Future: Technology Roadmap for Computational Fluid Dynamics", U.S. Department of Energy (DOE), Office of Industrial Technologies, Washington DC.
- Durst, H., 2001, "Reynolds Stress Under a Change of Frame of Reference", Physical Review E, 63, 056305, 1-5.
- Eggels, J.G.M., F. Unger, M.H. Weiss, J. Westerweel, R. J. Adrian, R. Friedrich, and F. T. M. Nieuwstadt, 1994, "Fully Developed Turbulent Pipe Flow: A Comparison Between Direct Numerical Simulation and Experiment", J. Fluid Mech., 254, 175-209.
- El-dein, D., S. Parks, C.A. Petty, and A. Bénard, 2004, "Simulation of Flow in a Pulsed-Jet Mixer Using a Volume-of-Fluid Model", 297-306, **Advances in Fluid Mechanics**, V, Editors: C. A. Brebbia, A. C. Mendes, and M. Rahman, WIT Press.
- El-dein, D., 2003, "Computational Fluid Dynamics Simulation of a Pulsed-Jet Mixer", MS Thesis, Michigan State University.
- El-Samni, O. A. and N. Kasagi, 2001, "The Effect of System Rotation with Three Orthogonal Rotating Axes on Turbulent Channel Flow", proceedings of ICFDP7.
- Faddeeva, V. N., 1959, Computational Methods of Linear Algebra, Dover, New York.
- Frazer, R. A., W. J. Duncan, and A. R. Collar, 1960, Elementary Matrices and Some Applications to Dynamics and Differential Equations, University Press, Cambridge.
- Gatski T.B., S. S. Sarkar, and C. G. Speziale, 1992 Studies in Turbulence, Springer, Berlin.

- Gatski, T. B., T. Jongen and L. Machiels 1998, "Predicting Nonlinear Effects with Linear and Nonlinear Eddy-Viscosity and Algebraic Stress Models", Flow, Turbulence and Combustion, 60, 215-234.
- Gatski, T. B. and T. Jongen, 2000, "Nonlinear Eddy Viscosity and Algebraic Stress Models for Solving Complex Turbulent Flows", Progress in Aerospace Sciences, 36, 655-682.
- Gatski, T. B., 2004, "Constitutive Equations for Turbulent Flows", Theoret. Comput. Fluid Dynamics, 18, 345-369.
- Gatski, T. B. and C. L. Rumsey, 2006, "On the Behavior of Two-Equation Models in Non-equilibrium Homogenous Turbulence", Phys. Fluids, 18, 065109.
- George W. K. and M. M. Gibson, 1992, "The Self-Preservation of Homogeneous Shear Flow Turbulence", Experiments in Fluids, 13, 229-238.
- Girimaji, S. S., 2004, "A New Perspective on Realizability of Turbulence Models", J. Fluid Mech., **512**, 191-210.
- Greenspan, 1968, Theory of Rotating Flows, Cambridge Press.
- Grundestam, O., 2004, "Development and Analysis of Turbulence Models for Flows with Strong Curvature and Rotation", Ph.D., Royal Institute of Technology, Sweden.
- Grundestam, O., and S. Wallin, 2008, "Direct Numerical Simulations of Rotating Turbulent Channel Flow", J. Fluid Mech., **598**, 177-199.
- Grundestam, O., S. Wallin, and A. V. Johansson, 2008, "A Priory Evaluations and Least-Squares Optimization of Turbulence Models for Fully Developed Rotating Channel Flow", European Journal of Mechanics B/Fluids 27, 75-95.
- Gunther, A., D. V. Papavassiliou, M. D. Warholic, and T. J. Hanratty, 1998, "Turbulent Flow in a Channel at a Low Reynolds Number", Experiments in Fluids, 25, 503-511.
- Gupta, A. K., D. G. Lilley, and N. Syred, 1984, **Swirl Flows**, Abacus Press, Cambridge, Massachusetts.
- Hamba F., 2006, "The Mechanism of Zero Mean Absolute Vorticity State in Rotating Channel Flow", Phys. Fluids, 18, 125104, 1-11.
- Hamba, F., 2006, "Euclidean Invariance and Weak Equillibrium Condition for the Algebraic Reynolds Stress Model", J. Fluid Mech., 569, 399-408.
- Hanjalic, K. and B. E. Launder, 1972, "A Reynolds Stress Model for Turbulence and its Application to Thin Shear Flows", J. Fluid Mech., **52** (4), 609-633.

- Hanjalic, K., 1994, "Advanced Turbulence Closure Models: A View of Current Status and Future Prospects", Int. J. Heat and Fluid flow, 15 (3), 178.
- Hanratty, T.J., 2003, "Workshop on Scientific Issues in Multiphase Flow", The University of Illinois at Urbana-Champaign, May 7-9, 2002, DOE Program on Engineering Physics.
- Hansen, K. G., C. H. Isben, T. Solberg, and B. H. Hjertager, 2003, "Eulerian/Eulerian CFD Simulation of a Cold Flowing FCC Riser", International Journal of Chemical Reactor Engineering, Vol. 1: A31 (http://www.bepress.com/ijcre/vol1/A31).
- Harris V. G., A. H. Graham, and S. Corrsin, 1977, "Further Experiments in Nearly Homogeneous Turbulent Shear Flow", J. Fluid. Mech., 81 (4), 657-687.
- Heschl, Ch., W. Sanz, and P. Klanatsky, 2005, "Implementation and Comparision of Different Turbulence Models for Three Dimensional Wall Jets with Fluent", CFD Forum, Bad Nauheim, Deutschland.
- Hill, J. C., and C. A. Petty, 1996, "Turbulent Transport of a Passive Scalar Field", Chem. Eng. Comm., **152-153**, 413-432.
- Hinze, J. O., 1975, **Turbulence**, 2nd Edition, McGraw-Hill, New York.
- Hirt, C.W., and B.D. Nichols, 1981, "Volume of Fluid (VOF) Method for Dynamics of Free Boundaries", J. Comput., Physics, 39, 210-225.
- Hoyas, S. and J. Jimenez, 2006, "Scaling of the Velocity Fluctuations in Turbulent Channels up to $Re_{\Gamma} = 2003$ ", Phys. Fluids, 18, 011702, 1-4.
- Huang, Y-N, and F. Durst, 2001, "Reynolds Stress Under a Change of Frame of Reference", Physical Review E, 63, 056305, 1-5.
- Hudy, L.M., A.M. Naguib, and W.M. Humphreys Jr., 2003, "Wall-Pressure-Array Measurements Beneath a Separating/Reattaching Flow Region", Phys. Fluids, 15 (3), 706-717.
- Hudy, L., A. M. Naguib, W.M. Humphreys and S.M. Bartram, 2005, "Particle Image Velocimetry Measurements of a Two/Three-dimensional Separating/Reattaching Boundary Layer Downstream of an Axisymmetric Backward-facing step", 43rd Aerospace Sciences and Exhibit, AIAA paper no. 2005-0114, Reno, NV, January 10 13.
- Ibbetson, A., and D. J. Tritton, 1975, "Experiments on Turbulence in a Rotating Fluid", J. Fluids Mech., 68 (4), 639-672.
- Iida O., K. Miyamoto, and Y. Nagano, 2007, "Structure of Turbulent Channel Flow under Spanwise System Rotation", Journal of Fluid Science and Technology, 2 (3), 547-557.

- Ilinca, F., D. Pelletier and A. Garon, 1997, "An Adaptive Finite Element Method For A Two-Equation Turbulence Model in Wall-Bounded Flows", International Journal for Numerical Methods in fluids, 24, 101-120.
- Iwamoto, K., Y. Suzuki and N. Kasagi, 2002, "Reynolds Number Effect on Wall Turbulence: Toward Effective Feedback Control", Int. J. Heat and Fluid Flow, 23, 678-689. Also see Iwamoto, K., 2002, "Database of Fully Developed Channel Flow", THTLAB Internal Report No. ILR-0201., THTLAB, The Univ. of Tokyo
- Jaberi, F.A. and P.J. Colucci, 2003, "Large Eddy Simulation of Heat and Mass Transport in Turbulent Flows, Part 1": Velocity Field," International Journal of Heat and Mass Transfer, 46, 1811-1825.
- Jacquin, L., O. Leuchter, C. Cambon, and J. Mathieu, 1990, "Homogeneous Turbulence in the Presence of Rotation", J. Fluid Mech., 220, 1-52.
- James, S., and F.A. Jaberi, 2000, "Large Scale Simulations of Nonpremixed Methane Jet Flames", Combustion and Flame, 123, 456-487.
- Jing-Lei, X., M. Yang, H. Yu-ning, 2008, "Non-Linear Turbulence Models for Predicting Strong Curvature Effects", Appl. Math. Mech., 29 (1), 31-42.
- Jongen, T., and G. Mompean, 1998, "Accounting for Reynolds stress and dissipation rate anisotropies in inertial and noninertial frames", Phys. Fluids, 10 (3), 674-684.
- Jongen, T., L. Machiels, T. B. Gatski, 1998, "Predicting Noninertial Effects with Linear and Nonlinear Eddy-Viscosity, and Algebraic Stress Models", Flow Turbulence and Combustion, 60, 215-234.
- Jovanovic, J., I. Otic, P. Bradshaw, 2003, "On the Anisotropy of Axisymmetric Strained Turbulence in the Dissipation Range", **125** (May), 401-413.
- Jovanovic, J., and R. Hillerbrand, 2005, "On Peculiar Property of the Velocity Fluctuations in Wall-Bounded Flows", Thermal Science, 9 (1), 3-12.
- Kantorovich, L. V. and G. P. Akilov, 1964, p. 627 in Functional Analysis in Normed Spaces, Pergamon Press, Oxford.
- Kasagi et al., DNS Database of Turbulence and Heat Transfer: (Tokyo, Japan) (http://www.thtlab.t.u-tokyo.ac.jp/)
- Kassinos, S. C., C. A. Langer, G. Kalitzin and G. Laccarino, 2006, "A Simplified Structure-Based Model Using Standard Turbulence", Int. J. Heat and Fluid Flow, 27, 653-660.
- Kim J., P. Moin, and R. D. Moser, 1987, "Turbulence statistics in fully developed channel flow at low Reynolds number", J. Fluid Mech. 177, 133-166.

- Kleinstreuer, C., 2003, **Two-Phase Flow: Theory and Applications**, Taylor and Fransis, N.Y.
- Ko. T., H.G. Choi, R. Bai, D.D. Joseph, 2002, "Finite Element Method Simulation of Turbulent Wavy Core-Annular Flows using a K-ω Turbulence Model Method", International Journal of Multiphase Flow, 28, 1205-1222.
- Koppula K. S., A. Bénard, and C. A. Petty (presenter), 2005, "Reynolds Stress Closure for Strongly Swirling Flows", Symposium [01J10]: Poster Session in Fluid Mechanics, Annual AIChE Meeting, October 30-November 4, 2005, Cincinnati Convention Center, Cincinnati, Ohio.
- Koppula K. S. (presenter), N. Gandi, A. Parihar, S. Moeykens, A. Bénard, C. A. Petty, 2006, "Integrating Computational Fluid Dynamics into the Engineering Curriculum: Demonstration Through Case Studies", Free Forum on engineering Education, Annual AIChE Meeting, November 15, 2006, San Francisco, California.
- Koppula K. S., A. Bénard, C. A. Petty (presenter), 2006, "Realizable Algebraic Reynolds Stress Model for Single Phase and Multiphase Turbulent Flows", Symposium on Turbulent Flows, Annual AIChE Meeting, November 14, 2006, San Francisco, California.
- Koppula K. S. (presenter), A. Bénard, C. A. Petty, 2007, "Realizable Reynolds Stress Closure for Turbulent Flows", Symposium on Turbulent Flows, Annual AIChE Meeting, November 6, 2007, Salt Lake City, Utah.
- Koppula K. S., A. Bénard, C. A. Petty, 2009, "Realizable Algebraic Reynolds Stress Closure", Chemical Engineering Science (accepted).
- Lamballais, E., M. Lesieur, and O. Metais, "Effects of Spanwise Rotation on the Vorticity Stretching in Transitional and Turbulent Channel Flow" Int. J. Heat and Fluid Flow, 17 (3), 325-332.
- Langer, C. A., S. C. Kassinos, W. C. Reynolds, 2003, "An Algebraic Structure-Based Turbulence Model", AFOSR Thermal and Fluid Sciences Affiliates & Sponsors Conference, February 5, Mechanical Engineering, Stanford University.
- Lathrop, D., J. Fineberg, and H. Swinney, 1992, "Turbulent Flow Between Concentric Rotating Cylinders at Large Reynolds Numbers", Phys. Rev. Letters, 68 (10), 1515.
- Launder, B. E. and D. B. Spalding, 1972, **Mathematical Models of Turbulence**, Academic Press.
- Launder, B. E. and D. B. Spalding, 1974, "The Numerical Computation of Turbulent Flows", Computer Methods in Applied Mechanics and Engineering, 3, 269-289.

- Launder, B. E. and B. I. Sharma, 1974, "Application of the Energy-Dissipation Model of Turbulence to the Calculation of Flow near a Spinning Disc", Letters in Heat and Mass Transfer, 1, 131-138.
- Li B.Y., N. S. Liu, X. Y. Lu, 2006, "Direct Numerical Simulations of Wall Normal Rotating Turbulent Channel Flow with Heat Transfer", International Journal of Heat and Mass Transfer, 49, 1162-1175.
- Liu, N. S., and X. Y. Lu, 2007, "Direct Numerical Simulation of Spanwise Rotating Turbulent Channel Flow with Heat Transfer", Int. J. Numer. Meth. Fluids, **53**, 1689-1706.
- Lumley, J., 1978, "Computational Modeling of Turbulent Flows", Adv. App. Mech., 18, 123.
- Mansour, N. N, and A. A. Wray, 1994, "Decay of Isotropic Turbulence at Low Reynolds Number", Phys. Fluids, 6 (2), 808-814.
- Marcus, P.S., 1984, "Simulation of Taylor-Couette flow: Part I. Numerical Methods and Comparison with Experiments", J. Fluid Mech., 146, 45-64.
- Moin, P., K. Mahesh, 1998, "Direct Numerical Simulation: A Tool in Turbulence Research", Annu. Rev. Fluid Mech., 30, 539-578.
- Monin, A.S. and A.M. Yaglom, 1965, Statistical Fluid Mechanics: Mechanics of Turbulence, Volume 1, MIT Press.
- Morinishi, Y., K. Nakabayashi, and S. Q. Ren, 2001, "Dynamics of Anisotropy on Decaying Homogeneous Turbulence Subjected to System Rotation", Phys. Fluids, 13, (10), 2912.
- Morize, C., F. Moisy, M. Rabaud, and J. Sommeria, 2007, "Dynamics of the Anisotropy in Decaying Rotating Turbulence with Confinement Effects", 18 Congrès Français de Mécanique, Grenoble, 27-31 August 2007.
- Morse, P.M. and H. Feshbach, 1953, **Methods of Theoretical Physics, Part I, McGraw-**Hill.
- Moser, R. D., J. Kim, N. N. Mansour, 1999, "Direct Numerical Simulation of Turbulent Channel Flow up to $Re_{\Gamma} = 590$ ", Phys. Fluids, 11 (4), 943-945.
- Moser et al., DNS Database for Turbulent Channel Flow: (Texas, U.S.A) (http://turbulence.ices.utexas.edu/MKM 1999.html; http://turbulence.ices.utexas.edu/)
- Nishino, K., M. Samada, K. Kasuya and K. Torri, 1996, "Turbulence Statistics in the Stagnation Region of an Axisymmetric Impinging Jet Flow", Int. J. Heat and Fluid Flow, 17, 193-201.

- Northrup, M.A., T.J. Kulp, and S.M.Angel, 1991, Fluorescent Particle Image Velocimetry: Application to Flow Measurement in Refractive Index-Matched Porous Media, Applied Optics, 30 (21), 3034-3040.
- Nsom, B., 1994, Transition from Circular Couette Flow to Taylor Vortex Flow in Dilute and Semi-Concentrated Suspensions of Stiff Fibers, J. Phys. II France, 4, 9-22.
- Oberlack, M., W. Cabot, B. A. Petersonreif and T. Weller, 2006, "Group Analysis, Direct Numerical Simulation and Modeling of a Turbulent Channel Flow with Streamwise Rotation", J. Fluid Mech., **562**, 383-403.
- Park, J. Y. and M. K. Chung, 1999, "A Model for the Decay of Rotating Homogeneous Turbulence", Phys. Fluids, 11 (6), 1544-1549.
- Parker, J. and P. Merati, 1996, An Investigation of Turbulent Taylor-Couette Flow Using Laser Doppler Velocimetry in a Refractive Index Matched Facility, Journal of Fluids Engineering, 118, 810-818.
- Parks, S.M., 1997, "Relaxation Model for Homogeneous Turbulent Flows", Ph.D. Dissertation, Michigan State University.
- Parks, S. M., K. Weispfennig, and C.A. Petty, 1998, "An Algebraic Preclosure Theory for the Reynolds Stress", Phys. Fluids, 10 (3), 645-653.
- Parks, S. M., and C. A. Petty, 1999, "Anisotropic Prestress Theory for Homogeneously Sheared Turbulent Flows", pp. 227 in **Turbulent Shear Flow Phenomena**, Editors: S. Bancrjee and E. K. Eaton, Begell House, New York.
- Pettersson-Reif. B. A., P. A. Durbin, and A. Ooi, 1999, "Modeling rotational effects in eddy-viscosity closures", Int. J. Heat and Fluid Flow, 20, 563-573.
- Pettersson-Reif., B. A., T. B. Gatski, and C. L. Rumsey, 2006, "On the Behavior of Two-Equation Models in Nonequilibrium Homogeneous Turbulence", Phys. Fluids, 18, 065109, 1-15.
- Petty, C. A., 1975, "A Statistical Theory for Mass Transfer Near Interfaces", Chem. Eng. Sci., 30, 1451.
- Petty C. A., and S. Lyons, 1985, "Predictions of Turbulent Drag Reduction for a Linear Viscoelastic Fluid", International Union of Theoretical and Applied Mechanics (1UTAM) Symposium, Essen, West Germany, 26-28 June 1984; Editor: B. Gampert, Springer-Verlag, The Influence of Polymer Additives on Velocity and Temperature Fields, p. 311.
- Petty, C. A., S. M. Parks, K. Weispfennig, 1999, "Passive Scalar Transport in Fully Developed Channel Flows", Proceedings of the Third ASME/JSME Joint Fluids Engineering Conference, FEDSM99-7757, San Francisco, CA, July 18-23.

- Petty, C.A, A. Bénard, and D. Eldin, 2004, "Realizable Algebraic Reynolds Stress", Session EJ Turbulence Modeling II, 57th Annual Meeting of the Division of Fluid Dynamics, American Physical Society Meeting, Seattle, November 21-23.
- Petty C. A. (presenter), A. Bénard, and K. S. Koppula, 2005 "Universal Realizable Reynolds Stress Model for Multiphase Fluids", 58th Annual Meeting of the Division of Fluid Dynamics, APS, November 20-22, 2005, Chicago, Illinois.
- Piquet, J., 1999, Turbulent Flows: Models and Physics, Springer, New York.
- Pope, S.B., 1975, "A More General Effective-Viscosity Hypothesis", J. Fluid Mech., 72, 331-340.
- Pope, S. B., 2000, Turbulent Flows, Cambridge University Press, Cambridge, UK.
- Poroseva, S. V., S. C. Kassinos, C. A. Langer and W. C. Reynolds, 2000, "Computation of Turbulent Flow in a Rotating Pipe using the Structure-Based Model", Center for Turbulence Research, Annual Research Briefs.
- Rahman, M. M. and T. Siikonen, 2006, "An Explicit Algebraic Reynolds Stress Model in Turbulence", Int J. Numer. Meth. Fluids, **52**, 1135-1157.
- Rahman, M. M., and T. Siikonen, 2006, "A Low-Reynolds Number Explicit Algebraic Stress Model", Transactions of the ASME, 128, 1364-1376.
- Recktenwald I., T. Weller, W. Schroder, M. Oberlack, 2007, "Comparision of Direct Numerical Simulations and Particle-image Velocimetry Data of Turbulent Channel Flow Rotating About the Streamwise Axis", Phys. Fluids, 19, 085114 (1-11).
- Reynolds, W. C., 1976, "Computation of Turbulent Flows", pp. 183-208, (#8087), Annual Reviews.
- Reynolds, W. C., 1987, "Fundamentals of Turbulence for Turbulence Modeling and Simulation", Computational Fluid Dynamics, Agard Report No. 755, pp. 1-67.
- Rivlin, R.S., 1955, "Further Remarks on the Stress Deformation Relations for Isotropic Materials", J. Arch. Ratl. Mech. Anal., 4, 681-702.
- Rodi, W. and N. N. Mansour, 1993, "Low Reynolds Number k-ε Modelling with the Aid of Direct Numerical Simulation Data" J. Fluid Mech., 250, 509-529.
- Rogallo, R. S. and P. Moin, 1984, "Numerical Simulation of Turbulent Flows", Annu. Rev. Fluid. Mech., 16, 99-137.
- Rohr J. J., E. C. Itsweire, K. N. Helland, and C. W. Vanatta, 1988, "An investigation of the growth of turbulence in a uniform-mean shear flow", J. Fluid. Mech., 187, 1-33.

- Ross, J. A., and B. E. Larock, 1997 "An Algebraic Stress Finite Element Model of Turbulent Flow", International Journal for Numerical Methods in Fluids, 24, 693-714.
- Rotta, J. C., 1951, "Statistische Theorie Nichthomogener Turbulenz", Z. Phys., 129, 547-572.
- Rumsey, C. L., T. B. Gatski, and J. H. Morrison, 2000, "Turbulence Model Predictions of Strongly Curved Flow in a U-Duct", AIAA Journal, 38 (8), 1394.
- Rung, T., F. Thiele, S. Fu., 1999 "On the realizability of Non Linear Stress-Strain relationships for Reynolds Stress Closures", Flow Turbulence and Combustion, 60, 333-359.
- Salhi, A. and T. Lilli, 1996, "Asymptotic Analysis of Equilibrium States for Rotating Turbulent Flows", Theoret. Comput. Fluid Dynamics, 8, 289-308.
- Salhi, A. and C. Cambon, 1997, "An Analysis of Rotating Shear Flow Using Linear Theory and DNS and LES Results", J. Fluid Mech., 347, 171-195.
- Salhi, A., C. Cambon, and C. G. Speziale, 1997, "Linear Stability Analysis of Plane Quadratic Flows in a Rotating Frame with Applications to Modeling", Phys. Fluids, 9 (8), 2300-2309.
- Salhi, A., and C. Cambon, 2007, "Anisotropic phase-mixing in homogeneous turbulence in a rapidly rotating or in a strongly stratified fluid: An analytical study", Phys. Fluids 19, 055102, 1-13.
- Sanci, N., Kugeler, K., Timm, W. & Schowalter, D., 2005, "Study of the Melt-Cool down in a Suggested Core Catcher Concept for a Helium Cooled Fast Breeder Reactor after a Hypothetical Severe Accident using Computational Fluid Dynamics Simulation", 13th International Conference on Nuclear Engineering, Beijing, China, May 16-20, 2005 ICONE13-50605.
- Schumann, U., 1977, "Realizability of Reynolds Stress Turbulence Models", Phys. Fluids, 20 (5), 721.
- Shaikmohammad I. T., D. Bandyopadhyay, K. S. Koppula, A. Benard (presenter), C. A. Petty, 2006, "Computational Fluid Dynamic Simulation of a Multiphase Fluid in Vertical Flow at High Reynolds Number", Poster Session in Fluid Mechanics, Annual AIChE Meeting, November 14, 2006, San Francisco, California.
- Shih, T-H and J. Zhu, 1994, "A New Reynolds Stress Algebraic Equation Model", NASA Lewis Research Center, NASA Technical Memorandum 106644, ICOMP-94-15; CMOTT-94-8 (30 pages).
- Shih, T-H, W.W. Liou, A. Shabbir, Z. Yang, and J. Zhu, 1995, "A New k-ε Eddy Viscosity Model for High Reynolds Number Turbulent Flows", Computers Fluids, 24 (3), 227-238.

- Shih, T. H, J. Zhu, W.W. Liou, K. H. Chen, N. S. Liu and J. Lumley, 1997, "Modeling of Turbulent Swirling Flows", Eleventh Symposium on Turbulent Shear Flows, Grenoble, France, 31-1 31-6.
- Shih, T. H., 1997, "Some Developments in Computational Modeling of Turbulent Flows" Fluid Dynamics Research, **20**, 67-96.
- Sjogren, T., and A. V. Johansson, 2000, "Development and Calibration of Algebraic Nonlinear Models for Terms in the Reynolds stress Transport Equations" Phys. Fluids, 12, 1554-1572.
- Smith, G. and A. Townsend, 1982, "Turbulent Couette Flow Between Concentric Cylinders at Large Taylor Numbers", J. Fluid Mech., 123, 187.
- Song, X., Shen, L., Murai, Y. Yamamoto, F., 1999, "Separation of Particle-Bubble Images in Multi-Phase Flow," in Proceedings of the Third International Workshop on PIV'99, Santa Barbara, Calif., 16 18 September, 15-18.
- Spalart, P. R. and C. G. Speziale, 1999, "A Note on Constraints in Turbulence Modelling", J. Fluid Mechanics, 391, 373-376.
- Speziale, C. G., 1985, "Modelling the Pressure Gradient-Velocity Correlation of Turbulence", Phys. Fluids, 28 (1), 69-71.
- Speziale, C. G., N. N. Mansour, and R. S. Rogallo, 1987, "The Decay of Isotropic Turbulence in a Rapidly Rotating Frame", Center for Turbulence Research, Proceedings of the Summer Program.
- Speziale, C. G., 1989, "Turbulence modeling in Noninertial Frames of Reference", Theoret. Compt. Fluid Dynamics, 1, 3-9.
- Speziale, C. G., 1991, "Analytical methods for the Development of Reynolds-Stress Closures in Turbulence", Ann. Rev. Fluid Mech., 23, 107.
- Speziale, C. G., R. Abid, and P. A. Durbin, 1993, "New Results on the Realizability of Reynolds Stress Turbulence Closures", ICASE Report 93-76, NASA CR-191548.
- Speziale, C. G., R. Abid, G. A. Blaisdell, 1996, "On the Consistency of Reynold's Stress Turbulence Closures with Hydrodynamic Stability Theory", Phys. Fluids, 8 (3), 781-788.
- Speziale, C. G. and X. Xu, 1996, "Towards the Development of Second-Order Closure Models for Non-Equilibrium Turbulent Flows", Int. J. Heat and Fluid Flow, 17, 238-244.
- Speziale, C. G. and T. B. Gatski, 1997, "Analysis and Modeling of Anisotropies in the Dissipation Rate of Turbulence", J. Fluid Mechanics, 344, 155-180.

- Speziale, C. G., 1998, "A review of material frame-indifference in mechanics", Appl. Mech. Rev. 51 (8), 489.
- Speziale, C. G., B. A. Younis, R. Rubinstein, and Y. Zhou, 1998, "On Consistency Conditions for Rotating Turbulent Flows", Phys. Fluids, 10 (8), 2108-2110.
- Speziale, C. G., 1998, "A Consistency Condition for Non-linear Algebraic Reynolds Stress Models in Turbulence" Int. J. Non-Linear Mechanics, 33 (4), 579-584.
- Speziale C. G., 1998, "Some Important Remarks Concerning Recent Work on Rotating Turbulence", Phys. Fluids, 10 (12), 3242-3244.
- Tavoularis, S., J. Bennett and S. Corrsin, 1978, "Velocity Derivative Skewness in Small Reynolds Number, Nearly Isotropic Turbulence", J. Fluid Mech., 88 (1), 63.
- Tavoularis, S. and U. Karnik, 1989, "Further Experiments on the Evolution of Turbulent Stresses and Scales in Uniformly Sheared Turbulence", J. Fluid Mech., 204, 457.
- Thais, L., G. Mompean, and L. Hean, 2005, "On the Consequenses of Material Frame-indifference in Algebraic Stress Models", Theoret. Comput. Fluid Dynamics, 19, 1-22.
- Theofanous, T.G., J.P. Sullivan, 1982, "Turbulence in Two-Phase Dispersed Flows," J. Fluid Mechanics, 116, 343-362.
- Truesdell, C. and W. Noll, 2004, Non-Linear Field Theories, Edited by S.S. Antman, Springer.
- Wallin S., 2000, "Engineering Turbulence Modelling for CFD with a Focus on Explicit Algebraic Reynolds Stress Models", Ph.D., Royal Institute of Technology, Sweden.
- Wallin S. and A. V. Johansson, 2002, "Modelling Streamline Curvature Effects in Explicit Algebraic Reynolds Stress Turbulence Models", Int. J. Heat and Fluid Flow 23, 721-730.
- Wei, T., P.Fife, J. Kliwicki, and P. McMurthy, 2005, "Properties of Mean Momentum Balance in Turbulent Boundary Layer, Pipe and Channel Flows", J. Fluid Mech., 522, 303-327.
- Weis, J., and K. Hutter, 2003, "On Euclidean Invariance of Algebraic Reynolds Stress Models in Turbulence", J. Fluid Mech., 476, 63-68.
- Weispfennig, K., 1997, "Relaxation/Retardation Model for Fully Developed Turbulent Channel Flow", Ph.D. dissertation, Michigan State University.
- Weispfennig, K., S. M. Parks, and C. A. Petty, 1999, "Isotropic Prestress for Fully Developed Channel Flows", Phys. Fluids, 11(5), 1262-1271.

- Wiegland, R. A., and H. M. Nagib, 1978, "Grid Generated Turbulence With and Without Rotation About the Streamwise Direction", IIT Fluid and Heat Transfer Report R78-1, Appendix B and C, Thesis.ST3B660, Illinois Institute of Technology, Chicago, Ill.
- Wu, H. and N. Kasagi, 2002, "Effects of Combined Streamwise and Spanwise Rotations on Turbulent Channel Flow", The fifth JSME-KSME Fluids Engineering Conference, Nov. 17-21, Nagoya, Japan.
- Wu, H. and N. Kasagi, 2004, "Effects of Arbitrary Directional System Rotation on Turbulent Channel Flow", Phys. Fluids, 16 (4), 979-990. Also see Wu, H. and N. Kasagi, 2004, "Turbulent Heat Transfer in a Channel Flow with Arbitrary System Rotation", Int. J. Heat Mass Transfer, 47, 4579-4591.
- Yang, X. and J. A. Domaradzki, 2004, "Large Eddy Simulations of Decaying Rotating Turbulence", Phys. Fluids, 16 (11), 4088-4104.
- Yang, X. D., and H. Y. Ma, 2003, "Computation of Strongly Swirling Confined Flows with Cubic Eddy- Vicosity Turbulence Models", Int. J. Numer. Meth. Fluids, 43, 1355-1370.
- Yang, X. D., and H. Y. Ma, and Y. N. Huang, 2005, "Prediction of Homogeneous Shear Flow and A Backward Facing Step Flow with Some Linear and Non-linear K-ε Turbulence Models, Communications in Nonlinear Science and Numerical Simulation, 10, 315-328.
- Yu, H., S. S. Girimaji, and L. S. Luo, 2005, "Lattice Boltzmann Simulations of Decaying Homogeneous Isotropic Turbulence", Physical Review E., 71, (016708), 1-5.

